Towards experimental therapies for retinal degenerative diseases

Koster, C.

Publication date
2022
Document Version
Final published version

Towards Experimental Therapies for Retinal Degenerative Diseases

Céline Koster

Towards Experimental Therapies for Retinal Degenerative Diseases

Céline Koster

ISBN: 978-94-6423-917-1
Cover & Layout: Angelique Ardjoen | www.aozoradesign.eu
Printed by: Proefschriftmaken | www.proefschriftmaken.nl

Towards experimental therapies for retinal degenerative diseases

ACADEMISCH PROEFSCHRIFT

ter verkrijging van de graad van doctor

aan de Universiteit van Amsterdam

op gezag van de Rector Magnificus

prof. dr. G.T.M. ten Dam

ten overstaan van een door het College voor Promoties ingestelde commissie,

in het openbaar te verdedigen in de Agnietenkapel

op vrijdag 16 september 2022, te 10.00 uur

door Céline Koster

geboren te Purmerend

Promotiecommissie

Promotor:	prof. dr. A.A.B. Bergen	AMC-UvA
Copromotor:	dr. K. Bharti	NIH-NEI
Overige leden:	prof. dr. C.J.F. Boon	AMC-UvA
	prof. dr. J.C. van Meurs	Erasmus Universiteit Rotterdam
	prof. dr. C.L. Mummery	Universiteit Leiden
	prof. dr. ir. T.H. Smit	AMC-UvA
	prof. dr. H. Tan	AMC-UvA
	prof. dr. J. Verhaagen	Vrije Universiteit Amsterdam
	dr. F.D. Verbraak	AMC-UvA

Faculteit der Geneeskunde

Gastopponent: Prof. Dr. C.D. van Karnebeek

verdedigingsceremonie 16 september 2022

"Ua ola loko i ke aloha"

Love gives life within

Voor Justin, mijn zoon

Voor Kees, mijn vader

Table of contents

Tell me and I forget.
Teach me and I remember.
Involve me and I learn.

— Benjamin Franklin

General introduction

1

Introduction

Hereditary retinal degenerative diseases is a term used to describe a genetically and clinically heterogeneous group of disorders that affect visual function. Retinal disorders are one of the leading causes of blindness worldwide. For a few conditions, treatments are available that mainly focus on arresting the progression of these diseases. However, there are no cures available that can reverse the retinal damage once that has occurred.

Once vision is lost, little to nothing can be done. The prospect of losing eyesight is extremely threatening. Patients lose their independent lifestyle, and therefore, their quality of life is severely reduced. Studies repeatedly show that blindness is considered the worst medical condition by the general population, with the highest impact on daily life [1, 2]. Losing eyesight is considered to have a higher impact on day-to-day life than other (chronic) conditions, such as dementia, cancer, arthritis, obesity or a stroke [3], see Figure 1.

Additionally, vision loss is associated with substantial direct costs for medical treatments, assistive devices, informal care, and indirect costs related to productivity loss, change in employment, and income loss [4]. Therefore, it is apparent that there is an unmet need for new treatment options for retinal degenerative diseases.

A

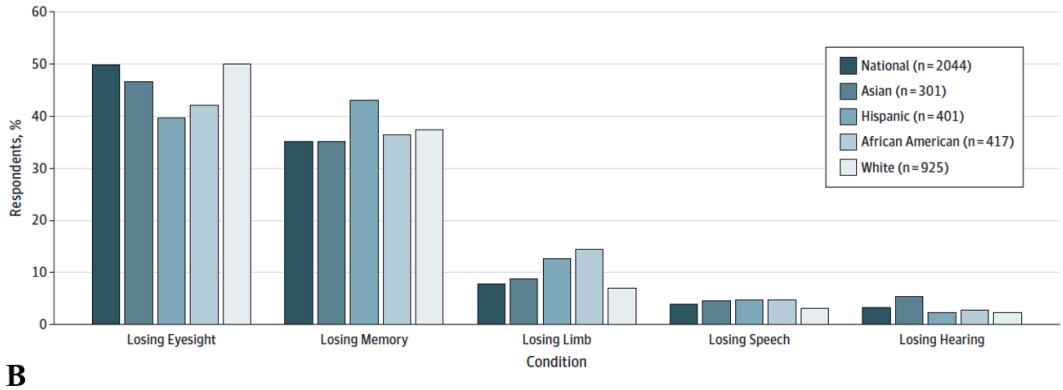

B

Condition	Mean EQ-5D score
Obesity	0.935
Any cancer history	0.896
Depression	0.887
Arthritis	0.847
Stroke	0.812
Visual impairment	0.779

Figure 1. A representation of the effect of vision loss compared to other conditions in the United States (**A**) and Europe (**B**). Losing eyesight or visual impairment is considered the worst medical condition than other conditions on both continents. **A**: a graphical overview of the response to the question: "which condition has the biggest effect on the day-to-day life?". On the X-axis, five conditions, which were used as answers to this question, are shown. On the Y-axis, the percentage of respondents is shown that consider the mentioned condition to have the biggest effect on the day-to-day life. The United States' population's response (national) and split up into ethnic groups (Asian, Hispanic, African American, White). For example, the dark bar on the left indicates that 50 % of the United States' population thinks losing eyesight has the biggest effect on the day-to-day life. Figure from Scott et al. [2]. **B**: a representation of the mean of the European Quality of Life–5 Dimensions Questionnaire (EQ-5D) score for a number of conditions. The EQ-5D score provides a simple descriptive profile and a single index value for the respondent's self-rated health status. The scores depicted here are scores from patients suffering from the named conditions. The higher the index value, the better the self-rated health status. Thus, visual impairment leads to the lowest self-reported health status of the conditions mentioned. Table adapted from Park et al. [3].

Structure and function of the healthy retina

The structure and function of the eye are tuned to enable optimal vision (Figure 2). When light enters the eye through the pupil, it first passes through the cornea and the lens. Both the lens and the cornea bend most of the high-intensity light to focus it correctly on the macular area of the retina. The retina lines the back of the eye and consists of nervous tissue consisting of two major layers: the neural retina and the retinal pigment epithelium (RPE). The neural retina consists of several stacked (cell) layers: the outer nuclear layer (ONL), the outer plexiform layer (OPL), the inner nuclear layer (INL), the inner plexiform layer (IPL) and the ganglion cell layer (GCL). These layers consist of many cell types, including the ganglion cells, amacrine cells, bipolar cells, horizontal cells, and the photoreceptors (PRs); see Figure 2 [5, 6].

In general, two types of PRs exist: rods and cones. Rods can function at a lower light intensity and are more concentrated in the peripheral area, including the perimacular area [7]. Cones are more concentrated in the macula area and are used for sharp and color vision [8]. Different types of cones exist, dividing up visual color information into red, green and blue signals. The RPE consists of a single monolayer of neuro-epithelial cells and is essential for a normal functioning retina. More detailed information about the RPE will be discussed below in the section 'A significant role for the retinal pigment epithelium'.

When light hits the retina, different cell layers work together to turn photons into electrical and neurochemical signals. As a single photon can activate a photoreceptor, most of the light that enters the eye and falls on the retina does not have an effect and will be absorbed by the underlying pigment in the RPE. Light of specific wavelengths will activate different types of PRs. The PRs send the electric and neurochemical signals to the cellular network of the neural retina, which includes horizontal, bipolar, and amacrine cells. Finally, the ganglion cells collect partly processed signals from the aforementioned cells, after which the electric and neurochemical signals are transported through the optic nerve to the brain [9]. The brain converts the incoming signals further into meaningful information and images.

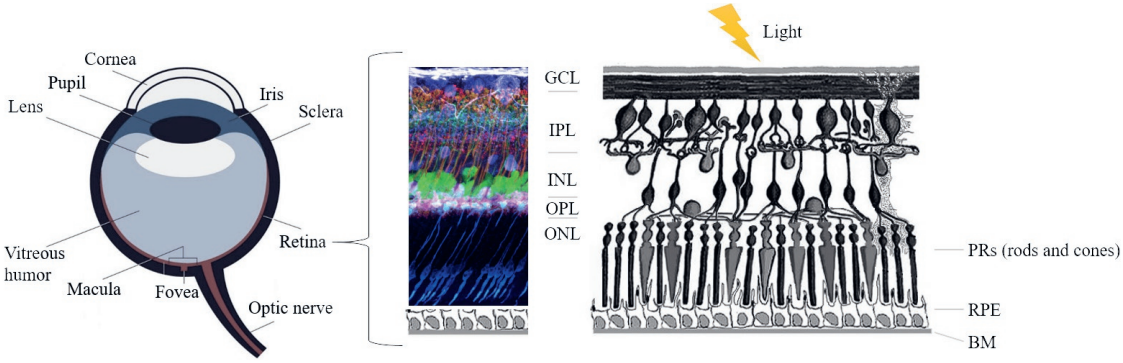

Figure 2. A schematic overview of the human eye's morphology (left) and a close-up overview of the retina (right). In the middle, a vertical section of a mouse retina is shown, including the labeling of the major retinal cell types: cone photoreceptors (blue), horizontal cells (pink), bipolar cells (red), amacrine cells (purple) and ganglion cells (white). ONL: outer nuclear layer; OPL: outer plexiform layer; INL: inner nuclear layer; IPL: inner plexiform layer; GCL: ganglion cell layer; PR: photoreceptor; RPE: retinal pigment epithelium and BM: Bruch's Membrane. The structure and function of the human, mouse and rat retinas are highly similar. Figure adapted from https://nei.nih.gov, Kolb et al. [6] and Hoon et al. [5].

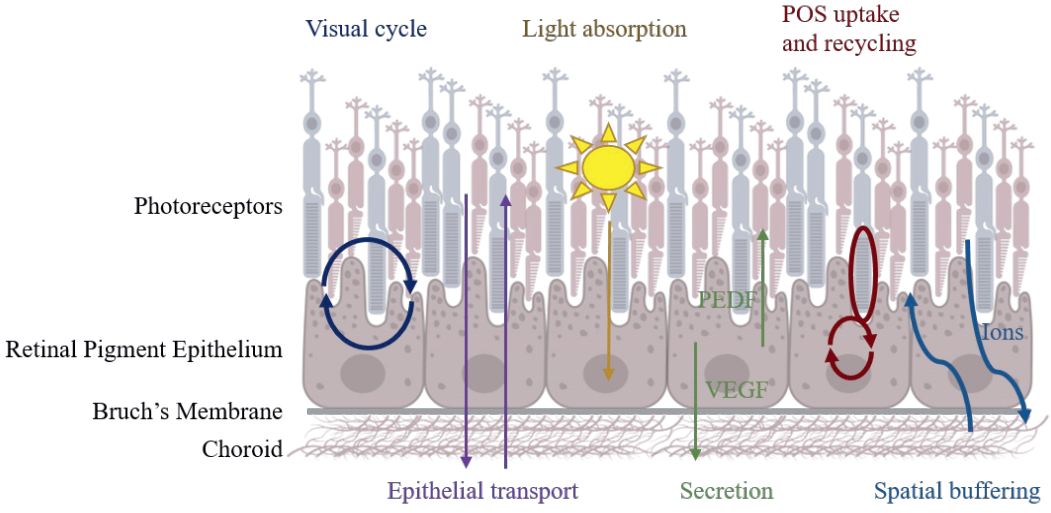

Figure 3. A schematic overview of the adjacent layers of the PR-RPE-BM-choroid complex, including (top to bottom) the following layers: the PRs, RPE, BM and choroid structure. The various essential functions of the RPE for normal vision are presented: the RPE is involved in the visual cycle, epithelial transport, the absorption of excessive light, the secretion of growth factors, the uptake of PR outer segments (POS), and spatial buffering. These crucial functionalities are discussed in detail below. Figure adapted from https://www.ucl.ac.uk and Strauss et al. [13].

A significant role for the retinal pigment epithelium

In the eye, the PRs are supported by the RPE, which absorbs excess light and maintains local homeostasis (see Figure 2). The RPE is a pigmented neuroepithelial single-cell layer lining the back of the eye [10]. The cells have a cobblestone morphology and are tightly linked together with intracellular tight junctions. The basal side of the RPE rests on a collagen- and elastin-rich extracellular matrix called the Bruch's Membrane (BM). Its apical side is facing the PRs. The RPE and its tight junctions are part of the blood-retina barrier. This barrier is exceptionally tight and restrictive [11]. It is a physical barrier that prevents neovascularization and penetration of the vessels from the choroid into the retina and regulates protein, water, and ion flow into and out of the retina. A functional blood-retina barrier is necessary to supply the PRs with selected nutrients and compounds such as glucose and vitamin A from the blood by active transport. Additionally, the RPE eliminates waste materials, metabolic end-products and physiological fluids [12, 13].

Topographical differences in the BM, PRs and the RPE occur throughout the retina. The PR density is higher in the center compared to the periphery. There is a sharp peak of cone PR cell density in the small central region of the macula, known as the fovea in the human eye. A PR cone density peak is absent in the rodent retina. Although the thickness of the RPE layer is relatively constant throughout the eye, the RPE cells' cross-sectional area is smaller in the center than in the periphery. Given the high, corresponsing density of photoreceptors in the central retina, the number of PRs per RPE cells remains the same throughout the retina. The BM is roughly two-fold thinner in the retina's central region than the periphery [11, 14]. These differences in the composition of the PRs, RPE, BM and choroid may account, in part, for pathological differences and symptoms between several retinal degenerative diseases.

The RPE has many critical functions. An overview is presented in Figure 3. Here, we will discuss six crucial functionalities of the RPE in detail: its involvement in the visual cycle, epithelial transport, the absorption of excessive light, the secretion of growth factors, the uptake of PR outer segments (POS), and spatial buffering.

First of all, the RPE is essential for a biologically and functionally active visual cycle (see Figure 5). The visual cycle is a critical process involving Vitamin A derivatives for keeping the PRs functioning. In the PRs, 11-*cis*-retinal is covalently bound to an opsin signaling protein, forming a visual pigment molecule. After activation, the visual pigment can activate several signaling pathways, generating a response to light. In the presence of light, the visual pigment is activated, and 11-*cis*-retinal is isomerized to all-*trans*-retinal. The formation of all-*trans*-retinal is essential to activate the PRs and initiate vision.

Light activation of a PR results in the depolarization of the PR membrane. Only an opsin protein coupled to 11-*cis*-retinal responds to light (see Figure 4). Neither the opsin protein itself nor all-*trans*-retinal are sensitive to light.

Therefore, a new molecule of 11-*cis*-retinal needs to be linked to the opsin protein to become light-sensitive again. PRs lack the reisomerization function to obtain a new molecule of 11-*cis*-retinal. Therefore, reisomerization from all-*trans*-retinal to 11-*cis*-retinal takes place in the RPE. After this process in the RPE, 11-*cis*-retinal is transported back to the PRs, binds to opsin and forms rhodopsin again [13, 15].

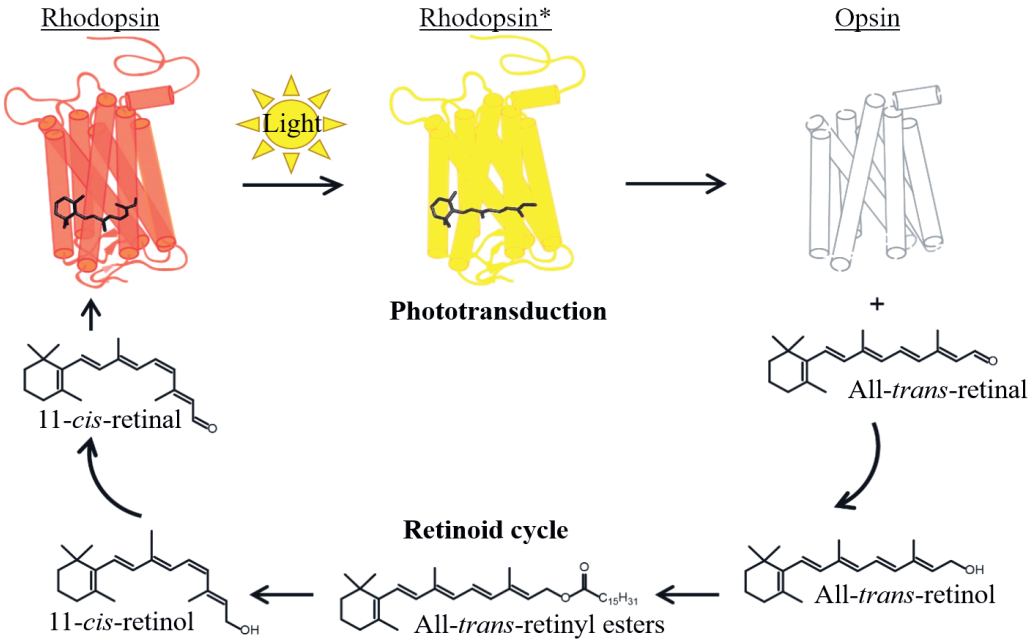

Figure 4. A schematic representation of rhodopsin photoactivation and regeneration. Only a rhodopsin protein couples to 11-*cis*-retinal (top left) responds to light, forming a photoactivated rhodopsin protein (Rhodopsin*). During this process, 11-*cis*-retinal isomerizes to all-*trans*-retinal. Neither the opsin protein itself nor all-*trans*-retinal are sensitive to light. Therefore, a new molecule of 11-*cis*-retinal needs to be linked to the rhodopsin protein. All-*trans*-retinal dissociates from the binding pocket of the rhodopsin protein forming free all-*trans*-retinal, which is reduced to all-*trans*-retinol by retinal dehydrogenases (RDHs) in the retinoid cycle. All-*trans*-retinol is esterified by lecithin retinol acyltransferase (LRAT) to all-*trans*-retinyl esters. These are converted to 11-*cis*-retinol by retinal pigment epithelium-specific protein 65 (RPE65) isomerase. Subsequently, 11-*cis*-retinol is reduced by RDHs to 11-*cis*-retinal, which can bind to a ligand-free opsin and become light-sensitive again. Figure adapted from Ortega and Jastrzebska [16].

Several proteins are involved in this cascade, including ABCA4, RDH8, RDH12, RDH14, RBP3, RLBP1, LRAT, RPE65, RDH5, and RDH11. ABCA4 and RLBP1 are involved in transporting the metabolites inside the cells, RBP3 is engaged in the transportation between the cells and *LRAT*, *RPE65* and the *RDH* genes are involved in the conversion of the metabolites [7, 17] (see Figure 4 and Figure 5). A defect in any of these genes can cause an impairment of the visual cycle and disturb the vision process.

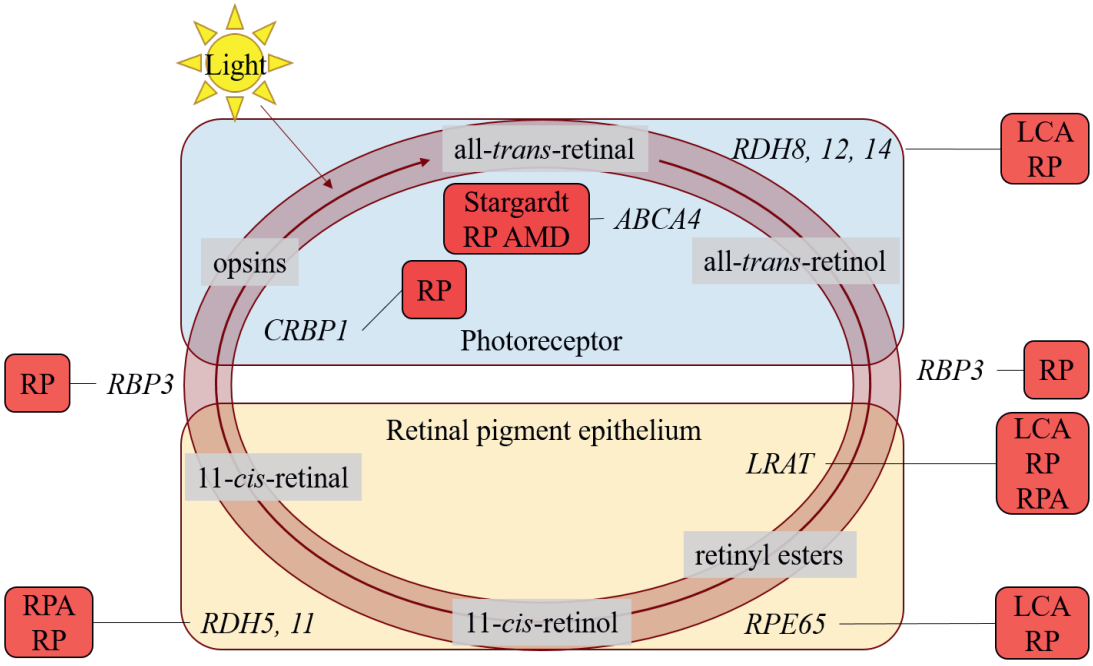

Figure 5. A schematic overview of the visual cycle in the PRs (on top) and the RPE (below). The visual cycle is a critical process involving vitamin A derivatives. In the PRs, 11-*cis*-retinal couples to an opsin protein, forming rhodopsin. Upon absorption of light, 11-*cis*-retinal is isomerized to all-*trans*-retinal. The retinol dehydrogenases (encoded by *RDH8*, *RDH12*, *RDH14*) reduce all-*trans*-retinal to all-*trans*-retinol, and this metabolite is moved to the RPE by retinoid-binding protein (encoded by *RBP3*). All-*trans*-retinol is also taken up from the blood by the RPE. In the RPE, it is esterified by lecithin:retinol acyltransferase (encoded by *LRAT*), after which it is re-converted to 11-*cis*-retinol by retinal pigment epithelium-specific 65 kDa protein (encoded by *RPE65*). Retinol dehydrogenases (encoded by *RDH5* and *RDH11*) convert 11-*cis*-retinol to 11-*cis*-retinal, and retinoid-binding protein moves it back to the PR. The disorders that have been implicated with mutations in these genes are indicated in the red boxes: Retinitis Pigmentosa (RP), Leber Congenital Amaurosis (LCA), Retinitis Punctata Albescens (RPA), Stargardt Disease and Age-related Macular Degeneration (AMD).

Furthermore, the tight and restrictive physical blood-retina barrier makes active transport of essential nutrients and compounds, such as glucose and vitamin A, from the blood to the PR and the rest of the retina necessary. Additionally, waste materials, metabolic end-products and accumulated water need to be eliminated. The RPE has an active role in this process [12, 13].

Third, the excess light emitted upon the retina during a large portion of the day causes local oxidative damage. The pigments that are localized inside the RPE absorb this excess light and protect the retina against oxidative damage. The light-absorbing pigment melanin takes care of the excess light absorption. This is referred to as the first line of defense against photo-oxidative damage. The second line of defense includes enzymatic and nonenzymatic antioxidants, such as carotenoids and ascorbate. These enzymes and compounds neutralize the molecules, also known as reactive oxygen species (ROS), that are an effect of oxidative stress. The third line of defense against photo-oxidative damage is the RPE cell's physiological ability to repair damaged DNA, proteins and lipids [13, 18].

Fourth, the RPE secretes several growth factors essential for maintaining the retinal structure and choriocapillaris' differentiated state. These factors include pigment epithelium-derived factor (PEDF), vascular endothelial growth factor (VEGF), fibroblast growth factors (FGF), connective tissue growth factors (CTGF), transforming growth factors (TGF), and insulin-like growth factor I (IGF-I) [13, 19]. PEDF helps to maintain the retinal and choriocapillaris structures in two ways. First, PEDF protects the RPE and neurons against glutamate-induced or hypoxia-induced apoptosis. Second, PEDF has antiangiogenic properties that prevent neovascularization by reducing VEGF-induced endothelial cell migration and proliferation via apoptosis [20, 21]. This stabilizes the endothelium of the choriocapillaris. PEDF is highly expressed by the RPE. In AMD eyes, lower levels of PEDF were found in the choroidal tissues and the vitreous compared to age-matched control eyes [21, 22]. The presence of VEGF and PEDF seems to be regulated by feedback mechanisms in a tightly controlled manner.

Together with VEGF and other molecules, PEDF is part of the angiogenic switch [23]. The angiogenic switch tightly controls angiogenesis. Angiogenesis is the formation of new blood vessels from preexisting vasculature. The RPE secretes VEGF in low concentrations in a healthy eye. It prevents endothelial cell apoptosis and is a stimulating factor for angiogenesis. Unbalanced VEGF and PEDF expressions are associated with many diseases involving neovascularization in the eye and irreversible visual impairment [13, 21, 23].

Fifth, the RPE is involved in phagocytosing the outer segments (OS) of the PRs. The PRs consist of multiple compartments: an elongated OS, connecting cilium, inner segment, cell body and synaptic terminal [24]. The PR OS consists of many densely packed discs and locally faces into the RPE. Structurally, the discs contain large amounts of rhodopsins and opsins. The functional light-sensitive visual (rhod)opsins are restricted to the OS. Because of the continuous light exposure, photo-damaged proteins and lipids are accumulated during the day inside the PR OS. The OSs are daily renewed from the base of the connecting cilium outward, shed from the PRs and are phagocytosed, digested, and recycled by the RPE [13, 25, 26].

Finally, the RPE is essential for maintaining the ion composition's homeostasis in the retina and the subretinal space. Changes in the ion composition rapidly occur in the retina due to all vision-related activities. In the darkness, K^+ ions entering the photoreceptors and the RPE through their Na^+/K^+-ATPases and the K^+ leaving the photoreceptors are in equilibrium, as are their counterions Na^+.

When exposed to light, photoreceptors hyperpolarize due to the closure of the cyclic nucleotide-gated Na^+-conducting cation channels, which are located in the membrane of the light-sensitive OSs. Due to the hyperpolarization, fewer K^+ ions leave the photoreceptors. Consequently, the K^+ concentration decreases in the subretinal space [13, 27, 28]. The RPE balances this out, together with the Müller cells, by active spatial buffering. It has been proposed that the other functions of the RPE (described above) are most likely also influenced by the spatial buffering activity of the RPE's ion channels [13, 27-29].

The involvement of the RPE in many retinal disorders illustrates the importance of this tissue for normal vision. Patients of all ages can be affected by diseases involving primarily the RPE. These disorders include rare, relatively early-onset monogenic disorders such as albinism [30], fundus albipunctatus [31], some types of retinitis pigmentosa (RP) [32], Stargardt disease [33], gyrate atrophy [34], and Best disease, also called vitelliform macular dystrophy [35]. However, the RPE is also involved in more common, complex, late-onset retinal diseases, such as age-related macular degeneration (AMD). In elderly patients, AMD affects 4 % of the population over 60 [36-38]. This thesis will focus on RPE disease pathology, illustrated by one specific genetic form of the monogenic disorder RP and the more complex retinal disease AMD.

RPE-associated retinitis pigmentosa (RPE-RP)

RP is a collective name for a group of retinal dystrophies, collectively characterized by night blindness, pigment clumping in the retina, concentric visual field loss, and reduced electroretinogram (ERG) amplitudes. The prevalence of RP is roughly 1:4,000. RP is one of the most common causes of inherited retinal disorders leading to legal blindness [39, 40]. RP may present itself within the first years of life, during the second decade or later. The first symptom often is night blindness [7, 41]. Biologically, RP is initially characterized by pigment deposits usually present in the retina's peripheral area. Subsequently, patients frequently experience concentric visual field loss. Patients often become photophobic and are facing reading challenges. As a result, patients may experience problems maintaining an independent lifestyle, reading is difficult, photophobia is intense, and finally, in the end-stage, a subset of patients becomes legally blind [7, 32, 41]. Typically, RP is a disease that progressively evolves over several decades.

The central area of the retina is usually relatively spared for a long time. Typical RP is often described as a rod-cone dystrophy, in which the PR rods are more affected than cones [41, 42]. Up to now, more than sixty disease genes have been implicated in rod-cone dystrophy RP (RetNet, https://sph.uth.edu/RetNet/; visited March 21st, 2022). These genes frequently encode proteins that play an essential role within the neural retina or the RPE [7, 43]. A subset of these disease genes/proteins plays a functional role in the visual cycle. As described above, in the section "A significant role for the retinal pigment epithelium", the visual cycle is essential to recycle the integral component of the phototransduction cascade 11-*cis*-retinal, see Figure 5. Besides RP, mutations in these genes have been implicated with subtypes of RP (Leber Congenital Amaurosis (LCA) and Retinitis Punctata Albescens (RPA), Stargardt Disease and AMD [7, 44-47].

Only for one subtype of RP, in which the *RPE65* gene is involved, a therapy is available, which has recently been approved by the FDA [48]; see more information in Chapter 6, “General discussion, prospects and conclusions” of this thesis. Unfortunately, this therapy is only applicable to a small subset of RP patients. No treatment is currently available for all other RP forms that stop the disease's progression or restore vision once lost. The currently successfully applied experimental therapeutic strategies aim to slow down or halt the degeneration process and treat the complications. Other treatments help the patients cope with the social and psychological impact of blindness [41].

Age-related macular degeneration (AMD)

AMD is a late-onset, degenerative and progressive disorder primarily affecting the macula area. It is one of the leading causes of severe visual impairment among the elderly in the western world. The disease affects 4 % of the population over 60. The number of AMD patients is rising due to the population's overall aging [49-51]. Clinically, AMD presents itself in several ways. It can affect one or both eyes. Symptoms develop gradually and are, therefore, sometimes initially missed. Initial symptoms include visual distortions, reduced central vision, blurriness or a well-defined blurry spot, difficulties while reading or recognizing faces and difficulty adapting to low light levels. Later, central vision is gradually lost, and patients can become fully blind in the end-stage of the disease.
Upon aging, a wide variety of subretinal deposits, frequently called drusen, develop, especially in the macular area [36]. Drusen are clinically defined depending on their size, color, autofluorescence and retinal location [52, 53]. Drusen can appear in the macula, peri-macular area, or periphery [36].

They can be divided into “hard” (<63 μm, round, clear edges), “intermediate” (63-125 μm) and “soft” drusen (>125 μm, ill-defined edges) [53]. The presence of a few (less than 5) small hard drusen in the macula is not necessarily a problem. However, when the numbers of hard drusen increase and/or become more like intermediate or soft drusen, the likelihood of the progression of advanced stages of AMD is increased significantly [36, 53].
During disease progression, the size and number of the sub-RPE deposits and pigmentary alterations progressively increase. The end-stages of AMD can be divided into "dry" and "wet" types. The majority (90 %) of the patients suffer from dry or geographic atrophic AMD. This type is characterized by drusen, pigment migration, progressive RPE atrophy, photoreceptor degeneration, and thinning of the choroid [49, 54]. The wet type of AMD is characterized by choroidal neovascularization. The new leaky blood vessels break locally through BM and cause pathological fluid accumulation, bleedings and fibrosis within the macula area [55].

AMD is a multifactorial disease, and multiple environmental and genetic risk factors have been identified. Environmental factors include age, smoking, body weight, diet and sunlight exposure. Genetic factors include ethnic origin and mutations or variants in genes that are associated with AMD’s development and progression. These factors are highlighted in more detail below.
Age is the most important demographic risk factor for AMD. Higher age is the main risk factor for AMD since aging is associated with structural and functional changes of the retina and can underly the development of AMD. However, the distinction between “normal” aging and AMD pathology is not a clear cut. Features of normal aging and disease may overlap and may be different for the involved cell types. Most individuals undergo changes continuously from adulthood to old age, without direct consequences. These normal age-related, non-pathogenic changes affect the overall fitness of cells and tissues, predisposing them to a pathogenic state. As a result, pathogenic changes cause (local) loss of function, leading to clinical consequences. The choroidal, BM, RPE and retinal cells undergo continuous aging changes that are not necessarily pathogenic.

This process is accelerated when specific AMD pathological processes set in [11]. Additionally, age contributes to the additive pathological effects of other risk factors over time [56, 57].

The second most important risk factor for AMD is smoking. Smoking is associated with at least a 3-6 fold increased risk of developing AMD, and it has been confirmed that a dose-response effect exists [58-63]. Cigarette smoke exerts its pathological effects, most likely through a number of biochemical pathways that result in the induction of retinal oxidative stress, induction of inflammation responses of the RPE cells and vascular changes in the choroidal vessels [60].

Thirdly, multi-ethnic studies show a prevalence difference of AMD between ethnic groups. AMD is most frequently found in Caucasians, Hispanics and Asians and the least in Africans [64, 65]. The increased presence of melanin in the RPE cells of Africans, compared to other groups, may act as a free radical scavenger or as a filter for radiation protecting the RPE cells and BM [60, 66]. Additional environmental risk factors include diet, BMI, previous cataract surgery, prior cardiovascular disease, gender, iris color, sunlight exposure, and hypertension [60, 67-75].

Many genes have been identified to be associated with AMD playing roles in maintaining retinal homeostasis and health but are, interestingly, not always exclusively retina-specific genes [67, 76-79]. More than half of the heritability can be explained by gene variants in 34 loci. These genes are primarily involved in extracellular matrix remodeling, the complement system, and lipid metabolism [80]. Variants of genes involved in the complement system have been identified to have (substantial) effects on AMD's risk. Especially common variants in the complement factor H (*CFH*) gene are highly associated. *CFH* knows protective allele variants and allele variants that increase the risk of developing AMD [60].

Additionally, variants in other genes, including complement factor I (*CFI*), complement component 2 (*C2*), complement component 3 (*C3*), and complement factor B (*CFB*), are associated with disease progression. A common genetic variant near the age-related maculopathy susceptibility (*ARMS2*) and high-temperature requirement A serine peptidase 1 (*HTRA1*) genes also has a strong effect on the risk of AMD [58, 81]. It is still not fully understood how the functions of either or both genes are related to AMD pathology. Studies suggest that the *ARMS2* gene may encode a protein that functions in the retina's mitochondria; however, it may also encode an extracellular protein [82, 83]. The *HTRA1* gene is involved in regulating extracellular matrix deposition and angiogenesis [84, 85].

Genes encoding proteins of lipid metabolism are also involved in the pathogenesis of AMD. These genes are probably involved in forming sub-RPE deposits [86-88]. For example, protective variants have been found in the ATP-binding cassette subfamily A member 1 (*ABCA1*) and the cholesteryl ester transfer protein (*CETP*) gene [89, 90]. The apolipoprotein E (*APOE*) gene has variants associated with a decreased risk and an increased risk of developing AMD. This gene is known to be polymorphic and is also associated with Alzheimer’s disease. Interestingly, the isoform associated with a decreased risk of developing Alzheimer’s disease (ε2 isoform) has an increased risk of developing AMD.

Vice versa, the ε4 isoform is associated with an increased risk of developing Alzheimer's disease and is protective in AMD. Although it is known that APOE transports lipids, cholesterol and fat-soluble vitamins, it is not yet fully understood why the ε2 and ε4 isoforms have opposite effects on AMD and Alzheimer's disease [60, 91, 92]. In addition to the genes mentioned here, many other genes in the pathways mentioned above are associated with AMD pathology [60, 80, 93].

Currently, no effective treatment is available for the dry form of AMD. For the wet form, a preventive treatment exists, which consists of (bi-)monthly intra-ocular anti-VEGF agent injections. *In vivo*, VEGF is responsible for driving the neovascularization via the proliferation of vascular endothelial cells, increased vessel permeability, migration and survival of the endothelial cells. The formation of these leaky choroidal vessels that penetrate the RPE cell layer is the main reason why wet AMD patients lose their vision. Monthly eye injections with anti-VEGF agents preserve the best visual outcome. However, intensive recurrent treatment may not be sustainable in the long term and is not patient-friendly. This treatment is based on arresting disease progression, not reversing it. Although some experimental therapeutic strategies are currently tested, a treatment resulting in a full stop or recovery is for both AMD forms not (yet) available [94].

In short: experimental therapeutic strategies RPE-RP and AMD

As stated above, besides for one subtype of the RPE-type RP (*RPE65*-RP), there are no treatments available for all other RPE-RP types and AMD. While some (experimental) therapies, including the anti-VEGF injections for wet AMD, are available, all treatment options focus on preventing and slowing down the disease progression instead of reversing the effects. Once retinal cells and vision are lost, nothing can be done. There are some potential treatments or strategies under development in the lab or in different stages of clinical trials. We can divide these experimental treatments into three major categories: gene therapy, drug therapy/dietary supplements, and cell-replacement therapy. The ultimate goal of all cures is to prevent or halt vision loss or restore vision. However, the different essential phases of preclinical research and clinical trials take a long time and are very expensive. Chapter 6 ("General discussion, prospects and conclusions") will give an extensive overview of the current status of the experimental therapies treating AMD or RPE-RP in the different clinical trial stages. So far, the results from most ongoing trials have been relatively disappointing: the "wonder drugs" do not exist yet. Most clinical trials and preclinical studies have been hampered by the lack of, or incomplete information from, fully representative *in vitro* or *in vivo* models [95-97]. Below, the currently available models, their applications, advantages and drawbacks are discussed.

Available experimental models

All experimental therapeutic strategies are first tested using *in vitro* and, subsequently, using *in vivo* models. The currently available models for retinal degenerative diseases include (post-mortem) human donor eyes, conventional cell (line) culture, organoid cultures and animal models. These categories are discussed in more detail below.

In vitro and *ex vivo* models: the use of human donor material, cell lines and retinal organoids

The studies on human donor eyes have been extremely useful to learn more about the (micro-) structures and function of the eye and the molecular and cellular pathology of ocular disease [37, 98-105]. However, there are several drawbacks to using post-mortem human donor eyes. They are usually scarce, and the available ones generally are aged or have an advanced or end-stage of the disease. Additionally, it is very difficult to manipulate the tissues or test to function or experimental therapeutic strategies concerning safety and efficacy, limiting their use.

The culture of (adherent) primary cells from donors' eyes, explant cultures, cell lines, and cells or cell lines originating from stem cells is an extremely useful *in vitro* tool. In RPE-related research, two types of adherent cells have been frequently used: primary cell lines and the ARPE19 cell line.

Primary cultures of fetal or adult RPE cells are isolated from human (fetal) donor eyes and are cultured and maintained *in vitro*. The isolated RPE cells retain the typical appearance of RPE but can become more motile fibroblast-like cells over time after repeated passaging. Besides the lack of donor material and the ethical issues facing fetal cells, the proliferation capacity of primary cells is another disadvantage. It is limited, and they tend to adopt mesenchymal fates over multiple passages [106].

For years, the popular ARPE-19 cell line was used as an *in vitro* model for RPE. ARPE-19 is an immortalized human RPE cell line that can form polarized epithelial cell layers when cultured properly. It was established from a primary RPE culture by using selective trypsinization resulting in cells that exhibit a strong growth potential. The cell line has a number of structural and functional characteristics of RPE cells, including the ability to phagocytose PR outer segments and secrete growth factors [107-109]. However, ARPE-19 cells also lack some essential characteristics of native RPE. The ARPE-19 cell line seems to degenerate after extensive passaging. It seems not to represent some of an RPE cell's (basal) functionalities, including the formation of a proper extracellular matrix and BM, which is reflected in a relative lack of barrier formation and low or absent expression of *RPE65* and *LRAT* [109]. Even though there are some drawbacks, the ARPE-19 cell line is still a widely, although more selectively used cell line to study molecular biological processes in RPE cells or the potential effects of experimental treatments *in vitro* [110-117].

There are a number of less frequently used RPE cell lines, such as the hTERT (human telomerase reverse transcriptase-immortalized) RPE-1 line [118, 119] and the RPE-J line (originating from Long Evans rats) [120], with their own limitations and advantages. However, the use of these is currently rapidly surpassed by the use of stem cell-derived RPE cells.

At this moment, many differentiation strategies are available to create many stem cell-derived retinal cell types and culture these in a 2D *in vitro* fashion [121-126]. Embryonic stem cells (ESCs), induced pluripotent stem cells (iPSCs) and adult retinal stem cells are currently being used [127, 128]. Despite extensive informed consent of the individuals involved, the use of human ESCs faces a number of ethical issues and discussions [129]. The introduction of iPSCs overcame many of these issues and has made it possible to use patient-specific materials to make stem cells. Retinal cell types can be made without using human embryonic tissues [130, 131].

Both iPSCs and ESCs are currently extremely valuable in research. However, iPSCs (and ESCs) can become genetically unstable. For example, genetic mutations were unexpectedly identified in the iPSCs that were supposed to be used in a clinical trial involving iPSC-derived RPE cells. The genetic alterations were unexpected, and the trial was postponed [132-134]. Genomic instability could occur at any stage of iPSC generation. Therefore, careful monitoring is essential to ensure safety for clinical applications [132, 135]. Under highly controlled protocols using iPSCs, it is possible to use the cells of several (genetic) patient groups and compare them and test, for example, the efficacy of the experimental therapies *in vitro*. Using adult stem cells, patient-specific materials could be developed as well. Adult stem cells have been identified in various tissues throughout the body, are multipotent and have a limited capacity for self-renewal and differentiation towards certain cell types [136]. A very small population of adult stem cells has been identified in the retina as well [137]. While these retinal stem cells can differentiate into the different cell types of the retina, they cannot grow indefinitely in *in vitro* cultures like ESCs and iPSCs. Therefore, they will have to be re-isolated from the retina [137]. Also, given the scarcity of these cells, using adult retinal stem cells as a source for retinal *in vitro* tissues might not outweigh the advantages of using iPSCs.

Overall, *in vitro* culture of (stem cell-derived) RPE cells has several advantages. The cells are usually highly accessible for experiments, and the use of RPE cell lines is generally relatively cheap. One significant advantage of cell cultures is the potentially endless source of available biological materials. However, cell lines do not fully represent the *in vivo* situation. Still, they can be used to get an idea about the processes involved in disease and to test the safety and efficacy of potential new experimental therapeutic approaches. A considerable disadvantage of 2D retinal culturing is that the models partially lack proper retinal organization and functionality. The cultures usually include only one cell type, making developing these features impossible [138].

A relatively new culture strategy was developed to overcome this issue involving stem cell-derived 3D cultures in a dish: retinal organoids. Organoids are defined as 3D cellular structures exhibiting function and morphology close to their respective *in vivo* counterparts [139]. The mechanism behind cells' ability to self-adhere and self-organize is strongly linked to the naturally occurring embryonic processes. Retinal organoids are the most recent, most advanced and probably the most physiologically representative *in vitro*-formed human biological structures resembling the retina. They consist of multiple retinal cell types and layers and, additionally, the RPE [140, 141]. Organoids are particularly useful for investigating the human retina's developmental aspects and disease modeling or pharmacological testing.

With the use of stem cells development of differentiation protocols resulting in retinal organoids, significant steps forward have been taken regarding the availability of human representative retinal *in vitro* models. For example, potential effects of experimental therapeutic approaches, such as administering drugs or applying gene therapy, could be tested in these (stem cell-derived) cell lines or retinal organoids before moving to *in vivo* animal models, reducing their necessary numbers tremendously [139]. However, it is still essential to test potential experimental therapeutic approaches *in vivo* using animal models before moving to the clinic.

The use of *in vivo* models

Human (disease) representative animal models can help significantly understand the molecular and cellular (patho-)mechanisms underlying a disorder and to develop or test new therapies. A large variety and number of animal models are currently available for studying retinal degenerative diseases. Some general information and considerations regarding the use of animals in the field will be discussed first, followed by a short discussion regarding some specific examples of RP and AMD animal models used.

In general, for an animal model to be useful for research, it should recapitulate (part of) the disease phenotype observed in human patients. Various animal models have different (dis)advantages. An ideal (animal) model would be (relatively) inexpensive, recapitulate the disease's pathobiology and functional changes, and disease progression in a reasonably rapid time course to allow efficient studies. So, what is the ideal animal model for studying retinal degenerative diseases?

Animal models for retinal degenerative diseases have been created in several species, including mice, rats, rabbits, pigs, dogs, cats, and non-human primates. It is essential to carefully consider the animal model choice in preclinical research [142]. To be useful in preclinical research, animal models for retinal degenerative diseases should ideally have similar anatomic features and light transduction mechanisms as humans. Such anatomic features include tissue organization as well as cellular specificities. Although all available animal models have a morphologically similar retinal structure, including all retinal layers and neuronal cell types, specific differences exist.

The animal models for retinal degeneration can be genetic or induced models in smaller or larger animals. Genetic models can be subdivided into two main categories: spontaneous mutants and genetically modified animals. The latter can be subdivided into animals from which the genome has been altered and transgenic animals. It is essential for genetic models that, although retinal degeneration is an eye disease, the mutation is germline transmissive and that a strain or species is obtained with the modification stably integrated into the genome. Additionally, one should consider that some genes are either duplicated or not present at all in some species' genomes when choosing an animal model. Induced models include models in which retinal degeneration is (manually) induced in (wildtype) animals using, for example, light exposure, lasers, mechanical scraping causing retinal injury or chemical compounds. In general, smaller rodent models are more cost-efficient than larger animal models. Disease progression in rodents is relatively quick, and genetic manipulation is relatively easy to perform. It takes only a few months to have doubled the numbers of rodents, such as mice and rats, making rodents time-efficient models. On the other hand, interventions such as ocular injections and ocular surgeries are more challenging to perform due to small eye size. Additionally, rodents lack particular human retinal features, such as the fovea or macula, and they have only two cone types and thus fewer than humans.

Only large animal models, including rabbits, cats, dogs, sheep, pigs and non-human primates, possess a central area in the eye corresponding to a foveal-like structure. Their eyes are anatomically very closely related to humans, and ocular interventions are less complicated to perform compared to the smaller rodent models. However, large animals are costly due to high food and housing costs and a slow reproduction rate. It takes at least six months to a year to obtain a small number of offspring. Additionally, the larger animal models are generally harder or ethically not desirable to modify genetically. On top of that, disease progression rate and therapeutic evaluation can span a considerable time interval, thereby increasing overall costs. Taken together, using larger animal species is a cost- and time-intensive investment.

Many available models have been reviewed extensively elsewhere [143-147]. A few genetic and induced models, fitting within the scope of this thesis, will be discussed in short below.

In short: available animal models for inherited RP

A mutation in a single relevant gene usually causes a monogenic subtype of RP. In recessively inherited RP, both copies of the gene need to have the disease-causing mutation for the disease to develop. In the absence of a spontaneously mutated gene, the mutation of interest can be introduced into the animal's genomic DNA. The strategy to genetically design an animal model to recapitulate the disease *in vivo* is relatively straightforward. In the case of recessively inherited RP, the modification should be introduced on both copies of the gene of interest. By doing so, several knockout mouse models were developed to model RP *in vivo*. For example, following this strategy, multiple mouse strains harboring a mutation in genes having a role in the visual cycle and phototransduction cascade have become available, including rhodopsin deficient ($Rho^{-/-}$) mice [148], the $Rpe65^{-/-}$ mice, and the $Lrat^{-/-}$ mice [149].

Moreover, recapitulating disease in an animal could also be done by introducing the disease-causing (human) gene into the animal's genome. Such animals are called knock-in (targeted insertion) or transgenic models (randomized insertion). For example, the S334ter-3 and P23H-3 rat strains express mutant human rhodopsin proteins as transgenic RP models [150]. Similarly, the P23H transgenic pig strain also expresses the human mutant rhodopsin protein and could be used as an animal model for RP.

In short: animal models for AMD

As described above in the section "Age-related macular degeneration (AMD)", and in contrast with RP, AMD is a multifactorial disease primarily affecting the RPE and secondarily the PRs, BM and the choriocapillaris. Multiple genetic and environmental factors are involved. Unfortunately, so far, no animal model is available that fully recapitulates all AMD features together *in vivo*. Nonetheless, many *in vivo* models for certain specific pathobiological aspects of AMD have been developed using genetically modified rodent strains, transgenic animals, chemically-based, and mechanical models. These include models for complement activity, retinal oxidative stress, aberrant lipid metabolism and extracellular matrix (BM) damage or disruption. A few examples of these models are discussed in short below.

Complement (dys)function as part of the AMD phenotype has been modeled in several mouse strains in which the involved genes are knocked out, such as *Cfh* [151] and *Ccr2* [152]. In addition, some models for retinal oxidative stress are available. These include *Sod1* [153] and *Sod2* [154] knockout mouse strains.

Moreover, since lipid metabolism and transport have been implicated in AMD, animal models with mutations in genes involved in these pathways, such as *ApoE* [155], are of interest. Finally, genetic, chemically or mechanically-induced models in rats, pigs and primates harming the BM and/or RPE are also used. Examples are the blue light-induced, laser-induced or surgical rupture of the RPE and/or BM [143]. Other models in small and large-eyed animals include cigarette smoke-induced, high fat diet-induced, aging-induced and sodium iodate-induced models [143, 156, 157]. As mentioned, all of the models discussed above aim to depict at least one of the features of AMD.

Conclusions

Taken together, retinal degenerative diseases of the RPE, such as RP and AMD, are of a tremendous societal impact and affect the quality of life of many individuals. At this moment, multiple experimental therapeutic strategies are under development, including gene therapy, dietary supplement or drug treatments, cell-replacement therapy, and combinations of these three. While human representative *in vitro* models, such as cell cultures and retinal organoids, become increasingly available, they do not (yet) fully represent the eye or vision in the context of the whole organism. Therefore, suitable animal models representing the disease's phenotype are still essential and required to test full visual function and experimental therapeutic's safety and efficacy *in vivo* before formal approval of a treatment by the FDA and EMA. Given the significant etiologic heterogeneity of AMD's and RP's patient populations, personalized strategies are currently a major research focus and of utmost importance for these patients.

Aim and outline of this thesis

This thesis will describe several studies related to the development and characterization of animal models for RPE-related retinal degenerative disorders, i.e., one sub-type of RP and AMD.

In the *in vivo* studies, we used our newly established, non-invasive screening facility for small animal models to gather insight into the disease pathology, including onset and progression for subsequent experimental therapeutic intervention. The non-invasive screening techniques used consist of four basic techniques: optical coherence tomography (OCT), scanning laser ophthalmoscopy (SLO), electroretinography (ERG) and vision-based behavioral assays. Where SLO and OCT are morphological readouts, ERG and vision-based behavioral assays are functional readouts. OCT is a laser-based imaging technique generating cross-sectional images of tissues with a high resolution. It is entirely non-invasive and can, therefore, provide *in vivo* images without impacting the tissue [158]. SLO is an imaging technique using infra-red and multicolor contrasts to obtain fundus photos of the eye. These fundus photos are also used for eye tracking and as a reference image for OCT applications. Additionally, using SLO, fluorescence imaging channels are used to visualize the vascular system [159].

ERG is used to obtain an electroretinogram of the functional activity of the retina upon a light stimulus. Using an active electrode, a reference electrode and a ground electrode, an electrical circuit is built. Using ERG, one can make statements about the functionality of the retina [160]. Lastly, vision-based behavioral assays are used to confirm that all signals obtained and created in the retina are processed in the brain [161].

In **chapter 2**, I performed a systematic review of studies using RPE transplantations in animals. I gathered full insight into what is known and what information is lacking to move forward. Additionally, we determined what parameters are essential to consider when performing RPE transplantations in preclinical animal models. We will use this information for the development of future studies and experiments. **Chapter 3** describes the development and characterization of a new rat model for the monogenic disease RP. This model was phenotyped in depth using the techniques described above. **Chapter 4** describes the extensive characterization of induced animal models for AMD. In both models (and chapters), we aimed to define a window of therapeutic possibility to test experimental therapies for retinal degenerative disease. Additionally, we describe the generation of a 3D-bio-printed tissue recapitulating the RPE, BM and Choroid complex and its integration into rat eyes in **chapter 5**. Lastly, **chapter 6** discusses the challenges and complexities that remain for the use of animal models and the application of experimental therapies for retinal degenerative disorders and diseases of the RPE.

References

1. Elsman, E. B. M.; van Rens, G.; van Nispen, R. M. A., Quality of life and participation of young adults with a visual impairment aged 18-25 years: comparison with population norms. *Acta Ophthalmol* **2019**, *97*, (2), 165-172.
2. Scott, A. W.; Bressler, N. M.; Ffolkes, S.; Wittenborn, J. S.; Jorkasky, J., Public Attitudes About Eye and Vision Health. *JAMA Ophthalmol* **2016**, *134*, (10), 1111-1118.
3. Park, S. J.; Ahn, S.; Woo, S. J.; Park, K. H., Extent of Exacerbation of Chronic Health Conditions by Visual Impairment in Terms of Health-Related Quality of Life. *JAMA Ophthalmol* **2015**, 133, (11), 1267-75.
4. Schakel, W.; van der Aa, H. P. A.; Bode, C.; Hulshof, C. T. J.; van Rens, G.; van Nispen, R. M. A., The Economic Burden of Visual Impairment and Comorbid Fatigue: A Cost-of-Illness Study (From a Societal Perspective). *Invest Ophthalmol Vis Sci* **2018**, *59*, (5), 1916-1923.
5. Hoon, M.; Okawa, H.; Della Santina, L.; Wong, R. O., Functional architecture of the retina: development and disease. *Prog Retin Eye Res* **2014**, *42*, 44-84.
6. Kolb, H.; Fernandez, E.; Nelson, R., The Organization of the Retina and Visual System (Online Book). In *Webvision: The Organization of the Retina and Visual System*, Kolb, H.; Fernandez, E.; Nelson, R., Eds. University of Utah Health Sciences Center Copyright: © 2020 Webvision . Salt Lake City (UT), 1995.
7. Verbakel, S. K.; van Huet, R. A. C.; Boon, C. J. F.; den Hollander, A. I.; Collin, R. W. J.; Klaver, C. C. W.; Hoyng, C. B.; Roepman, R.; Klevering, B. J., Non-syndromic retinitis pigmentosa. *Prog Retin Eye Res* **2018**, *66*, 157-186.
8. Ingram, N. T.; Sampath, A. P.; Fain, G. L., Why are rods more sensitive than cones? *J Physiol* **2016**, *594*, (19), 5415-26.
9. Vlasits, A. L.; Euler, T.; Franke, K., Function first: classifying cell types and circuits of the retina. *Curr Opin Neurobiol* **2019**, *56*, 8-15.
10. Sparrow, J. R.; Hicks, D.; Hamel, C. P., The retinal pigment epithelium in health and disease. *Curr Mol Med* **2010**, *10*, (9), 802-23.
11. Booij, J. C.; Baas, D. C.; Beisekeeva, J.; Gorgels, T. G.; Bergen, A. A., The dynamic nature of Bruch's membrane. *Prog Retin Eye Res* **2010**, *29*, (1), 1-18.
12. Cunha-Vaz, J.; Bernardes, R.; Lobo, C., Blood-retinal barrier. *Eur J Ophthalmol* **2011**, 21 Suppl 6, S3-9.
13. Strauss, O., The retinal pigment epithelium in visual function. *Physiol Rev* **2005**, 85, (3), 845-81.
14. Volland, S.; Esteve-Rudd, J.; Hoo, J.; Yee, C.; Williams, D. S., A comparison of some organizational characteristics of the mouse central retina and the human macula. *PLoS One* **2015**, *10*, (4), e0125631.
15. Saari, J. C., Vitamin A and Vision. *Subcell Biochem* **2016**, *81*, 231-259.
16. Ortega, J. T.; Jastrzebska, B., The Retinoid and Non-Retinoid Ligands of the Rod Visual G Protein-Coupled Receptor. *International Journal of Molecular Sciences* **2019**, *20*, (24).
17. Kiser, P. D.; Golczak, M.; Maeda, A.; Palczewski, K., Key enzymes of the retinoid (visual) cycle in vertebrate retina. *Biochim Biophys Acta* **2012**, *1821*, (1), 137-51.

18. Plafker, S. M.; O'Mealey, G. B.; Szweda, L. I., Mechanisms for countering oxidative stress and damage in retinal pigment epithelium. *Int Rev Cell Mol Biol* **2012**, *298*, 135-77.
19. Songstad, A. E.; Worthington, K. S.; Chirco, K. R.; Giacalone, J. C.; Whitmore, S. S.; Anfinson, K. R.; Ochoa, D.; Cranston, C. M.; Riker, M. J.; Neiman, M.; Stone, E. M.; Mullins, R. F.; Tucker, B. A., Connective Tissue Growth Factor Promotes Efficient Generation of Human Induced Pluripotent Stem Cell-Derived Choroidal Endothelium. *Stem Cells Transl Med* **2017**, *6*, (6), 1533-1546.
20. Mori, K.; Duh, E.; Gehlbach, P.; Ando, A.; Takahashi, K.; Pearlman, J.; Mori, K.; Yang, H. S.; Zack, D. J.; Ettyreddy, D.; Brough, D. E.; Wei, L. L.; Campochiaro, P. A., Pigment epithelium-derived factor inhibits retinal and choroidal neovascularization. *J Cell Physiol* **2001**, *188*, (2), 253-63.
21. Tong, J. P.; Yao, Y. F., Contribution of VEGF and PEDF to choroidal angiogenesis: a need for balanced expressions. *Clin Biochem* **2006**, *39*, (3), 267-76.
22. Bhutto, I. A.; McLeod, D. S.; Hasegawa, T.; Kim, S. Y.; Merges, C.; Tong, P.; Lutty, G. A., Pigment epithelium-derived factor (PEDF) and vascular endothelial growth factor (VEGF) in aged human choroid and eyes with age-related macular degeneration. *Exp Eye Res* **2006**, *82*, (1), 99-110.
23. Qazi, Y.; Maddula, S.; Ambati, B. K., Mediators of ocular angiogenesis. *J Genet* **2009**, 88, (4), 495-515.
24. Perkins, B. D.; Fadool, J. M., Photoreceptor structure and development analyses using GFP transgenes. *Methods Cell Biol* **2010**, *100*, 205-18.
25. Young, R. W., The renewal of photoreceptor cell outer segments. *J Cell Biol* **1967**, *33*, (1), 61-72.
26. Nguyen-Legros, J.; Hicks, D., Renewal of photoreceptor outer segments and their phagocytosis by the retinal pigment epithelium. *Int Rev Cytol* **2000**, *196*, 245-313.
27. Reichhart, N.; Strauss, O., Ion channels and transporters of the retinal pigment epithelium. *Exp Eye Res* **2014**, *126*, 27-37.
28. Wimmers, S.; Karl, M. O.; Strauss, O., Ion channels in the RPE. *Prog Retin Eye Res* **2007**, *26*, (3), 263-301.
29. Reichenbach, A.; Bringmann, A., New functions of Müller cells. *Glia* **2013**, *61*, (5), 651-78.
30. Figueroa, A. G.; McKay, B. S., GPR143 Signaling and Retinal Degeneration. *Adv Exp Med Biol* **2019**, *1185*, 15-19.
31. Schatz, P.; Preising, M.; Lorenz, B.; Sander, B.; Larsen, M.; Rosenberg, T., Fundus albipunctatus associated with compound heterozygous mutations in RPE65. *Ophthalmology* **2011**, *118*, (5), 888-94.
32. Talib, M.; van Schooneveld, M. J.; van Duuren, R. J. G.; Van Cauwenbergh, C.; Ten Brink, J. B.; De Baere, E.; Florijn, R. J.; Schalij-Delfos, N. E.; Leroy, B. P.; Bergen, A. A.; Boon, C. J. F., Long-Term Follow-Up of Retinal Degenerations Associated With LRAT Mutations and Their Comparability to Phenotypes Associated With RPE65 Mutations. *Transl Vis Sci Technol* **2019**, *8*, (4), 24.
33. Hussain, R. M.; Ciulla, T. A.; Berrocal, A. M.; Gregori, N. Z.; Flynn, H. W., Jr.; Lam, B. L., Stargardt macular dystrophy and evolving therapies. *Expert Opin Biol Ther* **2018**, *18*, (10), 1049-1059.
34. Tsang, S. H.; Aycinena, A. R. P.; Sharma, T., Inborn Errors of Metabolism: Gyrate Atrophy. *Adv Exp Med Biol* **2018**, *1085*, 183-185.
35. Guziewicz, K. E.; Sinha, D.; Gómez, N. M.; Zorych, K.; Dutrow, E. V.; Dhingra, A.; Mullins, R. F.; Stone, E. M.; Gamm, D. M.; Boesze-Battaglia, K.; Aguirre, G. D., Bestrophinopathy: An RPE-photoreceptor interface disease. *Prog Retin Eye Res* **2017**, *58*, 70-88.

36. Bergen, A. A.; Arya, S.; Koster, C.; Pilgrim, M. G.; Wiatrek-Moumoulidis, D.; van der Spek, P. J.; Hauck, S. M.; Boon, C. J. F.; Emri, E.; Stewart, A. J.; Lengyel, I., On the origin of proteins in human drusen: The meet, greet and stick hypothesis. *Prog Retin Eye Res* **2019**, *70*, 55-84.
37. Fisher, C. R.; Ferrington, D. A., Perspective on AMD Pathobiology: A Bioenergetic Crisis in the RPE. *Invest Ophthalmol Vis Sci* **2018**, *59*, (4), Amd41-amd47.
38. de Jong, P. T., Age-related macular degeneration. *N Engl J Med* **2006**, *355*, (14), 1474-85.
39. Tsujikawa, M.; Wada, Y.; Sukegawa, M.; Sawa, M.; Gomi, F.; Nishida, K.; Tano, Y., Age at onset curves of retinitis pigmentosa. *Arch Ophthalmol* **2008**, *126*, (3), 337-40.
40. Ferrari, S.; Di Iorio, E.; Barbaro, V.; Ponzin, D.; Sorrentino, F. S.; Parmeggiani, F., Retinitis pigmentosa: genes and disease mechanisms. *Curr Genomics* **2011**, *12*, (4), 238-49.
41. Hamel, C., Retinitis pigmentosa. *Orphanet J Rare Dis* **2006**, *1*, 40.
42. Hamel, C. P., Cone rod dystrophies. *Orphanet J Rare Dis* **2007**, *2*, 7.
43. Downes, S. M.; Nguyen, T.; Tai, V.; Broadgate, S.; Shah, M.; Al-Khuzaei, S.; MacLaren, R. E.; Shanks, M.; Clouston, P.; Halford, S., Genetic and Clinical Findings in an Ethnically Diverse Cohort with Retinitis Pigmentosa Associated with Pathogenic Variants in CERKL. *Genes (Basel)* **2020**, *11*, (12).
44. Sultan, N.; Ali, I.; Bukhari, S. A.; Baig, S. M.; Asif, M.; Qasim, M.; Naseer, M. I.; Rasool, M., A novel mutation in RDH5 gene causes retinitis pigmentosa in consanguineous Pakistani family. *Genes Genomics* **2018**, *40*, (5), 553-559.
45. Xie, Y. A.; Lee, W.; Cai, C.; Gambin, T.; Nõupuu, K.; Sujirakul, T.; Ayuso, C.; Jhangiani, S.; Muzny, D.; Boerwinkle, E.; Gibbs, R.; Greenstein, V. C.; Lupski, J. R.; Tsang, S. H.; Allikmets, R., New syndrome with retinitis pigmentosa is caused by nonsense mutations in retinol dehydrogenase RDH11. *Hum Mol Genet* **2014**, *23*, (21), 5774-80.
46. Klevering, B. J.; Deutman, A. F.; Maugeri, A.; Cremers, F. P.; Hoyng, C. B., The spectrum of retinal phenotypes caused by mutations in the ABCA4 gene. *Graefes Arch Clin Exp Ophthalmol* **2005**, *243*, (2), 90-100.
47. Littink, K. W.; van Genderen, M. M.; van Schooneveld, M. J.; Visser, L.; Riemslag, F. C.; Keunen, J. E.; Bakker, B.; Zonneveld, M. N.; den Hollander, A. I.; Cremers, F. P.; van den Born, L. I., A homozygous frameshift mutation in LRAT causes retinitis punctata albescens. *Ophthalmology* **2012**, *119*, (9), 1899-906.
48. Prado, D. A.; Acosta-Acero, M.; Maldonado, R. S., Gene therapy beyond VN: a new horizon of the treatment for inherited retinal disease. *Curr Opin Ophthalmol* **2020**, *31*, (3), 147-154.
49. García-Layana, A.; Cabrera-López, F.; García-Arumí, J.; Arias-Barquet, L.; Ruiz-Moreno, J. M., Early and intermediate age-related macular degeneration: update and clinical review. *Clin Interv Aging* **2017**, *12*, 1579-1587.
50. Wong, W. L.; Su, X.; Li, X.; Cheung, C. M.; Klein, R.; Cheng, C. Y.; Wong, T. Y., Global prevalence of age-related macular degeneration and disease burden projection for 2020 and 2040: a systematic review and meta-analysis. *Lancet Glob Health* **2014**, *2*, (2), e106-16.
51. Jonas, J. B.; Cheung, C. M. G.; Panda-Jonas, S., Updates on the Epidemiology of Age-Related Macular Degeneration. *Asia Pac J Ophthalmol (Phila)* **2017**, *6*, (6), 493-497.
52. Sarks, S. H., Ageing and degeneration in the macular region: a clinico-pathological study. *Br J Ophthalmol* **1976**, 60, (5), 324-41.

53. Bird, A. C.; Bressler, N. M.; Bressler, S. B.; Chisholm, I. H.; Coscas, G.; Davis, M. D.; de Jong, P. T.; Klaver, C. C.; Klein, B. E.; Klein, R.; et al., An international classification and grading system for age-related maculopathy and age-related macular degeneration. The International ARM Epidemiological Study Group. *Surv Ophthalmol* **1995**, *39*, (5), 367-74.
54. Curcio, C. A.; Medeiros, N. E.; Millican, C. L., Photoreceptor loss in age-related macular degeneration. *Invest Ophthalmol Vis Sci* **1996**, *37*, (7), 1236-49.
55. Khanna, S.; Komati, R.; Eichenbaum, D. A.; Hariprasad, I.; Ciulla, T. A.; Hariprasad, S. M., Current and upcoming anti-VEGF therapies and dosing strategies for the treatment of neovascular AMD: a comparative review. *BMJ Open Ophthalmol* **2019**, *4*, (1), e000398.
56. Ehrlich, R.; Harris, A.; Kheradiya, N. S.; Winston, D. M.; Ciulla, T. A.; Wirostko, B., Age-related macular degeneration and the aging eye. *Clin Interv Aging* **2008**, *3*, (3), 473-82.
57. Chou, R.; Dana, T.; Bougatsos, C.; Grusing, S.; Blazina, I., Screening for Impaired Visual Acuity in Older Adults: Updated Evidence Report and Systematic Review for the US Preventive Services Task Force. *Jama* **2016**, *315*, (9), 915-33.
58. Keenan, T. D.; Agrón, E.; Domalpally, A.; Clemons, T. E.; van Asten, F.; Wong, W. T.; Danis, R. G.; Sadda, S.; Rosenfeld, P. J.; Klein, M. L.; Ratnapriya, R.; Swaroop, A.; Ferris, F. L., 3rd; Chew, E. Y., Progression of Geographic Atrophy in Age-related Macular Degeneration: AREDS2 Report Number 16. *Ophthalmology* **2018**, *125*, (12), 1913-1928.
59. Jonasson, F.; Fisher, D. E.; Eiriksdottir, G.; Sigurdsson, S.; Klein, R.; Launer, L. J.; Harris, T.; Gudnason, V.; Cotch, M. F., Five-year incidence, progression, and risk factors for age-related macular degeneration: the age, gene/environment susceptibility study. *Ophthalmology* **2014**, *121*, (9), 1766-72.
60. Heesterbeek, T. J.; Lorés-Motta, L.; Hoyng, C. B.; Lechanteur, Y. T. E.; den Hollander, A. I., Risk factors for progression of age-related macular degeneration. *Ophthalmic Physiol Opt* **2020**, *40*, (2), 140-170.
61. Lechanteur, Y. T.; van de Ven, J. P.; Smailhodzic, D.; Boon, C. J.; Klevering, B. J.; Fauser, S.; Groenewoud, J. M.; van der Wilt, G. J.; den Hollander, A. I.; Hoyng, C. B., Genetic, behavioral, and sociodemographic risk factors for second eye progression in age-related macular degeneration. *Invest Ophthalmol Vis Sci* **2012**, *53*, (9), 5846-52.
62. Saunier, V.; Merle, B. M. J.; Delyfer, M. N.; Cougnard-Grégoire, A.; Rougier, M. B.; Amouyel, P.; Lambert, J. C.; Dartigues, J. F.; Korobelnik, J. F.; Delcourt, C., Incidence of and Risk Factors Associated With Age-Related Macular Degeneration: Four-Year Follow-up From the ALIENOR Study. *JAMA Ophthalmol* **2018**, *136*, (5), 473-481.
63. Vingerling, J. R.; Hofman, A.; Grobbee, D. E.; de Jong, P. T., Age-related macular degeneration and smoking. The Rotterdam Study. *Arch Ophthalmol* **1996**, *114*, (10), 1193-6.
64. Maller, J.; George, S.; Purcell, S.; Fagerness, J.; Altshuler, D.; Daly, M. J.; Seddon, J. M., Common variation in three genes, including a noncoding variant in CFH, strongly influences risk of age-related macular degeneration. *Nat Genet* **2006**, *38*, (9), 1055-9.
65. Lambert, N. G.; ElShelmani, H.; Singh, M. K.; Mansergh, F. C.; Wride, M. A.; Padilla, M.; Keegan, D.; Hogg, R. E.; Ambati, B. K., Risk factors and biomarkers of age-related macular degeneration. *Prog Retin Eye Res* **2016**, *54*, 64-102.

66. Group, A.-R. E. D. S. R., Risk factors associated with age-related macular degeneration. A case-control study in the age-related eye disease study: Age-Related Eye Disease Study Report Number 3. *Ophthalmology* **2000**, *107*, (12), 2224-32.
67. Leibowitz, H. M.; Krueger, D. E.; Maunder, L. R.; Milton, R. C.; Kini, M. M.; Kahn, H. A.; Nickerson, R. J.; Pool, J.; Colton, T. L.; Ganley, J. P.; Loewenstein, J. I.; Dawber, T. R., The Framingham Eye Study monograph: An ophthalmological and epidemiological study of cataract, glaucoma, diabetic retinopathy, macular degeneration, and visual acuity in a general population of 2631 adults, 1973-1975. *Surv Ophthalmol* **1980**, 24, (Suppl), 335-610.
68. Li, H.; Chintalapudi, S. R.; Jablonski, M. M., Current drug and molecular therapies for the treatment of atrophic age-related macular degeneration: phase I to phase III clinical development. *Expert Opin Investig Drugs* **2017**, *26*, (10), 1103-1114.
69. Johnson, E. J.; Neuringer, M.; Russell, R. M.; Schalch, W.; Snodderly, D. M., Nutritional manipulation of primate retinas, III: Effects of lutein or zeaxanthin supplementation on adipose tissue and retina of xanthophyll-free monkeys. *Invest Ophthalmol Vis Sci* **2005**, *46*, (2), 692-702.
70. Seddon, J. M.; Cote, J.; Davis, N.; Rosner, B., Progression of age-related macular degeneration: association with body mass index, waist circumference, and waist-hip ratio. *Arch Ophthalmol* **2003**, *121*, (6), 785-92.
71. Adams, M. K.; Simpson, J. A.; Aung, K. Z.; Makeyeva, G. A.; Giles, G. G.; English, D. R.; Hopper, J.; Guymer, R. H.; Baird, P. N.; Robman, L. D., Abdominal obesity and age-related macular degeneration. *Am J Epidemiol* **2011**, *173*, (11), 1246-55.
72. Chiu, C. J.; Milton, R. C.; Klein, R.; Gensler, G.; Taylor, A., Dietary carbohydrate and the progression of age-related macular degeneration: a prospective study from the Age-Related Eye Disease Study. *Am J Clin Nutr* **2007**, *86*, (4), 1210-8.
73. Kaushik, S.; Wang, J. J.; Flood, V.; Tan, J. S.; Barclay, A. W.; Wong, T. Y.; Brand-Miller, J.; Mitchell, P., Dietary glycemic index and the risk of age-related macular degeneration. *Am J Clin Nutr* **2008**, *88*, (4), 1104-10.
74. Merle, B. M. J.; Colijn, J. M.; Cougnard-Grégoire, A.; de Koning-Backus, A. P. M.; Delyfer, M. N.; Kiefte-de Jong, J. C.; Meester-Smoor, M.; Féart, C.; Verzijden, T.; Samieri, C.; Franco, O. H.; Korobelnik, J. F.; Klaver, C. C. W.; Delcourt, C., Mediterranean Diet and Incidence of Advanced Age-Related Macular Degeneration: The EYE-RISK Consortium. *Ophthalmology* **2019**, *126*, (3), 381-390.
75. Seddon, J. M.; Cote, J.; Rosner, B., Progression of age-related macular degeneration: association with dietary fat, transunsaturated fat, nuts, and fish intake. *Arch Ophthalmol* **2003**, *121*, (12), 1728-37.
76. Seddon, J. M.; Reynolds, R.; Yu, Y.; Daly, M. J.; Rosner, B., Risk models for progression to advanced age-related macular degeneration using demographic, environmental, genetic, and ocular factors. *Ophthalmology* **2011**, *118*, (11), 2203-11.
77. Lechanteur, Y. T.; van de Camp, P. L.; Smailhodzic, D.; van de Ven, J. P.; Buitendijk, G. H.; Klaver, C. C.; Groenewoud, J. M.; den Hollander, A. I.; Hoyng, C. B.; Klevering, B. J., Association of Smoking and CFH and ARMS2 Risk Variants With Younger Age at Onset of Neovascular Age-Related Macular Degeneration. *JAMA Ophthalmol* **2015**, *133*, (5), 533-41.

78. Seddon, J. M.; Francis, P. J.; George, S.; Schultz, D. W.; Rosner, B.; Klein, M. L., Association of CFH Y402H and LOC387715 A69S with progression of age-related macular degeneration. *Jama* **2007**, *297*, (16), 1793-800.

79. Yu, Y.; Reynolds, R.; Rosner, B.; Daly, M. J.; Seddon, J. M., Prospective assessment of genetic effects on progression to different stages of age-related macular degeneration using multistate Markov models. *Invest Ophthalmol Vis Sci* **2012**, *53*, (3), 1548-56.

80. Fritsche, L. G.; Igl, W.; Bailey, J. N.; Grassmann, F.; Sengupta, S.; Bragg-Gresham, J. L.; Burdon, K. P.; Hebbring, S. J.; Wen, C.; Gorski, M.; Kim, I. K.; Cho, D.; Zack, D.; Souied, E.; Scholl, H. P.; Bala, E.; Lee, K. E.; Hunter, D. J.; Sardell, R. J.; Mitchell, P.; Merriam, J. E.; Cipriani, V.; Hoffman, J. D.; Schick, T.; Lechanteur, Y. T.; Guymer, R. H.; Johnson, M. P.; Jiang, Y.; Stanton, C. M.; Buitendijk, G. H.; Zhan, X.; Kwong, A. M.; Boleda, A.; Brooks, M.; Gieser, L.; Ratnapriya, R.; Branham, K. E.; Foerster, J. R.; Heckenlively, J. R.; Othman, M. I.; Vote, B. J.; Liang, H. H.; Souzeau, E.; McAllister, I. L.; Isaacs, T.; Hall, J.; Lake, S.; Mackey, D. A.; Constable, I. J.; Craig, J. E.; Kitchner, T. E.; Yang, Z.; Su, Z.; Luo, H.; Chen, D.; Ouyang, H.; Flagg, K.; Lin, D.; Mao, G.; Ferreyra, H.; Stark, K.; von Strachwitz, C. N.; Wolf, A.; Brandl, C.; Rudolph, G.; Olden, M.; Morrison, M. A.; Morgan, D. J.; Schu, M.; Ahn, J.; Silvestri, G.; Tsironi, E. E.; Park, K. H.; Farrer, L. A.; Orlin, A.; Brucker, A.; Li, M.; Curcio, C. A.; Mohand-Saïd, S.; Sahel, J. A.; Audo, I.; Benchaboune, M.; Cree, A. J.; Rennie, C. A.; Goverdhan, S. V.; Grunin, M.; Hagbi-Levi, S.; Campochiaro, P.; Katsanis, N.; Holz, F. G.; Blond, F.; Blanché, H.; Deleuze, J. F.; Igo, R. P., Jr.; Truitt, B.; Peachey, N. S.; Meuer, S. M.; Myers, C. E.; Moore, E. L.; Klein, R.; Hauser, M. A.; Postel, E. A.; Courtenay, M. D.; Schwartz, S. G.; Kovach, J. L.; Scott, W. K.; Liew, G.; Tan, A. G.; Gopinath, B.; Merriam, J. C.; Smith, R. T.; Khan, J. C.; Shahid, H.; Moore, A. T.; McGrath, J. A.; Laux, R.; Brantley, M. A., Jr.; Agarwal, A.; Ersoy, L.; Caramoy, A.; Langmann, T.; Saksens, N. T.; de Jong, E. K.; Hoyng, C. B.; Cain, M. S.; Richardson, A. J.; Martin, T. M.; Blangero, J.; Weeks, D. E.; Dhillon, B.; van Duijn, C. M.; Doheny, K. F.; Romm, J.; Klaver, C. C.; Hayward, C.; Gorin, M. B.; Klein, M. L.; Baird, P. N.; den Hollander, A. I.; Fauser, S.; Yates, J. R.; Allikmets, R.; Wang, J. J.; Schaumberg, D. A.; Klein, B. E.; Hagstrom, S. A.; Chowers, I.; Lotery, A. J.; Léveillard, T.; Zhang, K.; Brilliant, M. H.; Hewitt, A. W.; Swaroop, A.; Chew, E. Y.; Pericak-Vance, M. A.; DeAngelis, M.; Stambolian, D.; Haines, J. L.; Iyengar, S. K.; Weber, B. H.; Abecasis, G. R.; Heid, I. M., A large genome-wide association study of age-related macular degeneration highlights contributions of rare and common variants. *Nat Genet* **2016**, *48*, (2), 134-43.

81. Grassmann, F.; Fleckenstein, M.; Chew, E. Y.; Strunz, T.; Schmitz-Valckenberg, S.; Göbel, A. P.; Klein, M. L.; Ratnapriya, R.; Swaroop, A.; Holz, F. G.; Weber, B. H., Clinical and genetic factors associated with progression of geographic atrophy lesions in age-related macular degeneration. *PLoS One* **2015**, *10*, (5), e0126636.

82. Kanda, A.; Chen, W.; Othman, M.; Branham, K. E.; Brooks, M.; Khanna, R.; He, S.; Lyons, R.; Abecasis, G. R.; Swaroop, A., A variant of mitochondrial protein LOC387715/ARMS2, not HTRA1, is strongly associated with age-related macular degeneration. *Proc Natl Acad Sci U S A* **2007**, *104*, (41), 16227-32.

83. Kortvely, E.; Hauck, S. M.; Behler, J.; Ho, N.; Ueffing, M., The unconventional secretion of ARMS2. *Hum Mol Genet* **2016**, *25*, (15), 3143-3151.

84. Canfield, A. E.; Hadfield, K. D.; Rock, C. F.; Wylie, E. C.; Wilkinson, F. L., HtrA1: a novel regulator of physiological and pathological matrix mineralization? *Biochem Soc Trans* **2007**, *35*, (Pt 4), 669-71.
85. Yang, Z.; Camp, N. J.; Sun, H.; Tong, Z.; Gibbs, D.; Cameron, D. J.; Chen, H.; Zhao, Y.; Pearson, E.; Li, X.; Chien, J.; Dewan, A.; Harmon, J.; Bernstein, P. S.; Shridhar, V.; Zabriskie, N. A.; Hoh, J.; Howes, K.; Zhang, K., A variant of the HTRA1 gene increases susceptibility to age-related macular degeneration. *Science* **2006**, *314*, (5801), 992-3.
86. van Leeuwen, E. M.; Emri, E.; Merle, B. M. J.; Colijn, J. M.; Kersten, E.; Cougnard-Gregoire, A.; Dammeier, S.; Meester-Smoor, M.; Pool, F. M.; de Jong, E. K.; Delcourt, C.; Rodrigez-Bocanegra, E.; Biarnés, M.; Luthert, P. J.; Ueffing, M.; Klaver, C. C. W.; Nogoceke, E.; den Hollander, A. I.; Lengyel, I., A new perspective on lipid research in age-related macular degeneration. *Prog Retin Eye Res* **2018**, *67*, 56-86.
87. Curcio, C. A., Soft Drusen in Age-Related Macular Degeneration: Biology and Targeting Via the Oil Spill Strategies. *Investigative Ophthalmology & Visual Science* **2018**, *59*, (4), AMD160-AMD181.
88. Curcio, C. A.; Messinger, J. D.; Sloan, K. R.; McGwin, G.; Medeiros, N. E.; Spaide, R. F., Subretinal drusenoid deposits in non-neovascular age-related macular degeneration: morphology, prevalence, topography, and biogenesis model. *Retina* **2013**, *33*, (2), 265-76.
89. Dietzel, M.; Pauleikhoff, D.; Arning, A.; Heimes, B.; Lommatzsch, A.; Stoll, M.; Hense, H. W., The contribution of genetic factors to phenotype and progression of drusen in early age-related macular degeneration. *Graefes Arch Clin Exp Ophthalmol* **2014**, *252*, (8), 1273-81.
90. Klein, R.; Myers, C. E.; Buitendijk, G. H.; Rochtchina, E.; Gao, X.; de Jong, P. T.; Sivakumaran, T. A.; Burlutsky, G.; McKean-Cowdin, R.; Hofman, A.; Iyengar, S. K.; Lee, K. E.; Stricker, B. H.; Vingerling, J. R.; Mitchell, P.; Klein, B. E.; Klaver, C. C.; Wang, J. J., Lipids, lipid genes, and incident age-related macular degeneration: the three continent age-related macular degeneration consortium. *Am J Ophthalmol* **2014**, *158*, (3), 513-24.e3.
91. Toops, K. A.; Tan, L. X.; Lakkaraju, A., Apolipoprotein E Isoforms and AMD. *Adv Exp Med Biol* **2016**, *854*, 3-9.
92. Bojanowski, C. M.; Shen, D.; Chew, E. Y.; Ning, B.; Csaky, K. G.; Green, W. R.; Chan, C. C.; Tuo, J., An apolipoprotein E variant may protect against age-related macular degeneration through cytokine regulation. *Environ Mol Mutagen* **2006**, *47*, (8), 594-602.
93. Gorin, M. B.; daSilva, M. J., Predictive genetics for AMD: Hype and hopes for genetics-based strategies for treatment and prevention. *Exp Eye Res* **2020**, *191*, 107894.
94. Cheung, G. C. M.; Lai, T. Y. Y.; Gomi, F.; Ruamviboonsuk, P.; Koh, A.; Lee, W. K., Anti-VEGF Therapy for Neovascular AMD and Polypoidal Choroidal Vasculopathy. *Asia Pac J Ophthalmol (Phila)* **2017**, *6*, (6), 527-534.
95. Rho, J.; Percelay, P.; Pilkinton, S.; Hollingsworth, T.; Kornblau, I.; Jablonski, M., An Overview of Age-Related Macular Degeneration: Clinical, Pre-Clinical Animal Models and Bidirectional Translation. *Animal Models in Medicine* **2021**.
96. Bergen, A. A., Nicotinamide, iRPE-in-a dish, and age-related macular degeneration therapy development. *Stem cell investigation* **2017**, *4*, 81.
97. Chader, G. J., Animal models in research on retinal degenerations: past progress and future hope. *Vision Research* **2002**, *42*, (4), 393-399.

98. Marmorstein, A. D.; Marmorstein, L. Y.; Sakaguchi, H.; Hollyfield, J. G., Spectral profiling of autofluorescence associated with lipofuscin, Bruch's Membrane, and sub-RPE deposits in normal and AMD eyes. *Invest Ophthalmol Vis Sci* **2002**, *43*, (7), 2435-41.
99. Bonilha, V. L.; Rayborn, M. E.; Bell, B. A.; Marino, M. J.; Pauer, G. J.; Beight, C. D.; Chiang, J.; Traboulsi, E. I.; Hollyfield, J. G.; Hagstrom, S. A., Histopathological comparison of eyes from patients with autosomal recessive retinitis pigmentosa caused by novel EYS mutations. Graefes Arch Clin Exp Ophthalmol 2015, 253, (2), 295-305.
100. Bonilha, V. L.; Rayborn, M. E.; Bell, B. A.; Marino, M. J.; Beight, C. D.; Pauer, G. J.; Traboulsi, E. I.; Hollyfield, J. G.; Hagstrom, S. A., Retinal histopathology in eyes from patients with autosomal dominant retinitis pigmentosa caused by rhodopsin mutations. *Graefes Arch Clin Exp Ophthalmol* **2015**, *253*, (12), 2161-9.
101. Mullins, R. F.; Kuehn, M. H.; Radu, R. A.; Enriquez, G. S.; East, J. S.; Schindler, E. I.; Travis, G. H.; Stone, E. M., Autosomal recessive retinitis pigmentosa due to ABCA4 mutations: clinical, pathologic, and molecular characterization. *Invest Ophthalmol Vis Sci* **2012**, *53*, (4), 1883-94.
102. Mitter, S. K.; Song, C.; Qi, X.; Mao, H.; Rao, H.; Akin, D.; Lewin, A.; Grant, M.; Dunn, W., Jr.; Ding, J.; Bowes Rickman, C.; Boulton, M., Dysregulated autophagy in the RPE is associated with increased susceptibility to oxidative stress and AMD. *Autophagy* **2014**, *10*, (11), 1989-2005.
103. Booij, J. C.; ten Brink, J. B.; Swagemakers, S. M.; Verkerk, A. J.; Essing, A. H.; van der Spek, P. J.; Bergen, A. A., A new strategy to identify and annotate human RPE-specific gene expression. *PLoS One* **2010**, *5*, (5), e9341.
104. Bennis, A.; Ten Brink, J. B.; Moerland, P. D.; Heine, V. M.; Bergen, A. A., Comparative gene expression study and pathway analysis of the human iris- and the retinal pigment epithelium. *PLoS One* **2017**, *12*, (8), e0182983.
105. van Soest, S. S.; de Wit, G. M.; Essing, A. H.; ten Brink, J. B.; Kamphuis, W.; de Jong, P. T.; Bergen, A. A., Comparison of human retinal pigment epithelium gene expression in macula and periphery highlights potential topographic differences in Bruch's membrane. *Mol Vis 2007*, **13**, 1608-17.
106. Shao, Z.; Wang, H.; Zhou, X.; Guo, B.; Gao, X.; Xiao, Z.; Liu, M.; Sha, J.; Jiang, C.; Luo, Y.; Liu, Z.; Li, S., Spontaneous generation of a novel foetal human retinal pigment epithelium (RPE) cell line available for investigation on phagocytosis and morphogenesis. *Cell Prolif* **2017**, *50*, (6).
107. Dunn, K. C.; Aotaki-Keen, A. E.; Putkey, F. R.; Hjelmeland, L. M., ARPE-19, a human retinal pigment epithelial cell line with differentiated properties. *Exp Eye Res* **1996**, *62*, (2), 155-69.
108. Mazzoni, F.; Safa, H.; Finnemann, S. C., Understanding photoreceptor outer segment phagocytosis: use and utility of RPE cells in culture. *Exp Eye Res* **2014**, *126*, 51-60.
109. Ablonczy, Z.; Dahrouj, M.; Tang, P. H.; Liu, Y.; Sambamurti, K.; Marmorstein, A. D.; Crosson, C. E., Human retinal pigment epithelium cells as functional models for the RPE in vivo. *Invest Ophthalmol Vis Sci* **2011**, *52,* (12), 8614-20.
110. Belgio, B.; Boschetti, F.; Mantero, S., Towards an In Vitro Retinal Model to Study and Develop New Therapies for Age-Related Macular Degeneration. *Bioengineering (Basel)* **2021**, *8*, (2).
111. Cornebise, C.; Courtaut, F.; Taillandier-Coindard, M.; Valls-Fonayet, J.; Richard, T.; Monchaud, D.; Aires, V.; Delmas, D., Red Wine Extract Inhibits VEGF Secretion and Its Signaling Pathway in Retinal ARPE-19 Cells to Potentially Disrupt AMD. *Molecules* **2020**, *25*, (23).

112. Ho, J.; Jang, K. H.; Koo, T. S.; Park, C.; Kim, Y. H.; Lee, J.; Kim, E., Protective effects of PARP1-inhibitory compound in dry age-related macular degeneration. *Biomed Pharmacother* **2021**, *133*, 111041.
113. Hu, L.; Guo, J.; Zhou, L.; Zhu, S.; Wang, C.; Liu, J.; Hu, S.; Yang, M.; Lin, C., Hydrogen Sulfide Protects Retinal Pigment Epithelial Cells from Oxidative Stress-Induced Apoptosis and Affects Autophagy. *Oxid Med Cell Longev* **2020**, *2020*, 8868564.
114. Pham, T. N. M.; Shin, C. Y.; Park, S. H.; Lee, T. H.; Ryu, H. Y.; Kim, S. B.; Auh, K.; Jeong, K. W., Solanum melongena L. Extract Protects Retinal Pigment Epithelial Cells from Blue Light-Induced Phototoxicity in In Vitro and In Vivo Models. *Nutrients* **2021**, *13*, (2).
115. Milićević, N.; Duursma, A.; Ten Asbroek, A.; Felder-Schmittbuhl, M. P.; Bergen, A. A., Does the circadian clock make RPE-mediated ion transport "tick" via SLC12A2 (NKCC1)? *Chronobiol Int* **2019**, *36*, (11), 1592-1598.
116. Milićević, N.; Mazzaro, N.; de Bruin, I.; Wils, E.; Ten Brink, J.; Asbroek, A. T.; Mendoza, J.; Bergen, A.; Felder-Schmittbuhl, M. P., Rev-Erbα and Photoreceptor Outer Segments modulate the Circadian Clock in Retinal Pigment Epithelial Cells. *Sci Rep* **2019**, *9*, (1), 11790.
117. Milićević, N.; Ten Brink, J. B.; Ten Asbroek, A.; Bergen, A. A.; Felder-Schmittbuhl, M. P., The circadian clock regulates RPE-mediated lactate transport via SLC16A1 (MCT1). *Exp Eye Res* **2020**, *190*, 107861.
118. Bodnar, A. G.; Ouellette, M.; Frolkis, M.; Holt, S. E.; Chiu, C. P.; Morin, G. B.; Harley, C. B.; Shay, J. W.; Lichtsteiner, S.; Wright, W. E., Extension of life-span by introduction of telomerase into normal human cells. *Science* **1998**, *279*, (5349), 349-52.
119. Jiang, X. R.; Jimenez, G.; Chang, E.; Frolkis, M.; Kusler, B.; Sage, M.; Beeche, M.; Bodnar, A. G.; Wahl, G. M.; Tlsty, T. D.; Chiu, C. P., Telomerase expression in human somatic cells does not induce changes associated with a transformed phenotype. *Nat Genet* **1999**, *21*, (1), 111-4.
120. Nabi, I. R.; Mathews, A. P.; Cohen-Gould, L.; Gundersen, D.; Rodriguez-Boulan, E., Immortalization of polarized rat retinal pigment epithelium. *J Cell Sci* **1993**, *104* (Pt 1), 37-49.
121. Osakada, F.; Ikeda, H.; Mandai, M.; Wataya, T.; Watanabe, K.; Yoshimura, N.; Akaike, A.; Sasai, Y.; Takahashi, M., Toward the generation of rod and cone photoreceptors from mouse, monkey and human embryonic stem cells. *Nat Biotechnol* **2008**, *26*, (2), 215-24.
122. Hirano, M.; Yamamoto, A.; Yoshimura, N.; Tokunaga, T.; Motohashi, T.; Ishizaki, K.; Yoshida, H.; Okazaki, K.; Yamazaki, H.; Hayashi, S.; Kunisada, T., Generation of structures formed by lens and retinal cells differentiating from embryonic stem cells. *Dev Dyn* **2003**, *228*, (4), 664-71.
123. Ikeda, H.; Osakada, F.; Watanabe, K.; Mizuseki, K.; Haraguchi, T.; Miyoshi, H.; Kamiya, D.; Honda, Y.; Sasai, N.; Yoshimura, N.; Takahashi, M.; Sasai, Y., Generation of Rx+/Pax6+ neural retinal precursors from embryonic stem cells. *Proc Natl Acad Sci U S A* **2005**, *102*, (32), 11331-6.
124. Shibata, S.; Hayashi, R.; Okubo, T.; Kudo, Y.; Katayama, T.; Ishikawa, Y.; Toga, J.; Yagi, E.; Honma, Y.; Quantock, A. J.; Sekiguchi, K.; Nishida, K., Selective Laminin-Directed Differentiation of Human Induced Pluripotent Stem Cells into Distinct Ocular Lineages. *Cell Rep* **2018**, *25*, (6), 1668-1679.e5.
125. Zhao, X.; Liu, J.; Ahmad, I., Differentiation of embryonic stem cells into retinal neurons. *Biochem Biophys Res Commun* **2002**, *297*, (2), 177-84.

126. Bennis, A.; Jacobs, J. G.; Catsburg, L. A. E.; Ten Brink, J. B.; Koster, C.; Schlingemann, R. O.; van Meurs, J.; Gorgels, T.; Moerland, P. D.; Heine, V. M.; Bergen, A. A., Stem Cell Derived Retinal Pigment Epithelium: The Role of Pigmentation as Maturation Marker and Gene Expression Profile Comparison with Human Endogenous Retinal Pigment Epithelium. *Stem Cell Rev Rep* **2017**, *13*, (5), 659-669.
127. Dalvi, S.; Galloway, C. A.; Singh, R., Pluripotent Stem Cells to Model Degenerative Retinal Diseases: The RPE Perspective. *Adv Exp Med Biol* **2019**, *1186*, 1-31.
128. Aladdad, A. M.; Kador, K. E., Adult Stem Cells, Tools for Repairing the Retina. *Curr Ophthalmol Rep* **2019**, *7*, (1), 21-29.
129. Ilic, D.; Ogilvie, C., Concise Review: Human Embryonic Stem Cells-What Have We Done? What Are We Doing? Where Are We Going? *Stem Cells* **2017**, *35*, (1), 17-25.
130. Takahashi, K.; Tanabe, K.; Ohnuki, M.; Narita, M.; Ichisaka, T.; Tomoda, K.; Yamanaka, S., Induction of pluripotent stem cells from adult human fibroblasts by defined factors. *Cell* **2007**, *131*, (5), 861-72.
131. Yu, J.; Vodyanik, M. A.; Smuga-Otto, K.; Antosiewicz-Bourget, J.; Frane, J. L.; Tian, S.; Nie, J.; Jonsdottir, G. A.; Ruotti, V.; Stewart, R.; Slukvin, II; Thomson, J. A., Induced pluripotent stem cell lines derived from human somatic cells. *Science* **2007**, *318*, (5858), 1917-20.
132. Yoshihara, M.; Hayashizaki, Y.; Murakawa, Y., Genomic Instability of iPSCs: Challenges Towards Their Clinical Applications. *Stem Cell Rev Rep* **2017**, *13*, (1), 7-16.
133. Garber, K., RIKEN suspends first clinical trial involving induced pluripotent stem cells. *Nat Biotechnol* **2015**, *33*, (9), 890-1.
134. Chakradhar, S., An eye to the future: Researchers debate best path for stem cell-derived therapies. *Nat Med* **2016**, *22*, (2), 116-9.
135. Gore, A.; Li, Z.; Fung, H. L.; Young, J. E.; Agarwal, S.; Antosiewicz-Bourget, J.; Canto, I.; Giorgetti, A.; Israel, M. A.; Kiskinis, E.; Lee, J. H.; Loh, Y. H.; Manos, P. D.; Montserrat, N.; Panopoulos, A. D.; Ruiz, S.; Wilbert, M. L.; Yu, J.; Kirkness, E. F.; Izpisua Belmonte, J. C.; Rossi, D. J.; Thomson, J. A.; Eggan, K.; Daley, G. Q.; Goldstein, L. S.; Zhang, K., Somatic coding mutations in human induced pluripotent stem cells. *Nature* **2011**, *471*, (7336), 63-7.
136. Yip, H. K., Retinal stem cells and regeneration of vision system. *Anat Rec (Hoboken)* **2014**, *297*, (1), 137-60.
137. Wallace, V. A., Stem cells: a source for neuron repair in retinal disease. *Can J Ophthalmol* **2007**, *42*, (3), 442-6.
138. Achberger, K.; Haderspeck, J. C.; Kleger, A.; Liebau, S., Stem cell-based retina models. *Adv Drug Deliv Rev* **2019**, *140*, 33-50.
139. Bartfeld, S.; Clevers, H., Stem cell-derived organoids and their application for medical research and patient treatment. *J Mol Med (Berl)* **2017**, *95*, (7), 729-738.
140. Collin, J.; Queen, R.; Zerti, D.; Dorgau, B.; Hussain, R.; Coxhead, J.; Cockell, S.; Lako, M., Deconstructing Retinal Organoids: Single Cell RNA-Seq Reveals the Cellular Components of Human Pluripotent Stem Cell-Derived Retina. *Stem Cells* **2019**, *37*, (5), 593-598.
141. Wagstaff, P. E.; Heredero Berzal, A.; Boon, C. J. F.; Quinn, P. M. J.; Ten Asbroek, A.; Bergen, A. A., The Role of Small Molecules and Their Effect on the Molecular Mechanisms of Early Retinal Organoid Development. *Int J Mol Sci* **2021**, *22*, (13).

142. Slijkerman, R. W.; Song, F.; Astuti, G. D.; Huynen, M. A.; van Wijk, E.; Stieger, K.; Collin, R. W., The pros and cons of vertebrate animal models for functional and therapeutic research on inherited retinal dystrophies. *Prog Retin Eye Res* **2015**, *48*, 137-59.
143. Pennesi, M. E.; Neuringer, M.; Courtney, R. J., Animal models of age related macular degeneration. *Mol Aspects Med* **2012**, *33*, (4), 487-509.
144. Niwa, M.; Aoki, H.; Hirata, A.; Tomita, H.; Green, P. G.; Hara, A., Retinal Cell Degeneration in Animal Models. *Int J Mol Sci* **2016**, *17*, (1).
145. Malek, G.; Busik, J.; Grant, M. B.; Choudhary, M., Models of retinal diseases and their applicability in drug discovery. *Expert Opin Drug Discov* **2018**, *13*, (4), 359-377.
146. Collin, G. B.; Gogna, N.; Chang, B.; Damkham, N.; Pinkney, J.; Hyde, L. F.; Stone, L.; Naggert, J. K.; Nishina, P. M.; Krebs, M. P., Mouse Models of Inherited Retinal Degeneration with Photoreceptor Cell Loss. *Cells* **2020**, *9*, (4).
147. Winkler, P. A.; Occelli, L. M.; Petersen-Jones, S. M., Large Animal Models of Inherited Retinal Degenerations: A Review. *Cells* **2020**, *9*, (4).
148. Sakami, S.; Maeda, T.; Bereta, G.; Okano, K.; Golczak, M.; Sumaroka, A.; Roman, A. J.; Cideciyan, A. V.; Jacobson, S. G.; Palczewski, K., Probing mechanisms of photoreceptor degeneration in a new mouse model of the common form of autosomal dominant retinitis pigmentosa due to P23H opsin mutations. *J Biol Chem* **2011**, 286, (12), 10551-67.
149. Fan, J.; Rohrer, B.; Frederick, J. M.; Baehr, W.; Crouch, R. K., Rpe65-/- and Lrat-/- mice: comparable models of leber congenital amaurosis. *Invest Ophthalmol Vis Sci* **2008**, *49*, (6), 2384-9.
150. LaVail, M. M.; Nishikawa, S.; Steinberg, R. H.; Naash, M. I.; Duncan, J. L.; Trautmann, N.; Matthes, M. T.; Yasumura, D.; Lau-Villacorta, C.; Chen, J.; Peterson, W. M.; Yang, H.; Flannery, J. G., Phenotypic characterization of P23H and S334ter rhodopsin transgenic rat models of inherited retinal degeneration. *Exp Eye Res* **2018**, *167*, 56-90.
151. Ding, J. D.; Kelly, U.; Landowski, M.; Toomey, C. B.; Groelle, M.; Miller, C.; Smith, S. G.; Klingeborn, M.; Singhapricha, T.; Jiang, H.; Frank, M. M.; Bowes Rickman, C., Expression of human complement factor H prevents age-related macular degeneration-like retina damage and kidney abnormalities in aged Cfh knockout mice. *Am J Pathol* **2015**, *185*, (1), 29-42.
152. Hu, Z.; Zhang, Y.; Wang, J.; Mao, P.; Lv, X.; Yuan, S.; Huang, Z.; Ding, Y.; Xie, P.; Liu, Q., Knockout of Ccr2 alleviates photoreceptor cell death in rodent retina exposed to chronic blue light. *Cell Death Dis* **2016**, *7*, (11), e2468.
153. Carver, K. A.; Lin, C. M.; Bowes Rickman, C.; Yang, D., Lack of the P2X(7) receptor protects against AMD-like defects and microparticle accumulation in a chronic oxidative stress-induced mouse model of AMD. *Biochem Biophys Res Commun* **2017**, *482*, (1), 81-86.
154. Biswal, M. R.; Justis, B. D.; Han, P.; Li, H.; Gierhart, D.; Dorey, C. K.; Lewin, A. S., Daily zeaxanthin supplementation prevents atrophy of the retinal pigment epithelium (RPE) in a mouse model of mitochondrial oxidative stress. *PLoS One* **2018**, *13*, (9), e0203816.
155. Plump, A. S.; Breslow, J. L., Apolipoprotein E and the apolipoprotein E-deficient mouse. *Annu Rev Nutr* **1995**, *15*, 495-518.
156. Zhou, P.; Kannan, R.; Spee, C.; Sreekumar, P. G.; Dou, G.; Hinton, D. R., Protection of retina by αB crystallin in sodium iodate induced retinal degeneration. *PLoS One* **2014**, *9*, (5), e98275.

157. Koster, C.; Wever, K. E.; Wagstaff, P. E.; Hirk, K.; Hooijmans, C. R.; Bergen, A. A., A Systematic Review on Transplantation Studies of the Retinal Pigment Epithelium in Animal Models. *Int J Mol Sci* **2020**, 21, (8).
158. Aumann, S.; Donner, S.; Fischer, J.; Müller, F., Optical Coherence Tomography (OCT): Principle and Technical Realization. In *High Resolution Imaging in Microscopy and Ophthalmology: New Frontiers in Biomedical Optics*, Bille, J. F., Ed. Springer Copyright 2019, The Author(s). Cham (CH), 2019; pp 59-85.
159. Fischer, J.; Otto, T.; Delori, F.; Pace, L.; Staurenghi, G., Scanning Laser Ophthalmoscopy (SLO). In *High Resolution Imaging in Microscopy and Ophthalmology: New Frontiers in Biomedical Optics*, Bille, J. F., Ed. Springer Copyright 2019, The Author(s). Cham (CH), 2019; pp 35-57.
160. Tsang, S. H.; Sharma, T., Electroretinography. *Adv Exp Med Biol* **2018**, *1085*, 17-20.
161. Leinonen, H.; Tanila, H., Vision in laboratory rodents-Tools to measure it and implications for behavioral research. *Behav Brain Res* **2018**, *352*, 172-182.

Out of the clutter, find simplicity.
From discord, find harmony.
In the middle of difficulty lies opportunity.

— Albert Einstein

A Systematic Review on Transplantation Studies of the Retinal Pigment Epithelium in Animal Models

Céline Koster, Kimberley E Wever, Philip E Wagstaff, Koen T van den Hurk, Carlijn R Hooijmans & Arthur A Bergen

Int. J. Mol. Sci. **2020**, accepted for publication, DOI: 10.3390/ijms21082719

2

Abstract

The retinal pigment epithelium (RPE) and the adjacent light-sensitive photoreceptors form a single functional unit lining the back of the eye. Both cell layers are essential for normal vision. RPE degeneration is usually followed by photoreceptor degeneration and vice versa. There are currently almost no effective therapies available for RPE disorders such as Stargardt disease, specific types of retinitis pigmentosa, and age-related macular degeneration. RPE replacement for these disorders, especially in later stages of the disease, may be one of the most promising future therapies. There is, however, no consensus regarding the optimal RPE source, delivery strategy, or the optimal experimental host in which to test RPE replacement therapy. Multiple RPE sources, delivery methods, and recipient animal models have been investigated, with variable results.

So far, a systematic evaluation of the (variables influencing) efficacy of experimental RPE replacement parameters is lacking. Here we investigate the effect of RPE transplantation on vision and vision-based behavior in animal models of retinal degenerated diseases. In addition, we aim to explore the effect of RPE source used for transplantation, the method of intervention, and the animal model which is used.

Methods: in this study, we systematically identified all publications concerning transplantation of RPE in experimental animal models targeting the improvement of vision (e.g., outcome measurements related to the morphology or function of the eye). A variety of characteristics, such as species, gender, and age of the animals but also cell type, number of cells, and other intervention characteristics were extracted from all studies. A risk of bias analysis was performed as well. Subsequently, all references describing one of the following outcomes were analyzed in depth in this systematic review: a-, b-, and c-wave amplitudes, vision-based, thickness analyses based on optical coherence tomography (OCT) data, and transplant survival based on scanning laser ophthalmoscopy (SLO) data. Meta-analyses were performed on the a- and b-wave amplitudes from electroretinography (ERG) data as well as data from vision-based behavioral assays. Results: original research articles met the inclusion criteria after two screening rounds.

Overall, most studies were categorized as unclear regarding the risk of bias, because many experimental details were poorly reported. Twenty-three studies reporting one or more of the outcome measures of interest were eligible for either descriptive (thickness analyses based on OCT data; $n = 2$) or meta-analyses. RPE transplantation significantly increased ERG a-wave (Hedges' g 1.181 (0.471–1.892), $n = 6$) and b-wave (Hedges' g 1.734 (1.295–2.172), $n = 42$) amplitudes and improved vision-based behavior (Hedges' g 1.018 (0.826–1.209), $n = 96$).

Subgroup analyses revealed a significantly increased effect of the use of young and adolescent animals compared to adult animals. Moreover, transplanting more cells (in the range of 10^5 versus in the range of 10^4) resulted in a significantly increased effect on vision-based behavior as well. The origin of cells mattered as well. A significantly increased effect was found on vision-based behavior when using ARPE-19 and OpRegen® RPE.

Conclusions: this systematic review shows that RPE transplantation in animal models for retinal degeneration significantly increases a- and b- wave amplitudes and improves vision-related behavior. These effects appear to be more pronounced in young animals, when the number of transplanted cells is larger and when ARPE-19 and OpRegen® RPE cells are used. We further emphasize that there is an urgent need for improving the reporting and methodological quality of animal experiments, to make such studies more comparable.

Introduction

The retinal pigment epithelium (RPE) is a neural epithelial cell layer lining the back of the eye [1]. The basal side of this polarized secretory cell layer rests on a collagen and elastin-rich extracellular matrix called the Bruch's membrane (BM). Its apical side faces the photoreceptors. Together with the photoreceptors, the RPE is vital for normal retinal function and vision. The physiological roles of the RPE include defense against local oxidative stress, transport of nutrients and ions over the blood-retinal barrier, synthesis and excretion of growth factors, phagocytosis of the photoreceptor outer segments and the capture, storage and metabolism of vitamin A derivatives [1].

The importance of the RPE in vision is illustrated by its role in many retinal disorders. Patients of all age groups can be affected by diseases of the RPE. These disorders include usually rare, early-onset monogenic disorders such as albinism [2], fundus albipunctatus [3], some types of retinitis pigmentosa (RP) [4], Stargardt disease [5], gyrate atrophy [6], and bestrophinopathy [7].

However, the RPE is also involved in more common complex retinal diseases, such as age-related macular degeneration (AMD). In elderly patients, AMD affects 4 % of the population over 60 and can be divided into dry and wet types. The majority of the patients suffer from dry or atrophic AMD which is characterized by the presence of drusen, pigment migration, and degeneration of the RPE and photoreceptors [8]. When dry AMD advances, the RPE degenerates almost completely and geographic atrophy characterized by RPE hypopigmentation and absence of the RPE sets in [9]. The wet types of AMD are characterized by choroidal neovascularization which causes bleedings, fluid accumulation and fibrosis within the macula [10]. Taken together, these RPE changes suggest that RPE dysfunction has a central role in AMD pathology and progression. Nonetheless, recent evidence suggests also that the photoreceptors, the choroid, as well as the blood contribute significantly to drusen formation and AMD disease pathology [11].

For the wet forms of AMD, a therapy exists which consists of monthly anti-VEGF injections. Monthly injections produce the best visual outcome, however intensive retreatment may not be sustainable in the long term. This treatment is based on hampering the disease progression however, a full cure is not available [12]. No effective treatment is currently available for the dry forms of AMD [8].

RPE Replacements as Experimental Therapies in AMD

To date, no effective treatments for RPE degeneration in dry AMD exists. RPE replacement may be a promising future therapeutic option [13]. Previously, either a free graft of autologous RPE and choroid taken from the mid-periphery [14,15] or a suspension of RPE cells [16] were transplanted to the macular area of diseased retinas, with some long-term functional restoration in some patients treated with a sheet. However, autologous RPE cell suspensions which were harvested in the nasal area and placed in the macula area did not settle. Therefore, any successful RPE replacement therapy for AMD should also consider the need to (temporarily) replace the underlying BM [17].

It has been shown that the integrity of the BM decreases with age. Several changes occur in ageing BM: it thickens, may become calcified, and lipids accumulate within the BM [18]. This aged BM may not support the survival and differentiation of transplanted RPE into a polarized cell layer. The fate of transplanted cells depends on their ability to make new BM (components), which can replace the host's BM. Temporarily restoring BM apart from the RPE would almost certainly be necessary, which implies further surgical manipulations beyond a simple subretinal injection of a cell suspension.

Therapeutic RPE replacement strategies are currently tested in usually small clinical trials (phase I) for AMD and in some types of RP (China: NCT02755428, NCT03944239, NCT03046407; United States of America: NCT01345006, NCT01344993, NCT02286089). These strategies include cell suspension injection, transplantation of autologous RPE sheets, and transplantation of RPE-scaffolds to the subretinal space [19]. In parallel, preclinical trials are ongoing in both animal models with smaller eyes, such as mice and rats, or larger eyes, such as rabbits, pigs, and primates. Each type of model appears to have its own pros and cons. Mice and rats have the advantage that they can be genetically manipulated, that maintenance of strains is relatively cheap, and that they have short generation times. At the same time, their eye size and lack of morphological resemblance to the human eye seem to be the biggest limitations. In larger animal models, the advantages are bigger eye size and a similar morphology as the human eye. The limitations are the lack of (genetic) models and the costs. A few laser-, mechanically-, and chemically-induced large animal models are available but not often used so far [20,21].
Finally, in AMD, not only the RPE is affected but also the composition of BM is changing [22] and the choroid is thinning [23]. Thus, the ageing of the BM and choriocapillaris, in addition to the ageing RPE and retina, should also be considered when performing transplantation experiments in AMD animal models. Generally, the animals used in transplantation studies are young and have a healthy BM and healthy choriocapillaris [24]. This does not fully reflect the human situation.

In summary, the best strategy to test and improve the efficacy of RPE cell transplantations as a treatment for retinal degenerative diseases is currently not clear. In recent years many animal experimental studies have been published to illustrate the safety and (limited) effectiveness. However, little consensus about the approach and analyses exists. Regardless, human clinical (phase I) trials have started based on these variable results. So far, no systematic meta-analysis has been published to analyze the effects of RPE transplantation therapy in animal models for retinal degenerative diseases. Such a review can be beneficial for future experimental designs and provides a more solid basis for future clinical studies. Therefore, in this systematic review, we investigate the effect of RPE transplantation on vision and vision-based behavior in animal models of retinal degenerative disorders. We aim to explore the effect of RPE source used for transplantation, the method of intervention, and the animal models which were used.

Materials and Methods

This review is reported according to the PRISMA guidelines [84]. The inclusion criteria and analyses were specified in advance and documented in a protocol, registered at PROSPERO (https://www.crd.york.ac.uk/prospero/display_record.php?RecordID=79628) on 15 December 2017 (PROSPERO registration number CRD42017079628).

Adjustments to the Review Protocol

After study selection according to the protocol's criteria, we found that the location of delivery correlated completely with the cell type which was transplanted. Therefore, and because of the large number of studies that were included, we decided to include all studies which transplanted RPE cells, which were all transplanted in the subretinal space, in this review. The other cell types will be analyzed in subsequent systematic reviews. We also conducted the following additional post hoc subgroup analyses (not listed in the original protocol): the effects of the number of cells that were transplanted, the follow-up time and whether or not immunosuppression was used.

Search Strategy

A comprehensive literature search was performed in PubMed, EMBASE (via OvidSP) and Web of Science to identify relevant articles until the 26th of September 2019. The search strategy (see Supplementary 1) consisted of the component "retinal degenerative diseases" and "cell transplantation replacing existing RPE". For PubMed and EMBASE, these were used in combination with a search filter for animal studies [51,85]. The search strategy was designed by information specialists at the Radboud University Medical Center (Nijmegen, the Netherlands) in collaboration with the medical library of the Amsterdam University Medical Centers (AUMC, location AMC, Amsterdam, The Netherlands).

Study Selection

After obtaining all references, duplicates were removed. Subsequently, unique references that were screened for relevance based on their title and abstract in Rayyan. A reference was included when it was an original full research article, using an animal model to study retinal degenerative diseases, included an appropriate control group receiving no treatment or a placebo/sham, it concerned a transplantation of cells replacing existing RPE, it reported outcome measurements related to the morphology or function of the eye. No language or publication date restrictions were made. In case of any doubt due to the absence of the abstract or insufficient information to make a valid judgment, references were included for full-text screening in Rayyan. Full-text copies of all publications eligible for inclusion were subsequently assessed and included when they met our pre-specified inclusion criteria.

Whenever necessary, studies in a language other than English were translated using Google Translate. In case of any doubts, a native speaker was asked to extract the data necessary for this review. For both screening phases, references were screened in duplicate by two independent reviewers and in case of disagreement between the reviewers, a third reviewer served as arbiter.

Study Characteristics

Study characteristics were extracted from the studies. Bibliographical information (author, year of publication, journal), animal model characteristics (species, strain, sex, age, weight, disease, control type, genotype, induction method), experimental characteristics (donor species, donor strain, cell type, number of transplanted cells/surface, administration place, type of intervention, carrier medium, injection volume, scaffold type, immune suppressors) and outcome characteristics (ERG, SLO, OCT, behavioral, transplant survival) were obtained. For all studies included in a meta-analysis, group averages (mean, standard deviation (STDEV), standard error (SE) number of animals per group (*n*), and the number of eyes per group (*n*)) were extracted for all outcome measures. When the SE was reported, the STDEV was recalculated from it using the number of eyes investigated. If a study reported data from several experimental groups, it was extracted as separate comparisons. Attempts were made to obtain original data by contacting authors if results were presented incompletely. If there was no reply within two weeks after sending a reminder, the data was not included in the meta-analysis. Graphically presented data was extracted as numerical data using ImageJ (version 1.8.0, National Institutes of Health, Bethesda, MD, United States of America).

Risk of Bias Assessment

The risk of bias was assessed for all studies which were included in the review after the full-text screening. The internal validity of the included studies was assessed in duplicate by two independent reviewers using SYRCLE's risk of bias tool [50]. This tool contains ten entries which are related to six types of bias (selection, performance, detection, attrition, reporting and 'other'). Disagreements between reviewers were resolved through discussion. For all studies, we determined whether the study used an external (other animal) or an internal (same animal, other eye) control group. For studies using an external control, all items of the risk of bias tool were scored. For studies using an internal control, all items except item 4 (random housing) were scored.

Some studies reported that one specific eye was always used as the experimental eye. This causes a high risk of bias for some items (e.g., 5 and 7). The risk of bias was assessed with the eye, which received the transplant, itself as an experimental unit and not the animal. Publication bias was assessed by visual inspection of the funnel plots and conducting Egger's regression test. Of note, since the effect measure used for both outcomes was Hedges' g, we used 1 divided by the square root of the total number of animals (1/sqrt n) as our precision estimate in publication bias analyses [86].

Data Analysis

Meta-analysis was performed whenever at least four or more independent studies reported on a specific outcome measure. As a consequence, meta-analysis could only be performed for three of our outcomes (the a-wave amplitude, the b-wave amplitude and the outcome of vision-based behavioral assays) using Comprehensive Meta-Analysis Software (CMA). Vision-based behavioral assays included optokinetic reflex, pupillometry, and visual water tasks. The effect size was expressed as a standardized mean difference (SMD (Hedges g); the mean of the experimental group minus the mean of the control group divided by the pooled STDEVs of the two groups) and its 95 % confidence interval (95 % CI). To enable assessment of sources of anticipated between-study heterogeneity, the individual effect sizes were subsequently pooled to obtain an overall SMD and 95 % CI. Because of the exploratory nature of animal studies, a random-effects model was used, which takes the anticipated between-study heterogeneity into account. Heterogeneity was addressed as I^2, i.e., the proportion of the total observed heterogeneity that can be explained by between-study heterogeneity.

Subgroup analyses were performed when subgroups contained a minimum of four independent comparisons. Subgroups were pre-specified in our protocol and analyses were planned for animal species, sex, age, intervention method (suspension/sheet), the cell type which was transplanted, type of animal model (genetic/induced), and genotype. In addition, some post hoc analyses were conducted for the number of cells, time after the intervention and whether immune suppressions were used (Y/N) as stated in the section adjustments made to the protocol. When a study contained multiple control groups, the control group undergoing the same surgical procedure as the experimental group (sham) was used. If multiple experimental groups were compared to the same control group, the number of animals in the control group was divided by the number of treatment groups, with a minimum of two animals in the control group and the number was rounded up. If the standard deviation was 0, the standard deviation of a similar group within that same reference was used in the meta-analysis. The *p*-value was adjusted for multiple testing, with an adjusted *p*-value of 0.05 and lower to be considered significant.

Results

Search and Study Selection

The study selection process is presented in Figure 1. We identified 9740 references. After removal of duplicates, we screened the titles and the abstracts of the remaining 6006 studies. After this first screening round, 5448 studies were excluded based on our predefined exclusion criteria. For the 558 remaining studies, we checked whether the full text was retrievable for full-text screening and whether those were original research articles. Three hundred and one studies were included for full-text screening.

Finally, we selected the 124 studies that used transplanted RPE cells in experimental animal models targeting the improvement of vision (e.g., outcome measurements related to the morphology or function of the eye). Subsequently, all references describing one of the following outcomes were analyzed in depth in this systematic review (n = 25): a-, b-, and c-wave amplitudes, vision-based behavior, thickness analyses based on optical coherence tomography (OCT) data and transplant survival based on scanning laser ophthalmoscopy (SLO) data. Meta-analyses were performed on the a- (n = 3) and b-wave amplitudes (n = 12) from electroretinography (ERG) data as well as data from vision-based behavioral assays (n = 16). Retina thickness analyses based on OCT data (n = 2) was analyzed by descriptive synthesis.

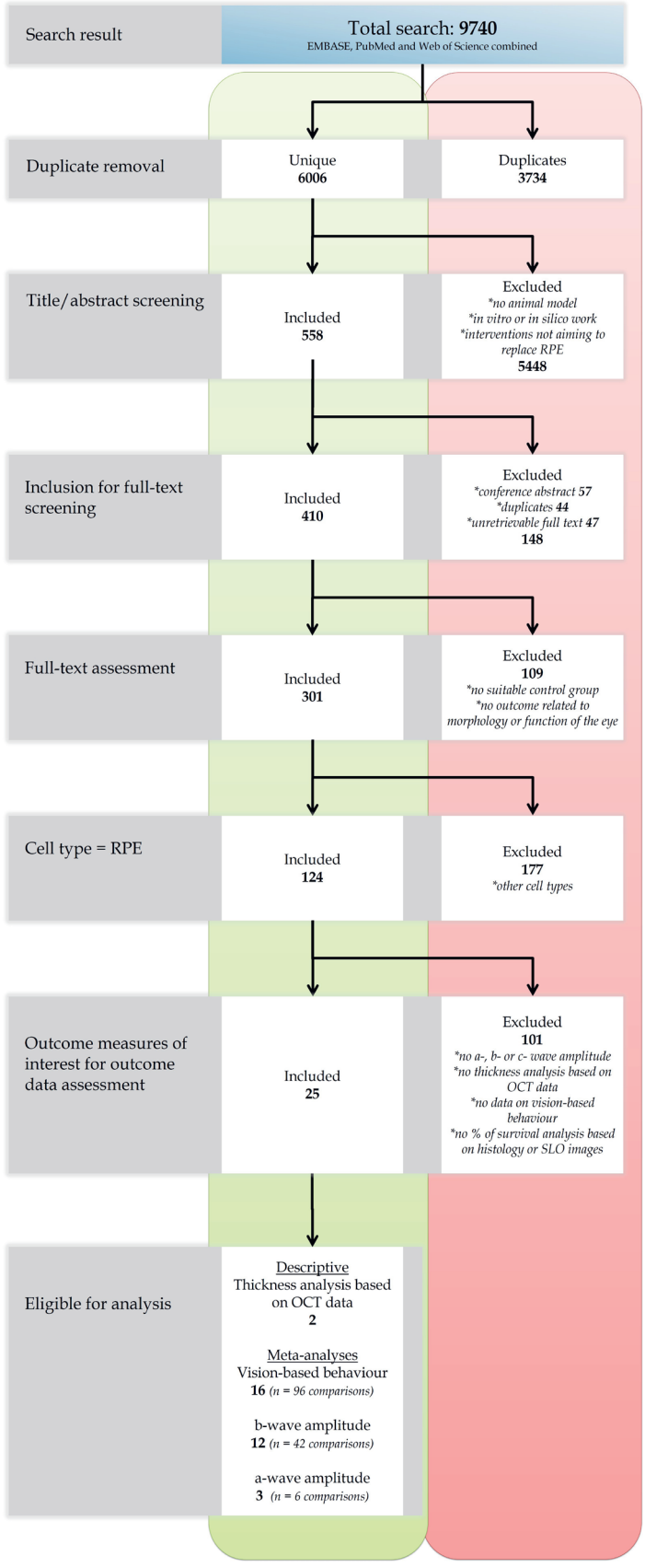

Figure 1.
Flow diagram of the study selection progress. For details of the selection process: see text.

Characteristics of the Included Studies

The characteristics of the 124 included studies are summarized in Tables S1 and S2, and Figure 2. In general, there was a large variation in study characteristics. Most studies were performed in rats (56 %). Other species included rabbit (25 %), mouse (11 %), pig (5 %), and other species (cat, dog, Macaca mulatta and Macaca fascicularis, all 1 %).

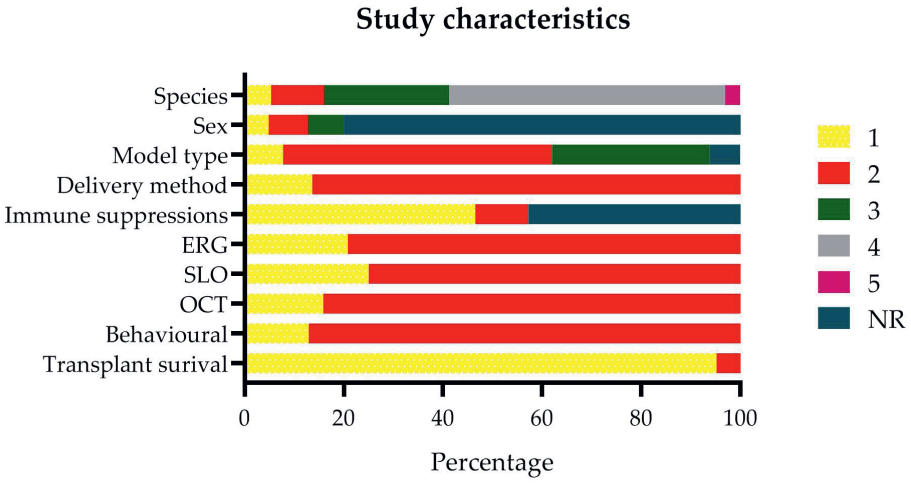

Figure 2. General study characteristics were extracted from the studies which were included in this systematic review. Species: 1 pig, 2 mouse, 3 rabbit, 4 rat, 5 other (cat, dog, Macaca mulatta, Macaca fascicularis). Sex: 1 female, 2 male, 3 both. Model type: 1 induced, 2 genetic, 3 not-applicable. Delivery method: 1 sheet, 2 suspension. Immune suppressions, ERG, SLO, OCT, behavioral and transplant survival: 1 yes, 2 no. NR = not reported.

In the majority of studies (80 %), the sex of animals used was not reported. When reported, roughly an equal number of males-only (8 %), females-only (5 %), and both sexes were used (7 %). Most studies were performed in genetic animal models, e.g., rats or mice (54 %). Chemically induced models were used in 8 % of all cases. Intervention methods included cells that were delivered in the subretinal space (100 %) as a suspension (86 %) or as a sheet (14 %) in rats, rabbits, pigs, cats, and Macaca mulatta. Immune suppression was used in at least half of all studies (47 %). Notably, 42 % did not report whether any suppression was used. All studies reported at least one of the following techniques to assess the outcome measures of interest: scanning laser ophthalmoscopy (SLO) was performed in 25 % of the studies; electroretinography (ERG) in 20 %; optical coherence tomography (OCT) in 16 %; a behavioral assay in 13 %; and, finally, transplant survival was determined in almost all studies (95 %). One outcome measure (retina thickness analysis based on OCT data) was selected for descriptive analysis. Out of 40 studies reporting any OCT data, only 2 performed a quantitative analysis on the retina thickness based on this data, which is not enough to perform a meta-analysis.

Moreover, three outcome measures (a-wave amplitude, b-wave amplitude, and vision-based behavior) were selected for our meta-analysis since enough studies reported these quantitative data. Out of 26 studies reporting ERG data, only 12 were suitable for meta-analysis on the b-wave amplitude and only 3 were suitable for meta-analysis on the a-wave amplitudes. The remainder of 15 studies did report some ERG data, but they did not report any formal statistics on a-, b-, or c-wave amplitudes, thereby prohibiting meta-analysis on the reported data. All (16) studies which reported behavioral data were selected for meta-analysis because quantitative data and statistics were available. An overview of the key study characteristics of the 25 studies which were eligible for analysis is summarized in Table 1. A more extensive summary of the study characteristics is shown in Tables S1 and S2.

Table 1. An overview of the study characteristics of the 25 studies which were eligible for in depth analysis.
WT = wildtype; NA = not applicable; NR = not reported; $NaIO_3$ = sodium iodate;
i.v. = intravenous; pRPE = primary RPE; hESC = human embryonic stem cell; BMSC = bone marrow-derived mesenchymal stem cell; 3D = three dimensions; SD = single dimension; CPCB-VN = parylene C membrane with vitronectin; PLGA = poly lactic-co-glycolic acid; N = no; Y = yes.

Author Year	Species	Genotype	Induction Method	Donor Species	Cell Type	Suspension or Sheet	Injection Volume (μL)	Scaffold	Immune Suppression	ERG	SLO	OCT	Behavioral
Abe2008 [25]	Rat	WT	Light	Rat	pRPE	Suspension	2	NA	N	Y	N	N	N
Carr2009 [26]	Rat	MERTK$^{-/-}$	NA	Human	pRPE	Suspension	2	NA	Y	N	N	N	Y
Coffey2002 [27]	Rat	MERTK$^{-/-}$	NA	Human	ARPE-19	Suspension	2	NA	Y	N	N	N	Y
Davis2017 [28]	Rat	MERTK$^{-/-}$	NA	Human	hESC-RPE	Suspension	1.5	NA	Y	N	N	N	Y
Duan2017 [29]	Rat	WT	$NaIO_3$; i.v.; 50 mg/kg	Human	hBMSC; BMSC-RPE; hESC-RPE	Suspension	2	NA	Y	y	N	N	N
Gouras2002 [30]	Mouse	RPE65$^{-/-}$	NA	Mouse	pRPE	Suspension	10	NA	NR	Y	N	N	N
Haruta2004 [31]	Rat	MERTK$^{-/-}$	NA	Monkey	hESC-RPE	Suspension	3	NA	Y	N	N	N	Y
Idelson2018 [32]	Rat	MERTK$^{-/-}$	NA	Human	hESC-RPE	Suspension	2–3	NA	Y	Y	Y	N	N
Kamao2014 [33]	Rat; Macaca fascilaris	MERTK$^{-/-}$; NR	NA; NR	Human; Monkey	pRPE	Suspension; Sheet	2; 100	none	Y; NR	Y; N	Y	N; Y	N
Klassen2001 [34]	Rat	MERTK$^{-/-}$; WT	NA	Rat	pRPE	Suspension	2	NA	NR	N	N	N	Y
Kole2018 [35]	Rat	MERTK$^{-/-}$	NA	Pig	pRPE	Suspension	2	NA	Y	Y	Y	Y	Y
Little1998 [36]	Rat	MERTK$^{-/-}$	NA	Human	pRPE	Sheet	3–5	NA	Y	N	N	N	Y
Lu2009 [37]	Rat; Mouse	MERTK$^{-/-}$; ELOVL4$^{-/-}$	NA	Human	pRPE	Suspension	2	NA	Y	N	N	N	Y
Lund2001 [38]	Rat	MERTK$^{-/-}$	NA	Human	ARPE-19; h1RPE7	Suspension	2	NA	Y	N	N	N	Y
Lund2006 [39]	Rat	MERTK$^{-/-}$	NA	Human	pRPE	Suspension	NR	NA	Y	Y	N	N	Y
Maeda2013 [40]	Mouse	LRAT$^{-/-}$; RPE65$^{-/-}$ Tyrc-2J/J	NA	Mouse; Human	pRPE; iPSC-RPE	Suspension	1.5	NA	Y	Y	Y	Y	N
M'Barek2017 [41]	Rat	MERTK$^{-/-}$	NA	Human	hESC-RPE	Sheet; Suspension	NA; 4	Gelatin; NA	Y	Y	N	Y	Y
McGill2004 [42]	Rat	MERTK$^{-/-}$	NA	Human	ARPE-19	Suspension	2	NA	Y	N	N	N	Y
McGill2017 [43]	Rat	MERTK$^{-/-}$	NA	Human	RPE (OpRegen)	Suspension	2	NA	Y	N	N	N	Y
Sauve2004 [44]	Rat	MERTK$^{-/-}$	NA	Human	ARPE-19	Suspension	2	NA	Y	Y	N	N	N
Sauve2006 [45]	Rat	MERTK$^{-/-}$	NA	Human	ARPE-19	Suspension	2	NA	Y	Y	N	N	N
Sharma2019 [46]	Rat; Pig	MERTK$^{-/-}$	Laser	Human	iPSC-RPE	Sheet; Suspension	2	PLGA	Y	Y	Y	Y	Y
Thomas2016 [47]	Rat	MERTK$^{-/-}$	NA	Human	pRPE	Sheet	NA	CPCB-VN	Y	N	N	N	Y
Wang2008 [48]	Rat	MERTK$^{-/-}$	NA	Human	ARPE-19	Suspension	3	NA	Y	N	N	N	Y
Wu2016 [49]	Rat	MERTK$^{-/-}$	NA	Human	3DRPE; SDRPE	Suspension	1–2	NA	Y	Y	N	N	N

The Methodological Quality of the Studies

Blinding and randomization of the experimental setup are essential measures to take to prevent statistical bias and underestimation or overestimation of the experimental data. However, both measures are infrequently reported in animal studies. We used SYRCLE's risk of bias tool [50] to determine the risk of bias in all included studies. This risk of bias assessment is, in summary, presented in Figure 3 and 4. We first assessed the reporting of four key study quality indicators, namely reporting of any randomization, any blinding, a sample size calculation and a conflict of interest statement. Only 7 % of all included studies reported the use of any form of randomization, 20 % reported the use of any blinding and not one study reported a sample size calculation. In addition, only 35 % of the studies reported a conflict of interest statement. Although some authors mentioned applying randomization or blinding in their experiments, few adequately specified the methodology used. As a result, the majority of studies were assessed to have an unclear risk of most types of bias (Figure 4).

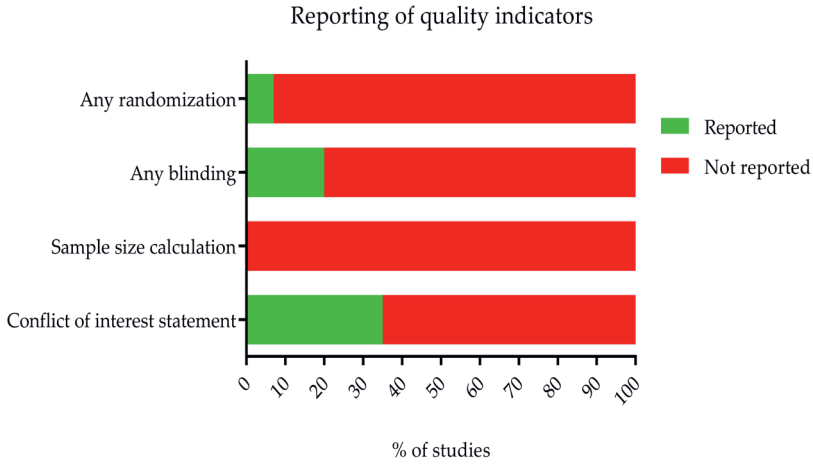

Figure 3. Reporting of four quality indicators in the 124 included studies. Only 7 % of studies reported the use of any form of randomization, 20 % reported the use of blinding and not one study reported a sample size calculation. In addition, only 35 % of the studies reported a conflict of interest statement.

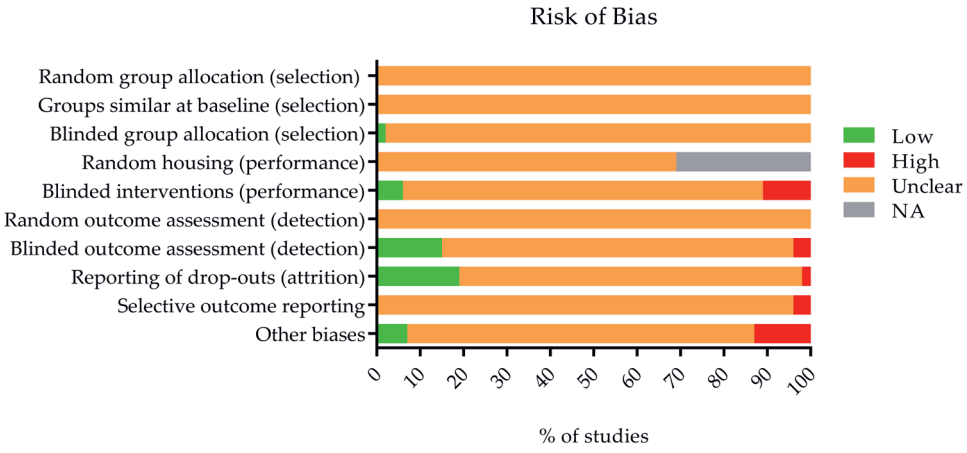

Figure 4. Using SYRCLE's risk of bias tool [51], the risk of selection, performance, detection, attrition and other biases was assessed for the studies included in this review. The proportion of studies (%) which have a low, unclear or high risk of bias in several categories. As a consequence of poor reporting of measures to reduce several types of bias, the analysis resulted in a high percentage of "unclear" risk of bias for most items. NA (not applicable) holds true for studies that used an internal control in their experiments (e.g. one eye experimental group, other eye control group). Random housing between the experimental and control group is in that case, obviously, impossible.

Descriptive Analysis

Retina Thickness Analysis Based on OCT Data

Twenty of the included studies reported OCT data. Only two of them showed a quantitative analysis of the thickness of the retina (or a retinal cell layer). Both studies showed an increased effect on the thickness of the ONL in the group receiving an RPE transplantation [35,41].

Meta-Analyses

A-wave and B-wave Amplitudes Extracted from ERG Data

Twenty-six studies reported ERG data. Fourteen [46,52–64] of them were excluded from meta-analysis since they did not report quantitative data or only showed single representative ERG traces. Three studies [25,29,39] reporting six experiments were included in the meta-analysis of the ERG a-wave amplitude, all of them using rats. See Supplementary 1 for all study characteristics of the individual studies. The forest plot, in which the graphical representation of the meta-analysis is presented, is shown in Figure 5. Additional data (individual Hedges' g (a measure for effect size using smaller sample sizes), lower- and upper limits) are shown in Table S3. For the a-wave meta-analysis, 45 experimental eyes and 22 control eyes were included. Group sizes were 5–14 (median = 5) for the experimental eyes and 3–8 (median = 8) for the control eyes.

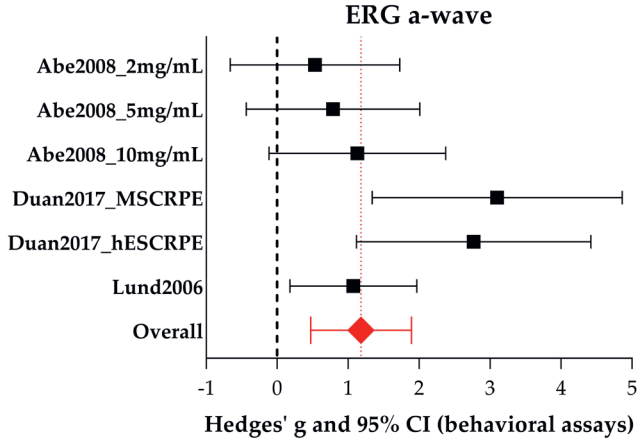

Figure 5. The meta-analysis of the effect of RPE transplantation on the size of the ERG a-wave amplitude. For every experimental group, Hedges' g (a measure for effect size using smaller sample sizes, black solid squares) and its 95 % confidence interval (CI) are graphically shown. The left side of the dashed black line (Hedges' g = 0) favors the control group (untreated or sham-operated) and the right side favors the experimental group (RPE transplantation). RPE transplantation significantly increases the a-wave amplitude (Hedges' g 1.181(0.471–1.892), red diamond).

Overall, RPE transplantation significantly increases a-wave amplitude (Hedges' g 1.181 (0.471–1.892), *n* = 6). Overall, between-study heterogeneity was low (I^2 = 26 %), but this could be partly due to the limited number of studies in this meta-analysis. Subgroup analysis was not conducted for a-wave amplitudes because the subgroups contained too few studies in order to draw meaningful conclusions (less than 4 studies per subgroup remained).

For the meta-analysis of ERG b-wave amplitude, twelve [25,29,30,32,33,35,39–41,44,45,49] studies reporting 42 experiments were included, of which 30 experiments were performed in rats and 12 in mice. See Supplementary 1 for all study characteristics of the individual studies. Four hundred and thirty-nine experimental eyes and 146 control eyes were included. The forest plot is shown in Figure 6.

Additional data (individual Hedges' g, lower- and upper limits) are presented in Table S4. Group sizes were 3–25 (median = 9) for the experimental eyes and 3–14 (median = 8) for the control eyes. Overall, RPE transplantation significantly increases b-wave amplitude (Hedges' g 1.734 (1.295–2.172), (*n* = 42). Between study heterogeneity was high (I^2 = 82 %). Subgroup analyses were performed and described below.

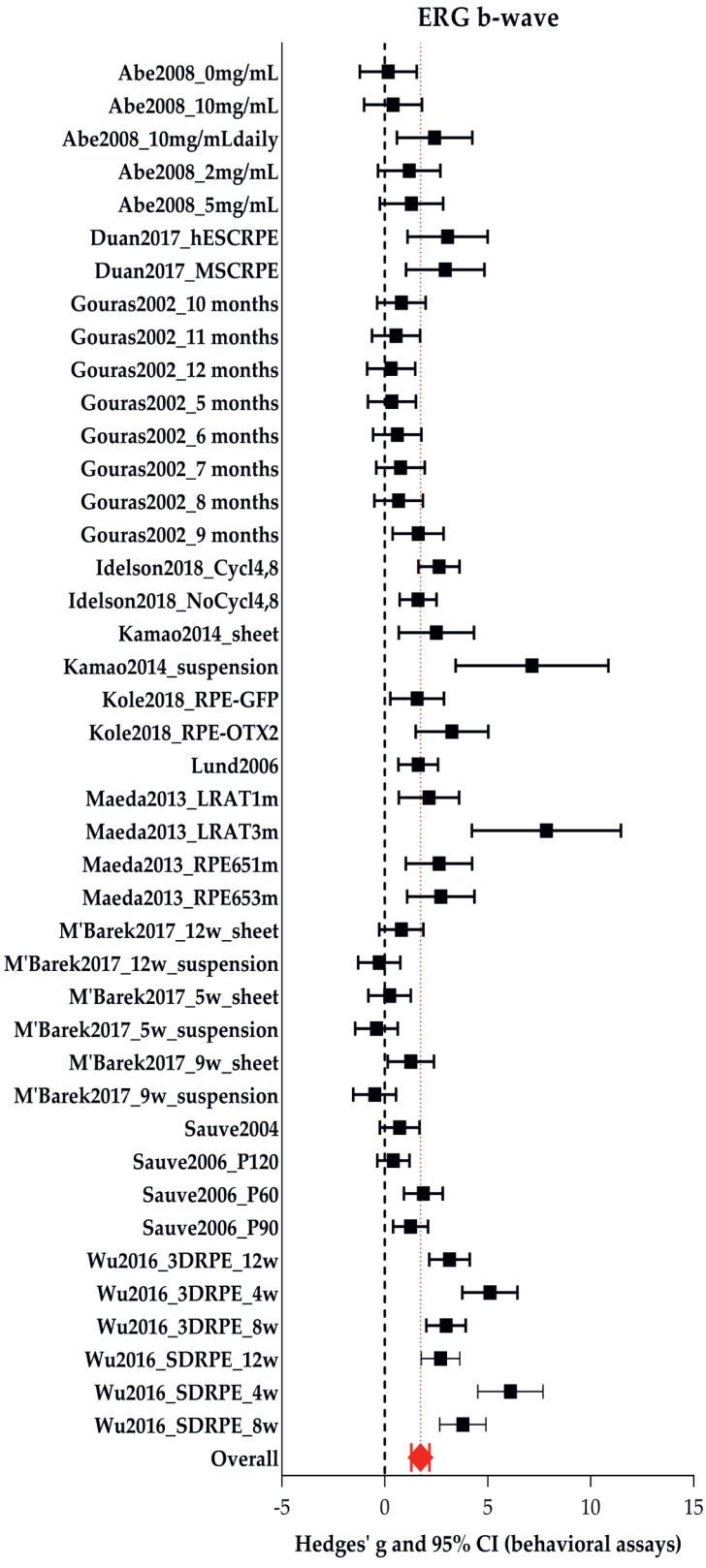

Figure 6. The meta-analysis on the effect of RPE transplantation on the ERG b-wave amplitude. For every experimental group, Hedges' g (a measure for effect size using smaller sample sizes, black solid squares) and its 95 % confidence interval (CI) are graphically shown. The left side of the dashed black line (Hedges' g = 0) favors the control group (untreated or sham-operated) and the right side favors the experimental group (RPE transplantation). Overall, an RPE transplantation increased the b-wave amplitude significantly (Hedges' g 1.734 (1.295–2.172), red diamond).

The use of both sexes increases the b-wave amplitude significantly (Hedges' g 3.500 (2.735–4.265), n = 8) compared to the use of males only (Hedges' g 1.029 (−0.019–2.077), n = 5, adjusted p-value 0.001), see Figure 7. No studies within this meta-analysis reported using females only. Additional data (number of experiments, I^2, Hedges' g, its lower- and upper limits) are shown in Table S5. We further identified that the effect on b-wave amplitude was larger in young animals (<20 days of age; Hedges' g 2.223 (1.591–2.855), n = 18) compared to adult animals (>2 months of age; Hedges' g 0.724 (−0.210–1.658), n = 8, adjusted p-value 0.047). No significant difference could be observed between young and adolescent animals (20 days–2 months of age) or between adolescent and adult animals. Subgroup analyses were also performed for species (mouse versus rat), model type (genetic versus induced), genotype (*Mertk*$^{-/-}$ versus *Rpe65*$^{-/-}$ versus wildtype), number of cells which was transplanted (in the range of 10^3 versus 10^4 versus 10^5), the cell type which was transplanted (ARPE-19 versus hESC-RPE versus pRPE versus BDNF-RPE), and the time after the intervention when the animals were analyzed (short-term (<30 days) versus middle-term (30–90 days) versus long-term (>90 days)). However, no significant differences were found. For other study characteristics, subgroups were too small (<4 studies) to perform subgroup analysis.

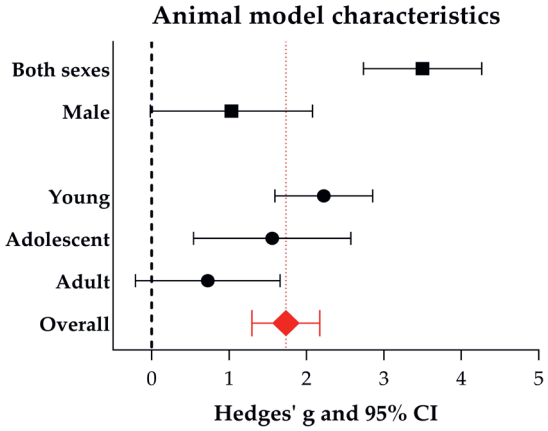

Figure 7. The effect of some animal model characteristics on the ERG b-wave amplitude. For every subgroup, Hedges' g (a measure for effect size using smaller sample sizes, black solid squares) and its 95 % confidence interval (CI) are graphically shown. The left side of the dashed black line (Hedges' g = 0) favors the control group (untreated or sham-operated) and the right side favors the experimental group (RPE transplantation). An overall beneficial effect of RPE transplantation on the b-wave amplitude was observed (Hedges' g 1.734 (1.295–2.172), red diamond). Significantly higher b-wave amplitudes were obtained when both sexes were used in the studies as compared to when males only were used (adjusted p-value 0.001). Significantly higher b-wave amplitudes were observed in young animals compared to adult animals (adjusted p-value 0.047).

Behavioral Assays

Results for the outcome measure vision-based behavior are summarized in Figure 8. and additional statistics data (individual Hedges' g, lower- and upper limits) can be found in Table S6. Sixteen studies [26–28,31,34–39,41–43,46–48] reporting 96 experiments were included in the meta-analysis. Ninety-one studies were performed in rats and five in mice. For all individual study characteristics see Supplementary 1. Group sizes were 4–59 (median = 8) and 2–21 (median = 7) for experimental eyes and control eyes respectively. In total, data of 1216 experimental eyes and 725 control eyes were available.

Overall, between study heterogeneity was high (I^2 = 73 %). We observed significantly increased vision-based behavior in RPE transplanted eyes versus control eyes (Hedges' g 1.018 (0.826–1.209), n = 96). Subgroup analysis revealed that the use of adolescent animals (20 days–2 months of age; Hedges'g w1.257 (1.032–1.481), n = 59) increased the outcome of vision-based behavior significantly compared to the use of adult animals (>2 months of age; Hedges' g 0.431 (0.136–0.725), n = 31, adjusted p-value 0.000033), see Figure 9. No studies included in the meta-analysis of vision-based behavior reported the use of young animals. Additional data (number of experiments, I^2, Hedges' g, its lower- and upper limits) are shown in Table S7.

In addition, subgroup analysis (Figure 10) showed that transplanting a larger number of RPE cells in the range of 10^5 (Hedges' g 1.694 (1.384–2.003), n = 32) yielded significant better vision-based behavior compared to the range of 10^4 cells (Hedges' g 0.811 (0.566–1.055), n = 47, adjusted p-value 0.000036). Furthermore, the origin of the RPE cells which were transplanted matters as well. The ARPE-19 cell line (Hedges' g 2.153 (1.597–2.709), n = 10) resulted in significant increased vision-based behavior compared to hESC-RPE cells (Hedges' g 0.783 (0.574–0.992), adjusted p-value 0.00035, n = 45).

Interestingly, OpRegen®-RPE (Lineage Cell Therapeutics), which is currently in a clinical trial phase I (NCT02286089) (Hedges' g 1.978 (1.551–2.406), n = 12), also resulted significantly in better vision-based behavior compared to hESC-RPE cells (adjusted p-value 0.000081) and primary RPE (Hedges' g 0.976 (0.529–1.423), n = 10, adjusted p-value 0.048). Additional data (number of experiments, I^2, Hedges' g, its lower- and upper limits) are shown in Table S7. Subgroup analyses were also performed for species (mouse versus rat), genotype (*Mertk*$^{-/-}$ versus *Elovl4*$^{-/-}$), the delivery method (suspension versus sheet) and the time after the intervention when the animals were screened (short-term (<30 days) versus middle-term (30–90 days) versus long-term (>90 days). However, no significant differences between subgroups were found. For the other study characteristics (sex and immune suppressions), subgroups were too small (<4 studies) to perform subgroup analysis.

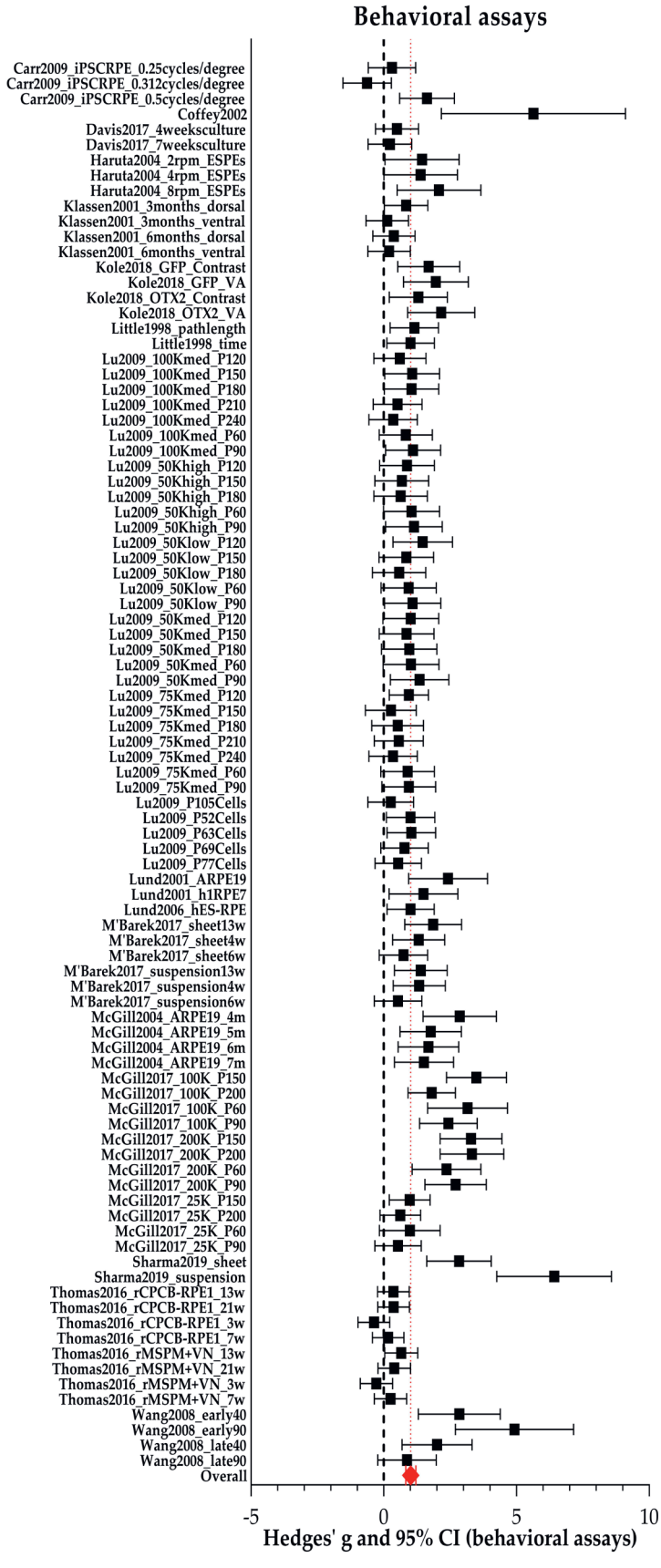

Figure 8. The meta-analysis on the effect of RPE transplantation on the outcome of vision-based behavioral assays. For every experimental group, Hedges' g (a measure for effect size using smaller sample sizes, black solid squares) and its 95 % confidence interval (CI) are graphically shown. The left side of the dashed black line (Hedges' g = 0) favors the control group (untreated or sham-operated) and the right side favors the experimental group (RPE transplantation). Overall, RPE transplantation increased vision-based behavior (Hedges' g 1.018 (0.826–1.209), red diamond).

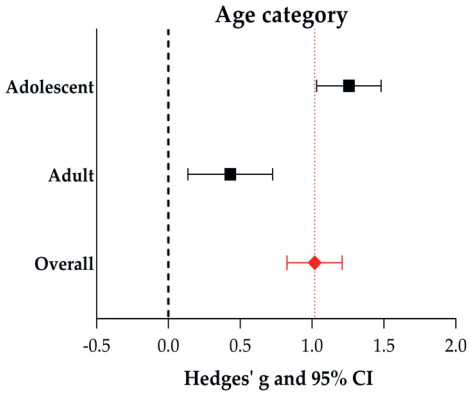

Figure 9. The effect of age on the outcome of vision-based behavioral assays. For every subgroup, Hedges' g (a measure for effect size using smaller sample sizes, black solid squares) and its 95 % confidence interval (CI) are graphically shown. The left side of the dashed black line (Hedges' g = 0) favors the control group (untreated or sham-operated) and the right side favors the experimental group (RPE transplantation). Overall, RPE transplantation increased vision-based behavior (Hedges' g 1.018 (0.826–1.209), red diamond). Significant better results were obtained when adolescent animals were used over adult animals (adjusted *p*-value 0.000033).

Publication Bias

Publication bias was assessed by visual inspection of the funnel plots shown in Figure 11, panel A (outcome vision-based behavioral assays) and B (ERG b-wave amplitude). Slight asymmetry can be observed for both outcomes. In addition, we performed Egger's test for small study effects, which indicated that small study effects are present for the outcome vision-based behavioral assays (p = 0.003) (Figure 11C), but not for the outcome ERG b-wave amplitude (p = 0.44) (Figure 11D). Data were insufficient to perform a similar analysis for the a-wave amplitude.

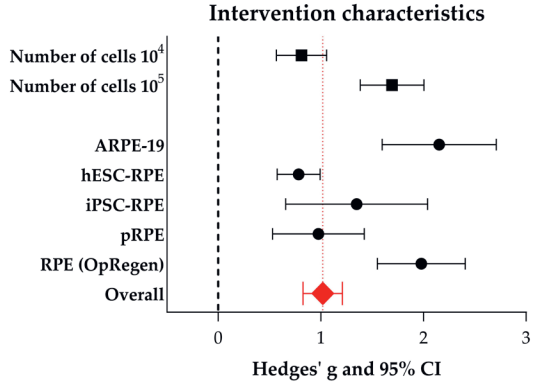

Figure 10. The effect of the number of transplanted cells and the origin of the cells on the outcome of vision-based behavioral assays. For every subgroup, Hedges' g (a measure for effect size using smaller sample sizes, black solid squares) and its 95 % confidence interval (CI) are graphically shown. The left side of the dashed black line (Hedges' g = 0) favors the control group (untreated or sham-operated) and the right side favors the experimental group (RPE transplantation). Overall, RPE transplantation increased vision-based behavior (Hedges' g 1.018 (0.826–1.209), red diamond). Significant better results were obtained when 10^5 cells were transplanted when compared to 10^4 cells (adjusted *p*-value 0.000036). The origin of the RPE cells which are transplanted matters as well, with ARPE-19 cells and OpRegen® RPE being the best options.

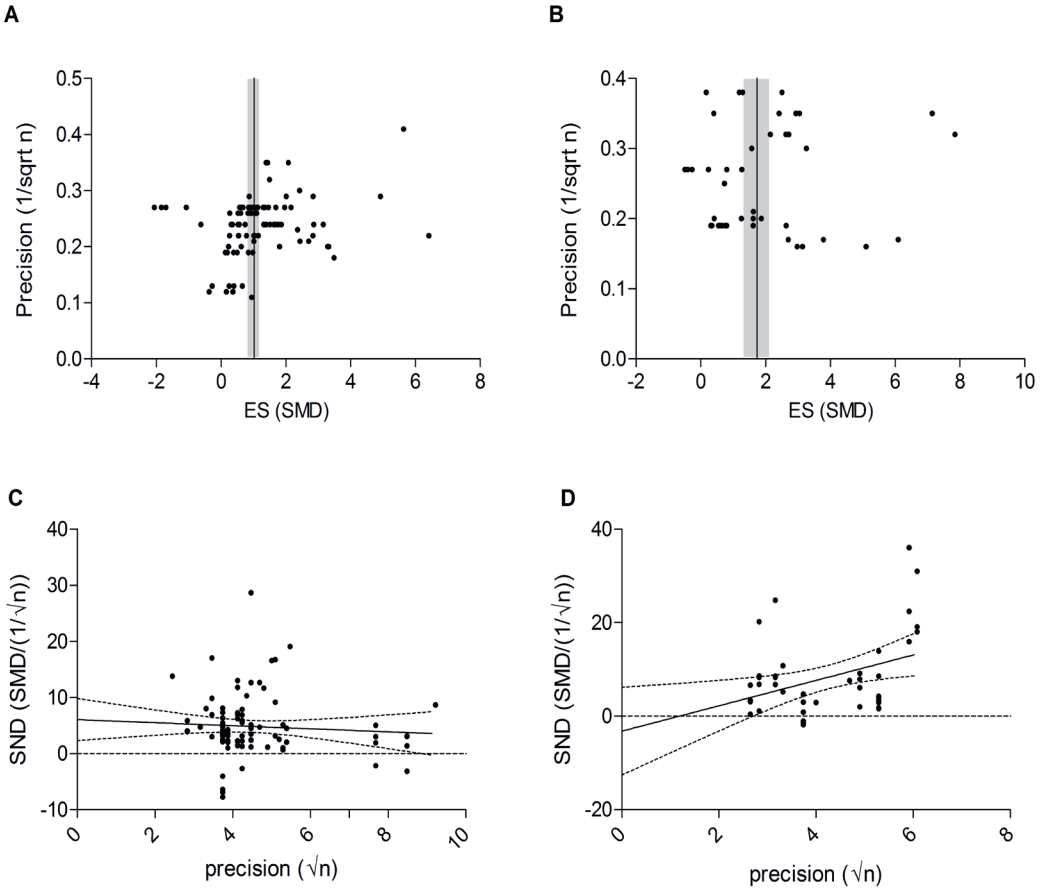

Figure 11. The funnel plots of studies which were included in the meta-analysis of (**A**) vision-based behavioral assays and (**B**) the b-wave amplitude. Publication bias was also assessed by Egger's regression test, which is based on plotting the standardized normalized difference (SND) on the y-axis and the precision (the square-root of the number of animals in an experimental group) on the x-axis in a funnel plot (**C**,**D**). Indication for publication bias was found for the vision-based behavioral studies (Egger's test, *p*-value = 0.003) and no indication for publication bias was found for the b-wave amplitude (Egger's test, *p*-value = 0.44).

Discussion

The first (autologous) RPE replacement studies in animal models were performed in the 1970s [65]. After primary failures, the transplantations of human RPE (hRPE) to the eyes of animal models showed some prevention of photoreceptor death, rescued visual function to some extent and had some protective effects. However, as a rule of the thumb, results were variable [62,66–68].

This systematic review and meta-analysis provide a quantitative summary of available preclinical *in vivo* evidence of the effect of RPE transplantations in animal models for retinal degeneration on the a-wave amplitude, the b-wave amplitude and vision-based behavioral assays. Our review shows a significant increase in these three outcomes after RPE transplantation. The high variation between studies can partially be explained by the age and sex of the animals which served as hosts, and additionally by the number of cells and origin of RPE which was transplanted into the subretinal space. The increase of the b-wave amplitude was significantly larger when both sexes were used, compared to males-only, and when young animals were used compared to adult animals. The effect on vision-based behavioral assays was significantly larger when adolescent animals were used compared to adult animals.

Moreover, the number of cells affects the intervention effect as well. A significantly larger effect on vision-based behavioral assays was found when more cells (in the range of 10^5 versus 10^4) was used and the cell type mattered as well; ARPE-19 and OpRegen® RPE seemed to be the better options. The other study characteristics which were selected for subgroup analysis upfront did not explain any proportions of heterogeneity significantly, or could not be analyzed due to insufficient data. It is also important to consider the fact that some of the subgroup effects differed between the two outcomes. We did find a general effect of age of the animal.

In both meta-analyses, a significantly larger effect was found for younger animals (young and adolescent) compared to adult animals. The other individual significant subgroup effects were not found in both meta-analyses. This could probably partly be explained by the fact of insufficient reporting of study characteristics. Moreover, insufficient reporting of study characteristics and the fact that most studies had an “unclear” risk of bias kept us from performing multiple subgroup analyses which might have explained some of the unexplained heterogeneity.

Methodological Limitations

Complete reporting of methodological details is essential to assess the risk of bias in original research articles and to determine the quality of the data. Reproducibility is very important in animal studies and variable results may be explained by differences in the methodology. However, insufficient reporting of methodology still occurs in the whole field of preclinical *in vivo* studies [65,66]. The risk of bias analysis within this systematic review revealed that details of most-importance regarding the study design are poorly reported, resulting in an "unclear" risk of bias for most (if not all) studies. Consequently, studies might have under- or overestimated their data which affects our meta-analysis [67].

Moreover, translational value to humans might be low because preclinical *in vivo* studies are generally not using sufficient animal numbers due to high costs [68,69]. Nonetheless, underpowered studies are included in this systematic review as well, because we wanted to give a full overview of the preclinical RPE transplantation field. Since none of the studies reported a power calculation or study protocol, the possibility cannot be excluded that the here presented meta-analyses suffer from an effect of such underpowering.

Analyses revealed moderate to severe levels of heterogeneity between studies. We used a random-effects model to account for this heterogeneity and used subgroup analyses to explore the causes. Exploring this heterogeneity is one of the added values of meta-analyses of animal studies and might help to inform the design of future animal studies and subsequent clinical trials. Some of our most important findings in this paper, the importance of animal age, the transplanted cell number and origin of RPE cells which are transplanted, are a consequence of the information we obtained from exploring the sources of heterogeneity. Some risk of publication bias was found for the vision-based assays. As a result, neutral and negative results could be underrepresented, and the translational value might be mediocre.

Delivery Methods: Cell Suspensions or Monolayers?

According to our meta-analysis, the delivery method for RPE cells is not straightforward. Frequently, cells are delivered by means of an injection into the eye, mostly in the subretinal space. Intravitreal injections are hardly used since the transplanted RPE cells have to pass the retinal layers to reach the host's RPE layer. Most recently it was postulated that RPE transplantation by means of a cell suspension injection might not be the most optimal procedure [69]. Dissociated cells that are injected into the subretinal space need to integrate into the host's RPE layer and form a strong and new functional epithelial layer. This might be too much to ask of these cells. Therefore, transplantation of a sheet of cells might be a better strategy [70].

This is a sheet of cells only or it is a combination of a carrier (artificial BM) with a monolayer of RPE cells. However, the use of an RPE monolayer comes with yet another complication: where an injection of a cell suspension is relatively simple, transplantation of a cell sheet (with or without a carrier) requires much more complex ocular surgery. Our meta-analyses revealed no significant difference of the effect of an RPE sheet versus an RPE suspension transplantation for both the b-wave amplitude (sheet n = 4 experimental groups, n = 3 studies; suspension n = 38 experimental groups, n = 12 studies) as the vision-based behavioral assays (sheet n = 11 experimental groups, n = 3 studies; suspension n = 85 experimental groups, n = 15 studies). However, we believe that we should take the limited amount of sheet transplantations compared to suspension transplantation into account when concluding anything on this matter.

Study Variables and Characteristics

Many factors contribute to cell survival following transplantation and improvement of the visual acuity of the patient. Normal RPE function is crucial for the maintenance of the outer blood-retinal barrier. In healthy eyes, the blood-retinal barrier provides an immune privilege and local tolerance to donor tissues. Nevertheless, non-matched cells are (eventually) rejected from the subretinal space over time unless systemic immune suppression is used [71]. Besides the delivery method, cell type, interventional timing, and site of graft placement are variables that could influence the outcomes of the trials. The clinical trials for cell-based therapies are in its infancy, so the extent of efficiency is unknown in humans. The main focus of these therapies is on the safety of the patients [19]. It is clear that current cell delivery systems need to be further improved and standardized.

RPE Cell Source and Immune Response

One important issue in transplantation is potential graft rejection. In summary, several different RPE cell sources have been used for transplantation purposes in animal models with variable success rates. These sources include autologous RPE, exogenic RPE, human donor RPE, cell lines such as ARPE-19 and RPE-J, stem cell-derived RPE (embryonic, induced pluripotent, adult), and progenitor cells. The first exogenous RPE transplantation study in animal models was performed by Li and Turner in 1988. They showed that healthy RPE cells from Long Evans rats can be grafted and can survive in the exogenous diseased retinal environment from the Royal College of Surgeons (RCS) rat [72,73]. However, human fetal RPE (hfRPE) cells transplanted into the eyes of rabbits resulted in inflammatory responses and rejected cells [74].

In more recent years, RPE cell lines, such as ARPE-19, and RPE cells, which were differentiated from stem cells, have been used for transplantation studies. These RPE lines yield, in principle, an unlimited transplantation source.

Our meta- and sub-group analysis showed that the cell type which is transplanted matters. The use of ARPE-19 and OpRegen® RPE cells resulted in a significantly increased effect compared to hESC-RPE and iPSC-RPE when looking at the outcomes of the vision-based behavioral assays. We should note here that ARPE-19 and OpRegen® RPE cells are a single cell type RPE source, whereas hESC-RPE and iPSC-RPE consist of more variable cell groups originating from multiple differentiation strategies [17,75,76]. Many recent papers state the advances in RPE differentiation protocols, however, there are still sources of variability. These sources include (stem) cell line, genetic background, passaging method, passage number, seeding density, and extracellular matrix [77,78]. This variability might explain the differences we find in our analysis between single cell types (ARPE-19 and OpRegen®) and more heterogeneous cell groups (hESC-RPE and iPSC-RPE).

Embryonic stem cell (ESC)-RPE cells or HLA-typed iPSCs can act as universal donors for large (sub-) populations since these cells are generally less immunogenic [79]. A number of safety studies showed that hESC-RPE cells could initiate an immune response in an AMD eye, possibly as an effect of the surgery or due to the diseased morphology [80]. Taken together, these data suggest that, despite the reputation of the eye as an immune-privileged site, non-autologous cells might be subject to graft rejection.
In humans, personalized or HLA-typed iPSC-RPE cells could overcome this problem fully since they are an autologous cell source. In animal models, the use of low immune suppression regimes is essential for the success of the experiment.

In our meta-analysis, we found that roughly only half of the studies included reported the use of immune suppression. Only a few studies reported not to use them, and roughly half the other studies did not report anything on the use of immune suppression. We could not perform subgroup analysis on the use of immune suppressions, because too little studies reported the use. Therefore, we cannot make a clear statement on this topic. We would, therefore, recommend reporting whether or not immune suppression is used.

Small Eyes, Big Eyes

In the smaller eyed animal models, such as mice and rats, subretinal injections are performed using glass pipettes or small (e.g. 33/34 GA) needles. Since a large part of the vitreous cavity is filled with the lens, only a little space is left to place needles and other instruments. Another difficulty is the exact visualization of the procedure through the pupil of the small eye. Therefore, the transplantation of RPE sheets with or without carriers is still a challenge in animals with small eyes, which is hard, but especially in rats not impossible, to overcome. In larger eyed animals, such as rabbits, pigs, and monkeys, the lens:vitreuscavity ratio is much smaller and more space is available to insert instruments. RPE sheets are usually placed using forceps or custom-made delivery tools [81–83]. Before placement of the graft, a complete vitrectomy is mostly performed, which is impossible in rodent eyes so far. Additionally, the transplantation site is enlarged by a subretinal injection using physiological salt. Vitreoretinal scissors are used to enable the implantation of the RPE sheet. Finally, multiple sclerotomies and retinotomies are required to perform a successful surgery. The surgery itself can be monitored using surgery microscopes with or without additional fundus visualization modules.

In general, the studies in which functionality of the retina and vision was analyzed in a quantitative manner all used small animal models, such as mice and rats. Larger animal species, such as rabbits and pigs, may be used to better resemble the eye morphology of humans and the surgical procedures that come with it. Both small and large animal models have their pros and cons. Experimental costs rise extensively when using larger animal models. In the future, data of smaller and larger animal species might be separately re-analyzed and re-examined.

Clinical Implications and Future Perspective

To our knowledge, this review is the first systematic overview of the effect of RPE transplantation in animal models for retinal degeneration. It provides useful insight into the methodology which is used worldwide in these preclinical *in vivo* studies. The unclear risk of bias is a reason to interpret the preclinical *in vivo* findings carefully. Overall, clinical trials are focusing on the safety and toxicology of RPE transplantations and consist still of too small groups to make clear statements about the efficacy (total number of enrolled patients 2–36, median = 12). Not all ongoing clinical trials are FDA approved (www.clinicaltrials.gov). We emphasize that there is an urgent need for improving the reporting and methodological quality of the conducted future animal experiments. Importantly, the effects of underpowering and publication bias should be avoided. Only on such a solid base, we can build designs of clinical trials which might be beneficial for patient groups.

Conclusions

This systematic review shows that RPE transplantation in animal models for retinal degeneration significantly increases a- and b- wave amplitudes and improves vision-related behavior. These effects appear to be more pronounced in young animals, when the number of transplanted cells is larger and when ARPE-19 and OpRegen® RPE cells are used.

Overall, this review clearly revealed that methodological details of animal experiments are often poorly reported. Although this is not unique to the ophthalmology field, it is worrying as a lack of reporting important methodological details will to some extent indicate neglected use of these methods to reduce bias, which can cause skewed results. This may seriously hamper drawing reliable conclusions from the included animal studies.

Supplementary Materials: please see Chapter 9: "Appendices".

Acknowledgments: we thank René Spijker and Alice Tillema for their help with setting up the search strategy. We thank Rob de Vries for his help during the whole process of the systematic review. Lastly, we thank Julia Menon and Darlyn Ranis for their help with the risk of bias analysis.

References

1. Sparrow, J.R.; Hicks, D.; Hamel, C.P. The retinal pigment epithelium in health and disease. *Curr. Mol. Med.* **2010**, *10*, 802–823.
2. Figueroa, A.G.; McKay, B.S. GPR143 Signaling and Retinal Degeneration. *Adv. Exp. Med. Biol.* **2019**, *1185*, 15–19.
3. Schatz, P.; Preising, M.; Lorenz, B.; Sander, B.; Larsen, M.; Rosenberg, T. Fundus albipunctatus associated with compound heterozygous mutations in RPE65. *Ophthalmology* **2011**, *118*, 888–894.
4. Talib, M.; van Schooneveld, M.J.; van Duuren, R.J.G.; Van Cauwenbergh, C.; Ten Brink, J.B.; De Baere, E.; Florijn, R.J.; Schalij-Delfos, N.E.; Leroy, B.P.; Bergen, A.A.; et al. Long-Term Follow-Up of Retinal Degenerations Associated with LRAT Mutations and Their Comparability to Phenotypes Associated with RPE65 Mutations. *Transl. Vis. Sci. Technol.* **2019**, *8*, 24.
5. Hussain, R.M.; Ciulla, T.A.; Berrocal, A.M.; Gregori, N.Z.; Flynn, H.W., Jr.; Lam, B.L. Stargardt macular dystrophy and evolving therapies. *Expert Opin. Biol. Ther.* **2018**, *18*, 1049–1059.
6. Tsang, S.H.; Aycinena, A.R.P.; Sharma, T. Inborn Errors of Metabolism: Gyrate Atrophy. *Adv. Exp. Med. Biol.* **2018**, *1085*, 183–185.
7. Guziewicz, K.E.; Sinha, D.; Gomez, N.M.; Zorych, K.; Dutrow, E.V.; Dhingra, A.; Mullins, R.F.; Stone, E.M.; Gamm, D.M.; Boesze-Battaglia, K.; et al. Bestrophinopathy: An RPE-photoreceptor interface disease. *Prog. Retin. Eye Res.* **2017**, *58*, 70–88.
8. Luo, M.; Chen, Y. Application of stem cell-derived retinal pigmented epithelium in retinal degenerative diseases: Present and future. *Int. J. Ophthalmol.* **2018**, *11*, 150–159.
9. Curcio, C.A.; Medeiros, N.E.; Millican, C.L. Photoreceptor loss in age-related macular degeneration. *Investig. Ophthalmol. Vis. Sci.* **1996**, *37*, 1236–1249.
10. Khanna, S.; Komati, R.; Eichenbaum, D.A.; Hariprasad, I.; Ciulla, T.A.; Hariprasad, S.M. Current and upcoming anti-VEGF therapies and dosing strategies for the treatment of neovascular AMD: A comparative review. *BMJ Open Ophthalmol.* **2019**, *4*, e000398.
11. Bergen, A.A.; Arya, S.; Koster, C.; Pilgrim, M.G.; Wiatrek-Moumoulidis, D.; van der Spek, P.J.; Hauck, S.M.; Boon, C.J.F.; Emri, E.; Stewart, A.J.; et al. On the origin of proteins in human drusen: The meet, greet and stick hypothesis. *Prog. Retin. Eye Res.* **2019**, *70*, 55–84.
12. Cheung, G.C.M.; Lai, T.Y.Y.; Gomi, F.; Ruamviboonsuk, P.; Koh, A.; Lee, W.K. Anti-VEGF Therapy for Neovascular AMD and Polypoidal Choroidal Vasculopathy. *Asia Pac. J. Ophthalmol.* **2017**, *6*, 527–534.
13. Dang, Y.; Zhang, C.; Zhu, Y. Stem cell therapies for age-related macular degeneration: The past, present, and future. *Clin. Interv. Aging* **2015**, *10*, 255–264.
14. van Meurs, J.C.; Van Den Biesen, P.R. Autologous retinal pigment epithelium and choroid translocation in patients with exudative age-related macular degeneration: Short-term follow-up. *Am. J. Ophthalmol.* **2003**, *136*, 688–695.
15. van Meurs, J.C.; Kirchhof, B.; MacLaren, R.E. Retinal Pigment Epithelium and Choroid Translocation in Patients with Age-Related Macular Degeneration. In *Ryan's Retina*, 6th ed.; Schachat, A., Ed.; Elsevier: Edinburgh, UK, 2018; pp. 2254–2265.

16. van Meurs, J.C.; ter Averst, E.; Hofland, L.J.; van Hagen, P.M.; Mooy, C.M.; Baarsma, G.S.; Kuijpers, R.W.; Boks, T.; Stalmans, P. Autologous peripheral retinal pigment epithelium translocation in patients with subfoveal neovascular membranes. *Br. J. Ophthalmol.* **2004**, *88*, 110–113.
17. Lee, E.; MacLaren, R.E. Sources of retinal pigment epithelium (RPE) for replacement therapy. *Br. J. Ophthalmol.* **2011**, *95*, 445–449.
18. Pauleikhoff, D.; Harper, C.A.; Marshall, J.; Bird, A.C. Aging changes in Bruch's membrane. A histochemical and morphologic study. *Ophthalmology* **1990**, *97*, 171–178.
19. Jones, M.K.; Lu, B.; Girman, S.; Wang, S. Cell-based therapeutic strategies for replacement and preservation in retinal degenerative diseases. *Prog. Retin. Eye Res.* **2017**, *58*, 1–27.
20. Shah, M.; Cabrera-Ghayouri, S.; Christie, L.A.; Held, K.S.; Viswanath, V. Translational Preclinical Pharmacologic Disease Models for Ophthalmic Drug Development. *Pharm. Res.* **2019**, *36*, 58.
21. Petrus-Reurer, S.; Bartuma, H.; Aronsson, M.; Westman, S.; Lanner, F.; Kvanta, A. Subretinal Transplantation of Human Embryonic Stem Cell Derived-retinal Pigment Epithelial Cells into a Large-eyed Model of Geographic Atrophy. *JoVE* **2018**, *131*, e56702.
22. Booij, J.C.; Baas, D.C.; Beisekeeva, J.; Gorgels, T.G.; Bergen, A.A. The dynamic nature of Bruch's membrane. *Prog. Retin. Eye Res.* **2010**, *29*, 1–18.
23. Arya, M.; Sabrosa, A.S.; Duker, J.S.; Waheed, N.K. Choriocapillaris changes in dry age-related macular degeneration and geographic atrophy: A review. *Eye Vis.* **2018**, *5*, 22.
24. Girman, S.V.; Wang, S.; Lund, R.D. Cortical visual functions can be preserved by subretinal RPE cell grafting in RCS rats. *Vis. Res.* **2003**, *43*, 1817–1827.
25. Abe, T.; Wakusawa, R.; Seto, H.; Asai, N.; Saito, T.; Nishida, K. Topical doxycycline can induce expression of BDNF in transduced retinal pigment epithelial cells transplanted into the subretinal space. *Investig. Ophthalmol. Vis. Sci.* **2008**, *49*, 3631–3639.
26. Carr, A.J.; Vugler, A.A.; Hikita, S.T.; Lawrence, J.M.; Gias, C.; Chen, L.L.; Buchholz, D.E.; Ahmado, A.; Semo, M.; Smart, M.J.; et al. Protective effects of human iPS-derived retinal pigment epithelium cell transplantation in the retinal dystrophic rat. *PLoS ONE* **2009**, *4*, e8152.
27. Coffey, P.J.; Girman, S.; Wang, S.M.; Hetherington, L.; Keegan, D.J.; Adamson, P.; Greenwood, J.; Lund, R.D. Long-term preservation of cortically dependent visual function in RCS rats by transplantation. *Nat. Neurosci.* **2002**, *5*, 53–56.
28. Davis, R.J.; Alam, N.M.; Zhao, C.; Muller, C.; Saini, J.S.; Blenkinsop, T.A.; Mazzoni, F.; Campbell, M.; Borden, S.M.; Charniga, C.J.; et al. The Developmental Stage of Adult Human Stem Cell-Derived Retinal Pigment Epithelium Cells Influences Transplant Efficacy for Vision Rescue. *Stem Cell Rep.* **2017**, *9*, 42–49.
29. Duan, P.; Zeng, Y.; Liu, Y.; Wang, Y.; Xu, H.; Yin, Z. Comparison of protective effects of hESCs-derived and hBMSCs-derived RPE cells on sodium iodate-injuried rat retina. *Int. J. Clin. Exp. Pathol.* **2017**, *10*, 5274–5284.
30. Gouras, P.; Kong, J.; Tsang, S.H. Retinal degeneration and RPE transplantation in Rpe65(-/-) mice. *Investig. Ophthalmol. Vis. Sci.* **2002**, *43*, 3307–3311.
31. Haruta, M.; Sasai, Y.; Kawasaki, H.; Amemiya, K.; Ooto, S.; Kitada, M.; Suemori, H.; Nakatsuji, N.; Ide, C.; Honda, Y.; et al. In vitro and in vivo characterization of pigment epithelial cells differentiated from primate embryonic stem cells. *Investig. Ophthalmol. Vis. Sci.* **2004**, *45*, 1020–1025.

32. Idelson, M.; Alper, R.; Obolensky, A.; Yachimovich-Cohen, N.; Rachmilewitz, J.; Ejzenberg, A.; Beider, E.; Banin, E.; Reubinoff, B. Immunological Properties of Human Embryonic Stem Cell-Derived Retinal Pigment Epithelial Cells. *Stem Cell Rep.* **2018**, *11*, 681–695.
33. Kamao, H.; Mandai, M.; Okamoto, S.; Sakai, N.; Suga, A.; Sugita, S.; Kiryu, J.; Takahashi, M. Characterization of human induced pluripotent stem cell-derived retinal pigment epithelium cell sheets aiming for clinical application. *Stem Cell Rep.* **2014**, *2*, 205–218.
34. Klassen, H.; Whiteley, S.J.; Young, M.J.; Lund, R.D. Graft location affects functional rescue following RPE cell transplantation in the RCS rat. *Exp. Neurol.* **2001**, *169*, 114–121.
35. Kole, C.; Klipfel, L.; Yang, Y.; Ferracane, V.; Blond, F.; Reichman, S.; Millet-Puel, G.; Clerin, E.; Ait-Ali, N.; Pagan, D.; et al. Otx2-Genetically Modified Retinal Pigment Epithelial Cells Rescue Photoreceptors after Transplantation. *Mol. Ther.* **2018**, *26*, 219–237.
36. Little, C.W.; Cox, C.; Wyatt, J.; del Cerro, C.; del Cerro, M. Correlates of photoreceptor rescue by transplantation of human fetal RPE in the RCS rat. *Exp. Neurol.* **1998**, *149*, 151–160.
37. Lu, B.; Malcuit, C.; Wang, S.; Girman, S.; Francis, P.; Lemieux, L.; Lanza, R.; Lund, R. Long-term safety and function of RPE from human embryonic stem cells in preclinical models of macular degeneration. *Stem Cells* **2009**, *27*, 2126–2135.
38. Lund, R.D.; Adamson, P.; Sauve, Y.; Keegan, D.J.; Girman, S.V.; Wang, S.; Winton, H.; Kanuga, N.; Kwan, A.S.; Beauchene, L.; et al. Subretinal transplantation of genetically modified human cell lines attenuates loss of visual function in dystrophic rats. *Proc. Natl. Acad. Sci. USA* **2001**, *98*, 9942–9947.
39. Lund, R.D.; Wang, S.; Klimanskaya, I.; Holmes, T.; Ramos-Kelsey, R.; Lu, B.; Girman, S.; Bischoff, N.; Sauve, Y.; Lanza, R. Human embryonic stem cell-derived cells rescue visual function in dystrophic RCS rats. *Cloning Stem Cells* **2006**, *8*, 189–199.
40. Maeda, T.; Lee, M.J.; Palczewska, G.; Marsili, S.; Tesar, P.J.; Palczewski, K.; Takahashi, M.; Maeda, A. Retinal pigmented epithelial cells obtained from human induced pluripotent stem cells possess functional visual cycle enzymes in vitro and in vivo. *J. Biol. Chem.* **2013**, *288*, 34484–34493.
41. Ben M'Barek, K.; Habeler, W.; Plancheron, A.; Jarraya, M.; Regent, F.; Terray, A.; Yang, Y.; Chatrousse, L.; Domingues, S.; Masson, Y.; et al. Human ESC-derived retinal epithelial cell sheets potentiate rescue of photoreceptor cell loss in rats with retinal degeneration. *Sci. Transl. Med.* **2017**, *9*, eaai7471.
42. McGill, T.J.; Lund, R.D.; Douglas, R.M.; Wang, S.; Lu, B.; Prusky, G.T. Preservation of vision following cell-based therapies in a model of retinal degenerative disease. *Vis. Res.* **2004**, *44*, 2559–2566.
43. McGill, T.J.; Bohana-Kashtan, O.; Stoddard, J.W.; Andrews, M.D.; Pandit, N.; Rosenberg-Belmaker, L.R.; Wiser, O.; Matzrafi, L.; Banin, E.; Reubinoff, B.; et al. Long-Term Efficacy of GMP Grade Xeno-Free hESC-Derived RPE Cells Following Transplantation. *Transl. Vis. Sci. Technol.* **2017**, *6*, 17.
44. Sauve, Y.; Lu, B.; Lund, R.D. The relationship between full field electroretinogram and perimetry-like visual thresholds in RCS rats during photoreceptor degeneration and rescue by cell transplants. *Vis. Res.* **2004**, *44*, 9–18.
45. Sauve, Y.; Pinilla, I.; Lund, R.D. Partial preservation of rod and cone ERG function following subretinal injection of ARPE-19 cells in RCS rats. *Vis. Res.* **2006**, *46*, 1459–1472.

46. Sharma, R.; Khristov, V.; Rising, A.; Jha, B.S.; Dejene, R.; Hotaling, N.; Li, Y.; Stoddard, J.; Stankewicz, C.; Wan, Q.; et al. Clinical-grade stem cell-derived retinal pigment epithelium patch rescues retinal degeneration in rodents and pigs. *Sci. Transl. Med.* **2019**, *11*, eaat5580.
47. Thomas, B.B.; Zhu, D.; Zhang, L.; Thomas, P.B.; Hu, Y.; Nazari, H.; Stefanini, F.; Falabella, P.; Clegg, D.O.; Hinton, D.R.; et al. Survival and Functionality of hESC-Derived Retinal Pigment Epithelium Cells Cultured as a Monolayer on Polymer Substrates Transplanted in RCS Rats. *Investig. Ophthalmol. Vis. Sci.* **2016**, *57*, 2877–2887.
48. Wang, S.; Lu, B.; Girman, S.; Holmes, T.; Bischoff, N.; Lund, R.D. Morphological and functional rescue in RCS rats after RPE cell line transplantation at a later stage of degeneration. *Investig. Ophthalmol. Vis. Sci.* **2008**, *49*, 416–421.
49. Wu, W.; Zeng, Y.; Li, Z.; Li, Q.; Xu, H.; Yin, Z.Q. Features specific to retinal pigment epithelium cells derived from three-dimensional human embryonic stem cell cultures—A new donor for cell therapy. *Oncotarget* **2016**, *7*, 22819–22833.
50. Hooijmans, C.R.; Rovers, M.M.; de Vries, R.B.; Leenaars, M.; Ritskes-Hoitinga, M.; Langendam, M.W. Syrcle's risk of bias tool for animal studies. *BMC Med. Res. Methodol.* **2014**, *14*, 43.
51. Hooijmans, C.R.; Tillema, A.; Leenaars, M.; Ritskes-Hoitinga, M. Enhancing search efficiency by means of a search filter for finding all studies on animal experimentation in PubMed. *Lab. Anim.* **2010**, *44*, 170–175.
52. Garcia Delgado, A.B.; De La Cerda, B.; Alba Amador, J.; Valdes Sanchez, M.L.; Fernandez-Munoz, B.; Relimpio Lopez, I.; Rodriguez De La Rua, E.; Diez Lloret, A.; Calado, S.M.; Sanchez Pernaute, R.; et al. Subretinal Transplant of Induced Pluripotent Stem Cell-Derived Retinal Pigment Epithelium on Nanostructured Fibrin-Agarose. *Tissue Eng. Part A* **2019**, *25*, 799–808.
53. Thomas, B.B.; Zhu, D.; Lin, T.C.; Kim, Y.C.; Seiler, M.J.; Martinez-Camarillo, J.C.; Lin, B.; Shad, Y.; Hinton, D.R.; Humayun, M.S. A new immunodeficient retinal dystrophic rat model for transplantation studies using human-derived cells. G*raefe's Arch. Clin. Exp. Ophthalmol.* **2018**, *56*, 2113–2125.
54. Wu, H.; Li, J.; Mao, X.; Li, G.; Xie, L.; You, Z. Transplantation of rat embryonic stem cell-derived retinal cells restores visual function in the Royal College of Surgeons rats. *Doc. Ophthalmol.* **2018**, *137*, 71–78.
55. Bhatt, N.S.; Newsome, D.A.; Fenech, T.; Hessburg, T.P.; Diamond, J.G.; Miceli, M.V.; Kratz, K.E.; Oliver, P.D. Experimental transplantation of human retinal pigment epithelial cells on collagen substrates. *Am. J. Ophthalmol.* **1994**, *117*, 214–221.
56. Carido, M.; Zhu, Y.; Postel, K.; Benkner, B.; Cimalla, P.; Karl, M.O.; Kurth, T.; Paquet-Durand, F.; Koch, E.; Munch, T.A.; et al. Characterization of a mouse model with complete RPE loss and its use for RPE cell transplantation. *Investig. Ophthalmol. Vis. Sci.* **2014**, *55*, 5431–5444.
57. Engelhardt, M.; Tosha, C.; Lopes, V.S.; Chen, B.; Nguyen, L.; Nusinowitz, S.; Williams, D.S. Functional and morphological analysis of the subretinal injection of retinal pigment epithelium cells. *Vis. Neurosci.* **2012**, *29*, 83–93.

58. Ilmarinen, T.; Hiidenmaa, H.; Koobi, P.; Nymark, S.; Sorkio, A.; Wang, J.H.; Stanzel, B.V.; Thieltges, F.; Alajuuma, P.; Oksala, O.; et al. Ultrathin Polyimide Membrane as Cell Carrier for Subretinal Transplantation of Human Embryonic Stem Cell Derived Retinal Pigment Epithelium. *PLoS ONE* **2015**, *10*, e0143669.
59. Jiang, L.Q.; Hamasaki, D. Corneal electroretinographic function rescued by normal retinal pigment epithelial grafts in retinal degenerative Royal College of Surgeons rats. I*nvestig. Ophthalmol. Vis. Sci.* **1994**, *35*, 4300–4309.
60. Li, Y.; Tsai, Y.T.; Hsu, C.W.; Erol, D.; Yang, J.; Wu, W.H.; Davis, R.J.; Egli, D.; Tsang, S.H. Long-term safety and efficacy of human-induced pluripotent stem cell (iPS) grafts in a preclinical model of retinitis pigmentosa. *Mol. Med.* **2012**, *18*, 1312–1319.
61. Peng, C.H.; Chuang, J.H.; Wang, M.L.; Jhan, Y.Y.; Chien, K.H.; Chung, Y.C.; Hung, K.H.; Chang, C.C.; Lee, C.K.; Tseng, W.L.; et al. Laminin modification subretinal bio-scaffold remodels retinal pigment epithelium-driven microenvironment in vitro and in vivo. *Oncotarget* **2016**, *7*, 64631–64648.
62. Pinilla, I.; Cuenca, N.; Sauve, Y.; Wang, S.; Lund, R.D. Preservation of outer retina and its synaptic connectivity following subretinal injections of human RPE cells in the Royal College of Surgeons rat. *Exp. Eye Res.* **2007**, *85*, 381–392.
63. Wang, N.K.; Tosi, J.; Kasanuki, J.M.; Chou, C.L.; Kong, J.; Parmalee, N.; Wert, K.J.; Allikmets, R.; Lai, C.C.; Chien, C.L.; et al. Transplantation of reprogrammed embryonic stem cells improves visual function in a mouse model for retinitis pigmentosa. *Transplantation* **2010**, *89*, 911–919.
64. Yamamoto, S.; Du, J.; Gouras, P.; Kjeldbye, H. Retinal pigment epithelial transplants and retinal function in RCS rats. *Investig. Ophthalmol. Vis. Sci.* **1993**, *34*, 3068–3075.
65. Muller-Jensen, K.; Mandelcorn, M.S. Membrane formation by autotransplanted retinal pigment epithelium (RPE). *Mod. Probl. Ophthalmol.* **1975**, *15*, 228–234.
66. Little, C.W.; Castillo, B.; DiLoreto, D.A.; Cox, C.; Wyatt, J.; del Cerro, C.; del Cerro, M. Transplantation of human fetal retinal pigment epithelium rescues photoreceptor cells from degeneration in the Royal College of Surgeons rat retina. *Investig. Ophthalmol. Vis. Sci.* **1996**, *37*, 204–211.
67. Wang, S.; Girman, S.; Lu, B.; Bischoff, N.; Holmes, T.; Shearer, R.; Wright, L.S.; Svendsen, C.N.; Gamm, D.M.; Lund, R.D. Long-term vision rescue by human neural progenitors in a rat model of photoreceptor degeneration. *Investig. Ophthalmol. Vis. Sci.* **2008**, *49*, 3201–3206.
68. Phillips, S.J.; Sadda, S.R.; Tso, M.O.; Humayan, M.S.; de Juan, E., Jr.; Binder, S. Autologous transplantation of retinal pigment epithelium after mechanical debridement of Bruch's membrane. *Curr. Eye Res.* **2003**, *26*, 81–88.
69. Stanzel, B.; Ader, M.; Liu, Z.; Amaral, J.; Aguirre, L.I.R.; Rickmann, A.; Barathi, V.A.; Tan, G.S.W.; Degreif, A.; Al-Nawaiseh, S.; et al. Surgical Approaches for Cell Therapeutics Delivery to the Retinal Pigment Epithelium and Retina. *Adv. Exp. Med. Biol.* **2019**, *1186*, 141–170.
70. Binder, S.; Stanzel, B.V.; Krebs, I.; Glittenberg, C. Transplantation of the RPE in AMD. *Prog. Retin. Eye Res.* **2007**, *26*, 516–554.
71. Enzmann, V.; Faude, F.; Wiedemann, P.; Kohen, L. Immunological problems of transplantation into the subretinal space. *Cells Tissues Organs* **1998**, *162*, 178–183.
72. Li, L.X.; Turner, J.E. Inherited retinal dystrophy in the RCS rat: Prevention of photoreceptor degeneration by pigment epithelial cell transplantation. *Exp. Eye Res.* **1988**, *47*, 911–917.

73. Li, L.; Turner, J.E. Optimal conditions for long-term photoreceptor cell rescue in RCS rats: The necessity for healthy RPE transplants. *Exp. Eye Res.* **1991**, *52*, 669–679.
74. Gabrielian, K.; Oganesian, A.; Patel, S.C.; Verp, M.S.; Ernest, J.T. Cellular response in rabbit eyes after human fetal RPE cell transplantation. *Graefe's Arch. Clin. Exp. Ophthalmol.* **1999**, *237*, 326–335.
75. Tang, Z.; Zhang, Y.; Wang, Y.; Zhang, D.; Shen, B.; Luo, M.; Gu, P. Progress of stem/progenitor cell-based therapy for retinal degeneration. *J. Transl. Med.* **2017**, *15*, 99.
76. M'Barek, K.B.; Habeler, W.; Monville, C. Stem Cell-Based RPE Therapy for Retinal Diseases: Engineering 3D Tissues Amenable for Regenerative Medicine. *Adv. Exp. Med. Biol.* **2018**, *1074*, 625–632.
77. Weed, L.S.; Mills, J.A. Strategies for retinal cell generation from human pluripotent stem cells. *Stem Cell Investig.* **2017**, *4*, 65.
78. Lane, A.; Philip, L.R.; Ruban, L.; Fynes, K.; Smart, M.; Carr, A.; Mason, C.; Coffey, P. Engineering efficient retinal pigment epithelium differentiation from human pluripotent stem cells. *Stem Cells Transl. Med.* **2014**, *3*, 1295–1304.
79. Drukker, M.; Katchman, H.; Katz, G.; Even-Tov Friedman, S.; Shezen, E.; Hornstein, E.; Mandelboim, O.; Reisner, Y.; Benvenisty, N. Human embryonic stem cells and their differentiated derivatives are less susceptible to immune rejection than adult cells. *Stem Cells* **2006**, *24*, 221–229.
80. Nazari, H.; Zhang, L.; Zhu, D.; Chader, G.J.; Falabella, P.; Stefanini, F.; Rowland, T.; Clegg, D.O.; Kashani, A.H.; Hinton, D.R.; et al. Stem cell based therapies for age-related macular degeneration: The promises and the challenges. *Prog. Retin. Eye Res.* **2015**, *48*, 1–39.
81. Koss, M.J.; Falabella, P.; Stefanini, F.R.; Pfister, M.; Thomas, B.B.; Kashani, A.H.; Brant, R.; Zhu, D.; Clegg, D.O.; Hinton, D.R.; et al. Subretinal implantation of a monolayer of human embryonic stem cell-derived retinal pigment epithelium: A feasibility and safety study in Yucatan minipigs. *Graefe's Arch. Clin. Exp. Ophthalmol.* **2016**, *254*, 1553–1565.
82. Stanzel, B.V.; Liu, Z.; Brinken, R.; Braun, N.; Holz, F.G.; Eter, N. Subretinal delivery of ultrathin rigid-elastic cell carriers using a metallic shooter instrument and biodegradable hydrogel encapsulation. *Investig. Ophthalmol. Vis. Sci.* **2012**, *53*, 490–500.
83. Sohn, E.H.; Jiao, C.; Kaalberg, E.; Cranston, C.; Mullins, R.F.; Stone, E.M.; Tucker, B.A. Allogenic iPSC-derived RPE cell transplants induce immune response in pigs: A pilot study. *Sci. Rep.* **2015**, *5*, 11791.
84. Moher, D.; Liberati, A.; Tetzlaff, J.; Altman, D.G.; The, P.G. Preferred Reporting Items for Systematic Reviews and Meta-Analyses: The PRISMA Statement. *PLoS Med.* **2009**, *6*, e1000097.
85. de Vries, R.B.; Hooijmans, C.R.; Tillema, A.; Leenaars, M.; Ritskes-Hoitinga, M. Updated version of the Embase search filter for animal studies. *Lab. Anim.* **2014**, *48,* 88.
86. Zwetsloot, P.P.; Van Der Naald, M.; Sena, E.S.; Howells, D.W.; IntHout, J.; De Groot, J.A.; Chamuleau, S.A.; MacLeod, M.R.; Wever, K.E. Standardized mean differences cause funnel plot distortion in publication bias assessments. *Elife* **2017**, *6*, e24260.

I'd rather dream large and fail than shoot for mediocre and never discover my limits.

— Diana Nyad

The Lrat$^{-/-}$ Rat: CRISPR/Cas9 Construction and Phenotyping of a New Animal Model for Retinitis Pigmentosa

Céline Koster, Koen T. van den Hurk, Colby F. Lewallen, Mays Talib, Jacoline B. ten Brink, Camiel J. F. Boon & Arthur A. Bergen

Int. J. Mol. Sci. **2021**, accepted for publication, DOI: 10.3390/ijms22137234

3

Abstract

Purpose: we developed and phenotyped a pigmented knockout rat model for lecithin retinol acyltransferase (LRAT) using CRISPR/Cas9. The introduced mutation (c.12delA) is based on a patient group harboring a homologous homozygous frameshift mutation in the *LRAT* gene (c.12delC), causing a dysfunctional visual (retinoid) cycle.

Methods: the introduced mutation was confirmed by DNA and RNA sequencing. The expression of *Lrat* was determined on both the RNA and protein level in wildtype and knockout animals using RT-PCR and immunohistochemistry. The retinal structure and function, as well as the visual behavior of the $Lrat^{-/-}$ and control rats, were characterized using scanning laser ophthalmoscopy (SLO), optical coherence tomography (OCT), electroretinography (ERG) and vision-based behavioral assays. Results: wildtype animals had high *Lrat* mRNA expression in multiple tissues, including the eye and liver. In contrast, hardly any expression was detected in $Lrat^{-/-}$ animals. LRAT protein was abundantly present in wildtype animals and absent in $Lrat^{-/-}$ animals. $Lrat^{-/-}$ animals showed progressively reduced ERG potentials compared to wildtype controls from two weeks of age onwards. Vison-based behavioral assays confirmed reduced vision. Structural abnormalities, such as overall retinal thinning, were observed in $Lrat^{-/-}$ animals. The retinal thickness in knockout rats was decreased to roughly 80 % by four months of age. No functional or structural differences were observed between wildtype and heterozygote animals.

Conclusions: our $Lrat^{-/-}$ rat is a new animal model for retinal dystrophy, especially for the *LRAT*-subtype of early-onset retinal dystrophies. This model has advantages over the existing mouse models and the RCS rat strain and can be used for translational studies of retinal dystrophies.

Introduction

Retinitis pigmentosa (RP), Leber congenital amaurosis (LCA), and retinitis punctata albescens (RPA) are severe early-onset retinal dystrophies that cause visual impairment, nystagmus, progressive nyctalopia, and finally, blindness. This heterogeneous retinal dystrophy disease group is characterized by damage to the retinal pigment epithelium (RPE)–photoreceptor (PR) complex. This results usually in progressive dysfunction of the rod photoreceptor cells, often followed by progressive cone degeneration. RP, LCA, and RPA are caused by mutations in virtually all genes encoding proteins acting in the retinoid cycle [1–4]. Indeed, for normal vision, a functionally valid retinoid cycle is essential: in the healthy situation, vitamin A (retinol) is the primary substrate for several functional retinoids' biosynthesis in the retinoid cycle. Then, the vitamin A-derivatives are shuttled from the RPE to the PRs. There, opsins are light-activated and the visual pigments transform the light energy in a cellular signal, initiating the visual cascade and resulting in a physiological response in the PR cell. After light activation, the cycle regenerates the visual pigments that are used after light activation of rhodopsin (see Figure 1). Upon photoactivation, a configurational change of the visual pigment 11-*cis*-retinal to all-*trans*-retinal is induced in the PR cells' outer segments. Subsequently, all-*trans*-retinal is reduced to all-*trans*-retinol and diffuses from the PRs back to to the RPE cells.

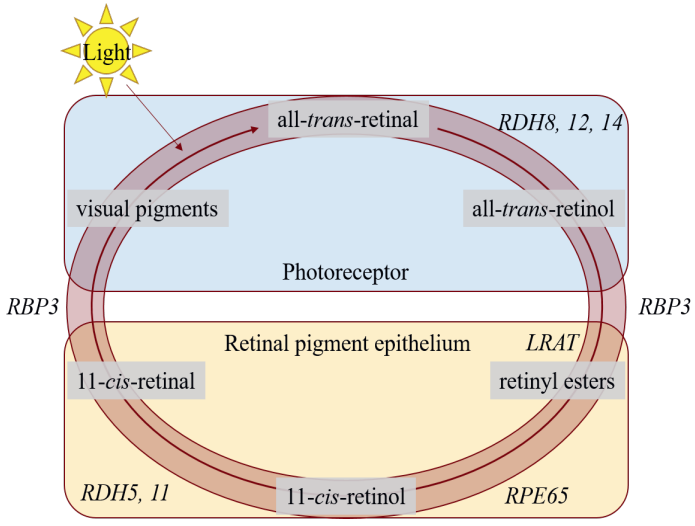

Figure 1. A schematic overview of the visual cycle in the photoreceptors (PRs) and the retinal pigment epithelium (RPE). In the PRs, 11-*cis*-retinal couples to an opsin protein, forming rhodopsin. Upon activation by photons, 11-*cis*-retinal is isomerized to all-*trans*-retinal. The retinol dehydrogenases (encoded by *RDH8*, *RDH12*, *RDH14*) reduce all-*trans*-retinal to all-*trans*-retinol, and this metabolite is moved to the RPE by retinoid-binding protein (encoded by *RBP3*). In the RPE, it is esterified by lecithin:retinol acyltransferase (encoded by *LRAT*), after which it is converted to 11-*cis*-retinol by retinal pigment epithelium-specific 65 kDa protein (encoded by *RPE65*). Retinol dehydrogenases (encoded by *RDH5* and *RDH11*) convert 11-*cis*-retinol to 11-*cis*-retinal, and retinoid-binding protein moves it back to the PR. For further explanation, see the text.

In the RPE, all-*trans*-retinol is esterified to all-*trans*-retinyl-ester by the enzyme lecithin:retinol acetyltransferase (LRAT), after which all-*trans*-retinyl-ester is subsequently the substrate for the enzyme retinal pigment epithelium-specific protein 65 kDa (RPE65). RPE65 converts all-*trans*-retinyl-ester to 11-*cis*-retinol, after which 11-*cis*-retinol is oxidized by retinol dehydrogenase (RDH) enzymes to 11-*cis*-retinal. Finally, to complete the cycle, 11-*cis*-retinal is shuttled back to the PRs, where it can be used for a new round of phototransduction.

Thus, LRAT as well as RPE65 are essential for the regeneration of functional visual pigment in the part of the retinoid cycle that takes place in the RPE. A defect in either enzyme leads to an impaired retinoid cycle [5,6]. Indeed, mutations in the *RPE65* gene have been implicated in 6–8 % of all LCA cases and up to 5 % of childhood-onset RP [2,7]. *RPE65*-associated retinal disorders are the first for which human gene therapy has become available [8,9], with many other retinal dystrophies, including *LRAT*-associated retinal disorders, to follow [10]. Mutations in the *LRAT* gene are rare and cause LCA, childhood-onset RP, and RPA-/fundus albipunctatus-like phenotypes in <1 % [2,3,7,11–13] (Figure 2). Interestingly, considerable phenotypic variability has been described in association with *LRAT* mutations [13].

The rat *Lrat* gene was characterized in 1999 by Ruiz and colleagues [14]. They described that the *Lrat* gene is highly expressed in several tissues, including the RPE in the eye, liver, heart, lung, skeletal muscle, skin, mammary tissue, testis, intestine, adrenal gland, and pancreas [14,15]. Multiple transcripts in a size range of 1.5–5 kb were identified in various human tissues, rodent tissues and cell lines. However, the translated protein from both the long and shorter transcripts contains 230 amino acids and is 25.8 kDa in size [14–17]. This demonstrates that the long 3'UTR after the ORF in the long transcripts did not affect the translation [17]. The widespread expression suggests a role for LRAT in several biological processes in multiple organs. However, patients with *LRAT* mutations only have retinal dystrophy and do not have other obvious pathogenic systemic abnormalities. The reason for this is not clear, but it suggests that the regulation of *LRAT* mRNA expression is complex and yet to be fully elucidated.

The c.12delC (NM_004744.4) mutation in the *LRAT* gene segregated perfectly in families with RPA, as shown by Littink and colleagues [4]. The mutation causes a frameshift and a premature stop codon 53 amino acids downstream (p.M5CfsX53), theoretically resulting in a truncated protein. These patients suffer from nyctalopia, decreased non-recordable scotopic electroretinography (ERG) measurements, and an overall decrease in visual sensitivity and acuity. Talib and colleagues examined patients with this homozygous mutation in the *LRAT* gene in a long-term follow-up study. Although the disease's progression was variable and slow, the follow-up showed that complete blindness was generally reached between 50 and 60 years of age [13]. The first symptoms started to show within the first decade of life in all patients, with nyctalopia being usually the first symptom within the first year of life. The clinical course of *LRAT*-associated phenotypes appears similar to the clinical course in patients with *RPE65* mutations [13].

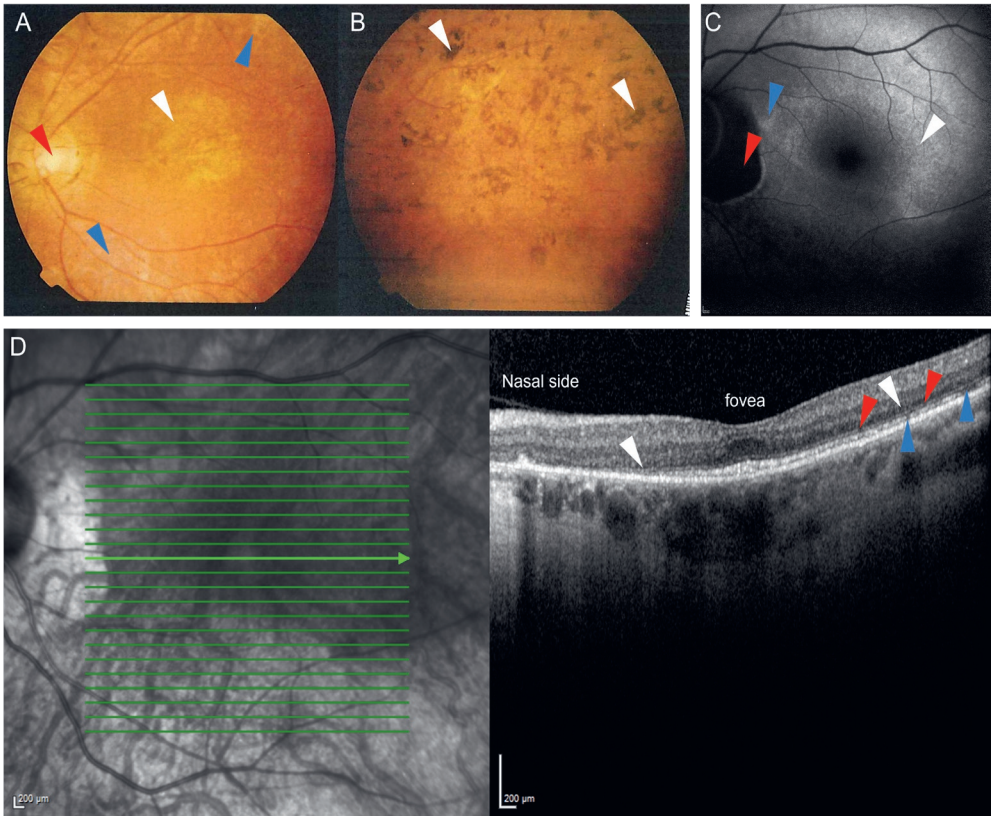

Figure 2. Representative fundus photographs (**A,B**), fundus autofluorescence image (**C**) and an optical coherence tomography (OCT) scan (**D**) of patients carrying the c.12delC mutation in LRAT suffering from LRAT-associated retinal dystrophy. Fundus photograph of the central (**A**) and peripheral area (**B**) of the left eye of a 39-year old patient. (**A**): atrophic alterations of the retinal pigment epithelium in the macula (white arrow) and around the vascular arcades (blue arrows), along with retinal atrophy around the optic disc, which shows some temporal pallor (red arrow) are visible. The vessels are attenuated. (**B**): the peripheral retina showed retinal atrophy and bone-spicule-like hyperpigmentation. (**C**): fundus autofluorescence image of a 57-year old patient, showing a subtle hyperautofluorescent ring around a relatively preserved central macula (white arrow) and a juxtapapillary patch of absent autofluorescence (red arrow), sharply outlined by a hyperautofluorescent border. The inferior posterior pole shows granular hypo-autofluorescence (blue arrow), indicating more atrophy of the retinal pigment epithelium in the area outside of the hyperautofluorescent ring. (**D**): spectral-domain OCT (SD-OCT) scan of a 57-year old patient, showing relative preservation of the outer nuclear layers, the external limiting membrane, and the ellipsoid zone at the level of the fovea. In the parafovea and perifovea, thinning of the outer nuclear layer is seen (white arrows), along with interruptions of the external limiting membrane (red arrows) and the ellipsoid zone (blue arrows). These interruptions, along with the outer nuclear layer thinning, increase towards the peripheral macula and are more profound on the nasal side.

The lack of human representative animal models severely hampers the development of effective treatments for retinal degenerative diseases. *Rpe65* and *Lrat* deficient mice have previously been used to study their RP-related phenotype and test potential experimental treatments' efficacies [5,6,18]. These strains show that the rods degenerate slowly, and the cones degenerate rapidly, with eventual complete loss of cone function [19]. Additionally, both strains had severely decreased to nearly absent ERG responses [5,6,18]. In these mouse strains, supplementation of visual cycle metabolites, such as retinoids [20] and 9-cis-retinyl acetate (QLT091001), seem to be efficacious to maintain the ERG responses as long as there is sufficient retinal integrity to support functional improvement [21,22]. Additionally, gene replacement therapy using adeno-associated viruses (AAVs) or lentiviruses have been used in *Rpe65*$^{-/-}$ [23–27] and *Lrat*$^{-/-}$ mice [22], resulting in the maintenance of retinal integrity and the improvement of ERG a- and b-wave amplitudes.

Experimental gene therapy is generally performed by careful intravitreal or subretinal injections in relavant host mice. However, mouse eyes are extremely small, hampering the effectiveness of these techniques. Furthermore, ocular surgery in mouse eyes, such as placing a sheet of RPE cells into the subretinal space, using commercially available devices, is nearly impossible. Consequently, bigger rat eyes are preferable for these types of experimental therapies. Their larger eye volume enables easier access for injections and makes work with commercially available surgical tools possible [28,29]. Despite this seeming advantage, only a limited number of genetic rat strains with inherited RD are attainable at the time of writing.

The Royal College of Surgeons (RCS) is a spontaneous genetic rat strain with inherited RD, and this model is currently widely used for testing the efficiency of therapies for RDs [30–32]. The strain harbors a mutation in the *Mertk* gene, which causes the RPE to fail to phagocytose the shed photoreceptor outer segments. Despite the apparent advantages of a rat model with larger eyes, photoreceptor debris in the RCS rat accumulates in the subretinal space, initiating spontaneous retinal degeneration and hampering experimental treatment modalities [33].

The work presented here entails the CRISPR/Cas9 mediated construction and characterization of a new *Lrat* deficient Brown Norway rat strain. Visual examination and follow-up of the knockout rat showed that it is a human-representative animal model for RP and, more specifically, RPA. The mutation (c.12delA), which we introduced, is based on a known patient group previously described by our group [4,13]. This new rat model could be used to develop potential (experimental) therapies to treat this specific patient group and patients harboring similar genotypes and/or phenotypes.

Materials and methods

Construction of the Animal Model

All animal experiments were conducted following the ARVO Statement for the Use of Animals in Ophthalmic and Vision Research and approved by the Netherlands' national committee. The previously detected deletion of a cytosine (C) of the 12th base pair (c.12delC) in the coding region of *LRAT* leads to a frameshift and a premature stop codon in exon 1 (p.M5CfsX53).

Homology analysis between the human *LRAT* and rat *Lrat* gene showed that the rat's equivalent of the human c.12delC mutation is c.12delA. This deletion is predicted to have a similar truncating effect (p.M5CfsX72) on the protein as the human variant. The *Lrat* mutant model (Brown Norway background) was produced in collaboration with GenOway (France) using a CRISPR/Cas9 approach to introduce the mutation according to the protocols published elsewhere [68,69]. The Cas9 nuclease and single guide RNA (sgRNA) were used to edit the *Lrat* gene localized to chromosome 2 (2q34). sgRNA was designed to target exon 1 of the *Lrat* gene using CRISPOR.org (http://crispor.tefor.net/; accessed on 16 February 2017), a web-based tool to select CRISPR/Cas9 target sequence: 5'-AAGGATGAAGAACTCAATGC-3'. Six predicted (27 September 2017) off-target sites have been identified from internal genOway process: Chr1:212689122-212689137; Chr2:150627149-150627164; Chr2:181905085-181905100; Chr9:60433155-60433170; Chr16:64050524-64050539, ChrX:28904421-28904436 (*genome* assembly *Rnor* 6.0). A short homologous single-stranded oligonucleotide (ssODN) carrying the c.12delA point mutation (CAGTTGCGGCCAGCGAGAAACTCTGGTCTTTAAAGGAT-GAAGAACAGTTGCTGGAGGCTGCGTCCCTCCTTCTGGAGAAGCTGCTCCTTATTTC) was used as a template for homology-directed repair.

sgRNA and ssODN were ordered from Integrated DNA Technologies (IDT, Coralville, IA, USA). Fertilized oocytes were collected from superovulated Brown Norway female rats previously mated with males. The gRNA (1 µM), ssODN (0.6 µM) and the Cas9 nuclease (0.4 µM, Alt-R™ S.p. Cas9 Nuclease V3, IDT) were then microinjected into the male pronucleus. Injected zygotes were cultivated overnight to the two-cell stage to assess sgRNA toxicity. The resulting two-cell embryos were reimplanted into pseudopregnant foster mothers at 0.5 days post-coitum. Standard surveyor assays were used to detect insertions and/or deletions at the targeted site in the genome. The targeted locus was amplified and sequenced to identify point mutant animals. Two founders harboring the c.12delA point mutation (*Lrat*$^{-/-}$) were identified and bred to generate heterozygous animals (*Lrat*$^{+/-}$). PCR amplification and Sanger sequencing of each predicted off-target site was realized, and no polymorphism was identified in the F1 generation.

Lrat$^{+/-}$ animals were used to expand a colony at our local animal facility. Homozygous *Lrat* knockout rats (*Lrat*$^{-/-}$) and their heterozygote (*Lrat*$^{+/-}$) and wildtype control (*Lrat*$^{+/+}$) littermates were born and reared at the VU University, Amsterdam. All animals were kept on a light cycle of 12 h on/12 h off and were fed ad libitum. The animals were followed over time for visual examination. Both males and females were used in these studies. At the start of the experiments, the rats were 15 days old, weighing 30–40 g.

Mutation Analysis and Expression of the *Lrat* Gene

According to standard protocols, we isolated genomic DNA from ear snips between 10 and 14 days of age using phenol extraction [34]. To confirm the introduced mutation in the experimental animals, we used PCR and sequencing. By PCR, a 365 bp product surrounding the point mutation was generated using forward primer (in 5'–3' direction) GCTGACCAACACTACATCCTC and reverse primer GGGTCCGTGACACTTCCAAC.
The fragment was sequenced (BigDye™) and analyzed using CodonCode software according to the manufacturer's protocol.

Lrat$^{+/+}$, *Lrat*$^{+/-}$, and *Lrat*$^{-/-}$ animals were terminated using CO_2 gas at 2.5 months of age. The liver, kidney, spleen, small intestine, lung, eye, brain, and testis were collected and placed on dry ice immediately. Total RNA was extracted using TRIzol Reagent (Ambion™) according to the manufacturer's protocol. The Nano-drop (ND-1000) was used to check the RNA's concentration and quality, and 200 ng total RNA was used for cDNA synthesis using Superscript III (Invitrogen™) and an oligodT according to the manufacturer's protocol. *Lrat* RNA presence was checked using two sets of specific primers for rat Lrat mRNA (from 5' –3' set 1: forward GCAGATACGGCTCTCCTAT; and reverse GCCAGA- CATCATCCACAAGC, and set 2: forward ACCTTGCACAGACCAGTTGC; and reverse: CAGTCTCGTGAAACTTCTC). The product was sequenced using Bigdye™ (according to the manufacturer's protocol), and the mutated sequence in *Lrat*$^{-/-}$ and *Lrat*$^{+/-}$ animals was confirmed. PCR reactions of the cDNA were performed using a multiplex set-up in which *Ef1a* served as a reference gene. In one PCR reaction, the *Lrat* and *Ef1a* PCR products were generated. The primers for *Ef1a* were made in an exon spanning design (from 5' –3' forward: CTGGCTTCACTGCTCAGGTG; and reverse: GGCTTGCCAGGGACCATGTC).

LRAT Detection Using Immunofluorescence

Lrat$^{+/+}$ and *Lrat*$^{-/-}$ animals were terminated using CO_2 gas at 2.5 months of age. The liver was collected and placed on dry ice immediately. Tissues were embedded in Optimal Cutting Temperature (O.C.T.)™ Compound (Tissue-Tek®) and cut into 5 µm sections using a cryostat ultramicrotome. The sections were fixed in 4 % PFA in 1× PBS at room temperature (RT) for 10 min. Incubation with the primary antibody for LRAT (1:200, custom-made by Biomatik, Kitchener, ON, CA) was performed in blocking buffer (1 % BSA, 0.2 % Triton™ X-100 in 1× PBS) for 90 min at RT. The secondary antibody (1:200, Goat-anti-Rabbit-Cy3, 111-166-003, Jackson ImmunoResearch, Ely, UK) was incubated in 0.2 % Triton™ in 1× PBS for 45 min in the dark at RT. The sections were embedded in Vectashield® mounting medium with DAPI (H-1200, Vector Laboratories, Burlingame, CA, USA) and imaged using a Leica TCS SP8 X confocal microscope.

The Experimental Set-Up, Randomization, Blinding, and Drop-Outs

Animals were given an identification number before entering the experiment. Investigators and caretakers were blinded for their genotype (e.g., experimental group). Males and females were housed separately in groups. Cage arrangements were determined randomly using the randomizing function of Microsoft Excel. Animals were followed over time using scanning laser ophthalmoscopy (SLO), optical coherence tomography (OCT), electroretinography (ERG), and vision-based behavioral measurements. At the start of every measurement, the measuring order was randomly determined using the randomizing function of Microsoft Excel. The rats were measured using SLO-OCT and ERG at a wide range of ages. *Lrat*$^{-/-}$ animals (n = 6) were measured weekly from 2 weeks of age onwards. *Lrat*$^{+/-}$ (n = 5) animals were measured at 16, 17, and 23 weeks of age only. Since only patients with a homozygous, and not heterozygous, c.12delC mutation suffer from RD, we did not expect a difference in these animals' visual phenotype compared to the *Lrat*$^{+/+}$ animals (n = 6) beforehand. A light/dark-box assay was done at 0.5, 1, 1.5, 2, and 3 months of age. At the end of the study, all animals were sacrificed, and the eyes and other tissues were collected for additional *in vitro* analyses. There were no drop-outs throughout the experiment.

Scanning Laser Ophthalmoscopy (SLO) and Optical Coherence Tomography (OCT) Measurements

SLO uses laser scanning microscopy to obtain images (fundus photos) of the retinal surface. OCT uses near-infrared light to obtain high-resolution two- and three-dimensional images within the retina. SLO-OCT measurements were performed using a commercially available system (Heidelberg Engineering Spectralis combined HRA+OCT, Heidelberg, DE), modified for use with animals (Medical Workshop, Utrecht, NL). Detailed methods are described elsewhere [35,36]. In short, animals were anesthetized with an intraperitoneal injection of a mixture of ketamine (22 mg/kg for animals <4 weeks of age; 65 mg/kg for animals ≥ 4 weeks of age) and xylazine (2.2 mg/kg for animals <4 weeks of age; 7.5 mg/kg for animals ≥ 4 weeks of age) diluted in 0.9 % NaCl.

The eyes were locally anesthetized using tetracaine-hydrochloride drops (1 % *w/v*) and were dilated using tropicamide (0.5 % *w/v*), and atropine (1 % *w/v*) drops. Hylocomod drops were applied to maintain corneal hydration at all times. A contact lens (5.2 mm in diameter; Cantor-Nissel, Brackley, UK) was placed. The standard 30° field of view equipment set was used. Animals were placed on a custom-made heated holder, eyes were kept moist using Hylocomod eye drops, and body temperature was monitored. Imaging was done using the Eye Explorer software version 1.9.14.0 (Heidelberg Engineering, Heidelberg,

DE). For fundus images, infra-red (820 nm) intensity was manually adjusted to prevent overexposure. OCT imaging was performed using a volume scan (57 frames, 786 A-scans, 30°× 25°, 61 scans, Δ120 µm, 8.8 scans per second). The reference arm was manually adjusted according to the manufacturer's instructions. The follow-up function was used whenever possible to ensure accurate thickness profiles between time points. Frame analysis was done on a total of five single OCT scans and corresponding thickness profiles. The chosen scans were the crossing of the optic nerve (ON = 0), the middle superior section (ON + 10), the superior section (ON + 20), the middle inferior section (ON - 10), and the inferior section (ON - 20). Within each selected OCT scan, retina thickness was determined on 1 mm intervals, with a 0.5 mm minimum distance from the optic nerve. The thickness values were averaged, normalized, and shown the standard error.

Electroretinography (ERG)

Using ERG, the electrical activity of the retina in response to a light stimulus is measured. The ERG arises from currents generated by the retinal neurons and glia. The animals were kept in total darkness in their home cage for at least 1 hour before scotopic ERG measurements and were anesthetized with an intraperitoneal injection of a mixture of ketamine (22 mg/kg for animals <4 weeks of age; 65 mg/kg for animals ≥ 4 weeks of age) and xylazine (2.2 mg/kg for animals <4 weeks of age; 7.5 mg/kg for animals ≥ 4 weeks of age) diluted in 0.9 % NaCl. The eyes were locally anesthetized using tetracaine-hydrochloride drops (1 % *w/v*) and were dilated using tropicamide (0.5 % *w/v*), and atropine (1 % *w/v*) drops. Hylocomod drops were applied to maintain corneal hydration at all times. The animals were placed in the RETImap full flash Ganzfeld (Roland Consult, Brandenburg an der Havel, DE) using a carrier table, which was kept at 37 °C. Body temperature was carefully monitored during all measurements. ERGs were recorded using gold electrodes, which were placed on the corneas of both eyes. Another gold electrode was placed in the animal's mouth serving as a reference for both eyes simultaneously. A needle was placed subcutaneously near the tail, which served as a ground electrode. See Supplementary Table S1 for the light intensities, the number of flashes used for averaging, and the flashes' interval. ERG traces were 350 ms long, utilizing 512 data points.

All ERG data were systematically analyzed, without human intervention, using a custom-made Matlab script. The data was zero-centered by averaging the signal before the stimulus (<20 ms) and subtracting the resultant from the entire trace. A low-pass filter (4^{th} order, 30 Hz (for the b-wave) and 235 Hz (for the a-wave)) was applied in both the forward and backward direction to remove noise and the oscillatory potentials (OPs). 30 Hz is well below the minimum expected frequency, and 235 Hz resembles the expected maximum frequency of OPs in rats [37]. The *findpeaks* function in Matlab was used to find the latencies of the a- and b-waves in the filtered data. The magnitudes of the unfiltered signal at the selected latencies were characterized as the values for b-wave and the absolute a-wave amplitude. The absolute a-wave was subtracted from the value of the b-wave amplitude to calculate the absolute b-wave amplitude.

Flicker properties were determined from the original, unfiltered trace. The time to the first peak (P1) and the second peak amplitude (P2) were identified. The (absolute) b-wave, a-wave, and flicker properties of each group, at each age, were averaged and normalized to the corresponding 30 cd·s/m^2 response from the wildtype control group (Supplementary Figure S5).

Light/Dark-Box Behavioral Assay

At the ages of 0.5, 1, 1.5, 2, and 3 months (for *Lrat*$^{-/-}$ and *Lrat*$^{+/+}$ animals) and 5 months (for *Lrat* $^{+/-}$ and *Lrat*$^{+/+}$), a vision-based behavioral assay was performed. A customized light/dark-box was used with dimensions of 100×50×40 cm (length×width×height). Half of the box was darkened. The box was placed in the same position in the room during every measurement to prevent possible light/shade interference. The animals were placed in the light area of the box and filmed for twenty minutes. Deep learning was used to extract key features. In short, a Faster Recursive Convolutional Neural Networks (Faster R-CNN) was used to locate and track the rat's head. The Faster R-CNN was developed using the resnet18 architecture and trained on 658 randomly sampled, annotated video frames. After the detector was trained, it was deployed on each video. A transition zone, dark zone, and light zone were determined. The transition zone was defined as a circle centered at the doorway base with a radius of 1.25 times the doorway's width. The rat was tracked in the light/dark box, and per frame, the rat's location was tracked. After tracking the rat's heads in each video, the data were processed using Matlab. A random subset of videos was selected to manually extract all parameters and compare the data to the values extracted via the Faster R-CNN-based algorithm. No significant differences were found between the manually extracted and automatically extracted parameters, confirming the automatic analysis's robustness.

Statistical Analyses Performed

Data were analyzed using one- or two-way ANOVA analyses, ANOVA analyses of the log-transformed data, and the Kruskal-Wallis analyses with posthoc Bonferroni to determine the statistical significance of all data. Similar *p*-values were obtained using all tests. *p*-values are reported: *: $p \leq 0.05$, **: $p \leq 0.01$, ***: $p \leq 0.001$, and ****: $p \leq 0.0001$.

Results

Generation of *Lrat* Knockout (KO) Rats

The *Lrat* mutation of interest was selected based on a mutation (c.12delC) occurring in a patient group's DNA within our hospital [4,13]. Bio-informatic homology analyses between human and rat genomic DNA sequences revealed that the rat's targeted mutation is c.12delA (Figure 3A). The alignments of the predicted peptides in patients and rats harbouring the deletion (c.12del) are shown in Figure 3B. For the complete alignments of human and rat mRNA and amino acid sequences, see Supplementary File 1.

Of 18 pups born after CRISPR/Cas9 editing, 4 carried mutations at the predicted 5' and/or 3' guide RNA target site, as judged from surveyor assays. The mutation of interest (c.12delA) was detected in two founders by sequencing a PCR product surrounding the predicted mutation (see Figure 4B).

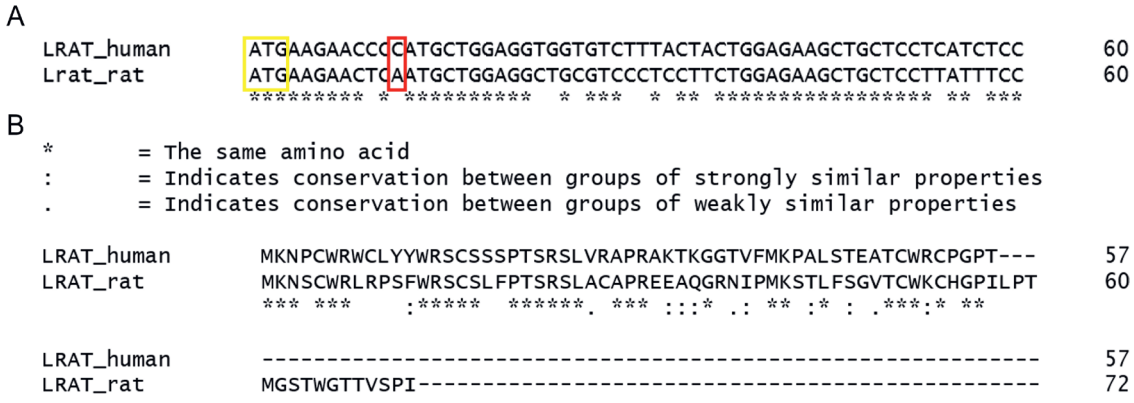

Figure 3. Alignment of the human and rat genomic DNA and protein sequences. (**A**): alignment of the first 60 nucleotides of the *LRAT* and *Lrat* ORF starting with the start codon (indicated by the yellow box). The red box indicates the nucleotide that is deleted in patients (c.12delC) and the rat equivalent (c.12delA). (**B**): alignment of the predicted resulting peptide in patients and rats harboring the deletion (c.12del). The single nucleotide deletion in the genomic DNA causes a frameshift from the fifth amino acid onwards and a truncated protein in both humans (57 amino acids) and rats (72 amino acids).

The DNA sequences' alignment in these two founders revealed that a local insertion and deletion were introduced in the Brown Norway rat's genome. Four nucleotides were deleted (c.10–13: TCAA), and three nucleotides were inserted at that spot (AGT), resulting in a silent mutation at p.4Ser and a frameshift afterward due to the targeted single nucleotide deletion (c.12delA). We found that the introduced mutation cosegregated with the disease phenotype through multiple generations without observing potential recombinations, which strongly suggests the introduced mutation's pathogenicity.

Intercrosses of heterozygotes (*Lrat*$^{+/-}$) rats produced homozygous *Lrat*$^{-/-}$ progeny in standard Mendelian ratios (see Supplementary Table S2). Homozygous (*Lrat*$^{-/-}$) crossings produced normal-sized litters, averaging 8 pups (6–12, median 8). *Lrat*$^{-/-}$ rats survived for over one year. No spontaneous phenotype was observed judging from their social behavior and health parameters (e.g., weight progression, see Supplementary Figure S1) under normal laboratory circumstances. This indicates that *Lrat*$^{-/-}$ rats have no readily apparent disease phenotype, as can be judged from standard laboratory observations.

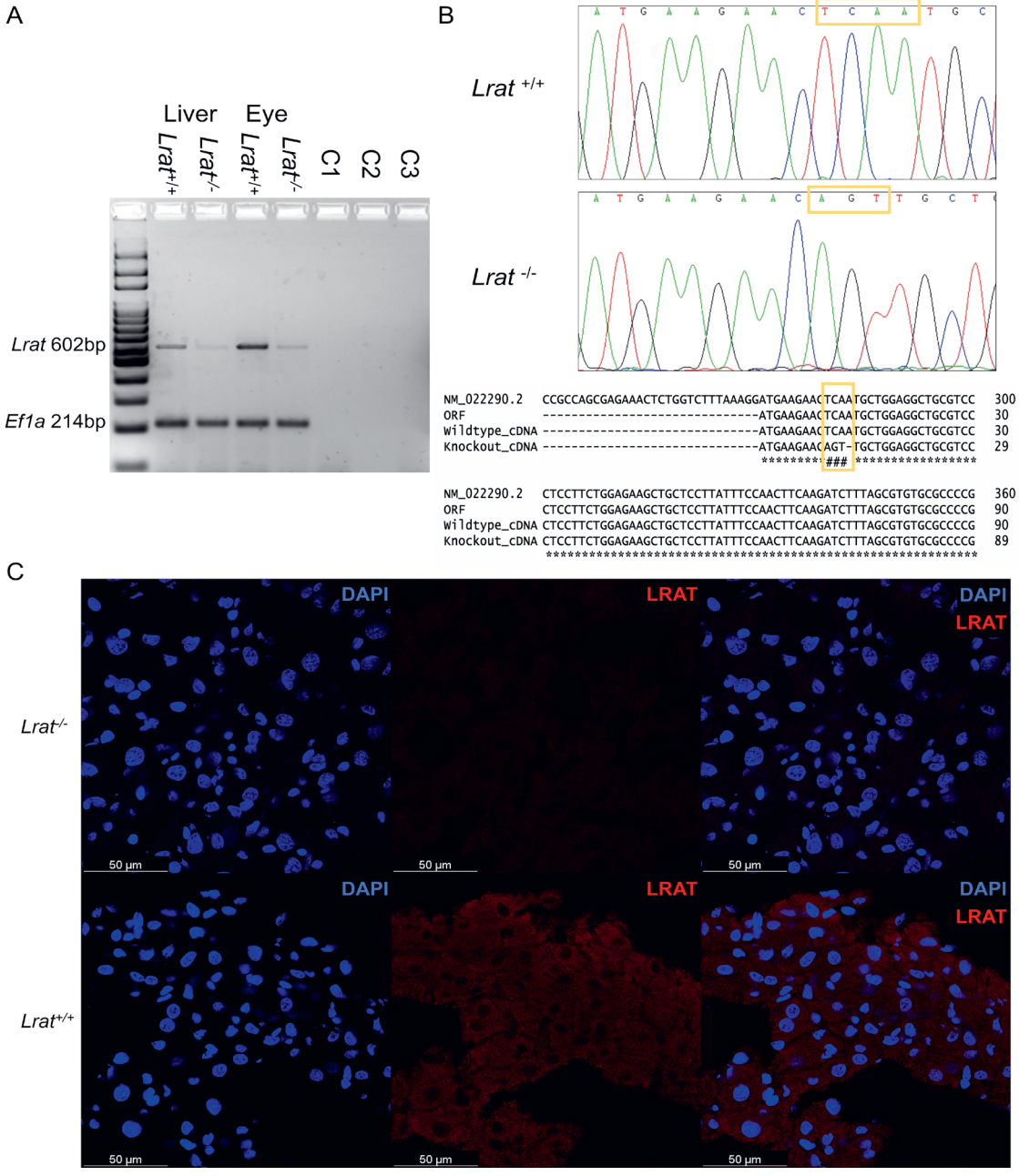

Figure 4. (**A**): mRNA expression of *Lrat* and *Ef1a* shown for $Lrat^{+/+}$ and $Lrat^{-/-}$ animals for liver and eye tissues. *Lrat* expression was found in both wildtype liver and eye tissues. Significantly less RNA is found in $Lrat^{-/-}$ tissues. C1–3: negative controls −/−cDNA in PCR reaction, −/−RNA in cDNA synthesis, and −/−SuperScriptIII in cDNA synthesis. (**B**): the presence of the introduced single nucleotide deletion and silent mutation in the *Lrat* mRNA of the Brown Norway rat was confirmed by Sanger sequencing. The rat reference sequence was retrieved from the NCBI database, Accession NM_02290.2. The open reading frame (ORF) of *Lrat* was determined using the ORFfinder (NCBI). (**C**): LRAT protein presence is confirmed in the liver of $Lrat^{+/+}$ animals and (almost completely) absent in $Lrat^{-/-}$ liver tissue.

Lrat Gene and Protein Expression in Rat Tissues of Wildtype, Heterozygous, and *Lrat* Knockout (KO) Rats

We analyzed the presence of *Lrat* mRNA using PCR in the liver and eye tissues of $Lrat^{+/+}$ and $Lrat^{-/-}$ animals. We found a high abundance of *Lrat* transcript in both tissues of the $Lrat^{+/+}$ animals (Figure 4A). Clearly, less *Lrat* transcript in $Lrat^{-/-}$ was observed. This observation was confirmed using a second set of RT-PCR primers. Other tissues of $Lrat^{-/-}$, $Lrat^{+/-}$, and $Lrat^{+/+}$ rats, including the kidneys, spleen, small intestine, lung, brain, and testis, were also tested for *Lrat* transcript presence, see Supplementary Figure S2. We found *Lrat* transcript to be abundant in the eyes, liver and testis. Less expression was found in lung tissue. After finding minimal *Lrat* mRNA in homozygous knockout tissues, we confirmed the single nucleotide deletion in the cDNA produced from whole mRNA samples of multiple animals. The sequences are shown in Figure 4B, including the alignment to the NCBI's reference sequence and our wildtype Brown Norway animals. In agreement with the mRNA expression, we observed, using immunofluorescence, that LRAT protein was abundantly present in liver sections of $Lrat^{+/+}$ animals and (almost completely) absent in liver sections of $Lrat^{-/-}$ animals (Figure 4C).

In Vivo Imaging of Retinal Structures Using Non-Invasive Scanning Laser Ophthalmoscopy (SLO) and Optical Coherence Tomography (OCT)

We assessed the retinal morphology of $Lrat^{-/-}$ rats and compared it to the retinal morphology of $Lrat^{+/+}$ and $Lrat^{+/-}$ rats over a timespan of 4 months with weekly intervals using non-invasive SLO and OCT. Representative fundus images and OCT scans of $Lrat^{+/+}$ and $Lrat^{-/-}$ animals of different ages (2.5, 4.5, 6.5, and 15 weeks of age) are presented in Figure 5. We observed an overall quantitative progressive degradation and significant thinning of the retina for $Lrat^{-/-}$ animals overtime, as judged by OCT images (Figure 6B). The thickness decrease is mostly due to the outer nuclear layer's degeneration, reflecting the loss of the PRs. At the same time, the inner plexiform layer and inner nuclear layer were similar to the wildtype controls. No apparent differences between the SLO and OCT images of $Lrat^{+/+}$ and $Lrat^{+/-}$ animals were seen (Supplementary Figure S3 and Figure 6B).

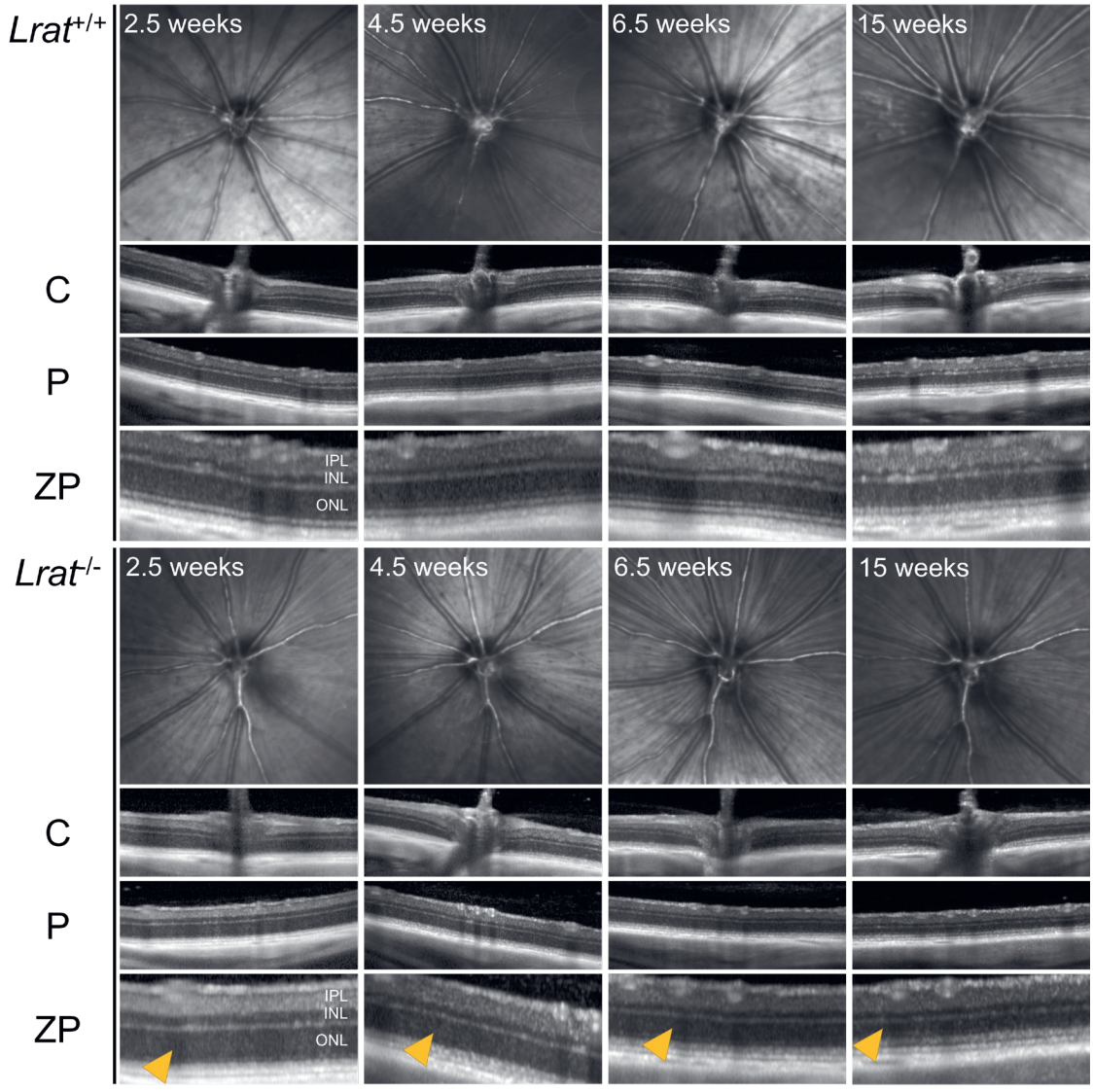

Figure 5. Representative qualitative SLO and OCT images of *Lrat*$^{+/+}$ and *Lrat*$^{-/-}$ rats at different ages. OCT scans from the same eye of the central area (C), including the optic disc and the peripheral area (P), are included for each genotype. Additionally, a more detailed image of the peripheral area is shown (ZP). It is possible to identify all retinal layers, including the inner plexiform layer (IPL), the inner nuclear layer (INL), and the outer nuclear layer (ONL) in both the wildtype and knockout animals from the OCT images. The layering of the retina becomes less distinct in the knockout animals over time. The retina of knockout animals degenerates over time and becomes thinner at later stages. Especially the ONL layer, representing the cell bodies of the PRs, becomes thinner over time (yellow arrows). For the thickness quantification, see Figure 6. No differences can be observed between wildtype and knockout SLO images.

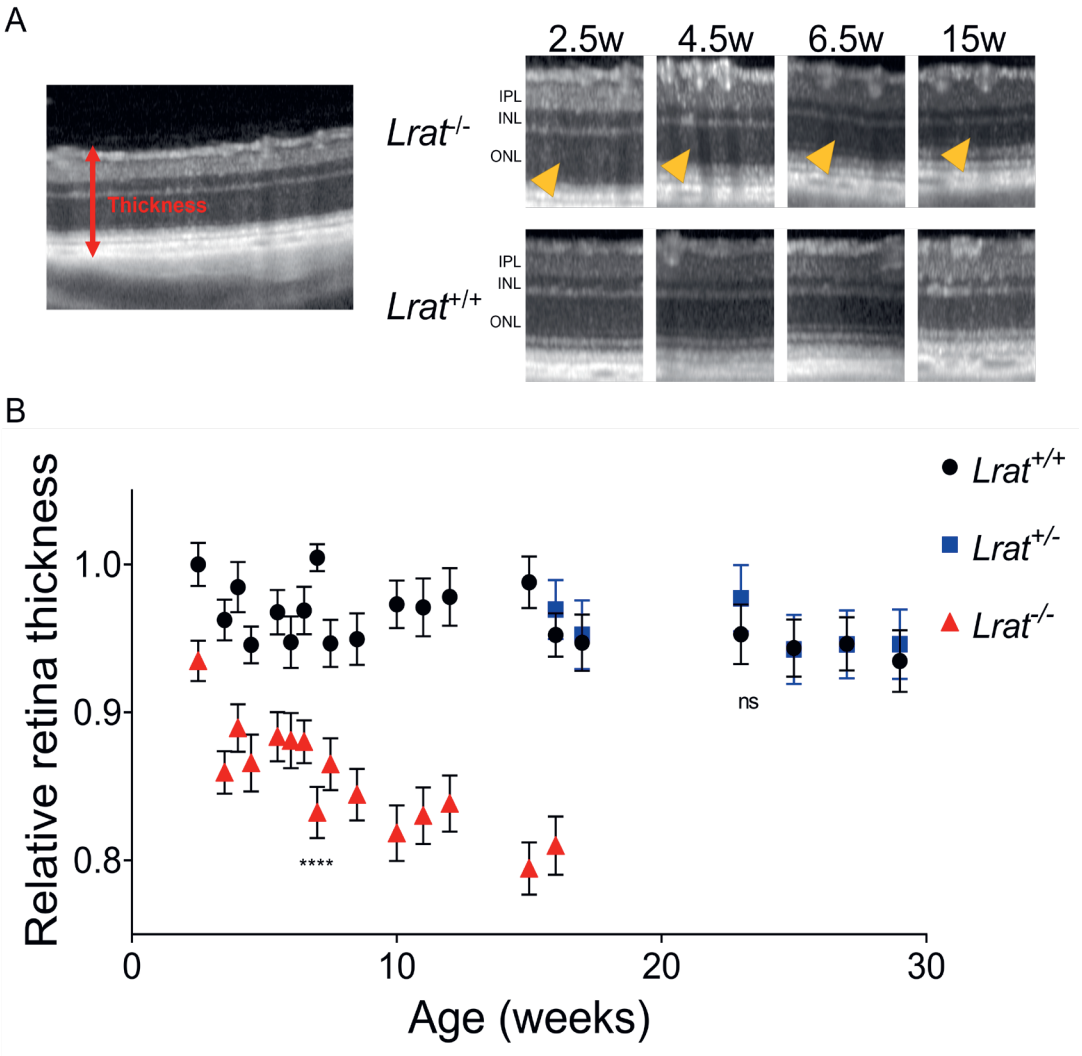

Figure 6. (**A**) quantitative representation of total retina thickness (**A**) at different ages of *Lrat*$^{+/+}$ (black circles), *Lrat*$^{+/-}$ (blue squares), and *Lrat*$^{-/-}$ (red triangles) animals. The left panel of A shows how the total thickness was determined. The chosen scans for determining total thickness were the crossing of the optic nerve (ON = 0), the middle superior section (ON + 10), the superior section (ON + 20), the middle inferior section (ON − 10), and the inferior section (ON − 20). Within each selected OCT scan, retina thickness was determined on 1 mm intervals, with a 0.5 mm minimum distance from the optic nerve. All values were normalized to the wildtype retina's thickness at 2 weeks of age and plotted with the standard error (panel (**B**)). Some variation between OCT measurements can be observed over time, although not significant within the wildtype and heterozygote animals. The retina of knockout animals degenerates over time and is significantly thinner than the retina of wildtype and heterozygous animals. The thinning is mostly due to the degeneration of the outer nuclear layer (ONL) (yellow arrows) (A). No significant differences are observed between wildtype and heterozygous animals. ns = non-significant; **** = p <0.0001. IPL: inner plexiform layer; INL: inner nuclear layer.

In Vivo Assessment of the Retinal Function Using Electroretinography (ERG)

We performed electrophysiological studies to assess the visual function of *Lrat*$^{-/-}$, *Lrat*$^{+/-}$ and *Lrat*$^{+/+}$ rats. We measured and analyzed the responses to scotopic stimuli at regular time points between 2 and 23 weeks of age. ERG traces are presented for *Lrat*$^{+/+}$ and *Lrat*$^{-/-}$ animals at 5 weeks of age (Figure 7A,B), showing several differences that were observed, including the complete absence of recordable a-waves, the almost complete lack of the b-waves, the absence of recordable oscillatory potentials, and the absence of a recordable response to a flicker (9 Hz) in *Lrat*$^{-/-}$ animals.

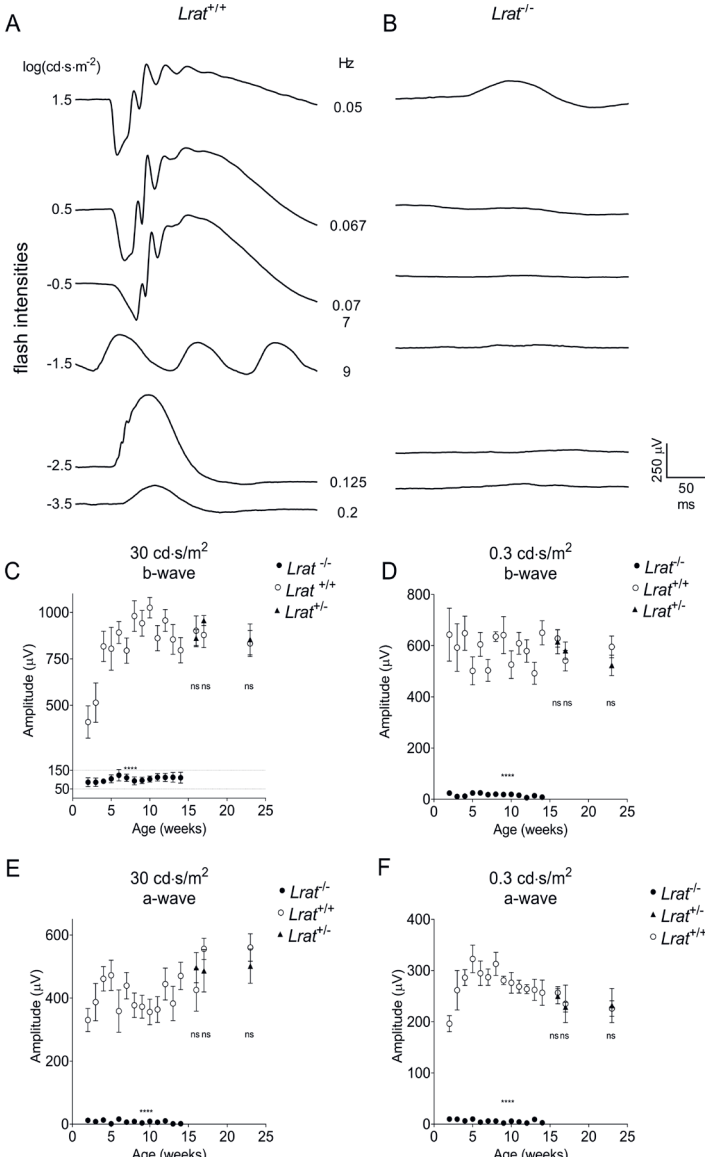

Figure 7. ERG responses of *Lrat*$^{+/+}$ (n = 6), *Lrat*$^{+/-}$ (n = 5), and *Lrat*$^{-/-}$ (n = 6) animals after a single light flash. Averaged traces with increasing flash intensities are plotted for *Lrat*$^{+/+}$ (**A**) and *Lrat*$^{-/-}$ animals (**B**) at 5 weeks of age. A-wave (**C**,**D**) and b-wave (**E**,**F**) amplitudes (µV) are plotted versus the age of the animals after a high light intensity flash (30 cd·s/m^2) (**C**,**E**) and a lower light intensity flash (0.3 cd·s/m^2) (**D**,**F**). No significant difference can be observed between the amplitudes of *Lrat*$^{+/+}$ (white circles) and *Lrat*$^{+/-}$ animals (triangles). *Lrat*$^{-/-}$ animals (black circles) have extremely decreased or not detectable ERG responses from 2 weeks of age onwards (**C**–**F**). No dark-adapted a-wave responses were recorded at all, and no b-wave response for 0.3 cd·s/m^2. ns = non-significant; **** = p <0.0001.

Wildtype control animals of various ages did not show any significant differences in ERG amplitudes between time points (n = 6; see Supplementary Figure S4). In contrast, differences were observed for the *Lrat*$^{-/-}$ animals. Hardly any responses were observed for this group at all time points. Only at the highest light intensity flash (30 cd·s/m^2) we observed a slight response for *Lrat*$^{-/-}$ animals. Dark-adapted a-wave amplitudes (Figure 7E,F) and b-wave amplitudes (Figure 7C,D) were quantified over time and presented in Figure 7D,F for 0.3 cd·s/m^2 and in Figure 7C,E for 30 cd·s/m^2. From the age of 2 weeks onwards, dark-adapted a-wave amplitudes were hardly recordable in *Lrat*$^{-/-}$ animals and b-wave amplitudes were strongly decreased in *Lrat*$^{-/-}$ animals compared to *Lrat*$^{+/+}$ animals. At 5 weeks of age, dark-adapted a-wave amplitudes were hardly recordable, and b-wave amplitudes were strongly decreased for *Lrat*$^{-/-}$ animals for all light intensities (Figure 8A,B). We also performed ERGs in heterozygous (*Lrat*$^{+/-}$) animals. However, no significant differences were observed between *Lrat*$^{+/-}$ and *Lrat*$^{+/+}$ animals. The relevant data are presented in Figure 7C–F and Supplementary Figure S5.

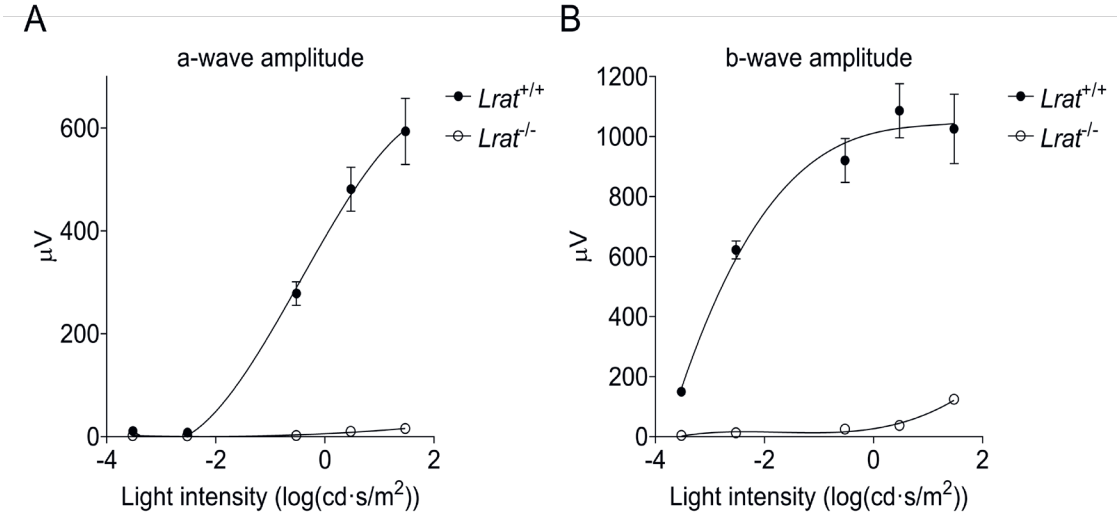

Figure 8. ERG responses of *Lrat*$^{+/+}$ (n = 6) (black circles) and *Lrat*$^{-/-}$ (n = 6) (white circles) animals at 2 weeks of age after a single light stimulus. Averaged a-wave (**A**) and b-wave (**B**) amplitudes per experimental group plotted against increasing light intensity. B-wave responses were extremely decreased, and a-wave responses were almost completely absent in *Lrat*$^{-/-}$ animals, indicating that these animals are blind from 2 weeks of age onwards.

Vision-Based Behavioral Analysis

We performed a light/dark box vision-based behavioral assay with *Lrat*$^{+/+}$, *Lrat*$^{+/-}$, and *Lrat*$^{-/-}$ animals at different ages (Figure 9). We did not observe significant differences between *Lrat*$^{+/+}$ and *Lrat*$^{+/-}$ for several test parameters such as time spent in the dark area, the light area, and the transition zone (Figure 9B). Clear and significant differences were observed between *Lrat*$^{+/+}$ and *Lrat*$^{-/-}$ animals (Figure 9C–H). *Lrat*$^{-/-}$ animals usually spend less time in the dark area (Figure 9C), more time in the light area (Figure 9D), and more time in the transition zone (Figure 9E) compared to *Lrat*$^{+/+}$ animals. Wildtype animals are more resistant to entering the lighted compartment (Figure 9F) compared to knockouts and less resistant to entering the darkened compartment (Figure 9G).

Moreover, *Lrat*$^{-/-}$ animals changed compartments more than *Lrat*$^{+/+}$ animals (Figure 9H). Altogether, these results indicate that *Lrat*$^{-/-}$ animals cannot distinguish between the light and the dark area of the box and, thus, do not prefer where to spend most of their time. Wildtype and heterozygote animals prefer to spend their time in the dark area, as expected from rats with normal vision.

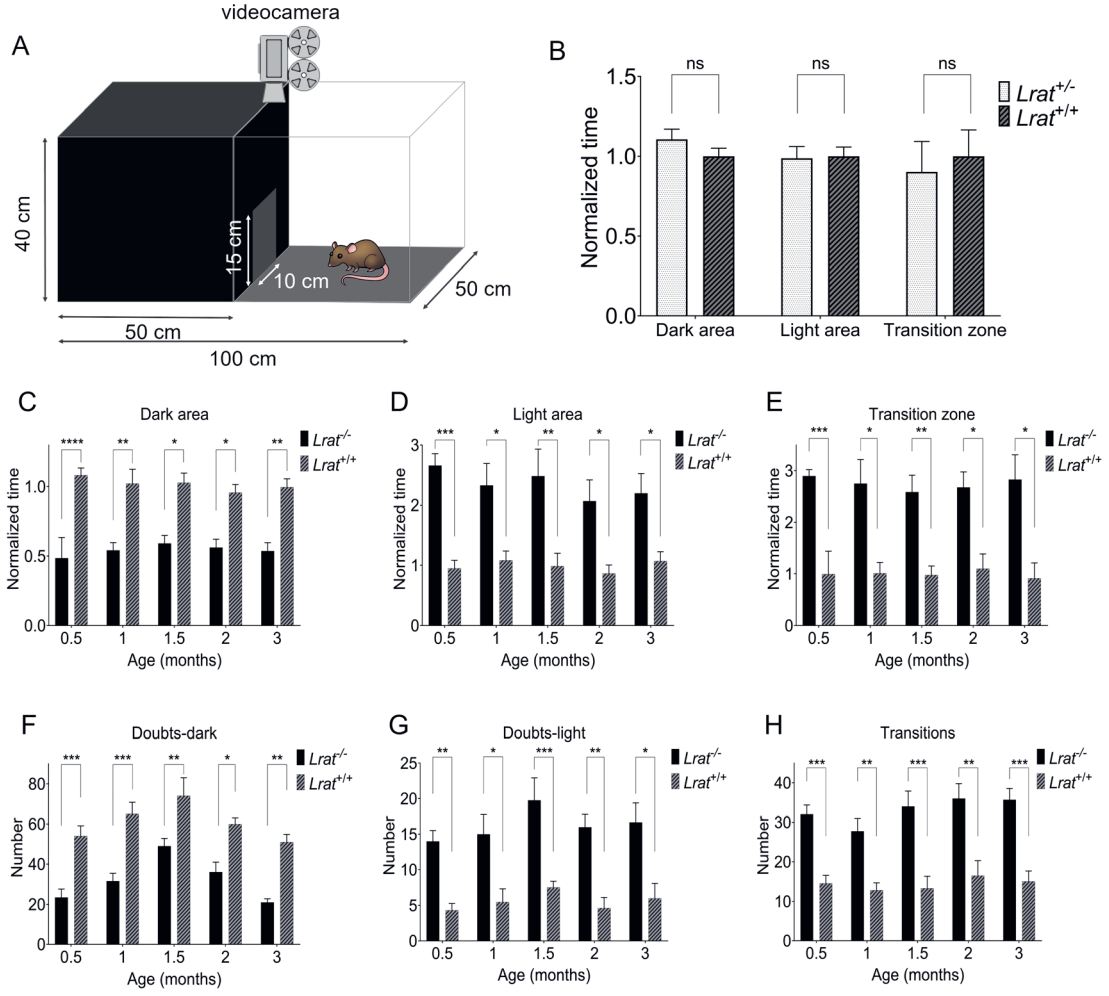

Figure 9. Light/dark box vision-based behavioral responses of *Lrat*$^{+/+}$ (n = 6), *Lrat*$^{+/-}$ (n = 5) and *Lrat*$^{-/-}$ (n = 6) animals. A schematic overview of the customized light/dark box used is presented in panel (**A**). No significant differences between *Lrat*$^{+/-}$ and *Lrat*$^{+/+}$ animals were observed for the time spent in any area at the age of 23 weeks (**B**). *Lrat*$^{-/-}$ spend more time in the dark area than the *Lrat*$^{+/+}$ animals (**C,D**). *Lrat*$^{-/-}$ spend more time in the transition zone (the area around the door) and switch compartment more than *Lrat*$^{+/+}$ animals (**E**). *Lrat*$^{+/+}$ animals doubt more to enter the light compartment (**F**) and less to enter the dark compartment (**G**) than *Lrat*$^{-/-}$ animals. *Lrat*$^{-/-}$ switch areas more often than *Lrat*$^{+/+}$ animals (**H**). Wildtype rats are more comfortable spending more time in a dark area. These data show that the knockout animals do not have the same preference, indicating that they cannot distinguish between the dark and light areas and are visually impaired. The data in panels (**B**–**E**) are normalized to the averaged *Lrat*$^{+/+}$ behavior of all measurements for each parameter separately. The wildtype animals' data were averaged for all measurements (all time points together) per parameter. This was possible since the behavior of the wildtype animals did not change significantly over time. These values were used for the normalization of the data of the *Lrat*$^{-/-}$ animals. ns = non-significant; * = p <0.05; ** = p <0.01; *** = p <0.001; **** = p ≤0.0001.

Discussion

In this study, we generated and phenotyped a new rat model for RP based on a mutation in the *LRAT* gene in our hospital's RPA patient group [4,13]. The rat equivalent of the human mutation (c.12delC) in *Lrat*, c.12delA, was successfully introduced in the Brown Norway rat strain using CRISPR/Cas9-based gene editing. The expression of *Lrat* was found in several tissues, including the liver, lung, testis, and eye, thereby confirming data from the literature [15–17,34]. Homozygous *Lrat* mutants were followed up by SLO-OCT, ERG, and vision-based behavioral tests.

We confirmed that the targeted mutation in both genomic DNA as cDNA in our $Lrat^{-/-}$ animals was the causative mutation for the *in vivo* vision-related phenotype that we observed in this strain. The introduced mutation (*Lrat* c.12delA) causes a frameshift and a predicted premature chain termination at position 72 (p.M5CfsX72). The mRNA is possibly degraded by nonsense-mediated decay [35]. Indeed, we observed significantly less mRNA expression in $Lrat^{-/-}$ tissues compared to the wildtype tissues. Immunohistochemistry data on liver sections showed the absence of LRAT protein. The remaining expression of *Lrat* mRNA in our knockout rat is an observation that we cannot explain readily yet and is a subject for further studies.

Nonetheless, it is well known that a small subset of specific mRNA species containing a premature chain termination escapes nonsense-mediated decay [35–39]. Another possible explanation might be related to the complex and partly unknown transcriptional machinery of the *Lrat* gene. Zolfaghari and coworkers (2002) found that the regulation of *Lrat* expression in different tissues is complex and occurs through a combination of mechanisms. They identified several potential signals for polyadenylation in the 3'UTR region of the *Lrat* transcript resulting in the expression of alternative smaller transcripts in specific tissues [17]. Possibly, minute quantities of alternatively spliced or regulated *Lrat* mRNA are induced by knocking out the gene, a phenomenon called transcriptional modulation.

Last but not least, our mutated $Lrat^{-/-}$ rat strain and patients harboring an *LRAT* mutation do not show an apparent additional phenotype besides vision-related problems. *Lrat* deficiency did not appear to adversely affect the long-term survival or fertility of male or female $Lrat^{-/-}$ rats. This suggests that the lack of functional LRAT protein might be compensated in other tissues besides the eye. Future in-depth studies on (the regulation of) *Lrat* expression and translation in the retina and other tissues may shed light on these issues.

In this study, we report the disease course of a new rat model for RP in detail using structural and functional phenotypic assessment of the retina and vision. In summary, the single nucleotide deletion in our $Lrat^{-/-}$ rat resulted in functionally blind rats, as measured by ERG and vision-based behavior assays, from two weeks of age onward. The functional retinal abnormalities measured by ERG precede the structural abnormalities as measured by OCT. Retinal degeneration started within three weeks of age (OCT) in $Lrat^{-/-}$ rats. At four months of age, their retinal thickness was significantly reduced to roughly 80 % of the original thickness.

Our *Lrat*$^{-/-}$ rat's phenotype is highly similar to that of a previously published *Lrat*$^{-/-}$ mouse model. This mouse model harbors a targeted mutation in which the whole first exon of the *Lrat* was replaced with a neomycin cassette. Similar to our rat model, the homozygous *Lrat*$^{-/-}$ mice are viable and fertile but blind from early-onset [6]. At the age of 6–8 weeks, in *Lrat*$^{-/-}$ mice, histological analysis revealed shorter (35 %) retinal rod outer segments than the wildtype controls. The *Lrat*$^{-/-}$ mice lost sensitivity of pupillary light responses and had abnormal electroretinograms. Besides thinning of the retina, relatively few morphological changes in the *Lrat*$^{-/-}$ mouse retina were visible from OCT images at an early age (6–8 weeks) under normal laboratory circumstances [6,19]. We obtained comparable results using OCT imaging in our *Lrat*$^{-/-}$ rat.

Although the *Lrat* c.12delA rat mutation was designed after a genetic defect in a human patient group, there is a considerable difference in the disease's onset and progression in humans and mice. The phenotype of patients harboring *LRAT* mutations is variable and relatively mild. Within the cohort carrying the c.12delC mutation, the first symptom usually presents itself within the early years of life, generally starting with nyctalopia. Later, patients have significantly decreased scotopic ERG measurements and an overall decrease in visual sensitivity. OCT showed normal architecture of the retinal layers. Funduscopy revealed significant variability in the quantity of white dots observed in the (mid-)peripheral fundus, which seemed to be dome-shaped hyperreflective lesions extending from the RPE as determined using OCT. The mean age of reaching blindness or severe visual impairment varies between 50 and 60 years of age. In other patient cohorts harboring other pathogenic *LRAT* mutations, this is broader: between childhood to 60 years of age [2,13,40]. In contrast to the clinical picture in our human patient group, both our new *Lrat*$^{-/-}$ rat and the previously published mouse strains reach functional blindness and retinal degeneration much sooner, during infancy if not directly after birth. Mice and rats open their eyes between 14–16 days of age. The phenotypic difference could perhaps be explained by the difference between rodent and human eyes. Since mice and rats are nocturnal mammals and humans are diurnal, mice and rats have many more rods than cones.

Rods are more efficient in responding to low light intensity conditions than cones. However, cones allow for greater visual acuity [41–43]. *Lrat*$^{-/-}$ rodents reach blindness relatively earlier in life than human patients. However, the first symptom for patients harboring an *LRAT* mutation usually is nyctalopia during infancy within the first year of life [13]. This can be explained by the fact that the rat's retina contains many more rods, which function better in lower light, than cones, which are responsible for color vision and work best in bright light. The absence of scotopic ERG responses in both rodents and humans lacking LRAT is a common characteristic. Finally, besides the absence of scotopic ERG responses, another similarity is the progressive retinal thinning as judged from OCT scans. In both human patients and our *Lrat*$^{-/-}$ rat strain, the ONL progressively degenerates [13].

Our newly developed model can be used for the development of therapeutic approaches for the *LRAT*-subtype of RP. This subtype is, at present, an incurable disease, as are most forms of RP. The only exception is the *RPE65*-subtype of RP, which is highly related to the *LRAT*-subtype [13]. For the *RPE65*-subtype of RP, AAV2-mediated augmentation gene therapy (voretigene nepravovec) is currently on the market [44,45]. From a biological point of view, the duration of the treatment effect is expected to last a lifetime. However, since extended patient follow-up data of treated patients are still scarce, there are still some uncertainties about the long-term impact of voretigene nepravovec [44]. Talib and colleagues (2019) suggested that patients with retinal degenerations caused by *LRAT* mutations may be particularly susceptible to treatments, such as gene-replacement therapy, since not (all) pathogenic mutations lead to early onset of severe visual dysfunction. Indeed, the patients suffering from RD, caused by the c.12delC mutation in *LRAT*, show long-term preservation of the outer retina, at least at the level of the fovea. This is potentially a favorable finding, as indicated by positive results of an ongoing therapeutic clinical trial (NCT01256697) in which patients with *RPE65*- and *LRAT*-subtype of RP receive oral synthetic 9-cis-retinoids [13]. In contrast to the *RPE65*-subtype of RP, the window of therapeutic opportunity for *LRAT*-RP patients can thus be extended to later decades of life [13]. However, the best therapeutic window in these patient groups needs to be determined still [46].

Since *Lrat* is expressed in the RPE, subretinal injections are more preferential over intravitreal injections for experimental therapies such as gene- and cell-replacement therapy. In mice, subretinal injections are generally challenging to perform with lower success rates than intravitreal injections. Moreover, it was recently suggested that suprachoroidal injections are possibly even more efficient than intravitreal and/or subretinal injections to target the RPE [47]. Suprachoroidal injections are a relatively new concept and need to be developed and fine-tuned in rodents. Experimental cell-based therapeutic studies may require either ocular injections or subretinal surgery. *In vivo* cell-therapeutic studies targeting (*Rpe65*$^{-/-}$ and *Lrat*$^{-/-}$ mediated) damage of RPE cells using injections of dissociated (RPE) cells resulted in variable outcomes [28,48,49].

More promising results were obtained with RPE cells transplanted as a monolayer with or without a carrier [50–54]. The procedures for transplanting cells as a sheet are more extensive than a relatively simple single subretinal injection. To transplant these tissues and scaffolds into mice's eyes is a significant, maybe not to overcome, technical challenge. Given the fact that the rat eye's volume (±50–55 µL) is roughly ten times as large as the mouse eye's volume (±4–5 µL) [55,56], in our hands, (all) ocular interventions are performed with a much higher success rate in rat eyes. We think that the more complex ocular interventions, such as sheet transplantations, are possible in rats' eyes, but not mice's eyes, given the currently commercially available instruments, indicating the need for larger eyed models, such as rats, to facilitate the exploration of novel therapies for RDs. Moreover, rats usually are the leading model for studies of physiology, pharmacology, toxicology, and neuroscience [57]. Indeed, it was suggested that rats are superior to mice as models for humans in neuroscience and behavioral assays [58–60]. Taken together, both the eye size and visual evaluation of (genetically manipulated) rats have substantial advantages over commonly used mice in preclinical studies studying RDs.

The number of suitable rat models for RP is scarce. We compared the retinal features of our *Lrat*$^{-/-}$ rat with those of the widely used Royal College of Surgeons (RCS) rat, which was the first described, and is a commonly used animal model for inherited retinal degeneration [30,31,61–67]. Additionally, it has been extensively used for testing the efficiency of the transplantation of RPE cells [32]. The RCS rat harbors a (spontaneous) mutation in the *Mertk* gene, which is uniquely and highly expressed in the RPE. *Mertk* deficient animals fail to phagocytose shed PR outer segments that accumulate in the subretinal space. Subsequently, the PRs die, which may interfere with the assessment of therapeutic strategies.
Despite the apparent advantages of a rat model with larger eyes, photoreceptor debris accumulates in the subretinal space, initiating spontaneous retinal degeneration and hampering experimental treatment modalities [33].

In conclusion, our newly developed *Lrat*$^{-/-}$ rat model is based on an existing patient population. It is an RD model without debris in the subretinal space. Crucially, the rat eye is large enough to perform complex procedures such as subretinal injections, suprachoroidal injections and RPE sheet transplantations. This model will be very useful for developing therapeutic approaches and determining therapeutic windows for this patient group, and possibly also for other RDs.

Supplementary Materials: please see Chapter 9: "Appendices".

Acknowledgments: the authors thank Mary van Schooneveld for the thourough clinical examination of the patients, Leon Begthel for his help during the *in vivo* studies and Roos-Sanne Verkerk for her hands-on help with the molecular biology work in the lab. Additionally, we thank Marije Wolvers for her help with the methodology and statistics.

References

1. Chelstowska, S.; Widjaja-Adhi, M.A.K.; Silvaroli, J.A.; Golczak, M. Impact of LCA-Associated E14L LRAT Mutation on Protein Stability and Retinoid Homeostasis. *Biochemistry* **2017**, *56*, 4489–4499.
2. Den Hollander, A.I.; Lopez, I.; Yzer, S.; Zonneveld, M.N.; Janssen, I.M.; Strom, T.M.; Hehir-Kwa, J.Y.; Veltman, J.A.; Arends, M.L.; Meitinger, T.; et al. Identification of novel mutations in patients with Leber congenital amaurosis and juvenile RP by genome-wide homozygosity mapping with SNP microarrays. *Investig. Ophthalmol. Vis. Sci.* **2007**, *48*, 5690–5698.
3. Dev Borman, A.; Ocaka, L.A.; Mackay, D.S.; Ripamonti, C.; Henderson, R.H.; Moradi, P.; Hall, G.; Black, G.C.; Robson, A.G.; Holder, G.E.; et al. Early onset retinal dystrophy due to mutations in LRAT: Molecular analysis and detailed phenotypic study. *Investig. Ophthalmol. Vis. Sci.* **2012**, *53*, 3927–3938.
4. Littink, K.W.; van Genderen, M.M.; van Schooneveld, M.J.; Visser, L.; Riemslag, F.C.; Keunen, J.E.; Bakker, B.; Zonneveld, M.N.; den Hollander, A.I.; Cremers, F.P.; et al. A homozygous frameshift mutation in LRAT causes retinitis punctata albescens. *Ophthalmology* **2012**, *119*, 1899–1906.
5. Redmond, T.M.; Yu, S.; Lee, E.; Bok, D.; Hamasaki, D.; Chen, N.; Goletz, P.; Ma, J.X.; Crouch, R.K.; Pfeifer, K. Rpe65 is necessary for production of 11-cis-vitamin A in the retinal visual cycle. *Nat. Genet.* **1998**, *20*, 344–351.
6. Batten, M.L.; Imanishi, Y.; Maeda, T.; Tu, D.C.; Moise, A.R.; Bronson, D.; Possin, D.; Van Gelder, R.N.; Baehr, W.; Palczewski, K. Lecithin-retinol acyltransferase is essential for accumulation of all-trans-retinyl esters in the eye and in the liver. *J. Biol. Chem.* **2004**, *279*, 10422–10432.
7. den Hollander, A.I.; Roepman, R.; Koenekoop, R.K.; Cremers, F.P. Leber congenital amaurosis: Genes, proteins and disease mechanisms. *Prog. Retin. Eye Res.* **2008**, *27*, 391–419.
8. Russell, S.; Bennett, J.; Wellman, J.A.; Chung, D.C.; Yu, Z.F.; Tillman, A.; Wittes, J.; Pappas, J.; Elci, O.; McCague, S.; et al. Efficacy and safety of voretigene neparvovec (AAV2-hRPE65v2) in patients with RPE65-mediated inherited retinal dystrophy: A randomised, controlled, open-label, phase 3 trial. *Lancet* **2017**, *390*, 849–860.
9. Maguire, A.M.; Russell, S.; Wellman, J.A.; Chung, D.C.; Yu, Z.F.; Tillman, A.; Wittes, J.; Pappas, J.; Elci, O.; Marshall, K.A.; et al. Efficacy, Safety, and Durability of Voretigene Neparvovec-rzyl in RPE65 Mutation-Associated Inherited Retinal Dystrophy: Results of Phase 1 and 3 Trials. *Ophthalmology* **2019**, *126*, 1273–1285.
10. Talib, M.; Boon, C.J.F. Retinal Dystrophies and the Road to Treatment: Clinical Requirements and Considerations. *Asia Pac. J. Ophthalmol.* **2020**, *9*, 159–179.
11. Thompson, D.A.; Li, Y.; McHenry, C.L.; Carlson, T.J.; Ding, X.; Sieving, P.A.; Apfelstedt-Sylla, E.; Gal, A. Mutations in the gene encoding lecithin retinol acyltransferase are associated with early-onset severe retinal dystrophy. *Nat. Genet.* **2001**, *28*, 123–124.
12. Senechal, A.; Humbert, G.; Surget, M.O.; Bazalgette, C.; Bazalgette, C.; Arnaud, B.; Arndt, C.; Laurent, E.; Brabet, P.; Hamel, C.P. Screening genes of the retinoid metabolism: Novel LRAT mutation in leber congenital amaurosis. *Am. J. Ophthalmol.* **2006**, *142*, 702–704.

13. Talib, M.; van Schooneveld, M.J.; van Duuren, R.J.G.; Van Cauwenbergh, C.; Ten Brink, J.B.; De Baere, E.; Florijn, R.J.; Schalij-Delfos, N.E.; Leroy, B.P.; Bergen, A.A.; et al. Long-Term Follow-Up of Retinal Degenerations Associated With LRAT Mutations and Their Comparability to Phenotypes Associated With RPE65 Mutations. *Transl. Vis. Sci. Technol.* **2019**, *8*, 24.
14. Ruiz, A.; Winston, A.; Lim, Y.H.; Gilbert, B.A.; Rando, R.R.; Bok, D. Molecular and biochemical characterization of lecithin retinol acyltransferase. *J. Biol. Chem*. **1999**, *274*, 3834–3841.
15. Zolfaghari, R.; Ross, A.C. Lecithin:retinol acyltransferase from mouse and rat liver. CDNA cloning and liver-specific regulation by dietary vitamin a and retinoic acid. *J. Lipid Res*. **2000**, *41*, 2024–2034.
16. Zolfaghari, R.; Ross, A.C. Cloning, gene organization and identification of an alternative splicing process in lecithin:retinol acyltransferase cDNA from human liver. *Gene* **2004**, *341*, 181–188.
17. Zolfaghari, R.; Wang, Y.; Chen, Q.; Sancher, A.; Ross, A.C. Cloning and molecular expression analysis of large and small lecithin:retinol acyltransferase mRNAs in the liver and other tissues of adult rats. *Biochem. J.* **2002**, *368*, 621–631.
18. Wright, C.B.; Chrenek, M.A.; Foster, S.L.; Duncan, T.; Redmond, T.M.; Pardue, M.T.; Boatright, J.H.; Nickerson, J.M. Complementation test of Rpe65 knockout and tvrm148. *Investig. Ophthalmol. Vis. Sci.* **2013**, *54*, 5111–5122.
19. Fan, J.; Rohrer, B.; Frederick, J.M.; Baehr, W.; Crouch, R.K. Rpe65$^{-/-}$ and Lrat$^{-/-}$ mice: Comparable models of leber congenital amaurosis. *Investig. Ophthalmol. Vis. Sci.* **2008**, *49*, 2384–2389.
20. Van Hooser, J.P.; Aleman, T.S.; He, Y.G.; Cideciyan, A.V.; Kuksa, V.; Pittler, S.J.; Stone, E.M.; Jacobson, S.G.; Palczewski, K. Rapid restoration of visual pigment and function with oral retinoid in a mouse model of childhood blindness. *Proc. Natl. Acad. Sci. USA* **2000**, *97*, 8623–8628.
21. Scholl, H.P.; Moore, A.T.; Koenekoop, R.K.; Wen, Y.; Fishman, G.A.; van den Born, L.I.; Bittner, A.; Bowles, K.; Fletcher, E.C.; Collison, F.T.; et al. Safety and Proof-of-Concept Study of Oral QLT091001 in Retinitis Pigmentosa Due to Inherited Deficiencies of Retinal Pigment Epithelial 65 Protein (RPE65) or Lecithin:Retinol Acyltransferase (LRAT). *PLoS ONE* **2015**, *10*, e0143846.
22. Batten, M.L.; Imanishi, Y.; Tu, D.C.; Doan, T.; Zhu, L.; Pang, J.; Glushakova, L.; Moise, A.R.; Baehr, W.; Van Gelder, R.N.; et al. Pharmacological and rAAV gene therapy rescue of visual functions in a blind mouse model of Leber congenital amaurosis. *PLoS Med.* **2005**, *2*, e333.
23. Roman, A.J.; Boye, S.L.; Aleman, T.S.; Pang, J.J.; McDowell, J.H.; Boye, S.E.; Cideciyan, A.V.; Jacobson, S.G.; Hauswirth, W.W. Electroretinographic analyses of Rpe65-mutant rd12 mice: Developing an in vivo bioassay for human gene therapy trials of Leber congenital amaurosis. *Mol. Vis.* **2007**, *13*, 1701–1710.
24. Kostic, C.; Crippa, S.V.; Pignat, V.; Bemelmans, A.P.; Samardzija, M.; Grimm, C.; Wenzel, A.; Arsenijevic, Y. Gene therapy regenerates protein expression in cone photoreceptors in Rpe65(R91W/R91W) mice. *PLoS ONE* **2011**, *6*, e16588.
25. Pang, J.; Boye, S.E.; Lei, B.; Boye, S.L.; Everhart, D.; Ryals, R.; Umino, Y.; Rohrer, B.; Alexander, J.; Li, J.; et al. Self-complementary AAV-mediated gene therapy restores cone function and prevents cone degeneration in two models of Rpe65 deficiency. *Gene* **2010**, *17*, 815–826.

26. Georgiadis, A.; Duran, Y.; Ribeiro, J.; Abelleira-Hervas, L.; Robbie, S.J.; Sünkel-Laing, B.; Fourali, S.; Gonzalez-Cordero, A.; Cristante, E.; Michaelides, M.; et al. Development of an optimized AAV2/5 gene therapy vector for Leber congenital amaurosis owing to defects in RPE65. *Gene* **2016**, *23*, 857–862.
27. Bemelmans, A.P.; Kostic, C.; Crippa, S.V.; Hauswirth, W.W.; Lem, J.; Munier, F.L.; Seeliger, M.W.; Wenzel, A.; Arsenijevic, Y. Lentiviral gene transfer of RPE65 rescues survival and function of cones in a mouse model of Leber congenital amaurosis. *PLoS Med.* **2006**, *3*, e347.
28. Li, Y.; Tsai, Y.T.; Hsu, C.W.; Erol, D.; Yang, J.; Wu, W.H.; Davis, R.J.; Egli, D.; Tsang, S.H. Long-term safety and efficacy of human-induced pluripotent stem cell (iPS) grafts in a preclinical model of retinitis pigmentosa. *Mol. Med.* **2012**, *18*, 1312–1319.
29. Ben M'Barek, K.; Habeler, W.; Plancheron, A.; Jarraya, M.; Regent, F.; Terray, A.; Yang, Y.; Chatrousse, L.; Domingues, S.; Masson, Y.; et al. Human ESC-derived retinal epithelial cell sheets potentiate rescue of photoreceptor cell loss in rats with retinal degeneration. *Sci. Transl. Med.* **2017**, *9*, 421.
30. Strauss, O.; Stumpff, F.; Mergler, S.; Wienrich, M.; Wiederholt, M. The Royal College of Surgeons rat: An animal model for inherited retinal degeneration with a still unknown genetic defect. *Acta Anat.* **1998**, *162*, 101–111.
31. D'Cruz, P.M.; Yasumura, D.; Weir, J.; Matthes, M.T.; Abderrahim, H.; LaVail, M.M.; Vollrath, D. Mutation of the receptor tyrosine kinase gene Mertk in the retinal dystrophic RCS rat. *Hum. Mol. Genet.* **2000**, *9*, 645–651.
32. Koster, C.; Wever, K.E.; Wagstaff, P.E.; Hirk, K.; Hooijmans, C.R.; Bergen, A.A. A Systematic Review on Transplantation Studies of the Retinal Pigment Epithelium in Animal Models. I*nt. J. Mol. Sci.* **2020**, *21*, 2719.
33. Valter, K.; Maslim, J.; Bowers, F.; Stone, J. Photoreceptor dystrophy in the RCS rat: Roles of oxygen, debris, and bFGF. *Investig. Ophthalmol. Vis. Sci.* **1998**, *39*, 2427–2442.
34. Owusu, S.A.; Ross, A.C. Retinoid Homeostatic Gene Expression in Liver, Lung and Kidney: Ontogeny and Response to Vitamin A-Retinoic Acid (VARA) Supplementation from Birth to Adult Age. *PLoS ONE* **2016**, *11*, e0145924.
35. Hu, J.; Li, P.; Shi, B.; Tie, J. Importin β1 mediates nuclear import of the factors associated with nonsense-mediated RNA decay. *Biochem. Biophys. Res. Commun.* **2021**, *542*, 34–39.
36. Gong, Q.; Stump, M.R.; Zhou, Z. Position of premature termination codons determines susceptibility of hERG mutations to nonsense-mediated mRNA decay in long QT syndrome. *Gene* **2014**, *539*, 190–197.
37. Zarraga, I.G.; Zhang, L.; Stump, M.R.; Gong, Q.; Vincent, G.M.; Zhou, Z. Nonsense-mediated mRNA decay caused by a frameshift mutation in a large kindred of type 2 long QT syndrome. *Heart Rhythm* **2011**, *8*, 1200–1206.
38. Seeger, T.; Shrestha, R.; Lam, C.K.; Chen, C.; McKeithan, W.L.; Lau, E.; Wnorowski, A.; McMullen, G.; Greenhaw, M.; Lee, J.; et al. A Premature Termination Codon Mutation in MYBPC3 Causes Hypertrophic Cardiomyopathy via Chronic Activation of Nonsense-Mediated Decay. *Circulation* **2019**, *139*, 799–811.

39. Ahmed, J.N.; Ali, R.G.; Warr, N.; Wilson, H.M.; Bellchambers, H.M.; Barratt, K.S.; Thompson, A.J.; Arkell, R.M. A murine Zic3 transcript with a premature termination codon evades nonsense-mediated decay during axis formation. *Dis. Model. Mech* **2013**, *6*, 755–767.
40. Koenekoop, R.K.; Sui, R.; Sallum, J.; van den Born, L.I.; Ajlan, R.; Khan, A.; den Hollander, A.I.; Cremers, F.P.; Mendola, J.D.; Bittner, A.K.; et al. Oral 9-cis retinoid for childhood blindness due to Leber congenital amaurosis caused by RPE65 or LRAT mutations: An open-label phase 1b trial. *Lancet* **2014**, *384*, 1513–1520.
41. Watson, C. Chapter 25—Visual System. In *The Mouse Nervous System*; Watson, C., Paxinos, G., Puelles, L., Eds.; *Academic Press: San Diego*, CA, USA, **2012**; pp. 646–652.
42. Carter-Dawson, L.D.; LaVail, M.M. Rods and cones in the mouse retina—I: Structural analysis using light and electron microscopy. *J. Comp. Neurol.* **1979**, *188*, 245–262.
43. Carter-Dawson, L.D.; LaVail, M.M. Rods and cones in the mouse retina—II: Autoradiographic analysis of cell generation using tritiated thymidine. *J. Comp. Neurol.* **1979**, *188*, 263–272.
44. Patel, U.; Boucher, M.; de Léséleuc, L.; Visintini, S. Voretigene Neparvovec: An Emerging Gene Therapy for the Treatment of Inherited Blindness. In *CADTH Issues in Emerging Health Technologies*; Canadian Agency for Drugs and Technologies in Health: Ottawa, ON, Canada, **2016**; pp. 1–11.
45. Miraldi Utz, V.; Coussa, R.G.; Antaki, F.; Traboulsi, E.I. Gene therapy for RPE65-related retinal disease. *Ophthalmic Genet.* **2018**, *39*, 671–677.
46. Kang, C.; Scott, L.J. Voretigene Neparvovec: A Review in RPE65 Mutation-Associated Inherited Retinal Dystrophy. *Mol. Diagn.* **2020**, *24*, 487–495.
47. Ding, K.; Shen, J.; Hafiz, Z.; Hackett, S.F.; e Silva, R.L.; Khan, M.; Lorenc, V.E.; Chen, D.; Chadha, R.; Zhang, M.; et al. AAV8- vectored suprachoroidal gene transfer produces widespread ocular transgene expression. *J. Clin. Investig.* **2019**, *129*, 4901–4911.
48. Maeda, T.; Lee, M.J.; Palczewska, G.; Marsili, S.; Tesar, P.J.; Palczewski, K.; Takahashi, M.; Maeda, A. Retinal pigmented epithelial cells obtained from human induced pluripotent stem cells possess functional visual cycle enzymes in vitro and in vivo. *J. Biol. Chem.* **2013**, *288*, 34484–34493.
49. Gouras, P.; Kong, J.; Tsang, S.H. Retinal degeneration and RPE transplantation in $Rpe65^{-/-}$ mice. *Investig. Ophthalmol. Vis. Sci.* **2002**, *43*, 3307–3311.
50. Ilmarinen, T.; Hiidenmaa, H.; Koobi, P.; Nymark, S.; Sorkio, A.; Wang, J.H.; Stanzel, B.V.; Thieltges, F.; Alajuuma, P.; Oksala, O.; et al. Ultrathin Polyimide Membrane as Cell Carrier for Subretinal Transplantation of Human Embryonic Stem Cell Derived Retinal Pigment Epithelium. *PLoS ONE* **2015**, *10*, e0143669.
51. Kamao, H.; Mandai, M.; Okamoto, S.; Sakai, N.; Suga, A.; Sugita, S.; Kiryu, J.; Takahashi, M. Characterization of human induced pluripotent stem cell-derived retinal pigment epithelium cell sheets aiming for clinical application. *Stem Cell Rep.* **2014**, *2*, 205–218.
52. Yaji, N.; Yamato, M.; Yang, J.; Okano, T.; Hori, S. Transplantation of tissue-engineered retinal pigment epithelial cell sheets in a rabbit model. *Biomaterials* **2009**, *30*, 797–803.
53. Kanemura, H.; Go, M.J.; Shikamura, M.; Nishishita, N.; Sakai, N.; Kamao, H.; Mandai, M.; Morinaga, C.; Takahashi, M.; Kawamata, S. Tumorigenicity studies of induced pluripotent stem cell (iPSC)-derived retinal pigment epithelium (RPE) for the treatment of age-related macular degeneration. *PLoS ONE* **2014**, *9*, e85336.

54. Diniz, B.; Thomas, P.; Thomas, B.; Ribeiro, R.; Hu, Y.; Brant, R.; Ahuja, A.; Zhu, D.; Liu, L.; Koss, M.; et al. Subretinal implantation of retinal pigment epithelial cells derived from human embryonic stem cells: Improved survival when implanted as a monolayer. *Investig. Ophthalmol. Vis. Sci.* **2013**, *54*, 5087–5096.
55. Kaplan, H.; Chiang, C.-W.; Chen, J.; Song, S.-K. Vitreous volume of the mouse measured by quantitative high-resolution MRI. *Investig. Ophthalmol. Vis. Sci.* **2010**, *51*, 4414.
56. Sha, O.; Kwong, W. Postnatal developmental changes of vitreous and lens volumes in Sprague-Dawley rats. *Neuroembryol. Aging* **2006**, *4*, 183–188.
57. Aitman, T.; Dhillon, P.; Geurts, A.M. A RATional choice for translational research? *Dis. Model. Mech.* **2016**, *9*, 1069–1072.
58. Ellenbroek, B.; Youn, J. Rodent models in neuroscience research: Is it a rat race? *Dis. Model. Mech.* **2016**, *9*, 1079–1087.
59. Timberlake, W. Integrating niche-related and general process approaches in the study of learning. *Behav. Process.* **2001**, *54*, 79–94.
60. Timberlake, W. Niche-related learning in laboratory paradigms: The case of maze behavior in Norway rats. *Behav. Brain Res.* **2002**, *134*, 355–374.
61. Sheedlo, H.J.; Gaur, V.; Li, L.X.; Seaton, A.D.; Turner, J.E. Transplantation to the diseased and damaged retina. *Trends Neurosci.* **1991**, *14*, 347–350.
62. Yu, D.Y.; Cringle, S.J. Retinal degeneration and local oxygen metabolism. *Exp. Eye Res.* **2005**, *80*, 745–751.
63. Nakazawa, M.; Hara, A.; Ishiguro, S.I. Optical Coherence Tomography of Animal Models of Retinitis Pigmentosa: From Animal Studies to Clinical Applications. *Biomed. Res. Int.* **2019**, *2019*, 8276140.
64. LaVail, M.M.; Yasumura, D.; Matthes, M.T.; Yang, H.; Hauswirth, W.W.; Deng, W.T.; Vollrath, D. Gene Therapy for MERTK- Associated Retinal Degenerations. *Adv. Exp. Med. Biol.* **2016**, *854*, 487–493.
65. Rösch, S.; Aretzweiler, C.; Müller, F.; Walter, P. Evaluation of Retinal Function and Morphology of the Pink-Eyed Royal College of Surgeons (RCS) Rat: A Comparative Study of in Vivo and in Vitro Methods. *Curr. Eye Res.* **2017**, *42*, 273–281.
66. Ryals, R.C.; Andrews, M.D.; Datta, S.; Coyner, A.S.; Fischer, C.M.; Wen, Y.; Pennesi, M.E.; McGill, T.J. Long-term Characterization of Retinal Degeneration in Royal College of Surgeons Rats Using Spectral-Domain Optical Coherence Tomography. *Investig. Ophthalmol. Vis. Sci.* **2017**, *58*, 1378–1386.
67. Zhao, T.; Li, Y.; Weng, C.; Yin, Z. The changes of potassium currents in RCS rat Müller cell during retinal degeneration. *Brain Res.* **2012**, *1427*, 78–87.
68. Remy, S.; Chenouard, V.; Tesson, L.; Usal, C.; Ménoret, S.; Brusselle, L.; Heslan, J.M.; Nguyen, T.H.; Bellien, J.; Merot, J.; et al. Generation of gene-edited rats by delivery of CRISPR/Cas9 protein and donor DNA into intact zygotes using electroporation. *Sci. Rep.* **2017**, *7*, 16554.
69. Kobayashi, T.; Namba, M.; Koyano, T.; Fukushima, M.; Sato, M.; Ohtsuka, M.; Matsuyama, M. Successful production of genome-edited rats by the rGONAD method. *BMC Biotechnol.* **2018**, *18*, 19.

The most beautiful and most profound religious emotion that we can experience is the sensation of the mystical. And this mysticality is the power of all true science.

— Albert Einstein

Sodium-Iodate Injection Can Replicate Retinal Degenerative Disease Stages in Pigmented Mice and Rats: Non-Invasive Follow-Up Using OCT and ERG

Céline Koster, Koen T. van den Hurk, Jacoline B. ten Brink, Colby F. Lewallen, Boris V. Stanzel, Kapil Bharti, & Arthur A. Bergen

Int. J. Mol. Sci. **2022**, accepted for publication, DOI: 10.3390/ijms23062918

4

Abstract

Purpose: the lack of suitable animal models for (dry) age-related macular degeneration (AMD) has hampered therapeutic research into the disease, so far. In this study, pigmented rats and mice were systematically injected with various doses of sodium iodate (SI). After injection, the retinal structure and visual function were non-invasively characterized over time to obtain in-depth data on the suitability of these models for studying experimental therapies for retinal degenerative diseases, such as dry AMD.

Methods: SI was injected into the tail vein (i.v.) using a series of doses (0–70 mg/kg) in adolescent C57BL/6J mice and Brown Norway rats. The retinal structure and function were assessed non-invasively at baseline (day 1) and at several time points (1–3, 5, and 10-weeks) post-injection by scanning laser ophthalmoscopy (SLO), optical coherence tomography (OCT), and electroretinography (ERG).

Results: after the SI injection, retinal degeneration in mice and rats yielded similar results. The lowest dose (10 mg/kg) resulted in non-detectable structural or functional effects. An injection with 20 mg/kg SI did not result in an evident retinal degeneration as judged from the OCT data. In contrast, the ERG responses were temporarily decreased but returned to baseline within two-weeks. Higher doses (30, 40, 50, and 70 mg/kg) resulted in moderate to severe structural RPE and retinal injury and decreased the ERG amplitudes, indicating visual impairment in both mice and rat strains.

Conclusions: after the SI injections, we observed dose-dependent structural and functional pathological effects on the retinal pigment epithelium (RPE) and retina in the pigmented mouse and rat strains that were used in this study. Similar effects were observed in both species. In particular, a dose of 30 mg/kg seems to be suitable for future studies on developing experimental therapies. These relatively easily induced non-inherited models may serve as useful tools for evaluating novel therapies for RPE-related retinal degenerations, such as AMD.

Introduction

Age-related macular degeneration (AMD) is one of the major causes of visual impairment in the developed world [1–5]. The irreversible and non-treatable vision loss that is associated with AMD is a significant social burden, with a projected number of people with the disease around 288 million in 2040 worldwide [6]. Early detection and prevention are critical in increasing the likelihood of retaining good and functional vision [1].

Despite decades of research worldwide, the complex pathogenesis of AMD has not been fully elucidated yet [7]. In the early and intermediate stages, pathological hallmarks of AMD include the appearance of soft subretinal deposits and pigment alterations in the macular area of the retinal pigment epithelium (RPE). In advanced stages of the disease, "wet" and "dry" AMD can be distinguished. Wet AMD, also called neovascular AMD, is characterized by the abnormal growth of new (leaky) blood vessels through the RPE or into the neural retina of the eye. Dry AMD, also called geographic atrophy, is characterized by progressive atrophy of the RPE accompanied by the degeneration of the adjacent neural retina and choriocapillaris. Clinically, "dry" AMD is the most common form, whereas the "wet" form affects roughly 10–15 % of the patients, depending on ethnic group [8–13]. AMD onset and progression can, most likely, be delayed by refraining from smoking and dietary modifications. The wet form of AMD can be delayed by repeated anti-VEGF medication, but, to date, no cure for AMD exists once retinal damage has occurred [14].

While AMD affects multiple cell layers in the retina and also has a systemic component, the involvement of the retinal pigment epithelium (RPE) is key [15]. The RPE is a multifunctional single neuroepithelial cell layer that acts as a metabolic interface and retinal-blood barrier between the choroid and the neurosensory retina [16]. On the apical side, the photoreceptor cells line the RPE. On the basal side, the interposing Bruch's membrane (BM) separates the RPE from the choroidal microvasculature (choriocapillaris).

It is well known that multiple risk factors drive the pathogenesis of AMD, most prominently age, smoking, and genetic risk variation in multiple genes [5]. The latter include genes that are implicated in oxidative stress handling (*GPX4*), the complement system (*C9*, *CFI*, *CFH*), lipid metabolism (*APOE*, *ABCA1*, *PLTP*), and components of the extracellular matrix (*ARMS2-HTRA1*, *VTN*, *COL15/8A1*, *MMP9*, *MMP19*, *TIMP3*) [17–24].

Indeed, epidemiological, genetic, functional, physiological, and pathological studies support the hypothesis that, in particular, oxidative stress affecting the RPE is one of the main initial drivers of AMD [25–31]. Oxidative stress refers to elevated intracellular levels of reactive oxygen species (ROS) that cause damage to lipids, proteins, and DNA [32]. Local oxidative RPE stress is invoked by environmental and endogenous factors. There are two environmental risk factors for AMD (smoking and a high-fat diet) that increase the oxidative stress upon the retina and RPE [26,33,34].

Endogenous local oxidative stress factors on the RPE and retina include the daily renewal and digestion of (oxidized) photoreceptor outer segments, their intrinsically high metabolic rate, high dissolved oxygen concentration, and dependency on mitochondrial oxidative phosphorylation for proper function [35,36]. As a result, with aging, the RPE contains relatively high concentrations of oxidation-modified lipids and proteins, which probably contribute to the development of AMD over time [35,37,38]. Moreover, as people age, BM's permeability also decreases and a lipid wall builds up, hindering the reciprocal transport of nutrients and (oxidized) waste products between the RPE to the choroid [39,40]. Consequently, these oxidized molecules accumulate and the immune system is activated to clear them [41]. An excess of ROS can lead to nuclear and mitochondrial DNA damage, autophagy decay, and apoptosis of the RPE and photoreceptors [42]. Taking all the literature data together, there is strong evidence that oxidative stress leads to local RPE damage and eventually contributes AMD pathology over time [25,26,28,32,36,42,43].

Due to the complexity of AMD, the pathobiology of the disease has not yet been fully defined. Consequently, animal disease models of AMD have been reduced to more or less representing the critical disease symptoms. Therapeutic research into AMD has been hampered by the lack of suitable experimental models, both *in vivo* and *in vitro* [44]. Recently, a partial AMD cellular phenotype was replicated *in vitro* using an induced pluripotent stem cell-derived RPE culture harboring disease-associated *CFH* variants [45].

As described above, multiple mechanisms have been implicated in AMD, which are not fully represented in any genetically-modified animal model for monogenic retinal disease [45–47]. Some of these models represent, more or less, part of the AMD phenotype, such as the presence of drusenoid deposits [48–51]. As an alternative, chemically-induced models have been generated. The oxidizing chemical sodium iodate, $NaIO_3$ (SI), causes necroptosis of the RPE cells and damage to its adjacent cell layers through oxidative stress-related processes [52–54]. As described above, this is a relevant mechanism for the development of dry AMD, especially geographic atrophy [55]. Consequently, such a model could be used for experimental therapeutic studies of retinal degenerative diseases, such as dry AMD. SI has been used in a wide variety of animals, injection methods, and doses. The SI-induced retinal degeneration model has been used to evaluate the transplantation of various experimental RPE-cell-based therapies [56–58]. However, comparing various published studies is often difficult due to notable differences in the experimental setup, such as the administration method, dosage, selected animals, and analyses time [59].

In this study, we further refined this model of SI-induced retinal degeneration to allow for reproducible induction by intravenous injection. We carefully followed the animals after the SI injection using non-invasive techniques. The post-injection retinal structure, morphology, and function were assessed at several time points in two different pigmented rodent species. This relatively easy and the rapidly induced non-inherited model may serve as a useful tool for evaluating novel therapies for retinal degenerations that are primarily caused by RPE failure.

Materials and Methods

Animals

C57BL/6J mice were purchased at the Jackson Laboratory, and Brown Norway rats were purchased at Charles River. All the animals were kept on a light cycle of 12 h on/12 h off and were fed ad libitum. These studies were conducted in accordance with the ARVO Statement for the use of Animals in Ophthalmic and Vision Research and approved by the Netherlands' national animal welfare committee (AVD1140020172044). Both males and females were used in the mouse studies. Given the availability of animals at the time of purchase, we only used male rats. There is no evidence in the literature that sex difference has a major influence on RPE damage in the context of our studies. Still, it can be considered a possible study limitation. Mice were 3–4-months old at the start of the experiment, weighing 17–20 g, whereas rats were 8-weeks old, weighing 230–260 g.

Sodium Iodate Treatment

Sodium iodate (SI) (Sigma-Aldrich, Hamburg, Germany, CAS number 7681-55-2, $NaIO_3$) was freshly diluted in 0.9 % sodium chloride (NaCl) into different doses and filter-sterilized directly before use. Electroretinography (ERG), scanning laser ophthalmoscopy (SLO), and spectral-domain optical coherence tomography (OCT) baseline measurements were recorded before the treatment. Subsequent to the baseline measurements, the animals were kept on a heating pad, and the tail vein was stimulated by a heating lamp. The animals were injected into the tail vein using a series of $NaIO_3$ doses in 100 µL 0.9 % NaCl, see Supplementary Table S1. The animals were randomly divided over the groups (using the tool at www.graphpad.com (accessed on 12 October 2017)).

Visual Follow-Up and Drop-Outs

The animals' retinal structure and visual function were followed over time using ERG and SLO-OCT measurements. The measurements were performed at day 1 (baseline), 1-week, 2-weeks, 3-weeks, 1-month, and 2-months post-injection. Daily health checks were done, and the weight was measured at least weekly. There were no drop-outs in the group of mice. A total of two rats received a dose of 70 mg/kg and were euthanized, according to the guidelines set in the license (AVD1140020172044), because their weight loss was more than 20 % within 3-days. They were excluded from the study.

Electroretinography

The animals were kept in total darkness for at least 2 h before the scotopic measurements and were anesthetized with a mixture of ketamine (65 mg/kg for rats; 100 mg/kg for mice) and xylazine (7.5 mg/kg for rats; 10 mg/kg for mice) intraperitoneally. The eyes were locally anesthetized using tetracaine-hydrochloride drops (1 % *w/v*) and were dilated using tropicamide (0.5 % *w/v*) and atropine (1 % *w/v*) drops. Hylocomod drops were applied to maintain corneal hydration at all times. From this moment onwards, the eye was kept moist using Hylocomod drops that were applied regularly on the animal's eye. The animals were placed in the RETImap full flash Ganzfeld (Roland Consult, Brandenburg, Germany) using a carrier table kept at 37 °C. The body temperature was carefully monitored during all the measurements. ERGs were recorded using a gold wire loop which was placed on the cornea of both eyes. A gold electrode was placed in the mouth serving as a reference electrode for both eyes. A subcutaneous needle near the tail served as a ground electrode. See Supplementary Table S2 for the light intensities, the number of traces that were used for averaging, and the flashes' interval. The ERG traces were 350 ms long utilizing 512 data points.

All the data were systematically analyzed, without human intervention, using a custom Matlab script. The data were zero-centered by averaging the signal before the stimulus (<20 ms) and subtracting the resultant from the entire trace. A low-pass filter (4^{th} order, 30 Hz (for the b-wave) and 235 Hz (for the a-wave)) was applied, in both the forward and backward direction, to remove noise and the oscillatory potentials (OPs) without phase-shifting the time-series data. The frequency 30 Hz is well below the minimum expected frequency, and 235 Hz resembles the expected maximum frequency of Ops in rats [103].

The *findpeaks* function in Matlab was used to find the latencies of the a- and b-waves in the filtered data. The magnitudes of the unfiltered signal at the selected latencies were characterized as the values for the b-wave and the absolute a-wave amplitude. The absolute a-wave was subtracted from the value of the b-wave amplitude to calculate the absolute b-wave amplitude. The Flicker properties were determined from the original, unfiltered trace, see Supplementary Figure S1. The time to the first peak (P1) and the amplitude of the second peak (P2) were identified. The b-wave, a-wave and flicker properties of each group, at each treatment day, were averaged and normalized to the corresponding 30 $cd{\cdot}s/m^2$ response from the control group (see Supplementary Figure S2).

Scanning Laser Ophthalmoscopy (SLO) and Optical Coherence Tomography (OCT)

The SLO and OCT measurements were done subsequently to the ERG measurements. Detailed methods are described elsewhere [104,105]. In short, we used a commercially available system (Spectralis® Heidelberg Engineering combined, Heidelberg, Germany) that was modified for use with animals (Medical Workshop, Groningen, The Netherlands). After ERG measurements, the animals received another tetracaine hydrochloride eye drop, and a contact lens (2.7 mm in diameter for mice, 5.2 mm in diameter for rats; Cantor-Nissel, Brackley, UK) was placed. The standard 30° field of view equipment set was used. The animals were placed on a custom-made heated holder, the eyes were kept moist using Hylocomod eye drops (Ursapharm, Saarland, Germany), and the body temperature was monitored. Imaging was done using the Eye Explorer software version 1.9.14.0 (Heidelberg Engineering, Heidelberg, Germany). For fundus imaging (infra-red reflection SLO), the intensity was adjusted to prevent overexposure. OCT imaging was performed using a volume scan (57 frames (ART), 786 A-scans, 30°×25°, 61 scans, Δ120 μm, 8.8 scans per second). The reference arm was adjusted according to the manufacturer's instructions. Whenever possible, the follow-up function was used to ensure the accurate thickness profiles between the time points. Frame analysis was done on a total of 5 single OCT scans and the corresponding thickness profiles. The chosen scans were the crossing of the optic nerve (ON = 0), the middle superior section (ON + 10), the superior section (ON + 20), the middle inferior section (ON–10), and the inferior section (ON–20). The total retinal thickness was determined within each selected OCT scan with 1 mm intervals, with a 0.5 mm minimum distance from the optic nerve. During recovery, the eyes were treated with Vidisic ® Carbogel eyegel (Bausch + Lomb; Brussel, Belgium).

Statistical Analyses Performed on OCT and ERG Data

The data were analyzed using one- or two-way ANOVA analyses, ANOVA analyses of the log-transformed data, and the Kruskal–Wallis analyses with a post hoc Bonferroni test to determine the statistical significance of all data. Similar *p*-values were obtained using all tests. *p*-values are reported: ns: not significant, *: $p \leq 0.05$, **: $p \leq 0.01$, ***: $p \leq 0.001$, and ****: $p \leq 0.0001$.

Results

Sodium Iodate (SI) Injections in Mice and Rats

A total of twelve three-to-four-month-old C57BL/6J and eighteen eight-week-old Brown Norway rats received a single intravenous injection with sodium iodate (SI). Additionally, four mice and four rats received a single intravenous injection with 0.9 % NaCl (saline; 0 mg/kg SI). This group served as a control group. A wide range of SI concentrations was used (0–70 mg/kg) to map a dose-dependent retinal degeneration and determine a potential model for experimental retinal tissue transplantations (see Supplementary Table S1). General health checks and weight progression graphs did not show any toxicologic effects up to 50 mg/kg (see Supplementary Figure S2). The animals were followed non-invasively after the injections using scanning laser ophthalmoscopy (SLO), optical coherence tomography (OCT), and electroretinography (ERG).

In Vivo Retinal Imaging Using an SLO-Based OCT System in Mice and Rats

To determine the retinal morphology after the SI treatment, the mice and rats were followed over time non-invasively using an SLO-based spectral domain-OCT system. Representative OCT images are shown for mice in Figure 1 and rats in Figure 2. At the baseline (day 1: before injection), well-defined retinal layers were visible for all the animals. The retinal morphology of the control animals (0 mg/kg group) did not change over time. Similarly, minor to no changes were visible for the 10 and 20 mg/kg groups.

In the 30 mg/kg groups, no retinal degeneration was visible on the OCT images within the first week. In contrast, at 13-days and later, RPE degeneration and disruption of the retinal layers started to show. The degeneration worsened over time without clear regeneration in the later stages. For the 40, 50, and 70 mg/kg groups, retinal thinning was visible within a week, and major retinal degeneration was visible from two-weeks onwards. The effects of the SI-treatments on the retinal structure were assessed using descriptive images (Figure 1 and 2) as well as a quantitative approach (Figure 3).

The retinal thickness was controlled and quantified consistently utilizing the manufacturer's software and compared between the treatment groups. Our data and analyses suggest that in the 10 and 20 mg/kg groups, the thickness of the retina did not change up to the end of the experiment (62-days). The 30 mg/kg dose appeared to cause a moderate late-onset (two-weeks post-treatment) retinal degeneration. The 40, 50, and 70 mg/kg dose groups showed a relative extreme thinning of the retina already within one week. Thinning of the retina did not seem to be reversible over time for the duration of the experiment (62-days post-injection).

Our data appears to show a preferential loss of the outer retinal layers. However, upon detailed analysis, we were not able to quantify this statistically. We obtained SLO images off all animals that were included in this study as well. However, we did not find any observable differences between the treatment groups (raw data available upon request). At the end of the experiment, we could compare all groups, and we annotated the retinal thinning as "none" in the 0, 10, and 20 mg/kg groups, "intermediate" in the 30 mg/kg group and "high" in the 40, 50, and 70 mg/kg groups.

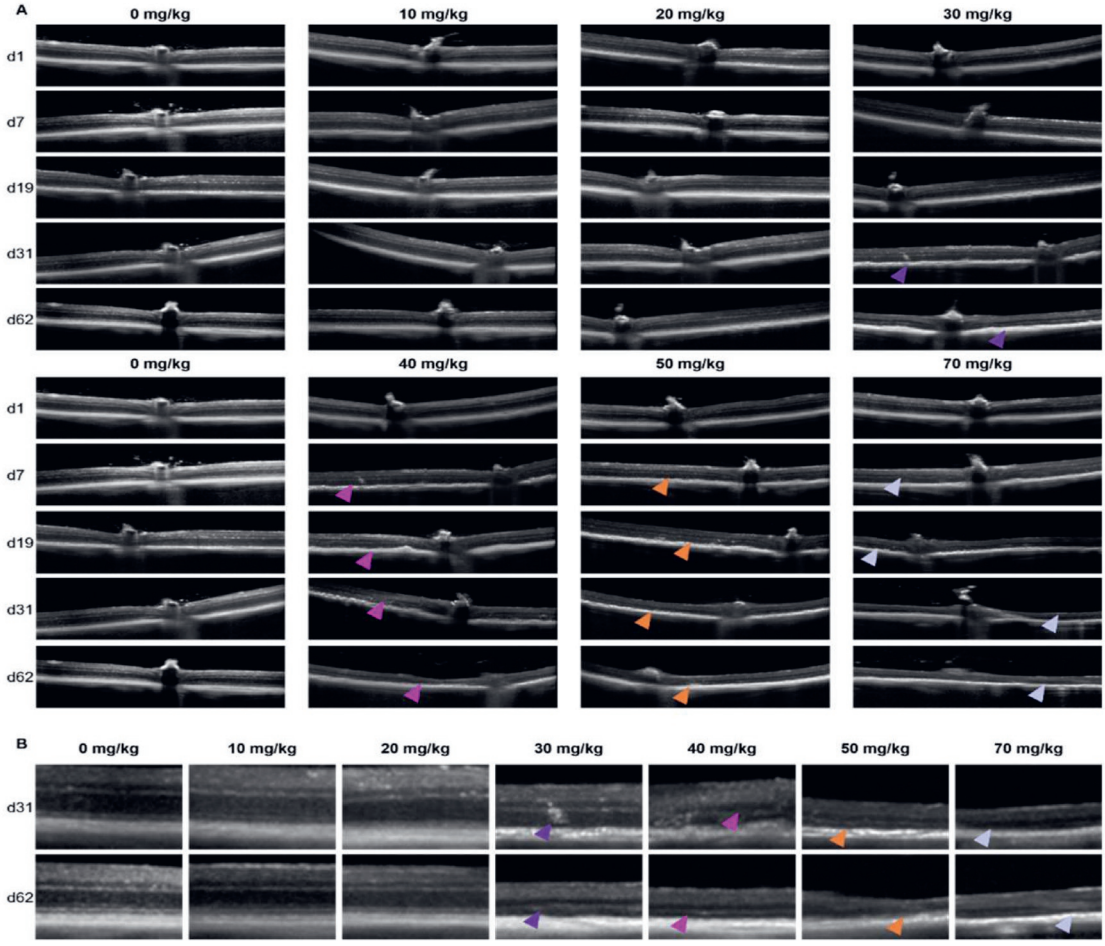

Figure 1. Representative serial OCT images of C57BL/6J mice of the central retina (**A**) and a magnification at the later timepoints (**B**) are shown. Serial scans are shown from single animals within the treatment group. In panel (**A**) the doses are horizontally shown in increasing concentration. The day of follow-up is shown vertically. No clear effects were observed for the 10 and 20 mg/kg groups compared to the control. Retinal degenerations was observed in all other groups. This is also better visible in panel (**B**), where the zoomed-in scans are shown per concentration SI (horizontally) and the later follow-up times (vertically). In the 30 mg/kg treatment group, retinal thinning started to show roughly 1 month post-injection (purple arrows). More drastic effects at the end of the experiments were observed for the 40 (pink arrows), 50 (orange arrows) and 70 mg/kg (lilac arrows) treatment groups. Quantification of the overall retinal thickness is shown in Figure 3.

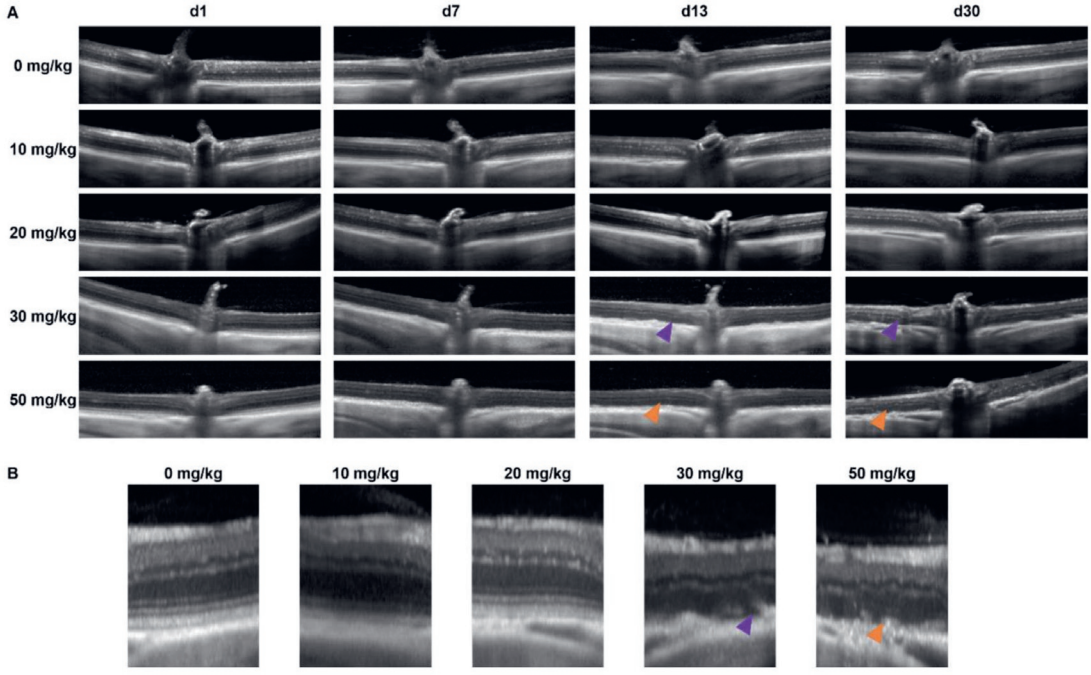

Figure 2. Representative serial OCT images of Brown Norway rats of the central retina (**A**) and a magnification at the later time points (**B**) are shown. Serial scans are shown from single animals within the treatment group. In panel (**A**) the doses are vertically shown in increasing concentration. The day of the follow-up is shown horizontally. No clear effects were observed for the 10 and 20 mg/kg groups compared to the control. Retinal degeneration is observed in both the 30 (purple arrows) and 50 mg/kg (orange arrows) groups at the later time points. Quantification of the overall retinal thickness is shown in Figure 3.

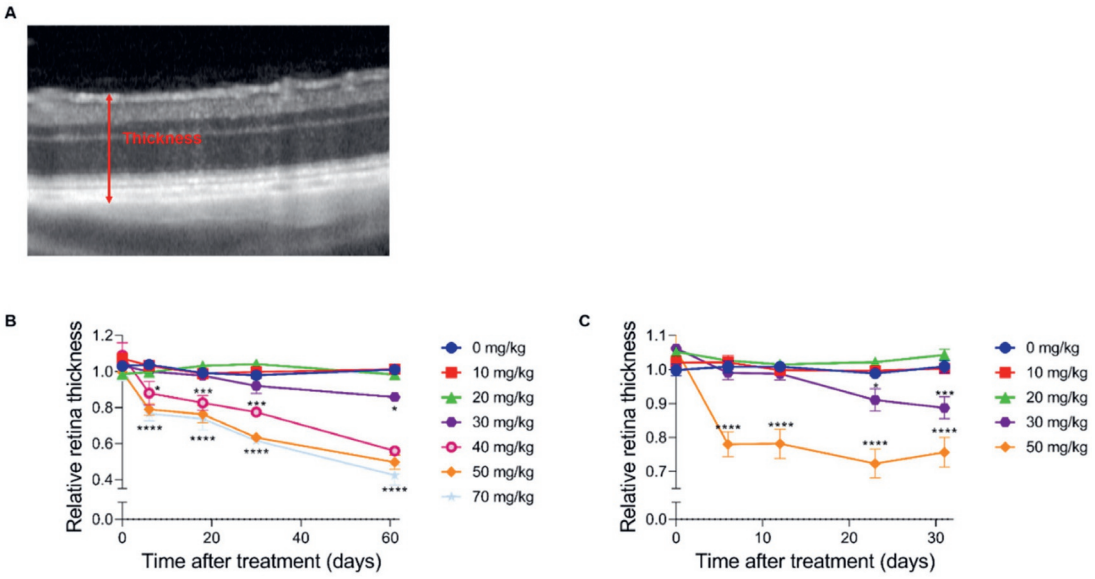

Figure 3. A quantitative analysis of the full retina thickness. The degeneration after SI injection was quantified in C57BL/6J mice (**B**) and Brown Norway rats (**C**) using the full thickness of the retina (red arrow) (**A**) (n = 4 per group). No significant effects were observed in both species for the 10 and 20 mg/kg treatment group compared to the control group (0 mg/kg). At two months post-injection, a thickness of ±90 % of its original thickness was observed in the 30 mg/kg treatment group. More dramatic effects were observed in the higher treatment groups (40, 50, and 70 mg/kg). The degeneration started to show within a week post-injection. A relative thickness of 40–60 % was observed two months post-injection. The results are presented as the mean ± the standard deviation. *: $p \leq 0.05$, ***: $p \leq 0.001$ and ****: $p \leq 0.0001$.

In Vivo Assessment of the Retinal Function Using ERG in Mice and Rats: A General Overview

We performed electrophysiological studies in both the mice and rats to assess the visual function after SI treatment. We measured between one week and two months post- injection. Scotopic ERG traces are presented for C57BL/6J mice (Figure 4) and Brown Norway rats (Figure 5). It appears that the lower doses (0 and 10 mg/kg) did not have an obvious impact on the electrophysiological response of the eye. However, a 20 mg/kg dose seemed to cause a temporary effect around day seven post-injection. Doses that were equal and greater than 30 mg/kg caused a non-recoverable and immediate decrease in the response magnitude. The higher doses (40, 50, and 70 mg/kg) almost completely eliminated the recordable a- and b-waves, oscillatory potentials, and 9 Hz-flicker responses in both species. Thus, we observed a dose-dependent functional effect after SI treatment. No significant differences between control rats and mice ERG responses were observed (see Supplementary Figure S2).

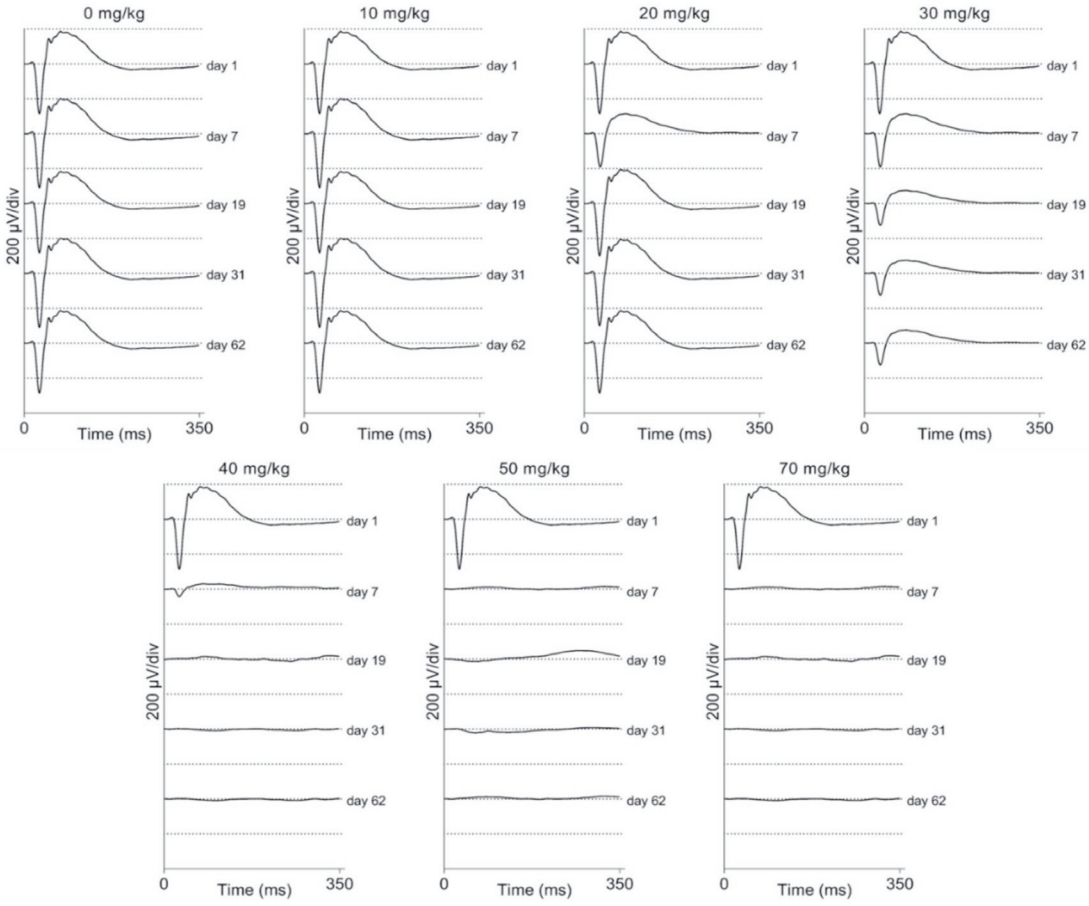

Figure 4. Averaged scotopic electroretinograms are shown for C57BL/6J mice (n = 4 per group). The averaged traces per treatment group and per day of follow-up are plotted. No difference can be observed between the 10 mg/kg group and the control group by eye. A temporary effect was seen for the 20 mg/kg group: a slightly decreased response was seen a week post-injection. A moderate effect was seen for the 30 mg/kg group: decreased responses were observed from seven-days post-injection onwards. This effect is larger later in time but seems stable after one-month post-injection. Direct and drastic effects were observed for higher treatment groups (40, 50, and 70 mg/kg). ERG responses were (almost) completely not recordable from one-week post-injection onwards. Similar effects were observed in ERG recordings from Brown Norway rats (Figure 5).

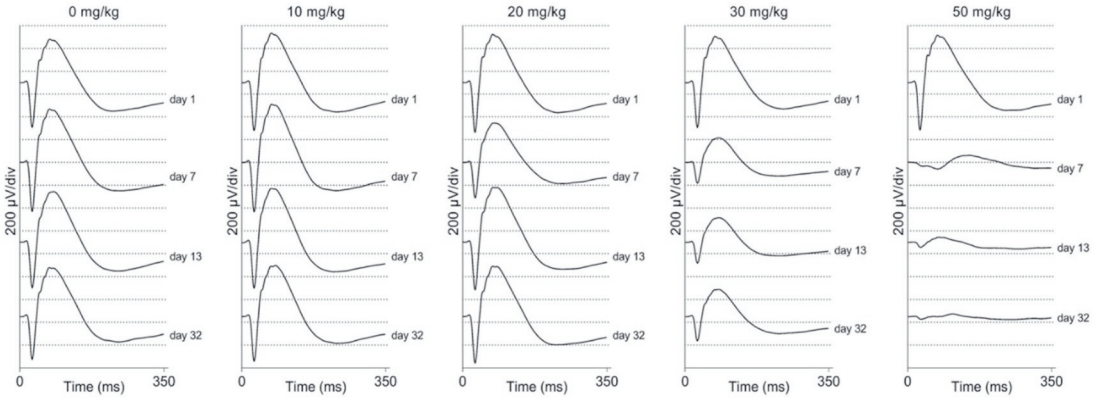

Figure 5. Averaged scotopic electroretinograms are shown for Brown Norway rats (n = 4 per group). The averaged traces per treatment group and per day of follow-up are plotted. No difference could be observed between the 10 mg/kg group and the control group by eye. A temporary effect was seen for the 20 mg/kg group: a slightly decreased response was seen a week post-injection. A moderate effect was seen for the 30 mg/kg group: decreased responses were observed from seven-days post-injection onwards. Direct and drastic effects were observed for the higher treatment group (50 mg/kg). The ERG responses were hardly recordable from one-week post-injection onwards. Similar effects were observed in the ERG recordings from C57BL/6J mice (Figure 4).

Electroretinographic Recordings Discussed in More Detail in SI-Treated C57BL/6J Mice

In C57BL/6J mice, a dose-dependent response for SI can be observed. A 10 mg/kg SI dose did not cause significant differences compared to the controls (see Figure 6 and 7). A dose of 20 mg/kg caused a significant decrease for the a-wave amplitude one-week post-injection for both the low (0.3 cd·s/m^2) and the high (30 cd·s/m^2) light intensity (Figure 6A,C). Although a slight drop of the b-wave amplitude was seen in this treatment group for both the low (0.0003 cd·s/m^2) and the high (30 cd·s/m^2) light intensity, it was not significant (Figure 6B,D). The effect of SI on the a- and b-wave amplitudes were not seen later in the experiment. A higher dose of 30 mg/kg caused a more moderate and permanent effect on the ERG amplitudes. At this dose, not only the a-wave but also the b-wave amplitude was significantly decreased from three-weeks post-injection onwards. Indeed, a reduction of roughly 50 % for both waves was observed. Even more extreme detrimental effects were observed for the higher doses (40, 50, and 70 mg/kg). From seven-days post-injection onwards, a- and b-wave amplitudes for low and high light intensities were significantly reduced. Reductions to <10 % of the original amplitude values were reached and remained permanently low throughout the experiment.

The effects of the intermediate (30 mg/kg) and high (40, 50, and 70 mg/kg) SI doses were observed from seven-days-post treatment for almost all the light intensities (see Figure 7A,D). From 19-days onwards, a moderate reduction was observed for the 30 mg/kg treatment group and a more extreme effect for the 40, 50, and 70 mg/kg treatment groups (Figure 7B,C,E,F). Finally, for C57BL/6J mice, Flicker (9 Hz) responses were also recorded, plotted, and analyzed. Similar dose-dependent functional effects were observed compared to the a- and b-wave amplitudes (see Supplementary Figure S3).

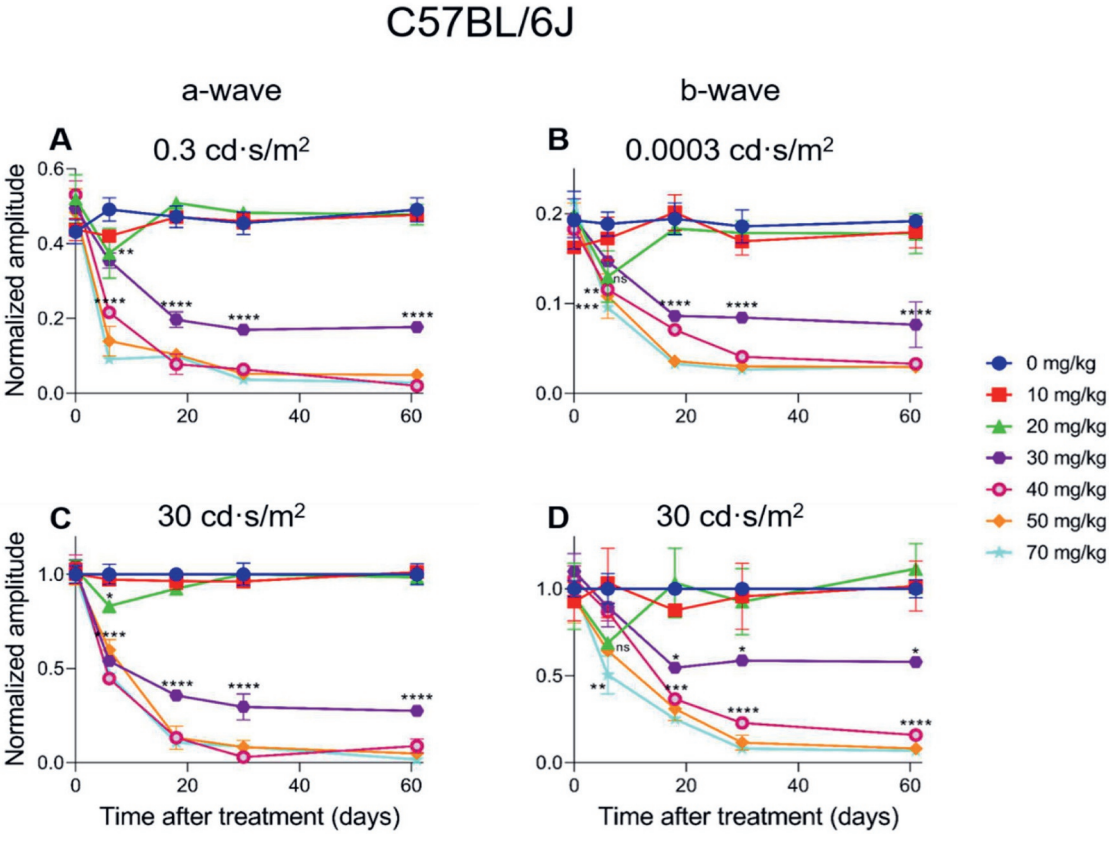

Figure 6. The normalized a- wave (**A**,**C**) and b-wave (**B**,**D**) amplitudes are plotted versus the time after treatment for all the treatment groups in C57BL/6J mice (n = 4 per group). The amplitudes are shown measured at 0.3 cd·s/m^2 (**A**) and 30 cd·s/m^2 (**C**) (a-wave) and 0.0003 cd·s/m^2 (**B**) and 30 cd·s/m^2 (**D**) (b-wave) including the standard deviations. No significant effect was observed for the 10 mg/kg group compared to the control. Although not significant for the b-wave, a temporary effect, and significant for the a-wave amplitude, was seen for the 20 mg/kg treatment group (**A**,**C**). This effect was not observed anymore later in the experiment. From seven-days post-injection onwards, significant decreased responses were observed for all the other treatment groups. The effects of the 30 mg/kg group was moderate and more prominently visible in the a-wave amplitude compared to the b-wave amplitude for both light intensities. Tremendous effects were seen for the higher treatment groups (40, 50, and 70 mg/kg). From three-weeks post-injection onwards, almost non-detectable a-wave amplitudes were observed and extremely decreased b-wave amplitudes. ns: not significant, *: $p \leq 0.05$, **: $p \leq 0.01$, ***: $p \leq 0.001$, and ****: $p \leq 0.0001$.

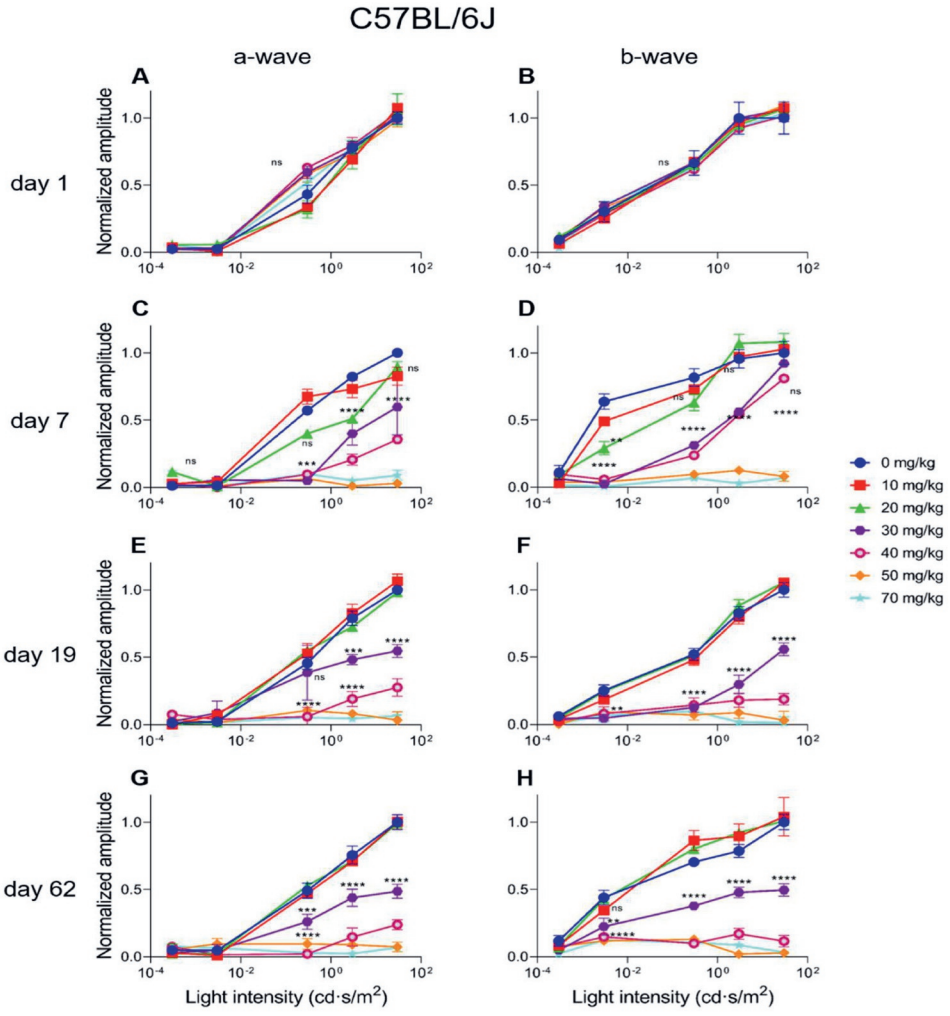

Figure 7. The normalized a-wave (**A**,**C**,**E**,**G**) and b-wave (**B**,**D**,**F**,**H**) amplitudes are plotted versus the light intensity for all the treatment groups in C57BL/6J mice (n = 4 per group). The amplitudes are shown ± the standard deviations. No significant differences can be observed at day 1 (baseline) between all the treatment groups. The treatment effects started to show from seven-days post-injection onwards. A slight effect was observed for the 20 mg/kg treatment group for both the a- and b-wave. The 30 and 40 mg/kg caused similar and moderate effects, and 50 and 70 mg/kg caused more extreme decreased amplitudes. From day 19 onwards, more long-term effects were visible. No significant differences were observed between the control, 10 mg/kg and 20 mg/kg groups. A significant and moderate effect was observed for the 30 mg/kg treatment group. Injection of 30 mg/kg SI caused a reduction of the a- and b-wave amplitudes of roughly 50 % at least up to two-months post-injection. More extreme effects were observed for the higher doses (40, 50 and 70 mg/kg). Reduced responses to 20 % to non-recordable ERG responses were observed in these groups. ns: not significant, **: $p \leq 0.01$, ***: $p \leq 0.001$, and ****: $p \leq 0.0001$.

Electroretinographic Recordings Discussed in More Detail in SI-Treated Brown Norway Rats

A dose-dependent electroretinographic response for SI could also be observed in the Brown Norway rats. A 10 mg/kg SI dose did not cause significant differences compared to the controls (see Figure 8 and 9). A dose of 20 mg/kg caused a significant decrease for the a-wave amplitude one-week post-injection for the low (0.3 cd·s/m^2) light intensity (Figure 8A). This effect was transient, as it was not seen later in the same experiment. Although drops of the a-wave amplitude at high light intensity (30 cd·s/m^2) and of the b-wave amplitude both at low (0.0003 cd·s/m^2) and high (30 cd·s/m^2) light intensities were observed, it was not significant (Figure 8B–D). Similar to our observations in mice, the 30 mg/kg dose in rats caused a moderate and temporally permanent effect on the ERG responses: both the a- and the b-wave amplitudes were significantly decreased from one-week post-injection onwards. Reductions of roughly 50–60 % were observed. The highest dose (50 mg/kg) in the rats caused a reduction of the a- and b-wave amplitudes to <10 % of the original amplitudes. This effect was stable throughout the experiment. Except for the 10 mg/kg treatment group, all the other treatment groups (20, 30, and 50 mg/kg) affected the a- and b-wave amplitudes at seven-days post-injection (Figure 9C,D). At 13-days post-treatment, no differences between the control and the 10 or 20 mg/kg groups were observed (Figure 9E,F). The 30 mg/kg group caused a moderate and stable reduction of the amplitudes for all the light intensities from seven-days post-injection onwards. Almost non-recordable amplitudes were observed for the 50 mg/kg treatment group (Figure 9C–H). Finally, the Flicker (9 Hz) responses were also plotted and analyzed for the Brown Norway rats. Similar dose-dependent functional effects were observed compared to the a- and b-wave amplitudes (see Supplementary Figure S4).

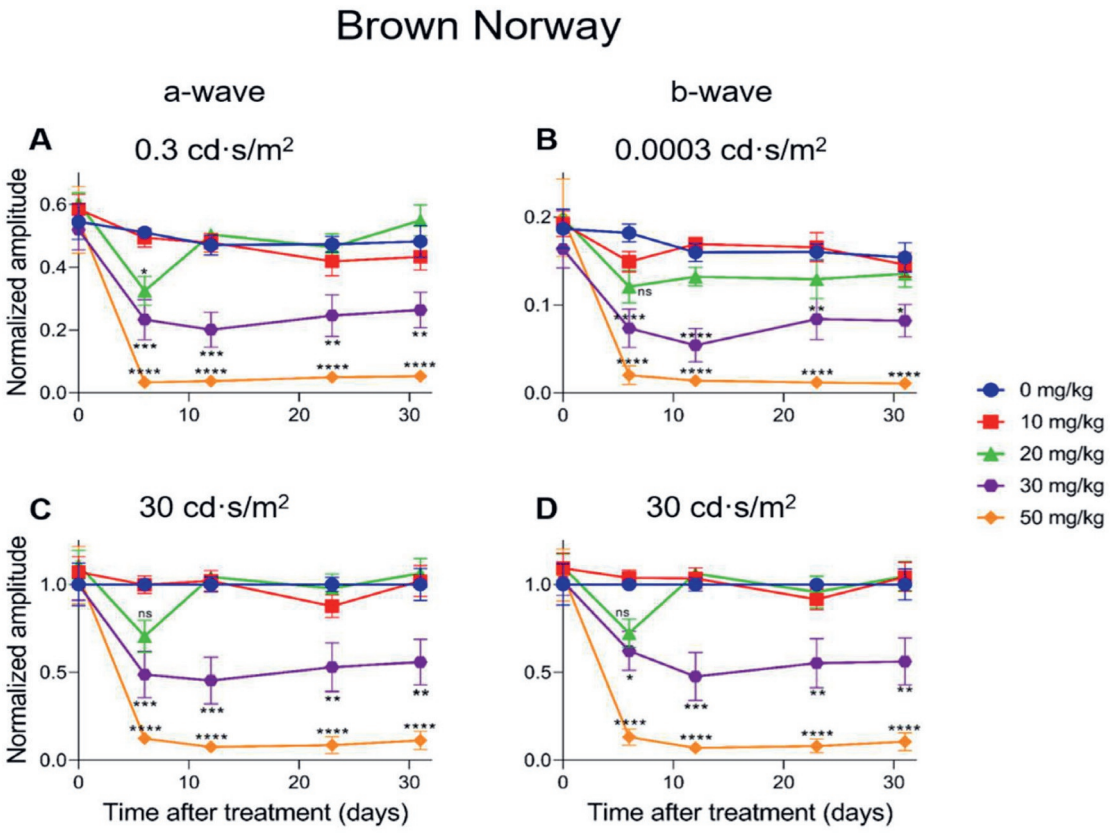

Figure 8. The normalized a-wave (**A**,**C**) and b-wave (**B**,**D**) amplitudes are plotted versus the time after treatment for all treatment groups in Brown Norway rats (n = 4 per group). The amplitudes are shown measured at 0.3 cd·s/m^2 and 30 cd·s/m^2 (a-wave) and 0.0003 cd·s/m^2 and 30 cd·s/m^2 (b-wave) including the standard deviations. No significant effect was observed for the 10 mg/kg group compared to the control. Although not always significant, a temporary effect and significant for the a-wave amplitude at 0.3 cd·s/m^2 was seen for the 20 mg/kg treatment group. This effect was not observed anymore later in the experiment. From seven-days post-injection onwards, significantly decreased responses were observed for all the other treatment groups. The effects of the 30 mg/kg group were moderate for both the a- and b-wave amplitudes at all light intensities. A tremendous effect was seen for the higher treatment group (50 mg/kg). From one-week post-injection onwards, the recorded a- and b-wave amplitudes decreased to less than 10 % of the original value. ns: not significant, *: $p \leq 0.05$, **: $p \leq 0.01$, ***: $p \leq 0.001$, and ****: $p \leq 0.0001$.

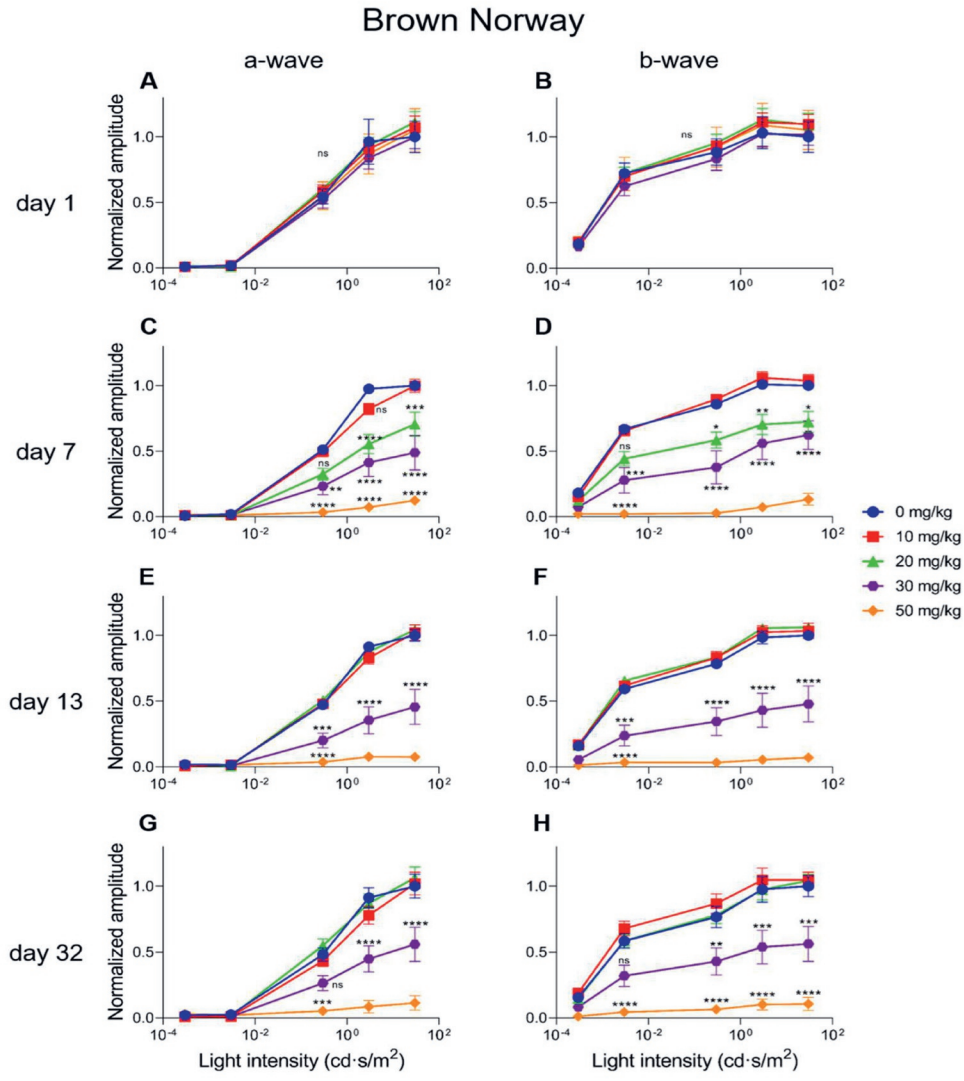

Figure 9. The normalized a-wave (**A**,**C**,**E**,**G**) and b-wave (**B**,**D**,**F**,**H**) amplitudes are plotted versus the light intensity for all the treatment groups in Brown Norway rats (n = 4 per group). The amplitudes are shown ± the standard deviations. No significant differences could be observed at day one (baseline) between all the treatment groups. The treatment effects started to show from seven-days post-injection onwards. A significant and clear effect was observed for the 20 mg/kg treatment group for both the a- and b-wave. A 30 mg/kg dose caused moderate effects, and 50 mg/kg caused more extreme decreased amplitudes. From day 13 onwards, more long-term effects were visible. No significant differences were observed (anymore) between the control, 10 mg/kg, and 20 mg/kg groups. A significant, stable, and moderate effect was observed for the 30 mg/kg treatment group. Injection of 30 mg/kg SI caused a reduction of the a- and b-wave amplitudes of roughly 50 % at least up to one-month post-injection. More extreme effects were observed for the higher dose (50 mg/kg). Almost non-recordable ERG responses were observed in this group. ns: not significant, *: $p \leq 0.05$, **: $p \leq 0.01$, ***: $p \leq 0.001$, and ****: $p \leq 0.0001.3$.

Discussion

Although numerous rodent models have been developed for (dry) AMD, until now, there is no animal model that is capable of fully representing the (progression of the) dry AMD disease phenotype. At the same time, a number of key mechanistic features of AMD, such as oxidative RPE stress and it consequences, resemble generalized dysfunction of the RPE or even normal physiological aging. Rodents, as also used in this study, share the overall retinal structure with humans and are genetically closely related [60]. A number of genetically-modified models for monogenic retinal degenerations may only represent part of the AMD phenotype [49,60–62]. The multifactorial nature of AMD complicates modeling its phenotype considerably [17,63]. Consequently, this lack of representative models severely hampers studies into the etiology and effective treatment modalities of the disease [17,44,63].

In this study, we generated and phenotyped two chemically-induced rodent models for retinal degeneration. C57BL/6J mice and Brown Norway rats were systemically injected intravenously with a wide range of SI doses (0, 10, 20, 30, 40, 50, and 70 mg/kg). They were followed up non-invasively over time by SLO-OCT and ERG. We observed a clear dose-dependent effect on the retinal structural integrity as judged from the OCT images and on the retinal function as judged from the ERG. In summary, we observed that the lower SI doses (0, 10, and 20 mg/kg) did not cause any long-term permanent effects, 30 mg/kg caused moderate effects on retinal structure and function, and higher doses (40, 50, and 70 mg/kg) caused extensive retinal degeneration and almost non-recordable ERG responses. We observed a dose-dependent effect as judged from the ERG data at earlier time points. Later in the experiment, the effects were similar for the higher doses (40, 50, and 70 mg/kg). Although 20 mg/kg did not result in any visible structural retinal damage, DNA fragmentation has been observed in the RPE layer by Koh et al. [64]. This may be functionally consistent with the temporary, although not always significant, quantitative drop that was observed in our ERG responses at the same dose. Indeed, a lower dose of SI may temporarily impact RPE functionality and survival. However, a 20 mg/kg dose is apparently not high enough to contribute to any long-term retinal degeneration. We observed overall similar effects in both species, even though the mice were older than the rats at the start of the experiment (3–4-months versus 8-weeks respectively). Although we cannot exclude an age effect influencing the results, we do not expect a tremendous difference in the outcome if we had included younger mice (e.g., 8-week-old) in our study. Similar results were obtained by Moriguchi et al., who included 8–12-week-old mice [65].

The SI-induced model is a widely used model for retinal degeneration and, more specifically, for AMD [48,52,66–69]. The model is, for example, used to study the efficacy of RPE transplantations for the treatment of retinal degeneration [59]. However, previously published studies are hard to compare due to differences in the experimental setup, species, strain, dose, administration route, and outcome parameters that have been used and studied [59]. Rodents, especially mice and rats, were most often used in these studies.

Among the mice studies, SI-based experiments have been published involving non- pigmented BALB/c mice and pigmented C57BL/6(J). The administration was usually done intravenously (tail vein, retro-orbital vein) or intraperitoneally. In these studies, the follow- up time varied between three-days and four-weeks, and most read-outs were histological. The SI doses varied between 10 and 50 mg/kg, and the higher doses (>30 mg/kg) were most frequently used [52,55,67,69–71]. SI injections in the retro-orbital vein resulted in quick and severe RPE and retinal damage, probably due to its proximity to the retina. For example, Wang and colleagues observed retinal degeneration when using a dose of 20 mg/kg based on histological data at eight-days post-injection [71]. There are some drawbacks to using the retro-orbital vein in experiments involving the eye. For example, anesthesia is always required, and swelling or injury of the eye may occur due to the injection. Since the eye is the subject of the study, in these cases, the animals need to be excluded from the study. In contrast, intravenous injections via the more distant tail vein require no anesthesia, a similar distribution is obtained, and there is no risk for eye damage due to the injection itself [72,73]. We and others did not observe structural damage at 20 mg/kg as measured by OCT. However, the affected ERG amplitudes at this time point do suggest lowered retinal functionality, also in our data. In both the aforementioned datasets, SI injections of 10 mg/kg did not cause any detectable effect [71]. Overall, our results are comparable to those that were obtained in other studies using pigmented mice.

To our knowledge, SI has only been used a few times before in Brown Norway rats [74–76]. Relatively high SI doses (35 and 40 mg/kg) and two different administration routes were used in these studies (intravenously and subretinally). An in-depth study giving an overview on the effect of a wide range of SI doses was, to our knowledge, lacking. The systemic intravenous injection caused an overall retinal degeneration in Brown Norway rats, comparable to our results at similar SI concentrations [74,75]. A subretinal injection with SI caused a local effect only [76]. Other rat strains have been used more extensively, such as the non-pigmented strains Wistar and Sprague Dawley and the pigmented strain Long Evans (pigmented hooded). Administration of SI was done intravenously (tail vein or retro-orbital vein), subretinally, or intraperitoneally. The follow-up times in these studies ranged from 1-week to 3-months, and doses varied from 25 to 75 mg/kg. A dose of 50 mg/kg was administered most [70,77–80].

A comparable study to our setup was performed using the non-pigmented Sprague Dawley strain by Koh et al. [64]. These rats were intravenously injected with 20, 40, 60, and 80 mg/kg SI and followed by ERG up to 10-days post-injection. Retinal morphology was determined by histology, at one time point only: 11-days post-injection. The results using the Sprague Dawley strain were similar to those in our study: little to no retinal damaging effect was observed for the 20 mg/kg dose and more prominent effects for 40 mg/kg and higher, as judged from histology. Unfortunately, the 30 mg/kg dose, which yielded the most interesting transient effect in our study, was not analyzed in the Sprague Dawley strain. Furthermore, little to no differences with our data were observed in the ERG responses between the highest doses: their experiment lasted 11-days, and a dose-dependent effect on the retinal morphology was observed. Additionally, more extensive damage was seen when a higher SI dose was used. Although OCT data is lacking in this study [64], the histological data are consistent with our findings in our *in vivo* OCT studies.

Administration of a >50 mg/kg SI dose affects the animals' general health and causes (temporarily) weight loss and doses of 100 mg/kg have been found to be lethal [64,81]. In the eye, the first known retinal cell layer to be affected by SI is the RPE. The RPE is extremely important for the normal function of the retina, as indicated by its role in many retinal degenerative diseases [7,43,44,82–85]. Severe damage to the RPE layer disrupts the blood-retina barrier and leads to impaired RPE-specific function. As the RPE-photoreceptor complex forms a single functional unit, impairment of the RPE leads to subsequent photoreceptor cell death. This secondary effect was also shown in our previous work reporting on a newly developed genetic rat model for retinitis pigmentosa (*Lrat*$^{-/-}$) [62].

Indeed, other layers of the retina besides the RPE are also eventually affected by SI. In our experiments, we observed thinning of the entire retina. This observation is in line with the observations by others who found SI-induced cell death among the photoreceptors, retinal ganglion cells, and bipolar cells [52,64,67]. Although a direct damaging effect of the systemic sodium iodate on the neural retina cannot be excluded, the most likely scenario is that higher doses of SI contribute to secondary cell death of neural retinal layers as a result of the initial damage to the RPE [64]. Indeed, it would be interesting to look into the sequence of damaging events in the retina. In our study, we were not able to make a definite statement about this. According to our OCT scans, the layers were disrupted due to SI administration. We could not make clear distinctions between the retinal layers in the eyes of the higher treatment groups at the later time points and quantify the degeneration per retinal layer.

Not only the RPE and the retina change with age. Also, the choroid and its vasculature undergo various changes during normal aging. These changes are more prominent and severe in AMD eyes [2]. As the main source of oxygen and nutrients for the outer retina, the choriocapillaris are essential for the survival of the photoreceptor cells and the RPE. It is known that, during normal aging, the choroid thins over time [86]. Moreover, more extensive thinning is observed in early AMD eyes and even more extreme thinning is observed in eyes with geographic atrophy, the endstage of (dry) AMD [87]. Age-related changes to the choroid (and the BM) may have significant roles in the development of AMD, as many of the changes in these tissues are more dramatic in diseased eyes [88]. The choriocapillaris might be affected even before RPE or photoreceptor cell loss [86–89]. Indeed, it has been shown in several animal models that SI not only induces RPE and retinal degeneration but also affects the choroid. Although it seems that it is not affecting the choriocapillaris directly, but rather via the RPE. No evidence was observed so far that the choriocapillaris degenerate over patches of healthy RPE [90,91]; only where RPE loss was observed and patches of scar tissue occurred, choriocapillaris atrophy was observed too. This observation led to the hypothesis that the choroid and its choriocapillaris depend on an intact and functioning RPE for its survival [90–96].

Apart from pigmented models, albino animals have also been widely used in SI studies in mice and rats. It has been postulated that SI reacts with melanin, increasing the conversion of glycine into glucoxylate, a potentially cell toxic compound [52,97]. Interestingly, although albino animals lack melanin, the effects of SI in albino animals seem to be more pronounced.

The most dramatic effects were observed using the (Han) Wistar rat [69,70]. Indeed, it appears that the albino retina is more susceptible to SI damage, especially in the central area of the retina where the light is focused [70,98]. Melanin pigment in the RPE has been implicated in protecting the entire retina, including the macula, from oxidative damage [16]. Melanin absorbs excess light and is a (co-)scavenger of oxidative stress-mediated free radicals [99,100]. In albino animals, the melanin pigment is absent. Also, a decline in pigment density is part of normal aging. As a result, the risk of developing AMD becomes higher with older age. Also, less pigmented human individuals may have an increased risk of developing AMD [101,102]. Although an overall comparable effect is reached in both pigmented and non-pigmented rodents, the choice of the model should be carefully made considering possible translational outcomes. Obviously, the majority of the human population has a pigmented RPE layer. This study gives an in-depth overview of the characteristics of the SI-induced model for retinal degeneration in pigmented rodents.

As discussed above, there are many similarities between dry AMD pathology and the effects of SI. Extreme RPE loss can be obtained depending on the dose, similar to geographic atrophy observed in late-stage AMD eyes. Additionally, not only the RPE but also the (outer) retina, the choroidal capillaries and BM are affected by SI [76]. Disease-related changes to these tissues have been observed in AMD eyes as well. Moreover, the mechanisms that are involved in SI-induced degeneration and atrophy (e.g., oxidative stress and melanin-related pathways) are also known to be involved in AMD pathology and development [5,26]. Further in-depth studies using these models will shed light on the dose-dependency and time windows of the cell types and tissues that are affected by SI, and its relationship with AMD.

In conclusion, SI-induced retinal degeneration in C57BL6/J mice and Brown Norway rats is relatively easy to establish and yields a reproducible model for retinal degenerative diseases, such as dry AMD. The SI-induced retinal degeneration was followed and characterized in depth using OCT and ERG measurements, yielding a detailed insight into the dose-effect of SI over time. This study demonstrates an SI-dose-dependent effect on the retina in both pigmented rat and mouse species; thus, the SI concentration can be selected to generate numerous disease states. No general model for the full disease spectrum of AMD exists yet. The SI-induced model that is presented in this work could be combined with other theorized AMD precursors (e.g., genetic modifications and environmental factors) to identify the critical stages during the evolution of the disease directly. Thus, our data are useful for identifying a therapeutic window and developing experimental therapies for AMD and other retinal degenerative diseases.

Supplementary Materials: please see Chapter 9: "Appendices".

Acknowledgments: the authors thank Leon Begthel and Roos-Sanne Verkerk for their hands-on help during the *in vivo* studies and with the molecular biology-related work in the lab.

References

1. Garcia-Layana, A.; Cabrera-Lopez, F.; Garcia-Arumi, J.; Arias-Barquet, L.; Ruiz-Moreno, J.M. Early and intermediate age-related macular degeneration: Update and clinical review. *Clin. Interv. Aging* **2017**, *12*, 1579–1587.
2. Fleckenstein, M.; Keenan, T.D.L.; Guymer, R.H.; Chakravarthy, U.; Schmitz-Valckenberg, S.; Klaver, C.C.; Wong, W.T.; Chew, E.Y. Age-related macular degeneration. *Nat. Rev. Dis. Primers* **2021**, *7*, 31.
3. Gorin, M.B.; Breitner, J.C.; De Jong, P.T.; Hageman, G.S.; Klaver, C.C.; Kuehn, M.H.; Seddon, J.M. The genetics of age-related macular degeneration. *Mol. Vis.* **1999**, *5*, 29.
4. Klein, R.; Myers, C.E.; Buitendijk, G.H.; Rochtchina, E.; Gao, X.; de Jong, P.T.; Sivakumaran, T.A.; Burlutsky, G.; McKean-Cowdin, R.; Hofman, A.; et al. Lipids, lipid genes, and incident age-related macular degeneration: The three continent age-related macular degeneration consortium. *Am. J. Ophthalmol.* **2014**, *158*, 513–524.e3.
5. de Jong, P.T. Age-related macular degeneration. *N. Engl. J. Med.* **2006**, *355*, 1474–1485.
6. Wong, W.L.; Su, X.; Li, X.; Cheung, C.M.; Klein, R.; Cheng, C.Y.; Wong, T.Y. Global prevalence of age-related macular degeneration and disease burden projection for 2020 and 2040: A systematic review and meta-analysis. *Lancet Glob. Health* **2014**, *2*, e106–e116.
7. Somasundaran, S.; Constable, I.J.; Mellough, C.B.; Carvalho, L.S. Retinal pigment epithelium and age-related macular degeneration: A review of major disease mechanisms. *Clin. Exp. Ophthalmol.* **2020**, *48*, 1043–1056.
8. Bergen, A.A.; Arya, S.; Koster, C.; Pilgrim, M.G.; Wiatrek-Moumoulidis, D.; van der Spek, P.J.; Hauck, S.M.; Boon, C.J.F.; Emri, E.; Stewart, A.J.; et al. On the origin of proteins in human drusen: The meet, greet and stick hypothesis. *Prog. Retin. Eye Res.* **2019**, *70*, 55–84.
9. Hageman, G.S.; Luthert, P.J.; Victor Chong, N.H.; Johnson, L.V.; Anderson, D.H.; Mullins, R.F. An integrated hypothesis that considers drusen as biomarkers of immune-mediated processes at the RPE-Bruch's membrane interface in aging and age-related macular degeneration. *Prog. Retin. Eye Res.* **2001**, *20*, 705–732.
10. Curcio, C.A. Soft Drusen in Age-Related Macular Degeneration: Biology and Targeting Via the Oil Spill Strategies. *Investig. Ophthalmol. Vis. Sci.* **2018**, *59*, Amd160–Amd181.
11. Curcio, C.A.; Johnson, M.; Rudolf, M.; Huang, J.D. The oil spill in ageing Bruch membrane. *Br. J. Ophthalmol.* **2011**, *95*, 1638–1645.
12. Pikuleva, I.A.; Curcio, C.A. Cholesterol in the retina: The best is yet to come. *Prog. Retin. Eye Res.* **2014**, *41*, 64–89.
13. Spaide, R.F.; Jaffe, G.J.; Sarraf, D.; Freund, K.B.; Sadda, S.R.; Staurenghi, G.; Waheed, N.K.; Chakravarthy, U.; Rosenfeld, P.J.; Holz, F.G.; et al. Consensus Nomenclature for Reporting Neovascular Age-Related Macular Degeneration Data: Consensus on Neovascular Age-Related Macular Degeneration Nomenclature Study Group. *Ophthalmology* **2020**, *127*, 616–636.
14. Brown, D.M.; Regillo, C.D. Anti-VEGF agents in the treatment of neovascular age-related macular degeneration: Applying clinical trial results to the treatment of everyday patients. *Am. J. Ophthalmol.* **2007**, *144*, 627–637.

15. Tisi, A.; Feligioni, M.; Passacantando, M.; Ciancaglini, M.; Maccarone, R. The Impact of Oxidative Stress on Blood-Retinal Barrier Physiology in Age-Related Macular Degeneration. *Cells* **2021**, *10*, 64.
16. Strauss, O. The retinal pigment epithelium in visual function. *Physiol. Rev.* **2005**, *85*, 845–881.
17. Fritsche, L.G.; Igl, W.; Bailey, J.N.; Grassmann, F.; Sengupta, S.; Bragg-Gresham, J.L.; Burdon, K.P.; Hebbring, S.J.; Wen, C.; Gorski, M.; et al. A large genome-wide association study of age-related macular degeneration highlights contributions of rare and common variants. *Nat. Genet.* **2016**, *48*, 134–143.
18. Thee, E.F.; Meester-Smoor, M.A.; Luttikhuizen, D.T.; Colijn, J.M.; Enthoven, C.A.; Haarman, A.E.G.; Rizopoulos, D.; Klaver, C.C.W. Performance of Classification Systems for Age-Related Macular Degeneration in the Rotterdam Study. *Transl. Vis. Sci. Technol.* **2020**, *9*, 26.
19. Vingerling, J.R.; Hofman, A.; Grobbee, D.E.; de Jong, P.T. Age-related macular degeneration and smoking. The Rotterdam Study. *Arch. Ophthalmol.* **1996**, *114*, 1193–1196.
20. Domalpally, A.; Agrón, E.; Pak, J.W.; Keenan, T.D.; Ferris, F.L., 3rd; Clemons, T.E.; Chew, E.Y. Prevalence, Risk, and Genetic Association of Reticular Pseudodrusen in Age-related Macular Degeneration: Age-Related Eye Disease Study 2 Report 21. *Ophthalmology* **2019**, *126*, 1659–1666.
21. Gorusupudi, A.; Nelson, K.; Bernstein, P.S. The Age-Related Eye Disease 2 Study: Micronutrients in the Treatment of Macular Degeneration. *Adv. Nutr.* **2017**, *8*, 40–53.
22. Yu, J.J.; Agrón, E.; Clemons, T.E.; Domalpally, A.; van Asten, F.; Keenan, T.D.; Cukras, C.; Chew, E.Y. Natural History of Drusenoid Pigment Epithelial Detachment Associated with Age-Related Macular Degeneration: Age-Related Eye Disease Study 2 Report No. 17. *Ophthalmology* **2019**, *126*, 261–273.
23. Dewan, A.; Liu, M.; Hartman, S.; Zhang, S.S.; Liu, D.T.; Zhao, C.; Tam, P.O.; Chan, W.M.; Lam, D.S.; Snyder, M.; et al. HTRA1 promoter polymorphism in wet age-related macular degeneration. *Science* **2006**, *314*, 989–992.
24. Yang, Z.; Camp, N.J.; Sun, H.; Tong, Z.; Gibbs, D.; Cameron, D.J.; Chen, H.; Zhao, Y.; Pearson, E.; Li, X.; et al. A variant of the HTRA1 gene increases susceptibility to age-related macular degeneration. *Science* **2006**, *314*, 992–993.
25. Blasiak, J.; Pawlowska, E.; Sobczuk, A.; Szczepanska, J.; Kaarniranta, K. The Aging Stress Response and Its Implication for AMD Pathogenesis. *Int. J. Mol. Sci.* **2020**, *21*, 8840.
26. Datta, S.; Cano, M.; Ebrahimi, K.; Wang, L.; Handa, J.T. The impact of oxidative stress and inflammation on RPE degeneration in non-neovascular AMD. *Prog. Retin. Eye Res.* **2017**, *60*, 201–218.
27. Fanjul-Moles, M.L.; López-Riquelme, G.O. Relationship between Oxidative Stress, Circadian Rhythms, and AMD. *Oxid. Med. Cell. Longev.* **2016**, *2016*, 7420637.
28. Hanus, J.; Anderson, C.; Wang, S. RPE necroptosis in response to oxidative stress and in AMD. *Ageing Res. Rev.* **2015**, *24 Pt B*, 286–298.
29. Kaarniranta, K.; Uusitalo, H.; Blasiak, J.; Felszeghy, S.; Kannan, R.; Kauppinen, A.; Salminen, A.; Sinha, D.; Ferrington, D. Mechanisms of mitochondrial dysfunction and their impact on age-related macular degeneration. *Prog. Retin. Eye Res.* **2020**, *79*, 100858.

30. Mitter, S.K.; Song, C.; Qi, X.; Mao, H.; Rao, H.; Akin, D.; Lewin, A.; Grant, M.; Dunn, W., Jr.; Ding, J.; et al. Dysregulated autophagy in the RPE is associated with increased susceptibility to oxidative stress and AMD. *Autophagy* **2014**, *10*, 1989–2005.
31. Zhang, Z.Y.; Bao, X.L.; Cong, Y.Y.; Fan, B.; Li, G.Y. Autophagy in Age-Related Macular Degeneration: A Regulatory Mechanism of Oxidative Stress. *Oxid. Med. Cell. Longev.* **2020**, *2020*, 2896036.
32. Schieber, M.; Chandel, N.S. ROS function in redox signaling and oxidative stress. *Curr. Biol.* **2014**, *24*, R453–R462.
33. Smith, C.J.; Hansch, C. The relative toxicity of compounds in mainstream cigarette smoke condensate. *Food Chem. Toxicol.* **2000**,*38*, 637–646.
34. Zhao, J.; Hopke, P.K. Concentration of reactive oxygen species (ROS) in mainstream and sidestream cigarette smoke. *Aerosol Sci. Technol.* **2012**, *46*, 191–197.
35. Lu, Z.G.; May, A.; Dinh, B.; Lin, V.; Su, F.; Tran, C.; Adivikolanu, H.; Ehlen, R.; Che, B.; Wang, Z.H.; et al. The interplay of oxidative stress and ARMS2-HTRA1 genetic risk in neovascular AMD. *Vessel Plus* **2021**, *5*, 4.
36. Léveillard, T.; Sahel, J.A. Metabolic and redox signaling in the retina. *Cell. Mol. Life Sci.* **2017**, *74*, 3649–3665.
37. Sparrow, J.R.; Boulton, M. RPE lipofuscin and its role in retinal pathobiology. *Exp. Eye Res.* **2005**, *80*, 595–606.
38. Vives-Bauza, C.; Anand, M.; Shiraz, A.K.; Magrane, J.; Gao, J.; Vollmer-Snarr, H.R.; Manfredi, G.; Finnemann, S.C. The age lipid A2E and mitochondrial dysfunction synergistically impair phagocytosis by retinal pigment epithelial cells. *J. Biol. Chem.* **2008**, *283*, 24770–24780.
39. Moore, D.J.; Clover, G.M. The effect of age on the macromolecular permeability of human Bruch's membrane. *Investig. Ophthalmol. Vis. Sci.* **2001**, *42*, 2970–2975.
40. Booij, J.C.; Baas, D.C.; Beisekeeva, J.; Gorgels, T.G.; Bergen, A.A. The dynamic nature of Bruch's membrane. *Prog. Retin. Eye Res.* **2010**, *29*, 1–18.
41. Miller, Y.I.; Choi, S.H.; Wiesner, P.; Fang, L.; Harkewicz, R.; Hartvigsen, K.; Boullier, A.; Gonen, A.; Diehl, C.J.; Que, X.; et al. Oxidation-specific epitopes are danger-associated molecular patterns recognized by pattern recognition receptors of innate immunity. *Circ. Res.* **2011**, *108*, 235–248.
42. Masuda, T.; Shimazawa, M.; Hara, H. Retinal Diseases Associated with Oxidative Stress and the Effects of a Free Radical Scavenger (Edaravone). *Oxid. Med. Cell. Longev.* **2017**, *2017*, 9208489.
43. Bermúdez, V.; Tenconi, P.E.; Giusto, N.M.; Mateos, M.V. Lipid Signaling in Retinal Pigment Epithelium Cells Exposed to Inflammatory and Oxidative Stress Conditions. Molecular Mechanisms Underlying Degenerative Retinal Diseases. *Adv. Exp. Med. Biol.* **2019**, *1185*, 289–293.
44. Bergen, A.A. Nicotinamide, iRPE-in-a dish, and age-related macular degeneration therapy development. *Stem Cell Investig.* **2017**, *4*, 81.
45. Sharma, R.; George, A.; Nimmagadda, M.; Ortolan, D.; Karla, B.-S.; Qureshy, Z.; Bose, D.; Dejene, R.; Liang, G.; Wan, Q.; et al. Epithelial phenotype restoring drugs suppress macular degeneration phenotypes in an iPSC model. *Nat. Commun.* **2021**, *12*, 7293.
46. Zeiss, C.J. Animals as models of age-related macular degeneration: An imperfect measure of the truth. *Vet. Pathol.* **2010**, *47*, 396–413.

47. Massengill, M.T.; Young, B.; Patel, D.; Jafri, F.; Sabogal, E.; Ash, N.; Li, H.; Ildefonso, C.J.; Lewin, A.S. Clinically Relevant Outcome Measures for the I307N Rhodopsin Mouse: A Model of Inducible Autosomal Dominant Retinitis Pigmentosa. *Investig. Ophthalmol. Vis. Sci.* **2018**, *59*, 5417–5430.
48. Fletcher, E.L.; Jobling, A.I.; Vessey, K.A.; Luu, C.; Guymer, R.H.; Baird, P.N. Animal models of retinal disease. *Prog. Mol. Biol. Transl. Sci.* **2011**, *100*, 211–286.
49. Pennesi, M.E.; Neuringer, M.; Courtney, R.J. Animal models of age related macular degeneration. *Mol. Asp. Med.* **2012**, *33*, 487–509.
50. Ramkumar, H.L.; Zhang, J.; Chan, C.C. Retinal ultrastructure of murine models of dry age-related macular degeneration (AMD). *Prog. Retin. Eye Res.* **2010**, *29*, 169–190.
51. van Lookeren Campagne, M.; LeCouter, J.; Yaspan, B.L.; Ye, W. Mechanisms of age-related macular degeneration and therapeutic opportunities. *J. Pathol.* **2014**, *232*, 151–164.
52. Machalińska, A.; Lubiński, W.; Kłos, P.; Kawa, M.; Baumert, B.; Penkala, K.; Grzegrzółka, R.; Karczewicz, D.; Wiszniewska, B.; Machaliński, B. Sodium iodate selectively injuries the posterior pole of the retina in a dose-dependent manner: Morphological and electrophysiological study. *Neurochem. Res.* **2010**, *35*, 1819–1827.
53. Kiuchi, K.; Yoshizawa, K.; Shikata, N.; Moriguchi, K.; Tsubura, A. Morphologic characteristics of retinal degeneration induced by sodium iodate in mice. *Curr. Eye Res.* **2002**, *25*, 373–379.
54. Zhou, R.; Li, Y.; Qian, H.; Maminishkis, A.; Jha, B.S.; Campos, M.M.; Amaral, J.; Stanzel, B.V.; Bharti, K. Sodium iodate-induced retina and choroid damage model in rabbits to test efficacy of RPE auto-transplants. *Investig. Ophthalmol. Vis. Sci.* **2016**, *57*, 2253.
55. Hanus, J.; Anderson, C.; Sarraf, D.; Ma, J.; Wang, S. Retinal pigment epithelial cell necroptosis in response to sodium iodate. *Cell Death Discov.* **2016**, *2*, 16054.
56. Park, U.C.; Cho, M.S.; Park, J.H.; Kim, S.J.; Ku, S.Y.; Choi, Y.M.; Moon, S.Y.; Yu, H.G. Subretinal transplantation of putative retinal pigment epithelial cells derived from human embryonic stem cells in rat retinal degeneration model. *Clin. Exp. Reprod. Med.* **2011**, *38*, 216–221.
57. Guan, Y.; Cui, L.; Qu, Z.; Lu, L.; Wang, F.; Wu, Y.; Zhang, J.; Gao, F.; Tian, H.; Xu, L.; et al. Subretinal transplantation of rat MSCs and erythropoietin gene modified rat MSCs for protecting and rescuing degenerative retina in rats. *Curr. Mol. Med.* **2013**, *13*, 1419–1431.
58. Petrus-Reurer, S.; Bartuma, H.; Aronsson, M.; Westman, S.; Lanner, F.; Andre, H.; Kvanta, A. Integration of Subretinal Suspension Transplants of Human Embryonic Stem Cell-Derived Retinal Pigment Epithelial Cells in a Large-Eyed Model of Geographic Atrophy. *Investig. Ophthalmol. Vis. Sci.* **2017**, *58*, 1314–1322.
59. Koster, C.; Wever, K.E.; Wagstaff, P.E.; Hirk, K.; Hooijmans, C.R.; Bergen, A.A. A Systematic Review on Transplantation Studies of the Retinal Pigment Epithelium in Animal Models. *Int. J. Mol. Sci.* **2020**, *21*, 2719.
60. Soundara Pandi, S.P.; Ratnayaka, J.A.; Lotery, A.J.; Teeling, J.L. Progress in developing rodent models of age-related macular degeneration (AMD). *Exp. Eye Res.* **2021**, *203*, 108404.
61. Veleri, S.; Lazar, C.H.; Chang, B.; Sieving, P.A.; Banin, E.; Swaroop, A. Biology and therapy of inherited retinal degenerative disease: Insights from mouse models. *Dis. Model. Mech.* **2015**, *8*, 109–129.

62. Koster, C.; van den Hurk, K.T.; Lewallen, C.F.; Talib, M.; Ten Brink, J.B.; Boon, C.J.F.; Bergen, A.A. The Lrat$^{-/-}$ Rat: CRISPR/Cas9 Construction and Phenotyping of a New Animal Model for Retinitis Pigmentosa. *Int. J. Mol. Sci.* **2021**, *22*, 7234.
63. Yan, Q.; Ding, Y.; Weeks, D.E.; Chen, W. AMD Genetics: Methods and Analyses for Association, Progression, and Prediction. *Adv. Exp. Med. Biol.* **2021**, *1256*, 191–200.
64. Koh, A.E.; Alsaeedi, H.A.; Rashid, M.B.A.; Lam, C.; Harun, M.H.N.; Saleh, M.; Luu, C.D.; Kumar, S.S.; Ng, M.H.; Isa, H.M.; et al. Retinal degeneration rat model: A study on the structural and functional changes in the retina following injection of sodium iodate. *J. Photochem. Photobiol. B* **2019**, *196*, 111514.
65. Moriguchi, M.; Nakamura, S.; Inoue, Y.; Nishinaka, A.; Nakamura, M.; Shimazawa, M.; Hara, H. Irreversible Photoreceptors and RPE Cells Damage by Intravenous Sodium Iodate in Mice Is Related to Macrophage Accumulation. *Investig. Ophthalmol. Vis. Sci.* **2018**, *59*, 3476–3487.
66. Ahn, S.M.; Ahn, J.; Cha, S.; Yun, C.; Park, T.K.; Kim, Y.J.; Goo, Y.S.; Kim, S.W. The effects of intravitreal sodium iodate injection on retinal degeneration following vitrectomy in rabbits. *Sci. Rep.* **2019**, *9*, 15696.
67. Balmer, J.; Zulliger, R.; Roberti, S.; Enzmann, V. Retinal Cell Death Caused by Sodium Iodate Involves Multiple Caspase-Dependent and Caspase-Independent Cell-Death Pathways. *Int. J. Mol. Sci.* **2015**, *16*, 15086–15103.
68. Cho, B.J.; Seo, J.M.; Yu, H.G.; Chung, H. Monocular retinal degeneration induced by intravitreal injection of sodium iodate in rabbit eyes. *Jpn. J. Ophthalmol.* **2016**, *60*, 226–237.
69. Chowers, G.; Cohen, M.; Marks-Ohana, D.; Stika, S.; Eijzenberg, A.; Banin, E.; Obolensky, A. Course of Sodium Iodate-Induced Retinal Degeneration in Albino and Pigmented Mice. *Investig. Ophthalmol. Vis. Sci.* **2017**, *58*, 2239–2249.
70. Redfern, W.S.; Storey, S.; Tse, K.; Hussain, Q.; Maung, K.P.; Valentin, J.P.; Ahmed, G.; Bigley, A.; Heathcote, D.; McKay, J.S. Evaluation of a convenient method of assessing rodent visual function in safety pharmacology studies: Effects of sodium iodate on visual acuity and retinal morphology in albino and pigmented rats and mice. *J. Pharmacol. Toxicol. Methods* **2011**, *63*, 102–114.
71. Wang, J.; Iacovelli, J.; Spencer, C.; Saint-Geniez, M. Direct effect of sodium iodate on neurosensory retina. *Investig. Ophthalmol. Vis. Sci.* **2014**, *55*, 1941–1953.
72. Steel, C.D.; Stephens, A.L.; Hahto, S.M.; Singletary, S.J.; Ciavarra, R.P. Comparison of the lateral tail vein and the retro-orbital venous sinus as routes of intravenous drug delivery in a transgenic mouse model. *Lab Anim.* **2008**, *37*, 26–32.
73. Yardeni, T.; Eckhaus, M.; Morris, H.D.; Huizing, M.; Hoogstraten-Miller, S. Retro-orbital injections in mice. *Lab Anim.* **2011**, *40*, 155–160.
74. Xiao, J.; Yao, J.; Jia, L.; Lin, C.; Zacks, D.N. Protective Effect of Met12, a Small Peptide Inhibitor of Fas, on the Retinal Pigment Epithelium and Photoreceptor After Sodium Iodate Injury. *Investig. Ophthalmol. Vis. Sci.* **2017**, *58*, 1801–1810.
75. Shen, Y.; Zhuang, P.; Xiao, T.; Chiou, G.C. Effect of cytokeratin 17 on retinal pigment epithelium degeneration and choroidal neovascularization. *Int. J. Ophthalmol.* **2016**, *9*, 363–368.

76. Bhutto, I.A.; Ogura, S.; Baldeosingh, R.; McLeod, D.S.; Lutty, G.A.; Edwards, M.M. An Acute Injury Model for the Phenotypic Characteristics of Geographic Atrophy. *Investig. Ophthalmol. Vis. Sci.* **2018**, *59*, Amd143–Amd151.
77. Kadkhodaeian, H.A.; Tiraihi, T.; Daftarian, N.; Ahmadieh, H.; Ziaei, H.; Taheri, T. Histological and Electrophysiological Changes in the Retinal Pigment Epithelium after Injection of Sodium Iodate in the Orbital Venus Plexus of Pigmented Rats. *J. Ophthalmic Vis. Res.* **2016**, *11*, 70–77.
78. Yang, Y.; Ng, T.K.; Ye, C.; Yip, Y.W.; Law, K.; Chan, S.O.; Pang, C.P. Assessing sodium iodate-induced outer retinal changes in rats using confocal scanning laser ophthalmoscopy and optical coherence tomography. *Investig. Ophthalmol. Vis. Sci.* **2014**, *55*, 1696–1705.
79. Tao, Z.; Dai, J.; He, J.; Li, C.; Li, Y.; Yin, Z.Q. The influence of $NaIO_3$-induced retinal degeneration on intra-retinal layer and the changes of expression profile/morphology of DA-ACs and mRGCS. *Mol. Neurobiol.* **2013**, *47*, 241–260.
80. Hariri, S.; Moayed, A.A.; Choh, V.; Bizheva, K. In vivo assessment of thickness and reflectivity in a rat outer retinal degeneration model with ultrahigh resolution optical coherence tomography. *Investig. Ophthalmol. Vis. Sci.* **2012**, *53*, 1982–1989.
81. Ou, Q.; Zhu, T.; Li, P.; Li, Z.; Wang, L.; Lian, C.; Xu, H.; Jin, C.; Gao, F.; Xu, J.Y.; et al. Establishment of Retinal Degeneration Model in Rat and Monkey by Intravitreal Injection of Sodium Iodate. *Curr. Mol. Med.* **2018**, *18*, 352–364.
82. Blasiak, J.; Reiter, R.J.; Kaarniranta, K. Melatonin in Retinal Physiology and Pathology: The Case of Age-Related Macular Degeneration. *Oxid. Med. Cell. Longev.* **2016**, *2016*, 6819736.
83. Wimmers, S.; Karl, M.O.; Strauss, O. Ion channels in the RPE. *Prog. Retin. Eye Res.* **2007**, *26*, 263–301.
84. Booij, J.C.; ten Brink, J.B.; Swagemakers, S.M.; Verkerk, A.J.; Essing, A.H.; van der Spek, P.J.; Bergen, A.A. A new strategy to identify and annotate human RPE-specific gene expression. *PLoS ONE* **2010**, *5*, e9341.
85. Ramos de Carvalho, J.E.; Klaassen, I.; Vogels, I.M.; Schipper-Krom, S.; van Noorden, C.J.; Reits, E.; Gorgels, T.G.; Bergen, A.A.; Schlingemann, R.O. Complement factor C3a alters proteasome function in human RPE cells and in an animal model of age-related RPE degeneration. *Investig. Ophthalmol. Vis. Sci.* **2013**, *54*, 6489–6501.
86. Chirco, K.R.; Sohn, E.H.; Stone, E.M.; Tucker, B.A.; Mullins, R.F. Structural and molecular changes in the aging choroid: Implications for age-related macular degeneration. *Eye* **2017**, *31*, 10–25.
87. Wakatsuki, Y.; Shinojima, A.; Kawamura, A.; Yuzawa, M. Correlation of Aging and Segmental Choroidal Thickness Measurement using Swept Source Optical Coherence Tomography in Healthy Eyes. *PLoS ONE* **2015**, *10*, e0144156.
88. Sarks, S.H. Ageing and degeneration in the macular region: A clinico-pathological study. *Br. J. Ophthalmol.* **1976**, *60*, 324–341.
89. Sohn, E.H.; Khanna, A.; Tucker, B.A.; Abràmoff, M.D.; Stone, E.M.; Mullins, R.F. Structural and biochemical analyses of choroidal thickness in human donor eyes. *Investig. Ophthalmol. Vis. Sci.* **2014**, *55*, 1352–1360.
90. Korte, G.E.; Reppucci, V.; Henkind, P. RPE destruction causes choriocapillary atrophy. *Investig. Ophthalmol. Vis. Sci.* **1984**, *25*, 1135–1145.

91. Peyman, G.A.; Vlchek, J.K.; Seth, N.V. Chorioretinal diffusion processes following pigment epithelial degeneration. *Investig. Ophthalmol.* **1975**, *14*, 58–62.
92. Noell, W.K. Experimentally Induced Toxic Effects on Structure and Function of Visual Cells and Pigment Epithelium. *Am. J. Ophthalmol.* **1953**, *36*, 103–116.
93. Grignolo, A.; Orzalesi, N.; Calabria, G.A. Studies on the fine structure and the rhodopsin cycle of the rabbit retina in experimental degeneration induced by sodium iodate. *Exp. Eye Res.* **1966**, *5*, 86–97.
94. Nilsson, S.E.; Knave, B.; Persson, H.E. Changes in ultrastructure and function of the sheep pigment epithelium and retina induced by sodium iodate. II. Early effects. *Acta Ophthalmol.* **1977**, *55*, 1007–1026.
95. Ringvold, A.; Olsen, E.G.; Flage, T. Transient breakdown of the retinal pigment epithelium diffusion barrier after sodium iodate: A fluorescein angiographic and morphological study in the rabbit. *Exp. Eye Res.* **1981**, *33*, 361–369.
96. Flage, T.; Ringvold, A. The retinal pigment epithelium diffusion barrier in the rabbit eye after sodium iodate injection. A light and electron microscopic study using horseradish peroxidase as a tracer. *Exp. Eye Res.* **1982**, *34*, 933–940.
97. Baich, A.; Ziegler, M. The effect of sodium iodate and melanin on the formation of glyoxylate. *Pigment Cell Res.* **1992**, *5*, 394–395.
98. Ikeda, H.; Adachi-Usami, E.; Saeki, M.; Takeda, N.; Kimura, T. Electrophysiological Studies on Light Damage in the Mouse Retina after Sodium Iodate Injection. *Ophthalmologica* **1994**, *208*, 220–225.
99. Mecklenburg, L.; Schraermeyer, U. An Overview on the Toxic Morphological Changes in the Retinal Pigment Epithelium after Systemic Compound Administration. *Toxicol. Pathol.* **2007**, *35*, 252–267.
100. Miceli, M.V.; Liles, M.R.; Newsome, D.A. Evaluation of Oxidative Processes in Human Pigment Epithelial Cells Associated with Retinal Outer Segment Phagocytosis. *Exp. Cell Res.* **1994**, *214*, 242–249.
101. Klein, R. Race/ethnicity and age-related macular degeneration. *Am. J. Ophthalmol.* **2011**, *152*, 153–154.
102. Klein, R.; Li, X.; Kuo, J.Z.; Klein, B.E.; Cotch, M.F.; Wong, T.Y.; Taylor, K.D.; Rotter, J.I. Associations of candidate genes to age-related macular degeneration among racial/ethnic groups in the multi-ethnic study of atherosclerosis. *Am. J. Ophthalmol.* **2013**, *156*, 1010–1020.e1.
103. Liu, K.; Akula, J.D.; Hansen, R.M.; Moskowitz, A.; Kleinman, M.S.; Fulton, A.B. Development of the electroretinographic oscillatory potentials in normal and ROP rats. *Investig. Ophthalmol. Vis. Sci.* **2006**, *47*, 5447–5452.
104. Fischer, M.D.; Huber, G.; Beck, S.C.; Tanimoto, N.; Muehlfriedel, R.; Fahl, E.; Grimm, C.; Wenzel, A.; Reme, C.E.; van de Pavert, S.A.; et al. Noninvasive, in vivo assessment of mouse retinal structure using optical coherence tomography. *PLoS ONE* **2009**, *4*, e7507.
105. Seeliger, M.W.; Beck, S.C.; Pereyra-Munoz, N.; Dangel, S.; Tsai, J.Y.; Luhmann, U.F.; van de Pavert, S.A.; Wijnholds, J.; Samardzija, M.; Wenzel, A.; et al. In vivo confocal imaging of the retina in animal models using scanning laser ophthalmoscopy. *Vis. Res.* **2005**, *45*, 3512–3519.

It is not the strongest of the species that survives, nor the most intelligent that survives. It is the one that is the most adaptable to change

— Charles Darwin

Bioprinted 3D Outer Retina Barrier Uncovers RPE-dependent Choroidal Phenotype in Advanced Macular Degeneration

Min Jae Song, Russ Quinn, Eric Nguyen, Christopher Hampton, Ruchi Sharma, Tea Soon Park, Céline Koster, Ty Voss, Carlos Tristan, Claire Malley, Anju Singh, Roba Dejene, Devika Bose, Paige Derr, Kristy Derr, Sam Michael, Francesca Barone, Arvydas Maminishkis, Ilyas Singec, Marc Ferrer, Kapil Bharti

In preprint. Submitted **2022**.

5

Abstract

Age-related macular degeneration (AMD), a leading cause of blindness, initiates in the outer-blood-retina-barrier (oBRB) formed by Retinal pigment epithelium (RPE), Bruch's membrane, and choriocapillaris. The mechanism of AMD initiation and progression remain poorly understood due to the lack of physiologically relevant oBRB models.

We engineered a native-like 3D-oBRB tissue by bioprinting endothelial cells, pericytes, and fibroblasts on the basal side of a biodegradable scaffold and establishing an RPE monolayer on top. In this 3D-oBRB, a fully-polarized RPE monolayer with apical processes and basal infoldings provides barrier resistance, induces fenestration and choroid-specific gene expression in the choriocapillaris, and supports the formation of a Bruch's-like membrane that allows tissue integration in rat eyes. Complement activation in the 3D-oBRB triggers dry-AMD phenotypes (including subRPE drusen and choriocapillaris degeneration), and hypoxia activated HIF-α induces wet-AMD phenotypes (choriocapillaris neovascularization). Anti-VEGF drug treatment suppresses neovascularization - validating this model for clinical translation and drug discovery.

Introduction

Age-related macular degeneration (AMD) affects over 196 million people worldwide and leads to blindness in advanced stages [1]. Atrophy of the retinal pigment epithelium (RPE) and the choriocapillaris of the choroid in advanced AMD stages trigger photoreceptor cell death leading to blindness [2,3]. With its functional tight junctions, the RPE monolayer and the choriocapillaris, separated by a proteinaceous (2-5 µm thick) Bruch's membrane, form the outer-blood-retina-barrier (oBRB) in the back of the eye [4]. RPE basal infoldings, Bruch's membrane, and fenestrations (60-80 nm pores) in the endothelial cell (EC) membrane allow unimpeded macromolecule and nutrient flow from the blood into the RPE - which regulates flow to the photoreceptors [4].

Dry AMD initiates by the accumulation of lipid/protein-rich drusen deposits, triggered by complement pathway activation, in the subRPE region [3,4]. Disease progression to the advanced stage geographic atrophy is hallmarked by RPE dropout that precedes choriocapillaris degeneration, leading to outer retina starvation [3]. In contrast, in advanced wet AMD (choroidal neovascularization, CNV) choriocapillaris hyperproliferate, grow under the RPE and occasionally break through RPE tight junctions leaking blood in the sub-retinal space [5]. This separates the photoreceptors from the RPE and deprives them of the RPE's functional and nutrient support resulting in photoreceptor degeneration [5]. The importance of vascular endothelial growth factor (VEGF) in CNV is underscored by the successful application of drugs that block VEGF signaling (Bevacizumab, Ranibizumab, and Aflibercept) [6,7]. However, the mechanism of increased VEGF secretion by human RPE remains elusive due to a lack of human-relevant models that accurately recapitulate CNV. Here, we developed a functionally validated 3D-oBRB utilizing bioprinting, tissue engineering, and directed differentiation of human induced pluripotent stem cells (iPSCs). The 3D-oBRB model recapitulates RPE-choriocapillaris interactions under healthy and dry and wet AMD stages.

Materials and methods

Donor tissues

Human cadaver eyes were obtained from the Advancing Sight Network (Alabama Eye Blank, Birmingham, AL). Use of cadaver eyes was exempt from the NIH Institutional Review Board approval.

Tissue culture media

RPE Maintenance Media (RPE-MM) components includes basal MEM alpha-modified media (Sigma-Aldrich, Cat# M-4526, St. Louis, MO) supplemented with N-2 supplement (1 % v/v, Gibco, Cat# 17502048, Waltham, MA), Glutamine, Penicillin and Streptomycin (1 % v/v, Sigma-Aldrich, Cat# G1146), Non-essential Amino Acids (5 mL, Sigma-Aldrich, Cat# M7145), a Taurine, Hydrocortisone and Triiodo-Thyronin cocktail dissolved in DPBS (125 mg/10 µg/0.0065 µg, Sigma-Aldrich, Cat#T-0625/H-0396/T-5516) and heat-inactivated fetal bovine serum (5 % v/v, FBS, Sigma-Aldrich, Cat#F4135-6X500ML/6505).

iPSC Endothelial Cell Media (iCell Media) consists of VascuLife Basal Medium (Thermo Fisher Scientific, Cat#LL-0003, Waltham, MA), growth factors from the VEGF LifeFactors® Supplement Kit (LifeLine Cell Technologies, Cat#LS-1020, Frederick, MD), and iCell Endothelial Cells Medium Supplement (Cellular Dynamics International, Cat#M1019, Madison, WI).

Note that fetal bovine serum and gentamycin were excluded from the LifeFactors® supplement kit. All Media was filtered through sterile 0.22 µm pore filters before use.

Cell/Tissue Culture

Human placental microvascular pericytes (Angio-Proteomie, Cat#cAP-0029, Boston, MA) were cultured on 25 cm^2 Easy Flasks (Thermo Fisher Scientific, Cat#156367) coated with quick coat solution (3 mL, Angio-Proteomie, Cat#cAP-01). Pericytes were cultured in RPE-MM, which is changed every other day. Pericytes were passaged up to three times prior to 3D bioprinting. iCell endothelial cells (Cellular Dynamics International, Cat#R1022) were cultured on 75 cm^2 Easy Flasks (Thermo Fisher Scientific, Cat#156499) coated with Fibronectin (Gibco, Cat#33016-015). The cells were cultured in the iCell Media with media changes occurring every other day. Cells were passaged at >70 % confluence by incubating cells in 0.25 % Trypsin-EDTA (1X, Gibco, Cat#.25200-056) for 5 minutes at 37 °C. The cells were then resuspended in iCell complete endothelial medium and centrifuged at 200 RCF for 5 minutes. The cells were passaged up to two times prior to 3D Bioprinting. The adult choroidal fibroblasts were isolated from cadaver human eyes which were procured from Alabama Eye Bank. Fibroblasts were cultured on Primaria tissue culture flasks (Corning, Cat#353824, Corning, NY) in RPE-MM.

iPSC derived Retinal Pigment Epithelium (iPSC-RPE) were purchased from Cellular Dynamics International. iPSC-RPE cells were seeded with initial density of 2.5×10^5 cells/well on a vitronectin coated transwell membrane (0.5 mg/mL, Thermo Fisher, Cat#A31804; Corning, Cat#3407). The medium was changed every other day. After two weeks of post-seeding, RPE maintenance media supplemented with Prostaglandin E2 (Tocris Biosciences, Cat#363-24-6, Bristol, United Kingdom) at a 100 μM concentration were fed to the iPSC-RPE cells for maturation.

Biodegradable scaffold and bioink

Scaffolds used to support 3D-oBRB were constructed by modifying commercially available trans-well inserts (Corning, Cat#3407). The permeable membranes included with the inserts were removed and replaced with 12-mm diameter circular sheets of biodegradable PDLGA scaffold (Polysciences, Cat#052218-6_1_20_20_55_24, Warrington, PA; Biosurfaces, Boston, MA). Following the removal of the transwell membranes, the transwell frames were dipped into Kwik-Cast silicone gel (World Precision Instruments, Cat#KWIK-CAST, Sarasota, FL), and the PDLGA scaffolds were attached to the frames. The gel solidified for 5 minutes with the scaffold facing up. Afterward, O-rings (Inner diameter: 10.4 mm, Outer diameter: 14.5 mm), which were 3-D printed using an Ultimaker2+ 3D Printer (Ultimaker, Utrecht,Netherlands), were treated on its inner surface using additional Kwik-Cast gel and attached to the basal side of the modified transwells. The gel solidified for 10 minutes, permanently attaching the scaffolds to the transwell frame. The scaffolds were coated on the apical side with vitronectin and incubated for an hour at room temperature, followed by an additional hour of incubation at 37 °C. Afterward, vitronectin from the apical side was aspirated and 4 mL of cell culture grade water was added to the bottom of the scaffold in well plates. The scaffolds were then incubated at 37 °C for 2 hours. Following incubation, the water was aspirated, and the scaffolds were dried overnight.

On the day of bioprinting, a 2.5 mg/mL fibrinogen solution (Sigma-Aldrich, Cat#F3879, St. Louis, MO) was prepared in DPBS (Calcium and Magnesium free, Thermo Fisher Scientific, Cat#14190144, Waltham, MA) to encapsulate cells during “choroid” printing. Aprotinin (0.075 U/mL, Sigma, Cat#A4529) was added to the fibrinogen solution, and the entire solution was filtered through a sterile 0.22 μm filter. Following filtration, a 300 mg sample of Novogel 2.0 (Organovo 3D Bioprinting Solutions, Cat#NVG-2.0, San Diego, CA) was carefully added to 5 mL of the fibrinogen solution. The solution was incubated in a 37 °C water bath to dissolve the Novogel powder. After dissolution, the completed 2.5 mg/mL fibrinogen solution was incubated at 37 °C for 1 to 2 hours prior to cell encapsulation. A 5.0 mg/mL fibrinogen solution was prepared identically to the 2.5 mg/mL solution above without the addition of Novogel powder. This solution was placed at 4 °C until bioprinting.

Bioprinting of "choroid" and 3D-oBRB maturation

Following assembly of the scaffolds and immediately before bioprinting, the scaffolds were treated in a Plasma Etch PE-50 oxygen-plasma etcher at maximum power (150W, Plasma Etch, Inc., Carson City, NV) for 30 minutes under 10 CC/min O^2 flow to sterilize and improve surface hydrophilicity.

Fibroblasts, endothelial cells, and pericytes were trypsinized from cell culture flasks as described previously. Cells were encapsulated at the following densities in the 2.5 mg/mL fibrinogen solution: 1.0 to 1.2 × 10^7 Fibroblasts/mL; 5.0 to 7.0 × 10^6 Endothelial cells/mL; and 5.0 to 7.0 × 10^5 Pericytes/mL. The three cell types were combined and centrifuged at 500 RCF for 4 minutes before resuspension in the 2.5 mg/mL fibrinogen solution. Resuspension and mixing were conducted using a sterile spatula (Corning, Cat#3004) to prevent air bubble formation in the suspension. The cell suspension transferred to a sterile Hamilton Gastight syringe without air bubbles (Hamilton, Cat#1750). The syringe was then sealed and placed at 4 °C for 12-15 minutes with the dispensing side facing up. A NovoGen MMX Bioprinter™ (Organovo, San Diego, CA) was used to extrude the solution onto the biodegradable polymer scaffolds.

After the structure was printed, 360 µL of 5 mg/mL fibrinogen solution was added to a 40 uL aliquot of 10 U/mL thrombin. 170 uL of the 5 mg/mL fibrin gel with thrombin was then added directly to the printed structure to form a supporting fibrin gel structure between printing lanes.
It solidified for 15-20 minutes. Printing Medium, which consists of a 1:2 ratio of iCell media and serum-free RPE-MM that was supplemented with 1.67 % heat-inactivated FBS, thrombin (0.5 U/mL, Sigma, Cat#T6884), rh ANG-1 (100 ng/mL, R&D Systems, Cat#923-AN, Minneapolis, MN), VEGF (85 ng/mL, R&D systems, Cat#293-VE-500), and aprotinin, was then added to the well (0.5 mL apically, and 3.5 mL basally) and laced at room temperature 2 hours. The samples were then placed in a 37 °C, 5 % CO_2 incubator overnight.

Bioprinted 3D-oBRB tissues consist of multiple cell types such as endothelial cells, pericytes, fibroblasts, and iPSC-RPE and were incubated under a complex medium changing schedule (Table 1). RPE cells were seeded on the apical side of the PDLGA scaffold at day 7 after bioprinting. 2.5 × 10^5 RPE cells were added to each bioprinted tissue in suspension of RPE-MM. The RPE growth and maintenance media were used according to table S1. Printing Media was applied to the apical and basal sides of the tissue on the day of the print. Tissues were then fed on the apical and basal sides using Vascular Development Media (VDM), which has the same composition as Printing Media but with thrombin removed, from day 2 to day 7. On day 7, the apical sides of the tissues were fed using 5 % RPE, while the basal sides of the tissues were fed using Vascular Growth Media with Aprotinin (VGM+AP), which excludes ANG-1 and VEGF from VDM. On day 14, the apical sides of the tissues continued to be fed using 5 % RPE, while basal sides of the tissues were fed using VGM which excludes Aprotinin from VGM+AP. On day 21, media conditions were identical to the previous week, except that the 5 % RPE medium was supplemented with Prostaglandin E2 at a 100 µM concentration on the apical side. From day 29 onward, media conditions were identical to the previous week, except that Vascular maintenance media (VMM), which excludes VEGF completely, replaced VGM medium on the basal side.

Rat Transplantation

The tissue was gently wash with BSS+ (*Alcon* Inc, Cat#00065079515) and a thin layer of Healon PRO (Johnson & Johnson Vision Care Inc) was used to protect it during manipulation. A 1.5 mm (Acuderm Inc Cat#P1525) puncher was used to cut the dose to deliver from the cultured tissue. RNU rats from Charles River Laboratories, Inc., Wilmington, MA were used in this study. The animals (n = 4, males, between 250 and 300 g) were anesthetized with i.p. injection of Ketamine (65 mg/kg, VetONE Inc, Cat#13985-702-10) and 7.5 mg/kg Xylazine (7.5 mg/kg, Akorn Inc, 59399-111-50). Animals were then placed on a shaped foam holder and the body was covered to avoid body temperature drop. Isoflurane was administered in mask, 1 % with an oxygen flow rate of 300 mL/min, to maintain anesthesia. Eyes were exposed and secured by a suture tide around the eyeball. Proparacaine (0.5 %, Novartis, Cat#61314-016-01) was used as local anesthetic and the pupil were dilated with Phenylephrine (Paragon Biotek, 4270210215) and Tropicamide (Novartis, Cat#T2018-39) eye drops. GenTeal lubricant eye gel (Alcon, Cat#US-GNT-VLC-2000008) and a glass cover slip were used as a lens substitute to visually access the back of the eye. A 2.2 mm knife was used for sclerotomy, vitreous was replaced with 2 % Hyaluronic acid (HA) (Sigma Aldrich, Cat#H7630) and the retina was detached with 0.5 % HA.

The tissue was then delivered in the subretinal space with end-grasping ophthalmic forceps. The retina was flattened with 2 % HA. The suture used to expose the eye was removed and topic Neo-Poly-Bac (Bausch & Lomb, Cat#*IWM044525*) ophthalmic ointment was used to prevent infections. Animals were kept in a warm, dark and quiet environment until complete recover from anesthesia, then were single caged until the end of the experiment. Two weeks after surgery animals were euthanized by CO_2 overdose and perfused with 1,1'-dioctadecyl-3,3,3',3'-tetramethylindocarbocyanine perchlorate (DiI) (Sigma Aldrich, Cat#42364) a lipophilic carbocyanine dye, which incorporates into endothelial cell membranes upon contact (Li et al., 2008). The dye was prepared and administered as previously described by Li, followed by 4% PFA perfusion. Eyes were collected and fixed in 4 % PFA overnight

Modeling Wet and Dry AMD

We modeled wet and dry AMD on four-week-old tissue using a chemical stressor or complement competent human serum, respectively. For Wet-AMD, ML228 (2 μM) was introduced to the apical side of RPE and treated for four days, and Bevacizumab (0.284 mg/mL, NIH clinical center) was treated with ML228 after the four days of the ML228 treatment. ML228 was treated every day and Bevacizumab was treated every other day. For Dry AMD, complement competent human serum (5 %) was treated to both apical and basal side of the tissue with everyday media change. The total inducing period for both AMD models is two weeks.

Trans-Epithelial Resistance measurements and fixation

The junctional integrity of 3D-oBRB tissues or iPSC-RPE monolayers were examined prior to fixation. Trans-Epithelial Resistance (TER) was measured using an EVOM2 Epithelial Volt/ohm meter (World Precision Instruments, Cat#300523) and an Endohm-245NAP well container (World Precision Instruments). Afterward, tissue samples were incubated in 4 % PFA in 1× PBS at 4 °C overnight for fixation and were washed three times for 10 minutes in 1× PBS. At this point, whole tissue samples were either Cryosectioned (See: Cryosectioning) or Paraffin-sectioned (See: Paraffin-sectioning) or immunostained (See: Immunostaining). If whole tissue samples were to be immunostained directly, samples were permeabilized using in 0.5 % Triton X-100 (Thermo Fisher Scientific, Cat#85112) solution in 1× PBS. Samples were punched out using a biopsy punch,transferred to the 24 well and blocked in 5 % goat serum, 0.1 % Triton X-100 and 1 % BSA in 1× PBS for 1 hour at room temperature. Afterward, the samples were washed three times for 10 minutes in 1× PBS.

Microscopy

Time lapse images of GFP labeled endothelial cells were taken by aEVOS Auto FL (Thermo Fisher Scientific, NY). Time-course immunofluorescent images for quantification were taken by using Leica TCS-SP8 (Leica, Wetzlar, Germany) and Zeiss LSM710 (Zeiss, Oberkochen, Germany) confocal microscopes. 3D reconstructed images with high magnification (×25) were taken by SP8 confocal microscope (Leica). Transmission electron microscopy with glutaraldehyde fixed samples was taken by the NEI core facility using a JEM-1010 electron microscope (JEOL, Peabody, MA).

Histology and immunofluorescence

Cryosectioning

Fixed tissue samples were punched from transwell inserts using a 10-mm biopsy punch and incubated in 15 % sucrose, followed by 30 % sucrose until the water was sufficiently removed from the tissue sample (approximately 1-hour incubation per solution). Rat Ocular Tissue was extracted from animals, and then flash frozen. Afterward, the tissues were embedded in Optical Cutting Temperature Embedding Medium (Thermo Fisher Scientific, Cat#23-730-571) and frozen using dry ice for a minimum of 90 minutes. The samples were stored in -80 °C until sectioning. The tissues were cut to to 12-µm-thickness slices and loaded onto glass slides using a cryostat (Leica, Germany) at -30 °C cutting temperature and -15 °C sample head temperature. Prior to staining, tissue slices were heated on a hot plate to 37 °C for 30 minutes to secure the section to the glass slide. The tissues were then either H&E stained using an automated H&E Staining machine (Bond RX; Leica, Germany), or immunostained. During immunostaining, the slices were blocked and permeabilized using 0.5 % Triton X-100 (Thermo Fisher Scientific, Cat#85112) prior to the application of primary and secondary antibodies.

Paraffin Sectioning

Fixed samples were permeabilized for 30 minutes in 0.5 % Triton X-100 (Thermo Fisher Scientific, Cat#85112). After permeabilization, samples were punched out from transwell inserts using a 10-mm biopsy punch and stored in 24-well plates. Samples were then blocked in 5 % goat serum, 0.1 % Triton X-100 and 1 % BSA in 1× PBS for 1 hour at room temperature. Afterward, the samples were washed three times for 10 minutes in 1× PBS.

Vibratome Sectioning

Fixed 3D-oBRB and Rat Ocular tissues were embedded in 6.8 % *w/v* Type 7-A Agarose (Sigma-Aldrich, Cat# A0701) and cut into 100 µm sections on the Leica VT 1200S vibratome (Leica, Wetzlar, Germany). Sectioned samples were blocked, permeabilized, and washed prior to staining as described previously.

Immunostaining

Primary antibodies were diluted in 1× PBS containing 0.1 % Triton-X-100 and 1 % BSA and 3D-oBRB tissues, or iPSC-RPE monolayers were incubated at 4 °C overnight. Primary antibodies included Mouse anti-PLVAP (FELS, 1:50, Abcam, Cat#AB81719); Rabbit anti-CD31 (1:50, Abcam, Cat#AB28364); Mouse anti CD31 (1:50, Agilent, Cat#M0823); Rabbit anti-Laminin (1:50; Abcam, Cat#AB11575); Mouse anti E-cadherin (1:100; Abcam; Cat#AB40772); mouse anti-ZO-1 (1:100; Thermo Fisher Scientific, Cat#33-9100); rabbit anti-ZO-1 (1:50; Thermo Fisher Scientific, Cat#61-7300) Mouse anti-Collagen-IV (1:50; Abcam, Cat#AB6311); Rabbit anti-Elastin (1:50 Abcam, Cat#AB21610); Rabbit anti-APOE (1:50; Abcam, Cat#AB52607), Rabbit anti-VEGF (1:50; Thermo Fisher Scientific, Cat#807), Mouse anti-STEM121 (1:100; Takara Bio, Cat#Y40410), Rabbit anti-VWF (1:100; Dako, Cat#GA52761-2) and Alexa-Fluor™ 647-Phalloidin (26 nM, Thermo Fisher Scientific, Cat#A22287).

Blocking controls were performed using primary antibody buffers without the use of primary antibodies. Samples were then washed three times for 10 minutes in 1× PBS. Secondary antibodies were diluted (PBS containing 0.1 % Triton-X-100 and 1 % BSA). Secondary antibodies included Alexa-fluor™ Goat anti Rabbit 647 (Invitrogen, Cat#A21244); Goat anti Rabbit 594 (Life Technologies, Cat#A11012); Goat anti Rabbit 555 (Invitrogen, Cat#A32732); Goat anti-Rabit 488 (Invitrogen, Cat#A11008); Goat anti-mouse 647 (Invitrogen, Cat#A32728); Goat anti-mouse 595 (Invitrogen, Cat#A11032); Goat anti-mouse 555 (Invitrogen, Cat#A21422); Goat anti Mouse 488 (Invitrogen, Cat#A32723). Secondary antibodies were incubated with Hoescht 33342 nuclear stain (1:2000) in the dark at room temperature for 4 hours. Samples were washed 3 times for 10 minutes in 1× PBS. Cryosectioned, Parafilm-sectioned and whole tissue samples were mounted using Fluoromount G (Southern Biotech, Cat#0100-01, Birmingham, AL) following immunostaining.

Quantification

Angiogenesis quantification

Fluorescent images of vasculature at 4, 6, and 8 days after bioprinting, either non-treated or treated with varying doses of VEGF were quantified using MATLAB version 2019b (Mathworks, Natick, MA). Six line probes, numbered 1 to 6, were created in the acellular spaces between printed stripes. Fluorescence intensity peaks with a threshold (100 in 8-bit gray scale) that overlapped with the line probes were quantified in each image (Fig. S2). The counted peaks from each line number were averaged per each vascular micrograph, representing the "edges" to "centers" of the acellular space. To determine the directionality and persistence of blood vessel migration into the acellular regions, an angiogenesis index was created to quantify mean blood vessel length perpendicular to the printed stripes.Confocal images were processed as maximum intensity projection images and the angiogenesis index was measured using MATLAB (Mathworks). Briefly, regions of interest were defined in acellular spaces as a space within 250 pixels of a line probe generated through the center of the spaces. Acellular spaces that overlapped with out-of-focus endothelial cell clusters were excluded from analysis (Figure S5b). Blood vessels were defined as objects that were greater than 20 pixels in length and expanded to within a mean distance of 85 pixels of the line probe. Angiogenesis index was calculated using maximum ferret angle of each blood vessel relative to the line probe and maximum ferret diameter of each blood vessel [equation (1)].

$$(1)\ Index = |sin\,(MaxFerretAngle) \times MaxFerretDiameter|$$

FELS immunostaining quantification for the analysis of vascular network in 3D-oBRB tissues

Immunostaining images of CD31 and FELS were analyzed using ImageJ to quantify the vascular networks in 3D-oBRB tissues. Any CD31-labeled images taken one week after bioprinting were contrasted with isolating the brightest 80 % of pixels (Leica TCS-SP8 and Zeiss LSM710) from the background. For the rest of the time points, CD31-labelled images were contrasted with isolating the brightest 20 % of pixels from the background. FELS-labeled images were contrasted with separating the brightest 5 % of pixels from the background at all time points. The area ratios were taken between FELS-positive area/image and the combined area of CD31 and FELS-positive signal to quantify the area of CD31 that was co-occupied by FELS.

VEGF Immunostaining Quantification

Z-stacks of the VEGF-A-stained cryosectioned tissue slices were analyzed using ImageJ. The images were converted into maximum intensity projection images before quantification. For image quantification, a Gaussian Blur Filter (radius 4.0 px) was applied to reduce noise in the images. The average pixel brightness along the thickness of the slice was quantified for each slice to identify areas of high VEGF concentration in the slices. Phalloidin 647 staining was used to identify the apical (RPE) and basal (choroid) ends of the tissue slices.

Cytokine Quantification

To quantify the cytokine secretion from iPSC-RPE monolayers and 3D-oBRB tissues, apical and basal media were collected at 48-hour, 96-hour, and 2-week timepoints and frozen at - 80 °C until the assay was performed. Once thawed, the samples were centrifuged at 1400 RPM for 5 minutes to remove possible cell debris from sample supernatant. The assay was carried out using a Millioplex MAP Kits per the manufacturer's instructions (Millipore-Sigma, Cat# HCYTOMAG-60K) analyzed at the NIH Flow Cytometry Core Facility.

Vascular Density Quantification

3D reconstruction of tissues was conducted on confocal images taken with 20× or 25× magnification, and area fractions of CD31 expression were calculated in each focal plane. For estimating distance from RPE region, beginning focal plane of vasculature was manually determined by comparing to z-stack images with ZO-1 expression by RPE. Thresholding was performed on z-stack images of the CD31 channel by Otsu thresholding method in ImageJ. Step size of the distance from RPE was determined as 5 μm to adjust z-step size differences between samples.

Quantification of Extracellular Matrix Deposition

RPE monoculture and 3D-oBRB tissues in 24 transwell plates were fixed with 4 % PFA after 5 weeks from RPE seeding on transwell membrane or bioprinted “choroid”. The z-stacks of confocal images from the apical side of RPE to the basal side of RPE were taken with the same microscope settings among the treatment groups. Mean intensity of Elastin and Collagen IV expression were measured using ImageJ.

Single cell RNA sequencing

Endothelial cell Isolation from 3D-oBRB tissues

The endothelial isolation was performed by digesting the 3D-oBRB tissues. The digestion solution was created using 1.5 mg/mL Collagenase II (Gibco, Cat#17101-015), 0.5 mg/mL DNAse I (Worthington Biochemical Corporation, Cat# 54D14897, Lakewood, NJ) and 0.2 mg/mL Dispase I (Sigma, Cat#D4818) in PBS. Tissues were removed with a sterile scalpel, placed in a 50 mL conical tube. Digestion solution was added (approximately 10 mL/6 tissues) and the samples were rocked on an orbital shaker at 37 °C for 30 minutes. Following the incubation, the suspension is given 20mL of media and is then centrifuged at 1000 RPM for 5 minutes. Endothelial cells were then purified using magnetic assisted cell sorting (Miltenyl Biotec, Cat#130-042-401) protocol supplied by Miltenyl Biotec, counted, and analyzed with assistance from the NCATS Stem Cell Translation Laboratory.

Single-cell RNA Library Preparation

Single-cell suspensions were loaded on a Chromium Controller (10X Genomics) to generate single-cell gel bead-in-emulsions (GEMs) and barcoding. GEMs were transferred to PCR 8-tube strips, and GEM-reverse transcription was performed in a C1000 Touch Thermal Cycler (BioRad). GEMs were lysed in recovery buffer, and single-stranded cDNA was cleaned up using silane DynaBeads (Thermo Fisher Scientific). cDNA was amplified in a C1000 Touch Thermal Cycler (BioRad). Amplified cDNA was cleaned up using the SPRIselect Reagent (Beckman Coulter). Post cDNA amplification QC and quantification were done using a High Sensitivity D5000 ScreenTape Assay (Agilent) on a 4200 TapeStation System (Agilent). Library Construction was done by fragmentation at 32 °C for 5 min, end repair, and A-tailing at 65 °C for 30 min. Post fragmentation, end repair, and A-tailing double-sided size selection were done using the SPRIselect Reagent (Beckman Coulter). Adaptor ligation was done at 20 °C for 15 min. Post ligation cleaned up using the SPRIselect Reagent (Beckman Coulter). Sample indexing was done using the i7 Sample Index Plate (Chromium) in a C1000 Touch Thermal Cycler (BioRad). Post sample index PCR double sided size selection done using the SPRIselect Reagent (Beckman Coulter). Post library construction quantification was done using a High Sensitivity D1000 ScreenTape Assay (Agilent) on a 4200 TapeStation System (Agilent). Sequencing libraries were quantified by quantitative PCR using the KAPA library quantification kit for Illumina platforms (KAPA Biosystems) on a QuantStudio 12K Flex Real-Time PCR System (Thermo Fisher Scientific). Libraries were loaded on an Illumina HiSeq 3000 using the following: 98bp Read1, 8bp i7 Index, and 26bp Read2.

The cellranger software package from 10X Genomics, Inc. (version 3.0.1) was used to process raw BCL files from single-cell sequencing as follows. This work used the computational resources of the NIH HPC Biowulf cluster (http://hpc.nih.gov). Demultiplexing and FASTQ generation were done with the mkfastq command, and the count command created gene expression matrices. Dense matrices were created with the mat2csv command. Embryonic stem cell and iPSC lines were analyzed in the Seurat R package (Stuart et al. 2018 https://www.biorxiv.org/content/10.1101/460147v1; Seurat 2.3.4; R 3.5.2).

Further data visualizations were made in R and with the ggplot2 package (3.1.0) (Table S2). Gene set enrichment analysis was performed using GSEA v4.0.3 (Broad Institute, Inc., MIT),the gene set databases C2 and C5 (MSigDB v6.2), which are the curated and Gene Ontology sets, and EnrichR 20. Endothelial and RPE single cell RNA-Seq phenotypes for 2D vs 3D-oBRB cells were coded as 0 and 1 respectively for a test of enrichment by ranked differential gene expression. Significantly enriched phenotypes were selected based on whether there was a nominal P value of <0.5 and a false discovery rate <25 % between 2D and 3D-oBRB datasets. Log2 ratio of classes was used for the ranking metric and otherwise default parameters were used. When comparing cytokine gene expression levels to cytokine detection levels in media, we extracted expression data was extracted for gene symbols that corresponded to the Luminex cytokine detection Assays performed previously. Only apical media was considered in these results. Only RPE gene expression data was considered in these results.

Single cell RNAseq Analysis

Gene List Construction

The ECM gene list was created by finding the gene ontology annotation for "extracellular matrix" (http://www.informatics.jax.org/go/term/GO:0031012), then narrowing that list to those genes that are also RPE characteristic genes [27] and genes found in the CYCLOPS database [22] to be expressed in the tissues "RPE fetal" and "RPE adult" at levels >2× levels that were found in at least 70 other tissues in the database. Selected genes must also exceed a minimum TPM threshold of 100. Afterward, the gene list was reduced to those pertaining to ECM proteins, matrix metalloproteinases, tissue-inhibitor matrix metalloproteinases, and ECM crosslinking proteins. Endothelial cell signature genes were derived from literature searches related to choroidal maturation [21], arterial and venous specification [19], as well as angiogenesis [23].

PCA Cluster Analysis

Statistical comparisons between 2D and 3D-oBRB gene expression and Gene Enrichment analysis were performed in RStudio using the Seurat Gene Expression Analysis Package) and EnrichR. Single Cell samples were filtered to exclude samples with less than 200 unique RNA features, more than 6,000 unique RNA features, and more than 5 % mitochondrial genome content. Afterward, samples were clustered using PCA (15 principal components analyzed) followed by tSNE. Endothelial cell clusters were identified using the Louvain algorithm at 0.2 resolution and RPE cell clusters were identified using 0.6 resolution. Gene enrichment was determined using the FindAllMarkers Seurat function. Genes in clusters with greater than 1.5-fold upregulation over the cell population average were processed in EnrichR to identify enriched biological processes (GO Biological Process 2018). Biological processes in clusters did not have 25 sufficiently upregulated genes were determined using comparisons with similar culture formats (i.e. 2D vs 2D or 3D-oBRB vs 3D-oBRB) only.

Statistical Analysis

All the data analyzed were unpaired (that is, the samples were independent from each other). Before conducting multiple comparison tests, the Brown–Forsythe test was performed to determine the homogeneity of variance between the datasets. One-way and Two-way ANOVA was performed prior to any post-hoc statistical comparison. To compare multiple datasets, Tukey's multiple comparisons test was used as a single-step multiple comparison procedure to find means significantly different from each other.

The Bonferroni post-hoc test was used to detect significant differences in the Line-Probe Angiogenesis quantifications. To compare datasets with a vehicle control, Dunnett's test was used to find means significantly different from the control. Student's T-Test was used to find significant differences between two single conditions. All statistical tests were two-tailed (two-sided tests). All statistical analyses were performed using Graphpad Prism version 8.2.0 for Windows (GraphPad Software, San Diego, CA) or Microsoft® Excel® for Microsoft 365 MSO (16.0.13001.20266) 32-bit (Microsoft, Redmond, WA). P <0.05 was considered significant. Variances between each group of data were represented by the standard deviation unless otherwise stated. Each statistical analysis method was indicated in individual quantification sections. Comparisons between ANG-1 and treated and non-treated conditions were performed using individual Sidak's Multiple Comparisons Tests on the day 4, 6, and 8 timepoints. Statistical comparisons between 2D and 3D-oBRB cytokine detection were performed using Sidak's Multiple Comparisons Test for each assayed gene.

Calculations were performed using Graphpad Prism ver. 8.2.0 (GraphPad Software, Inc). Sample sizes to ensure adequate power were as follows: initial angiogenesis formation between printed structures, n = 5 tissue replicates; ANG-1 modulating angiogenesis, n = 4 tissue replicates; Immunofluorescence of ECM proteins, n = 3; Outer-BRB maturation by RPE and printed choroid, n = 3 tissue replicates; Bevacizumab treatment on choroidal neovascularization model, n = 3 tissue replicates per condition; APOE deposition and dry AMD, n = 3 tissue replicates per condition; Single Cell RNASeq, n = 3012 2D RPE cells, n = 4380 3D-oBRB RPE cells, n = 5369 2D Endothelial cells, n = 1294 3D-oBRB Endothelial cells. Samples were excluded from analysis if they were determined to be outliers through Grubbs' outlier test.

Results

Design of 3D outer blood-retina barrier (3D-oBRB)

To develop a functional 3D-oBRB, we included the four key cell types (RPE, ECs, pericytes, and fibroblasts) in our tissue design (Figure 1A) [8,9]. The identity of iPSC-derived ECs (iECs), iPSC-derived RPE (iRPE), primary ECs, pericytes, and fibroblasts was confirmed using cell type-specific markers (CD31, ETV2, vWF – ECs; NG2, PDGFR-ß, COL-I – pericytes; VIMENTIN, COL-I, PDGFR-ß (negative) – fibroblasts; MITF, TYRP1, ZO-1, RPE65, EZRIN – RPE, Figure S1) [10-12]. A biodegradable scaffold made of thermally fused electrospun poly-(lactic-co-glycolic acid) (PLGA) fibers of 400-500 nm diameter supported the formation of a polarized RPE monolayer on one side and a capillary-bed derived from 3D-printed bioink of ECs, pericytes, and fibroblasts on the other side (Figure 1A and S2A, B). As the tissue matured, the degrading scaffold was gradually replaced by extracellular matrix (ECM) secreted by RPE and ECs forming a Bruch's membrane-like structure between the RPE and the capillary-bed.

Manufacturing and functional maturation of the 3D-oBRB took 42 days (Figure 1A). The printing surface was prepared a day before bioprinting by replacing the snapwell membrane with a 12 mm PLGA scaffold disc (Figure 1A; methods). The scaffold's RPE side was coated with vitronectin (50 μg/mL) to aid cell attachment. To enhance scaffold hydrophilicity - needed for bioink attachment, scaffold was treated with oxygen plasma (5 cc/min, 30mins). Improved hydrophilicity was confirmed by the dispersal of a water droplet (Figure 1A, S2C, D).

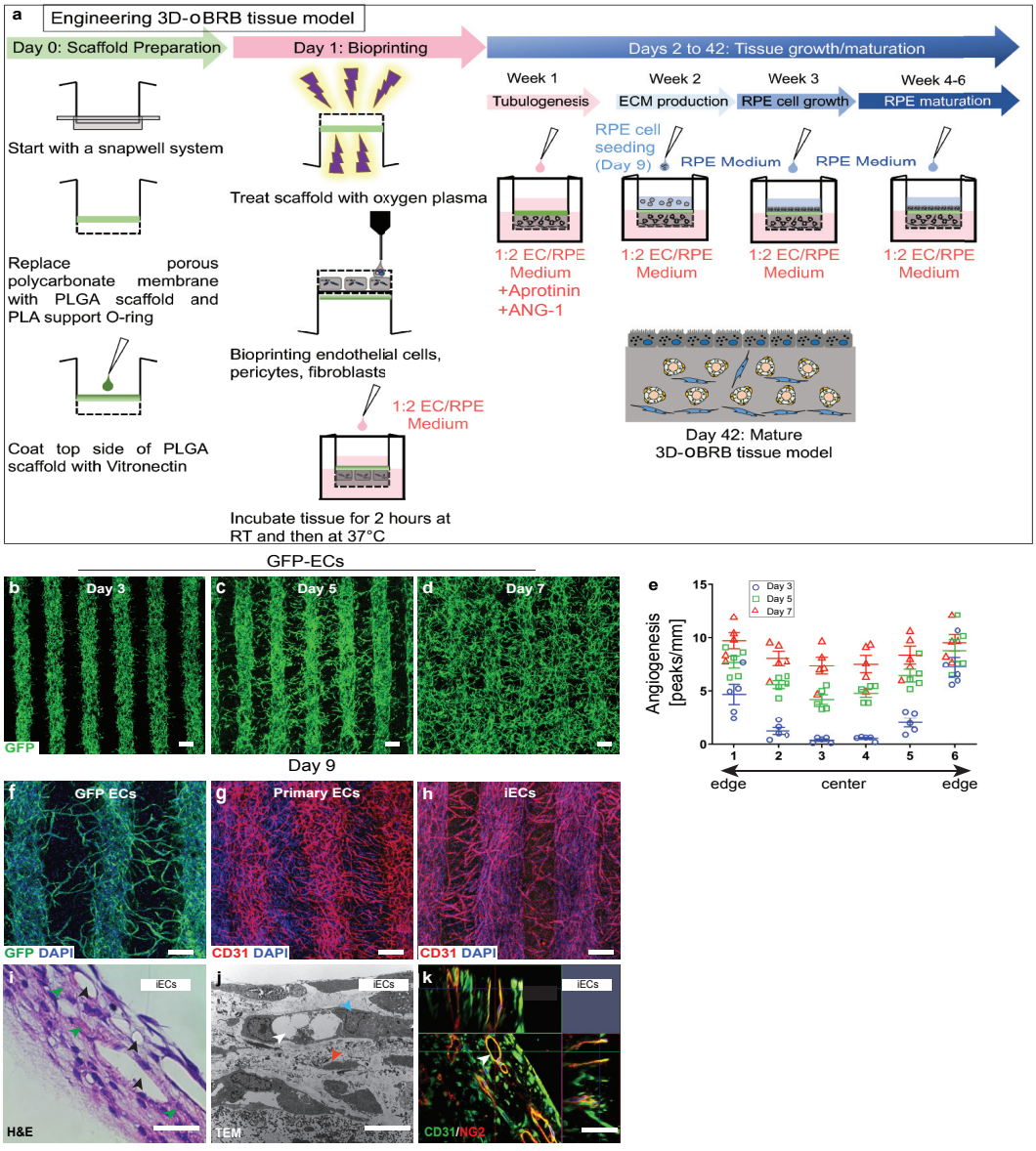

Figure 1. Design of 3D-oBRB. (**A**): bioprinting workflow with human endothelial cells (ECs) and RPE. (**B-D**): vascular development of GFP expressing primary ECs on day 3 (**A**), day 5 (**B**) and day 7 (**C**) after printing. Scale bars, 500 µm. (**E**): angiogenesis between printed stripes (n = 5). #p <0.05 in day 3 vs. day 5, †p <0.05 in day 5 vs. day 7, *p <0.05 in day 3 vs. day 7. (**F-H**): vascular formation of GFP-positive ECs (green, **F**), primary ECs (CD31 - red, **G**), and iPSC-derived ECs (iECs, CD31 – red, **H**) and nuclei (blue). Scale bars, 500 µm. (**I**): H&E images of 10 µm thick cross section of iECs derived vascular tissue (day 7). Vasculature is marked with black arrowheads, and ECM components are marked with green arrowheads. Scale bar, 50 µm. (**J**): transmission electron microscope (TEM) images of iECs derived vascular tissue at day 7. White arrowhead shows a capillary, blue arrowhead marks pericytes, and red arrowhead labels fibroblasts. Scale bar, 300 nm. (**K**): orthogonal views of confocal images of 100 µm thick tissue sections stained with CD31 (ECs; green) and NG2 (pericytes; red). White arrowheads mark patent EC-derived capillaries. Scale bar, 50 µm. Statistical significance was attributed to values of p <0.05 as determined by two-way ANOVA and Bonferroni post-hoc pair comparison. All error bars indicate STE.

Engineering 3D capillary-bed

To produce a dense capillary-bed of 5-20 μm lumen diameter [13], we sought to bioprint a high density of mixed ECs, pericytes and fibroblasts (12/6/0.6 million fibroblasts/EC's/pericytes per mL of bioink). To achieve a homogenous bioink with such high cell density, we designed a temperature-sensitive hydrogel by mixing a gelatin-based hydrogel (Novogel, 60 mg/mL) with fibrinogen (2.5 mg/mL) at 37 °C reduced hydrogel viscosity allowing bioink homogeneity and easier loading in the printing syringe. Cooling the syringe down to 10 °C increased bioink viscosity allowing for easy printing of desired structures. During tissue culture at 37 °C, Novogel dissolved and fibrin continued to provide the 3D architecture needed to support capillary-bed formation. However, fibrin degraded after four days leading to capillary-bed collapse, as confirmed by the clumping of GFP-expressing ECs (Figure S3A, B). The addition of recombinant aprotinin (25 μg/mL), a known fibrinolysis inhibitor, prevented tissue collapse giving fibroblasts time to secrete ECM that enabled a stable capillary network (Figure S3C, D).

A striped bioprinting pattern facilitated capillary growth quantification outwards from the printed stripes into the acellular hydrogel (movie S1; Figure S4). A MATLAB-based algorithm was developed for angiogenesis quantification (Methods). Bioprinted tissue was treated with VEGF (85 ng/mL) for three or seven days, to determine the optimal treatment window for capillary growth. Capillary sprouting was evident in printed ECs with three-days of VEGF treatment, but these sprouts did not form a contiguous capillary-network and disintegrated by day 7 (arrowheads, Figure S4A). In comparison, seven-days treatment increased capillary angiogenesis resulting in anastomosis between two printed stripes (arrowheads, Figure S4B, movie S1). Quantification revealed 1.5-2× folder higher angiogenesis on the edges of the printed tissues and 5-10× fold more angiogenesis in the center of the acellular structure after seven-days VEGF treatment as compared to three-days treatment (Figure S4A-E), establishing the use of exogenous VEGF for seven days.

Exogenous VEGF treatment supported EC angiogenesis, but it also increased EC migration resulting in sole ECs that didn't incorporate into capillaries [14] (Figure S5A and B - circle). To prevent this undesirable EC migration, we supplemented tissues with recombinant angiopoietin-1 (ANG-1; 100 ng/mL), a well-known EC migration inhibitor. Expectedly, ANG-1 initially slowed down capillary sprouting (arrowheads Figure S5A and C), but it did not disrupt capillary formation. In fact, by day 8 the number of capillaries increased in ANG-1 treated Group 2 as compared to without it (Group 1) (Figure S5 B, D). This allowed more precise analysis of the angiogenesis kinetics excluding individual EC signal.

To monitor the time course of angiogenesis, we analyzed the GFP-expressed ECs on days 3, 5 and 7 post-printing. By day 3, capillaries grew in a gradient with 5-6 capillary peaks/mm close to the printed stripe edge the and no peaks in the center of the acellular zone (p <0.001; Figure 1B, E, S6A). By day 5, the capillary gradient between stripe edges and the acellular area center was shallowed with 8 peaks/mm on edges and 4 peaks/mm in the center (p <0.05; Figure 1C, E, S6B).

By day 7, no statistically significant difference between edges (9 peaks/mm) and center (10 peaks/mm) was evident (p >0.05; Figure 1D, E, S6C). A comparative analysis of capillary networks derived from GFP-expressing ECs, non-GFP expressing ECs, and iECs revealed similar capillary confluency and angiogenesis throughout the tissue (Figure 1F-H). Together, this confirmed robustness of our bioprinting protocol across different ECs. Histological analysis (H&E staining) of tissue sections confirmed capillaries with 5-20 μm lumen diameters (black arrowheads) and interstitial spaces filled with cells and ECM (green arrowheads; Figure 1I). Transmission electron microscopy (TEM) of tissue cross-sections confirmed iECs derived capillaries (white arrowhead) with a pericyte (blue arrowhead) wrapped around, and fibroblasts (red arrowhead) in interstitial spaces (Figure 1J). This observation was further confirmed in confocal images of 100 μm thick tissue slices where pericytes (NG2, red) were found to colocalize with iEC (CD31, green) derived intact capillaries (arrowhead; Figure 1K, movie S2).

Overall, this data shows that our bioink composed of Novogel, fibrinogen mixed with fibroblasts, ECs, and pericytes (2:1:0.1 ratio) forms a robust capillary-network with both primary and iPSC-ECs.

Development of 3D-oBRB

To complete the 3D-oBRB, iPSC-derived RPE cells were seeded and matured [12] on the Vitronectin-coated scaffold side. TEM confirmed iRPE cells-initiated polarization and pigmentation within three weeks after seeding (Figure 2A). By six weeks, known structural features of RPE maturation and polarization were evident: dense apical processes (ap), tight junctions (tj) between neighboring cells, apically located stage IV melanosomes (ml), and basal infoldings (bi) - a critical native-RPE feature that cannot be reproduced in RPE grown on plastic substrates [15] (Figure 2B). Similar to the native-BRB, RPE basal infoldings were in continuum with the ECM that had replaced the scaffold and formed a Bruch's membrane (BM)-like structure (Figure 2B) [16]. Immunostaining for the tight junction marker E-CADHERIN and the apical process marker EZRIN further confirmed RPE monolayer junctional maturity and polarization (Figure 2C). Concurrent with the RPE maturation, capillary confluency was evident in CD31 immunostained 3D rendered tissue images (Figure 2D). High expression of FELS, a fenestration marker [17], colocalized with CD31 suggested the formation of fenestration in our 3D-oBRB model (Figure 2E, movie S3). Histological analysis revealed the structure of the entire 3D-oBRB with a 2-4 μm thick BM-like acellular ECM region sandwiched between an RPE monolayer on top and a 40-50 μm thick vascular tissue with capillaries (cl) running along various tissue planes (Figure 2F). To confirm functionality of the 3D-oBRB tight junctions, we measured tissue resistance to current flow (trans-epithelial resistance - TER), produced by functional tight junctions between neighboring RPE cells. TER of the tissue with vasculature and no iRPE layer was 53.4 (±1.36) Ohms·cm^2. The presence of the iRPE monolayer increased the tissue TER to 740.4 (±155.99) Ohms·cm^2, comparable to the TER of iRPE monolayer without the vascularized tissue 873.7 (±67.82) Ohms·cm^2 (Figure 2G). Finally, to confirm capillaries' functionality in this 3D-oBRB, we transplanted the intact tissue in the choroid of immunocompromised rats. Two weeks post-transplantation, animals were perfused with DiI in the left heart ventricle to label all the vessels; and choroid was analyzed histologically. Anti-human STEM121 labeling with GFP-expressed ECs in 10 μm cryosections identified human capillaries perfused with DiI suggesting anastomosis and integration with rat capillaries (Figure 2H). This was further confirmed by 100 μm sections that revealed different size human capillaries anastomosed and integrated within rat capillaries (Figure 2I, S7A, B). Overall, TEM, immunostaining, barrier resistance, and transplantation confirmed the formation of a functional 3D-oBRB with polarized RPE monolayer and functionally lumenized capillaries.

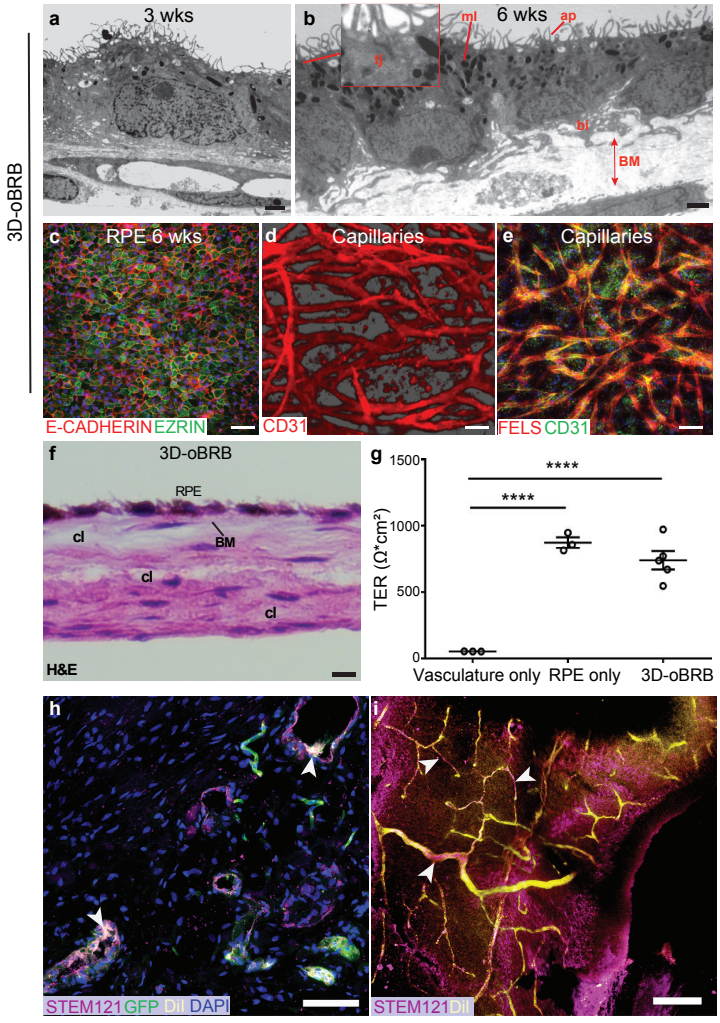

Figure 2. Engineering of 3D oBRB. (**A**,**B**): TEM images of 3D-oBRB maturity at week 3 (**A**) and 6 (**B**) with RPE pigmentation: melanin (ml), RPE apical processes (ap), RPE basal infoldings (bl), tight junction (tj) formation and Bruch's membrane (BM). Scale bars, 1 μm (**A**), 2 μm (**B**) (n = 3) (**C**): immunostaining for RPE maturity markers E-CADHERIN (red) and EZRIN (green) in 6-week-old tissues. Scale bar, 50 μm. (**D**): 3D-rendered image of CD31 (red) immunostained capillary-bed in 6-week-old 3D-oBRB. Scale bar, 50 μm. (n = 4) (**E**): immunostaining for capillary-maturation marker FELS (red) co-labeled with EC marker CD31 (green) of confocal images of vascular networks labeled with CD31 (red). Scale bar, 50 μm. (n = 3) (**F**): H&E staining of 6-week-old tissues containing capillaries (cl), RPE, and Bruch's membrane (BM). Scale bar, 10 μm. (**G**): transepithelial resistance (TER) of 3D-oBRB compared to vascular and 2D-RPE (n = 3). (**H**): GFP signal in human ECs and immunostaining with STEM121 (magenta) detect human capillaries that are perfused with DiI (yellow) in 10 μm cryosections of rat choroid transplanted with 3D-oBRB. Scale bar 75 μm. (n = 8 eyes from 4 animals). (**I**): immunostaining for STEM121 (magenta) detects human capillaries integrated with rat capillaries detected by Dil (yellow) perfusion in 100 μm vibratome sections of transplanted rat choroid. Scale bar 100 μm. Statistical significance was attributed to values of p <0.05 as determined by one-way ANOVA with Tukey's multiple-comparisons test. ****p <0.0001, All error bars indicate STE.

RPE cells induce capillary fenestration in 3D-oBRB

Strong FELS expression in fully-mature 3D-oBRB (Figure 2E) suggested the presence of fenestration in capillaries. To better characterize the fenestration process, we performed a temporal analysis of FELS expression in 3D-oBRB constructs (Figure S8A-D). CD31 co-immunostaining revealed minimal FELS expression in capillaries for the first two weeks post-printing (Figure S8A, B). Coincidental with iRPE monolayer polarization (Figure 2A), FELS expression became prominent starting week three (Figure S8C, D). To confirm if FELS expression led to fenestration in fully-mature 3D-oBRB, we performed ultrastructural analysis of capillaries (Figure 3A, B). TEM revealed 50-80 nm thinned areas in the EC capillary membrane reminiscent of fenestration in native choroidal capillaries (arrowheads Figure 3B) [18]. To further confirm if FELS expression was affected by the RPE presence, we cultured the vascular tissue with (Figure 3C, D, G) or without the RPE (Figure 3E, F, G). CD31 and FELS co-immunostaining revealed a confluent capillary bed with higher capillary number and thickness, and a 2.5-fold higher FELS expression in tissues that contained the RPE as compared to tissues that lacked the RPE monolayer where vasculature collapsed (Figure 3D, F, G). Overall, this work provides the first direct evidence that human RPE cells induce fenestration in an iEC-derived capillary-network.

RPE-dependent fenestration formation in our 3D-oBRB suggested that iECs acquire a choroidal fate. To investigate this possibility, we compared the transcriptome profiles of iECs within the 3D-oBRB and 2D monocultures (without RPE) using scRNAseq. Clustering samples by t-distributed stochastic neighbor embedding (tSNE) plots revealed three different EC populations in the 3D-oBRB, likely based on location in the tissue: fully-mature (FM) ECs expressed several choroidal and arterial maturation genes; partially-mature (PM) ECs expressed fewer arterial maturation genes; and inflamed (Inf) ECs expressed inflammatory genes in addition to arterial maturation genes (Figure 3H, I, Table S3). Detailed analysis revealed genes relevant for ECM (*COL3A1*, *COL6A1*, *COL1A1*), EC maturation (*LOX*, *VEGFA*, *GJA4*, *ACE*), choroidal phenotype (*APOE*, *PLVAP*, *TIMP1*), angiogenesis (downregulated - *ENG*, *ACTB*, *MMP1*; upregulated - *ADAM17*, *ITGAV*), and arterial maturation (*EPSA1*, *KDR*, *EFNB2*, and *NOTCH1*) showed the most differential expression among the 531 genes that were significantly different between 2D and 3D iEC transcriptomes (Figure 3I, S9, S10) [19-23]. Overall, these findings suggest that our 3D-oBRB construct capillaries matured and attained an arterial and choroidal phenotype.

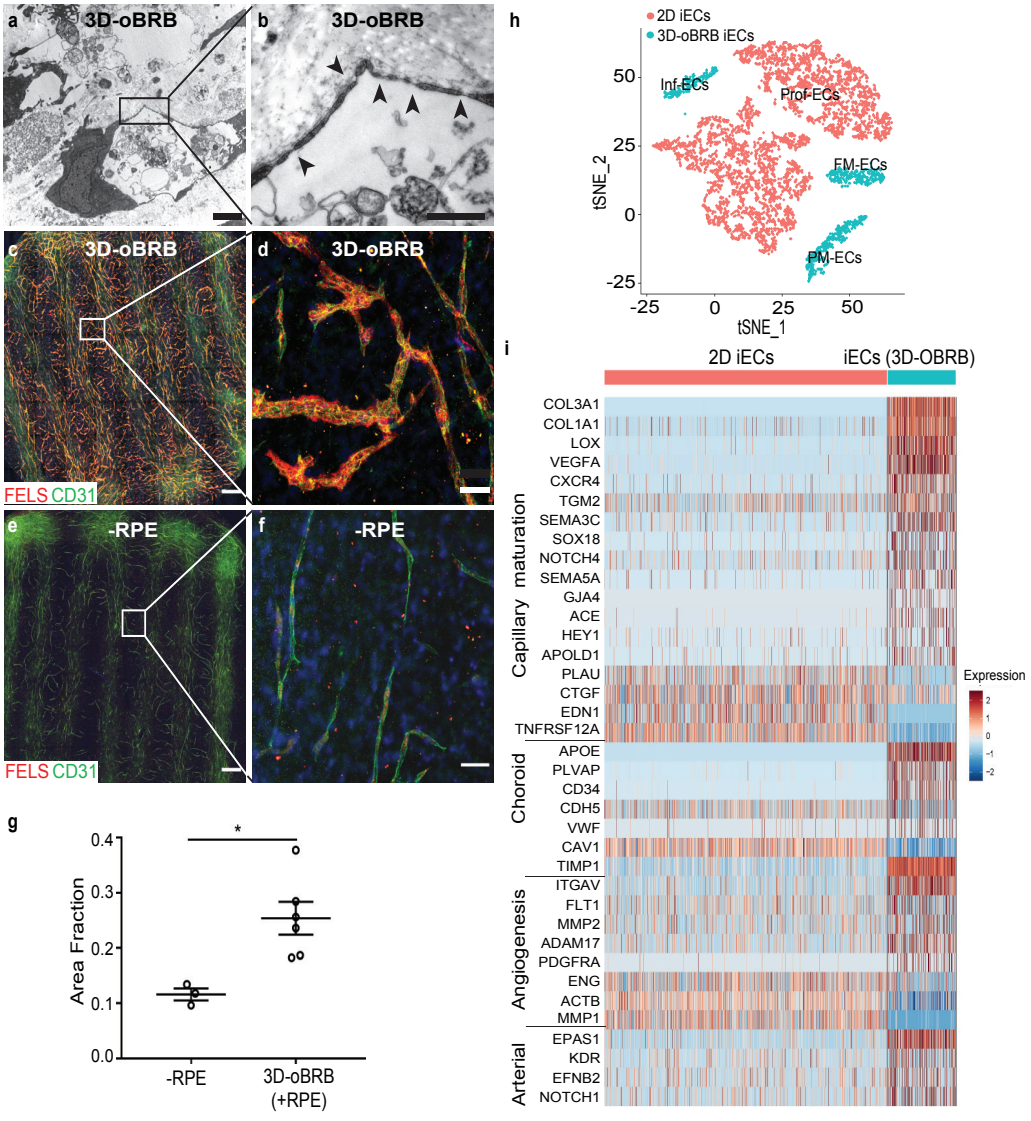

Figure 3. Capillary maturation in 3D-oBRB. (**A**, **B**): TEM images highlight fenestration (arrowheads) in iECs with in 3D-oBRB capillaries at week 6. Scale bars, 2 μm (**A**), 500nm (**B**). (n = 3). (**C**-**F**): immunostaining for FELS (red) and CD31 (green) in 3D-oBRB (with RPE; **C**, **D**) or just the vasculature (without RPE; **E**, **F**). Scale bars, 500 μm (**C**, **E**) and 50 μm (**D**, **F**). (**G**): area fraction of FELS and CD31 expression in vascular regions with or without RPE. (n = 3). (**H**): TSNE plots from sc-RNA seq of 2D iECs and iECs from 3D-oBRB. (**I**): gene expression differences between 2D iECs and iECs from 3D-oBRB for genes related to endothelial maturation, choroid, angiogenesis, and arterial development. Statistical significance was attributed to values of P <0.05 as determined by unpaired t-test. Data depicts results from n = 3012 cells (2D RPE), n = 4380 cells (3D-oBRB RPE), n = 5369 cells (2D iECs), and n = 1294 cells (3D-OBRB iECs). *p <0.05, All error bars indicate STE.

Bruch's membrane formation in 3D-oBRB

TEM suggested the formation of a Bruch's membrane-like structure between the RPE and the capillary-bed (Figure 2B). We confirmed strong immunostaining for ECM components of native Bruch's membrane including FIBRONECTIN, LAMININ, COLLAGEN IV (COL IV), and ELASTIN [16,24] (Figure 4A-D, movie S4). 3D rendering of ELASTIN and LAMININ immunostained images further revealed an acellular membranous zone underneath the RPE monolayer (movie S4). Quantification revealed a 15× higher COL IV expression and 4× higher ELASTIN expression in 3D-oBRB as compared to 2D-iRPE (Figure 4 E-I). To determine the cellular origin of Bruch's membrane, we analyzed ECM-related gene expression in scRNAseq data. iRPE contributed to ECM proteins like *COL8A1* and *EFEMP1* - involved in Doyne honeycomb retinal dystrophy [25] whereas iECs were the major source of ECM proteins including *COL8A1*, *COL8A2*, *COL9A3*, *COL11A1*, *ELN* (Figure S10A, B) [26-28]. All together this data shows that our 3D model enabled the creation of a Bruch's membrane-like structure *in vitro* that further enabled close interactions between RPE and choriocapillaris.

The presence of a Bruch's membrane-like structure prompted the question if iRPE grown on a natural ECM behave differently than iRPE grown on plastic substrates [15]. scRNAseq data confirmed this hypothesis. 46 out of the previously reported 157 RPE signature-genes [29] were 1.5-4 log2 fold-higher in iRPE in the 3D-oBRB than 2D iRPE. Most notable were components of the visual cycle (*RPE65*, *RDH5*, *RBP1*, *RLBP1*, *RDH11*), angiogenic and non-angiogenic genes (*VEGFA*, *ENPP2* and *SERPINF1*), components of the Bruch's membrane (*EFEMP1*, *ITGAV*, *ITM2b* and *TIMP1*), and exosome assembly genes (*HSP90B1*, *LAMP2*, *SDCBP*) (Figure 4J, K, S11A, B). Overall, this data provides additional evidence that as part of the 3D-oBRB both iECs and iRPE attain more native-like properties including the formation of a Bruch's membrane equivalent structure.

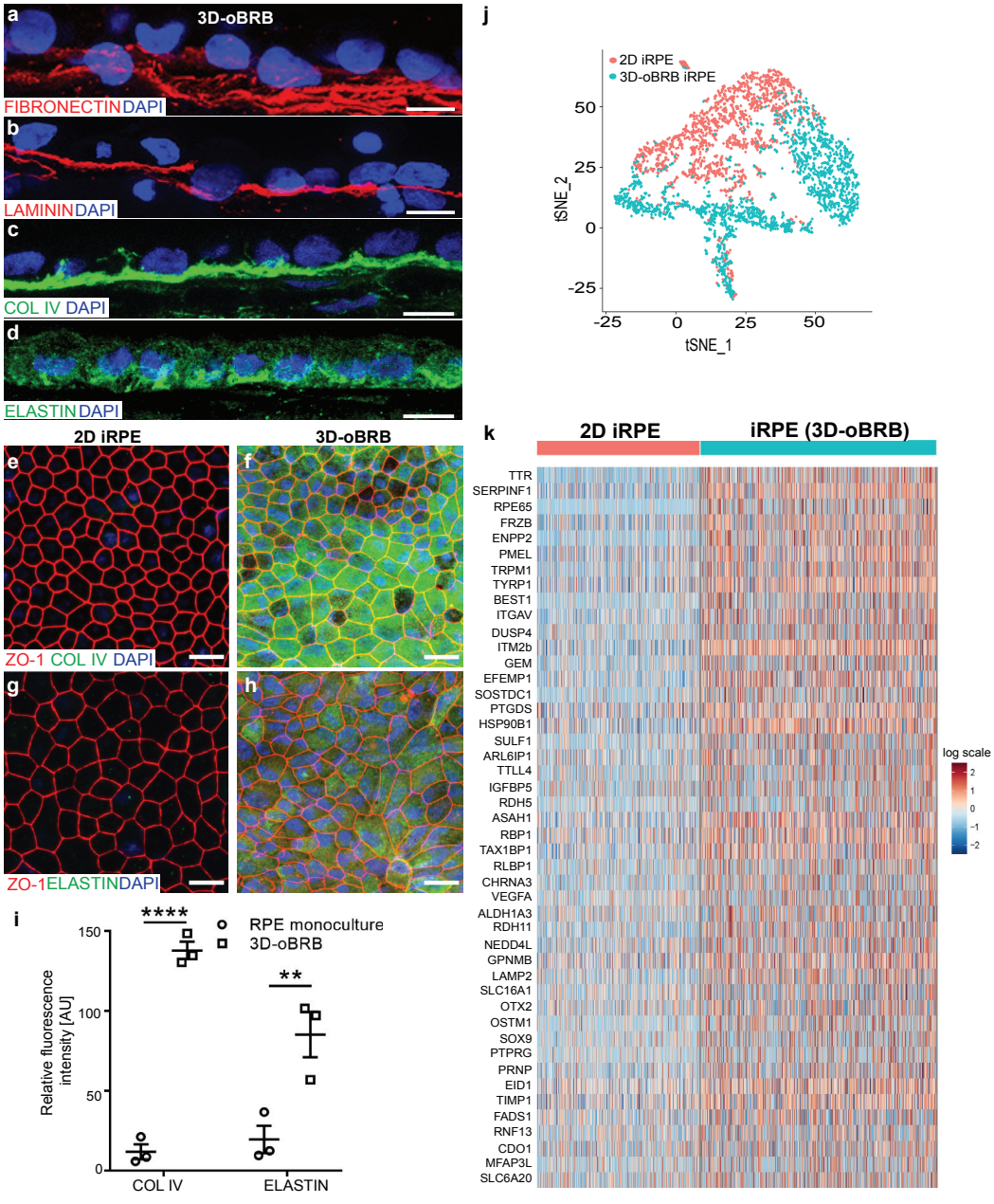

Figure 4. RPE maturity in 3D-oBRB. (**A-D**): cross sections of 3D-oBRB immunostained for Bruch's membrane proteins FIBRONECTIN (**A**), LAMININ (**B**), COLLAGEN IV (COL IV) (**C**), and ELASTIN (**D**). Nuclei stained with DAPI. Scale bars, 10 µm. (**E-H**): 2D RPE monoculture (**E**, **G**) and 3D-oBRB (**F**, **H**), co-immunostained for COL IV (green) or ELASTIN with ZO-1 (red), and nuclei (blue). Scale bars, 30 µm. (**I**): fluorescence mean intensity comparison of ELASTIN and COL IV immunostaining in 2D-iRPE and 3D-oBRB models. (n = 3). (**J**): TSNE plots from sc-RNA seq of 2D-iRPE and RPE in 3D-oBRB. (**K**): gene expression of RPE signature genes, comparison between 2D-iRPE and RPE in 3D-oBRB. Statistical significance was attributed to values of p <0.05 as determined by two-way ANOVA and Sidak's multiple comparison test. **p <0.01, ****p <0.0001. All error bars indicate STE

3D-oBRB recapitulates choroidal phenotypes seen in dry and wet AMD

Drusen - a hallmark of dry AMD - accumulates under the RPE within the Bruch's membrane [30]. Complement competent human serum (CC-HS), has recently been linked to drusen formation [31]. Treatment of 3D-oBRB with 5 % CC-HS induced APOE positive drusen-like deposits within the Bruch's membrane, as confirmed by histological analysis of 3D-oBRB in *en-face* view (APOE - purple, Figure 5A, D), cross-sections (white lines, APOE - purple, Figure 5G), and 3D rendered images (APOE - purple, movie S5). CC-HS treatment also led to RPE atrophy in 3D-oBRB (compare F-ACTIN – green Figure 5B, E). Consistent with RPE atrophy, capillary degeneration was evident with CC-HS treatment (arrowheads; CD31 – red, Figure 5C, F and G). Lastly, these structural changes in the 3D-oBRB led to a loss in its barrier resistance, as confirmed by a 20× drop in TER (p <0.01; Figure 5H). Overall, these results validated 3D-oBRB as a physiologically relevant dry AMD model including subRPE drusen deposits, loss of barrier resistance, RPE atrophy, and capillary degeneration.

It is thought that hypoxia in the back of the eye leads to stabilization and nuclear translocation of the transcription factor HIF-1α in the RPE [32]. HIF-1α increases the expression and secretion of VEGF [33], which leads to wet AMD. However, there is no direct proof to support this hypothesis for human ocular tissues. We sought to recreate wet AMD using RPE-specific hypoxia in the 3D-oBRB model. Treatment of the iRPE apical side with ML228 (2 μM), a known HIF-1α activator [34], led to HIF-1α activation in <5 % of cells by 48 hours; by 96 hours elevated HIF-1α protein levels was evident in 25 % of cells (Figure S12A, B, D, E). Continued treatment of ML228 for two weeks resulted in HIF-1α activation in majority of iRPE cells and dropped iRPE monolayer TER close to zero; in comparison the TER of vehicle-treated cells wasn't changed (Figure S12C, F, G). Consistently, HIF-1α expressing cells also lost their epithelial phenotype, as confirmed by the loss of typical hexagonal morphology, unorganized ZO-1 expression, and an increase in cell size (Figure S12E, F, and H).

Treatment of mature 3D-oBRB (on the apical side) with ML228 produced outcomes similar to seen in 2D-iRPE, including disruption of tight junctions and a 3-fold drop in tissue TER (Figure 5I, J, O). Unlike 2D iRPE, in the 3D-oBRB model the TER did not drop to zero suggesting a protective effect of the capillary-bed on iRPE barrier resistance (Figure S12G, 5O). Activation of HIF-1α in the RPE of a mature 3D-oBRB initiated a CNV-like response with capillaries hyperproliferating towards the iRPE monolayer, as confirmed by image-based analysis of z-planes (Figure 5K, L; yellow to red color of the code shows capillaries that are in the subRPE zone – white circles). Cross-sections of 3D rendered images of tissues clearly revealed capillaries hyperproliferating into the Bruch's membrane and expanding into the subRPE zone (Figure 5M, N - arrowheads; movie S6). To determine if the CNV-like response seen in our hypoxic 3D-oBRB model was VEGF induced, we measured VEGF secretion in ML228 treated 3D-OBRB. ML228 treatment led to a 5-fold increase in the apical VEGF secretion (Figure 5P), while basal VEGF secretion did not change with ML228 treatment (Figure 5Q). Quantification of VEGF immunostaining revealed that most of the basally secreted VEGF accumulated around capillaries, likely binding to its cognate receptor - leading to CNV-like phenotype (Figure 5R). Overall, the above data confirmed that our 3D-oBRB is able to recapitulate both dry and wet AMD phenotypes *in vitro*.

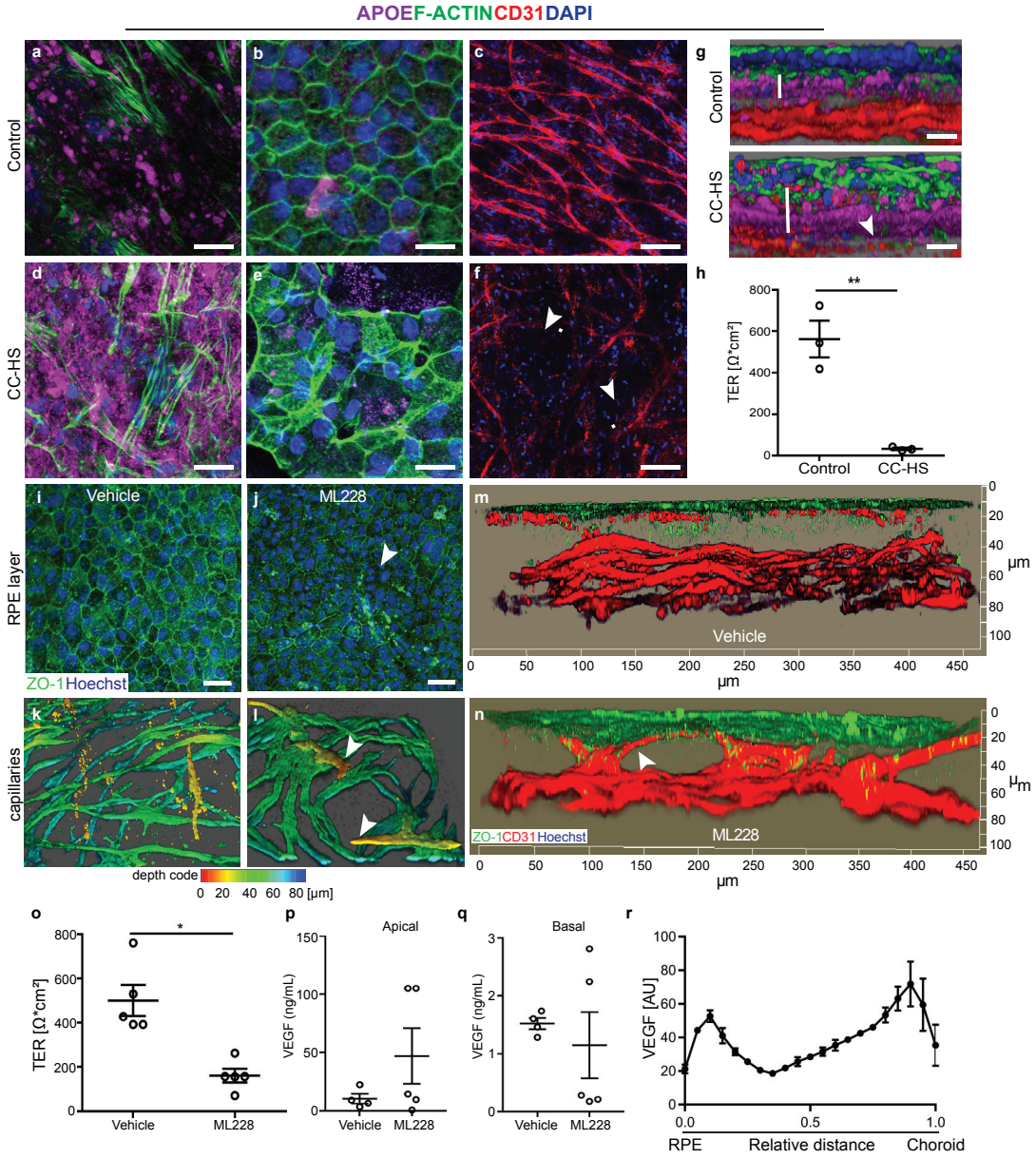

Figure 5. RPE dependent choroid degeneration in dry and wet AMD models of 3D-oBRB. (**A-G**) *En face* (**A-F**), cross-section (**G**) views of APOE (magenta), CD31 (red) immunostaining, F-ACTIN (green), Hoechst (blue) in complement competent human serum (CC-HS) treated and control 3D-oBRB. Arrowheads mark degenerated RPE and capillaries. Scale bars, 100µm. (**G**) white vertical lines mark Bruch's membrane. Scale bars, 10µm. (n = 3) (**H**): TER of control and CC-HS treated 3D-oBRB (n = 3). (**I**, **J**): Confocal images of RPE from 3D-oBRB, immunostained with ZO-1 (green) and Hoechst (blue). Arrowhead marks lost ZO-1 signal. Scale bars, 30 µm. (**K**, **L**): Depth code of 3D reconstructed confocal images. Color gradient along z-axis (100 µm depth) starting from subRPE zone (red) to the end of choroid (blue); in vehicle-treated 3D-oBRB (**K**) and in ML228 treated 3D-oBRB (**L**). Arrowheads mark capillaries in the sub-RPE region. Scale bars, 100 µm. (**M**, **N**): side view images of CNV, immunostained with ZO-1 (green) and CD31(red). Scale in x-axis, 50µm and in z-axis, 10µm. (**I-N**): (n = 5) (**O**): TER measurement on vehicle or ML228 treated 3D-oBRB (n = 5). (**P**, **Q**): apical (**P**) and basal (**Q**) VEGF secretion in vehicle and ML228 treated 3D-oBRB (n = 4). (**R**): Fluorescence intensity of VEGF staining in cryosectioned 3D-oBRB tissue slice. Quantification of subRPE region (0.0 fractional distance) to the bottom of the choroid layer (1.0 fractional distance) (n = 3). Statistical significance was attributed to values of p <0.05 as determined by paired t-test (**O**, **P**, **Q**) or two-way ANOVA and Sidak's multiple comparison test (**G**, **H**). *p <0.05, ***p <0.001, ****p <0.0001. All error bars indicate STE (**G**, **O**, **P**, **Q**, **R**).

Bevacizumab halts CNV in the 3D-oBRB disease model

To validate our CNV model for drug discovery, we asked whether we could replicate the efficacy of an anti-VEGF monoclonal antibody (bevacizumab), used for the treatment of wet AMD [6]. We co-treated 2D iRPE and 3D-oBRBs with ML228 and a clinical dose (0.3 mg/mL) of bevacizumab. Bevacizumab had little, if any, effect reversing ML228-induced 2D iRPE atrophy (Figure 6A-D). In contrast, in the 3D-oBRB bevacizumab co-treatment with ML228 partially recovered RPE epithelial phenotype as confirmed by regained epithelial morphology in ZO-1 immunostained images (arrowheads, Figure 6E-G) and doubled TER values of ML228+ bevacizumab co-treated tissues (Figure 6D). 3D reconstruction of tissue cross-sections revealed a noticeable reduction in CNV with bevacizumab and ML228 co-treatment as compared to ML228 treatment alone (arrowhead, Figure 6H-J, movie S6). Image-based quantification of vascular density in each focal plane showed a 3-fold higher (p <0.05) capillary density within 5µm of the iRPE monolayer in ML228 treated samples that were suppressed entirely in bevacizumab and ML228 co-treated samples (Figure 6K). There was no significant difference in vascular density deeper than 10 microns in the tissue (Figure 6K, S13A-C). Overall, these results suggest that hypoxia induced CNV seen in our 3D-oBRB is primarily VEGF induced and can be suppressed by the clinically used drug bevacizumab. All together, these results validate the utility of our tissue for discovering new drugs to treat AMD.

Figure 6. Bevacizumab treatment suppresses wet-AMD in 3D-oBRB. (**A-C**): RPE monoculture at 2 weeks treated with DMSO as a vehicle control (**A**), ML228 (2 µM) (**B**), and ML228 (2µM)+bevacizumab (0.284 mg/ml) (**C**), immunostained for HIF-1α (red), ZO-1 (green), and nuclei stained with Hoechst (blue). Scale bars, 30 µm. (n = 3). (**D**): TER measurement comparison between 2D-iRPE and 3D-oBRB for ML228 amd ML228+bevacizumab treated samples. TER values were normalized to vehicle treated 3D-oBRBs. (2D-iRPE, n = 3; 3D-oBRB, n = 6). (**E-G**): Maximum intensity projection images of RPE of 3D-oBRB, immunostained with ZO-1 (green) and stained with Hoechst for nuclei (blue). Degenerated and recovered RPE are marked with arrowheads in (**F**, **G**). Scale bars, 25 µm. (**H-J**): side view of 3D reconstructed images of vehicle (**H**), ML228 (**I**), and ML228+bevacizumab (**J**) treated 3D-oBRB tissues, immunostained with ZO-1 (green) and CD31(red). Arrowheads in (**I**) mark hyperproliferating capillaries and in (**J**) mark retracted capillaries. Scale in x-axis, 50 µm and in z-axis, 10 µm. (**E-J**): (n = 4). (**K**): vascular area fraction was calculated from CD31 positive area in each z-stack. (n = 5). Statistical significance was attributed to values of p <0.05 as determined by unpaired t-test (**M**) or two-way ANOVA and Sidak's multiple comparison test (**D**, **H**, **L**). *p <0.05, **p <0.01, ****p <0.0001. All error bars indicate STE.

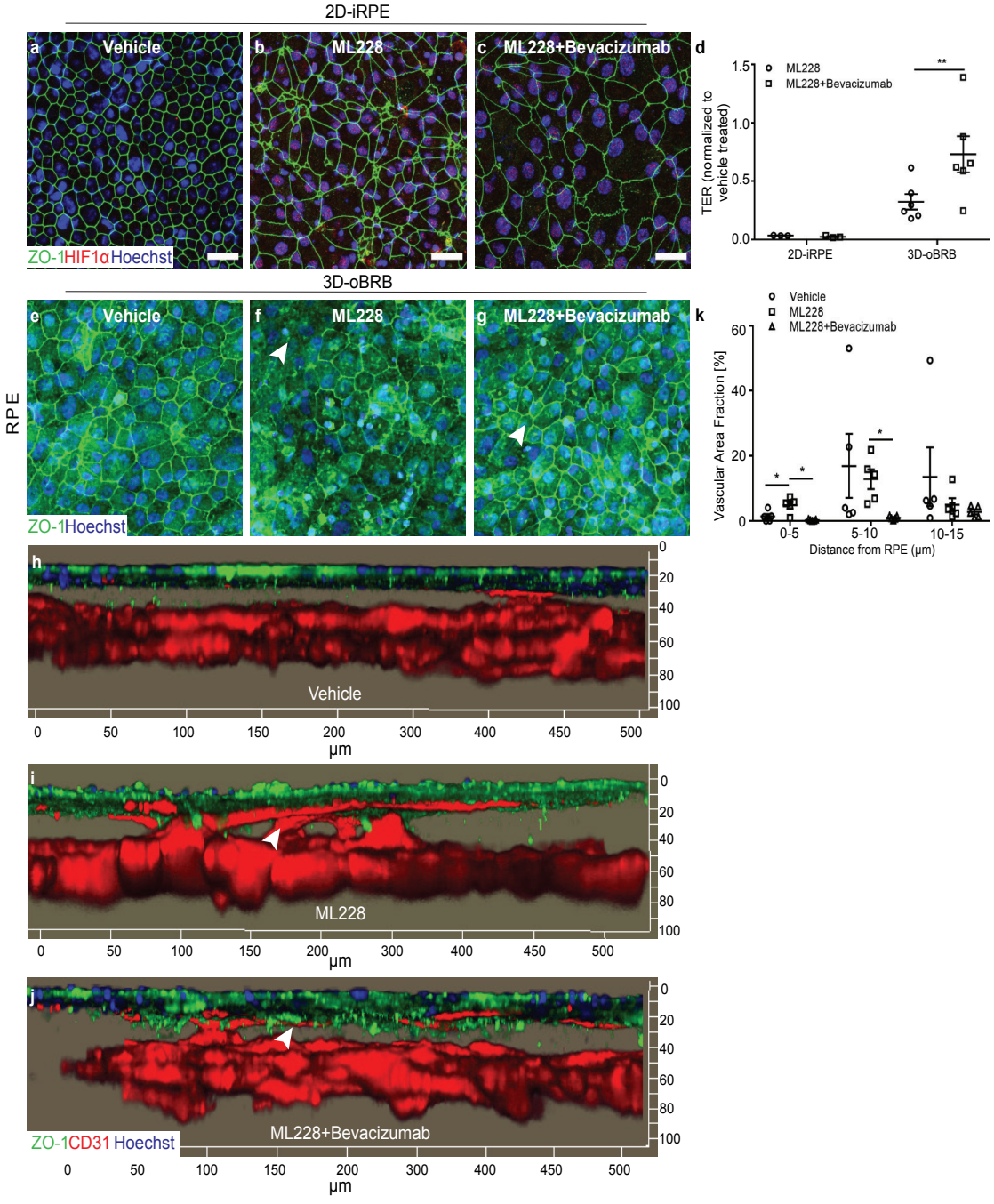
2D-iRPE
a Vehicle
b ML228
c ML228+Bevacizumab
ZO-1HIF1αHoechst
d
ML228
ML228+Bevacizumab
TER (normalized to vehicle treated)
1.5
1.0
0.5
0.0
**
2D-iRPE
3D-oBRB
3D-oBRB
RPE
e Vehicle
f ML228
g ML228+Bevacizumab
ZO-1Hoechst
k
Vehicle
ML228
ML228+Bevacizumab
Vascular Area Fraction [%]
60
40
20
0
*
*
*
0-5
5-10
10-15
Distance from RPE (μm)
h
Vehicle
i
ML228
j
ML228+Bevacizumab
ZO-1CD31 Hoechst
0
20
40
60
80
100
0
50
100
150
200
300
400
450
500
μm

Discussion

3D-oBRB recapitulated key native features that have not been previously replicated *in vitro*:

1. a fully mature and polarized RPE monolayer with basal infoldings that are critical for metabolite transport and membrane trafficking. Consistently, an increased expression of exosome transport genes was seen in iRPE in the 3D-oBRB. Basal infoldings are lost in diseases like choroideremia and AMD, underscoring the importance of our 3D-oBRB for studying both monogenic and polygenic eye diseases [35];
2. a Bruch's membrane that mediates RPE and capillary interactions. Its hydraulic conductivity ensures the free flow of nutrients, metabolites and cytokines between the two tissues [28]. With age and in AMD, loss of Bruch's membrane hydraulic conductivity disrupts communication between the two tissues and is thought to be the cause of outer retina degeneration [36]. Our 3D-oBRB replicates degenerative changes in the Bruch's membrane (APOE deposits and angiogenic invasion) and allows the possibility of discovering how such changes contribute to disease; and
3. a capillary-bed with a functional lumen, fenestration, choroid-specific gene expression and ability to integrate upon transplantation. Loss of fenestration is associated with AMD risk-alleles and advanced AMD [18]. Our model provides direct evidence that fenestration is dependent on the presence of healthy RPE and a possibility of understanding the role of AMD risk-alleles via the use of patient iPSCs.

These features were possible due to the introduction of several innovative bioengineering attributes:

1. a biodegradable scaffold provided two bioactive surfaces allowing RPE monolayer growth on one side and bioink printing on the opposite side. Scaffold micropores allowed RPE and ECs to deposit ECM leading to the formation of a Bruch's membrane to recreate a native-like tissue architecture [2];
2. the mixture of gelatin and fibrin provided a temperature-sensitive hydrogel with high fluidity at room temperature for developing a homogenously concentrated bioink of ECs, pericytes, and fibroblasts and low fluidity at 10 °C for relatively easier bioprinting. Fibrin maintained the 3D tissue structure until fibroblasts secreted sufficient ECM to provide substrate for a stable capillary-bed;
3. a combination of relevant cell types at appropriate ratio: 2:1 fibroblasts to ECs and 1:10 pericytes to ECs allowed easier EC migration and angiogenesis through a native-like ECM structure and sustained long-term capillaries of the correct lumen size (5-20 μm). RPE cells provided VEGF for capillary growth, confluency, fenestration, and choroidal phenotype.

Our 3D-oBRB constructs recapitulated AMD phenotypes and shed light on disease mechanisms that could not be addressed previously due to the lack of appropriate *in vitro* model systems. In 3D-oBRB, drusen accumulated within the Bruch's membrane, similar to the observation in AMD eyes [2,3].

This allowed monitoring of drusen impact on Bruch's membrane. RPE atrophy led to choroid degeneration, providing a direct proof of observations made in AMD cadaver eyes that suggested RPE atrophy precedes choroid degeneration. The data from our model suggests that complement inhibition might be a potential therapeutic strategy at an earlier disease stage before the RPE atrophy begins. Our model also provides direct proof supporting previous work that suggested CNV is induced by abnormal VEGF secretion by RPE cells [37,38]. We provide additional insight into CNV by showing higher VEGF secretion induced by RPE hypoxia; and binding of basally secreted VEGF to ECs – combined these data suggest a combination of HIF-1α inhibitor with a VEGF-receptor blocker will be a more effective in CNV, especially where anti-VEGF agents have failed.

Here we have developed a relatively complete model of the oBRB and validated its clinical relevance by demonstrating the efficacy of a clinically used anti-VEGF antibody. A fully-syngeneic 3D-oBRB derived from AMD-patient iPSCs will help provide a more comprehensive understanding of disease pathology and help determine the role of genetics in disease manifestation.

Supplementary Materials: please see Chapter 9: "Appendices".

References

1. Wong, W.L.; Su, X.; Li, X.; Cheung, C.M.; Klein, R.; Cheng, C.Y.; Wong, T.Y. Global prevalence of age-related macular degeneration and disease burden projection for 2020 and 2040: A systematic review and meta-analysis. *Lancet Glob. Health* **2014**, *2*, e106–e116.
2. McLeod, D. S.; Grebe, R.; Bhutto, I.; Merges, C.; Baba, T.; Lutty, G. A. Relationship between RPE and choriocapillaris in age-related macular degeneration. *Investig. Ophthalmol. Vis. Sci.* **2009**, *50*, 4982-4991.
3. Bhutto, I.; Lutty, G. Understanding age-related macular degeneration (AMD): relationships between the photoreceptor/retinal pigment epithelium/Bruch's membrane/choriocapillaris complex. *Mol. Aspects. Med.* **2012**, *33*, 295-317.
4. Song, M. J.; Bharti, K. Looking into the future: Using induced pluripotent stem cells to build two and three dimensional ocular tissue for cell therapy and disease modeling. *Brain research* **2016**, *1638 (Pt A)*, 2–14.
5. Farecki, M. L.; Gutfleisch, M.; Faatz, H.; Rothaus, K.; Heimes, B.; Spital, G.; Lommatzsch, A.; Pauleikhoff, D. Characteristics of type 1 and 2 CNV in exudative AMD in OCT-Angiography. *Graefes Arch. Clin. Exp. Ophthalmol.* **2017**, *255*, 913–921.
6. Kovach, J. L.; Schwartz, S. G.; Flynn, H. W., Jr.; Scott, I. U. Anti-VEGF Treatment Strategies for Wet AMD. *J. Ophthalmol.* **2012**, *2012*, 786870.
7. Barben, M.; Samardzija, M.; Grimm, C. The Role of Hypoxia, Hypoxia-Inducible Factor (HIF), and VEGF in Retinal Angiomatous Proliferation. *Adv. Exp. Med. Biol.* **2018**, *1074*, 177–183.
8. Campbell, M.; Humphries, P. The blood-retina barrier: tight junctions and barrier modulation. *Adv. Exp. Med. Biol.* **2012**, *763*, 70-84.
9. Nickla, D. L.; Wallman, J. The multifunctional choroid. *Prog. Retin. Eye Res.* **2010**, *29*, 144-68.
10. Hoshino, A.; Chiba, H.; Nagai, K.; Ishii, G.; Ochiai, A. Human vascular adventitial fibroblasts contain mesenchymal stem/progenitor cells. *Biochem. Biophys. Res. Commun.* **2008**, *368*, 305-10.
11. Orlova, V. V.; van den Hil, F. E.; Petrus-Reurer, S.; Drabsch, Y.; Ten Dijke, P.; Mummery, C. L. Generation, expansion and functional analysis of endothelial cells and pericytes derived from human pluripotent stem cells. *Nat. Protoc.* **2014**, *9*, 1514-31.
12. Sharma, R.; Khristov, V.; Rising, A.; Jha, B. S.; Dejene, R.; Hotaling, N.; Li, Y.; Stoddard, J.; Stankewicz, C.; Wan, Q.; Zhang, C.; Campos, M. M.; Miyagishima, K. J.; McGaughey, D.; Villasmil, R.; Mattapallil, M.; Stanzel, B.; Qian, H.; Wong, W.; Chase, L.; Bharti, K. Clinical-grade stem cell-derived retinal pigment epithelium patch rescues retinal degeneration in rodents and pigs. *Sci. Transl. Med.* **2019**, *11*, 5580.
13. Shiihara, H.; Sonoda, S.; Terasaki, H.; Kakiuchi, N.; Yamashita, T.; Uchino, E.; Murao, F.; Sano, H.; Mitamura, Y.; Sakamoto, T. Quantitative analyses of diameter and running pattern of choroidal vessels in central serous chorioretinopathy by en face images. *Sci. Rep.* **2020**, *10*, 9591.
14. Lamalice, L.; Le Boeuf, F.; Huot, J. Endothelial cell migration during angiogenesis. *Circ. Res.* **2007**, *100*, 782-94.

15. Maminishkis, A.; Chen, S.; Jalickee, S.; Banzon, T.; Shi, G.; Wang, F. E.; Ehalt, T.; Hammer, J. A.; Miller, S. S; Confluent monolayers of cultured human fetal retinal pigment epithelium exhibit morphology and physiology of native tissue. *Invest. Ophthalmol. Vis. Sci.* **2006**, *47*, 3612-24.
16. Campochiaro, P. A.; Jerdon, J. A.; Glaser, B. M. The extracellular matrix of human retinal pigment epithelial cells in vivo and its synthesis in vitro. *Invest. Ophthalmol. Vis. Sci.* **1986**, *27*, 1615-21.
17. Choi, W.; Mohler, K. J.; Potsaid, B.; Lu, C. D.; Liu, J. J.; Jayaraman, V.; Cable, A. E.; Duker, J. S.; Huber, R.; Fujimoto, J. G. Choriocapillaris and choroidal microvasculature imaging with ultrahigh speed OCT angiography. *PLoS One* **2013**, *8*, e81499.
18. Grebe, R.; Mughal, I.; Bryden, W.; McLeod, S.; Edwards, M.; Hageman, G. S.; Lutty, G. Ultrastructural analysis of submacular choriocapillaris and its transport systems in AMD and aged control eyes. *Exp. Eye Res.* **2019**, *181*, 252-262.
19. dela Paz, N. G.; D'Amore, P. A. Arterial versus venous endothelial cells. *Cell Tissue Res.* **2009**, *335*, 5.
20. Kuleshov, M. V.; Jones, M. R.; Rouillard, A. D.; Fernandez, N. F.; Duan, Q.; Wang, Z.; Koplev, S.; Jenkins, S. L.; Jagodnik, K. M.; Lachmann, A.; McDermott, M. G.; Monteiro, C. D.; Gundersen, G. W.; Ma'ayan, A. Enrichr: a comprehensive gene set enrichment analysis web server 2016 update. *Nucleic Acids Res.* **2016**, *44*, w9097.
21. Songstad, A. E.; Wiley, L. A.; Duong, K.; Kaalberg, E.; Flamme-Wiese, M. J.; Cranston, C. M.; Riker, M. J.; Levasseur, D.; Stone, E. M.; Mullins, R. F.; Tucker, B. A. Generating iPSC-Derived Choroidal Endothelial Cells to Study Age-Related Macular Degeneration. *Invest. Ophthalmol. Vis. Sci.* **2015**, *56*, 8258-67.
22. Swamy, V.; McGaughey, D. Eye in a Disk: eyeIntegration Human Pan-Eye and Body Transcriptome Database Version 1.0. *Invest. Ophthalmol. Vis. Sci.* **2019**, *60*, 3236-3246.
23. Zanotelli, M. R.; Ardalani, H.; Zhang, J.; Hou, Z.; Nguyen, E. H.; Swanson, S.; Nguyen, B. K.; Bolin, J.; Elwell, A.; Bischel, L. L.; Xie, A. W.; Stewart, R.; Beebe, D. J.; Thomson, J. A.; Schwartz, M. P.; Murphy, W. L. Stable engineered vascular networks from human induced pluripotent stem cell-derived endothelial cells cultured in synthetic hydrogels. *Acta Biomater* **2016**, *35*, 32-41.
24. Curcio A.C, J. M. in Retina Vol. Vol. 1, Part 2: Basic Science and Translation to Therapy, (ed SriniVas R. Sadda Stephen J. Ryan, David R. Hinton, Andrew P. Schachat, SriniVas R. Sadda, C.P. Wilkinson, Peter Wiedemann, Andrew P. Schachat) Ch. 20, 465-481 (London: Elsevier. 5th ed., 2013).
25. Michaelides, M.; Hunt, D. M.; Moore, A. T. The genetics of inherited macular dystrophies. *J. Med. Genet.* **2003**, *40*, 654-50.
26. Corominas, J.; Colijn, J. M.; Geerlings, M. J.; Pauper, M.; Bakker, B.; Amin, N.; Lores Motta, L.; Kersten, E.; Garanto, A.; Verlouw, J.; van Rooij, J.; Kraaij, R.; de Jong, P.; Hofman, A.; Vingerling, J. R.; Schick, T.; Fauser, S.; de Jong, E. K.; van Duijn, C. M.; Hoyng, C. B.; den Hollander, A. I. Whole-Exome Sequencing in Age-Related Macular Degeneration Identifies Rare Variants in COL8A1, a Component of Bruch's Membrane. *Ophthalmology* **2018**, *125*, 1433-1443.
27. Miyagishima, K. J.; Wan, Q.; Corneo, B.; Sharma, R.; Lotfi, M. R.; Boles, N. C.; Hua, F.; Maminishkis, A.; Zhang, C.; Blenkinsop, T.; Khristov, V.; Jha, B. S.; Memon, O. S.; D'Souza, S.; Temple, S.; Miller, S. S.; Bharti, K. In Pursuit of Authenticity: Induced Pluripotent Stem Cell-Derived Retinal Pigment Epithelium for Clinical Applications. *Stem Cells Transl. Med.* **2016**, *5*, 1562-1574.

28. Booij, J. C.; Baas, D. C.; Beisekeeva, J.; Gorgels, T. G.; Bergen, A. A. The dynamic nature of Bruch's membrane. *Prog. Retin. Eye Res.* **2010**, *29*, 1-18.
29. Strunnikova, N. V.; Maminishkis, A.; Barb, J. J.; Wang, F.; Zhi, C.; Sergeev, Y.; Chen, W.; Edwards, A. O.; Stambolian, D.; Abecasis, G.; Swaroop, A.; Munson, P. J.; Miller, S. S. Transcriptome analysis and molecular signature of human retinal pigment epithelium. *Hum. Mol. Genet. 2010*, **19**, 2468-86.
30. Anderson, D. H.; Ozaki, S.; Nealon, M.; Neitz, J.; Mullins, R. F.; Hageman, G. S.; Johnson, L. V. Local cellular sources of apolipoprotein E in the human retina and retinal pigmented epithelium: implications for the process of drusen formation. *Am. J. Ophthalmol.* **2001**, *131*, 767-81.
31. Johnson, L. V.; Forest, D. L.; Banna, C. D.; Radeke, C. M.; Maloney, M. A.; Hu, J.; Spencer, C. N.; Walker, A. M.; Tsie, M. S.; Bok, D.; Radeke, M. J.; Anderson, D. H. Cell culture model that mimics drusen formation and triggers complement activation associated with age-related macular degeneration. *Proc. Natl. Acad. Sci. U. S. A.* **2011**, *108*, 18277-18282.
32. Vadlapatla, R. K.; Vadlapudi, A. D.; Mitra, A. K. Hypoxia-inducible factor-1 (HIF-1): a potential target for intervention in ocular neovascular diseases. *Curr. Drug Targets* **2013**, *14*, 919-935.
33. Mammadzada, P.; Corredoira, P. M.; Andre, H. The role of hypoxia-inducible factors in neovascular age-related macular degeneration: a gene therapy perspective. *Cell. Mol. Life Sci.* **2020**, *77*, 819-833.
34. Chilov, D.; Camenisch, G.; Kvietikova, I.; Ziegler, U.; Gassmann, M.; Wenger, R. H. Induction and nuclear translocation of hypoxia-inducible factor-1 (HIF-1): heterodimerization with ARNT is not necessary for nuclear accumulation of HIF-1alpha. *J. Cell. Sci.* **1999**, *112 (Pt 8)*, 1203-12.
35. Wavre-Shapton, S. T.; Tolmachova, T.; Lopes da Silva, M.; Futter, C. E.; Seabra, M. C. Conditional ablation of the choroideremia gene causes age-related changes in mouse retinal pigment epithelium. *PLoS One* **2013**, *8*, e57769.
36. Huang, J. D.; Presley, J. B.; Chimento, M. F.; Curcio, C. A.; Johnson, M. Age-related changes in human macular Bruch's membrane as seen by quick-freeze/deep-etch. *Exp. Eye Res.* **2007**, *85*, 202-218.
37. Spilsbury, K.; Garrett, K. L.; Shen, W. Y.; Constable, I. J.; Rakoczy, P. E. Overexpression of vascular endothelial growth factor (VEGF) in the retinal pigment epithelium leads to the development of choroidal neovascularization. *Am. J. Pathol.* **2000**, *157*, 135-144.
38. Sun, L.; Huang, T.; Xu, W.; Sun, J.; Lv, Y.; Wang, Y. Advanced glycation end products promote VEGF expression and thus choroidal neovascularization via Cyr61-PI3K/AKT signaling pathway. *Sci. Rep.* **2017**, *7*, 14925.

If you don't like something change it;
if you can't change it, change the way you think about it.

— Mary Engelbreit

General conclusions, discussion and prospects

6

The main aim of this thesis was to make steps forward towards developing experimental therapies for retinal degenerative diseases and, more in particular, for AMD and the RPE-RP subtype. In the last decade, great deal of scientific efforts have been put into the generation, development and characterization of experimental therapeutic strategies and suitable models, *in vitro* and *in vivo*, to test their safety and efficacy. This thesis describes the generation of *in vitro* and *in vivo* models for AMD and RPE-RP, their characteristics and applications. This chapter discusses and places the currently available models and experimental therapeutic strategies for both diseases into a broader perspective. Additionally, some future research prospectives are addressed as well. First, I discuss the available (experimental) therapeutic strategies currently available for RPE-RP and AMD

Experimental therapeutic strategies for RPE-RP and AMD

As stated before in this thesis in Chapter 1, "General introduction," there is a large unmet need to develop curative treatments for most retinal degenerative diseases. While some therapies, including anti-VEGF injections for wet AMD and the gene-replacement therapy for the RPE65-RP subtype, are available, most treatment options focus on preventing and slowing down the disease progression instead of reversing the effects. Once retinal cells and vision are lost, nothing can be done. Below, three major categories of (potential) treatments and strategies, currently in the clinic, under development in the lab or in different stages of clinical trials are discussed. These categories include experimental gene therapy, drug therapy/ dietary supplements, and cell-replacement therapy. The ultimate goal of all cures is to prevent or halt vision loss or restore vision.

Gene therapy

Over the last years, the interest in the potential of (ocular) gene therapy has grown considerably. In general, gene therapy is a broad term used for many therapy types that involve the transfer of genetic material to a patient to treat an (ocular) disease. Gene therapy is most useful when the condition of interest is (directly) caused by a mutation in a specific gene, and intact living cells are still present in a structurally undamaged tissue. Gene therapy is especially promising for treating eye diseases due to the accessibility and the immune-privileged nature of the eye and the compartmentalization of this organ [1, 2].

Gene therapy can be classified in many ways. These include sorting by class of the disease (genetic disease versus complex acquired disorder), based on the characteristics of the strategy of gene delivery (integrating versus non-integrating) and whether the gene therapy is applied *in vivo* (directly into the patient) or *ex vivo* (in cultured cells taken from the patient that are subsequently transplanted back). In this chapter, I describe three examples of gene therapy (presented in Figure 1). These types are gene-replacement therapy, gene suppression therapy and genome editing.

Gene-replacement therapy can be used in cases where the mutation in the disease gene causes a loss-of-function defect. A functional copy of the defective gene is expressed to replace the defective gene (Figure 1A).

Gene suppression therapy can be used in cases where mutation causes a gain-of-function deficiency (e.g., the mutated protein is toxic and causes the disease) (Figure 1B). Suppression can, for example, be achieved by RNA interference technologies using, for example, microRNAs, short-hairpin RNAs and exon skipping oligonucleotides [3-5].

Genome editing is currently technically possible using various editing techniques. A mutated gene can be corrected by these strategies (Figure 1C). Strategies to correct the mutation directly include homologous recombination via a donor template or via prime- or base-editing. These strategies are emerging techniques and are not yet often used in the clinic.

Gene-replacement therapy is, at the moment, the most plausible type of gene therapy to make it to the clinic for recessively inherited RPE-RP or, perhaps, in rare AMD cases. Therefore, I will focus on this type of gene therapy strategy further in this chapter. The other two types of gene therapy, gene suppression and genome editing, are extensively reviewed elsewhere [6-12].

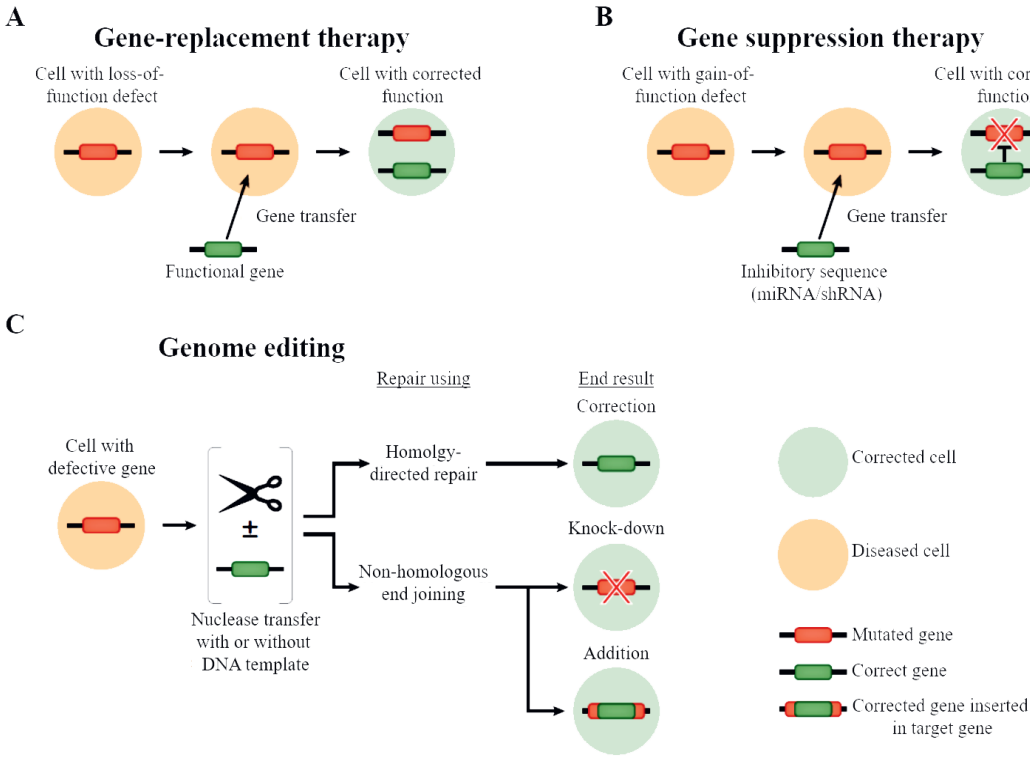

Figure 1. Three common examples of gene therapy include (**A**) gene-replacement therapy, (**B**) gene suppression therapy and (**C**) genome editing. **A**: a functional copy of a gene is provided to the diseased cells without affecting the diseased gene itself. **B**: the diseased gene can be suppressed by reducing the expression by RNA interference technology using microRNAs (miRNA) or short-hairpin RNAs (shRNA), exon skipping oligonucleotides. **C**: the mutation is corrected in the diseased gene using a nuclease with or without a DNA template. The nuclease will introduce a double-strand break at the target site. The DNA is repaired by either the non-homologous end joining (NHEJ) pathway without a DNA template or by the homology-directed repair (HDR) pathway using a DNA template. Additionally, recently developed strategies such as base-editing and prime-editing belong also to this category. Figure adapted from Anguela et al. [13].

The strategy of gene-replacement therapy is to deliver a functional copy of the gene to replace the defective version. Gene-replacement therapy can be delivered in several ways (see Figure 2). The delivery methods can be divided into viral and non-viral delivery. Non-viral delivery usually involves a circular double-stranded plasmid DNA encoding the gene of interest. This piece of DNA is directly delivered into the target tissue or cell type mediated by lipid-based particles, peptide-based particles or polymer-based particles by endocytosis or phagocytosis of the target cells. Moreover, in specific cell types, "naked" RNA or DNA could be endocytosed or phagocytosed as well [14]. The RPE has both endocytic and phagocytic capacities in the eye, while the PRs are predominantly endocytic [15-18].

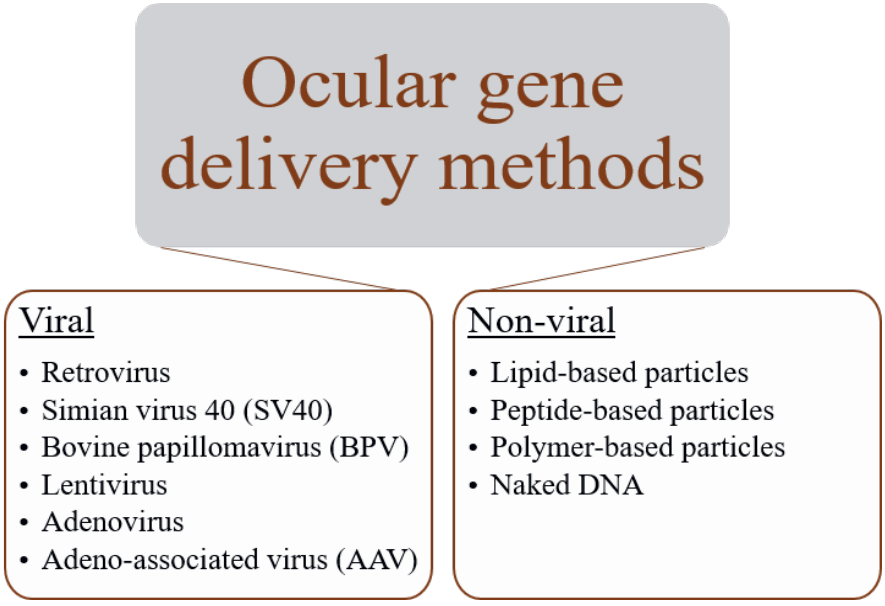

Figure 2. Gene therapy constructs can be delivered using viral- and non-viral-based delivery methods. Non-viral methods include the delivery of plasmid DNA encoding the gene of interest in a lipid-based, peptide-based or polymer-based particle. These DNA-particle complexes are phagocytosed or endocytosed by the tissue of interest. Additionally, naked (plasmid) DNA can also be endocytosed or phagocytosed. Viral delivery includes the use of integrating and non-integrating vectors. Retroviruses, Simian viruses (SV40), bovine papillomaviruses (BPV), and lentiviruses integrate into the genomic DNA, making their use less desirable for (ocular) gene therapy. The non-integrating adenoviruses and, in particular, adeno-associated viruses (AAV) have emerged as favorites for direct gene delivery.

Viral vectors have been invaluable for delivering copies of genes *in vivo*. Viral vectors can be divided into integrating and non-integrating vectors. Integrating viral vectors include retrovirus, lentivirus and simian virus (SV40). Non-integrating vectors include adenovirus and adeno-associated virus (AAV) [19]. An overview of the viral characteristics is shown in Table 1. Most viruses integrate randomly into host chromosomes, resulting in potential mutagenesis. Therefore, integration of the viral genome into the host's genome is, in general, not desired for *in vivo* gene therapy [20]. Since AAVs are currently considered the most efficient and safest for delivering gene therapy [12], I will focus on the presently available (experimental) gene therapies for RPE-RP and AMD using AAVs.

Table 1. An overview of the characteristics of viral vectors that could be used to deliver gene-replacement therapy.
AAV = adeno-associated virus.

Feature	Retrovirus	Lentivirus	Simian virus	Adenovirus	AAV
Viral genome	RNA	RNA	DNA	DNA	DNA
Cell division required?	Yes	Yes	No	No	No
Packaging limit	8 kb	8 kb	3 kb	8-30 kb	5 kb
Immune response?	Minor	Minor	Minor	Extensive	Minor
Genome integration	Yes	Yes	Yes	Poor	Poor
Long-term expression	Yes	Yes	Yes	No	Yes

AAVs have emerged as a favored non-integrating virus vector for direct gene delivery. AAVs only cause a very mild immune response *in vivo*, supporting the apparent lack of pathogenicity during gene delivery. In general, mitotic cells lose the expression of the introduced gene during cell division. Therefore, integrating the augmented gene into the genome in mitotic cells is needed for stable long-term expression [13]. The retina mostly consists of long-lived post-mitotic cells. Therefore a long-term stable expression can be achieved without integrating the transferred gene into the genome. Depending on the serotype, AAVs can infect many different cell types, both mitotic (dividing) and post-mitotic (quiescent) cells *in vivo*. Additionally, the transduction of various (retinal) tissues can be tuned using the different available AAV serotypes, and cell type-specific expression can be regulated using different types of promotors. Using AAVs, long-term stable expression can be reached *in vivo*.

A major drawback of AAV vectors is their limited cloning capacity (<4.7 kb), limiting their use in gene delivery to smaller-sized genes. Also, antibodies against AAVs may attenuate the efficacy of AAV-mediated gene therapy [21-23].

After 15 years of functional- and preclinical research and extensive clinical trials, the FDA approved a specific gene-replacement treatment [Voretigene neparvovec (VN)] for one subtype of RP caused by mutations in the *RPE65* gene [24]. The therapy involves gene-replacement therapy by subretinal injections with an AAV serotype 2 (AAV2) vector carrying the complementary DNA encoding RPE65 protein. Patients have visual improvements for up to four years after VN treatment. Long-term follow-up studies are needed to determine the durability of VN in the long run [25, 26]. For a more in-depth discussion about VN, see below the section "What can we learn from Voretigene neparvovec?".

While a treatment is now available for the *RPE65*-RP type, (gene-) therapy is not yet available for all other RP patient groups. However, some experimental therapies are under development in the lab and/or in clinical trials. Additionally, similar to VN, clinical trials involving gene replacement therapy strategies are currently recruiting, active or recently completed (see Table 2).

Table 2. An overview of the clinical trials which are currently going on involving gene therapy for retinitis pigmentosa (RP) and age-related macular degeneration (AMD). *USH2A* = usherin gene (Usher Syndrome Type-2A). *RHO* = rhodopsin gene. *RPGR* = retinitis pigmentosa GTPase regulator gene. *PDE6A/B* = phosphodiesterase 6A/B gene. *RLBP1* = retinaldehyde binding protein 1 gene. *CD59* = MAC inhibitory protein gene. *CFI* = complement factor I gene. NCT = national clinical trial number (registration of clinical trials at https://clinicaltrials.gov).

Gene therapy type	Disease	Gene involved	NCT number	Status at time of writing
Suppression	RP	*USH2A*	NCT03780257	Active, not recruiting
Suppression	RP	*RHO*	NCT04123626	Recruiting
Replacement	RP	*RPGR*	NCT03316560	Recruiting
Replacement	RP	*RPGR*	NCT03584165	Enrolling by invitation
Replacement	RP	*RPGR*	NCT04671433	Recruiting
Replacement	RP	*RPGR*	NCT04312672	Recruiting
Replacement	RP	*RPGR*	NCT03252847	Completed
Replacement	RP	*RPGR*	NCT03116113	Completed
Replacement	RP	*RPGR*	NCT04517149	Recruiting
Replacement	RP	*PDE6A*	NCT04611503	Recruiting
Replacement	RP	*PDE6B*	NCT03328130	Recruiting
Replacement	RP	*RLBP1*	NCT03374657	Recruiting
Replacement	Dry AMD	*CD59*	NCT03144999	Completed
Replacement	Dry AMD	*CFI*	NCT03846193	Recruiting
Replacement	Dry AMD	*CFI*	NCT04566445	Recruiting
Replacement	Dry AMD	*CFI*	NCT04437368	Recruiting
Suppression	Wet AMD	*VEGF*	NCT01024998	Completed
Suppression	Wet AMD	*VEGF*	NCT01494805	Completed
Suppression	Wet AMD	*VEGF*	NCT03066258	Active, not recruiting

Because an RP generally is a monogenic disorder, gene therapy targets are relatively easily identified. However, as described in Chapter 1, "General introduction" of this thesis, AMD is a more complex multifactorial disease, and effective gene therapy targets are harder to identify. Although it is not yet precisely clear, the complement system that plays a crucial role in the innate immune system [27, 28], is involved in the pathology of AMD [29, 30]. A limited number of complement-based gene replacement therapies for dry AMD have made it to clinical trials (see Table 2), but results have been, so far, disappointing. For wet from of AMD, the gene therapy target is primarily VEGF. AAV vectors carry proteins that cause local reduction of VEGF levels [31]. Some of these AAV-mediated gene therapy strategies for wet AMD are currently being tested in clinical trials (see Table 2). The anti-VEGF medication presently used to treat wet AMD often has to be applied monthly or bi-monthly by direct eye injections. Therefore, this therapy is very patient-unfriendly. The gene therapies that may reduce VEGF levels may replace the patient-unfriendly anti-VEGF medications in the future.

Differences in the outcomes of clinical trials involving gene-replacement therapy targeting RP or AMD generally occur often. The reasons behind the differences likely reflect the differences in the gene expression vector's design, the final formulation, the surgical procedure, and the perioperative immunomodulatory regimen. These variables may affect the vector amount delivered to the target cells, the potential immune response, or other parameters that affect the clinical outcome. Additionally, it was postulated that the patients' age in the clinical trials also matters [13]. Moreover, more potential gene therapy targets may be identified regarding AMD. Additional (pre-)clinical studies need to be performed to answer these crucial questions.

Dietary supplementation

Besides gene therapy, dietary supplements can (potentially) slow down the onset or progression of retinal degeneration. For some AMD and RP patient groups and a number of genetic metabolic eye disorders, such as gyrate atrophy, the aforementioned strategies may be beneficial [32-36]. For example, the supplemental dietary administration of high-dose oxidants, omega-3-fatty acids, and zinc seems beneficial in AMD patients [37, 38]. Additionally, other supplements that may have some beneficial effects in RP patients are neuro-protective taurine [39], docosahexaenoic acid (DHA) [40] and lutein [41, 42].

In the context of this thesis, two supplements will be discussed in more detail below: Vitamin A (and its derivatives) supplementation in RP, involved in the visual cycle, and zinc supplementation in AMD, involved in the complement system. Some recent extensive overviews regarding the therapeutic effects of diet and other supplements on AMD and RP progression can be found elsewhere [43-55].

Vitamin A (derivative) supplementation in RP

Vitamin A has been a compound of interest since the first half of the 20th century because of its involvement in the visual cycle (see Chapter 1, "General introduction"). The general term vitamin A is a frequently used word for a group of unsaturated nutritional compounds, including retinol, retinal, retinoic acid, and provitamin A carotenoids. Vitamin A deficiency itself is a serious and widespread public health problem in a large part of the world's population: it is the leading cause of preventable blindness in children, most pronounced in developing countries [56]. Vitamin A deficiency causes night blindness and structural degeneration of the retina and thus mimics the visual defects seen in RP cases due to some mutations in the visual cycle [57]. Moreover, both a lack or an overdose of vitamin A in pregnant women can cause malformations and even miscarriage [58].

A possible improvement in ERG measurements of RP patients after daily vitamin A supplementation was observed in 1993 [59]. However, the results of this study have been an issue of intense debate given the absence of genetic subtyping of patients and design issues [60-65]. To illustrate this point, vitamin A supplementation was found to be potentially harmful to RP patients harboring mutations in the *ABCA4* gene due to over-accumulation of toxic byproducts [66]. More recently, vitamin A has also been used in two other studies combined with lutein [42] or the omega-3 fatty acid DHA [67]. Supplementation of lutein and vitamin A seemed to have a beneficial effect, whereas supplementation of DHA and vitamin A did not make a difference for RP patients. The trials included participants with RP of all forms of genetic predisposition. Thus, the potential beneficial or harmful effects of vitamin A supplementation in most genetic RP sub-types remain unclear [55].

More recently, a derivative of vitamin A, 9-*cis*-retinyl acetate (QLT091001), was orally administered to a subset of RP patients harboring a mutation in the *RPE65* or *LRAT* genes (NCT01014052, NCT01521793, NCT01543906): in *RPE65*- and *LRAT*-RP patients, the compromised production of 11-*cis*-retinal is replaced by QLT091001 (see Figure 4 and 5 in Chapter 1, "General introduction").

Therefore, the essential biochemical steps in the visual cycle performed by the RPE65 and LRAT proteins are skipped. Indeed, a subset of the patients suffering from RP caused by mutations in RPE65 or LRAT showed a degree of visual recovery after QLT091001 administration within two months of treatment. No "serious" side effects were registered. The observed side effects included headache (94 %), photophobia (28 %), nausea and vomiting (17 %) [68]. A structure-function relationship was also observed: the longer the outer segment length of the PR layer, the more chance of a positive effect of QLT091001. This suggests that PR integrity is a predictor of the efficacy of QLT091001 in *RPE65*- and *LRAT*-RP patients [68, 69]. The effectiveness and evaluation of this treatment's side effects in humans await further clinical trials.

Supplementation of vitamin A or its derivatives will probably be effective for many subtypes of RP. Nowadays, most ophthalmologists are hesitant to prescribe vitamin A supplements, especially when the underlying genotype of the patients may not be beneficial or is not known. Apart from the aforementioned detrimental effect in patients with RP caused by mutations in *RPE65* or *LRAT*, vitamin A supplementation will not be useful in patients harboring mutations in the *RBP3* gene. When the transporting protein RBP3 is involved, not the amount or presence of the visual cycle's metabolites is an issue, but their localization. Therefore, supplementation of vitamin A or its derivatives will probably not be beneficial for these patients. Additionally, RP can also be caused by mutations in genes not involved in the visual cycle. For those patients, vitamin A supplementation will also probably not have an effect. Finally, for vitamin A supplementation to have an impact, remaining living retinal cells are required. This is not the case for all RP subtypes, especially in advanced disease stages. Obviously, more research is required to determine which subsets of RP patients possibly benefit or not from supplementing vitamin A derivatives.

Zinc Supplementation in AMD

Zinc is an essential element for the structure and function of many enzymes and protein complexes [70, 71]. The eye has a relatively high zinc content, primarily in the RPE, but zinc is also stored in the ganglion cells, the horizontal cells, the amacrine cells, the Müller cells, and the PR outer segments [72-74]. The effect of zinc supplementation on the RPE has been examined in several *in vitro* studies with mixed results [75-78]. Zinc may positively affect complement-mediated inflammation and, therefore, AMD pathogenesis. However, the exact mechanisms remain to be elucidated [70, 79, 80]. Zinc has been shown to be involved in other key functions of the RPE, such as its phagocytic function and dealing with oxidative stress [75, 81]. Recently, the regulatory pathways that might be involved in mediating the positive effects of long-term zinc supplementation in AMD may have been identified in an *in vitro* study [75].

Dietary intake of zinc has most likely a beneficial effect on delaying the progression of AMD [37, 82, 83]. Besides a general effect on relevant enzyme activity, the patient's individual genetic background may play a role in the effect of zinc supplementation on the onset and progression of AMD. For example, zinc supplementation in patients bearing a high-risk variant of the *CFH* gene may be extra beneficial [84]. In contrast, another observational study was inconclusive regarding the effect of zinc supplementation in AMD [85]. At the moment, one ongoing clinical trial recruiting AMD patients (NCT04177069) aims to test the impact of Visucomplex Plus, which contains zinc, among other supplements. Overall, further research is needed to determine zinc's role in AMD pathogenesis and the possible beneficial effect of zinc supplementation.

Small molecule drugs

Small molecule drugs are defined as compounds with a low molecular weight capable of modulating biochemical processes to diagnose, treat, or prevent diseases [86]. For example, the small molecule groups include anti-inflammatory agents, complement system inhibitors, visual cycle modulators, and antioxidants. They are usually designed and/or developed to intervene in signaling pathways. For example, anti-VEGF agents are the standard treatment for wet AMD to slow down the progression of neovascularization [87]. Several (recently identified) signaling pathways associated with AMD pathobiology are presently targeted in clinical trials (NCT04626128, NCT02556424, NCT04590196, NCT03056079 and NCT03630315) [88, 89]. Indeed, the small molecule drug E10030, an inhibitor of platelet-derived growth factor (PDGF), was studied in combination with VEGF inhibitors to treat wet AMD in a phase III clinical trial (NCT01944839) after being successful in phase I and II trials (NCT02859441, NCT00569140).

RPE-replacement therapy

Both in RPE-RP and AMD, RPE cell function is initially implicated and severely compromised in the advanced disease stages, and local cell death occurs. In this case, RPE cell replacement is the only promising (future) therapeutic option for both disorders. The main goal of retinal cell-replacement therapy is to replace dead cells and, in combination with other therapies, prevent further cell death. The PRs, RPE, BM and choriocapillaris are a single functional unit. If one of these layers is dysfunctional, it will cause a secondary loss of the other layers. In dry AMD, it seems that the RPE is the first layer to be lost [90]. Replacing the RPE in time could therefore prevent the secondary loss of other cell layers. Correct structural and functional integration of "new" RPE cells into the already damaged host retina is essential for this to succeed. The "new" RPE cells can have several origins, including autologous RPE, donor RPE and stem-cell-derived RPE.

Previously, surgical translocation of more peripheral (autologous) RPE patches into the macula area within the same (human) eye has been tried, with variable but encouraging results [91]. Drawbacks of this approach are the length of the surgery time, the risk of complications due to the complexity of de procedures and the fact that the health of the RPE cells used for translocation might be sub-optimal. The transplantation of human donor RPE cells has not reached the clinic on a larger scale, probably due to the limited availability of viable cells and/or suitable matching donors.

Recently, technological developments present the opportunity to generate RPE cells from unlimited sources, including embryonic stem cells (ESCs), induced pluripotent stem cells (iPSCs), and adult stem cells [88]. All three stem cell types can form RPE cells. However, since ESCs are isolated from fetal tissues, they are subject to ethical concerns [92]. Apart from the ethical considerations, iPSCs have another advantage over ESCs: iPSCs are patient-specific cells, and the risk of tissue rejection after transplantation decreases tremendously [93]. On the other hand, recent evidence suggests that iPSCs are possibly more genetically unstable than ESCs [94]. Some degree of heterogeneity and variability exists between all patient iPSC lines and, therefore, also between the retinal tissues generated from them.

The healthy eye is considered an immune-privileged site. The immune privilege is maintained by the inner- (I) and the outer (O)-blood-retinal-barrier (BRB). The IBRB consists of the deep, the intermediate and the superficial plexus retinal vessels. The OBRB consists of the choroidal capillaries, the BM and the RPE [95]. To uphold the immune privilege, it is of great importance that the damage to the BRBs is minimized during all procedures.

Moreover, since the RPE is involved in both RPE-RP and AMD pathology, the BRB's integrity may not be (completely) maintained in preclinical (animal) models or many patients [95]. Local retinal damage may result in cell loss, transient immune system involvement, fibrosis, and/or scar formation, which must be considered before considering RPE transplantation.

After transplantation, the already activated immune system may hamper proper functional integration and may be a problem in a yet-to-be-defined number of cases. Even when transplanted cells are HLA-matched, immunosuppressive medication and microglial activation inhibiting agents might still be essential during and/or after these procedures to enhance graft survival after transplantation [96].

The transplantation of stem cell-derived RPE cells into the subretinal space of AMD patients has been tried in several phase I/II clinical trials, see Table 3. Favorably, evidence of uncontrolled cell growth after transplantation was not found in any of these studies. Cells survived for at least four months, and no immune-mediated transplant rejection was observed. Some visual improvement was seen in a few patients. The results were encouraging but highly variable and not statistically significant [97-100]. The drawbacks of these studies are that patients were enrolled in the end-stage of the disease, only a few patients were enrolled, and the patients did not have a similar phenotype at baseline [97-102]. Apart from these study design difficulties, the variable outcome obtained could also be explained by the lack of reliable preclinical research data: there is little to no consensus about the many parameters that must be determined, influencing potential (pre-)clinical outcomes [103]. The FDA and EMA recently implemented specific regulations for human (ocular) stem cell replacement therapy to potentially enter clinical trials and/or to forbid trials based on unreliable and incomplete preclinical data. We reviewed all preclinical studies performing RPE transplantations into the subretinal space in a systematic review, including meta-analyses, in Chapter 2 of this thesis. Based on these results and combined with the literature, we conclude that RPE cells transplanted as a sheet on a suitable scaffold instead of injected as a dissociated cell suspension in the eye of preclinical models is a better strategy [103-105].

Table 3. An overview of the clinical trials which are currently going on involving retinal pigment epithelium (RPE) cell-replacement therapy for retinitis pigmentosa (RP), age-related macular degeneration (AMD) and Stargardt disease. NCT = national clinical trial number (registration of clinical trials at https://clinicaltrials.gov.) FDA = Food and Drug Administration. EMA = European Medicines Agency. IS = immune-suppressive agents applied. Status = status at the time of writing. HuPrim = human primary. hESC = human embryonic stem cell. ASC = adult stem cell. SCNT = somatic cell nuclear transfer. NR = not reported.

Disease	RPE source	Suspension or sheet?	NCT number	FDA/EMA approval	IS	Status
RP	HuPrim	Suspension	NCT03566147	No	NR	Unknown
RP	hESC	Suspension	NCT03944239	No	NR	Unknown
RP	hESC	Suspension	NCT03944239	No	NR	Unknown
Dry AMD	ASC	Suspension	NCT04627428	Yes	Yes	Recruiting
Dry AMD	iPSC	Sheet, PLGA	NCT04339764	Yes	NR	Recruiting
Dry AMD	SCNT-hESC	Suspension	NCT03305029	No	NR	Unknown
Dry AMD	hESC	Suspension	NCT02755428	No	NR	Unknown
Dry AMD	hESC	Suspension	NCT03046407	No	NR	Unknown
Dry-AMD	hESC	Suspension	NCT02286089	Yes	Yes	Active
Dry AMD	hESC	Suspension	NCT01674829	No	NR	Unknown
AMD, Stargardt	hESC	Suspension	NCT02749734	No	NR	Unknown
Stargardt	hESC	Suspension	NCT01469832	Yes	Yes	Completed
Stargardt	hESC	Suspension	NCT02941991	Yes	Yes	Completed
Stargardt	hESC	Suspension	NCT01345006	Yes	Yes	Completed
Stargardt	hESC	Suspension	NCT01344993	Yes	Yes	Completed
Stargardt	hESC	Suspension	NCT01625559	No	Yes	Unknown

The current challenges faced in developing RPE cell-replacement therapy include RPE survival and their functional behavior, the complexity of the procedure, safety, long-term functionality, the optimum window of treatments, and costs. The use of ESCs has been proven to be challenging from an ethical and political perspective. On the other hand, there are also several considerations about using iPSC-derived transplants. Although these cells are considered autologous and patient-specific, they are heterogeneous because of their varying genetic background, epi-genetic profile, and potential sub-chromosomal instability after *in vitro* cultures [106, 107]. Due to the persistence of undifferentiated iPSCs (and ESCs) at the end of the differentiation protocol, tumorigenesis was of significant concern. However, Li and colleagues showed no tumors developed after transplantation in a preclinical model of RP [108]. The novel reprogramming strategies significantly reduced the risk of tumorigenesis, including membrane-permeable peptides and episomal plasmids that do not integrate into the genome [106, 109]. Nonetheless, since safety always needs to be guaranteed, iPSCs are still under consideration for their (general) use in cell transplantation studies, and further research is needed in this area [94].

Combination therapy

In some cases, combination therapy, combining two (or more) of the therapeutic strategies described above, could be an option. For example, patients suffering from an advanced (RPE-)RP stage may benefit from gene therapy to prevent further progression. At the same time, these patients may also benefit from cell-replacement therapy to replace the degenerated tissues. Moreover, this approach could also be useful for selected AMD patients with a strong and clear genetic component implicated in their disease.

A similar example includes RPE-replacement therapy using an autologous iPSC-based approach in a patient with a clear genetic cause of the disease. In this case, it might be more efficient to apply the gene therapy in the lab before transplanting the tissue to the patient's eye. The genetic defect will, by doing so, be repaired before transplantation. This approach might also be less invasive for the patient.

Transplanting multiple cell types and tissue layers could be considered as well as a combination therapy in cell-replacement therapies. For example, in AMD, the malfunction of the RPE, BM and the choriocapillaris complex precedes the loss of macular PRs [110]. Following this thought, it might be possible that only a healthy RPE, BM and choriocapillaris could rescue the macular PRs. Indeed, Van Meurs and Van den Biesen translocated autologous RPE and the mid-peripheral healthy RPE, including the underlying tissues: a full-thickness patch of RPE, BM choriocapillaris and choroid. Many followed this approach and published promising but variable results [111-116]. Chapter 5 of this thesis describes the generation of a 3D tissue including the RPE, an artificial BM and an endothelium with functional vessels, simulating the RPE-BM-choroid complex. These tissues were generated from stem cells, and a translocation in the patient's eye will, therefore, not be necessary, reducing the risk of post-operative adverse effects. Before starting future clinical trials using these tissues, additional preclinical studies in suitable animal models must be performed.

As a last example, for late-stage wet AMD patients, an RPE-replacement therapy combined with anti-VEGF treatment could also be more beneficial than either RPE-replacement or anti-VEGF therapy alone. The RPE-replacement therapy could replace the already damaged tissues, and the anti-VEGF treatment could prevent further progressive damage to this new tissue in the future. Although such combination therapies might be more beneficial for patients, this has to be tested in the available preclinical (animal) models first.

Summary – experimental therapeutic strategies

There is a need to improve RPE-type RP and AMD experimental studies and clinical trials involving gene replacement, supplements, drug or cell-replacement therapy. For gene(-replacement) therapy, improvement of molecular correction strategies (i.e., prime editing), vector design and delivery strategy are essential. Cell-replacement therapy also still faces multiple challenges, including the best differentiation strategy to create RPE cells from stem cells, deciding on the best delivery strategy (e.g., suspension or sheet) and, in the case of a sheet, the best cellular carrier type.

It is hard to conclude anything from preclinical studies and clinical trials. This is due to the small number of patients included, the lack of reporting and the differences in the experimental setup (e.g., inclusion criteria, visual acuity at baseline, progression of the disease, disease subtype, follow-up time, outcome parameters etc.). Additionally, most clinical trials and preclinical studies have been hampered by the lack of (information from) fully representative *in vitro* or *in vivo* models [117, 118].

Finally, the complex physiopathology, multifactorial nature and the lack of suitable biomarkers for AMD add to the difficulty of defining one or more therapeutic strategies.

The development of translational models for RPE-RP and AMD

Most, if not all, therapeutic entities have to be tested in representative *in vivo* models before moving forward to the first phases of clinical trials, as determined by regulatory requirements. For the RPE-RP subtype and AMD, there is currently no alternative EMA or FDA-accepted type of model available that can replace preclinical animal experiments.

Recently, a new class of stem cell-derived human representative *in vitro* models, i.e., retinal organoids, has been developed that reduces the need for animal models. Retinal organoids consist of multiple human retinal cell types and layers and, additionally, the RPE [119, 120]. Organoids are particularly useful for investigating the human retina's developmental aspects and disease modeling or pharmacological testing. For example, the potential effects of experimental therapeutic approaches, such as administering drugs or applying gene therapy, could be tested in these retinal organoids before moving to *in vivo* animal models [121].

Despite the features and attributes of the current retinal organoid models, many challenges need to be overcome before they can be considered genuinely physiological models. For example, the immature photoreceptor outer segment morphology, the lack of extracellular matrix, the problems that arise with long-term culturing, the absence of immune cells, proper ECM and the absence of vascular tissue are issues to improve upon. Moreover, modeling the naturally occurring communication between the retina and the brain *in vitro* needs to be investigated in more detail. Taken together, while the first generation of retinal (and brain) organoids have been successfully generated, multiple improvements are still essential.

Chapter 3 of this thesis describes the successful generation and characterization of a new genetic rat model for the RPE subtype of RP. This model was developed to represent a group of (Dutch) RP patients and harbors the genomic mutation found in this patient group (*LRAT*c12delC). We found that the phenotype of this model is very similar to the patients that are suffering from this type of RP [122]. Therefore, this model could be used to test the safety and efficacy of experimental therapeutic strategies that are currently being developed to treat this patient group. This rat strain could also be used as a model for other patient groups harboring other mutations in the *LRAT* gene. At the same time, one should consider the pathologic heterogeneity found in the RP patients with different mutations in the *LRAT* gene [123]. From an experimental therapeutic perspective, it is always best to develop "fully" representative models for each subcategory of the disease. However, in terms of time and costs, this is a severe limitation of developing "the best" models. And even with an "optimal" animal model, the results cannot be translated directly to humans [124].

As described in Chapter 1 of this thesis, and in contrast with RP, AMD is a multifactorial disease. Multiple genetic and environmental factors are involved. So far, no animal model is available that fully recapitulates all AMD features together *in vivo*. Nonetheless, many *in vivo* models for certain specific pathobiological aspects of AMD have been developed using genetically modified rodent strains, transgenic animals, chemically-based and mechanical models. Chapter 4 of this thesis describes the generation and in-depth characterization of an inducible model of AMD using two rodent strains, e.g., mice and rats. The chemical agent used for this model, sodium-iodate (SI), is causing AMD-like retinal degeneration through the oxidative stress pathway. Various degrees of RPE cell loss can be obtained depending on SI dose, similar to various degrees of RPE loss seen in different stages of AMD. In addition, not only the RPE but also the (outer) retina, the choroidal capillaries and the BM are affected by SI [125], a phenomenon that can also be seen in AMD [126, 127]. Further detailed studies using these models are needed to fine-tune the relationship between SI dose, retinal damage and AMD.

Taken together, it is clear that each (animal) model has its pros and cons when used in preclinical research for retinal degenerative diseases. The choice of the most optimal preclinical model depends on the scientific or clinical questions asked and the results of the relevant ongoing *in vivo* experiments. This will serve our understanding of the molecular mechanisms behind the disorders, develop potential treatments, and prevent unnecessary use of research animals, which are all important goals to achieve.

What can we learn from Voretigene neparvovec?

The FDA recently approved gene-replacement therapy, voretigene neparvovec (VN), for treating RPE-RP patients harboring biallelic mutations in the *RPE65* gene [128]. Using VN as an example, we can learn a lot from all the (pre)clinical experiments that have been done to get here. Moreover, we can (and should) use this information to develop a similar therapy for other RPE-RP subtypes, such as the *LRAT*-RP subtype, efficiently.

VN involves gene-replacement therapy by subretinal injections with an AAV serotype 2 (AAV2) vector carrying the complementary DNA encoding *RPE65*. The medicine is injected into the subretinal space via pars plana vitrectomy (1.5×10^{12} viral genomes) [26]. Patients have various degrees of visual improvement for up to four years after VN treatment [26, 129, 130]. In 65 % of the patients treated with VN, a stable visual improvement was observed for up to one year after treatment. Side effects were also observed: in 66 % of the patients, who received VN, adverse ocular reactions were registered. The most common incidences were conjunctival hyperemia, cataract, increased ocular pressure, retinal tear, thinning of the corneal stroma, a macular hole, subretinal deposits, eye inflammation, eye irritation, eye pain and maculopathy. The majority of these side effects were minor, and no harmful immune responses were reported [25, 26].

Although visual improvements have been reported consistently, long-term follow-up studies in patients are needed to determine the durability of VN in the long run [25, 26, 129, 131-135]. Additionally, whether treatment protects against progressive retinal degeneration remains to be determined. It was shown that retinal degeneration in the treated zone was rescued 5-11 years later in dogs suffering from a spontaneous mutation in the *RPE65* gene after gene-replacement therapy [136]. However, the treatment was applied before the onset of retinal degeneration. The optimal timing of the intervention is, so far, unclear in human patients. It was suggested that early intervention could result in the best efficacy. However, this should be balanced against the surgical risks in young children who may still have reasonably well-preserved eyesight [25, 123, 137]. Nevertheless, even the oldest patient treated so far did show some visual improvement after one year of follow-up [26].

Currently, VN is applied only once, showing a stable expression for at least four years [137]. It is unclear whether two or repeated treatments could improve outcomes and not cause severe side effects due to repeated surgical administration and, for example, activation of the immune system [25].

Although most of the reported adverse reactions in VN-treated patients were transient and minor, Gange and coworkers recently reported perifoveal chorioretinal atrophy after subretinal injection of VN in 10 patients harboring mutations in the *RPE65* gene [135], see Figure 3 (A – F). The mean age of this patient group was 11.6 years (range 5 – 20 years). Perifoveal chorioretinal atrophy was identifiable at an average of 4.7 months (range 1 week – 1 year) post-injection and progressively worsened in all cases up to at least the last follow-up examination (mean follow-up 11.3 months; range 4 – 18 months).

Despite the atrophy, the visual acuity improved or remained stable in 83 % of the patients. Progressive chorioretinal atrophy has been described so far only once before after treatment with AAV2-based gene therapy. One patient developed progressive chorioretinal atrophy 6 months after treatment with a higher dose (1.5×10^{12} viral genomes) of another AAV2 vector (rAAV2/2.hRPE65p.hRPE65) [138]. Since functionality has been a major outcome measurement in most clinical trials, possible (local) atrophy after injection could have been missed or simply not reported.

The observed post-treatment retinal atrophy can be caused by a number of factors, including surgical delivery, immune response to the vector, patient characteristics and direct toxicity of the AAV2 vector to the PRs and the RPE [135].

First, surgical delivery strategy is another possible contributing factor to potential side effects. For example, the delivery rate seems to be very important to consider. It appears that a higher injection rate might cause more atrophy than a slower injection rate [140]. Since the delivery rate is determined by multiple factors, including injection pressure, cannula size (thickness and length) and intraocular pressure, it is hard to control these parameters in clinical trials. The importance of each parameter needs to be determined.

Secondly, inflammation or an immune response to AAV vectors was previously observed in small subgroups of patients treated with VN or other gene therapy trials [130, 139]. However, post-operative inflammation is unlikely to be the sole cause of the atrophy since clinical signs could only be found in about 10 % of the eyes that developed progressive chorioretinal atrophy [135].

Next, patient characteristics, including age, myopia and disease status, could influence the toxic effect of the AAV vector. For example, high myopia could cause thinning of the RPE-choriocapillaris complex and may therefore predispose these eyes to vector toxicity [135]. Furthermore, it was postulated that VN might affect young children's developing retina differently than a developed retina in older children and adults [142].

Finally, the AAV delivery vector might have toxic effects itself. The ocular toxicity of various AAV vectors was tested by Xiong et al. in mice and found a dose-dependent RPE degradation and outer nuclear layer thinning in some cases. The effect was more extreme when RPE-specific or broadly active promotors (like the CAG promotor used in VN) were used. Although AAV2 was not specifically tested, similar effects were observed using several AAV serotypes [141].

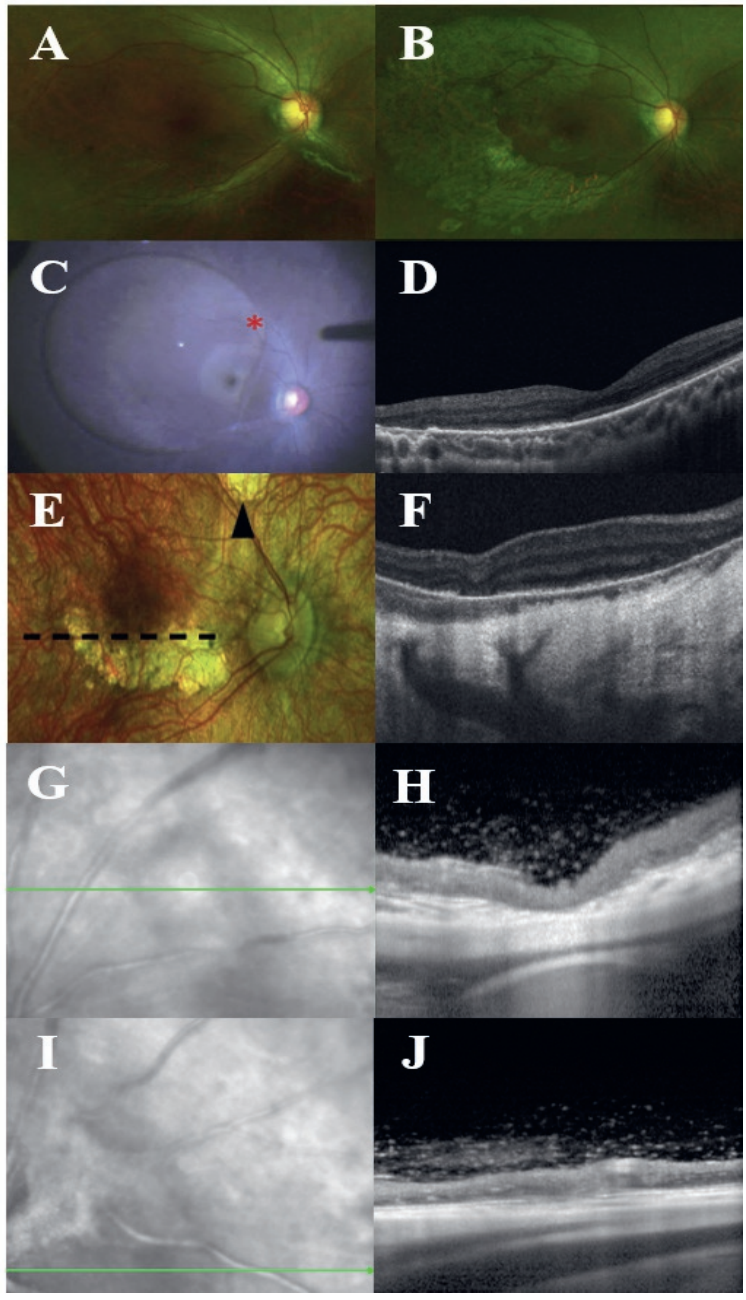

Figure 3. The potential toxic effects of AAV-based gene-replacement therapy in patients suffering from the *RPE65*-RP subtype treated with VN (**A**-**F**) and in wildtype Brown Norway rats injected with AAV2 (**G**, **H**) or AAV2.7m8 (**I**, **J**) loaded with green fluorescent protein (GFP). The CAG promoter was used in all cases. Progressive chorioretinal atrophy was observed 1.5 years post-operative (**B**) compared to baseline fundus images (**A**) after subretinal injection with VN. The intraoperative photograph (**C**) demonstrates the extent of the subretinal bleb. The red asterisk indicates the bleb initiation site. The OCT image (**D**) shows areas with outer retinal loss and increased signal transmission from the choroid correlating with the atrophy identified using the fundus image (**B**). Similar effects are found in a myopic eye post-injection (**E**, **F**). Clear atrophy is observed 1 year post-operative using fundus (**E**) and an OCT image (**F**). The dotted line demonstrates the position of the corresponding OCT image. Similar effects are also observed in Brown Norway subretinally injected with AAV2 (**G**, **H**) and AAV2.7m8 (**I**, **J**). Clear toxicity can be observed 35 days post-injection using fundus (**G**, **I**) and OCT (**H**, **J**) images. Equivalent doses of the AAV vectors were used throughout all conditions. Figure partly adapted (**A** – **F**) from Gange et. al (2021) [135] supplemented with preliminary data by Koster et. al (unpublished) (**G** – **J**).

Working towards experimental therapeutic strategies to treat retinal degenerative diseases, we are currently looking into the possibility of applying AAV-based gene-replacement therapy in patients suffering from the *LRAT*-RP subtype, similar to VN treatment for the *RPE65*-RP subtype. We are developing a gene-replacement treatment using two AAV serotypes (AAV2 and AAV2.7m8). Unfortunately, we also found toxicity after injecting AAVs into the subretinal space of rats, which is very similar to the progressive chorioretinal atrophy as seen by others [135, 141], see Figure 3 (G – J) (Koster et al. unpublished data). Before 2019, there were, to our knowledge, no reports studying the potential ocular toxicity of AAV vectors. VN was approved in 2017 by the FDA, based on studies reporting visual improvements in preclinical models. However, these publications lack the potential toxicity results. Further (preclinical) studies are necessary to determine what ocular, surgical delivery, and vector-related parameters predispose patients to this and other complications using AAV-based gene-replacement therapeutic strategies.

Conclusions

In conclusion, even though many scientific efforts have gone into translational research to develop potential new experimental therapies for retinal degenerative diseases, there is still much to learn. We still lack fully human representative models that are fully characterized to test experimental therapeutic strategies. Although several clinical trials are currently ongoing in different phases, results are often inconsistent due to various reasons. There is a need for standardized protocols in both preclinical and clinical research to ensure reproducibility and consistency.

References

1. Boye, S. E.; Boye, S. L.; Lewin, A. S.; Hauswirth, W. W., A comprehensive review of retinal gene therapy. *Mol Ther* **2013**, *21*, (3), 509-19.
2. Akyol, E.; Lotery, A., Gene, Cell and Antibody-Based Therapies for the Treatment of Age-Related Macular Degeneration. *Biologics* **2020**, *14*, 83-94.
3. Sangermano, R.; Garanto, A.; Khan, M.; Runhart, E. H.; Bauwens, M.; Bax, N. M.; van den Born, L. I.; Khan, M. I.; Cornelis, S. S.; Verheij, J.; Pott, J. R.; Thiadens, A.; Klaver, C. C. W.; Puech, B.; Meunier, I.; Naessens, S.; Arno, G.; Fakin, A.; Carss, K. J.; Raymond, F. L.; Webster, A. R.; Dhaenens, C. M.; Stöhr, H.; Grassmann, F.; Weber, B. H. F.; Hoyng, C. B.; De Baere, E.; Albert, S.; Collin, R. W. J.; Cremers, F. P. M., Deep-intronic ABCA4 variants explain missing heritability in Stargardt disease and allow correction of splice defects by antisense oligonucleotides. *Genet Med* **2019**, *21*, (8), 1751-1760.
4. Jaber, V. R.; Zhao, Y.; Sharfman, N. M.; Li, W.; Lukiw, W. J., Addressing Alzheimer's Disease (AD) Neuropathology Using Anti-microRNA (AM) Strategies. *Mol Neurobiol* **2019**, *56*, (12), 8101-8108.
5. Jiang, L.; Frederick, J. M.; Baehr, W., RNA interference gene therapy in dominant retinitis pigmentosa and cone-rod dystrophy mouse models caused by GCAP1 mutations. *Front Mol Neurosci* **2014**, *7*, 25.
6. Pena, S. A.; Iyengar, R.; Eshraghi, R. S.; Bencie, N.; Mittal, J.; Aljohani, A.; Mittal, R.; Eshraghi, A. A., Gene therapy for neurological disorders: challenges and recent advancements. *J Drug Target* **2020**, *28*, (2), 111-128.
7. Richardson, R.; Smart, M.; Tracey-White, D.; Webster, A. R.; Moosajee, M., Mechanism and evidence of nonsense suppression therapy for genetic eye disorders. *Exp Eye Res* **2017**, *155*, 24-37.
8. Geisler, A.; Fechner, H., MicroRNA-regulated viral vectors for gene therapy. *World J Exp Med* **2016**, *6*, (2), 37-54.
9. Peddle, C. F.; Fry, L. E.; McClements, M. E.; MacLaren, R. E., CRISPR Interference-Potential Application in Retinal Disease. *Int J Mol Sci* **2020**, *21*, (7).
10. Yu, W.; Wu, Z., Ocular delivery of CRISPR/Cas genome editing components for treatment of eye diseases. *Adv Drug Deliv Rev* **2021**, *168*, 181-195.
11. Cho, G. Y.; Justus, S.; Sengillo, J. D.; Tsang, S. H., CRISPR in the Retina: Evaluation of Future Potential. *Adv Exp Med Biol* **2017**, *1016*, 147-155.
12. Botto, C.; Rucli, M.; Tekinsoy, M. D.; Pulman, J.; Sahel, J. A.; Dalkara, D., Early and late stage gene therapy interventions for inherited retinal degenerations. *Prog Retin Eye Res* **2022**, *86*, 100975.
13. Anguela, X. M.; High, K. A., Entering the Modern Era of Gene Therapy. *Annu Rev Med* **2019**, *70*, 273-288.
14. Sahu, B.; Chug, I.; Khanna, H., The Ocular Gene Delivery Landscape. *Biomolecules* **2021**, *11*, (8).
15. Dunlap, D. D.; Maggi, A.; Soria, M. R.; Monaco, L., Nanoscopic structure of DNA condensed for gene delivery. *Nucleic Acids Res* **1997**, *25*, (15), 3095-101.
16. Farjo, R.; Skaggs, J.; Quiambao, A. B.; Cooper, M. J.; Naash, M. I., Efficient Non-Viral Ocular Gene Transfer with Compacted DNA Nanoparticles. *PLOS ONE* **2006**, *1*, (1), e38.

17. Hollyfield, J. G.; Varner, H. H.; Rayborn, M. E.; Liou, G. I.; Bridges, C. D., Endocytosis and degradation of interstitial retinol-binding protein: differential capabilities of cells that border the interphotoreceptor matrix. *Journal of Cell Biology* **1985**, *100*, (5), 1676-1681.
18. Young, R. W., The renewal of photoreceptor cell outer segments. *J Cell Biol* **1967**, *33*, (1), 61-72.
19. Finer, M.; Glorioso, J., A brief account of viral vectors and their promise for gene therapy. *Gene Ther* **2017**, *24*, (1), 1-2.
20. Romano, G., Development of safer gene delivery systems to minimize the risk of insertional mutagenesis-related malignancies: a critical issue for the field of gene therapy. *ISRN Oncol* **2012**, *2012*, 616310-616310.
21. Afione, S. A.; Conrad, C. K.; Kearns, W. G.; Chunduru, S.; Adams, R.; Reynolds, T. C.; Guggino, W. B.; Cutting, G. R.; Carter, B. J.; Flotte, T. R., In vivo model of adeno-associated virus vector persistence and rescue. *J Virol* **1996**, *70*, (5), 3235-41.
22. Flotte, T. R.; Barraza-Ortiz, X.; Solow, R.; Afione, S. A.; Carter, B. J.; Guggino, W. B., An improved system for packaging recombinant adeno-associated virus vectors capable of in vivo transduction. *Gene Ther* **1995**, *2*, (1), 29-37.
23. Wagner, J. A.; Messner, A. H.; Moran, M. L.; Daifuku, R.; Kouyama, K.; Desch, J. K.; Manley, S.; Norbash, A. M.; Conrad, C. K.; Friborg, S.; Reynolds, T.; Guggino, W. B.; Moss, R. B.; Carter, B. J.; Wine, J. J.; Flotte, T. R.; Gardner, P., Safety and biological efficacy of an adeno-associated virus vector-cystic fibrosis transmembrane regulator (AAV-CFTR) in the cystic fibrosis maxillary sinus. *Laryngoscope* **1999**, *109*, (2 Pt 1), 266-74.
24. Prado, D. A.; Acosta-Acero, M.; Maldonado, R. S., Gene therapy beyond VN: a new horizon of the treatment for inherited retinal disease. *Curr Opin Ophthalmol* **2020**, *31*, (3), 147-154.
25. Ciulla, T. A.; Hussain, R. M.; Berrocal, A. M.; Nagiel, A., Voretigene neparvovec-rzyl for treatment of RPE65-mediated inherited retinal diseases: a model for ocular gene therapy development. *Expert Opin Biol Ther* **2020**, *20*, (6), 565-578.
26. Russell, S.; Bennett, J.; Wellman, J. A.; Chung, D. C.; Yu, Z. F.; Tillman, A.; Wittes, J.; Pappas, J.; Elci, O.; McCague, S.; Cross, D.; Marshall, K. A.; Walshire, J.; Kehoe, T. L.; Reichert, H.; Davis, M.; Raffini, L.; George, L. A.; Hudson, F. P.; Dingfield, L.; Zhu, X.; Haller, J. A.; Sohn, E. H.; Mahajan, V. B.; Pfeifer, W.; Weckmann, M.; Johnson, C.; Gewaily, D.; Drack, A.; Stone, E.; Wachtel, K.; Simonelli, F.; Leroy, B. P.; Wright, J. F.; High, K. A.; Maguire, A. M., Efficacy and safety of voretigene neparvovec (AAV2-hRPE65v2) in patients with RPE65-mediated inherited retinal dystrophy: a randomised, controlled, open-label, phase 3 trial. *Lancet* **2017**, *390*, (10097), 849-860.
27. Noris, M.; Remuzzi, G., Overview of complement activation and regulation. *Semin Nephrol* **2013**, *33*, (6), 479-92.
28. Sarma, J. V.; Ward, P. A., The complement system. *Cell Tissue Res* **2011**, *343*, (1), 227-35.
29. Wu, J.; Sun, X., Complement system and age-related macular degeneration: drugs and challenges. *Drug Des Devel Ther* **2019**, *13*, 2413-2425.
30. Dunkelberger, J. R.; Song, W. C., Complement and its role in innate and adaptive immune responses. *Cell Res* **2010**, *20*, (1), 34-50.
31. Ludwig, P. E.; Freeman, S. C.; Janot, A. C., Novel stem cell and gene therapy in diabetic retinopathy, age related macular degeneration, and retinitis pigmentosa. *Int J Retina Vitreous* **2019**, *5*, 7.

32. Elnahry, A. G.; Tripathy, K., Gyrate Atrophy Of The Choroid and Retina. In *StatPearls*, StatPearls Publishing Copyright© 2021, StatPearls Publishing LLC.: Treasure Island (FL), 2021.
33. Tsang, S. H.; Aycinena, A. R. P.; Sharma, T., Inborn Errors of Metabolism: Gyrate Atrophy. *Adv Exp Med Biol* **2018**, *1085*, 183-185.
34. Brosnan, J. T.; Brosnan, M. E., Creatine: endogenous metabolite, dietary, and therapeutic supplement. *Annu Rev Nutr* **2007**, *27*, 241-61.
35. Gaby, A. R., Nutritional therapies for ocular disorders: Part Three. *Altern Med Rev* **2008**, *13*, (3), 191-204.
36. Hayasaka, S.; Kodama, T.; Ohira, A., Retinal risks of high-dose ornithine supplements: a review. *Br J Nutr* **2011**, *106*, (6), 801-11.
37. Group, A.-R. E. D. S. R., A randomized, placebo-controlled, clinical trial of high-dose supplementation with vitamins C and E, beta carotene, and zinc for age-related macular degeneration and vision loss: AREDS report no. 8. *Arch Ophthalmol* **2001**, *119*, (10), 1417-36.
38. Souied, E. H.; Aslam, T.; Garcia-Layana, A.; Holz, F. G.; Leys, A.; Silva, R.; Delcourt, C., Omega-3 Fatty Acids and Age-Related Macular Degeneration. *Ophthalmic Res* **2015**, *55*, (2), 62-9.
39. Pasantes-Morales, H.; Quiroz, H.; Quesada, O., Treatment with taurine, diltiazem, and vitamin E retards the progressive visual field reduction in retinitis pigmentosa: a 3-year follow-up study. *Metab Brain Dis* **2002**, *17*, (3), 183-97.
40. Hoffman, D. R.; Locke, K. G.; Wheaton, D. H.; Fish, G. E.; Spencer, R.; Birch, D. G., A randomized, placebo-controlled clinical trial of docosahexaenoic acid supplementation for X-linked retinitis pigmentosa. *Am J Ophthalmol* **2004**, *137*, (4), 704-18.
41. Bahrami, H.; Melia, M.; Dagnelie, G., Lutein supplementation in retinitis pigmentosa: PC-based vision assessment in a randomized double-masked placebo-controlled clinical trial [NCT00029289]. *BMC Ophthalmol* **2006**, *6*, 23.
42. Berson, E. L.; Rosner, B.; Sandberg, M. A.; Weigel-DiFranco, C.; Brockhurst, R. J.; Hayes, K. C.; Johnson, E. J.; Anderson, E. J.; Johnson, C. A.; Gaudio, A. R.; Willett, W. C.; Schaefer, E. J., Clinical trial of lutein in patients with retinitis pigmentosa receiving vitamin A. *Arch Ophthalmol* **2010**, *128*, (4), 403-11.
43. Carneiro, Â.; Andrade, J. P., Nutritional and Lifestyle Interventions for Age-Related Macular Degeneration: A Review. *Oxid Med Cell Longev* **2017**, *2017*, 6469138.
44. Desmettre, T., Geographic Atrophy and micronutritional supplements: A complex relationship. *J Fr Ophtalmol* **2019**, *42*, (10), 1111-1115.
45. Eisenhauer, B.; Natoli, S.; Liew, G.; Flood, V. M., Lutein and Zeaxanthin-Food Sources, Bioavailability and Dietary Variety in Age-Related Macular Degeneration Protection. *Nutrients* **2017**, *9*, (2).
46. Evans, J. R.; Lawrenson, J. G., Antioxidant vitamin and mineral supplements for slowing the progression of age-related macular degeneration. *Cochrane Database Syst Rev* **2017**, *7*, (7), Cd000254.
47. Evans, J. R.; Lawrenson, J. G., Antioxidant vitamin and mineral supplements for preventing age-related macular degeneration. *Cochrane Database Syst Rev* **2017**, *7*, (7), Cd000253.
48. Heitmar, R.; Brown, J.; Kyrou, I., Saffron (Crocus sativus L.) in Ocular Diseases: A Narrative Review of the Existing Evidence from Clinical Studies. *Nutrients* **2019**, *11*, (3).

49. Kaarniranta, K.; Pawlowska, E.; Szczepanska, J.; Jablkowska, A.; Błasiak, J., Can vitamin D protect against age-related macular degeneration or slow its progression? *Acta Biochim Pol* **2019**, *66*, (2), 147-158.
50. Lister, T., Nutritional, Alternative, and Complementary Therapies for Age-related Macular Degeneration. *Integr Med (Encinitas)* **2019**, *18*, (6), 30-36.
51. Mukhtar, S.; Ambati, B. K., The value of nutritional supplements in treating Age-Related Macular Degeneration: a review of the literature. *Int Ophthalmol* **2019**, *39*, (12), 2975-2983.
52. Rojas-Fernandez, C. H.; Tyber, K., Benefits, Potential Harms, and Optimal Use of Nutritional Supplementation for Preventing Progression of Age-Related Macular Degeneration. *Ann Pharmacother* **2017**, *51*, (3), 264-270.
53. Veritti, D.; Sarao, V.; Samassa, F.; Danese, C.; Löwenstein, A.; Schmidt-Erfurth, U.; Lanzetta, P., State-of-the art pharmacotherapy for non-neovascular age-related macular degeneration. *Expert Opin Pharmacother* **2020**, *21*, (7), 773-784.
54. Neelam, K.; Dey, S.; Sim, R.; Lee, J.; Au Eong, K. G., Fructus lycii: A Natural Dietary Supplement for Amelioration of Retinal Diseases. *Nutrients 2021*, **13**, (1).
55. Zhao, Y.; Feng, K.; Liu, R.; Pan, J.; Zhang, L.; Lu, X., Vitamins and Mineral Supplements for Retinitis Pigmentosa. *J Ophthalmol* **2019**, *2019*, 8524607.
56. Wiseman, E. M.; Bar-El Dadon, S.; Reifen, R., The vicious cycle of vitamin a deficiency: A review. *Crit Rev Food Sci Nutr* **2017**, *57*, (17), 3703-3714.
57. Sandberg, M. A.; Johnson, E. J.; Berson, E. L., The relationship of macular pigment optical density to serum lutein in retinitis pigmentosa. *Invest Ophthalmol Vis Sci* **2010**, *51*, (2), 1086-91.
58. Bastos Maia, S.; Rolland Souza, A. S.; Costa Caminha, M. F.; Lins da Silva, S.; Callou Cruz, R.; Carvalho Dos Santos, C.; Batista Filho, M., Vitamin A and Pregnancy: A Narrative Review. *Nutrients* **2019**, *11*, (3).
59. Berson, E. L.; Rosner, B.; Sandberg, M. A.; Hayes, K. C.; Nicholson, B. W.; Weigel-DiFranco, C.; Willett, W., A Randomized Trial of Vitamin A and Vitamin E Supplementation for Retinitis Pigmentosa. *Archives of Ophthalmology* **1993**, *111*, (6), 761-772.
60. Norton, E. W., A randomized trial of vitamin A and vitamin E supplementation for retinitis pigmentosa. *Arch Ophthalmol* **1993**, *111*, (11), 1460; author reply 1463-5.
61. Marmor, M. F., A randomized trial of vitamin A and vitamin E supplementation for retinitis pigmentosa. *Arch Ophthalmol* **1993**, *111*, (11), 1460-1; author reply 1463-5.
62. Clowes, D. D., A randomized trial of vitamin A and vitamin E supplementation for retinitis pigmentosa. *Arch Ophthalmol* **1993**, *111*, (11), 1461-2; author reply 1462-5.
63. Fielder, A. R., A randomized trial of vitamin A and vitamin E supplementation for retinitis pigmentosa. *Arch Ophthalmol* **1993**, *111*, (11), 1463; author reply 1463-6.
64. Gamel, J. W.; Barr, C. C., A randomized trial of vitamin A and vitamin E supplementation for retinitis pigmentosa. *Arch Ophthalmol* **1993**, *111*, (11), 1462-3.
65. Massof, R. W.; Finkelstein, D., Supplemental vitamin A retards loss of ERG amplitude in retinitis pigmentosa. *Arch Ophthalmol* **1993**, *111*, (6), 751-4.

66. Radu, R. A.; Yuan, Q.; Hu, J.; Peng, J. H.; Lloyd, M.; Nusinowitz, S.; Bok, D.; Travis, G. H., Accelerated accumulation of lipofuscin pigments in the RPE of a mouse model for ABCA4-mediated retinal dystrophies following Vitamin A supplementation. *Invest Ophthalmol Vis Sci* **2008**, *49*, (9), 3821-9.
67. Berson, E. L.; Rosner, B.; Sandberg, M. A.; Weigel-DiFranco, C.; Moser, A.; Brockhurst, R. J.; Hayes, K. C.; Johnson, C. A.; Anderson, E. J.; Gaudio, A. R.; Willett, W. C.; Schaefer, E. J., Clinical trial of docosahexaenoic acid in patients with retinitis pigmentosa receiving vitamin A treatment. *Arch Ophthalmol* **2004**, *122*, (9), 1297-305.
68. Scholl, H. P.; Moore, A. T.; Koenekoop, R. K.; Wen, Y.; Fishman, G. A.; van den Born, L. I.; Bittner, A.; Bowles, K.; Fletcher, E. C.; Collison, F. T.; Dagnelie, G.; Degli Eposti, S.; Michaelides, M.; Saperstein, D. A.; Schuchard, R. A.; Barnes, C.; Zein, W.; Zobor, D.; Birch, D. G.; Mendola, J. D.; Zrenner, E., Safety and Proof-of-Concept Study of Oral QLT091001 in Retinitis Pigmentosa Due to Inherited Deficiencies of Retinal Pigment Epithelial 65 Protein (RPE65) or Lecithin:Retinol Acyltransferase (LRAT). *PLoS One* **2015**, *10*, (12), e0143846.
69. Wen, Y.; Birch, D. G., Outer Segment Thickness Predicts Visual Field Response to QLT091001 in Patients with RPE65 or LRAT Mutations. *Transl Vis Sci Technol* **2015**, *4*, (5), 8.
70. Blasiak, J.; Pawlowska, E.; Chojnacki, J.; Szczepanska, J.; Chojnacki, C.; Kaarniranta, K., Zinc and Autophagy in Age-Related Macular Degeneration. *Int J Mol Sci* **2020**, *21*, (14).
71. Bafaro, E.; Liu, Y.; Xu, Y.; Dempski, R. E., The emerging role of zinc transporters in cellular homeostasis and cancer. *Signal Transduct Target Ther* **2017**, *2*, 17029-.
72. Roehlecke, C.; Valtink, M.; Frenzel, A.; Goetze, D.; Knels, L.; Morawietz, H.; Funk, R. H., Stress responses of human retinal pigment epithelial cells to glyoxal. *Graefes Arch Clin Exp Ophthalmol* **2016**, *254*, (12), 2361-2372.
73. Ripps, H.; Chappell, R. L., Review: Zinc's functional significance in the vertebrate retina. *Mol Vis* **2014**, *20*, 1067-74.
74. Organisciak, D.; Wong, P.; Rapp, C.; Darrow, R.; Ziesel, A.; Rangarajan, R.; Lang, J., Light-induced retinal degeneration is prevented by zinc, a component in the age-related eye disease study formulation. *Photochem Photobiol* **2012**, *88*, (6), 1396-407.
75. Pao, P.-J.; Emri, E.; Abdirahman, S. B.; Soorma, T.; Zeng, H.-H.; Hauck, S. M.; Thompson, R. B.; Lengyel, I., The effects of zinc supplementation on primary human retinal pigment epithelium. *Journal of Trace Elements in Medicine and Biology* **2018**, *49*, 184-191.
76. Song, J.; Lee, S. C.; Kim, S. S.; Koh, H. J.; Kwon, O. W.; Kang, J. J.; Kim, E. K.; Shin, S.-H.; Lee, J. H., Zn2+ -induced cell death is mediated by the induction of intracellular ROS in ARPE-19 cells. *Current Eye Research* **2004**, *28*, (3), 195-201.
77. Tate, D. J.; Miceli, M. V.; Newsome, D. A.; Alcock, N. W.; Oliver, P. D., Influence of zinc on selected cellular functions of cultured human retinal pigment epithelium. *Current Eye Research* **1995**, *14*, (10), 897-903.
78. Bozym, R. A.; Chimienti, F.; Giblin, L. J.; Gross, G. W.; Korichneva, I.; Li, Y.; Libert, S.; Maret, W.; Parviz, M.; Frederickson, C. J.; Thompson, R. B., Free zinc ions outside a narrow concentration range are toxic to a variety of cells in vitro. *Experimental Biology and Medicine* **2010**, *235*, (6), 741-750.

79. Kauppinen, A.; Paterno, J. J.; Blasiak, J.; Salminen, A.; Kaarniranta, K., Inflammation and its role in age-related macular degeneration. *Cell Mol Life Sci* **2016**, *73*, (9), 1765-86.
80. Jarosz, M.; Olbert, M.; Wyszogrodzka, G.; Młyniec, K.; Librowski, T., Antioxidant and anti-inflammatory effects of zinc. Zinc-dependent NF-κB signaling. *Inflammopharmacology* **2017**, *25*, (1), 11-24.
81. Tate, D. J., Jr.; Miceli, M. V.; Newsome, D. A., Zinc protects against oxidative damage in cultured human retinal pigment epithelial cells. *Free Radic Biol Med* **1999**, *26*, (5-6), 704-13.
82. van Leeuwen, R.; Boekhoorn, S.; Vingerling, J. R.; Witteman, J. C.; Klaver, C. C.; Hofman, A.; de Jong, P. T., Dietary intake of antioxidants and risk of age-related macular degeneration. *Jama* **2005**, *294*, (24), 3101-7.
83. Tan, J. S.; Wang, J. J.; Flood, V.; Rochtchina, E.; Smith, W.; Mitchell, P., Dietary antioxidants and the long-term incidence of age-related macular degeneration: the Blue Mountains Eye Study. *Ophthalmology* **2008**, *115*, (2), 334-41.
84. Ho, L.; van Leeuwen, R.; Witteman, J. C.; van Duijn, C. M.; Uitterlinden, A. G.; Hofman, A.; de Jong, P. T.; Vingerling, J. R.; Klaver, C. C., Reducing the genetic risk of age-related macular degeneration with dietary antioxidants, zinc, and ω-3 fatty acids: the Rotterdam study. *Arch Ophthalmol* **2011**, *129*, (6), 758-66.
85. Assel, M. J.; Li, F.; Wang, Y.; Allen, A. S.; Baggerly, K. A.; Vickers, A. J., Genetic Polymorphisms of CFH and ARMS2 Do Not Predict Response to Antioxidants and Zinc in Patients with Age-Related Macular Degeneration: Independent Statistical Evaluations of Data from the Age-Related Eye Disease Study. *Ophthalmology* **2018**, *125*, (3), 391-397.
86. Ngo, H. X.; Garneau-Tsodikova, S., What are the drugs of the future? *Medchemcomm* **2018**, *9*, (5), 757-758.
87. Brown, D. M.; Regillo, C. D., Anti-VEGF agents in the treatment of neovascular age-related macular degeneration: applying clinical trial results to the treatment of everyday patients. *Am J Ophthalmol* **2007**, *144*, (4), 627-37.
88. Li, H.; Chintalapudi, S. R.; Jablonski, M. M., Current drug and molecular therapies for the treatment of atrophic age-related macular degeneration: phase I to phase III clinical development. *Expert Opin Investig Drugs* **2017**, *26*, (10), 1103-1114.
89. Waugh, N.; Loveman, E.; Colquitt, J.; Royle, P.; Yeong, J. L.; Hoad, G.; Lois, N., Treatments for dry age-related macular degeneration and Stargardt disease: a systematic review. *Health Technol Assess* **2018**, *22*, (27), 1-168.
90. Bhutto, I.; Lutty, G., Understanding age-related macular degeneration (AMD): relationships between the photoreceptor/retinal pigment epithelium/Bruch's membrane/choriocapillaris complex. *Mol Aspects Med* **2012**, *33*, (4), 295-317.
91. van Meurs, J. C.; ter Averst, E.; Hofland, L. J.; van Hagen, P. M.; Mooy, C. M.; Baarsma, G. S.; Kuijpers, R. W.; Boks, T.; Stalmans, P., Autologous peripheral retinal pigment epithelium translocation in patients with subfoveal neovascular membranes. *Br J Ophthalmol* **2004**, *88*, (1), 110-3.
92. Volarevic, V.; Markovic, B. S.; Gazdic, M.; Volarevic, A.; Jovicic, N.; Arsenijevic, N.; Armstrong, L.; Djonov, V.; Lako, M.; Stojkovic, M., Ethical and Safety Issues of Stem Cell-Based Therapy. *Int J Med Sci* **2018**, *15*, (1), 36-45.

93. Medvedev, S. P.; Shevchenko, A. I.; Zakian, S. M., Induced Pluripotent Stem Cells: Problems and Advantages when Applying them in Regenerative Medicine. *Acta Naturae* **2010**, *2*, (2), 18-28.
94. Yoshihara, M.; Hayashizaki, Y.; Murakawa, Y., Genomic Instability of iPSCs: Challenges Towards Their Clinical Applications. *Stem Cell Rev Rep* **2017**, *13*, (1), 7-16.
95. Tisi, A.; Feligioni, M.; Passacantando, M.; Ciancaglini, M.; Maccarone, R., The Impact of Oxidative Stress on Blood-Retinal Barrier Physiology in Age-Related Macular Degeneration. *Cells* **2021**, *10*, (1), 64.
96. Xian, B.; Huang, B., The immune response of stem cells in subretinal transplantation. *Stem Cell Res Ther* **2015**, *6*, 161.
97. Schwartz, S. D.; Hubschman, J. P.; Heilwell, G.; Franco-Cardenas, V.; Pan, C. K.; Ostrick, R. M.; Mickunas, E.; Gay, R.; Klimanskaya, I.; Lanza, R., Embryonic stem cell trials for macular degeneration: a preliminary report. *Lancet* **2012**, *379*, (9817), 713-20.
98. Schwartz, S. D.; Regillo, C. D.; Lam, B. L.; Eliott, D.; Rosenfeld, P. J.; Gregori, N. Z.; Hubschman, J. P.; Davis, J. L.; Heilwell, G.; Spirn, M.; Maguire, J.; Gay, R.; Bateman, J.; Ostrick, R. M.; Morris, D.; Vincent, M.; Anglade, E.; Del Priore, L. V.; Lanza, R., Human embryonic stem cell-derived retinal pigment epithelium in patients with age-related macular degeneration and Stargardt's macular dystrophy: follow-up of two open-label phase 1/2 studies. *Lancet* **2015**, *385*, (9967), 509-16.
99. Schwartz, S. D.; Tan, G.; Hosseini, H.; Nagiel, A., Subretinal Transplantation of Embryonic Stem Cell-Derived Retinal Pigment Epithelium for the Treatment of Macular Degeneration: An Assessment at 4 Years. *Invest Ophthalmol Vis Sci* **2016**, *57*, (5), ORSFc1-9.
100. Sung, Y.; Lee, M. J.; Choi, J.; Jung, S. Y.; Chong, S. Y.; Sung, J. H.; Shim, S. H.; Song, W. K., Long-term safety and tolerability of subretinal transplantation of embryonic stem cell-derived retinal pigment epithelium in Asian Stargardt disease patients. *Br J Ophthalmol* **2021**, *105*, (6), 829-837.
101. Tang, Z.; Zhang, Y.; Wang, Y.; Zhang, D.; Shen, B.; Luo, M.; Gu, P., Progress of stem/progenitor cell-based therapy for retinal degeneration. *J Transl Med* **2017**, *15*, (1), 99.
102. Wang, Y.; Tang, Z.; Gu, P., Stem/progenitor cell-based transplantation for retinal degeneration: a review of clinical trials. *Cell Death Dis* **2020**, *11*, (9), 793.
103. Koster, C.; Wever, K. E.; Wagstaff, P. E.; Hirk, K.; Hooijmans, C. R.; Bergen, A. A., A Systematic Review on Transplantation Studies of the Retinal Pigment Epithelium in Animal Models. *Int J Mol Sci* **2020**, *21*, (8).
104. Diniz, B.; Thomas, P.; Thomas, B.; Ribeiro, R.; Hu, Y.; Brant, R.; Ahuja, A.; Zhu, D.; Liu, L.; Koss, M.; Maia, M.; Chader, G.; Hinton, D. R.; Humayun, M. S., Subretinal implantation of retinal pigment epithelial cells derived from human embryonic stem cells: improved survival when implanted as a monolayer. *Invest Ophthalmol Vis Sci* **2013**, *54*, (7), 5087-96.
105. Ben M'Barek, K.; Habeler, W.; Plancheron, A.; Jarraya, M.; Regent, F.; Terray, A.; Yang, Y.; Chatrousse, L.; Domingues, S.; Masson, Y.; Sahel, J. A.; Peschanski, M.; Goureau, O.; Monville, C., Human ESC-derived retinal epithelial cell sheets potentiate rescue of photoreceptor cell loss in rats with retinal degeneration. *Sci Transl Med* **2017**, *9*, (421).
106. Garg, A.; Yang, J.; Lee, W.; Tsang, S. H., Stem Cell Therapies in Retinal Disorders. *Cells* **2017**, *6*, (1).

107. Kim, K.; Doi, A.; Wen, B.; Ng, K.; Zhao, R.; Cahan, P.; Kim, J.; Aryee, M. J.; Ji, H.; Ehrlich, L. I.; Yabuuchi, A.; Takeuchi, A.; Cunniff, K. C.; Hongguang, H.; McKinney-Freeman, S.; Naveiras, O.; Yoon, T. J.; Irizarry, R. A.; Jung, N.; Seita, J.; Hanna, J.; Murakami, P.; Jaenisch, R.; Weissleder, R.; Orkin, S. H.; Weissman, I. L.; Feinberg, A. P.; Daley, G. Q., Epigenetic memory in induced pluripotent stem cells. *Nature* **2010**, *467*, (7313), 285-90.
108. Li, Y.; Tsai, Y. T.; Hsu, C. W.; Erol, D.; Yang, J.; Wu, W. H.; Davis, R. J.; Egli, D.; Tsang, S. H., Long-term safety and efficacy of human-induced pluripotent stem cell (iPS) grafts in a preclinical model of retinitis pigmentosa. *Mol Med* **2012**, *18*, (1), 1312-9.
109. Ito, D.; Okano, H.; Suzuki, N., Accelerating progress in induced pluripotent stem cell research for neurological diseases. *Ann Neurol* **2012**, *72*, (2), 167-74.
110. van Meurs, J. C.; Van Den Biesen, P. R., Autologous retinal pigment epithelium and choroid translocation in patients with exudative age-related macular degeneration: short-term follow-up. *Am J Ophthalmol* **2003**, *136*, (4), 688-95.
111. Heussen, F.; Fawzy, N.; Joeres, S.; Lux, A.; Maaijwee, K.; Meurs, J. C.; Kirchhof, B.; Joussen, A., Autologous translocation of the choroid and RPE in age-related macular degeneration: 1-year follow-up in 30 patients and recommendations for patient selection. *Eye* **2008**, *22*, (6), 799-807.
112. Joussen, A. M.; Heussen, F. M.; Joeres, S.; Llacer, H.; Prinz, B.; Rohrschneider, K.; Maaijwee, K. J.; van Meurs, J.; Kirchhof, B., Autologous translocation of the choroid and retinal pigment epithelium in age-related macular degeneration. *American journal of ophthalmology* **2006**, *142*, (1), 17-30. e8.
113. Joussen, A. M.; Joeres, S.; Fawzy, N.; Heussen, F. M.; Llacer, H.; van Meurs, J. C.; Kirchhof, B., Autologous translocation of the choroid and retinal pigment epithelium in patients with geographic atrophy. *Ophthalmology* **2007**, *114*, (3), 551-560.
114. Maaijwee, K.; Heimann, H.; Missotten, T.; Mulder, P.; Joussen, A.; van Meurs, J., Retinal pigment epithelium and choroid translocation in patients with exudative age-related macular degeneration: long-term results. *Graefe's Archive for Clinical and Experimental Ophthalmology* **2007**, *245*, (11), 1681-1689.
115. Caramoy, A.; Liakopoulos, S.; Menrath, E.; Kirchhof, B., Autologous translocation of choroid and retinal pigment epithelium in geographic atrophy: long-term functional and anatomical outcome. *British journal of ophthalmology* **2010**, *94*, (8), 1040-1044.
116. van Zeeburg, E. J.; Maaijwee, K. J.; Missotten, T. O.; Heimann, H.; van Meurs, J. C., A free retinal pigment epithelium–choroid graft in patients with exudative age-related macular degeneration: results up to 7 years. *American journal of ophthalmology* **2012**, *153*, (1), 120-127. e2.
117. Bergen, A. A., Nicotinamide, iRPE-in-a dish, and age-related macular degeneration therapy development. *Stem cell investigation* **2017**, *4*, 81.
118. Cabral de Guimaraes, T. A.; Daich Varela, M.; Georgiou, M.; Michaelides, M., Treatments for dry age-related macular degeneration: therapeutic avenues, clinical trials and future directions. *British Journal of Ophthalmology* **2022**, *106*, (3), 297-304.
119. Collin, J.; Queen, R.; Zerti, D.; Dorgau, B.; Hussain, R.; Coxhead, J.; Cockell, S.; Lako, M., Deconstructing Retinal Organoids: Single Cell RNA-Seq Reveals the Cellular Components of Human Pluripotent Stem Cell-Derived Retina. *Stem Cells* **2019**, *37*, (5), 593-598.

120. Wagstaff, P. E.; Heredero Berzal, A.; Boon, C. J. F.; Quinn, P. M. J.; Ten Asbroek, A.; Bergen, A. A., The Role of Small Molecules and Their Effect on the Molecular Mechanisms of Early Retinal Organoid Development. *Int J Mol Sci* **2021**, *22*, (13).
121. Bartfeld, S.; Clevers, H., Stem cell-derived organoids and their application for medical research and patient treatment. *J Mol Med (Berl)* **2017**, *95*, (7), 729-738.
122. Koster, C.; van den Hurk, K. T.; Lewallen, C. F.; Talib, M.; Ten Brink, J. B.; Boon, C. J. F.; Bergen, A. A., The Lrat(-/-) Rat: CRISPR/Cas9 Construction and Phenotyping of a New Animal Model for Retinitis Pigmentosa. *Int J Mol Sci* **2021**, *22*, (13).
123. Talib, M.; van Schooneveld, M. J.; van Duuren, R. J. G.; Van Cauwenbergh, C.; Ten Brink, J. B.; De Baere, E.; Florijn, R. J.; Schalij-Delfos, N. E.; Leroy, B. P.; Bergen, A. A.; Boon, C. J. F., Long-Term Follow-Up of Retinal Degenerations Associated With LRAT Mutations and Their Comparability to Phenotypes Associated With RPE65 Mutations. *Transl Vis Sci Technol* **2019**, *8*, (4), 24.
124. Shanks, N.; Greek, R.; Greek, J., Are animal models predictive for humans? *Philosophy, Ethics, and Humanities in Medicine* **2009**, *4*, (1), 2.
125. Bhutto, I. A.; Ogura, S.; Baldeosingh, R.; McLeod, D. S.; Lutty, G. A.; Edwards, M. M., An Acute Injury Model for the Phenotypic Characteristics of Geographic Atrophy. *Investigative Ophthalmology & Visual Science* **2018**, *59*, (4), AMD143-AMD151.
126. de Jong, P. T. V. M., Age-Related Macular Degeneration. *New England Journal of Medicine* **2006**, *355*, (14), 1474-1485.
127. Datta, S.; Cano, M.; Ebrahimi, K.; Wang, L.; Handa, J. T., The impact of oxidative stress and inflammation on RPE degeneration in non-neovascular AMD. *Progress in Retinal and Eye Research* **2017**, *60*, 201-218.
128. Darrow, J. J., VN: FDA documents reveal the value of a costly gene therapy. *Drug Discov Today* **2019**, *24*, (4), 949-954.
129. Maguire, A. M.; Russell, S.; Chung, D. C.; Yu, Z. F.; Tillman, A.; Drack, A. V.; Simonelli, F.; Leroy, B. P.; Reape, K. Z.; High, K. A.; Bennett, J., Durability of Voretigene Neparvovec for Biallelic RPE65-Mediated Inherited Retinal Disease: Phase 3 Results at 3 and 4 Years. *Ophthalmology* **2021**, *128*, (10), 1460-1468.
130. Maguire, A. M.; Russell, S.; Wellman, J. A.; Chung, D. C.; Yu, Z. F.; Tillman, A.; Wittes, J.; Pappas, J.; Elci, O.; Marshall, K. A.; McCague, S.; Reichert, H.; Davis, M.; Simonelli, F.; Leroy, B. P.; Wright, J. F.; High, K. A.; Bennett, J., Efficacy, Safety, and Durability of Voretigene Neparvovec-rzyl in RPE65 Mutation-Associated Inherited Retinal Dystrophy: Results of Phase 1 and 3 Trials. *Ophthalmology* **2019**, *126*, (9), 1273-1285.
131. Gao, J.; Hussain, R. M.; Weng, C. Y., Voretigene Neparvovec in Retinal Diseases: A Review of the Current Clinical Evidence. *Clin Ophthalmol* **2020**, *14*, 3855-3869.
132. Kang, C.; Scott, L. J., Voretigene Neparvovec: A Review in RPE65 Mutation-Associated Inherited Retinal Dystrophy. *Mol Diagn Ther* **2020**, *24*, (4), 487-495.
133. Kortüm, F. C.; Kempf, M.; Jung, R.; Kohl, S.; Ott, S.; Kortuem, C.; Sting, K.; Stingl, K., Short term morphological rescue of the fovea after gene therapy with voretigene neparvovec. *Acta Ophthalmol* **2022**, *100*, (3), e807-e812.

134. Weng, C. Y., Bilateral Subretinal Voretigene Neparvovec-rzyl (VN) Gene Therapy. *Ophthalmol Retina* **2019**, *3*, (5), 450.
135. Gange, W. S.; Sisk, R. A.; Besirli, C. G.; Lee, T. C.; Havunjian, M.; Schwartz, H.; Borchert, M.; Sengillo, J. D.; Mendoza, C.; Berrocal, A. M.; Nagiel, A., Perifoveal Chorioretinal Atrophy after Subretinal Voretigene Neparvovec-rzyl for RPE65-Mediated Leber Congenital Amaurosis. *Ophthalmology Retina* **2022**, *6*, (1), 58-64.
136. Cideciyan, A. V.; Jacobson, S. G.; Beltran, W. A.; Sumaroka, A.; Swider, M.; Iwabe, S.; Roman, A. J.; Olivares, M. B.; Schwartz, S. B.; Komáromy, A. M.; Hauswirth, W. W.; Aguirre, G. D., Human retinal gene therapy for Leber congenital amaurosis shows advancing retinal degeneration despite enduring visual improvement. *Proc Natl Acad Sci U S A* **2013**, *110*, (6), E517-25.
137. Maguire, A. M.; High, K. A.; Auricchio, A.; Wright, J. F.; Pierce, E. A.; Testa, F.; Mingozzi, F.; Bennicelli, J. L.; Ying, G. S.; Rossi, S.; Fulton, A.; Marshall, K. A.; Banfi, S.; Chung, D. C.; Morgan, J. I.; Hauck, B.; Zelenaia, O.; Zhu, X.; Raffini, L.; Coppieters, F.; De Baere, E.; Shindler, K. S.; Volpe, N. J.; Surace, E. M.; Acerra, C.; Lyubarsky, A.; Redmond, T. M.; Stone, E.; Sun, J.; McDonnell, J. W.; Leroy, B. P.; Simonelli, F.; Bennett, J., Age-dependent effects of RPE65 gene therapy for Leber's congenital amaurosis: a phase 1 dose-escalation trial. *Lancet* **2009**, *374*, (9701), 1597-605.
138. Bainbridge, J. W.; Mehat, M. S.; Sundaram, V.; Robbie, S. J.; Barker, S. E.; Ripamonti, C.; Georgiadis, A.; Mowat, F. M.; Beattie, S. G.; Gardner, P. J.; Feathers, K. L.; Luong, V. A.; Yzer, S.; Balaggan, K.; Viswanathan, A.; de Ravel, T. J.; Casteels, I.; Holder, G. E.; Tyler, N.; Fitzke, F. W.; Weleber, R. G.; Nardini, M.; Moore, A. T.; Thompson, D. A.; Petersen-Jones, S. M.; Michaelides, M.; van den Born, L. I.; Stockman, A.; Smith, A. J.; Rubin, G.; Ali, R. R., Long-term effect of gene therapy on Leber's congenital amaurosis. *N Engl J Med* **2015**, *372*, (20), 1887-97.
139. Cehajic-Kapetanovic, J.; Xue, K.; Martinez-Fernandez de la Camara, C.; Nanda, A.; Davies, A.; Wood, L. J.; Salvetti, A. P.; Fischer, M. D.; Aylward, J. W.; Barnard, A. R.; Jolly, J. K.; Luo, E.; Lujan, B. J.; Ong, T.; Girach, A.; Black, G. C. M.; Gregori, N. Z.; Davis, J. L.; Rosa, P. R.; Lotery, A. J.; Lam, B. L.; Stanga, P. E.; MacLaren, R. E., Initial results from a first-in-human gene therapy trial on X-linked retinitis pigmentosa caused by mutations in RPGR. *Nat Med* **2020**, *26*, (3), 354-359.
140. Scruggs, B. A.; Jiao, C.; Cranston, C. M.; Kaalberg, E.; Wang, K.; Russell, S. R.; Wiley, L. A.; Mullins, R. F.; Stone, E. M.; Tucker, B. A.; Sohn, E. H., Optimizing Donor Cellular Dissociation and Subretinal Injection Parameters for Stem Cell-Based Treatments. *Stem Cells Transl Med* **2019**, *8*, (8), 797-809.
141. Xiong, W.; Wu, D. M.; Xue, Y.; Wang, S. K.; Chung, M. J.; Ji, X.; Rana, P.; Zhao, S. R.; Mai, S.; Cepko, C. L., AAV cis-regulatory sequences are correlated with ocular toxicity. *Proc Natl Acad Sci U S A* **2019**, *116*, (12), 5785-5794.
142. Testa, F.; Melillo, P.; Della Corte, M.; Di Iorio, V.; Brunetti-Pierri, R.; Citro, A.; Ferrara, M.; Karali, M.; Annibale, R.; Banfi, S.; Rossi, S.; Simonelli, F., Voretigene Neparvovec Gene Therapy in Clinical Practice: Treatment of the First Two Italian Pediatric Patients. *Transl Vis Sci Technol* **2021**, *10*, (10), 11.

The way to get started is to quit talking and begin doing.

— Walt Disney

English summary

7

Towards Experimental Therapies for Retinal Degenerative Diseases

This thesis describes part of the preclinical road that is essential in developing experimental therapies for retinal degenerative diseases such as age-related macular degeneration (AMD) and a specific type of retinitis pigmentosa (RPE-RP). The retinal pigment epithelium (RPE) plays a significant role in the pathology of both diseases. Indeed, patients of all ages can be affected by conditions involving (primarily) the RPE. This thesis is focused on RPE disease pathology, illustrated by the complex retinal disease AMD and a specific genetic form of the monogenic disorder RP. Many experimental therapeutic strategies are being developed to treat AMD and RPE-RP; however, gene therapy and cell-replacement therapy can be considered important strategies for these diseases, especially because of the curative nature of these two treatment modalities. In this thesis, we first used a systematic approach to identify and analyze all preclinical studies that have been published regarding RPE cell-replacement strategy to treat retinal degenerative diseases (Chapter 2). We next used a genome-editing technique to create a new animal model for an RPE-RP subtype and characterized the model in-depth (Chapter 3). Additionally, we describe an induced preclinical model for AMD and its in-depth characterization (Chapter 4). As a final step, we describe the generation of a 3D-bio-printed tissue recapitulating the RPE and underlying tissues and its transplantation and integration into rat eyes (Chapter 5). Below, a short summary is presented for each chapter of this thesis.

In **Chapter 1**, I briefly introduce retinal degenerative diseases and their tremendous impact on patients' quality-of-life. The structure and function of the healthy retina are described. The involvement of the RPE in many retinal degenerative diseases can be understood easily by reading about all the essential tasks that the RPE performs in maintaining normal vision. The pathology and disease etiology of the RPE-RP subtype and AMD are discussed, and some experimental therapeutic strategies are briefly considered. In Chapter 1, I also discuss the available experimental models and their application in research on retinal degenerative diseases. Both *in vitro* and *in vivo* models are summarized. While human representative *in vitro* models, such as cell cultures and retinal organoids, become increasingly available, they do not fully represent the eye or vision in the context of a whole organism. Therefore, suitable animal models representing the disease's phenotype are still essential and required to test full visual function and experimental therapeutic's safety and efficacy *in vivo* before formal treatment approval. Given the significant etiologic heterogeneity of AMD's and RP's patient populations, personalized strategies are currently a major research focus and of utmost importance for these patients. A full in-depth discussion about therapeutic strategies and their future directions can be found in **Chapter 6**.

In **Chapter 2**, all available preclinical studies involving animal models and RPE transplantation as cell-replacement therapy are reviewed. RPE-replacement for AMD and the RPE-RP subtypes, especially in the later stages of the disease, may be one of the most promising experimental therapeutic strategies once significant portions of vision are lost. There is, however, no consensus regarding the optimal RPE source, delivery strategy, or the optimal experimental host in which to test the RPE-replacement therapy. Indeed, multiple RPE sources, delivery methods, and recipient animal models have been investigated with variable results. So far, a systematic evaluation of the (variables influencing) efficacy of experimental RPE-replacement parameters was lacking. In this chapter, we investigated the effect of RPE transplantation on vision and vision-based behavior in animal models for retinal degenerative diseases. In addition, we explored the impact of the RPE source used for transplantation, the method of intervention, and the animal model used for testing. To study this, we systematically identified all publications concerning transplantation of the RPE in experimental animal models targeting an improvement in vision. A variety of characteristics, such as species, gender, and age of the animals, but also cell type, number of cells, and other intervention characteristics were extracted from all studies. A risk of bias in the analyses was performed as well. Overall, most studies were categorized as unclear regarding the risk of bias because many experimental details were poorly reported. Meta-analyses were performed on the a- and b-wave amplitudes from electroretinography (ERG) data as well as data from vision-based behavioral assays. RPE transplantation significantly increased ERG a-wave and b-wave amplitudes and vision-based behavior. Subgroup analyses revealed a significantly increased effect of using young and adolescent animals compared to adult animals. Moreover, transplanting more cells (in the range of 10^5 versus in the range of 10^4) resulted in a significantly increased effect on vision-based behavior as well. The origin of cells matters as well. A significantly increased effect was found on vision-based behavior when using ARPE-19 and OpRegen® RPE. The conclusion of this chapter is that RPE transplantation in animal models for retinal degeneration is safe and may also be beneficial. Still, there is an urgent need to improve the methodological and reporting quality of animal experiments to make such studies more comparable.

In **Chapter 3**, the development and characterization of a new animal model for the RPE-RP subtype involving an autosomal recessive mutation causing this disease are described. Using CRISPR/Cas9 genome editing, we constructed and phenotyped a pigmented knockout rat model for lecithin retinol acyltransferase (LRAT) (*Lrat*$^{-/-}$ rats). The introduced mutation (c.12delA) is based on a Dutch patient cohort harboring a homologous homozygous frameshift mutation in the *LRAT* gene (c.12delC). This mutation causes a dysfunctional visual (retinoid) cycle. We confirmed the mutation in the transgenic rat by DNA and RNA sequencing. The expression of *Lrat* was determined on both the RNA and protein levels in wildtype and knockout rats using RT-PCR and immunohistochemistry. Wildtype animals had a high *Lrat* mRNA expression in multiple tissues, including the eye and the liver. In contrast, hardly any expression was detected in *Lrat*$^{-/-}$ animals. LRAT protein was abundantly present in wildtype animals and absent in *Lrat*$^{-/-}$ animals.

The retinal structure and function and the vision-based behavior of the *Lrat*$^{-/-}$ and control rats were characterized using scanning laser ophthalmoscopy (SLO), optical coherence tomography (OCT), ERG, and a vision-based behavioral assay. The retinal thickness in *Lrat*$^{-/-}$ animals was decreased to roughly 80 % by four months of age compared to the wildtype controls. *Lrat*$^{-/-}$ animals also showed progressively reduced ERG potentials from two weeks of age onwards. The vision-based behavioral assay confirmed reduced vision. No functional or structural differences were observed between wildtype and heterozygote animals, as was expected based on patient data. This pigmented rat model is a new animal model for retinal dystrophy, especially for the *LRAT*-subtype of early-onset retinal dystrophies. The model has advantages over existing mouse models and rat strains and can be used for future translational and therapeutic studies of the *LRAT*-RP type.

In **Chapter 4**, the generation and characterization of inducible models for AMD are described. Pigmented mice and rats were systemically injected with various doses of sodium iodate (SI). This agent is known to cause retinal degeneration through oxidative stress pathways. Oxidative stress in the RPE is an important driver of AMD pathology. After injection, the animal models' retinal structure and visual function were non-invasively characterized over time to obtain in-depth data about the experimental therapeutic suitability for (dry) AMD and other RPE-based retinal diseases. A series of doses (0 – 70 mg/kg) was injected into adolescent pigmented mice and rats' tail veins (i.v.). The retinal structure and function were assessed non-invasively using SLO, OCT and ERG. We found that the degree of retinal degeneration after injection was similar in the two species. The lowest dose (10 mg/kg) resulted in non-detectable structural or functional effects. An injection with 20 mg/kg SI did not result in an evident retinal degeneration as judged from OCT data. However, at this dose, ERG responses were temporarily decreased but returned to baseline within two weeks. Higher doses (30, 40, 50 and 70 mg/kg) resulted in moderate to severe structural RPE and retinal damage as well as decreased ERG amplitudes, indicating visual impairment in both mice and rat strains. The conclusion of this chapter is that a dose-dependent structural and functional pathological effect could be observed on the RPE and the retina after SI injections. In particular, a dose of 30 mg/kg seems suitable for future studies on developing experimental therapies. These relatively easily induced non-inherited models may be useful for evaluating novel therapies for RPE-related retinal degenerations, such as AMD and the RPE-RP subtype.

In **Chapter 5**, the construction of a native-like 3D tissue representing the outer-blood-retina barrier (oBRB) is described. The oBRB consists of a monolayer of RPE and its tight junctions. The RPE is flanked by the photoreceptor layer on the apical side, and the Bruch's membrane and the choriocapillaris on the basal side. It is thought that the RPE is primarily affected in AMD, followed by degeneration of the adjacent tissues. Nonetheless, the mechanism of AMD initiation and progression remains poorly understood due to the lack of physiologically relevant oBRB models. We constructed a 3D-oBRB tissue model by bioprinting endothelial cells, pericytes, and fibroblasts on the basal side of a biodegradable scaffold and establishing an RPE monolayer on top. In this 3D-oBRB, a fully-polarized RPE monolayer with apical processes, basal infoldings and tight junctions provides relevant barrier resistance. It induces fenestration and choroid-specific gene expression in the choriocapillaris. Further, it supports the formation of a (natural) Bruch's-like membrane that allows tissue integration in rat eyes. Complement activation in the 3D-oBRB triggers dry-AMD-like phenotypes (including subRPE drusen and choriocapillaris degeneration), and hypoxia-induced wet-AMD-like phenotypes (choriocapillaris neovascularization). Anti-VEGF drug treatment suppressed neovascularization in the 3D-oBRB tissues. The 3D-oBRB construct essentially recapitulates AMD phenotypes and sheds light on disease mechanisms that could not be addressed previously due to the lack of appropriate in vitro model systems. A fully-syngeneic 3D-oBRB derived from AMD-patient iPSCs may shed light on a more comprehensive understanding of disease pathology.

In **Chapter 6**, I discuss the currently considered experimental therapeutic strategies for retinal degenerative diseases and, more specifically, for AMD and the RPE-RP subtype. Even though much scientific effort has been put into translational research to develop new experimental therapies for retinal degenerative disorders, there is still much to learn. We currently lack detailed and systemic information about the preclinical models and their therapeutic potential. Although several clinical trials are currently ongoing in different phases, results are often inconsistent due to various reasons. To ensure reproducibility and consistency, we need more standardized systematic protocols in both preclinical and clinical research.

Be who you are and say what you feel,
because those who mind don't matter
and those who matter don't mind.

— Dr. Seuss

Nederlandse samenvatting

8

De ontwikkeling van experimentele therapiën voor degeneratieve netvliesziekten

Dit proefschrift beschrijft een deel van het preklinische onderzoek welke essentieel is voor het ontwikkelen van experimentele therapieën voor degeneratieve netvliesziekten, zoals leeftijd gerelateerde maculadegeneratie (LMD) en een specifiek type van retinitis pigmentosa (RP-RPE). Een laagje netvliescellen, het retinaal pigment epitheel (RPE), speelt een belangrijke rol in de pathologie van beide ziektes. Patiënten van alle leeftijden kunnen te maken krijgen met oogziektes waarbij (hoofdzakelijk) het RPE is aangedaan. In dit proefschrift staat de pathologie RPE-ziektes centraal. Dit wordt geïllustreerd door de complexe netvliesziekte LMD en een meer specifieke genetische variant van de monogene aandoening RP. Veel experimentele therapieën worden op dit moment ontwikkeld om LMD en RPE-RP te kunnen behandelen. Gentherapie en regeneratieve celtherapie kunnen worden gezien als veel belovende strategieën om deze ziektes te kunnen (gaan) behandelen. Dit komt doordat deze therapieën gericht zijn op genezing. De overige therapeutische strategieën zijn vooral gericht op het behandelen van symptomen. In dit proefschrift, hebben we allereerst, met een systematische aanpak, alle voorheen gepubliceerde preklinische studies op het gebied van regeneratieve RPE celtherapie voor degeneratieve netvliesziekten gelezen en geanalyseerd (Hoofdstuk 2). Ook hebben we, door middel van genetische modificatie, een nieuw diermodel voor een RPE-RP subtype gemaakt. Dit model hebben we uitgebreid gekarakteriseerd (Hoofdstuk 3). Vervolgens beschrijven we een geïnduceerd preklinisch model voor LMD en de uitgebreide karakterisatie van dit model (Hoofdstuk 4). Als een laatste stap in dit proefschrift beschrijven we een driedimensionaal (3D) weefsel dat gemaakt is met behulp van een bioprinter. Dit weefsel is een model voor het RPE en de onderliggende weefsels. Tenslotte hebben we dit weefsel getransplanteerd in een rattenoog en beschrijven we de integratie ervan (Hoofdstuk 5). Hieronder volgt een korte samenvatting per hoofdstuk van dit proefschrift.

Hoofdstuk 1 bevat een korte introductie over degeneratieve netvliesziekten en de enorme impact die deze ziektes hebben op de kwaliteit van leven van patiënten. Ook staat de structuur en de functie van het gezonde netvlies beschreven. Het RPE is betrokken bij veel degeneratieve netvliesziekten. Dit kan makkelijk worden begrepen door te lezen over alle essentiële taken die het RPE heeft om normaal te kunnen zien. De pathologie en de etiologie van de ziektes LMD en RPE-RP worden beschreven en een aantal experimentele therapeutische strategieën worden kort genoemd. In Hoofdstuk 1 worden de beschikbare experimentele modellen en hun toepasbaarheid in onderzoek naar degeneratieve netvliesziekten beschreven. Zowel *in vitro* (in een kweekschaaltje) als *in vivo* (dier) modellen worden beschreven en samengevat. Er komen steeds meer (humane) representatieve *in vitro* modellen, zoals celkweken en netvlies organoïden, beschikbaar. Toch kunnen deze (nog) niet model staan voor een compleet oog of de mogelijkheid tot (therapeutisch in)zicht in de context van een levend organisme. Daarom zijn diermodellen die het fenotype van de ziekte representeren nog steeds noodzakelijk om te gebruiken.

Alleen *in vivo* kan "het zien" worden getest en of de experimentele therapieën veilig en effectief zijn. Binnen de LMD en RPE-RP patiënten populaties bestaan er grote etiologische verschillen. Mede hierom zijn gepersonaliseerde behandelingsstrategieën ontzettend belangrijk voor deze patiënten en wordt er binnen het onderzoeksveld momenteel veel focus op gelegd. Een uitgebreide uiteenzetting van mogelijke (toekomstige) therapeutische strategieën kan worden gevonden in **Hoofdstuk 6**.

In **Hoofdstuk 2** is een uiteenzetting te vinden van alle in de literatuur beschikbare preklinische studies over diermodellen en de transplantatie van het RPE als regeneratieve celtherapie. Het vervangen van de RPE cellaag in LMD en het RPE-RP subtype, voornamelijk in de vergevorderde stadia van deze ziektes, is de meest belovende experimentele therapeutische aanpak: met name als al een groot gedeelte van het zicht verloren is gegaan. Op het moment is er echter geen algemene overeenstemming over de optimale bron van de RPE cellen, de plaatsingsstrategie, of het beste diermodel om de RPE celtherapie te kunnen testen. Meerdere RPE cel bronnen, transplantatiestrategieën en diermodellen zijn inmiddels gebruikt in dit onderzoeksveld, met wisselende resultaten. Tot dusver was een systematische evaluatie van de efficiëntie van RPE celtherapie en de variabelen die dit beïnvloeden nog niet beschikbaar. In dit hoofdstuk, hebben we het effect van RPE transplantatie op het zicht in diermodellen van degeneratieve netvliesziekten systematisch onderzocht en beschreven. Ook hebben we bekeken wat de impact is van de bron van de RPE cellen op de effectiviteit van de celtherapie evenals de plaatsingsstrategie en het diermodel dat werd gebruikt. Om dit te onderzoeken, hebben we systematisch alle publicaties betreffende RPE transplantaties in diermodellen geïdentificeerd. Meerdere studie eigenschappen zoals diersoort, geslacht, leeftijd van de dieren, maar ook celtype, het aantal cellen en andere eigenschappen van de interventie zijn van alle studies verzameld. Er is ook gekeken naar het risico op bias in de geïncludeerde studies: over het algemeen moesten de meeste studies in de categorie "onduidelijk" worden geplaatst. Dit werd vooral veroorzaakt doordat veel experimentele details niet of nauwelijks werden gerapporteerd. Meta-analyses zijn gedaan op de gemeten a- en b-wave amplitudes uit electroretinogrammen (ERG) en op gedragsstudies waar het zicht invloed op heeft.

RPE transplantatie verbeterde significant de ERG a- en b-wave amplitudes en ook het visueel gebaseerde gedrag van de dieren. Een subgroep analyse liet zien dat een groter effect kon worden behaald als er jonge en jong-volwassen dieren werden gebruikt in vergelijking met volwassen dieren. Ook bleek dat het transplanteren van meer cellen (10^5 versus 10^4) een significant groter effect had in de gedragsstudies. De bron van de getransplanteerde cellen maakte ook zeker een verschil op de efficiëntie van de transplantatie. Een significant groter effect werd gevonden in de gedragsstudies als ARPE-19 cellen en OpRegen® RPE cellen werden gebruikt. De conclusie van dit hoofdstuk is dat het transplanteren van RPE cellen in diermodellen voor netvliesdegeneratie veilig is en efficiënt kan zijn. Ondanks dat is er nog steeds een grote noodzaak om de kwaliteit van de methodologie en het rapporteren van experimentele opzet van dierproeven te verbeteren. Alleen dan kunnen zulke studies goed met elkaar worden vergeleken en kunnen vervolgstappen beter bepaald worden.

In **Hoofdstuk 3** staat de ontwikkeling en karakterisatie van een nieuw diermodel voor een RPE-RP subtype (het LRAT-RP subtype) uitgebreid beschreven. De genetische mutatie die bij dit subtype betrokken is, erft autosomaal recessief over. Door middel van CRISPR/Cas9 werd een ratmodel gecreëerd (*Lrat*$^{-/-}$ ratten) dat een mutatie heeft in het gen voor het eiwit lecithine retinol acyltransferase (LRAT). De geïntroduceerde mutatie (c.12delA) is gebaseerd op een Nederlandse patiëntengroep die een homozygote frameshift mutatie hebben in het *LRAT* gen (c.12delC). Deze mutatie veroorzaakt een verstoorde en niet functionele visuele (retinoïde) cyclus. We hebben bevestigd dat de mutatie in het rattenmodel aanwezig is door middel van het sequensen van het DNA en RNA. Ook hebben we de mate van expressie van *Lrat* bepaald op zowel het RNA niveau als het eiwit niveau in wildtype en gemuteerde ratten door middel van RT-PCR en immuunhistochemie. Wildtype dieren hadden hoge expressie van *Lrat* mRNA in meerdere soorten weefsels, zoals het oog en de lever, maar *Lrat*$^{-/-}$ dieren hadden dit vrijwel niet. Het LRAT eiwit was in grote hoeveelheid aanwezig in wildtype dieren en niet aanwezig in *Lrat*$^{-/-}$ dieren. De structuur en functie van het netvlies van *Lrat*$^{-/-}$ en controle ratten werden gekarakteriseerd door middel van scanning laser oftalmoscopie (SLO), optische coherentie tomografie (OCT) en ERG. Het visueel gedrag van de dieren werd in kaart gebracht door middel van gedragsexperimenten.

Na vier maanden was de dikte van de retina in *Lrat*$^{-/-}$ dieren afgenomen tot ongeveer 80 % in vergelijking met gezonde controles. Ook hadden *Lrat*$^{-/-}$ dieren progressief gereduceerde ERG potentialen vanaf de leeftijd van twee weken. De visuele gedragsexperimenten bevestigden dat de *Lrat*$^{-/-}$ ratten minder goed kunnen zien. Er was geen structureel of functioneel netvliesverschil tussen heterozygote en wildtype dieren. Dit was ook niet de verwachting op basis van de patiënten data. Dit gepigmenteerde rattenmodel is een nieuw model voor het *LRAT*-RP subtype en van vroeg optredende netvliesdystrofieën. Dit model heeft meerdere voordelen ten opzichte van bestaande muis- en ratmodellen en het kan gebruikt worden voor translationele en therapeutische studies van *LRAT*-RP.

In **Hoofdstuk 4** wordt het genereren en karakteriseren van een geïnduceerd model voor LMD beschreven. Gepigmenteerde muizen en ratten werden systemisch geïnjecteerd met verschillende doses van natriumjodaat (NJ) zout. Van dit middel is bekend dat het netvliesdegeneratie veroorzaakt door middel van oxidatieve stress. Omdat oxidatieve stress in het RPE een belangrijke oorzaak is van de pathologie van LMD, kan dit geïnduceerde model LMD representeren in wetenschappelijk onderzoek. Na de injectie werden de netvliesstructuur en de visuele functie over een tijdsperiode niet-invasief gemeten. Op deze manier werd er gedetailleerde informatie verkregen over de geschiktheid van deze modellen om model te staan voor (droge) LMD en andere netvliesaandoeningen waarin het RPE een rol speelt. Verschillende doses zout (0 – 70 mg/kg) werden geïnjecteerd in de staartaders van jong-volwassen muizen en ratten (i.v.).

De structuur en de functie van het netvlies werden niet-invasief beoordeeld door middel van SLO, OCT en ERG. We ontdekten dat de mate van netvliesdegeneratie na injectie vergelijkbaar was in de twee hiervoor genoemde diersoorten. De laagste dosis (10 mg/kg) veroorzaakte geen meetbaar structureel of functioneel effect. Een injectie van 20 mg/kg NJ resulteerde in een zeer minimale netvliesdegeneratie volgens de OCT beelden. Bij deze dosis namen de ERG amplitudes wel tijdelijk af, maar keerden ze binnen twee weken weer terug naar de uitgangswaarde. Injecties van de hogere doses (30, 40, 50 en 70 mg/kg) resulteerden in een matige tot ernstige structurele schade aan het RPE en aan het netvlies. Verminderde ERG amplitudes wijzen op een functioneel visuele afwijking bij zowel de muizen als de ratten. De conclusie van dit hoofdstuk is dat een systemische injectie met NJ een dosisafhankelijke structureel en functioneel pathologisch effect heeft op het RPE en het netvlies. Een dosis van 30 mg/kg lijkt een geschikte dosis voor toekomstig onderzoek naar de ontwikkeling van experimentele therapieën. Deze relatief gemakkelijk te induceren niet-erfelijke modellen kunnen erg nuttig zijn voor het evalueren van nieuwe therapieën voor RPE-gerelateerde ziekten van het netvlies, zoals LMD en het RPE-RP subtype.

In **Hoofdstuk 5** wordt de constructie van een 3D weefsel beschreven dat de buitenste bloed-netvlies-barrière (bBNB) vertegenwoordigt. De bBNB bestaat uit het RPE en zijn cel-cel contacten ("tight junctions"). Het RPE wordt geflankeerd door de fotoreceptor cellaag aan de apicale zijde en het membraan van Bruch en de choriocapillaris aan de basale zijde. Er wordt gedacht dat in eerste instantie voornamelijk het RPE is aangetast bij LMD, gevolgd door de degeneratie van de aangrenzende weefsels. Het mechanisme van de initiatie en de progressie van LMD blijft nog niet volledig begrepen, vooral vanwege het ontbreken van fysiologisch relevante modellen voor de bBNB en flankerende weefsels. We hebben een 3D weefselmodel geconstructureerd voor de bBNB door middel van endotheelcellen, pericyten en fibroblasten aan de basale kant van een biologisch afbreekbare houder te bioprinten en er een RPE cellaag bovenop te plaatsen. In deze 3D-bBNB is een volledig gepolariseerde RPE cellaag met apicale processen, basale instulpingen en tight junctions te vinden met een relevante barrièreweerstand. Ook wordt in dit weefsel de organisatie en de specifieke genexpressie van het choroid in de choriocapillaris geïnduceerd. Verder ondersteunt het de vorming van een natuurlijk Bruch-achtig membraan dat de weefselintegratie in rattenogen mogelijk maakt. Activatie van het complementsysteem in het 3D-bBNB initieert droge LMD-achtige fenotypes (inclusief subRPE drusen en degeneratie van de choriocapillaris), en hypoxie-geïnduceerde natte LMD-achtige fenotypes (neovascularisatie van de choriocapillaris). Behandeling met anti-VEGF middelen onderdrukt deze neovascularisatie in 3D-bBNB weefsels. Het nieuwe 3D-bBNB weefsel bootst in essentie LMD fenotypen na, waardoor de ziektemechanismen nu beter begrepen kunnen worden. Een volledig syngeen 3D-bBNB weefsel dat gemaakt is uit stamcellen van LMD patiënten kan licht werpen op een meer uitgebreid begrip van de pathologie en het verloop van deze ziekte.

Hoofdstuk 6 gaat in op de momenteel gangbare experimentele therapeutische strategieën voor degeneratieve netvliesziekten en, meer specifiek, voor LMD en het RPE-RP subtype. Hoewel er veel wetenschappelijke inspanning gestoken is in translationeel onderzoek om nieuwe experimentele therapieën voor degeneratieve netvliesaandoeningen te ontwikkelen, valt er nog veel te leren. Het ontbreekt ons op dit moment aan systematische data en gedetailleerde informatie over de (nieuw ontwikkelde) preklinische modellen en het therapeutisch potentieel van experimentele therapieën. Hoewel er momenteel verschillende klinische onderzoeken lopen in verschillende fasen, zijn de resultaten tot nu toe om verschillende redenen vaak variabel en inconsistent. Om de reproduceerbaarheid en consistentie te garanderen, zijn betere, meer gestandaardiseerde en systematische protocollen essentieel voor zowel het preklinische als het klinische onderzoek.

The work of today is the history of tomorrow,
and we are its makers.

— Juliette Gordon Low

Appendices

Abbreviation index

Supplementary data

List of authors with affiliations

PhD portfolio

Funding

Acknowledgements / Dankwoord

9

Abbreviation index

3D	Three dimensional
2D	Two dimensional
AAV	Adeno-associated virus
ABCA1/4	ATP-binding cassette subfamily A member 1/4
ACE	Angiotensin-converting enzyme
ACTB	Actin bèta
ADAM1	A disintegrin and metalloprotease 1
AMD	Age-related macular degeneration
ANOVA	Analysis of variance
AP	Aprotinin
APOE	Apolipoprotein E
ARMS2	Age-related maculopathy susceptibility 2
ARRIVE	Animal Research: Reporting of In Vivo Experiments
ASC	Adult stem cell
ATP	Adenosine tri-phosphate
BCL	Binary base call
BMSC	Bone marrow-derived mesenchymal stem cell
BM	Bruch's membrane
BMI	Body mass index
BPV	Bovine papilloma virus
BRB	Blood-retina-barrier
BSA	Bovine aerum albumin
BSS	Balanced salt solution
c.12delA	Deletion of coding nucleotide 12 adenosine
c.12delC	Deletion of coding nucleotide 12 cytosine
C2/3/9	Complement component 2/3/9
CAG promoter	CMV immediate enhancer / β-actin promoter
Ccr2	C-C chemokine receptor type 2
CD31	Cluster of differentation 31
CD59	MAC inhibitory protein
cDNA	Complementary DNA
CC-HS	Complement competent human serum
CETP	Cholesteryl transfer protein
CFH/Cfh	Complement factor H

CFI	Complement factor I
CI	Confidence interval
CMA	Comprehensive meta-analysis software
CMV	Cytomegalovirus
CNV	Choroidal neovascularization
COL15	Collagen type XV
COL1A1	Collagen type I alpha 1 chain
COL3A1	Collagen type III alpha 1 chain
COL6A1	Collagen type VI alpha 1 chain
COL8A1	Collagen type VIII alpha 1 chain
COL8A2	Collagen type VIII alpha 2 chain
COL9A3	Collagen type IX alpha 3 chain
COL11A1	Collagen type XI alpha 1 chain
CPCB	Parylene C membrane
CRISPR/Cas9	Clustered regularly interspaced short palindromic repeats/ CRISPR associated protein 9
CTGF	Connective tissue growth factor
Cycl	Cyclosporine
DiI	1,1'-dioctadecyl-3,3,3',3'-tetramethylindocarbocyanine perchlorate
DAPI	4',6-Diamidino-2-Phenylindole
DHA	Docosahexaenoic acid
DNA	Deoxyribonucleic acid
DPBS	Dulbecco's phosphate buffered saline
EC	Endothelial cell
ECM	Extracellular matrix
EDTA	Ethylenediaminetetraacetic acid
EF1A	Elongation factor 1-alpha
EFEMP1	EGF-containing fibulin-like extracellular matrix protein 1
EFNB2	EphrinB2
EGF	Epidermal growth factor
ELN	Elastin
EMA	European medicines agency
ENG	Endoglin
ENPP2	Ectonucleotide Pyrophosphatase/Phosphodiesterase 2
EPSA1	Endothelial PAS-domain containing protein 1
ERG	Electroretinography

ETV2	ETS variant transcription factor 2
EQ-5D	European quality of life-5 dimensions questionnaire
Faster R-CNN	Faster recursive convolutional neural networks
FBS	Fetal bovine serum
FDA	Food and drug administration
FGF	Fibroblast growth factor
FM	Fully-mature
GA	Gauge
GCL	Ganglion cell layer
GEM	Gel bead-in-emulsions
GFP	Green fluorescent protein
GJA4	Gap junction alpha-4
GPX4	Glutathion peroxidase 4
gRNA	Guide RNA
H&E	Hematoxylin & eosin
HA	Hyaluronic Acid
HDR	Homology directed repair
Hedges' g	Measure of effect size
hESC	Human embryonic stem cell
hfRPE	Human fetal retinal pigment epithelium
HIF-1α	Hypoxia-inducible factor 1-alpha
HLA	Human leukocyte antigen
HSP90B1	Heat Shock Protein 90 Beta Family Member 1
hTERT	Human Telomerase reverse transcriptase
HTRA1	High-temperature requirement A serine peptidase 1
HuPrim	Human primary
i.v.	Intravenous
i.p.	Intraperitoneally
I^2	Measure of heterogeneity
IBRB	Inner blood-retina-barrier
IG-F-I	Insulin-like growth factor I
INL	Inner nuclear layer
IPL	Inner plexiform layer
iPSC	Induced pluripotent stem cell
IS	Immune-suppressive agents
ITGAV	Integrin alpha V

ITM2b	Integral membrane protein 2B
kb	Kilobases
KDR	Kinase insert domain receptor
KO	Knockout
LAMP2	Lysosome-associated membrane protein 2
LCA	Leber congenital amaurosis
LOX	Lysyl oxidase
LRAT/Lrat	Lecithin retinol acyltransferase
MEM	Minimum essential medium
MERTK	Proto-oncogene tyrosine-protein kinase mer
MiRNA	MicroRNA
MITF	Melanocyte inducing transcription factor
ML228	Hypoxia inducible factor pathway activator
MMP1/9/19	Matrix metallopeptidase 1/9/19
mRNA	messenger RNA
MSC	Mesenchymal stem cell
MSPM	Mesh-supported parylene C membrane
NA	Not applicable
NCT	National clinical trial number
Neo-Poly-Bac	Neomycin-polymyxin-bacitracin
NG2	Neural glial antigen 2
NHEJ	Non-homologous end joining
NOTCH1	Notch homolog 1, translocation-associated
NR	Not reported
OBRB	Outer-blood-retina-barrier
O.C.T.	Optimal cutting temperature
OCT	Optical coherence tomography
ON	Optic nerve
ONL	Outer nuclear layer
OP	Oscillatory potentials
OPL	Outerplexiform layer
ORF	Open reading frame
OS	Outer segments
OTX2	Orthodenticle homeobox 2
p.M5CfsX53	Frameshift from aminoacid 5 onwards (methionine) resulting in a premature stopcodon 53 aminoacids downstream

p.M5CfsX72	Frameshift from aminoacid 5 onwards (methionine) resulting in a premature stopcodon 72 aminoacids downstream
PBS	Phosphate-buffered saline
PCA	Principal component analysis
PCR	Polymerase chain reaction
PDE6A/B	Phosphodiesterase 6A/B
PDGFR-β	Platelet-derived growth factor-bèta
PDGF	Platelet-derived growth factor
PDLGA	Poly(DL-lactic-co-glycolic)
PEDF	Pigment epithelium-derived factor
PFA	Paraformaldehyde
PhD	Doctor of Philosopy
PLGA	Poly lactic-co-glycolic acid
PLTP	Phospholipid transfer protein
PLVAP	Plasmalemma vesicle associated protein
PM	Partially-mature
POS	Photoreceptor outer segments
PR	Photoreceptor
PROSPERO	International prospective register of systematic reviews
pRPE	Primary retinal pigment epithelium
QC	Quality control
QLT091001	9-cis-retinyl acetate
RBP3	Retinoid-binding protein 3
RCF	Relative centrifugal force
RCS	Royal college of surgeons
RD	Retinal degeneration
RDH	Retinol dehydrogenase
Rh / ANG-1	Recombinant human angiopoietin-1
Rho	Rhodopsin
RLBP1	Retinaldehyde-binding protein 1
RNA	Ribonucleic acid
ROS	Reactive oxygen species
RP	Retinitis pigmentosa
RPA	Retinitis punctata albescens
RPE	Retinal pigment epithelium

RPE65/Rpe65	Retinal pigment epithelium-specific protein 65 kilodalton
RPE-MM	RPE maintenance medium
RPGR	Retinitis Pigmentosa GTpase regulator
RPM	Rotations per minute
RT	Room temperature
RT-PCR	Reverse transcriptase-polymerase chain reaction
SCNT	Somatic cell nuclear transfer
SD	Single dimension
STDEV	Standard deviation
SDCBP	Syndecan binding protein
SD-OCT	Spectral domain optical coherence tomography
SE	Standard error
Ser	Serine
SERPINF1	Serpin family F member 1
sgRNA	Single guide RNA
shRNA	Short-hairpin RNA
SI	Sodium iodate
SLO	Scanning laser ophthalmoscopy
SMD	Standard mean dierence
Sod1/2	Superoxide dismutax 1/2
ssODN	Single-stranded oligonucleotide
SV40	Simian virus 40
SYRCLE	Systematic review center for laboratory animal experimentation
TGF	Transforming growth factor
TIMP1/3	Tissue inhibitor of matrix metalloproteinases 1/3
TEM	Transmission electron microscopy
TER	Trans-epithelial resistance
TPM	Transcripts per million
tSNE	T-distributed stochastic neighbor embedding
TYRP1	Tyrosinase-related protein 1
USH2A	Usherin
UTR	Untranslated region
VDM	Vascular development media
VEGF	Vascular endothelial growth factor
VDG	Vascular growth media

VMM	Vasular maintenance media
VN	Voretigene neparvovec
VTN	Vitronectin
VWF	Von Willebrand factor
ZO-1	Zonula occludens protein 1

Supplementary data — Chapter 2

A Systematic Review on Transplantation Studies of the Retinal Pigment Epithelium in Animal Models.

Supplementary 1
Search strategy in PubMed, EMBASE, and Web of Science

PubMed.

	Macula(r) Degeneration/Retina(l) Degeneration
#1	"Retinal Degeneration"[Mesh:NoExp] OR "Macular Degeneration"[Mesh] OR (("Photoreceptor Cells"[Mesh] OR "Retina"[Mesh] OR photoreceptor[tiab] OR photoreceptors[tiab] OR photo-receptor[tiab] OR photo-receptors[tiab] OR macula*[tiab] OR retina*[tiab]) AND (degenera*[tiab] OR atroph*[tiab] OR dystroph*[tiab] OR necrosis[tiab] OR necrotic[tiab]))
	Retina(l) Pigment Epithelium
#2	"Retinal Pigment Epithelium"[Mesh] OR "Pigment Epithelium of Eye"[Mesh:noexp] OR retina progenitor cell*[tiab] OR retinal progenitor cell*[tiab] OR pigment epithel*[tiab] OR pigmented epithel*[tiab] OR RPE[tiab] OR IPE[tiab] OR RPE- J[tiab] OR RPEJ[tiab] OR ARPE-19[tiab] OR ARPE19[tiab]
	Cell or Tissue Transplantation
#3	"Transplants"[Mesh] OR "Cell- and Tissue-Based Therapy"[Mesh] OR "Transplantation"[Mesh] OR "transplantation"[Subheading] OR graft*[tiab] OR xenograft*[tiab] OR autograft*[tiab] OR xeno-graft*[tiab] OR auto-graft*[tiab] OR transplant*[tiab] OR xenotransplant*[tiab] OR autotransplant*[tiab] OR xeno-transplant*[tiab] OR auto-transplant*[tiab] OR retinotomy[tiab] OR autologous translocation[tiab] OR cell therap*[tiab] OR cell based therap*[tiab] OR cell-based therap*[tiab]
	Injections with Relevant Cell Types
#4	"Injections"[Mesh] OR inject*[tiab]) AND ("Stem Cells"[Mesh] OR "Photoreceptor Cells"[Mesh] OR stem cell*[tiab] OR progenitor cell*[tiab] OR neuroprogenitor cell*[tiab] OR epithelial cell*[tiab] OR epithelium cell*[tiab] OR RPE[tiab] OR IPE[tiab] OR RPE-J[tiab] OR RPEJ[tiab] OR ARPE-19[tiab] OR ARPE19[tiab]) OR ((subretinal*[tiab] OR sub-retinal*[tiab] OR intravitreal*[tiab]) AND bleb[tiab])
#5	**SYRCLE Animal Filter**
#6	**#1OR#2**
#7	**#3OR#4**
#8	**#6 AND #7**
#9	**#8 AND #5**
#10	**#9 NOT Review[ptyp]**

EMBASE

	Macula(r) Degeneration/Retina(l) Degeneration
#1	exp retina degeneration/ or ((exp photoreceptor cell/ or exp retina/) and (degenera* or atroph* or dystroph* or necrosis or necrotic).ti,ab,kw.) or ((photoreceptor or photoreceptors or photo-receptor or photo-receptors or macula* or retina*) and (degenera* or atroph* or dystroph* or necrosis or necrotic)).ti,ab,kw.
	Retina(l) Pigment Epithelium
#2	retinal pigment epithelium/ or exp pigment epithelium/ or (retina progenitor cell* or retinal progenitor cell* or pigment epithel* or pigmented epithel* or RPE or IPE or RPE-J or RPEJ or ARPE-19 or ARPE19).ti,ab,kw.
	Cell or Tissue Transplantation
#3	exp transplantation/ or cell therapy/ or (xeno-graft* or auto-graft* or xenograft* or autograft* or transplant* or xenotransplant* or autotransplant* or xeno-transplant* or auto- transplant* or graft* or retinotomy or autologous translocation or cell therap* or cell based therap*). ti,ab,kw.
	Injections with Relevant Cell Types
#4	(exp intraocular drug administration/ or injection/ or inject*.ti,ab,kw.) AND (exp stem cell/ or exp photoreceptor cell/ or (stem cell* or progenitor cell* or neuroprogenitor cell* or epithelial cell* or epithelium cell* or RPE or IPE or RPE-J or RPEJ or ARPE-19 or ARPE19) or ((subretinal* or sub-retinal* or intravitreal*) and bleb).ti,ab,kw.)
#5	**SYRCLE Animal Filter**
#6	**#1OR#2**
#7	**#3OR#4**
#8	**#6 AND #7**
#9	**#8 AND #5**

Web of Science

	Macula(r) degeneration/Retina(l) degeneration or Retina(l) Pigment Epithelium
#1	TS=(((photoreceptor OR photoreceptors OR photo-receptor OR photo-receptors OR macula* OR retina*) AND (degenera* OR atroph* OR dystroph* OR necrosis OR necrotic)) OR "retina progenitor cell*" OR "retinal progenitor cell*" OR pigment epithel* OR pigmented epithel* OR RPE OR IPE OR RPE-J OR RPEJ OR ARPE-19 OR ARPE19)Indexes=SCI-EXPANDED, SSCI, A&HCI, ESCI Timespan=All years
	Cell or Tissue Transplantation or Injections With Relevant Cell Types
#2	TS=(graft* OR xenograft* OR autograft* OR xeno-graft* OR auto-graft* OR transplant* OR xenotransplant* OR autotransplant* OR xeno-transplant* OR auto- transplant* OR retinotomy OR “autologous translocation” OR “cell therap*” OR “cell based therap*” OR cell-based therap* OR (inject* AND ("stem cell*" OR "progenitor cell*" OR "neuroprogenitor cell*" OR epithelial cell* OR epithelium cell* OR RPE OR IPE OR RPE-J OR RPEJ OR ARPE-19 OR ARPE19)) OR ((subretinal* OR sub-retinal* OR intravitreal*) AND bleb))Indexes=SCI-EXPANDED, SSCI, A&HCI, ESCI Timespan=All years

	Adapted Animal Filter
#3	spoonbill OR platalea OR leucorodia OR blackbird OR turdus OR merula OR “blue tit” OR cyanistes OR pigeon OR pigeons OR columba OR pintail OR anas OR starling OR sturnus OR owl OR “athene noctua” OR pochard OR ferina OR cockatiel OR nymphicus OR hollandicus OR skylark OR alauda OR tern OR sterna OR teal OR crecca OR oystercatcher OR haematopus OR ostralegus OR shrew OR shrews OR sorex OR araneus OR crocidura OR russula OR “european mole” OR talpa OR chiroptera OR bat OR bats OR eptesicus OR serotinus OR myotis OR dasycneme OR daubentonii OR pipistrelle OR pipistrellus OR cat OR cats OR felis OR catus OR feline OR dog OR dogs OR canis OR canine OR canines OR otter OR otters OR lutra OR badger OR badgers OR meles OR fitchew OR fitch OR foumart OR foulmart OR ferrets OR ferret OR polecat OR polecats OR mustela OR putorius OR weasel OR weasels OR fox OR foxes OR vulpes OR “common seal” OR phoca OR vitulina OR “grey seal” OR halichoerus OR horse OR horses OR equus OR equine OR equidae OR donkey OR donkeys OR mule OR mules OR pig OR pigs OR swine OR swines OR hog OR hogs OR boar OR boars OR porcine OR piglet OR piglets OR sus OR scrofa OR llama OR llamas OR lama OR glama OR deer OR deers OR cervus OR elaphus OR cow OR cows OR “bos taurus” OR “bos indicus” OR bovine OR bull OR bulls OR cattle OR bison OR bisons OR sheep OR sheeps OR “ovis aries” OR ovine OR lamb OR lambs OR mouflon OR mouflons OR goat OR goats OR capra OR caprine OR chamois OR rupicapra OR leporidae OR lagomorpha OR lagomorph OR rabbit OR rabbits OR oryctolagus OR cuniculus OR laprine OR hares OR lepus OR rodentia OR rodent OR rodents OR murinae OR mouse OR mice OR mus OR musculus OR murine OR woodmouse OR apodemus OR rat OR rats OR rattus OR norvegicus OR “guinea pig” OR “guinea pigs” OR cavia OR porcellus OR hamster OR hamsters OR mesocricetus OR cricetulus OR cricetus OR gerbil OR gerbils OR jird OR jirds OR meriones OR unguiculatus OR jerboa OR jerboas OR jaculus OR chinchilla OR chinchillas OR beaver OR beavers OR castor fiber OR “castor canadensis” OR sciuridae OR squirrel OR squirrels OR sciurus OR chipmunk OR chipmunks OR marmot OR marmots OR marmota OR suslik OR susliks OR spermophilus OR cynomys OR cottonrat OR cottonrats OR sigmodon OR vole OR voles OR microtus OR myodes OR glareolus OR primate OR primates OR prosimian OR prosimians OR lemur OR lemurs OR lemuridae OR loris OR “bush baby” OR “bush babies” OR bushbaby OR bushbabies OR galago OR galagos OR anthropoidea OR anthropoids OR simian OR simians OR monkey OR monkeys OR marmoset OR marmosets OR callithrix OR cebuella OR tamarin OR tamarins OR saguinus OR leontopithecus OR “squirrel monkey” OR “squirrel monkeys” OR saimiri OR “night monkey” OR “night monkeys” OR “owl monkey” OR “owl monkeys” OR douroucoulis OR aotus OR “spider monkey” OR “spider monkeys” OR ateles OR baboon OR baboons OR papio OR “rhesus monkey” OR macaque OR macaca OR mulatta OR cynomolgus OR fascicularis OR “green monkey” OR “green monkeys” OR chlorocebus OR vervet OR vervets OR pygerythrus OR hominoidea OR ape OR apes OR hylobatidae OR gibbon OR gibbons OR siamang OR siamangs OR nomascus OR symphalangus OR hominidae OR orangutan OR orangutans OR pongo OR chimpanzee OR chimpanzees OR “pan troglodytes” OR bonobo OR bonobos OR pan paniscus OR gorilla OR gorillas OR troglodytes)Indexes=SCI-EXPANDED, SSCI, A&HCI, ESCI Timespan=All years
#4	**#1AND#2AND#3**
#5	**#4 Refined by: DOCUMENT TYPES: (ARTICLE)**

Table S1. Study characteristcs part 1. Study information and model characteristics.

Author Year	Journal	Study Type	Control Type	Species	Strain/ Breed	Sex	Age	Weight	Genetic or Induced Model	Genotype	Induction Method
Abe1999 [1]	Tohoku J Exp Med	External	Sham	Rat	RCS	NR	NR	250-300 g	Genetic	MERTK-/-	NA
Abe2005 [2]	Cell Transplant	External	Sham	Rat	Sprague Dawley	NR	3 months	NR	NA	WT	NA
Abe2008 [3]	IOVS	External	Sham	Rat	Sprague Dawley	male	NR	NR	Induced	WT	Light
Bhatt1994 [4]	Am J Ophthalmol	External	Sham	Rabbit	New Zealand White	NR	NR	2-3 kg	NA	WT	NA
Carido2014 [5]	IOVS	Internal	Sham	Mouse	C57BL/6	NR	10-11 weeks	NR	Induced	WT	NaIO3; i.v.; 70 mg/kg,
Carr2009 [6]	PLoS One	External	Sham	Rat	RCS	NR	22-23 days	NR	Genetic	MERTK-/-	NA
Castillo1997 [7]	Exp Neurol	External	Sham	Rat	RCS	NR	21 days; 25 days	NR	Genetic	MERTK-/-	NA
Cho2019 [8]	Regulatory Toxicology and Pharmacology	External	Sham	Pig	Laboratory minipig	NR	16 months	30 kg	NA	WT	NA
Coffey2002 [9]	Nat Neurosci	External	Sham	Rat	RCS	NR	NR	NR	Genetic	MERTK-/-	NA
Cong2008 [10]	IOVS	Internal	Sham	Rabbit	Pigmented	NR	NR	NR	NA	WT	NA
Crafoord1999 [11]	Acta Ophthalmol Scand	Internal	Untreated	Rabbit	New Zealand White	male	NR	2.0-2.5 kg	NA	WT	NA
Crafoord2000 [12]	Acta Ophthalmol Scand	Internal	Not clear	Rabbit	New Zealand White	NR	NR	2.0-2.9 kg	NA	WT	NA
Davis2016 [13]	J Ocul Pharmacol Ther	External	Sham	Rat	RCS	NR	30 days	NR	Genetic	MERTK-/-	NA
Davis2017 [14]	Stem Cell Reports	External	Sham	Rat	RCS	NR	29-32 days	NR	Genetic	MERTK-/-	NA
Del Priore2003 [15]	Curr Eye Res	Internal	Untreated	Rabbit	Albino	NR	NR	2-4 kg	NA	WT	NA
Del Priore2003 [16]	IOVS	Internal	Untreated	Rabbit	Albino	NR	NR	2-4 kg	NA	WT	NA
Diniz2013 [17]	IOVS	Internal	Untreated	Rat	Nude	both	28-40 days	NR	Genetic	RNU	NA

Duan2017 [18]	Int J Clin Exp Pathol	External	Sham	Rat	Long-Evans	NR	35-40 days	NR	Induced	WT	NaIO3; i.v.; 50 mg/kg
Dunaief1995 [19]	Hum Gene Ther	Internal	Untreated	Rat	RCS	NR	15-25 days	NR	Genetic	MERTK-/-	NA
Durlu1997 [20]	Cell Transplant	External	Sham	Rabbit; Rat	Albino; RCS	both ; NR	NR; 23 days	2.0-2.5 kg; NR	NA; Genetic	WT; MERTK-/-	NA
el Dirini1992 [21]	Graefes Arch Clin Exp Ophthalmol	Internal	Untreated	Rabbit	Albino	both	NR	2-3 kg	NA	WT	NA
Engelhardt2012 [22]	Vis Neurosci	Baseline	Baseline	Mouse	BALB/c	NR	32; 65 days	NR	NR	WT	NA
Enzmann2000 [23]	Curr Eye Res	External	Sham	Rabbit	New Zealand White	NR	NR	NR	NA	WT	NA
Gabrielian1999 [24]	Graefes Arch Clin Exp Ophthalmol	External	Sham	Rabbit	Pigmented	NR	NR	NR	NA	WT	NA
Garcia Delgado2019 [25]	Tissue Engineering - Part A	Internal	Untreated	Mouse; Pig	NR	NR	NR	NR	NR	NR	NR
Gaur1992 [26]	Exp Eye Res	External	Sham	Rat	RCS	NR	17 days	NR	Genetic	MERTK-/-	NA
Gias2007 [27]	Eur J Neurosci	External	Untreated	Rat	RCS	NR	21-23 days	NR	Genetic	MERTK-/-	NA
Girman2003 [28]	Vision Res	External	Sham	Rat	RCS	NR	3-4 weeks	NR	Genetic	MERTK-/-	NA
Girman2005 [29]	Vision Res	External	Untreated	Rat	RCS	NR	3-4 weeks	NR	Genetic	MERTK-/-	NA
Gouras1992 [30]	Graefes Arch Clin Exp Ophthalmol	Not clear	Not clear	Rabbit	Albino	NR	adult	NR	NA	WT	NA
Gouras2002 [31]	IOVS	External	Sham	Mouse	C57BL/6	NR	neonatal	NR	Genetic	RPE65 -/-	NA
Grisanti1997 [32]	IOVS	Not clear	Untreated	Mouse	C57BL/6	male	7-10 weeks	NR	NA	WT	NA
Grisanti2002 [33]	Jpn J Ophthalmol	External	Sham	Rat	RCS	NR	17-19 days	NR	Genetic	MERTK-/-	NA
Hao2011 [34]	Int J Ophthalmol	External	Sham	Rat	Sprague Dawley	male	NR	250g	Induced	WT	Chemical; STZ
Haruta2004 [35]	IOVS	External	Sham	Rat	RCS	NR	4 weeks	NR	Genetic	MERTK-/-	NA
Idelson2018 [36]	Stem Cell Reports	Not clear	Not clear	Rat	RCS	NR	3 weeks	NR	Genetic	MERTK-/-	NA

Ilmarinen2015 [37]	PLoS One	External	Sham	Rat; Rabbit	RCS; New Zealand White	NR	22-29 days; NR	NR; 3.1-3.9 kg	Genetic; NA	MERTK-/-; WT	NA
Ilmarinen2019 [38]	Acta Ophthalmol	External	Sham	Rabbit	Chinchilla Bastard; Dutch-Belted	both	2-5 months	2-2,5 kg	NA	WT	NA
Jiang1994 [39]	IOVS	External	Sham	Rat	RCS	NR	20 days	NR	Genetic	MERTK-/-	NA
Kamao2014 [40]	Stem Cell Reports	Internal	Sham	Rat; Macaca fascilaris	RCS; Macaca fascilaris	NR	3 weeks; NR	NR	Genetic; NR	MERTK-/-; NR	NA; NR
Kanemura2014 [41]	PLoS One	Internal	Other cell type	Rat	RNU	female	3 weeks	NR	Genetic	NA	NA
Kennelly2017 [42]	Cell Transplant	External	Sham	Mouse	C57BL/6	male	NR	NR	NA	WT	NA
Klassen2001 [43]	Exp Neurol	External	Untreated	Rat	RCS; Long Evans	NR	4 weeks; adult	NR	Genetic; NA	MERTK-/-; WT	NA
Kohen1997 [44]	Ophthalmic Res	Internal	Untreated	Rabbit	New Zealand White	NR	NR	NR	NA	WT	NA
Kole2018 [45]	Molecular Therapy	Internal	Untreated	Rat	RCS	both	18 days	NR	Genetic	MERTK-/-	NA
Koss2016 [46]	Graefes Arch Clin Exp Ophthalmol	External	Sham	Pig	Yucatán mini	female	8 weeks	24-35 kg	NA	NA	NA
Lai1999 [47]	IOVS	External	Sham	Rabbit	Pigmented	NR	adult	NR	NA	WT	NA
Lai2000 [48]	IOVS	Internal	Sham	Rabbit	NR	NR	NR	NR	NR	NR	NR
Lane1989 [49]	Eye (Lond)	Internal	Not clear	Pig	Mini	NR	NR	NR	NA	NA	NA
Lavail1992 [50]	Exp Eye Res	External	Sham	Rat	RCS	both	16-19 days	NR	Genetic	MERTK-/-	NA
Li1988 [51]	Exp Eye Res	External	Untreated	Rat	RCS	NR	26 days	NR	Genetic	MERTK-/-	NA
Li1991 [52]	Curr Eye Res	External	Sham	Rat	RCS	NR	26 days	NR	Genetic	MERTK-/-	NA
Li1991 [53]	Exp Eye Res	External	Sham	Rat	RCS	NR	10-48 days	NR	Genetic	MERTK-/-	NA
Li1993 [54]	IOVS	External	Sham	Mouse	B6 (Albino)	NR	33 days	NR	Genetic	rds/rds	NA
Li2012 [55]	Mol Med	External	Sham	Mouse	B6 (Albino)	NR	2 days	NR	Genetic	Rpe65rd12; Prkdcscid	NA

Li2015 [56]	Exp Eye Res	External	Sham	Rat	Long-Evans	both	adult	200 g	Induced	WT	Laser
Lin1996 [57]	Curr Eye Res	External	Sham	Rat	RCS	NR	22-23 days	NR	Genetic	MERTK-/-	NA
Little1996 [58]	IOVS	External	Sham	Rat	RCS	male	24 days	NR	Genetic	MERTK-/-	NA
Little1998 [59]	Exp Neurol	External	Sham	Rat	RCS	male	29 days	NR	Genetic	MERTK-/-	NA
Liu2014 [60]	Biomaterials	Internal	Untreated	Rabbit	Chinchilla Bastard; New Zealand White	female	NR	1.5-2kg	NA	WT	NA
Lopez1987 [61]	IOVS	Not clear	Not clear	Rabbit	Pigmented	NR	adult	NR	NA	WT	NA
Lopez1989 [62]	IOVS	Internal	Untreated	Rat	RCS	NR	15-25 days	NR	Genetic	MERTK-/-	NA
Lu2009 [63]	Stem Cells	External	Sham	Rat; Mouse	RCS; C57BL/6	NR	21 days; 28 days	NR	Genetic	MERTK-/-; ELOVL4-/-	NA
Lund2001 [64]	Proc Natl Acad Sci U S A	External	Sham	Rat	RCS	NR	3-4 weeks	NR	Genetic	MERTK-/-	NA
Lund2006 [65]	Cloning Stem Cells	External	Sham	Rat	RCS	NR	21-23 days	NR	Genetic	MERTK-/-	NA
Maeda2013 [66]	J Biol Chem	External	Sham	Mouse	C57BL/6	NR	NR	NR	Genetic	LRAT-/-; RPE65-/-; Tyrc-2J/J	NA
Majji2000 [67]	Graefes Arch Clin Exp Ophthalmol	Internal	Untreated	Rabbit	Pigmented	NR	NR	2-3 kg	Induced	WT	Mechanical
M'Barek2017 [68]	Science Translational Medicine	External	Sham	Rat	RCS; RNU	NR	p28; adult	NR	Genetic	MERTK-/-	NA
McGill2004 [69]	Vision Res	External	Sham	Rat	RCS	NR	NR	NR	Genetic	MERTK-/-	NA
McGill2017 [70]	Transl Vis Sci Technol	External	Sham	Rat	RCS	NR	21-25 days	NR	Genetic	MERTK-/-	NA
Oganesian1999 [71]	Arch Ophthalmol	Internal	Sham	Rabbit	Albino; Pigmented	NR	NR	NR	NA	WT	NA
Osusky1995 [72]	Graefes Arch Clin Exp Ophthalmol	External	Sham	Rabbit	New Zealand White	NR	NR	NR	NA	WT	NA
Park2011 [73]	Clin Exp Reprod Med	Not clear	Not clear	Rat	Sprague Dawley	NR	6 weeks	NR	Induced	WT	NaIO3; i.v.; 50 mg/kg

Peng2016 [74]	Oncotarget	Internal	Untreated	Pig	NR	NR	10-12 weeks	25-30 kg	NA	NA	NA
Petrus-Reurer2017 [75]	IOVS	External	Sham	Rabbit	New Zealand White	NR	5 months	3.5-4 kg	Induced	WT	NaIO3
Phillips2003 [76]	Curr Eye Res	Internal	Untreated	Rabbit	Dutch Belted	NR	NR	1.5-2kg	Induced	WT	Mechanical
Pinilla2007 [77]	Exp Eye Res	External	Sham	Rat	RCS	NR	21 days; 30 days	NR	Genetic	MERTK-/-	NA
Plaza Reyes2016 [78]	Stem Cell Reports	Not clear	Not clear	Rabbit	New Zealand White	NR	5 months	3.5-4 kg	NA	WT	NA
Ribeiro2013 [79]	Ophthalmic Surgery Lasers & Imaging Retina	External	Sham	Rat	RCS	NR	27-29 days	NR	Genetic	MERTK-/-	NA
Saigo2004 [80]	IOVS	External	Sham	Rat	Sprague Dawley	NR	3 months	250g	NA	WT	NA
Sauve2002 [81]	Neuroscience	External	Sham	Rat	RCS	NR	1 month	NR	NR	MERTK-/-	NA
Sauve2004 [82]	Vision Res	External	Sham	Rat	RCS	NR	NR	NR	Genetic	MERTK-/-	NA
Sauve2006 [83]	Vision Res	External	Sham	Rat	RCS	NR	21-23 days	NR	Genetic	MERTK-/-	NA
Schmack2009 [84]	Mol Vis	External	Sham	Mouse	C57BL/6	fem ale	2 months; 12 months	18-20g; 25-30g	Genetic	dCcl-2	NA
Schraermeyer2000 [85]	Graefes Arch Clin Exp Ophthalmol	External	Untreated	Rat	RCS	NR	14-18 days	NR	Genetic	MERTK-/-	NA
Seaton1992 [86]	IOVS	External	Sham	Rat	RCS	NR	26 days	NR	Genetic	MERTK-/-	NA
Seaton1994 [87]	IOVS	External	Sham	Rat	RCS	NR	3 months	NR	Genetic	MERTK-/-	NA
Sharma2019 [88]	Science Translational Medicine	External	Sham	Rat; Pig	RCS; RNU	NR	21-28 days	NR	Genetic; Induced	MERTK-/-	Laser
Sheedlo1989 [89]	Exp Eye Res	External	Untreated	Rat	RCS	NR	26 days	NR	Genetic	MERTK-/-	NA
Sheedlo1989 [90]	Prog Clin Biol Res	External	Sham	Rat	RCS	NR	26 days	NR	Genetic	MERTK-/-	NA

Sheedlo1991 [91]	J Neural Transplant Plast	External	Sham	Rat	RCS	NR	10 days; 17 days; 26 days; 39 days; 43 days; 61 days; 68 days	NR	Genetic	MERTK-/-	NA
Sheedlo1993 [92]	Exp Eye Res	External	Sham	Rat	RCS	NR	22-26 days	NR	Genetic	MERTK-/-	NA
Sheedlo1993 [93]	J Neurosci Res	External	Sham	Rat	RCS	NR	26 days	NR	Genetic	MERTK-/-	NA
Sheng1995 [94]	IOVS	External	Untreated	Macaca Mulatta; Rabbit	Macaca mullata; NR	NR	NR; adult	NR; 1-2 kg	NR	NR	NA
Shiragami1998 [95]	Br J Ophthalmol	Not clear	Not clear	Rabbit	Albino	NR	5-10 months	2-3 kg	NA	WT	NA
Sohn2015 [96]	Sci Rep	Internal	Sham	Pig	Yucatán mini	NR	12-14 weeks	NR	NA	NA	NA
Stanzel2014 [97]	Stem Cell Reports	External	Sham	Rabbit	Chinchilla Bastard	female	NR	2-2.5 kg	NA	WT	NA
Sun2015 [98]	Stem Cells	Internal	Sham	Mouse	C3H/HeJ	NR	14 days	NR	Genetic	rd1, Pde66rd1-/-	NA
Suzuki2017 [99]	Biomater Sci	Internal	Untreated	Rat	Sprague-Dawley	male	NR	250-300 g	NR	WT	NA
Thomas2016 [100]	IOVS	External	Untreated	Rat	RCS	NR	27-29 days	NR	Genetic	MERTK-/-	NA
Thomas2018 [101]	Graefes Arch Clin Exp Ophthalmol	External	Sham	Rat	RCSxRNU	NR	28-30 days	NR	Genetic	MERTK-/- and Fox1n-/-	NA
Thumann2009 [102]	Biomaterials	External	Not clear	Rabbit	NR	NR	NR	NR	NR	NR	NR
Thumann2009 [103]	Graefes Arch Clin Exp Ophthalmol	External	Sham	Rat	RCS	NR	23 days	NR	Genetic	MERTK-/-	NA
Verdugo2001 [104]	Cell Transplant	External	Sham	Dog	Beagles/crossbred	NR	adult	NR	NA	NR	NA
Vugler2008 [105]	Exp Neurol	Internal	Untreated	Rat	RCS	NR	23 days	NR	Genetic	MERTK-/-	NA
Wang2004 [106]	Exp Eye Res	Internal	Sham	Cat	Domestic, shot-haired	female	NR	2-5 kg	NA	NR	NA

Wang2005 [107]	IOVS	External	Sham	Rat	RCS	NR	NR	NR	Genetic	MERTK-/-	NA
Wang2005 [108]	J Comp Neurol	External	Sham	Rat	RCS	NR	23 days	NR	Genetic	MERTK-/-	NA
Wang2008 [109]	IOVS	External	Sham	Rat	RCS	NR	21 days; 60 days	NR	Genetic	MERTK-/-	NA
Wang2010 [110]	Transplantation	External	Sham	Mouse	B6	NR	5 days	NR	Genetic	rd12	NA
Wang2016 [111]	Philos Trans A Math Phys Eng Sci	External	Untreated	Rat	RCS; Sprague Dawley	NR	3 weeks	NR	Genetic	MERTK-/-	NA
Warncke2004 [112]	Virchows Arch	Not clear	Not clear	Rat	RCS	NR	NR	NR	Genetic	MERTK-/-	NA
Wen2005 [113]	Mol Vis	Internal	Untreated	Mouse	C57BL/6; Balb/c	NR	adult	NR	NA	WT	NA
Westenskow 2016 [114]	Stem Cells Int	External	Untreated	Rat	RCS	NR	3 weeks	NR	Genetic	MERTK-/-	NA
Wong2002 [115]	Can J Ophthalmol	Internal	Untreated	Rabbit	New Zealand White	NR	NR	2.5-3.5 kg	NA	WT	NA
Wongpichedchai1992 [116]	IOVS	Internal	Untreated	Rabbit	Pigmented	NR	NR	2.5-3 kg	NA	WT	NA
Wu2016 [117]	Oncotarget	External	Sham	Rat	RCS	both	21 days	NR	Genetic	MERTK-/-	NA
Wu2018 [118]	Docu Ophthalmol	External	Sham	Rat	RCS	NR	7 weeks	NR	Genetic	MERTK-/-	NA
Yaji2009 [119]	Biomaterials	Not clear	Not clear	Rabbit	Japanese White	male	NR	2 kg	NA	WT	NA
Yamaguchi1992 [120]	Jpn J Ophthalmol	Not clear	Not clear	Rabbit	New Zealand White	NR	NR	NR	NA	WT	NA
Yamaguchi1993 [121]	Jpn J Ophthalmol	External	Sham	Rat	Fischer 344	male	3 months	NR	NA	WT	NA
Yamamoto1993 [122]	IOVS	External	Sham	Rat	RCS	NR	16-20 days	NR	Genetic	MERTK-/-	NA
Ye1993 [123]	Curr Eye Res	Internal	Untreated	Rabbit	New Zealand White	both	NR	1.8-2.3 kg	NA	WT	NA
Zhang1998 [124]	IOVS	External	Sham	Rat	RCS	NR	19-21 days	NR	Genetic	MERTK-/-	NA

Table S2. Study characteristcs part 2. Intervention information and outcome measures.

AuthorYear	Donor Species	Cell Type	Number of Transplanted Cells/Surface	Suspension or Sheet	Medium	Injection Volume (µL)	Scaffold Type	Immuunsuppressors Used?	ERG	SLO	OCT	Behavioural	Transplant Survival
Abe1999 [1]	Human	3DRPE; SDRPE	1.00E+05	suspension	PBS	1-2	NA	Y	Y	N	N	N	Y
Abe2005 [2]	Human	ARPE-19	NR	suspension	Medium	NR	NA	Y	Y	N	N	N	Y
Abe2008 [3]	Human	ARPE-19; h1RPE7	1.00E+05	suspension	NR	2	NA	Y	N	N	N	N	Y
Bhatt1994 [4]	Human	ARPE-19; h1RPE7	2.00E+05	suspension	Ham F10	2	NA	Y	N	N	N	Y	Y
Carido2014 [5]	Human	ARPE-19; hSCs; fibroblast	2.00E+05	suspension	DMEM:F12 (1:1)	2	NA	Y	N	N	N	N	Y
Carr2009 [6]	Human; Rat	ARPE-19; Schwann	2.00E+04	suspension	NR	2	NA	Y; N	N	N	N	N	Y
Castillo1997 [7]	Human	ARPE-19; Schwann cells; fibroblasts	2E+05; 2E+04	suspension	DMEM:F12 (1:1); DMEM	2	NA	Y	N	N	N	Y	Y
Cho2019 [8]	Human	ARPE-19	2.00E+05	suspension	DMEM:F12 (1:1)	3	NA	Y	N	N	N	Y	Y
Coffey2002 [9]	Human	ARPE-19	NR	suspension	Medium. serum-	2	NA	Y	N	N	N	N	Y
Cong2008 [10]	Human	ARPE-19	2.00E+05	suspension	Ham F10	2	NA	Y	Y	N	N	N	N
Crafoord1999 [11]	Human	ARPE-19	2.00E+05	suspension	DMEM:F12 (1:1)	2	NA	Y	N	N	N	N	Y
Crafoord2000 [12]	Human	ARPE-19	NR	suspension	Ham F10	2	NA	Y	N	N	N	Y	Y
Davis2016 [13]	Human	ARPE-19	2.00E+05	suspension	Ham F10	2	NA	Y	Y	N	N	N	N
Davis2017 [14]	Human	ARPE-19	2 x 2 mm	sheet	NA	NA	equine collagen type I	N	N	N	N	N	Y
Del Priore2003 [15]	Human	dRPE	NR	sheet	NR	NA	PDMS; PDMS-Laminin	Y	Y	N	Y	N	N
Del Priore2003 [16]	Human	h1RPE7	2.00E+05	suspension	Ham F10	2	NA	Y	N	N	N	N	Y

Diniz2013 [17]	Human	hBMSC; BMSC-RPE; hESC-RPE	5.00E+04	suspension	PBS	2	NA	Y	y	N	N	N	Y
Duan2017 [18]	Human	HeLa; iPSC; iPSC-RPE	10; 1 x 1 mm (0.8E+04-1.5E+04)	suspension; sheet	DMEM:F12 (1:1)	2	NA; none	NR	N	N	N	N	Y
Dunaief1995 [19]	Human	hESC-RPE	1E+05 - 2E+05	suspension	PBS	1-2	NA	NR	Y	N	Y	N	Y
Durlu1997 [20]	Human	hESC-RPE	6E+05; 1.2E+06	suspension	BSS	150	NA	Y	N	Y	Y	N	Y
el Dirini1992 [21]	Human	hESC-RPE	NR	suspension	BSS	1.5	NA	Y	N	N	N	Y	Y
Engelhardt2012 [22]	Monkey	hESC-RPE	3.00E+04	suspension	PBS	3	NA	Y	N	N	N	Y	Y
Enzmann2000 [23]	Human	hESC-RPE	0.6-1E+05	suspension	NR	2-3	NA	Y	Y	Y	N	N	Y
Gabrielian1999 [24]	Human	hESC-RPE	NR	sheet	NA	NA	PET	Y	N	Y	Y	N	Y
Garcia Delgado2019 [25]	Human	hESC-RPE	1.00E+05	sheet	X-VIVO	NR	CPCB-RPE1	Y	N	N	Y	N	Y
Gaur1992 [26]	Human	hESC-RPE	5E+04; 20E+04	sheet; suspension	NA; CO_2 independent medium	NA; 4	Gelatin; NA	Y	Y	N	Y	Y	Y
Gias2007 [27]	Human	hESC-RPE	NR	sheet	NA	NA	Parylene	Y	N	Y	Y	N	Y
Girman2003 [28]	Human; Rat	IPE; ARPE-19	8E+04-1E+05	suspension	NR	1	NA	Y	N	N	N	N	Y
Girman2005 [29]	Human	iPSC-RPE	1 mm2; 1 cm2	sheet	NA	NA	Fibrin Agarose	Y	Y	Y	N	N	Y
Gouras1992 [30]	Human	iPSC-RPE	1E+04; 1E+05	sheet; suspension	BSS	2	PLGA	Y	Y	Y	Y	Y	Y
Gouras2002 [31]	Pig	iPSC-RPE	2.50E+05	suspension	NR	NR	NA	Y	N	N	N	N	Y
Grisanti1997 [32]	Human	iPSC-RPE; fetal NSCs; MSCs	1.00E+05	suspension	GMEM	1	NA	Y	N	N	N	N	Y
Grisanti2002 [33]	Human	iPSC-RPE; hESC-RPE	1.00E+05	suspension	DMEM:F12 (1:1)	2	NA	NR	Y	N	Y	N	Y
Hao2011 [34]	Mouse	mESC-RPE	1.00E+03	suspension	NR	1	NA	NR	Y	N	N	N	Y
Haruta2004 [35]	Rat	rESC-RPE; rESC-PR	1.00E+05	suspension	PBS	1	NA	NR	Y	N	N	N	Y
Idelson2018 [36]	Rat	RPE	4.00E+04	suspension	HBSS	2	NA	N	N	N	N	N	Y
Ilmarinen2015 [37]	Rat	RPE	4.00E+04	suspension	HBSS	2	NA	N	Y	N	N	N	Y

Ilmarinen2019 [38]	Human	RPE	NR	sheet	10% glucose	NR	collagen	N	Y	N	N	N	Y
Jiang1994 [39]	Human	RPE	1.00E+05	suspension	a-MEM	2	NA	Y	N	N	N	Y	Y
Kamao2014 [40]	Human	RPE	NR	suspension	DMEM low glucose	2	NA	Y	N	N	N	N	Y
Kanemura2014 [41]	Rabbit	RPE	1.00E+05	suspension	BSS	25	NA	NR	N	Y	Y	N	Y
Kennelly2017 [42]	Rabbit	RPE	2E+04-3E+04	aggregates	EBSS	20	NA	NR	N	Y	N	N	Y
Klassen2001 [43]	Rabbit	RPE	2.00E+04	suspension	EBSS	20	NA	Y; N	N	Y	N	N	Y
Kohen1997 [44]	Human	RPE	5.00E+04	suspension	BSS	1	NA	Y	N	N	N	N	Y
Kole2018 [45]	Pig	RPE	4.00E+04	aggregates	DMEM	10	NA	Y	N	Y	N	N	Y
Koss2016 [46]	Pig	RPE	4.00E+04	aggregates	DMEM	10	NA	Y; N	N	Y	N	N	Y
Lai1999 [47]	Human	RPE	1E+05; 1 x 0.4 mm (2.7E+03)	suspension; sheet	DMEM:F12 (1:1); NA	2; NA	NA; Parylene-vitronectin	NR	N	Y	N	N	Y
Lai2000 [48]	Rat	RPE	5.00E+04	suspension	MEM	10-20	NA	NR	N	N	N	N	Y
Lane1989 [49]	Bovine	RPE	2E+04; 2.5E+04	suspension	HBSS	15; 1	NA	NR	N	N	N	N	Y
Lavail1992 [50]	Rabbit	RPE	5.00E+03	suspension	PBS	20	NA	N	N	N	N	N	Y
Li1988 [51]	NR	RPE	3.00E+04	suspension	PBS	1	NA	Y	Y	Y	Y	N	Y
Li1991 [52]	Rabbit	RPE	6E+04-8E+04	suspension	PBS	30	NA	NR	N	N	N	N	N
Li1991 [53]	Human	RPE	1.8E+04; 3.75E+03; 7.5E+04	suspension	HBSS	15	NA	NR	N	N	N	N	Y
Li1993 [54]	Rat	RPE	6.00E+04	suspension	CMF-HBSS	1	NA	NR	N	N	N	N	Y
Li2012 [55]	Rabbit	RPE	1.00E+05	suspension	MEM	5-10	NA	Y	N	N	N	N	Y
Li2015 [56]	Mouse	RPE	5E+03-7.5E+03	suspension	HBSS	10	NA	NR	Y	N	N	N	Y
Lin1996 [57]	Mouse	RPE	3.00E+05	suspension	HBSS	3	NA	NR	N	N	N	N	Y
Little1996 [58]	Pig	RPE	5.00E+04	suspension	HBSS	1.5	NA	NR	N	N	N	N	Y
Little1998 [59]	Mouse	RPE	4.00E+04	aggregates	DMEM	20	NA	Y	N	N	N	N	Y
Liu2014 [60]	Human	RPE	1E+05; 1 x 4 mm	suspension; sheet	RPEbasic medium; NA	2; NA	NA; Polyimide	Y	Y	N	N; Y	N	Y
Lopez1987 [61]	Rat	RPE	NR	sheet	HBSS	0.5	none	NR	Y	N	N	N	Y

Lopez1989 [62]	Human; Monkey	RPE	1 x 1 mm (1E+05); 1 x 2 mm (5E+04)	suspension; sheet	DMEM:F12 (1:1)	2; 100	none	Y; NR	Y; N	Y	N; Y	N	Y
Lu2009 [63]	Mouse	RPE	1.00E+05	suspension	DMEM	2	NA	N	N	N	N	N	Y
Lund2001 [64]	Rat	RPE	NR	suspension	NR	2	NA	NR	N	N	N	Y	Y
Lund2006 [65]	Rabbit	RPE	6E+04-8E+04	suspension	NR	30	NA	NR	N	N	N	N	Y
Maeda2013 [66]	Pig	RPE	5.00E+04	suspension	HBSS	2	NA	Y	Y	Y	Y	Y	Y
Majji2000 [67]	Human	RPE	1.00E+05	suspension	BSS	10	NA	NR	N	Y	N	N	Y
M'Barek2017 [68]	Human	RPE	5.00E+04	suspension	NR	50	NA	Y; N	N	Y	N	N	Y
McGill2004 [69]	Pig	RPE	4.00E+03	suspension	NR	100	NA	N	N	N	N	N	Y
McGill2017 [70]	Rat	RPE	6.00E+04	suspension	CMF-HBSS	1	NA	NR	N	N	N	N	Y
Oganesian1999 [71]	Rat	RPE	4E+04-6E+04	suspension	NR	1	NA	NR	N	N	N	N	Y
Osusky1995 [72]	Rat	RPE	6.00E+04	suspension	CMF-HBSS	1	NA	NR	N	N	N	N	Y
Park2011 [73]	Rat	RPE	3E+04; 6E+04; 1.2E+05	suspension	CMF-HBSS	1; 2; 4	NA	NR	N	N	N	N	Y
Peng2016 [74]	Mouse	RPE	6.00E+04	suspension	HBSS	1	NA	NR	N	N	N	N	Y
Petrus-Reurer2017 [75]	Rat	RPE	5.00E+05	suspension	DMEM:F12 (1:1)	5	NA	Y	N	Y	N	N	Y
Phillips2003 [76]	Rat	RPE	8E+04-1E+05	suspension	CMF-HBSS	1	NA	Y	N	N	N	N	Y
Pinilla2007 [77]	Human	RPE	NR	fragments	DMEM	3	none	Y	N	Y	N	N	Y
Plaza Reyes2016 [78]	Human	RPE	NR	sheet	DMEM	3-5	NA	Y	N	N	N	Y	Y
Ribeiro2013 [79]	Human	RPE	2 x 1.1 mm	sheet	NA	NA	NF-PET-p; NF-PLCL-P	NR	N	N	Y	N	Y
Saigo2004 [80]	Rabbit	RPE	2.00E+05	suspension	MEM	50-100	NA	NR	N	N	N	N	Y
Sauve2002 [81]	Rat	RPE	NR	suspension	MEM	NR	NA	NR	N	N	N	N	Y
Sauve2004 [82]	Human	RPE	5E+03. 2E+04. 5E+04. 7.5E+04. 1E+05	suspension	BSS	2	NA	Y	N	N	N	Y	Y
Sauve2006 [83]	Human	RPE	2.00E+04	suspension	Medium	NR	NA	Y	Y	N	N	Y	Y
Schmack2009 [84]	Rabbit	RPE	NR	suspension	NR	NR	NA	NR	N	N	N	N	Y

Schraermeyer2000 [85]	Human	RPE	NR	aggregates	NR	NR	NA	NR	N	Y	N	N	Y
Seaton1992 [86]	Rabbit	RPE	4.00E+04	suspension	NR	20	NA	NR	N	N	N	N	Y
Seaton1994 [87]	Human	RPE	1.00E+05	suspension	NR	5	NA	Y	N	N	N	N	Y
Sharma2019 [88]	Human	RPE	5.00E+04	suspension	PBS	50	NA	Y	N	Y	Y	N	Y
Sheedlo1989 [89]	Rabbit	RPE	NR	suspension	BSS	NR	NA	NR	N	Y	N	N	Y
Sheedlo1989 [90]	Rat	RPE	4.00E+04	suspension	HBSS	2	NA	NR	N	N	N	N	Y
Sheedlo1991 [91]	Mouse	RPE	1.00E+05	suspension	HBSS	2	NA	NR	N	Y	N	N	Y
Sheedlo1993 [92]	Rat	RPE	6.00E+04	suspension	BSS	1	NA	NR	N	N	N	N	Y
Sheedlo1993 [93]	Rat	RPE	4E+04-6E+04	suspension	CMF-HBSS	1	NA	NR	N	N	N	N	Y
Sheng1995 [94]	Rat	RPE	6.00E+04	suspension	CMF-HBSS	1	NA	NR	N	N	N	N	Y
Shiragami1998 [95]	Rat	RPE	4E+04-6E+04	suspension	NR	1	NA	NR	N	N	N	N	Y
Sohn2015 [96]	Rat	RPE	4E+04-6E+04	suspension	CMF-HBSS	1	NA	NR	N	N	N	N	Y
Stanzel2014 [97]	Rat	RPE	6.00E+04	suspension	HBSS	1	NA	NR	N	N	N	N	Y
Sun2015 [98]	Rat	RPE	6.00E+04	suspension	CMF-HBSS	1	NA	NR	N	N	N	N	Y
Suzuki2017 [99]	Rat	RPE	6.00E+04	suspension	CMF-HBSS	1	NA	NR	N	N	N	N	Y
Thomas2016 [100]	Human	RPE	disc: 2-4 mm diameter	sheet	BSS	NA	none	NR	N	Y	N	N	Y
Thomas2018 [101]	Rabbit	RPE	5E+04-1E+05	suspension	PBS	100	NA	NR	N	N	N	N	Y
Thumann2009 [102]	Human	RPE	2.2 x1.1 mm (6E+0+03-8E+0+03)	sheet	Gelatin	NA	PET	Y; N	N	Y	Y	N	Y
Thumann2009 [103]	Human	RPE	NR	sheet	NA	NA	Parylene-vitronectin	Y	N	N	N	Y	Y
Verdugo2001 [104]	Dog	RPE	1E+05-4.6E+06	suspension	DMEM	10-200	NA	Y	N	Y	N	N	Y
Vugler2008 [105]	Human	RPE	1.00E+05	suspension	NR	2	NA	Y	N	N	N	N	Y
Wang2004 [106]	Cat	RPE	2 x 3 mm	sheet	NA	NA	Gelatin (32.5%)	Y	N	Y	N	N	Y
Wang2005 [107]	Human	RPE	NR	suspension	NR	NR	NA	NR	N	N	N	N	N
Wang2005 [108]	Human	RPE	NR	suspension	NR	10	NA	NR	N	N	N	N	Y
Wang2008 [109]	Mouse	RPE	1.00E+05	suspension	HBSS	2	NA	NR	N	N	N	N	Y

Wang2010 [110]	Human	RPE	NR	suspension	PBS	0.5	NA	Y	N	N	N	N	Y
Wang2016 [111]	Human	RPE	1.00E+06	suspension	BSS	200	NA	NR	N	Y	N	N	Y
Warncke2004 [112]	Rabbit	RPE	6E+04-1.4E+05	suspension	PBS	30-40	NA	NR	N	N	N	N	Y
Wen2005 [113]	Rabbit	RPE	NR; 1E+05	sheet; suspension	NR	200	none	Y	N	N	N	N	Y
Westenskow2016 [114]	Rabbit	RPE	NR	suspension	HBSS	10	NA	Y	N	N	N	N	Y
Wong2002 [115]	Rat	RPE	1.00E+05	suspension	CMF-HBSS	2	NA	NR	N	N	N	N	Y
Wongpichedchai1992 [116]	Rat	RPE	NR	suspension	DMEM	NR	NA	NR	Y	N	N	N	Y
Wu2016 [117]	Rabbit	RPE	2.10E+04	suspension	PBS	40	NA	NR	N	N	N	N	Y
Wu2018 [118]	Rat	RPE	2E+04-6E+04	suspension	MEM	0.6-2	NA	NR	N	N	N	N	Y
Yaji2009 [119]	Human	RPE (OpRegen)	2.5E+04; 1E+05; 2E+05	suspension	BSS	2	NA	Y	N	N	N	Y	Y
Yamaguchi1992 [120]	Human	RPE; ESC; NHDF	5.00E+04	suspension	PBS	50	NA	Y; N	N	Y	Y	N	Y
Yamaguchi1993 [121]	Human; Rat	RPE; IPE	8.00E+04	suspension	F12	2	NA	N	N	N	N	N	N
Yamamoto1993 [122]	Mouse; Human	RPE; iPSC-RPE	3E+04; 7.5E+04	suspension	HBSS	1.5	NA	Y	Y	Y	Y	N	Y
Ye1993 [123]	Human; Mouse	RPE; mESC	1.00E+03	suspension	NR	1	NA	NR	Y	Y	N	N	Y
Zhang1998 [124]	Human	RPE-J	disc: 0.2 mm diameter	sheet	NA	NA	PDMS. nanosheet	NR	N	N	Y	N	Y

References

1. Abe, T.; Takeda, Y.; Yamada, K.; Akaishi, K.; Tomita, H.; Sato, M.; Tamai, M., Cytokine gene expression after subretinal transplantation. *The Tohoku journal of experimental medicine* **1999**, *189*, (3), 179-89.
2. Abe, T.; Saigo, Y.; Hojo, M.; Kano, T.; Wakusawa, R.; Tokita, Y.; Tamai, M., Protection of photoreceptor cells from phototoxicity by transplanted retinal pigment epithelial cells expressing different neurotrophic factors. *Cell transplantation* **2005**, *14*, (10), 799-808.
3. Abe, T.; Wakusawa, R.; Seto, H.; Asai, N.; Saito, T.; Nishida, K., Topical doxycycline can induce expression of BDNF in transduced retinal pigment epithelial cells transplanted into the subretinal space. *Investigative ophthalmology & visual science* **2008**, *49*, (8), 3631-9.
4. Bhatt, N. S.; Newsome, D. A.; Fenech, T.; Hessburg, T. P.; Diamond, J. G.; Miceli, M. V.; Kratz, K. E.; Oliver, P. D., Experimental transplantation of human retinal pigment epithelial cells on collagen substrates. *American journal of ophthalmology* **1994**, *117*, (2), 214-21.
5. Carido, M.; Zhu, Y.; Postel, K.; Benkner, B.; Cimalla, P.; Karl, M. O.; Kurth, T.; Paquet-Durand, F.; Koch, E.; Munch, T. A.; Tanaka, E. M.; Ader, M., Characterization of a mouse model with complete RPE loss and its use for RPE cell transplantation. *Investigative ophthalmology & visual science* **2014**, *55*, (8), 5431-44.
6. Carr, A. J.; Vugler, A. A.; Hikita, S. T.; Lawrence, J. M.; Gias, C.; Chen, L. L.; Buchholz, D. E.; Ahmado, A.; Semo, M.; Smart, M. J.; Hasan, S.; da Cruz, L.; Johnson, L. V.; Clegg, D. O.; Coffey, P. J., Protective effects of human iPS-derived retinal pigment epithelium cell transplantation in the retinal dystrophic rat. *PloS one* **2009**, *4*, (12), e8152.
7. Castillo, B. V., Jr.; del Cerro, M.; White, R. M.; Cox, C.; Wyatt, J.; Nadiga, G.; del Cerro, C., Efficacy of nonfetal human RPE for photoreceptor rescue: a study in dystrophic RCS rats. *Experimental neurology* **1997**, *146*, (1), 1-9.
8. Cho, S. M.; Lee, H. B.; Choi, H. J.; Ryu, J. E.; Lee, H. J.; Park, H. K.; Lee, M. J.; Lee, J.; Lee, H. J.; Kim, H. S.; Lee, J. Y.; Son, W. C., Subretinal transplantation of human embryonic stem cell-derived retinal pigment epithelium (MA09-hRPE): A safety and tolerability evaluation in minipigs. *Regulatory Toxicology and Pharmacology* **2019**, *106*, 7-14.
9. Coffey, P. J.; Girman, S.; Wang, S. M.; Hetherington, L.; Keegan, D. J.; Adamson, P.; Greenwood, J.; Lund, R. D., Long-term preservation of cortically dependent visual function in RCS rats by transplantation. *Nature neuroscience* **2002**, *5*, (1), 53-6.
10. Cong, L.; Sun, D.; Zhang, Z.; Jiao, W.; Rizzolo, L. J.; Peng, S., A novel rabbit model for studying RPE transplantation. *Investigative ophthalmology & visual science* **2008**, *49*, (9), 4115-25.
11. Crafoord, S.; Algvere, P. V.; Seregard, S.; Kopp, E. D., Long-term outcome of RPE allografts to the subretinal space of rabbits. *Acta ophthalmologica Scandinavica* **1999**, *77*, (3), 247-54.
12. Crafoord, S.; Algvere, P. V.; Kopp, E. D.; Seregard, S., Cyclosporine treatment of RPE allografts in the rabbit subretinal space. *Acta ophthalmologica Scandinavica* **2000**, *78*, (2), 122-9.

13. Davis, R. J.; Blenkinsop, T. A.; Campbell, M.; Borden, S. M.; Charniga, C. J.; Lederman, P. L.; Frye, A. M.; Aguilar, V.; Zhao, C.; Naimark, M.; Kiehl, T. R.; Temple, S.; Stern, J. H., Human RPE Stem Cell-Derived RPE Preserves Photoreceptors in the Royal College of Surgeons Rat: Method for Quantifying the Area of Photoreceptor Sparing. *Journal of ocular pharmacology and therapeutics: the official journal of the Association for Ocular Pharmacology and Therapeutics* **2016**, *32*, (5), 304-9.
14. Davis, R. J.; Alam, N. M.; Zhao, C.; Muller, C.; Saini, J. S.; Blenkinsop, T. A.; Mazzoni, F.; Campbell, M.; Borden, S. M.; Charniga, C. J.; Lederman, P. L.; Aguilar, V.; Naimark, M.; Fiske, M.; Boles, N.; Temple, S.; Finnemann, S. C.; Prusky, G. T.; Stern, J. H., The Developmental Stage of Adult Human Stem Cell-Derived Retinal Pigment Epithelium Cells Influences Transplant Efficacy for Vision Rescue. *Stem cell reports* **2017**, *9*, (1), 42-49.
15. Del Priore, L. V.; Sheng, Y.; Johnson, E.; Jacoby, D.; Edge, A.; Suzuki, T.; Geng, L.; Tezel, T. H.; Kaplan, H. J., Identification of transplanted retinal pigment epithelium with a novel chromosomal marker. *Current eye research* **2003**, *26*, (2), 125-31.
16. Del Priore, L. V.; Ishida, O.; Johnson, E. W.; Sheng, Y.; Jacoby, D. B.; Geng, L.; Tezel, T. H.; Kaplan, H. J., Triple immune suppression increases short-term survival of porcine fetal retinal pigment epithelium xenografts. *Investigative ophthalmology & visual science* **2003**, *44*, (9), 4044-53.
17. Diniz, B.; Thomas, P.; Thomas, B.; Ribeiro, R.; Hu, Y.; Brant, R.; Ahuja, A.; Zhu, D.; Liu, L.; Koss, M.; Maia, M.; Chader, G.; Hinton, D. R.; Humayun, M. S., Subretinal implantation of retinal pigment epithelial cells derived from human embryonic stem cells: improved survival when implanted as a monolayer. *Investigative ophthalmology & visual science* **2013**, *54*, (7), 5087-96.
18. Duan, P.; Zeng, Y.; Liu, Y.; Wang, Y.; Xu, H.; Yin, Z., Comparison of protective effects of hESCs-derived and hBMSCs-derived RPE cells on sodium iodate-injuried rat retina. *Int J Clin Exp Pathol* **2017**, *10*, (5), 5274-5284.
19. Dunaief, J. L.; Kwun, R. C.; Bhardwaj, N.; Lopez, R.; Gouras, P.; Goff, S. P., Retroviral gene transfer into retinal pigment epithelial cells followed by transplantation into rat retina. *Human gene therapy* **1995**, *6*, (9), 1225-9.
20. Durlu, Y. K.; Tamai, M., Transplantation of retinal pigment epithelium using viable cryopreserved cells. *Cell transplantation* **1997**, *6*, (2), 149-62.
21. 21. el Dirini, A. A.; Wang, H. M.; Ogden, T. E.; Ryan, S. J., Retinal pigment epithelium implantation in the rabbit: technique and morphology. *Graefe's archive for clinical and experimental ophthalmology = Albrecht von Graefes Archiv fur klinische und experimentelle Ophthalmologie* **1992**, *230*, (3), 292-300.
22. Engelhardt, M.; Tosha, C.; Lopes, V. S.; Chen, B.; Nguyen, L.; Nusinowitz, S.; Williams, D. S., Functional and morphological analysis of the subretinal injection of retinal pigment epithelium cells. *Visual neuroscience* **2012**, *29*, (2), 83-93.
23. Enzmann, V.; Faude, F.; Wiedemann, P.; Kohen, L., The local and systemic secretion of the pro-inflammatory cytokine interleukin-6 after transplantation of retinal pigment epithelium cells in a rabbit model. *Current eye research* **2000**, *21*, (1), 530-4.

24. Gabrielian, K.; Oganesian, A.; Patel, S. C.; Verp, M. S.; Ernest, J. T., Cellular response in rabbit eyes after human fetal RPE cell transplantation. *Graefe's archive for clinical and experimental ophthalmology = Albrecht von Graefes Archiv fur klinische und experimentelle Ophthalmologie* **1999**, *237*, (4), 326-35.
25. Garcia Delgado, A. B.; De La Cerda, B.; Alba Amador, J.; Valdes Sanchez, M. L.; Fernandez-Munoz, B.; Relimpio Lopez, I.; Rodriguez De La Rua, E.; Diez Lloret, A.; Calado, S. M.; Sanchez Pernaute, R.; Bhattacharya, S. S.; Diaz Corrales, F. J., Subretinal Transplant of Induced Pluripotent Stem Cell-Derived Retinal Pigment Epithelium on Nanostructured Fibrin-Agarose. *Tissue Engineering - Part A* **2019**, *25*, (9), 799-808.
26. Gaur, V.; Agarwal, N.; Li, L.; Turner, J. E., Maintenance of opsin and S-antigen gene expression in RCS dystrophic rats following RPE transplantation. *Experimental eye research* **1992**, *54*, (1), 91-101.
27. Gias, C.; Jones, M.; Keegan, D.; Adamson, P.; Greenwood, J.; Lund, R.; Martindale, J.; Johnston, D.; Berwick, J.; Mayhew, J.; Coffey, P., Preservation of visual cortical function following retinal pigment epithelium transplantation in the RCS rat using optical imaging techniques. *The European journal of neuroscience* **2007**, *25*, (7), 1940-8.
28. Girman, S. V.; Wang, S.; Lund, R. D., Cortical visual functions can be preserved by subretinal RPE cell grafting in RCS rats. *Vision research* **2003**, *43*, (17), 1817-27.
29. Girman, S. V.; Wang, S.; Lund, R. D., Time course of deterioration of rod and cone function in RCS rat and the effects of subretinal cell grafting: a light- and dark-adaptation study. *Vision research* **2005**, *45*, (3), 343-54.
30. Gouras, P.; Du, J.; Kjeldbye, H.; Yamamoto, S.; Zack, D. J., Reconstruction of degenerate rd mouse retina by transplantation of transgenic photoreceptors. *Investigative ophthalmology & visual science* **1992**, *33*, (9), 2579-86.
31. 31. Gouras, P.; Kong, J.; Tsang, S. H., Retinal degeneration and RPE transplantation in Rpe65(-/-) mice. *Investigative ophthalmology & visual science* **2002**, *43*, (10), 3307-11.
32. Grisanti, S.; Ishioka, M.; Kosiewicz, M.; Jiang, L. Q., Immunity and immune privilege elicited by cultured retinal pigment epithelial cell transplants. *Investigative ophthalmology & visual science* **1997**, *38*, (8), 1619-26.
33. Grisanti, S.; Szurman, P.; Jordan, J.; Kociok, N.; Bartz-Schmidt, K. U.; Heimann, K., Xenotransplantation of retinal pigment epithelial cells into RCS rats. *Japanese journal of ophthalmology* **2002**, *46*, (1), 36-44.
34. Hao, L. N.; Zhang, Y. Q.; Shen, Y. H.; Li, M. Q.; Yang, T.; Zhao, Z. H.; Wang, Z. Y.; Wang, Y. H.; He, S. Z., Toxicity of endogenous peroxynitrite and effects of puerarin on transplanted retinal pigment epithelial sheets in the subretinal space in mice. *International journal of ophthalmology* **2011**, *4*, (3), 250-4.
35. Haruta, M.; Sasai, Y.; Kawasaki, H.; Amemiya, K.; Ooto, S.; Kitada, M.; Suemori, H.; Nakatsuji, N.; Ide, C.; Honda, Y.; Takahashi, M., In vitro and in vivo characterization of pigment epithelial cells differentiated from primate embryonic stem cells. *Investigative ophthalmology & visual science* **2004**, *45*, (3), 1020-5.

36. Idelson, M.; Alper, R.; Obolensky, A.; Yachimovich-Cohen, N.; Rachmilewitz, J.; Ejzenberg, A.; Beider, E.; Banin, E.; Reubinoff, B., Immunological Properties of Human Embryonic Stem Cell-Derived Retinal Pigment Epithelial Cells. *Stem cell reports* **2018**, *11*, (3), 681-695.
37. Ilmarinen, T.; Hiidenmaa, H.; Koobi, P.; Nymark, S.; Sorkio, A.; Wang, J. H.; Stanzel, B. V.; Thieltges, F.; Alajuuma, P.; Oksala, O.; Kataja, M.; Uusitalo, H.; Skottman, H., Ultrathin Polyimide Membrane as Cell Carrier for Subretinal Transplantation of Human Embryonic Stem Cell Derived Retinal Pigment Epithelium. *PloS one* **2015**, *10*, (11), e0143669.
38. Ilmarinen, T.; Thieltges, F.; Hongisto, H.; Juuti-Uusitalo, K.; Koistinen, A.; Kaarniranta, K.; Brinken, R.; Braun, N.; Holz, F. G.; Skottman, H.; Stanzel, B. V., Survival and functionality of xeno-free human embryonic stem cell-derived retinal pigment epithelial cells on polyester substrate after transplantation in rabbits. *Acta ophthalmologica* **2019**, *97*, (5), e688-e699.
39. Jiang, L. Q.; Hamasaki, D., Corneal electroretinographic function rescued by normal retinal pigment epithelial grafts in retinal degenerative Royal College of Surgeons rats. *Investigative ophthalmology & visual science* **1994**, *35*, (13), 4300-9.
40. Kamao, H.; Mandai, M.; Okamoto, S.; Sakai, N.; Suga, A.; Sugita, S.; Kiryu, J.; Takahashi, M., Characterization of human induced pluripotent stem cell-derived retinal pigment epithelium cell sheets aiming for clinical application. *Stem cell reports* **2014**, *2*, (2), 205-18.
41. Kanemura, H.; Go, M. J.; Shikamura, M.; Nishishita, N.; Sakai, N.; Kamao, H.; Mandai, M.; Morinaga, C.; Takahashi, M.; Kawamata, S., Tumorigenicity studies of induced pluripotent stem cell (iPSC)-derived retinal pigment epithelium (RPE) for the treatment of age-related macular degeneration. *PloS one* **2014**, *9*, (1), e85336.
42. Kennelly, K. P.; Holmes, T. M.; Wallace, D. M.; O'Farrelly, C.; Keegan, D. J., Early Subretinal Allograft Rejection Is Characterized by Innate Immune Activity. *Cell Transplantation* **2017**, *26*, (6), 983-1000.
43. Klassen, H.; Whiteley, S. J.; Young, M. J.; Lund, R. D., Graft location affects functional rescue following RPE cell transplantation in the RCS rat. E*xperimental neurology* **2001**, *169*, (1), 114-21.
44. Kohen, L.; Enzmann, V.; Faude, F.; Wiedemann, P., Mechanisms of graft rejection in the transplantation of retinal pigment epithelial cells. *Ophthalmic research* **1997**, *29*, (5), 298-304.
45. Kole, C.; Klipfel, L.; Yang, Y.; Ferracane, V.; Blond, F.; Reichman, S.; Millet-Puel, G.; Clerin, E.; Ait-Ali, N.; Pagan, D.; Camara, H.; Delyfer, M. N.; rot, E. F.; Sahel, J. A.; Goureau, O.; Leveillard, T., &ITOtx2&IT-Genetically Modified Retinal Pigment Epithelial Cells Rescue Photoreceptors after Transplantation. *Molecular Therapy* **2018**, *26*, (1), 219-237.
46. Koss, M. J.; Falabella, P.; Stefanini, F. R.; Pfister, M.; Thomas, B. B.; Kashani, A. H.; Brant, R.; Zhu, D.; Clegg, D. O.; Hinton, D. R.; Humayun, M. S., Subretinal implantation of a monolayer of human embryonic stem cell-derived retinal pigment epithelium: a feasibility and safety study in Yucatan minipigs. *Graefe's archive for clinical and experimental ophthalmology = Albrecht von Graefes Archiv fur klinische und experimentelle Ophthalmologie* **2016**, *254*, (8), 1553-65.
47. Lai, C. C.; Gouras, P.; Doi, K.; Lu, F.; Kjeldbye, H.; Goff, S. P.; Pawliuk, R.; Leboulch, P.; Tsang, S. H., Tracking RPE transplants labeled by retroviral gene transfer with green fluorescent protein. *Investigative ophthalmology & visual science* **1999**, *40*, (9), 2141-6.

48. Lai, C. C.; Gouras, P.; Doi, K.; Tsang, S. H.; Goff, S. P.; Ashton, P., Local immunosuppression prolongs survival of RPE xenografts labeled by retroviral gene transfer. *Investigative ophthalmology & visual science* **2000**, *41*, (10), 3134-41.
49. Lane, C.; Boulton, M.; Marshall, J., Transplantation of retinal pigment epithelium using a pars plana approach. *Eye (London, England)* **1989**, *3* (Pt 1), 27-32.
50. Lavail, M. M.; Li, L.; Turner, J. E.; Yasumura, D., Retinal pigment epithelial cell transplantation in RCS rats: normal metabolism in rescued photoreceptors. *Experimental eye research* **1992**, *55*, (4), 555-62.
51. Li, L. X.; Turner, J. E., Inherited retinal dystrophy in the RCS rat: prevention of photoreceptor degeneration by pigment epithelial cell transplantation. *Experimental eye research* **1988**, *47*, (6), 911-7.
52. Li, L. X.; Sheedlo, H. J.; Gaur, V.; Turner, J. E., Effects of macrophage and retinal pigment epithelial cell transplants on photoreceptor cell rescue in RCS rats. *Current eye research* **1991**, *10*, (10), 947-58.
53. Li, L.; Turner, J. E., Optimal conditions for long-term photoreceptor cell rescue in RCS rats: the necessity for healthy RPE transplants. *Experimental eye research* **1991**, *52*, (6), 669-79.
54. Li, L.; Sheedlo, H. J.; Turner, J. E., Retinal pigment epithelial cell transplants in retinal degeneration slow mice do not rescue photoreceptor cells. *Investigative ophthalmology & visual science* **1993**, *34*, (6), 2141-5.
55. Li, Y.; Tsai, Y. T.; Hsu, C. W.; Erol, D.; Yang, J.; Wu, W. H.; Davis, R. J.; Egli, D.; Tsang, S. H., Long-term safety and efficacy of human-induced pluripotent stem cell (iPS) grafts in a preclinical model of retinitis pigmentosa. *Molecular medicine (Cambridge, Mass.)* **2012**, *18*, 1312-9.
56. Li, F.; Zeng, Y.; Xu, H.; Yin, Z. Q., Subretinal transplantation of retinal pigment epithelium overexpressing fibulin-5 inhibits laser-induced choroidal neovascularization in rats. *Experimental eye research* **2015**, *136*, 78-85.
57. Lin, N.; Fan, W.; Sheedlo, H. J.; Aschenbrenner, J. E.; Turner, J. E., Photoreceptor repair in response to RPE transplants in RCS rats: outer segment regeneration. *Current eye research* **1996**, *15*, (10), 1069-77.
58. Little, C. W.; Castillo, B.; DiLoreto, D. A.; Cox, C.; Wyatt, J.; del Cerro, C.; del Cerro, M., Transplantation of human fetal retinal pigment epithelium rescues photoreceptor cells from degeneration in the Royal College of Surgeons rat retina. *Investigative ophthalmology & visual science* **1996**, *37*, (1), 204-11.
59. Little, C. W.; Cox, C.; Wyatt, J.; del Cerro, C.; del Cerro, M., Correlates of photoreceptor rescue by transplantation of human fetal RPE in the RCS rat. *Experimental neurology* **1998**, *149*, (1), 151-60.
60. Liu, Z.; Yu, N.; Holz, F. G.; Yang, F.; Stanzel, B. V., Enhancement of retinal pigment epithelial culture characteristics and subretinal space tolerance of scaffolds with 200 nm fiber topography. *Biomaterials* **2014**, *35*, (9), 2837-50.
61. Lopez, R.; Gouras, P.; Brittis, M.; Kjeldbye, H., Transplantation of cultured rabbit retinal epithelium to rabbit retina using a closed-eye method. *Investigative ophthalmology & visual science* **1987**, *28*, (7), 1131-7.

62. Lopez, R.; Gouras, P.; Kjeldbye, H.; Sullivan, B.; Reppucci, V.; Brittis, M.; Wapner, F.; Goluboff, E., Transplanted retinal pigment epithelium modifies the retinal degeneration in the RCS rat. *Investigative ophthalmology & visual science* **1989**, *30*, (3), 586-8.
63. Lu, B.; Malcuit, C.; Wang, S.; Girman, S.; Francis, P.; Lemieux, L.; Lanza, R.; Lund, R., Long-term safety and function of RPE from human embryonic stem cells in preclinical models of macular degeneration. *Stem cells (Dayton, Ohio)* **2009**, *27*, (9), 2126-35.
64. Lund, R. D.; Adamson, P.; Sauve, Y.; Keegan, D. J.; Girman, S. V.; Wang, S.; Winton, H.; Kanuga, N.; Kwan, A. S.; Beauchene, L.; Zerbib, A.; Hetherington, L.; Couraud, P. O.; Coffey, P.; Greenwood, J., Subretinal transplantation of genetically modified human cell lines attenuates loss of visual function in dystrophic rats. *Proceedings of the National Academy of Sciences of the United States of America* **2001**, *98*, (17), 9942-7.
65. Lund, R. D.; Wang, S.; Klimanskaya, I.; Holmes, T.; Ramos-Kelsey, R.; Lu, B.; Girman, S.; Bischoff, N.; Sauve, Y.; Lanza, R., Human embryonic stem cell-derived cells rescue visual function in dystrophic RCS rats. *Cloning and stem cells* **2006**, *8*, (3), 189-99.
66. Maeda, T.; Lee, M. J.; Palczewska, G.; Marsili, S.; Tesar, P. J.; Palczewski, K.; Takahashi, M.; Maeda, A., Retinal pigmented epithelial cells obtained from human induced pluripotent stem cells possess functional visual cycle enzymes in vitro and in vivo. *The Journal of biological chemistry* **2013**, *288*, (48), 34484-93.
67. Majji, A. B.; de Juan, E., Jr., Retinal pigment epithelial autotransplantation: morphological changes in retina and choroid. *Graefe's archive for clinical and experimental ophthalmology = Albrecht von Graefes Archiv fur klinische und experimentelle Ophthalmologie* **2000**, *238*, (9), 779-91.
68. Ben M'Barek, K.; Habeler, W.; Plancheron, A.; Jarraya, M.; Regent, F.; Terray, A.; Yang, Y.; Chatrousse, L.; Domingues, S.; Masson, Y.; Sahel, J. A.; Peschanski, M.; Goureau, O.; Monville, C., Human ESC-derived retinal epithelial cell sheets potentiate rescue of photoreceptor cell loss in rats with retinal degeneration. *Sci Transl Med* **2017**, *9*, (421).
69. McGill, T. J.; Lund, R. D.; Douglas, R. M.; Wang, S.; Lu, B.; Prusky, G. T., Preservation of vision following cell-based therapies in a model of retinal degenerative disease. *Vision research* **2004**, *44*, (22), 2559-66.
70. McGill, T. J.; Bohana-Kashtan, O.; Stoddard, J. W.; Andrews, M. D.; Pandit, N.; Rosenberg-Belmaker, L. R.; Wiser, O.; Matzrafi, L.; Banin, E.; Reubinoff, B.; Netzer, N.; Irving, C., Long-Term Efficacy of GMP Grade Xeno-Free hESC-Derived RPE Cells Following Transplantation. *Translational vision science & technology* **2017**, *6*, (3), 17.
71. Oganesian, A.; Gabrielian, K.; Ernest, J. T.; Patel, S. C., A new model of retinal pigment epithelium transplantation with microspheres. *Archives of ophthalmology (Chicago, Ill. : 1960)* **1999**, *117*, (9), 1192-200.
72. Osusky, R.; Jiang, M.; Buchi, E. R.; Spee, C.; Ye, J.; Ryan, S. J., beta-Galactosidase transgene expression in transplanted rabbit retinal pigment epithelial cells in vivo. *Graefe's archive for clinical and experimental ophthalmology = Albrecht von Graefes Archiv fur klinische und experimentelle Ophthalmologie* **1995**, *233*, (4), 220-5.

73. Park, U. C.; Cho, M. S.; Park, J. H.; Kim, S. J.; Ku, S. Y.; Choi, Y. M.; Moon, S. Y.; Yu, H. G., Subretinal transplantation of putative retinal pigment epithelial cells derived from human embryonic stem cells in rat retinal degeneration model. *Clinical and experimental reproductive medicine* **2011**, *38*, (4), 216-21.
74. Peng, C. H.; Chuang, J. H.; Wang, M. L.; Jhan, Y. Y.; Chien, K. H.; Chung, Y. C.; Hung, K. H.; Chang, C. C.; Lee, C. K.; Tseng, W. L.; Hwang, D. K.; Hsu, C. H.; Lin, T. C.; Chiou, S. H.; Chen, S. J., Laminin modification subretinal bio-scaffold remodels retinal pigment epithelium-driven microenvironment in vitro and in vivo. *Oncotarget* **2016**, *7*, (40), 64631-64648.
75. Petrus-Reurer, S.; Bartuma, H.; Aronsson, M.; Westman, S.; Lanner, F.; Andre, H.; Kvanta, A., Integration of Subretinal Suspension Transplants of Human Embryonic Stem Cell-Derived Retinal Pigment Epithelial Cells in a Large-Eyed Model of Geographic Atrophy. *Investigative ophthalmology & visual science* **2017**, *58*, (2), 1314-1322.
76. Phillips, S. J.; Sadda, S. R.; Tso, M. O.; Humayan, M. S.; de Juan, E., Jr.; Binder, S., Autologous transplantation of retinal pigment epithelium after mechanical debridement of Bruch's membrane. *Current eye research* **2003**, *26*, (2), 81-8.
77. Pinilla, I.; Cuenca, N.; Sauve, Y.; Wang, S.; Lund, R. D., Preservation of outer retina and its synaptic connectivity following subretinal injections of human RPE cells in the Royal College of Surgeons rat. *Experimental eye research* **2007**, *85*, (3), 381-92.
78. Plaza Reyes, A.; Petrus-Reurer, S.; Antonsson, L.; Stenfelt, S.; Bartuma, H.; Panula, S.; Mader, T.; Douagi, I.; Andre, H.; Hovatta, O.; Lanner, F.; Kvanta, A., Xeno-Free and Defined Human Embryonic Stem Cell-Derived Retinal Pigment Epithelial Cells Functionally Integrate in a Large-Eyed Preclinical Model. *Stem cell reports* **2016**, *6*, (1), 9-17.
79. Ribeiro, R. M.; Oregon, A.; Diniz, B.; Fernandes, R. B.; Koss, M. J.; Charafeddin, W.; Hu, Y. T.; Thomas, P.; Thomas, B. B.; Maia, M.; Chader, G. J.; Hinton, D. R.; Humayun, M. S., In Vivo Detection of hESC-RPE Cells via Confocal Near-Infrared Fundus Reflectance. O*phthalmic Surgery Lasers & Imaging Retina* **2013**, *44*, (4), 380-384.
80. Saigo, Y.; Abe, T.; Hojo, M.; Tomita, H.; Sugano, E.; Tamai, M., Transplantation of transduced retinal pigment epithelium in rats. I*nvestigative ophthalmology & visual science* **2004**, *45*, (6), 1996-2004.
81. Sauve, Y.; Girman, S. V.; Wang, S.; Keegan, D. J.; Lund, R. D., Preservation of visual responsiveness in the superior colliculus of RCS rats after retinal pigment epithelium cell transplantation. *Neuroscience* **2002**, *114*, (2), 389-401.
82. Sauve, Y.; Lu, B.; Lund, R. D., The relationship between full field electroretinogram and perimetry-like visual thresholds in RCS rats during photoreceptor degeneration and rescue by cell transplants. *Vision research* **2004**, *44*, (1), 9-18.
83. Sauve, Y.; Pinilla, I.; Lund, R. D., Partial preservation of rod and cone ERG function following subretinal injection of ARPE-19 cells in RCS rats. *Vision research* **2006**, *46*, (8-9), 1459-72.
84. Schmack, I.; Berglin, L.; Nie, X.; Wen, J.; Kang, S. J.; Marcus, A. I.; Yang, H.; Lynn, M. J.; Kapp, J. A.; Grossniklaus, H. E., Modulation of choroidal neovascularization by subretinal injection of retinal pigment epithelium and polystyrene microbeads. *Molecular vision* **2009**, *15*, 146-61.

85. Schraermeyer, U.; Kayatz, P.; Thumann, G.; Luther, T. T.; Szurman, P.; Kociok, N.; Bartz-Schmidt, K. U., Transplantation of iris pigment epithelium into the choroid slows down the degeneration of photoreceptors in the RCS rat. *Graefe's archive for clinical and experimental ophthalmology = Albrecht von Graefes Archiv fur klinische und experimentelle Ophthalmologie* **2000**, *238*, (12), 979-84.
86. Seaton, A. D.; Turner, J. E., RPE transplants stabilize retinal vasculature and prevent neovascularization in the RCS rat. *Investigative ophthalmology & visual science* **1992**, *33*, (1), 83-91.
87. Seaton, A. D.; Sheedlo, H. J.; Turner, J. E., A primary role for RPE transplants in the inhibition and regression of neovascularization in the RCS rat. *Investigative ophthalmology & visual science* **1994**, *35*, (1), 162-9.
88. Sharma, R.; Khristov, V.; Rising, A.; Jha, B. S.; Dejene, R.; Hotaling, N.; Li, Y.; Stoddard, J.; Stankewicz, C.; Wan, Q.; Zhang, C.; Campos, M. M.; Miyagishima, K. J.; McGaughey, D.; Villasmil, R.; Mattapallil, M.; Stanzel, B.; Qian, H.; Wong, W.; Chase, L.; Charles, S.; McGill, T.; Miller, S.; Maminishkis, A.; Amaral, J.; Bharti, K., Clinical-grade stem cell-derived retinal pigment epithelium patch rescues retinal degeneration in rodents and pigs. *Science Translational Medicine* **2019**, *11*.
89. Sheedlo, H. J.; Li, L. X.; Turner, J. E., Functional and structural characteristics of photoreceptor cells rescued in RPE-cell grafted retinas of RCS dystrophic rats. *Experimental eye research* **1989**, *48*, (6), 841-54.
90. Sheedlo, H. J.; Li, L.; Turner, J. E., Photoreceptor cell rescue in the RCS rat by RPE transplantation: a therapeutic approach in a model of inherited retinal dystrophy. *Progress in clinical and biological research* **1989**, *314*, 645-58.
91. Sheedlo, H. J.; Li, L.; Turner, J. E., Photoreceptor cell rescue at early and late RPE-cell transplantation periods during retinal disease in RCS dystrophic rats. *Journal of neural transplantation & plasticity* **1991**, *2*, (1), 55-63.
92. Sheedlo, H. J.; Li, L.; Turner, J. E., Effects of RPE age and culture conditions on support of photoreceptor cell survival in transplanted RCS dystrophic rats. *Experimental eye research* **1993**, *57*, (6), 753-61.
93. Sheedlo, H. J.; Li, L.; Barnstable, C. J.; Turner, J. E., Synaptic and photoreceptor components in retinal pigment epithelial cell transplanted retinas of Royal College of Surgeons dystrophic rats. *Journal of neuroscience research* **1993**, *36*, (4), 423-31.
94. Sheng, Y.; Gouras, P.; Cao, H.; Berglin, L.; Kjeldbye, H.; Lopez, R.; Rosskothen, H., Patch transplants of human fetal retinal pigment epithelium in rabbit and monkey retina. *Investigative ophthalmology & visual science* **1995**, *36*, (2), 381-90.
95. Shiragami, C.; Matsuo, T.; Shiraga, F.; Matsuo, N., Transplanted and repopulated retinal pigment epithelial cells on damaged Bruch's membrane in rabbits. *The British journal of ophthalmology* **1998**, **82**, (9), 1056-62.
96. Sohn, E. H.; Jiao, C.; Kaalberg, E.; Cranston, C.; Mullins, R. F.; Stone, E. M.; Tucker, B. A., Allogenic iPSC-derived RPE cell transplants induce immune response in pigs: a pilot study. *Scientific reports* **2015**, *5*, 11791.

97. Stanzel, B. V.; Liu, Z.; Somboonthanakij, S.; Wongsawad, W.; Brinken, R.; Eter, N.; Corneo, B.; Holz, F. G.; Temple, S.; Stern, J. H.; Blenkinsop, T. A., Human RPE stem cells grown into polarized RPE monolayers on a polyester matrix are maintained after grafting into rabbit subretinal space. *Stem cell reports* **2014**, 2, (1), 64-77.
98. Sun, J.; Mandai, M.; Kamao, H.; Hashiguchi, T.; Shikamura, M.; Kawamata, S.; Sugita, S.; Takahashi, M., Protective Effects of Human iPS-Derived Retinal Pigmented Epithelial Cells in Comparison with Human Mesenchymal Stromal Cells and Human Neural Stem Cells on the Degenerating Retina in rd1 mice. *Stem cells (Dayton, Ohio)* **2015**, *33*, (5), 1543-53.
99. Suzuki, J.; Nagai, N.; Nishizawa, M.; Abe, T.; Kaji, H., Electrochemical manipulation of cell populations supported by biodegradable polymeric nanosheets for cell transplantation therapy. *Biomaterials science* **2017**, *5*, (2), 216-222.
100. Thomas, B. B.; Zhu, D.; Zhang, L.; Thomas, P. B.; Hu, Y.; Nazari, H.; Stefanini, F.; Falabella, P.; Clegg, D. O.; Hinton, D. R.; Humayun, M. S., Survival and Functionality of hESC-Derived Retinal Pigment Epithelium Cells Cultured as a Monolayer on Polymer Substrates Transplanted in RCS Rats. *Investigative ophthalmology & visual science* **2016**, *57*, (6), 2877-87.
101. Thomas, B. B.; Zhu, D.; Lin, T. C.; Kim, Y. C.; Seiler, M. J.; Martinez-Camarillo, J. C.; Lin, B.; Shad, Y.; Hinton, D. R.; Humayun, M. S., A new immunodeficient retinal dystrophic rat model for transplantation studies using human-derived cells. *Graefe's Archive for Clinical and Experimental Ophthalmology*. **2018**.
102. Thumann, G.; Viethen, A.; Gaebler, A.; Walter, P.; Kaempf, S.; Johnen, S.; Salz, A. K., The in vitro and in vivo behaviour of retinal pigment epithelial cells cultured on ultrathin collagen membranes. *Biomaterials* **2009**, *30*, (3), 287-94.
103. Thumann, G.; Salz, A. K.; Walter, P.; Johnen, S., Preservation of photoreceptors in dystrophic RCS rats following allo- and xenotransplantation of IPE cells. *Graefe's archive for clinical and experimental ophthalmology = Albrecht von Graefes Archiv fur klinische und experimentelle Ophthalmologie* **2009**, *247*, (3), 363-9.
104. Verdugo, M. E.; Ailing, J.; Lazar, E. S.; del Cerro, M.; Ray, J.; Aguirre, G., Posterior segment approach for subretinal transplantation or injection in the canine model. *Cell transplantation* **2001**, *10*, (3), 317-27.
105. Vugler, A.; Carr, A. J.; Lawrence, J.; Chen, L. L.; Burrell, K.; Wright, A.; Lundh, P.; Semo, M.; Ahmado, A.; Gias, C.; da Cruz, L.; Moore, H.; Andrews, P.; Walsh, J.; Coffey, P., Elucidating the phenomenon of HESC-derived RPE: anatomy of cell genesis, expansion and retinal transplantation. *Experimental neurology* **2008**, *214*, (2), 347-61.
106. Wang, H.; Yagi, F.; Cheewatrakoolpong, N.; Sugino, I. K.; Zarbin, M. A., Short-term study of retinal pigment epithelium sheet transplants onto Bruch's membrane. *Experimental eye research* **2004**, *78*, (1), 53-65.
107. Wang, S.; Lu, B.; Wood, P.; Lund, R. D., Grafting of ARPE-19 and Schwann cells to the subretinal space in RCS rats. *Investigative ophthalmology & visual science* **2005**, *46*, (7), 2552-60.
108. Wang, S.; Lu, B.; Lund, R. D., Morphological changes in the Royal College of Surgeons rat retina during photoreceptor degeneration and after cell-based therapy. *The Journal of comparative neurology* **2005**, *491*, (4), 400-17.

109. Wang, S.; Lu, B.; Girman, S.; Holmes, T.; Bischoff, N.; Lund, R. D., Morphological and functional rescue in RCS rats after RPE cell line transplantation at a later stage of degeneration. *Investigative ophthalmology & visual science* **2008**, *49*, (1), 416-21.
110. Wang, N. K.; Tosi, J.; Kasanuki, J. M.; Chou, C. L.; Kong, J.; Parmalee, N.; Wert, K. J.; Allikmets, R.; Lai, C. C.; Chien, C. L.; Nagasaki, T.; Lin, C. S.; Tsang, S. H., Transplantation of reprogrammed embryonic stem cells improves visual function in a mouse model for retinitis pigmentosa. *Transplantation* **2010**, *89*, (8), 911-9.
111. Wang, J.; Westenskow, P. D.; Fang, M.; Friedlander, M.; Siuzdak, G., Quantitative metabolomics of photoreceptor degeneration and the effects of stem cell-derived retinal pigment epithelium transplantation. *Philosophical transactions. Series A, Mathematical, physical, and engineering sciences* **2016**, *374*, (2079).
112. Warncke, B.; Valtink, M.; Weichel, J.; Engelmann, K.; Schafer, H., Experimental rat model for therapeutic retinal pigment epithelium transplantation--unequivocal microscopic identification of human donor cells by in situ hybridisation of human-specific Alu sequences. *Virchows Archiv : an international journal of pathology* **2004**, *444*, (1), 74-81.
113. Wen, J.; McKenna, K. C.; Barron, B. C.; Langston, H. P.; Kapp, J. A., Use of superparamagnetic microbeads in tracking subretinal injections. *Molecular vision* **2005**, *11*, 256-62.
114. Westenskow, P. D.; Bucher, F.; Bravo, S.; Kurihara, T.; Feitelberg, D.; Paris, L. P.; Aguilar, E.; Lin, J. H.; Friedlander, M., iPSC-Derived Retinal Pigment Epithelium Allografts Do Not Elicit Detrimental Effects in Rats: A Follow-Up Study. *Stem cells international* **2016**, *2016*, 8470263.
115. Wong, C. A.; Potter, M. J.; Cui, J. Z.; Chang, T. S.; Ma, P.; Maberley, A. L.; Ross, W. H.; White, V. A.; Samad, A.; Jia, W.; Hornan, D.; Matsubara, J. A., Induction of proliferative vitreoretinopathy by a unique line of human retinal pigment epithelial cells. Canadian journal of ophthalmology. *Journal canadien d'ophtalmologie* **2002**, *37*, (4), 211-20.
116. Wongpichedchai, S.; Weiter, J. J.; Weber, P.; Dorey, C. K., Comparison of external and internal approaches for transplantation of autologous retinal pigment epithelium. *Investigative ophthalmology & visual science* **1992**, *33*, (12), 3341-52.
117. Wu, W.; Zeng, Y.; Li, Z.; Li, Q.; Xu, H.; Yin, Z. Q., Features specific to retinal pigment epithelium cells derived from three-dimensional human embryonic stem cell cultures - a new donor for cell therapy. **Oncotarget 2016**, *7*, (16), 22819-33.
118. Wu, H.; Li, J.; Mao, X.; Li, G.; Xie, L.; You, Z., Transplantation of rat embryonic stem cell-derived retinal cells restores visual function in the Royal College of Surgeons rats. *Documenta Ophthalmologica* **2018**, *137*, (2), 71-78.
119. Yaji, N.; Yamato, M.; Yang, J.; Okano, T.; Hori, S., Transplantation of tissue-engineered retinal pigment epithelial cell sheets in a rabbit model. *Biomaterials* **2009**, *30*, (5), 797-803.
120. Yamaguchi, K.; Yamaguchi, K.; Young, R. W.; Gaur, V. P.; Greven, C. M.; Slusher, M. M.; Turner, J. E., Vitreoretinal surgical technique for transplanting retinal pigment epithelium in rabbit retina. *Japanese journal of ophthalmology* **1992**, *36*, (2), 142-50.
121. Yamaguchi, K.; Yamaguchi, K.; Gaur, V. P.; Turner, J. E., Retinal pigment epithelial cell transplantation into aging retina: a possible approach to delay age-related cell death. *Japanese journal of ophthalmology* **1993**, *37*, (1), 16-27.

122. Yamamoto, S.; Du, J.; Gouras, P.; Kjeldbye, H., Retinal pigment epithelial transplants and retinal function in RCS rats. *Investigative ophthalmology & visual science* **1993**, *34*, (11), 3068-75.
123. Ye, J.; Wang, H.-M.; Ogden, T. E.; Ryan, S. J., Allotransplantation of rabbit retinal pigment epithelial cells double-labelled with 5-bromodeoxyuridine (BrdU) and natural pigment. *Current eye research* **1993**, *12*, (7), 629-639.
124. Zhang, X.; Bok, D., Transplantation of retinal pigment epithelial cells and immune response in the subretinal space. *Investigative ophthalmology & visual science* **1998**, *39*, (6), 1021-7.

Supplementary 3

Table S3. Additional statistics data on the meta-analysis of the effect of RPE transplantation on the a-wave amplitude.

Experiment Name	Lower Limit	Hedges' g	Upper Limit
Abe2008_0mg/mL [1]	−1.169	0	1.169
Abe2008_2mg/mL [1]	−0.662	0.533	1.727
Abe2008_5mg/mL [1]	−0.437	0.787	2.011
Abe2008_10mg/mL [1]	−0.115	1.130	2.376
Duan2017_MSCRPE [2]	1.340	3.100	4.861
Duan2017_hESCRPE [2]	1.118	2.770	4.421
Lund2006 [3]	0.180	1.074	1.968
Overall	0.471	1.181	1.892

Table S5. Additional statistics data on the subgroup analysis of the b-wave amplitude meta-analysis.

Subgroup	Experiments (#)	I^2	Lower Limit	Hedges' g	Upper Limit
Both sexes	8	82	2.735	3.500	4.265
Male	5	75	−0.019	1.029	2.077
Young	18	13	1.591	2.223	2.855
Adolescent	6	86	0.541	1.557	2.573
Adult	8	63	−0.210	0.724	1.658
Overall	42	70	1.295	1.734	2.172

Table S4.
Additional statistics data on the meta-analysis of the effect of RPE transplantation on the b-wave amplitude.

Experiment Name	Lower Limit	Hedges'g	Upper Limit
Abe2008_0mg/mL [1]	−1.215	0.168	1.552
Abe2008_10mg/mL [1]	−1.004	0.401	1.806
Abe2008_10mg/mLdaily [1]	0.591	2.419	4.246
Abe2008_2mg/mL [1]	−0.326	1.189	2.704
Abe2008_5mg/mL [1]	−2.420	1.297	2.837
Duan2017_hESCRPE [2]	1.104	3.049	4.993
Duan2017_MSCRPE [2]	1.036	2.940	4.843
Gouras2002_10 months [4]	−0.377	0.804	1.986
Gouras2002_11 months [4]	−0.623	0.548	1.720
Gouras2002_12 months [4]	−0.857	0.309	1.474
Gouras2002_5 months [4]	−0.82	0.346	1.512
Gouras2002_6 months [4]	−0.567	0.606	1.780
Gouras2002_7 months [4]	−0.414	0.765	1.945
Gouras2002_8 months [4]	−0.503	0.673	1.849
Gouras2002_9 months [4]	0.381	1.619	2.856
Idelson2018_Cycl4.8 [5]	1.637	2.633	3.630
Idelson2018_NoCycl4.8 [5]	0.719	1.616	2.514
Kamao2014_sheet [6]	0.687	2.507	4.328
Kamao2014_suspension [6]	3.445	7.149	10.85
Kole2018_RPE-GFP [7]	0.274	1.576	2.877
Kole2018_RPE-OTX2 [7]	1.495	3.260	5.026
Lund2006 [3]	0.662	1.626	2.590
Maeda2013_LRAT1m [8]	0.684	2.147	3.609
Maeda2013_LRAT3m [8]	4.232	7.850	11.47
Maeda2013_RPE651m [8]	1.025	2.632	4.240
Maeda2013_RPE653m [8]	1.083	2.718	4.353
M'Barek2017_12w_sheet [9]	−0.264	0.802	1.868
M'Barek2017_12w_suspension [9]	−1.297	−0.269	0.759
M'Barek2017_5w_sheet [9]	−0.793	0.234	1.261
M'Barek2017_5w_suspension [9]	-1.437	−0.403	0.631
M'Barek2017_9w_sheet [9]	0.141	1.267	2.393
M'Barek2017_9w_suspension [9]	−1.530	−0.490	0.549
Sauve2004 [10]	−0.233	0.728	1.688
Sauve2006_P120 [11]	−0.364	0.418	1.200
Sauve2006_P60 [11]	0.935	1.871	2.808
Sauve2006_P90 [11]	0.404	1.254	2.104
Wu2016_3DRPE_12w [12]	2.162	3.145	4.129
Wu2016_3DRPE_4w [12]	3.760	5.104	6.447
Wu2016_3DRPE_8w [12]	2.019	2.974	3.930
Wu2016_SDRPE_12w [12]	1.773	2.704	3.635
Wu2016_SDRPE_4w [12]	4.514	6.096	7.679
Wu2016_SDRPE_8w [12]	2.671	3.791	4.910
Overall	1.295	1.734	2.172

Table S6. Additional statistics data on the meta-analysis of the effect of RPE transplantation on the b-wave amplitude.

Experiment Name	Lower Limit	Hedges' g	Upper Limit
Carr2009_iPSCRPE_0.25cycles/degree [13]	−0.584	0.307	1.198
Carr2009_iPSCRPE_0.312cycles/degree [13]	−1.534	−0.626	0.283
Carr2009_iPSCRPE_0.5cycles/degree [13]	0.595	1.628	2.661
Coffey2002 [14]	2.171	5.638	9.106
Davis2017_4weeksculture [15]	−0.315	0.497	1.309
Davis2017_7weeksculture [15]	−0.589	0.233	1.055
Haruta2004_2rpm_ESPEs [16]	0.043	1.439	2.836
Haruta2004_4rpm_ESPEs [16]	0.004	1.388	2.772
Haruta2004_8rpm_ESPEs [16]	0.501	2.078	3.656
Klassen2001_3months_dorsal [17]	0.021	0.841	1.662
Klassen2001_3months_ventral [17]	−0.666	0.131	0.927
Klassen2001_6months_dorsal [17]	−0.416	0.382	1.179
Klassen2001_6months_ventral [17]	−0.598	0.199	0.997
Kole2018_GFP_Contrast [7]	0.529	1.692	2.857
Kole2018_GFP_VA [7]	0.741	1.962	3.183
Kole2018_OTX2_Contrast [7]	0.208	1.301	2.394
Kole2018_OTX2_VA [7]	0.895	2.161	3.427
Little1998_pathlength [18]	0.239	1.151	2.063
Little1998_time [18]	0.112	1.008	1.904
Lu2009_100Kmed_P120 [19]	−0.372	0.607	1.586
Lu2009_100Kmed_P150 [19]	0.040	1.068	2.097
Lu2009_100Kmed_P180 [19]	0.019	1.044	2.069
Lu2009_100Kmed_P210 [19]	−0.400	0.521	1.441
Lu2009_100Kmed_P240 [19]	−0.558	0.354	1.266
Lu2009_100Kmed_P60 [19]	−0.172	0.827	1.827
Lu2009_100Kmed_P90 [19]	0.070	1.103	2.136
Lu2009_50Khigh_P120 [19]	−0.157	0.876	1.909
Lu2009_50Khigh_P150 [19]	−0.335	0.678	1.690
Lu2009_50Khigh_P180 [19]	−0.374	0.634	1.643
Lu2009_50Khigh_P60 [19]	−0.009	1.046	2.100
Lu2009_50Khigh_P90 [19]	0.068	1.135	2.202
Lu2009_50Klow_P120 [19]	0.344	1.465	2.586
Lu2009_50Klow_P150 [19]	−0.181	0.849	1.879
Lu2009_50Klow_P180 [19]	−0.425	0.579	1.583
Lu2009_50Klow_P60 [19]	−0.102	0.938	1.979

Lu2009_50Klow_P90 [19]	0.026	1.086	2.146
Lu2009_50Kmed_P120 [19]	−0.035	1.016	2.066
Lu2009_50Kmed_P150 [19]	−0.173	0.859	1.889
Lu2009_50Kmed_P180 [19]	−0.084	0.959	2.002
Lu2009_50Kmed_P60 [19]	−0.027	1.024	2.076
Lu2009_50Kmed_P90 [19]	0.247	1.347	2.448
Lu2009_75Kmed_P120 [19]	0.207	0.942	1.678
Lu2009_75Kmed_P150 [19]	−0.692	0.267	1.227
Lu2009_75Kmed_P180 [19]	−0.448	0.525	1.498
Lu2009_75Kmed_P210 [19]	−0.359	0.565	1.488
Lu2009_75Kmed_P240 [19]	−0.560	0.351	1.263
Lu2009_75Kmed_P60 [19]	−0.108	0.899	1.906
Lu2009_75Kmed_P90 [19]	−0.070	0.942	1.955
Lu2009_P105Cells [19]	−0.595	0.265	1.126
Lu2009_P52Cells [19]	0.098	1.010	1.922
Lu2009_P63Cells [19]	0.125	1.041	1.957
Lu2009_P69Cells [19]	−0.109	0.781	1.672
Lu2009_P77Cells [19]	−0.330	0.543	1.416
Lund2001_ARPE19 [20]	0.938	2.421	3.905
Lund2001_h1RPE7 [20]	0.198	1.495	2.793
Lund2006_hES-RPE [20]	0.122	1.009	1.897
M'Barek2017_sheet13w [9]	0.792	1.862	2.932
M'Barek2017_sheet4w [9]	0.336	1.315	2.294
M'Barek2017_sheet6w [9]	−0.172	0.741	1.654
M'Barek2017_suspension13w [9]	0.403	1.394	2.385
M'Barek2017_suspension4w [9]	0.353	1.335	2.317
M'Barek2017_suspension6w [9]	−0.360	0.537	1.434
McGill2004_ARPE19_4m [21]	1.482	2.863	4.244
McGill2004_ARPE19_5m [21]	0.614	1.769	2.925
McGill2004_ARPE19_6m [21]	0.543	1.684	2.824
McGill2004_ARPE19_7m [21]	0.399	1.512	2.625
McGill2017_100K_P150 [22]	2.362	3.491	4.620
McGill2017_100K_P200 [22]	0.911	1.804	2.697
McGill2017_100K_P60 [22]	1.653	3.155	4.657
McGill2017_100K_P90 [22]	1.350	2.436	3.523
McGill2017_200K_P150 [22]	2.126	3.290	4.453
McGill2017_200K_P200 [22]	2.125	3.321	4.517
McGill2017_200K_P60 [22]	1.068	2.362	3.656

McGill2017_200K_P90 [22]	1.549	2.705	3.862
McGill2017_25K_P150 [22]	0.210	0.975	1.740
McGill2017_25K_P200 [22]	−0.144	0.622	1.387
McGill2017_25K_P60 [22]	−0.163	0.982	2.126
McGill2017_25K_P90 [22]	−0.335	0.538	1.410
Sharma2019_sheet [23]	1.619	2.834	4.049
Sharma2019_suspension [23]	4.258	6.417	8.575
Thomas2016_rCPCB-RPE1_13w [24]	−0.236	0.361	0.958
Thomas2016_rCPCB-RPE1_21w [24]	−0.226	0.371	0.968
Thomas2016_rCPCB-RPE1_3w [24]	−0.967	−0.370	0.227
Thomas2016_rCPCB-RPE1_7w [24]	−0.429	0.165	0.76
Thomas2016_rMSPM+VN_13w [24]	0.038	0.657	1.276
Thomas2016_rMSPM+VN_21w [24]	−0.217	0.395	1.007
Thomas2016_rMSPM+VN_3w [24]	−0.889	−0.279	0.33
Thomas2016_rMSPM+VN_7w [24]	−0.358	0.251	0.86
Wang2008_early40 [25]	1.299	2.843	4.388
Wang2008_early90 [25]	2.694	4.923	7.153
Wang2008_late40 [25]	0.691	2.009	3.326
Wang2008_late90 [25]	−0.228	0.873	1.975
Overall	0.826	1.018	1.209

Table 7. Additional statistics data on the subgroup analysis of the behavioural meta-analysis.

Subgroup	Experiment (#)	I^2	Lower Limit	Hedges'g	Upper Limit
Adolescent	59	66	1.032	1.257	1.481
Adult	31	70	0.136	0.431	0.725
Number of Cells 10^4	47	58	0.566	0.811	1.055
Number of Cells 10^5	32	77	1.384	1.694	2.003
ARPE-19	10	53	1.597	2.153	2.709
hESC-RPE	45	0	0.574	0.783	0.992
iPSC-RPE	5	92	0.658	1.348	2.039
pRPE	10	49	0.529	0.976	1.423
RPE (OpRegen)	12	79	1.551	1.978	2.406
Overall	96	73	1.018	0.826	1.209

References

1. Abe. T.; Wakusawa. R.; Seto. H.; Asai. N.; Saito. T.; Nishida. K.. Topical doxycycline can induce expression of BDNF in transduced retinal pigment epithelial cells transplanted into the subretinal space. *Investigative ophthalmology & visual science* **2008**. *49*. (8). 3631-9.
2. Duan. P.; Zeng. Y.; Liu. Y.; Wang. Y.; Xu. H.; Yin. Z.. Comparison of protective effects of hESCs-derived and hBMSCs-derived RPE cells on sodium iodate-injuried rat retina. *Int J Clin Exp Pathol* **2017**. *10*. (5). 5274-5284.
3. Lund. R. D.; Wang. S.; Klimanskaya. I.; Holmes. T.; Ramos-Kelsey. R.; Lu. B.; Girman. S.; Bischoff. N.; Sauve. Y.; Lanza. R.. Human embryonic stem cell-derived cells rescue visual function in dystrophic RCS rats. *Cloning and stem cells* **2006**. *8*. (3). 189-99.
4. Gouras. P.; Kong. J.; Tsang. S. H.. Retinal degeneration and RPE transplantation in Rpe65(-/-) mice. *Investigative ophthalmology & visual science* **2002**. *43*. (10). 3307-11.
5. Idelson. M.; Alper. R.; Obolensky. A.; Yachimovich-Cohen. N.; Rachmilewitz. J.; Ejzenberg. A.; Beider. E.; Banin. E.; Reubinoff. B.. Immunological Properties of Human Embryonic Stem Cell-Derived Retinal Pigment Epithelial Cells. *Stem cell reports* **2018**. *11*. (3). 681-695.
6. Kamao. H.; Mandai. M.; Okamoto. S.; Sakai. N.; Suga. A.; Sugita. S.; Kiryu. J.; Takahashi. M.. Characterization of human induced pluripotent stem cell-derived retinal pigment epithelium cell sheets aiming for clinical application. *Stem cell reports* **2014**. *2*. (2). 205-18.
7. Kole. C.; Klipfel. L.; Yang. Y.; Ferracane. V.; Blond. F.; Reichman. S.; Millet-Puel. G.; Clerin. E.; Ait-Ali. N.; Pagan. D.; Camara. H.; Delyfer. M. N.; rot. E. F.; Sahel. J. A.; Goureau. O.; Leveillard. T.. &ITOtx2&IT-Genetically Modified Retinal Pigment Epithelial Cells Rescue Photoreceptors after Transplantation. *Molecular Therapy* **2018**. *26*. (1). 219-237.
8. Maeda. T.; Lee. M. J.; Palczewska. G.; Marsili. S.; Tesar. P. J.; Palczewski. K.; Takahashi. M.; Maeda. A.. Retinal pigmented epithelial cells obtained from human induced pluripotent stem cells possess functional visual cycle enzymes in vitro and in vivo. *The Journal of biological chemistry* **2013**. *288*. (48). 34484-93.
9. Ben M'Barek. K.; Habeler. W.; Plancheron. A.; Jarraya. M.; Regent. F.; Terray. A.; Yang. Y.; Chatrousse. L.; Domingues. S.; Masson. Y.; Sahel. J. A.; Peschanski. M.; Goureau. O.; Monville. C.. Human ESC-derived retinal epithelial cell sheets potentiate rescue of photoreceptor cell loss in rats with retinal degeneration. *Sci Transl Med* **2017**. *9*. (421).
10. Sauve. Y.; Lu. B.; Lund. R. D.. The relationship between full field electroretinogram and perimetry-like visual thresholds in RCS rats during photoreceptor degeneration and rescue by cell transplants. *Vision research* **2004**. *44*. (1). 9-18.
11. Sauve. Y.; Pinilla. I.; Lund. R. D.. Partial preservation of rod and cone ERG function following subretinal injection of ARPE-19 cells in RCS rats. *Vision research* **2006**. *46*. (8-9). 1459-72.
12. Wu. W.; Zeng. Y.; Li. Z.; Li. Q.; Xu. H.; Yin. Z. Q.. Features specific to retinal pigment epithelium cells derived from three-dimensional human embryonic stem cell cultures - a new donor for cell therapy. *Oncotarget* **2016**. *7*. (16). 22819-33.

13. Carr. A. J.; Vugler. A. A.; Hikita. S. T.; Lawrence. J. M.; Gias. C.; Chen. L. L.; Buchholz. D. E.; Ahmado. A.; Semo. M.; Smart. M. J.; Hasan. S.; da Cruz. L.; Johnson. L. V.; Clegg. D. O.; Coffey. P. J.. Protective effects of human iPS-derived retinal pigment epithelium cell transplantation in the retinal dystrophic rat. *PloS one* **2009**. *4*. (12). e8152.
14. Coffey. P. J.; Girman. S.; Wang. S. M.; Hetherington. L.; Keegan. D. J.; Adamson. P.; Greenwood. J.; Lund. R. D.. Long-term preservation of cortically dependent visual function in RCS rats by transplantation. *Nature neuroscience* **2002**. *5*. (1). 53-6.
15. Davis. R. J.; Alam. N. M.; Zhao. C.; Muller. C.; Saini. J. S.; Blenkinsop. T. A.; Mazzoni. F.; Campbell. M.; Borden. S. M.; Charniga. C. J.; Lederman. P. L.; Aguilar. V.; Naimark. M.; Fiske. M.; Boles. N.; Temple. S.; Finnemann. S. C.; Prusky. G. T.; Stern. J. H.. The Developmental Stage of Adult Human Stem Cell-Derived Retinal Pigment Epithelium Cells Influences Transplant Efficacy for Vision Rescue. *Stem cell reports* **2017**. *9*. (1). 42-49.
16. Haruta. M.; Sasai. Y.; Kawasaki. H.; Amemiya. K.; Ooto. S.; Kitada. M.; Suemori. H.; Nakatsuji. N.; Ide. C.; Honda. Y.; Takahashi. M.. In vitro and in vivo characterization of pigment epithelial cells differentiated from primate embryonic stem cells. *Investigative ophthalmology & visual science* **2004**. *45*. (3). 1020-5.
17. Klassen. H.; Whiteley. S. J.; Young. M. J.; Lund. R. D.. Graft location affects functional rescue following RPE cell transplantation in the RCS rat. *Experimental neurology* **2001**. *169*. (1). 114-21.
18. Little. C. W.; Cox. C.; Wyatt. J.; del Cerro. C.; del Cerro. M.. Correlates of photoreceptor rescue by transplantation of human fetal RPE in the RCS rat. *Experimental neurology 1998*. **149**. *(1)*. 151-60.
19. Lu. B.; Malcuit. C.; Wang. S.; Girman. S.; Francis. P.; Lemieux. L.; Lanza. R.; Lund. R.. Long-term safety and function of RPE from human embryonic stem cells in preclinical models of macular degeneration. *Stem cells (Dayton. Ohio)* **2009**. *27*. (9). 2126-35.
20. Lund. R. D.; Adamson. P.; Sauve. Y.; Keegan. D. J.; Girman. S. V.; Wang. S.; Winton. H.; Kanuga. N.; Kwan. A. S.; Beauchene. L.; Zerbib. A.; Hetherington. L.; Couraud. P. O.; Coffey. P.; Greenwood. J.. Subretinal transplantation of genetically modified human cell lines attenuates loss of visual function in dystrophic rats. *Proceedings of the National Academy of Sciences of the United States of America* **2001**. *98*. (17). 9942-7.
21. McGill. T. J.; Lund. R. D.; Douglas. R. M.; Wang. S.; Lu. B.; Prusky. G. T.. Preservation of vision following cell-based therapies in a model of retinal degenerative disease. *Vision research* **2004**. *44*. (22). 2559-66.
22. McGill. T. J.; Bohana-Kashtan. O.; Stoddard. J. W.; Andrews. M. D.; Pandit. N.; Rosenberg-Belmaker. L. R.; Wiser. O.; Matzrafi. L.; Banin. E.; Reubinoff. B.; Netzer. N.; Irving. C.. Long-Term Efficacy of GMP Grade Xeno-Free hESC-Derived RPE *Cells Following Transplantation. Translational vision science & technology* **2017**. *6*. (3). 17.
23. Sharma. R.; Khristov. V.; Rising. A.; Jha. B. S.; Dejene. R.; Hotaling. N.; Li. Y.; Stoddard. J.; Stankewicz. C.; Wan. Q.; Zhang. C.; Campos. M. M.; Miyagishima. K. J.; McGaughey. D.; Villasmil. R.; Mattapallil. M.; Stanzel. B.; Qian. H.; Wong. W.; Chase. L.; Charles. S.; McGill. T.; Miller. S.; Maminishkis. A.; Amaral. J.; Bharti. K.. Clinical-grade stem cell-derived retinal pigment epithelium patch rescues retinal degeneration in rodents and pigs. *Science Translational Medicine* **2019**. *11*.

24. Thomas. B. B.; Zhu. D.; Zhang. L.; Thomas. P. B.; Hu. Y.; Nazari. H.; Stefanini. F.; Falabella. P.; Clegg. D. O.; Hinton. D. R.; Humayun. M. S.. Survival and Functionality of hESC-Derived Retinal Pigment Epithelium Cells Cultured as a Monolayer on Polymer Substrates Transplanted in RCS Rats. *Investigative ophthalmology & visual science* **2016**. *57*. (6). 2877-87.
25. Wang. S.; Lu. B.; Girman. S.; Holmes. T.; Bischoff. N.; Lund. R. D.. Morphological and functional rescue in RCS rats after RPE cell line transplantation at a later stage of degeneration. *Investigative ophthalmology & visual science* **2008**. *49*. (1). 416-21.

Supplementary data — Chapter 3

The Lrat$^{-/-}$ Rat: CRISPR/Cas9 Construction and Phenotyping of a New Animal Model for Retinitis Pigmentosa

Supplementary Figures and Tables

Supplementary Table S1: An overview of the scotopic ERG settings which were used throughout the experiment.

Intensity (cd/m²)	Averaged	Interval (Hz)
0.0003	20	0.2
0.003	18	0.125
0.03	14	9 (Flicker)
0.3	15	0.077
3	12	0.067
30	8	0.05

Supplementary Table S2: The progeny from Lrat$^{+/-}$ × Lrat$^{+/-}$ breeding results compared to the standard Mendelian frequencies. No significant deviation were observed (p >0.9, according to the Chi-Square Test).

Genotype	WT (*Lrat*$^{+/+}$)	Heterozygous (*Lrat*$^{+/-}$)	Homozygous (*Lrat*$^{-/-}$)	Males:Females
Total	34	66	37	64:71
Expected	25%	50%	25%	1:1
Actual	24.8%	48.2%	27.0%	1:1.1

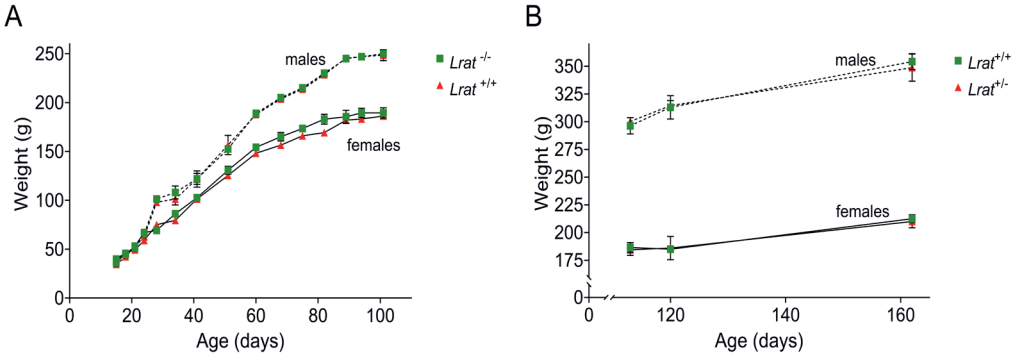

Supplementary Figure S1: The weight progression of Lrat$^{-/-}$ versus Lrat$^{+/+}$ animals (n = 3 males and n = 3 females) (**A**) and Lrat$^{+/-}$ versus Lrat$^{+/+}$ animals (n = 3 males and n = 2 females) (**B**). No significant differences in weight progression was observed between the genotypes.

Supplementary Figure S2: Expression analysis of *Lrat* mRNA in the liver, eyes, testis, brain, kidney, spleen, lung and small intestine of *Lrat*$^{+/+}$ (WT), *Lrat*$^{+/-}$ (HZ) and *Lrat*$^{-/-}$ (KO) rats. *Ef1a* was used as a reference gene. *Lrat* mRNA was abundantly present in the liver, eye and testis. Little expression was seen in lung tissue (yellow arrows), and no expression was observed in the brain, kidney, spleen and small intestine. Less expression of *Lrat* was seen in KO tissues compared to WT and HZ tissues.

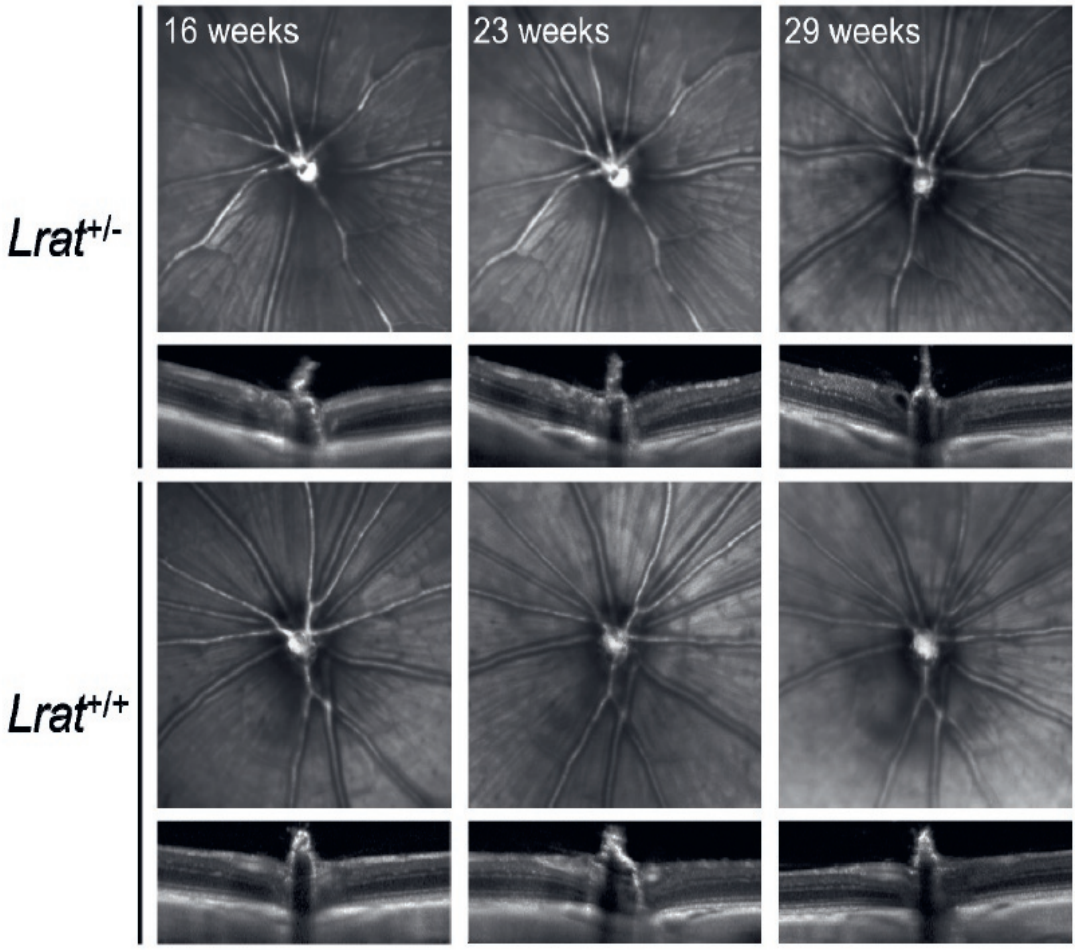

Supplementary Figure S3: Representative SLO and OCT images of *Lrat*$^{+/+}$ and *Lrat*$^{+/-}$ rats at different ages. It is possible to clearly identify all retinal layers in both the wildtype and heterozygous animals from the OCT images. No differences were observed between the thickness of the retina between wildtype and heterozygous animals. For the quantification, see Figure 6. No differences were observed for SLO images as well.

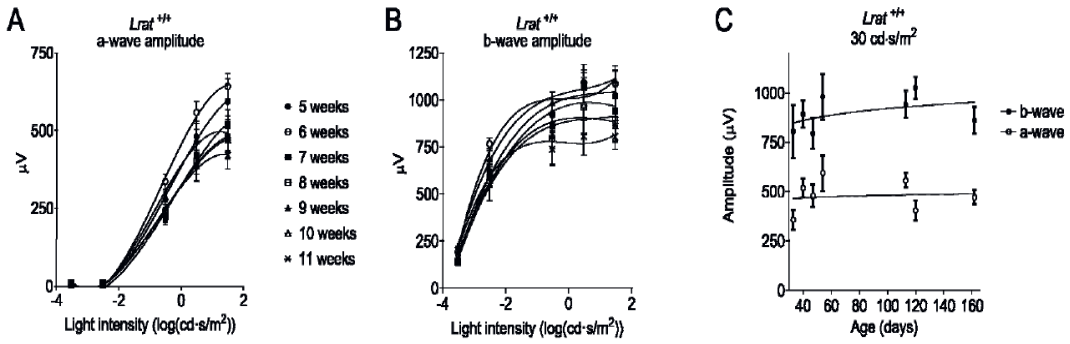

Supplementary Figure S4: Single flash ERG responses of increasing light intensities (**A** and **B**) of *Lrat*$^{+/+}$ animals at different ages (n = 6). The measured a- and b-wave amplitudes at the highest light intensity (30 cd·s/m^2) is plotted against age (**C**). No significant differences (2-way ANOVA) between the several ages of wildtype animals for a-wave or b-wave amplitudes were observed.

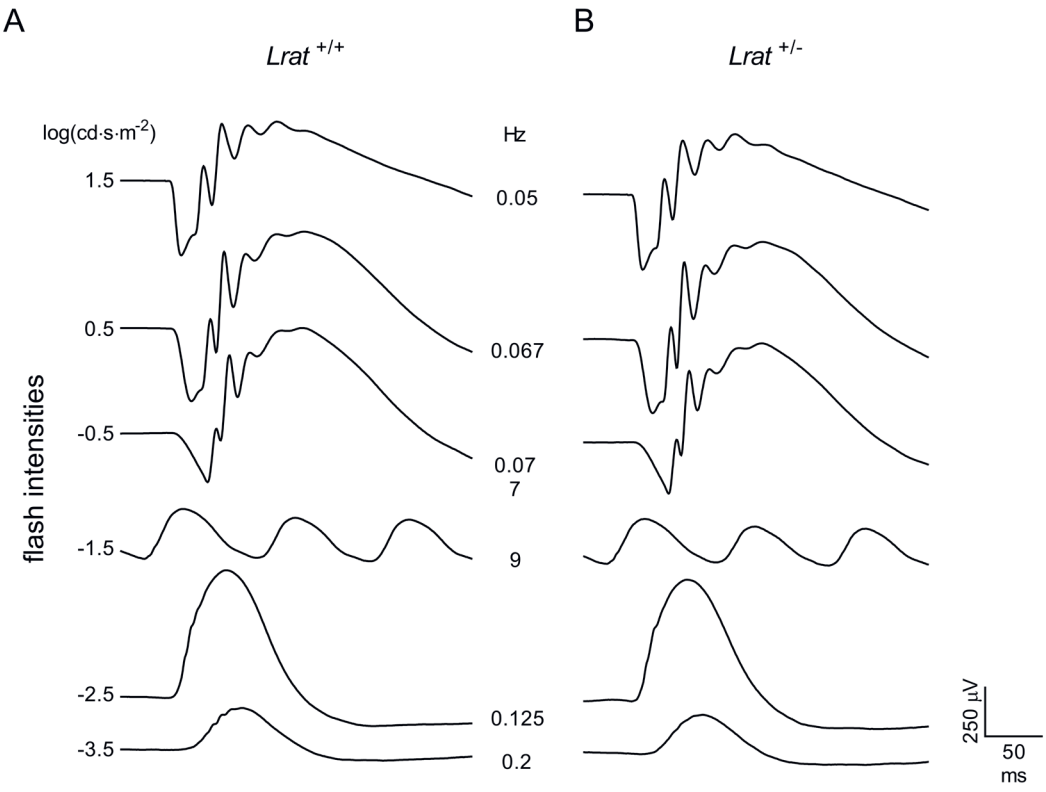

Supplementary Figure S1: Scotopic ERG responses of single flash and flicker stimuli. Averaged traces (duration of 350 ms) (n = 5 per group) with increasing flash intensities (-3.5 – 1.5 log(cd·s·m^{-2}) are plotted for *Lrat*$^{+/+}$ (**A**) and *Lrat*$^{+/-}$ animals (**B**) at the age of 23 weeks. Based on this data, no differences were observed between *Lrat*$^{+/+}$ and *Lrat*$^{+/-}$ animals.

Alignment of wildtype and knockout cDNA sequences

NM_022290.2 = NCBI reference sequence
ORF = Open reading frame
= Serine

```
NM_022290.2                CCGCCAGCGAGAAACTCTGGTCTTTAAAGGATGAAGAACTCAATGCTGGAGGCTGCGTCC   300
ORF                        ------------------------------ATGAAGAACTCAATGCTGGAGGCTGCGTCC   30
Wildtype_cDNA              ------------------------------ATGAAGAACTCAATGCTGGAGGCTGCGTCC   30
Knockout_cDNA              ------------------------------ATGAAGAACAGT-TGCTGGAGGCTGCGTCC   29
                                                          *********### ******************

NM_022290.2                CTCCTTCTGGAGAAGCTGCTCCTTATTTCCAACTTCAAGATCTTTAGCGTGTGCGCCCCG   360
ORF                        CTCCTTCTGGAGAAGCTGCTCCTTATTTCCAACTTCAAGATCTTTAGCGTGTGCGCCCCG   90
Wildtype_cDNA              CTCCTTCTGGAGAAGCTGCTCCTTATTTCCAACTTCAAGATCTTTAGCGTGTGCGCCCCG   90
Knockout_cDNA              CTCCTTCTGGAGAAGCTGCTCCTTATTTCCAACTTCAAGATCTTTAGCGTGTGCGCCCCG   89
                           ************************************************************

NM_022290.2                GGAGGAGGCACAGGGAAGAAACATCCCTATGAAATCAACTCTTTTCTCCGGGGTGACGTG   420
ORF                        GGAGGAGGCACAGGGAAGAAACATCCCTATGAAATCAACTCTTTTCTCCGGGGTGACGTG   150
Wildtype_cDNA              GGAGGAGGCACAGGGAAGAAACATCCCTATGAAATCAACTCTTTTCTCCGGGGTGACGTG   150
Knockout_cDNA              GGAGGAGGCACAGGGAAGAAACATCCCTATGAAATCAACTCTTTTCTCCGGGGTGACGTG   149
                           ************************************************************

NM_022290.2                TTGGAAGTGTCACGGACCCATTTTACCCACTATGGGATCTACCTGGGGGACAACCGTGTC   480
ORF                        TTGGAAGTGTCACGGACCCATTTTACCCACTATGGGATCTACCTGGGGGACAACCGTGTC   210
Wildtype_cDNA              TTGGAAGTGTCACGGACCCATTTTACCCACTATGGGATCTACCTGGGGGACAACCGTGTC   210
Knockout_cDNA              TTGGAAGTGTCACGGACCCATTTTACCCACTATGGGATCTACCTGGGGGACAACCGTGTC   209
                           ************************************************************

NM_022290.2                GCCCATCTAATGCCTGACATCCTGTTGGCCCTGACCAGTGACAAGGAACGCACTCAGAAG   540
ORF                        GCCCATCTAATGCCTGACATCCTGTTGGCCCTGACCAGTGACAAGGAACGCACTCAGAAG   270
Wildtype_cDNA              GCCCATCTAATGCCTGACATCCTGTTGGCCCTGACCAGTGACAAGGAACGCACTCAGAAG   270
Knockout_cDNA              GCCCATCTAATGCCTGACATCCTGTTGGCCCTGACCAGTGACAAGGAACGCACTCAGAAG   269
                           ************************************************************

NM_022290.2                GTGGTCTCCAACAAGCGTCTCCTCCCAGGAGTCATTTGCAAGGTGGCCAGCATCCGTGTG   600
ORF                        GTGGTCTCCAACAAGCGTCTCCTCCCAGGAGTCATTTGCAAGGTGGCCAGCATCCGTGTG   330
Wildtype_cDNA              GTGGTCTCCAACAAGCGTCTCCTCCCAGGAGTCATTTGCAAGGTGGCCAGCATCCGTGTG   330
Knockout_cDNA              GTGGTCTCCAACAAGCGTCTCCTCCCAGGAGTCATTTGCAAGGTGGCCAGCATCCGTGTG   329
                           ************************************************************

NM_022290.2                GACACAGTAGAGGACTTTGCCTATGGAGCGGACATCCTCGTCAATCACCTAGACGAGACT   660
ORF                        GACACAGTAGAGGACTTTGCCTATGGAGCGGACATCCTCGTCAATCACCTAGACGAGACT   390
Wildtype_cDNA              GACACAGTAGAGGACTTTGCCTATGGAGCGGACATCCTCGTCAATCACCTAGACGAGACT   390
Knockout_cDNA              GACACAGTAGAGGACTTTGCCTATGGAGCGGACATCCTCGTCAATCACCTAGACGAGACT   389
                           ************************************************************

NM_022290.2                CTCAAGAAGAAGTCCTTGCTCAATGAGGAGGTGGCACGCAGAGCAGAGCAGCAGTTGGGG   720
ORF                        CTCAAGAAGAAGTCCTTGCTCAATGAGGAGGTGGCACGCAGAGCAGAGCAGCAGTTGGGG   450
Wildtype_cDNA              CTCAAGAAGAAGTCCTTGCTCAATGAGGAGGTGGCACGCAGAGCAGAGCAGCAGTTGGGG   450
Knockout_cDNA              CTCAAGAAGAAGTCCTTGCTCAATGAGGAGGTGGCACGCAGAGCAGAGCAGCAGTTGGGG   449
                           ************************************************************

NM_022290.2                CTGACCCCCTACAGCCTACTGTGGAACAACTGCGAACACTTTGTGACCTACTGCAGATAC   780
ORF                        CTGACCCCCTACAGCCTACTGTGGAACAACTGCGAACACTTTGTGACCTACTGCAGATAC   510
Wildtype_cDNA              CTGACCCCCTACAGCCTACTGTGGAACAACTGCGAACACTTTGTGACCTACTGCAGATAC   510
Knockout_cDNA              CTGACCCCCTACAGCCTACTGTGGAACAACTGCGAACACTTTGTGACCTACTGCAGATAC   509
                           ************************************************************

NM_022290.2                GGCTCTCCTATCAGTCCGCAGGCTGAGAAGTTTCACGAGACTGTGAAGATACTCATTCGT   840
ORF                        GGCTCTCCTATCAGTCCGCAGGCTGAGAAGTTTCACGAGACTGTGAAGATACTCATTCGT   570
Wildtype_cDNA              GGCTCTCCTATCAGTCCGCAGGCTGAGAAGTTTCACGAGACTGATAGAAGGAGAGCCGTA   570
Knockout_cDNA              GGCTCTCCTATCAGTCCGCAGGCTGAGAAGTTTCACGAGACTG----------------   552
                           ******************************************

NM_022290.2                GATCAGAGAAGTTGTCTTGCTTCAGCTGTCTTGGGATTAGTGTCTATTATCTACACAGGC   900
ORF                        GATCAGAGAAGTTGTCTTGCTTCAGCTGTCTTGGGATTAGTGTCTATTATCTACACAGGC   630
Wildtype_cDNA              TGCTGTGGGTGTCA-------------------------------------------------   584
Knockout_cDNA              ------------------------------------------------------------   552
```

Alignment of wildtype cDNA sequences using forward and reverse primers

NM_022290.2 = NCBI reference sequence
ORF = Open reading frame

```
ORF                    ------------------------------ATGAAGAACTCAATGCTGGAGGCTGCGTCC   30
NM_022290.2            CCGCCAGCGAGAAACTCTGGTCTTTAAAGGATGAAGAACTCAATGCTGGAGGCTGCGTCC   300
Wildtype_cDNA_forward  ------------------------------ATGAAGAACTCAATGCTGGAGGCTGCGTCC   30
Wildtype_cDNA_reverse  ------------------------------ATGAAGAACTCAATGCTGGAGGCTGCGTCC   30
                                                      ********************************

ORF                    CTCCTTCTGGAGAAGCTGCTCCTTATTTCCAACTTCAAGATCTTTAGCGTGTGCGCCCCG   90
NM_022290.2            CTCCTTCTGGAGAAGCTGCTCCTTATTTCCAACTTCAAGATCTTTAGCGTGTGCGCCCCG   360
Wildtype_cDNA_forward  CTCCTTCTGGAGAAGCTGCTCCTTATTTCCAACTTCAAGATCTTTAGCGTGTGCGCCCCG   90
Wildtype_cDNA_reverse  CTCCTTCTGGAGAAGCTGCTCCTTATTTCCAACTTCAAGATCTTTAGCGTGTGCGCCCCG   90
                       ************************************************************

ORF                    GGAGGAGGCACAGGGAAGAAACATCCCTATGAAATCAACTCTTTTCTCCGGGGTGACGTG   150
NM_022290.2            GGAGGAGGCACAGGGAAGAAACATCCCTATGAAATCAACTCTTTTCTCCGGGGTGACGTG   420
Wildtype_cDNA_forward  GGAGGAGGCACAGGGAAGAAACATCCCTATGAAATCAACTCTTTTCTCCGGGGTGACGTG   150
Wildtype_cDNA_reverse  GGAGGAGGCACAGGGAAGAAACATCCCTATGAAATCAACTCTTTTCTCCGGGGTGACGTG   150
                       ************************************************************

ORF                    TTGGAAGTGTCACGGACCCATTTTACCCACTATGGGATCTACCTGGGGGACAACCGTGTC   210
NM_022290.2            TTGGAAGTGTCACGGACCCATTTTACCCACTATGGGATCTACCTGGGGGACAACCGTGTC   480
Wildtype_cDNA_forward  TTGGAAGTGTCACGGACCCATTTTACCCACTATGGGATCTACCTGGGGGACAACCGTGTC   210
Wildtype_cDNA_reverse  TTGGAAGTGTCACGGACCCATTTTACCCACTATGGGATCTACCTGGGGGACAACCGTGTC   210
                       ************************************************************

ORF                    GCCCATCTAATGCCTGACATCCTGTTGGCCCTGACCAGTGACAAGGAACGCACTCAGAAG   270
NM_022290.2            GCCCATCTAATGCCTGACATCCTGTTGGCCCTGACCAGTGACAAGGAACGCACTCAGAAG   540
Wildtype_cDNA_forward  GCCCATCTAATGCCTGACATCCTGTTGGCCCTGACCAGTGACAAGGAACGCACTCAGAAG   270
Wildtype_cDNA_reverse  GCCCATCTAATGCCTGACATCCTGTTGGCCCTGACCAGTGACAAGGAACGCACTCAGAAG   270
                       ************************************************************

ORF                    GTGGTCTCCAACAAGCGTCTCCTCCCAGGAGTCATTTGCAAGGTGGCCAGCATCCGTGTG   330
NM_022290.2            GTGGTCTCCAACAAGCGTCTCCTCCCAGGAGTCATTTGCAAGGTGGCCAGCATCCGTGTG   600
Wildtype_cDNA_forward  GTGGTCTCCAACAAGCGTCTCCTCCCAGGAGTCATTTGCAAGGTGGCCAGCATCCGTGTG   330
Wildtype_cDNA_reverse  GTGGTCTCCAACAAGCGTCTCCTCCCAGGAGTCATTTGCAAGGTGGCCAGCATCCGTGTG   330
                       ************************************************************

ORF                    GACACAGTAGAGGACTTTGCCTATGGAGCGGACATCCTCGTCAATCACCTAGACGAGACT   390
NM_022290.2            GACACAGTAGAGGACTTTGCCTATGGAGCGGACATCCTCGTCAATCACCTAGACGAGACT   660
Wildtype_cDNA_forward  GACACAGTAGAGGACTTTGCCTATGGAGCGGACATCCTCGTCAATCACCTAGACGAGACT   390
Wildtype_cDNA_reverse  GACACAGTAGAGGACTTTGCCTATGGAGCGGACATCCTCGTCAATCACCTAGACGAGACT   390
                       ************************************************************

ORF                    CTCAAGAAGAAGTCCTTGCTCAATGAGGAGGTGGCACGCAGAGCAGAGCAGCAGTTGGGG   450
NM_022290.2            CTCAAGAAGAAGTCCTTGCTCAATGAGGAGGTGGCACGCAGAGCAGAGCAGCAGTTGGGG   720
Wildtype_cDNA_forward  CTCAAGAAGAAGTCCTTGCTCAATGAGGAGGTGGCACGCAGAGCAGAGCAGCAGTTGGGG   450
Wildtype_cDNA_reverse  CTCAAGAAGAAGTCCTTGCTCAATGAGGAGGTGGCACGCAGAGCAGAGCAGCAGTTGGGG   450
                       ************************************************************

ORF                    CTGACCCCCTACAGCCTACTGTGGAACAACTGCGAACACTTTGTGACCTACTGCAGATAC   510
NM_022290.2            CTGACCCCCTACAGCCTACTGTGGAACAACTGCGAACACTTTGTGACCTACTGCAGATAC   780
Wildtype_cDNA_forward  CTGACCCCCTACAGCCTACTGTGGAACAACTGCGAACACTTTGTGACCTACTGCAGATAC   510
Wildtype_cDNA_reverse  CTGACCCCCTACAGCCTACTGTGGA----------------------------------   475
                       *************************

ORF                    GGCTCTCCTATCAGTCCGCAGGCTGAGAAGTTTCACGAGACTGTGAAGATACTCATTCGT   570
NM_022290.2            GGCTCTCCTATCAGTCCGCAGGCTGAGAAGTTTCACGAGACTGTGAAGATACTCATTCGT   840
Wildtype_cDNA_forward  GGCTCTCCTATCAGTCCGCAGGCTGAGAAGTTTCACGAGACTGATAGAAGGAGAGCCGTA   570
Wildtype_cDNA_reverse  ------------------------------------------------------------   475

ORF                    GATCAGAGAAGTTGTCTTGCTTCAGCTGTCTTGGGATTAGTGTCTATTATCTACACAGGC   630
NM_022290.2            GATCAGAGAAGTTGTCTTGCTTCAGCTGTCTTGGGATTAGTGTCTATTATCTACACAGGC   900
Wildtype_cDNA_forward  TGCTGTGGGTGTCA----------------------------------------------   584
Wildtype_cDNA_reverse  ------------------------------------------------------------   475
```

Alignment of knockout cDNA sequences using forward and reverse primers

NM_022290.2 = NCBI reference sequence
ORF = Open reading frame
= Serine

```
NM_022290.2               CCGCCAGCGAGAAACTCTGGTCTTTAAAGGATGAAGAACTCAATGCTGGAGGCTGCGTCC   300
ORF                       ------------------------------ATGAAGAACTCAATGCTGGAGGCTGCGTCC    30
Knockout_cDNA_forward     ------------------------------ATGAAGAACAGT-TGCTGGAGGCTGCGTCC    28
Knockout_cDNA_reverse     ------------------------------ATGAAGAACAGT-TGCTGGAGGCTGCGTCC    29
                                                         *********### ******************

NM_022290.2               CTCCTTCTGGAGAAGCTGCTCCTTATTTCCAACTTCAAGATCTTTAGCGTGTGCGCCCCG   360
ORF                       CTCCTTCTGGAGAAGCTGCTCCTTATTTCCAACTTCAAGATCTTTAGCGTGTGCGCCCCG    90
Knockout_cDNA_forward     CTCCTTCTGGAGAAGCTGCTCCTTATTTCCAACTTCAAGATCTTTAGCGTGTGCGCCCCG    88
Knockout_cDNA_reverse     CTCCTTCTGGAGAAGCTGCTCCTTATTTCCAACTTCAAGATCTTTAGCGTGTGCGCCCCG    89
                          ************************************************************

NM_022290.2               GGAGGAGGCACAGGGAAGAAACATCCCTATGAAATCAACTCTTTTCTCCGGGGTGACGTG   420
ORF                       GGAGGAGGCACAGGGAAGAAACATCCCTATGAAATCAACTCTTTTCTCCGGGGTGACGTG   150
Knockout_cDNA_forward     GGAGGAGGCACAGGGAAGAAACATCCCTATGAAATCAACTCTTTTCTCCGGGGTGACGTG   148
Knockout_cDNA_reverse     GGAGGAGGCACAGGGAAGAAACATCCCTATGAAATCAACTCTTTTCTCCGGGGTGACGTG   149
                          ************************************************************

NM_022290.2               TTGGAAGTGTCACGGACCCATTTTACCCACTATGGGATCTACCTGGGGGACAACCGTGTC   480
ORF                       TTGGAAGTGTCACGGACCCATTTTACCCACTATGGGATCTACCTGGGGGACAACCGTGTC   210
Knockout_cDNA_forward     TTGGAAGTGTCACGGACCCATTTTACCCACTATGGGATCTACCTGGGGGACAACCGTGTC   208
Knockout_cDNA_reverse     TTGGAAGTGTCACGGACCCATTTTACCCACTATGGGATCTACCTGGGGGACAACCGTGTC   209
                          ************************************************************

NM_022290.2               GCCCATCTAATGCCTGACATCCTGTTGGCCCTGACCAGTGACAAGGAACGCACTCAGAAG   540
ORF                       GCCCATCTAATGCCTGACATCCTGTTGGCCCTGACCAGTGACAAGGAACGCACTCAGAAG   270
Knockout_cDNA_forward     GCCCATCTAATGCCTGACATCCTGTTGGCCCTGACCAGTGACAAGGAACGCACTCAGAAG   268
Knockout_cDNA_reverse     GCCCATCTAATGCCTGACATCCTGTTGGCCCTGACCAGTGACAAGGAACGCACTCAGAAG   269
                          ************************************************************

NM_022290.2               GTGGTCTCCAACAAGCGTCTCCTCCCAGGAGTCATTTGCAAGGTGGCCAGCATCCGTGTG   600
ORF                       GTGGTCTCCAACAAGCGTCTCCTCCCAGGAGTCATTTGCAAGGTGGCCAGCATCCGTGTG   330
Knockout_cDNA_forward     GTGGTCTCCAACAAGCGTCTCCTCCCAGGAGTCATTTGCAAGGTGGCCAGCATCCGTGTG   328
Knockout_cDNA_reverse     GTGGTCTCCAACAAGCGTCTCCTCCCAGGAGTCATTTGCAAGGTGGCCAGCATCCGTGTG   329
                          ************************************************************

NM_022290.2               GACACAGTAGAGGACTTTGCCTATGGAGCGGACATCCTCGTCAATCACCTAGACGAGACT   660
ORF                       GACACAGTAGAGGACTTTGCCTATGGAGCGGACATCCTCGTCAATCACCTAGACGAGACT   390
Knockout_cDNA_forward     GACACAGTAGAGGACTTTGCCTATGGAGCGGACATCCTCGTCAATCACCTAGACGAGACT   388
Knockout_cDNA_reverse     GACACAGTAGAGGACTTTGCCTATGGAGCGGACATCCTCGTCAATCACCTAGACGAGACT   389
                          ************************************************************

NM_022290.2               CTCAAGAAGAAGTCCTTGCTCAATGAGGAGGTGGCACGCAGAGCAGAGCAGCAGTTGGGG   720
ORF                       CTCAAGAAGAAGTCCTTGCTCAATGAGGAGGTGGCACGCAGAGCAGAGCAGCAGTTGGGG   450
Knockout_cDNA_forward     CTCAAGAAGAAGTCCTTGCTCAATGAGGAGGTGGCACGCAGAGCAGAGCAGCAGTTGGGG   448
Knockout_cDNA_reverse     CTCAAGAAGAAGTCCTTGCTCAATGAGGAGGTGGCACGCAGAGCAGAGCAGCAGTTGGGG   449
                          ************************************************************

NM_022290.2               CTGACCCCCTACAGCCTACTGTGGAACAACTGCGAACACTTTGTGACCTACTGCAGATAC   780
ORF                       CTGACCCCCTACAGCCTACTGTGGAACAACTGCGAACACTTTGTGACCTACTGCAGATAC   510
Knockout_cDNA_forward     CTGACCCCCTACAGCCTACTGTGGAACAACTGCGAACACTTTGTGACCTACTGCAGATAC   508
Knockout_cDNA_reverse     CTGACCCCCTACAGCCTACTGTGG-----------------------------------   473
                          *************************

NM_022290.2               GGCTCTCCTATCAGTCCGCAGGCTGAGAAGTTTCACGAGACTGTGAAGATACTCATTCGT   840
ORF                       GGCTCTCCTATCAGTCCGCAGGCTGAGAAGTTTCACGAGACTGTGAAGATACTCATTCGT   570
Knockout_cDNA_forward     GGCTCTCCTATCAGTCCGCAGGCTGAGAAGTTTCACGAGACTGA----------------   552
Knockout_cDNA_reverse     ------------------------------------------------------------   473
```

Alignment of the wildtype human and rat Lrat ORF nucleotide sequences

```
LRAT_human      ATGAAGAACCCCATGCTGGAGGTGGTGTCTTTACTACTGGAGAAGCTGCTCCTCATCTCC      60
Lrat_rat        ATGAAGAACTCAATGCTGGAGGCTGCGTCCCTCCTTCTGGAGAAGCTGCTCCTTATTTCC      60
                ********* * **********  * ***  * ** ***************** ** ***

LRAT_human      AACTTCACGCTCTTTAGTTCGGGCGCCGCGGGCGAAGACAAAGGGAGGAACAGTTTTTAT      120
Lrat_rat        AACTTCAAGATCTTTAGCGTGTGCGCCCCGGGAGGAGGCACAGGGAAGAAACATCCCTAT      120
                ******* * *******   * ***** **** * ** ** ***** ***   *   ***

LRAT_human      GAAACCAGCTCTTTCCACCGAGGCGACGTGCTGGAGGTGCCCCGGACCCACCTGACCCAC      180
Lrat_rat        GAAATCAACTCTTTTCTCCGGGGTGACGTGTTGGAAGTGTCACGGACCCATTTTACCCAC      180
                **** ** ****** * *** ** ****** **** *** * ********  * ******

LRAT_human      TATGGCATCTACCTAGGAGACAACCGTGTTGCCCACATGATGCCCGACATCCTGTTGGCC      240
Lrat_rat        TATGGGATCTACCTGGGGGACAACCGTGTCGCCCATCTAATGCCTGACATCCTGTTGGCC      240
                ***** ******** ** *********** *****  * ***** ***************

LRAT_human      CTGACAGACGACATGGGGCGCACGCAGAAGGTGGTCTCCAACAAGCGTCTCATCCTGGGC      300
Lrat_rat        CTGACCAGTGACAAGGAACGCACTCAGAAGGTGGTCTCCAACAAGCGTCTCCTCCCAGGA      300
                *****    **** **  ***** ***************************** ***  **

LRAT_human      GTTATTGTCAAAGTGGCCAGCATCCGCGTGGACACAGTGGAGGACTTCGCCTACGGAGCT      360
Lrat_rat        GTCATTTGCAAGGTGGCCAGCATCCGTGTGGACACAGTAGAGGACTTTGCCTATGGAGCG      360
                ** ***  *** ************** *********** ******** ***** *****

LRAT_human      AACATCCTGGTCAATCACCTGGACGAGTCCCTCCAGAAAAAGGCACTGCTCAACGAGGAG      420
Lrat_rat        GACATCCTCGTCAATCACCTAGACGAGACTCTCAAGAAGAAGTCCTTGCTCAATGAGGAG      420
                 ******* *********** ****** * *** **** *** *  ******* ******

LRAT_human      GTGGCGCGGAGGGCTGAAAAGCTGCTGGGCTTTACCCCCTACAGCCTGCTGTGGAACAAC      480
Lrat_rat        GTGGCACGCAGAGCAGAGCAGCAGTTGGGGCTGACCCCCTACAGCCTACTGTGGAACAAC      480
                ***** ** ** ** **  *** * ****  * ************** ************

LRAT_human      TGCGAGCACTTCGTGACCTACTGCAGATATGGCACCCCGATCAGTCCCCAGTCCGACAAG      540
Lrat_rat        TGCGAACACTTTGTGACCTACTGCAGATACGGCTCTCCTATCAGTCCGCAGGCTGAGAAG      540
                ***** ***** ****************** *** * ** ******** *** * ** ***

LRAT_human      TTTTGTGAGACTGTGAAGATAATTATTCGTGATCAGAGAAGTGTTCTTGCTTCAGCAGTC      600
Lrat_rat        TTTCACGAGACTGTGAAGATACTCATTCGTGATCAGAGAAGTTGTCTTGCTTCAGCTGTC      600
                ***   *************** * ******************  ************ ***

LRAT_human      TTGGGATTGGCGTCTATAGTCTGTACGGGCTTGGTATCATACACTACCCTTCCTGCAATT      660
Lrat_rat        TTGGGATTAGTGTCTATTATCTACACAGGCCTGGCATCATATATGACCCTTCCTGCAGTC      660
                ******** * ******  ***  ** *** *** ****** *  ************ *

LRAT_human      TTTATTCCATTCTTCCTATGGAT---GGCTGGCTAA                            693
Lrat_rat        TGCATCCCGTTCTGCTTGTGGATGATGTCTGGCTAG                            696
                *  ** ** **** * * *****   * ********
```

Alignment of the wildtype human and rat LRAT ORF amino acid sequences

```
*       = The same amino acid
:       = Indicates conservation between groups of strongly similar properties
.       = Indicates conservation between groups of weakly similar properties

LRAT_human      MKNPMLEVVSLLLEKLLLISNFTLFSSGAAGEDKGRNSFYETSSFHRGDVLEVPRTHLTH      60
Lrat_rat        MKNSMLEAASLLLEKLLLISNFKIFSVCAPGGGTGKKHPYEINSFLRGDVLEVSRTHFTH      60
                *** ***..**************.:**  * * ..*::  ** .** ******* ***:**

LRAT_human      YGIYLGDNRVAHMMPDILLALTDDMGRTQKVVSNKRLILGVIVKVASIRVDTVEDFAYGA      120
Lrat_rat        YGIYLGDNRVAHLMPDILLALTSDKERTQKVVSNKRLLPGVICKVASIRVDTVEDFAYGA      120
                ************:*********.*  ***********: *** *****************

LRAT_human      NILVNHLDESLQKKALLNEEVARRAEKLLGFTPYSLLWNNCEHFVTYCRYGTPISPQSDK      180
Lrat_rat        DILVNHLDETLKKKSLLNEEVARRAEQQLGLTPYSLLWNNCEHFVTYCRYGSPISPQAEK      180
                :********:*:**:***********: **:*******************:*****::*

LRAT_human      FCETVKIIIRDQRSVLASAVLGLASIVCTGLVSYTTLPAIFIPFFLWMAG-              230
Lrat_rat        FHETVKILIRDQRSCLASAVLGLVSIIYTGLASYMTLPAVCIPFCLWMMSG              231
                * *****:****** ********.**: ***.** ****: *** *** .
```

Alignment of the mutant human and rat LRAT ORF nucleotide sequences

```
LRAT_human      ATGAAGAACCCATGCTGGAGGTGGTGTCTTTACTACTGGAGAAGCTGCTCCTCATCTCCA      60
Lrat_rat        ATGAAGAACTCATGCTGGAGGCTGCGTCCCTCCTTCTGGAGAAGCTGCTCCTTATTTCCA      60
                ********* ***********  * ***  * ** ***************** ** ****

LRAT_human      ACTTCACGCTCTTTAGTTCGGGCGCCGCGGGCGAAGACAAAGGGAGGAACAGTTTTTATG      120
Lrat_rat        ACTTCAAGATCTTTAGCGTGTGCGCCCCGGGAGGAGGCACAGGGAAGAAACATCCCTATG      120
                ****** * *******   * ***** **** * ** ** ***** ***   *   ****

LRAT_human      AAACCAGCTCTTTCCACCGAGGCGACGTGCTGGAGGTGCCCCGGACCCACCTGA------      174
Lrat_rat        AAATCAACTCTTTTCTCCGGGGTGACGTGTTGGAAGTGTCACGGACCCATTTTACCCACT      180
                *** ** ****** * *** ** ****** **** *** * ********  * *

LRAT_human      ----------------------------------------                          174
Lrat_rat        ATGGGATCTACCTGGGGGACAACCGTGTCGCCCATCTAA                           219
```

Alignment of the mutant human and rat LRAT theoretic ORF amino acid sequences

```
*       = The same amino acid
:       = Indicates conservation between groups of strongly similar properties
.       = Indicates conservation between groups of weakly similar properties

LRAT_human       MKNPCWRWCLYYWRSCSSSPTSRSLVRAPRAKTKGGTVFMKPALSTEATCWRCPGPT---      57
LRAT_rat         MKNSCWRLRPSFWRSCSLFPTSRSLACAPREEAQGRNIPMKSTLFSGVTCWKCHGPILPT      60
                 *** ***    :*****  ******. *** :::* .: ** :* : .***:* **

LRAT_human       ------------                                                      57
LRAT_rat         MGSTWGTTVSPI                                                      72
```

Supplementary data — Chapter 4

Sodium-Iodate Injection Can Replicate Retinal Degenerative Disease Stages in Pigmented Mice and Rats: Non-Invasive Follow-Up Using OCT and ERG

Supplementary Table S1. An overview of the experimental groups.

Species	Strain	Number of animals	Treatment
Mouse	C57BL/6J	4	0.9% NaCl
		4	10 mg/kg
		4	20 mg/kg
		4	30 mg/kg
		4	40 mg/kg
		4	50 mg/kg
		4	70 mg/kg
Rat	Brown Norway	4	0.9% NaCl
		4	10 mg/kg
		4	20 mg/kg
		4	30 mg/kg
		4	50 mg/kg
		2	70 mg/kg

Supplementary Table S2. An overview of the settings for electroretinography measurements.

Intensity (cd/m²)	Averaged	Interval (Hz)
0.0003	20	0.2
0.003	18	0.125
0.03	14	9 (Flicker)
0.3	15	0.077
3	12	0.067
10	8	0.05
30	8	0.05

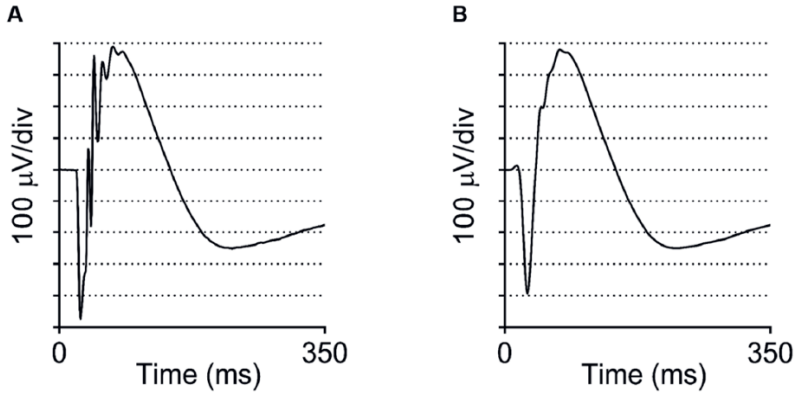

Supplementary Figure S1. An example of an ERG trace before (**A**) and after (**B**) data filtering is shown. The trace belongs to an untreated Brown Norway rat from which the ERG is measured at 30 cd·s/m^2. The oscillatory potentials are filtered out to determine the latencies of the a- and b-wave (in **B**). Subsequently, the latencies are used to determine the values of the amplitudes in the unfiltered data (**A**).

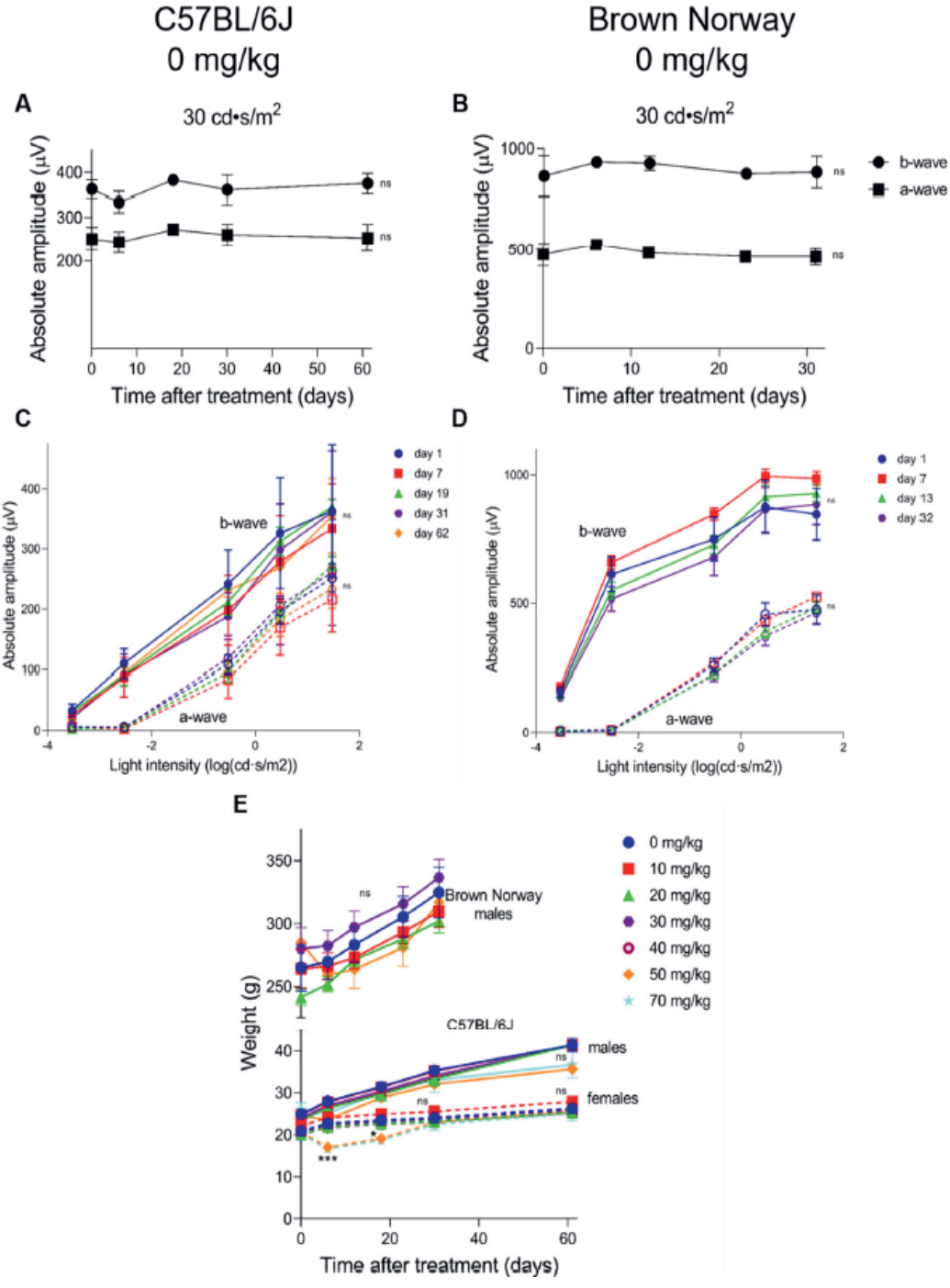
C57BL/6J
0 mg/kg
Brown Norway
0 mg/kg
A
30 cd•s/m2
Absolute amplitude (µV)
Time after treatment (days)
ns
B
30 cd•s/m2
b-wave
a-wave
C
b-wave
a-wave
day 1
day 7
day 19
day 31
day 62
Light intensity (log(cd·s/m2))
D
day 1
day 7
day 13
day 32
E
Brown Norway
males
C57BL/6J
males
females
Weight (g)
0 mg/kg
10 mg/kg
20 mg/kg
30 mg/kg
40 mg/kg
50 mg/kg
70 mg/kg

Supplementary Figure S2. The absolute values for the a- and b-wave amplitudes at the highest light intensity (30 cd·s/m^2) over time (**A** and **B**) and versus the light intensities (**C** and **D**) are shown for both mice (**A** and **C**) and rats (**B** and **D**) (n = 4 per group). No significant differences can be observed over time within the control groups (0 mg/kg SI) for both species. In **E**, the weight progression of both rats and mice is shown. Within the group of mice, a significant drop in weight progression is seen for the highest doses (50 and 70 mg/kg). At 3 weeks post-injection, no difference can be observed between all groups of mice. For the rats, there is no significant difference in weight progression visible. However, the 70 mg/kg group (n = 2) was excluded from the study since they lost >20% of their weight within 3 days post-injection, reaching a humane endpoint. All data points are plotted with standard deviations (although not always visible in the graph). If not visible, it means that their value is not larger than the symbol that is used in the graph. *ns*: not significant.

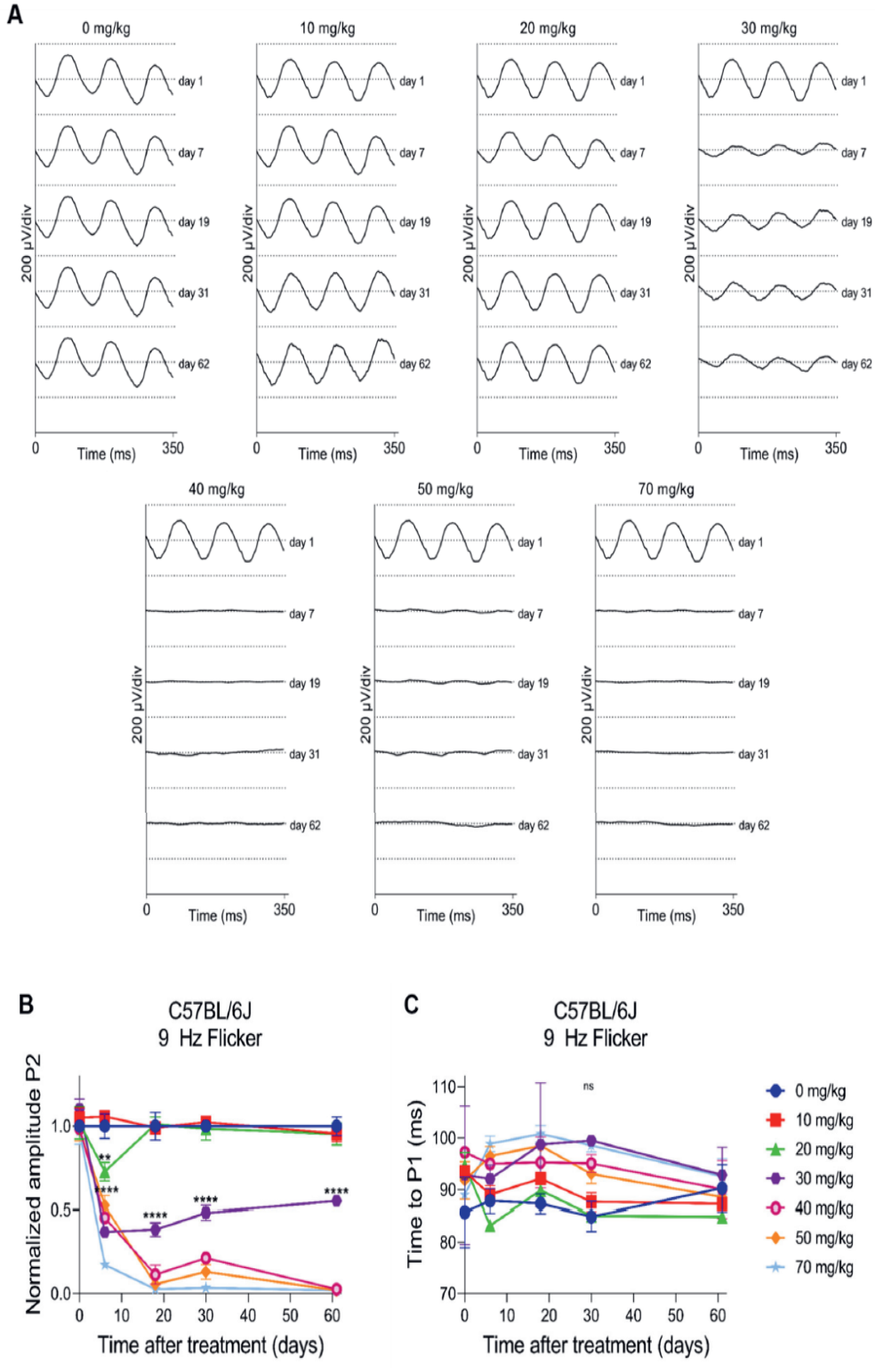
A
0 mg/kg
10 mg/kg
20 mg/kg
30 mg/kg
40 mg/kg
50 mg/kg
70 mg/kg
day 1
day 7
day 19
day 31
day 62
200 µV/div
0
Time (ms)
350
B
C57BL/6J
9 Hz Flicker
Normalized amplitude P2
Time after treatment (days)
C
C57BL/6J
9 Hz Flicker
Time to P1 (ms)
ns
Time after treatment (days)
0 mg/kg
10 mg/kg
20 mg/kg
30 mg/kg
40 mg/kg
50 mg/kg
70 mg/kg

Supplementary Figure S3. ERG Flicker data (9 Hz) is shown for C57BL/6J mice (n = 4 per group). From the traces (**A**), it is clear that by eye, there is no clear difference between the 10 mg/kg group and the control group (0 mg/kg). A slight effect of SI-treatment is seen for the 20 mg/kg group after a week. However, this effect is gone after two weeks. Moderate effects of SI-treatment are seen for the 30 mg/kg group already within a week post-injection. This effect seems stable over time. The tremendous impact is seen for the higher doses (40, 50 and 70 mg/kg). Flicker responses are (almost) completely absent already within a week after injection. These observations were confirmed by quantifying the data (**B** and **C**): No significant differences were observed between the 10 mg/kg group and the control group. A significant drop in P2 amplitude was observed for the 20 mg/kg group. A quick and moderate effect is seen for the 30 mg/kg group, with no significant difference between the last two time points. The higher doses (40, 50 and 70 mg/kg) cause an immediate and tremendous effect with hardly any measurable activity from 20 days post-injection onwards. No significant differences were observed for the time to P1 between all treatment groups. *ns*: not significant, **: $p \leq 0.01$, and ****: $p \leq 0.0001$.

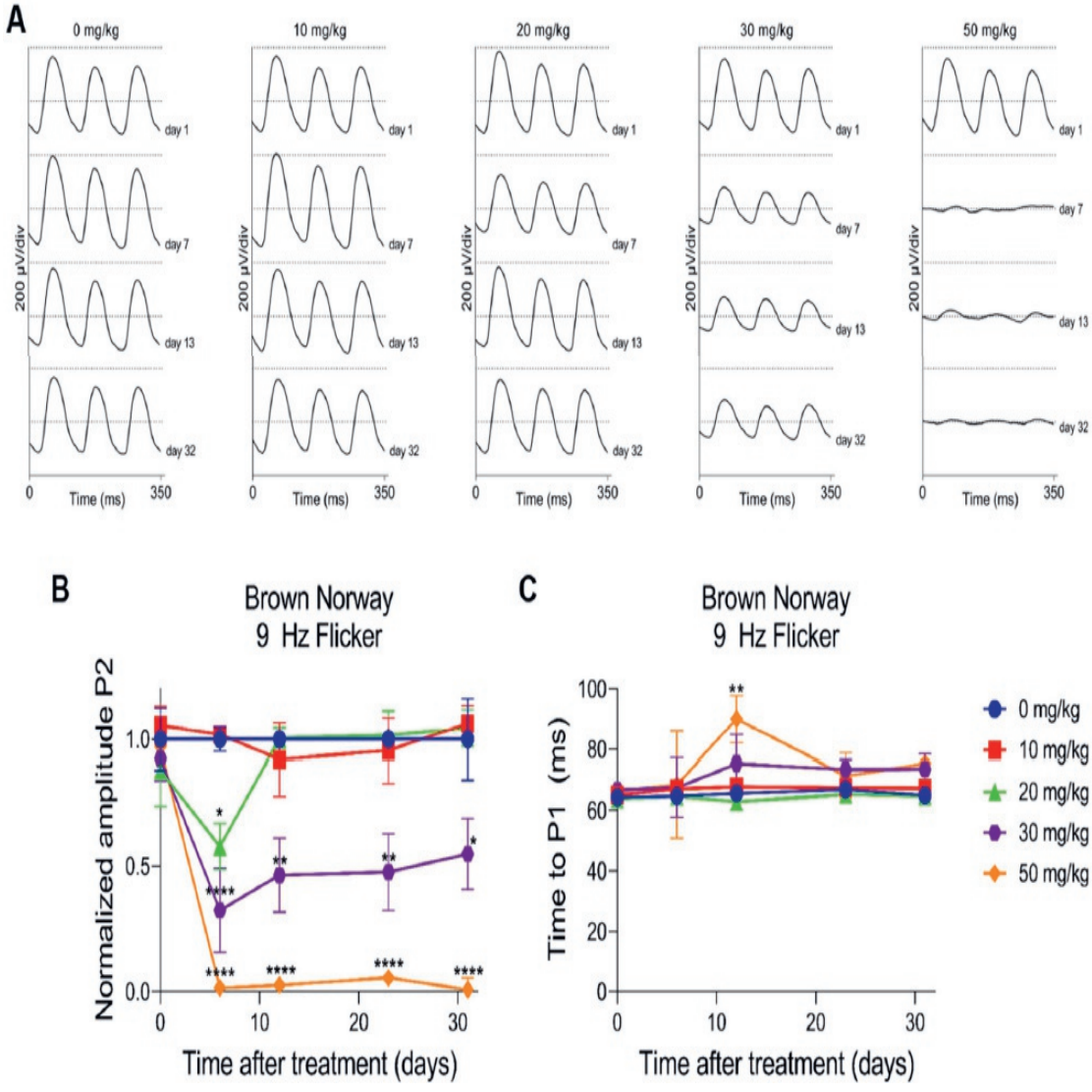
A
0 mg/kg
10 mg/kg
20 mg/kg
30 mg/kg
50 mg/kg
day 1
day 7
day 13
day 32
200 µV/div
0
Time (ms)
350
B
Brown Norway
9 Hz Flicker
Normalized amplitude P2
1.0
0.5
0.0
0
10
20
30
Time after treatment (days)
C
Brown Norway
9 Hz Flicker
Time to P1 (ms)
100
80
60
40
20
0
Time after treatment (days)
0 mg/kg
10 mg/kg
20 mg/kg
30 mg/kg
50 mg/kg

Supplementary Figure S4. ERG Flicker data (9 Hz) is shown for Brown Norway rats (n = 4 per group). From the traces (**A**), it is clear that by eye, there is no clear difference between the 10 mg/kg group and the control group (0 mg/kg). A slight effect of SI-treatment is seen for the 20 mg/kg group after a week. However, this effect is gone after two weeks. Moderate effects of SI-treatment are seen for the 30 mg/kg group already within a week post-injection. This effect seems stable over time. The tremendous impact is seen for the higher dose (50 mg/kg). Flicker responses are (almost) completely absent already within a week after injection. These observations were confirmed by quantifying the data (**B** and **C**): No significant differences were observed between the 10 mg/kg group and the control group. A significant drop in P2 amplitude was observed for the 20 mg/kg group. A quick and moderate effect is seen for the 30 mg/kg group, with no significant difference between the last three time points. The higher dose (50 mg/kg) causes an immediate and tremendous effect with hardly any measurable activity from already 7 days post-injection onwards. A significant difference was observed for the time to P1 between the 50 mg/kg group and the control group. However, it is debatable whether this parameter could be observed properly within this dataset. No other significant differences could be observed between the other groups. *ns*: not significant, *: $p \leq 0.05$, **: $p \leq 0.01$, and ****: $p \leq 0.0001$.

Supplementary data — Chapter 5

Bioprinted 3D Outer Retina Barrier Uncovers RPE-dependent Choroidal Phenotype in Advanced Macular Degeneration

Supplementary Table 1. Media treatment schedule for maintenance of 3D-oBRB.

Day(s)	Basal Conditions	Apical Conditions
1	Printing Medium	Printing Medium
2-7	VDM	VDM
8-14	VGM+AP	RPE-MM + AP
15-21	VGM	RPE-MM
22-29	VGM	RPE-MM + Prostaglandin E2
29-Fixation	VMM	RPE-MM + Prostaglandin E2

Supplementary Table 2. Libraries generated for single cell RNA-seq.

Library ID	Library Concentration (ng/ul)	Library Average Size (bp)	Sequence Modality(e.g. PE50-6-50)	Tube Label	Sample ID*	Sample Barcode Index1: I7 Sequence
IS0011	2nM	*455*	(PE) 26-8-98mer	2D iEndo	CT_3878_S1	SI-GA-A6
IS0011	2nM	*479*	(PE) 26-8-98mer	2D iRPE	CT_3878_S2	SI-GA-B6
IS0011	2nM	*454*	(PE) 26-8-98mer	3D iEndo	CT_3878_S3	SI-GA-C6
IS016	2nM	*508*	(PE) 26-8-98mer	3D iRPE		SI-GA-F7

Supplementary Table 3. Significant genes relevant to vascular maturation. p****<0.0001. Data depicts results from n = 5369 cells (2D iECs), and n = 1294 cells (3D-oBRB iECs).

Partially-Mature (PM)	
Gene	**Average LogFC**
TTR****	3.293097084
PTGDS****	2.91023027
SERPINF1****	2.746884668
PMEL****	2.728151531
TYRP1****	2.473397492
SLC2A1****	2.447382476
RBP1****	2.277384475
DCT****	2.266739064
APOE****	2.191424756
ELN****	2.184219482
CDKN1C****	2.184180543
GPNMB****	2.155826338
FRZB****	2.036587593
TIMP3****	2.020232723
NPC2****	1.971437309
NEAT1****	1.877960021
TRPM3****	1.868956372
RPS4Y1****	1.748429142
SFRP1****	1.71339181
MIF****	1.626987544
FOS****	1.61485332
VEGFA****	1.604315395
CRYAB****	1.596007132
NDUFA4L2****	1.584758503
EGR1****	1.583968974
CST3****	1.583860234
SCD****	1.576730172
KCNQ1OT1****	1.569869951
AKAP12****	-1.509372337
TUBB4B****	-1.516117864
LGALS1****	-1.524191678
TUBB6****	-1.535855664
SMS****	-1.564620788
GNG11****	-1.573524516
JPT1****	-1.578619298
ECSCR****	-1.610296939
TPM1****	-1.705061753
CAV1****	-1.720755414
CLIC1****	-1.806758255
MT1E****	-1.829130034
ARHGDIB****	-1.833353979
S100A16****	-1.854543401
SRGN****	-1.855853186
SERPINE1****	-2.011057296
TUBA1B****	-2.085073696
MT2A****	-2.165154694
HMGA1****	-2.202244352
MMP1****	-2.466878261

Fully-Mature (FM)	
Gene	**Average LogFC**
IGFBP3****	2.839701836
ESM1****	2.603010821
IGF2****	2.598543141
INSR****	2.394917281
HLA-B****	2.255402078
TCF4****	2.052826873
CD93****	2.036025929
PECAM1****	1.99525718
ACKR3****	1.990773556
PLVAP****	1.970377307
NEAT1****	1.965910456
SPRY1****	1.962680299
ANGPT2****	1.961169986
RGCC****	1.929979405
HSPG2****	1.871711824
COL4A1****	1.851158264
TP53I11****	1.834864472
RFLNB****	1.820297661
CXCR4****	1.812145964
CD34****	1.811398119
SPARC****	1.763536864
DEPP1****	1.746571776
PXDN****	1.745320416
UNC5B****	1.703681255
FLT1****	1.662451028
B2M****	1.655103184
COL4A2****	1.63152531
ADGRF5****	1.620363791
GJA1****	1.588797246
SPP1****	1.559651451
ANXA2****	-1.532336179
TUBA1B****	-1.76975269
MMP1****	-1.885111478
MT1E****	-2.016514401
MT2A****	-2.294959755
HMGA1****	-2.481583463

Inflamed (Inf)	
Gene	**Average LogFC**
COL3A1****	3.790343782
IGFBP5****	3.767910699
COL1A2****	3.456215894
MGP****	3.436031728
STATH****	3.376360389
COL1A1****	3.35150075
TIMP1****	3.271068336
STC1****	2.761122651
COL6A2****	2.651220963
SAA1****	2.634649398
SERPINE2****	2.597995887
COL6A1****	2.573399435
AREG****	2.445094854
COL6A3****	2.305247798
DCN****	2.254222597
FN1****	2.220866953
IGF2****	2.062980648
TFPI2****	1.856624892
PLAC9****	1.830906964
LUM****	1.806349544
NDUFA4L2****	1.791817577
LOX****	1.785051044
CXCL2****	1.741603755
TGM2****	1.731212221
PDGFRB****	1.730017382
CXCL1****	1.707399258
MEG3****	1.706864124
PLAT****	1.696673351
SAA2****	1.675952576
CXCL8****	1.661135865
SPARC****	1.655768294
PAPPA****	1.637425773
EGR1****	1.628629962
FDCSP****	1.57565212
FOS****	1.574482144
F3****	1.529745697
COL5A2****	1.502431491
ARHGDIB****	-1.500379729
STMN1****	-1.526635755
SMS****	-1.555392149
TPM1****	-1.594545485
ECSCR****	-1.59696695
JPT1****	-1.607577918
S100A16****	-1.755430391
TUBA1B****	-1.910956266
MMP1****	-2.286670634
HMGA1****	-2.461526253

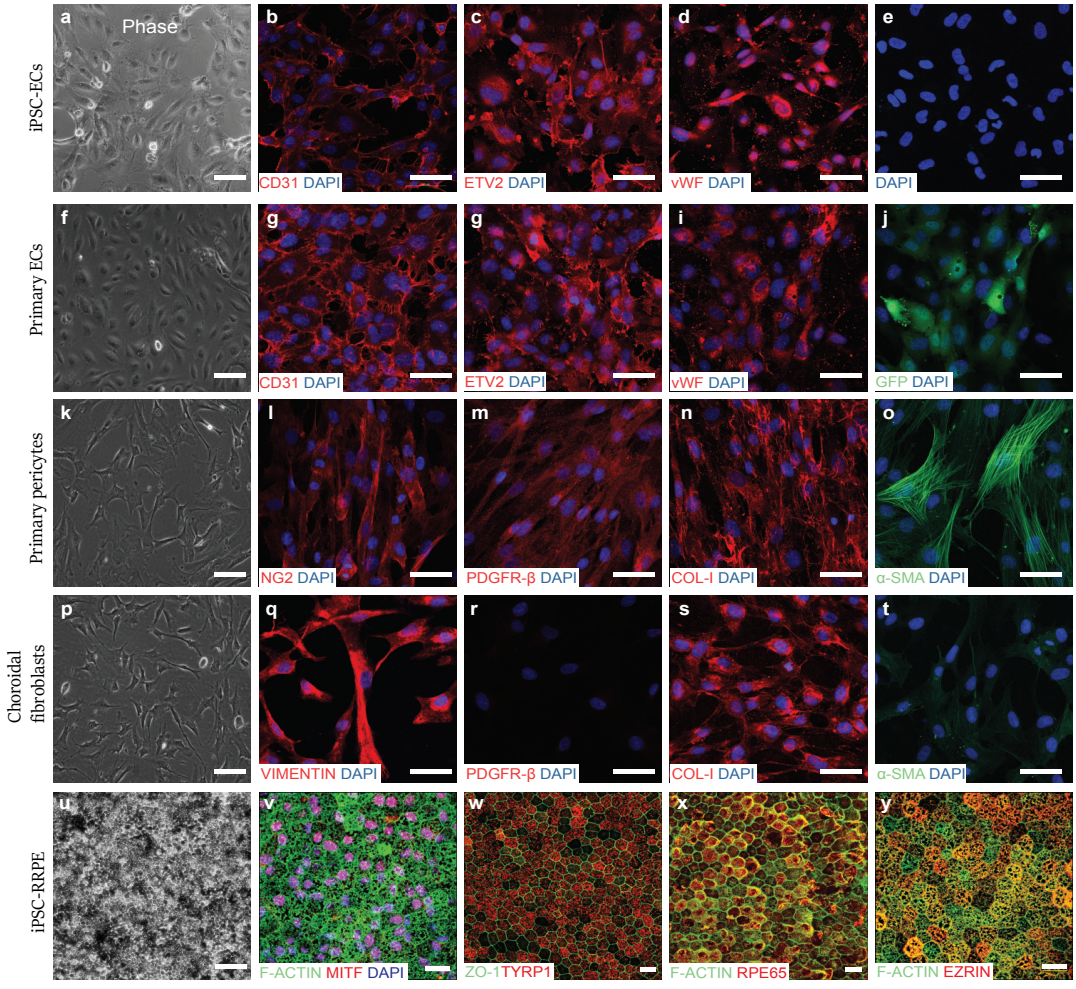

Supplementary Figure 1. Representative images of iPSC-derived endothelial cells (iECs), primary endothelial cells (EC), retinal pericyte, choroid fibroblast, and iRPE. **A-J**: phase contrast images of iECs (**A**) (n = 5) and primary ECs (**F**) (n = 4). Immunostaining for iEC and GFP+ primary ECs with CD31 (**B**,**G**) (n = 3), ETV2 (**C**, **H**) (n = 3), vWF (**D**,**I**) (n = 3). GFP expression in primary ECs (**J**) (n = 4). DAPI (**B-E**, **G-J**). **K-O**: phase contrast image of primary pericytes (**K**) (n = 5). Immunostaining of primary pericytes with NG2 (**L**), PDGFR-β (**M**), COL-1 (**N**), and α-SMA (**O**) (**L-O** n = 3). DAPI (**L-O**). **P-T**: phase contrast image of choroidal fibroblasts (**P**) (n = 5). Immunostaning of choroidal fibroblasts with VIMENTIN (**Q**), lacking PDGFR-β expression (**R**), and positive expression for COL-1 (**S**) and lacking α-SMA (**T**) (**Q-T** n = 3). DAPI (**Q-T**). **U-Y**: phase contrast image of iPSC-derived RPE (iRPE) cells (**U**). Immunostaining of iRPE cells with MITF (red) F-ACTIN (green) (**V**), ZO-1 (green) and TYRP1 (red) (**W**), F-ACTIN (green) and RPE65 (red) (**X**), and F-ACTIN green and Ezrin (red) (**Y**). DAPI (**V-Y**). Scale bars, 50 μm.

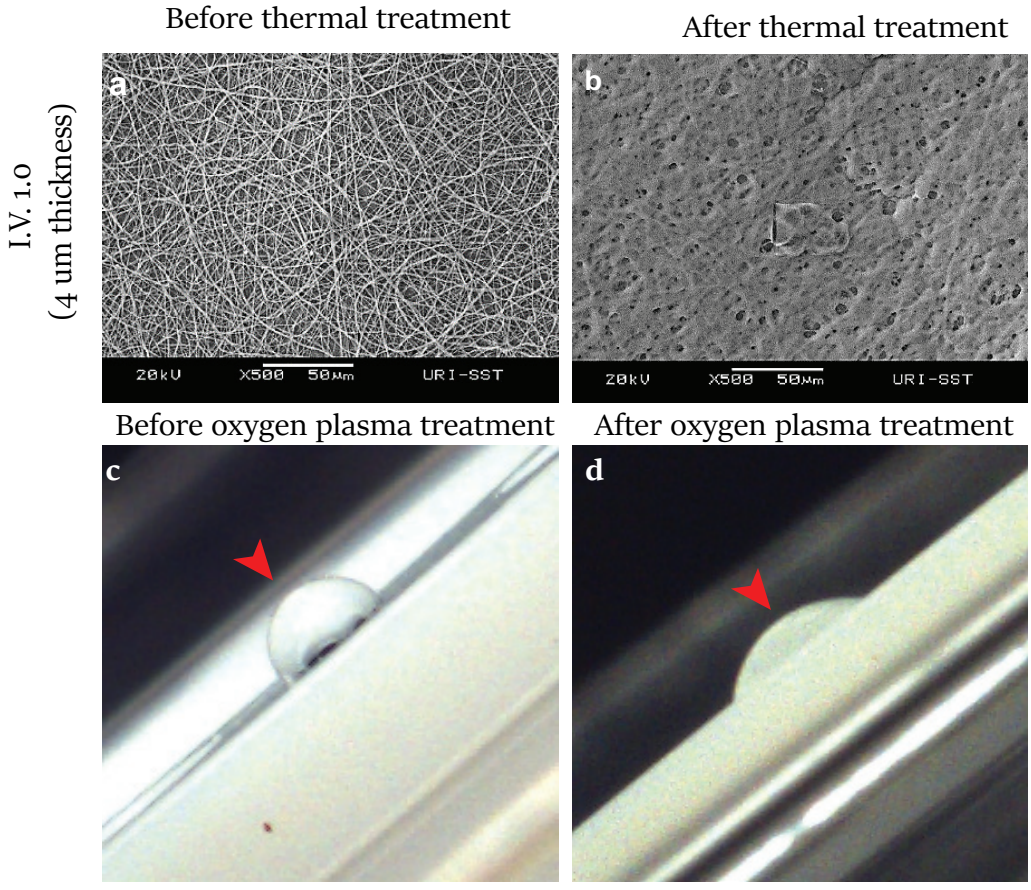

Supplementary Figure 2. Scaffold preparation for bioprinting.

A,**B**: microstructure of PLGA electrospun scaffolds without or with heat treatment **C**,**D**: oxygen-plasma treatment-induced hydrophilicity on Teflon. Red arrowheads mark water droplet before and after the treatment. Scale bars, 50 µm.

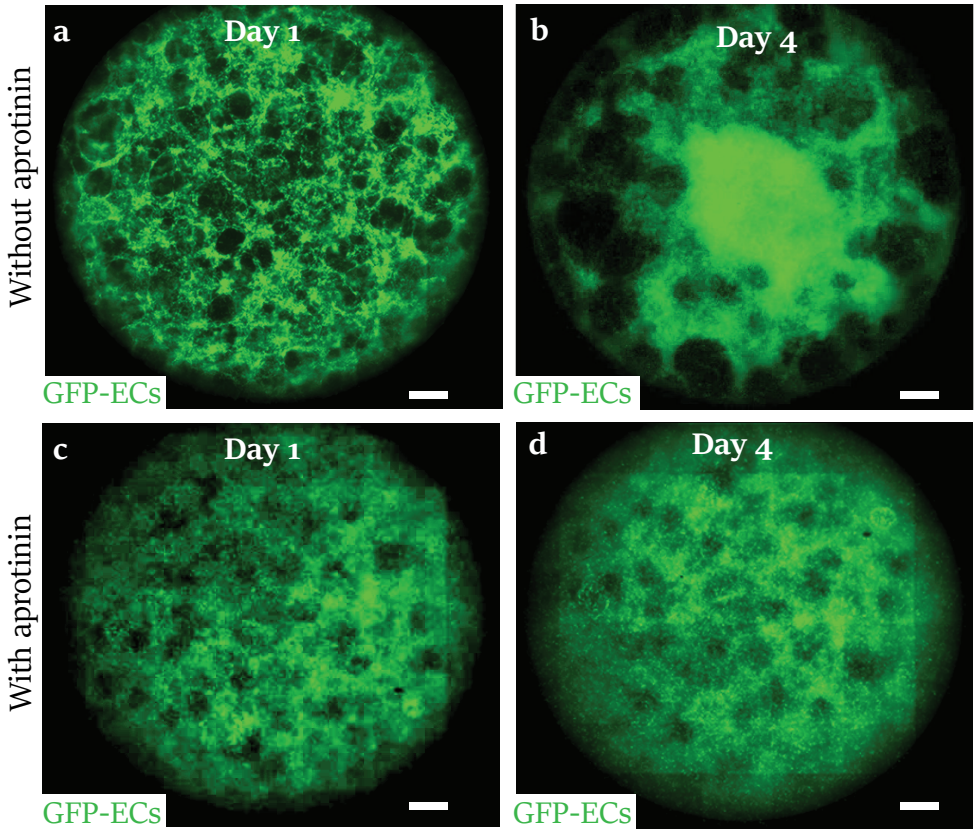

Supplementary Figure 3. Aprotinin stabilizes 3D vasculature. GFP positive endothelial cells were embedded in fibrin gels consisting of 2.5 mg/ml of FIBRINOGEN and 0.5 U/ml of THROMBIN. Cultures were incubated with or without aprotinin. Images represent entire well area in a 24 well plate. Images were taken at day 1 (**A**,**C**) and day 4 (**B**,**D**).
Scale bars, 2 mm.

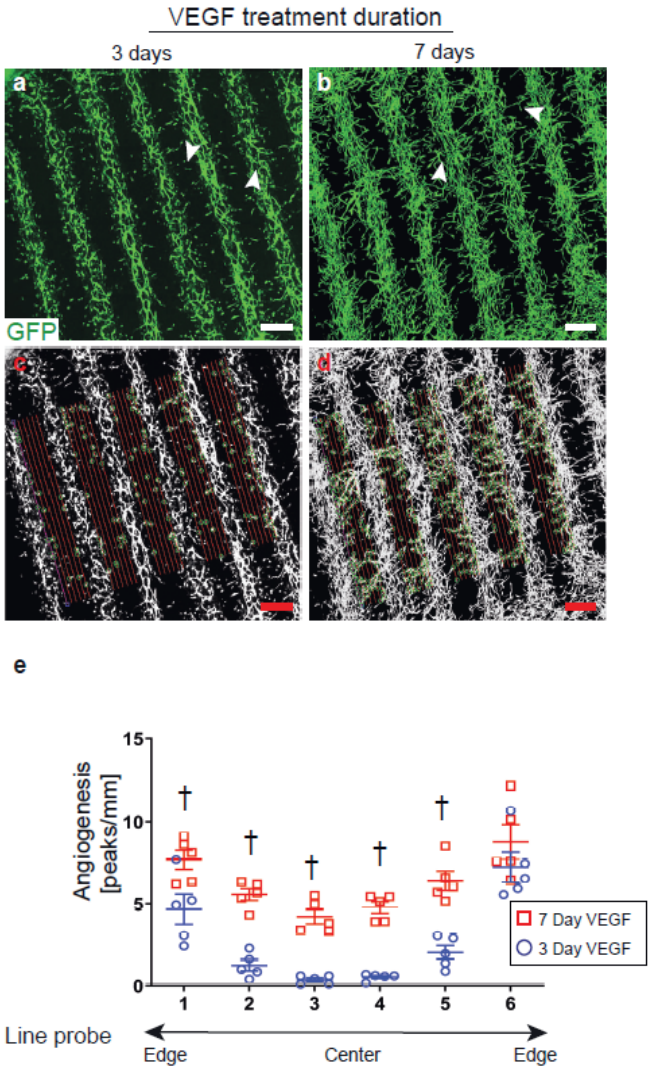

Supplementary Figure 4. VEGF promotes angiogenesis printed tissue. **A**,**B**: GFP positive ECs showing angiogenesis with 3 days (**A**) or 7 days (**B**) days of VEGF (85 ng/mL) treatment. Arrow heads mark ECs derived capillaries expanding from the printed structure. Scale bars, 500 µm. **C-E**, Image quantification of angiogenesis. Fluorescence intensity is measured along six red line probes between printed stripes. Statistical significance was attributed to values of p <0.05 as determined by two-way ANOVA and Sidak's multiple comparison test. †p <0.05, (n = 5), error bars indicate STE.

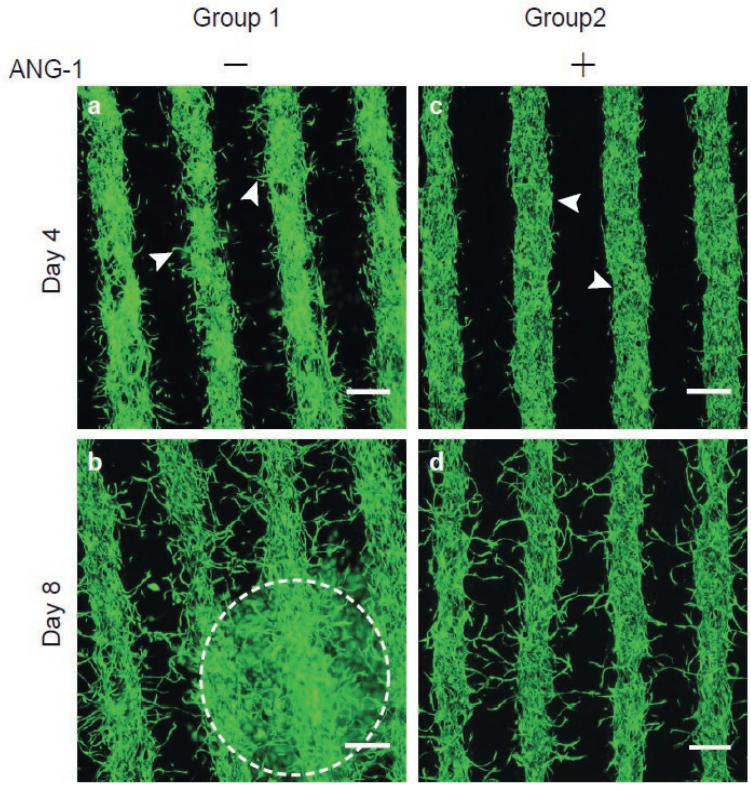

Supplementary Figure 5. Angiopoietin-1 reduces EC migration. **A-D**: vascular development for 8 days with ANG-1 (100 ng/ml) treatment. Arrow heads mark branching out capillaries sprouting from the printed structure. Dotted-circle markes single cell migration. Scale bars, 500 μm. n = 3.

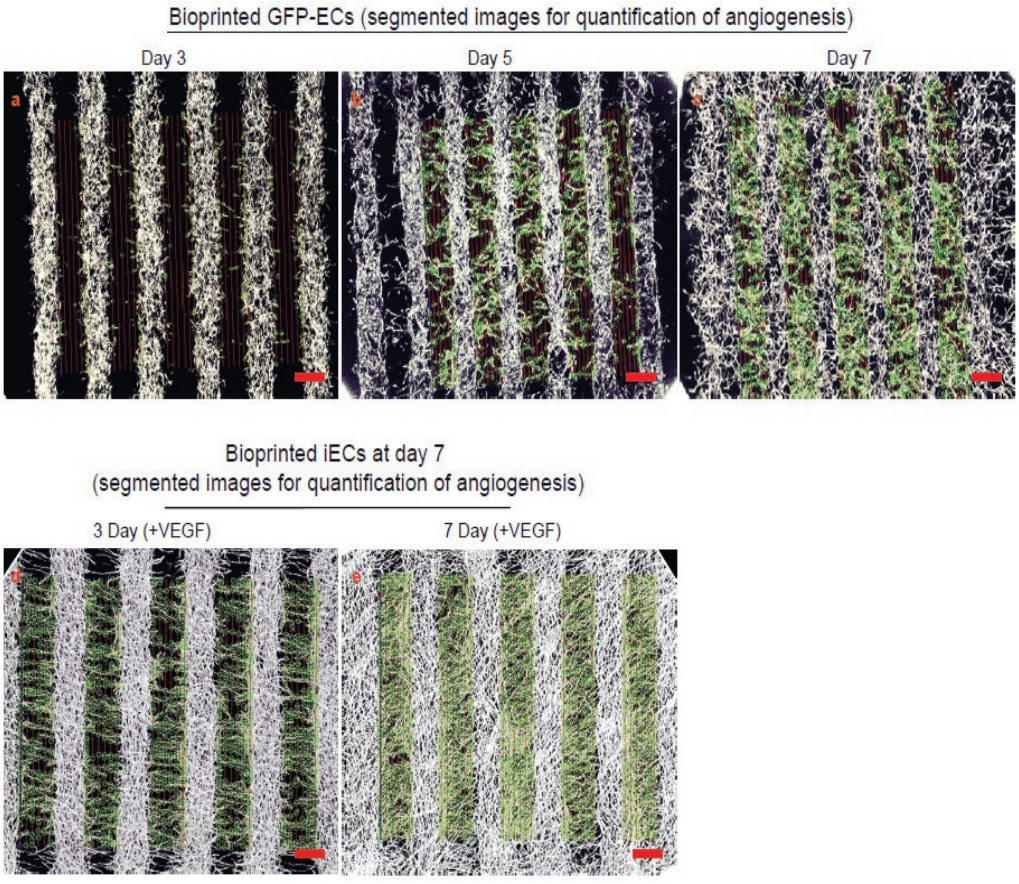

Supplementary Figure 6. Angiogenesis quantification. **A-E**: fluorescence intensity is measured along six red line probes between printed stripes from day 3 to 7 of angiogenesis (A-C) and with 3 or 7 days of VEGF treatment (**D**, **E**). **A-C**: n =5. **D**,**E**: n =4. Line probes (red; 100 μm apart) were placed in each gap between stripes of the printed geometry. Each line probe detects number of peaks of GFP intensity above a threshold. Line 1 and 6, 2 and 5, 3 and 4 mark edges, intermediate, and center of each gap, respectively. Scale bars, 500 μm.

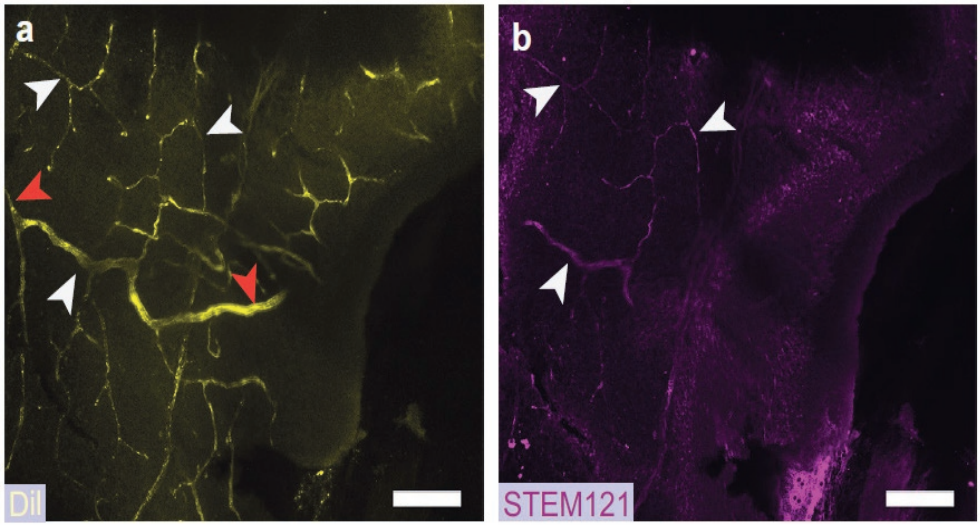

Supplementary Figure 7. A,**B**: DiI (yellow) signal marks rat capillaries and immunostaining for STEM121 (magenta) detects human capillaries integrated with rat capillaries.

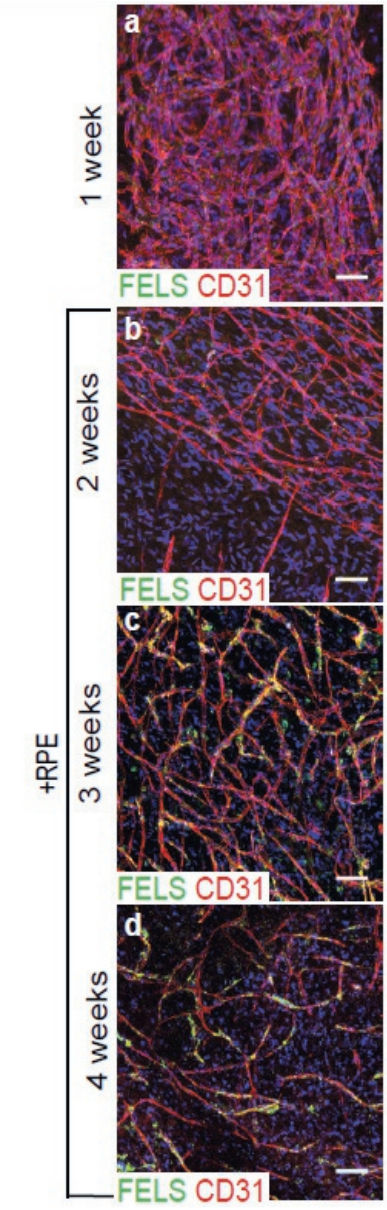

Supplementary Figure 8. Time course of fenestration marker expression in 3D-oBRB. **A-D**: 3D vascular growth within tissues fixed at week 1 (**A**), week 2 (**B**), week 3 (**C**), and week 4 (**D**). Tissues were immunostained with FELS (green) and CD31 (red).
Scale bars, 50 μm. n = 3.

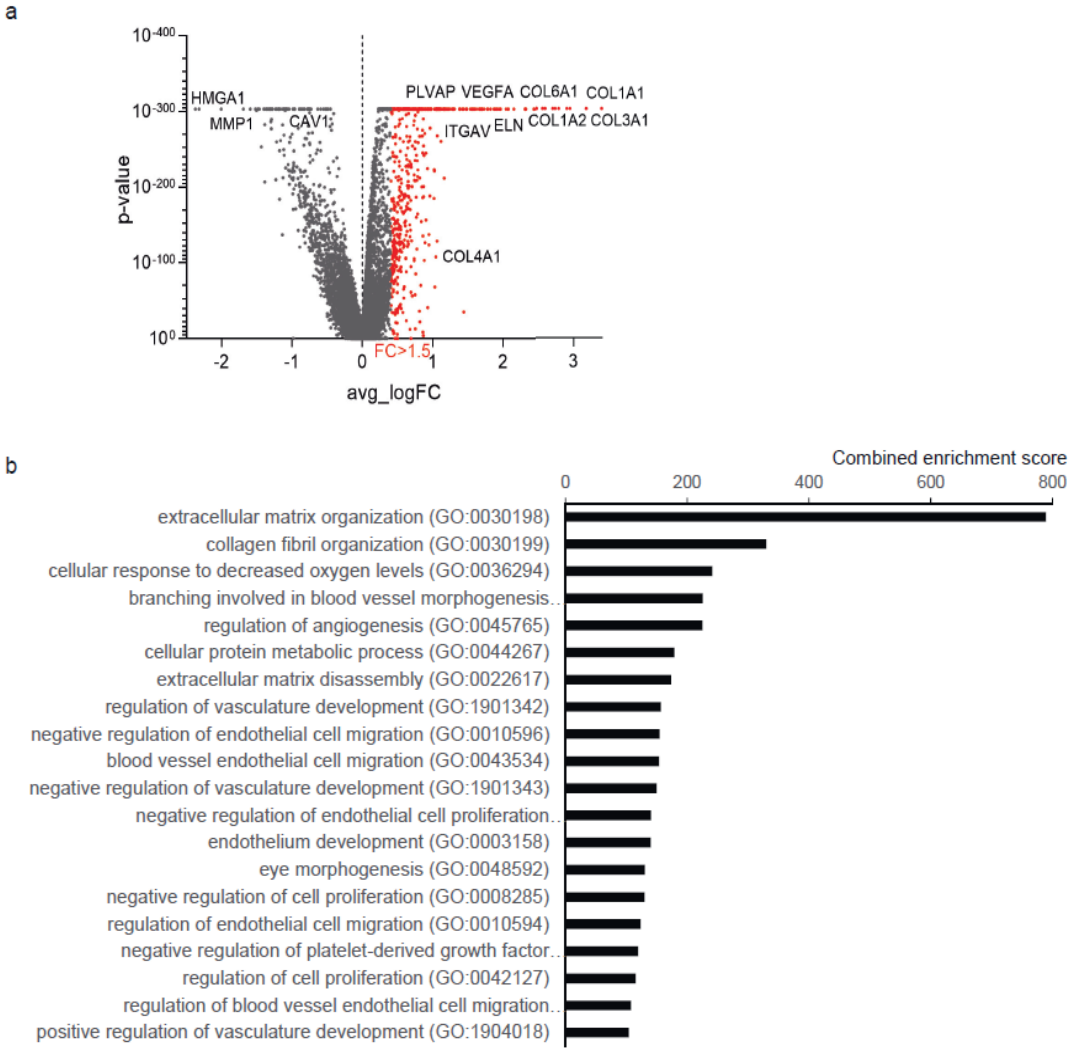

Supplementary Figure 9. Comparative analysis of gene expression between 2D-iECs and iECs from 3D-oBRB. **A**: volcano plot of 21,792 genes. Red dots indicate genes that demonstrated greater than 1.5 log-fold change (531 genes) from 2D monoculture. **B**: Relevant Gene Ontology Biological Process categories (scores>100) using 531 genes (FC>1.5) by Enrichr[20]. Data depicts results from n = 5369 cells (2D iECs), and n = 1294 cells (3D-oBRB iECs).

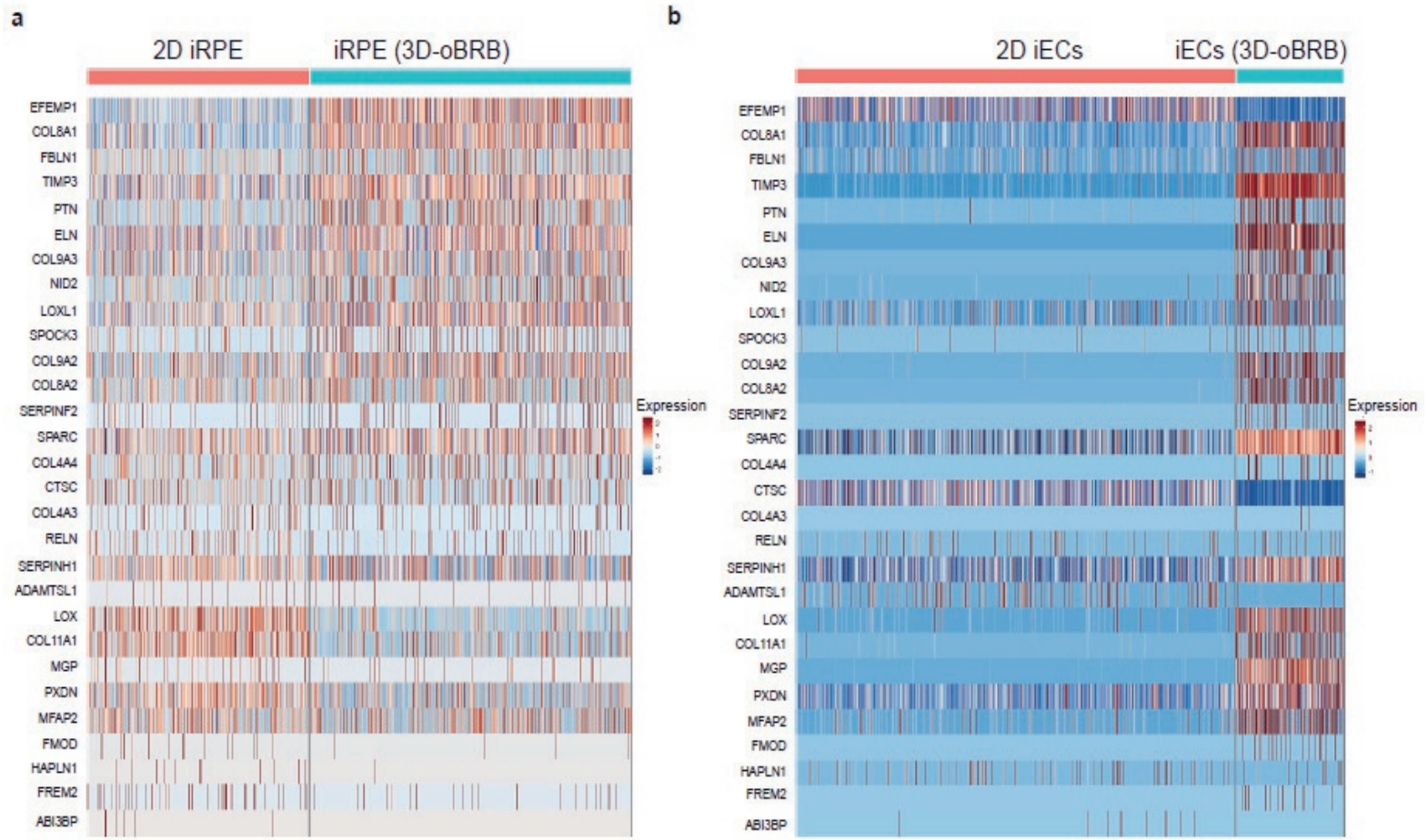

Supplementary Figure 10

Supplementary Figure 10. ECM related gene expressions in iEC and iRPE in 2D and in 3D-oBRB. **A**: ECM gene expression comparisons between 2D iRPE and iRPE in 3D-oBRB. Average log fold change and significance calculations performed between RPE monocultures and oBRB performed using the Seurat gene analysis package. **B**: ECM gene expression comparisons between 2D iECs and iECs from 3D-oBRB. Average log fold change and significance (p <0.05) calculations performed between 2D iECs and 3D-oBRB performed using the Seurat gene analysis package. Data depicts results from n = 3012 cells (2D RPE), n = 4380 cells (3D-oBRB RPE), n = 5369 cells (2D iECs), and n = 1294 cells (3D-oBRB iECs).

a

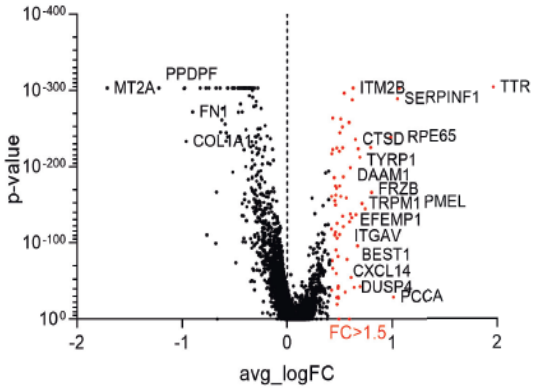

b

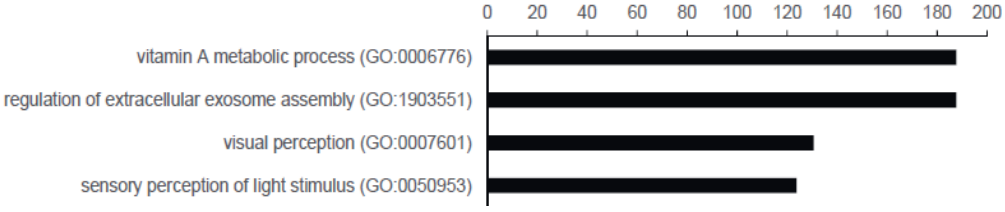

Supplementary Figure 11. Comparative analysis of genes significantly different between 2D iRPE and iRPE cells from 3D-oBRB. **A**: volcano plot of 21,321 genes. Red dots indicate genes greater than 1.5 log-fold changes (69 genes) in iRPE from 3D-oBRB as compared to 2D-iRPE. **B**: Relevant Gene Ontology Biological Process categories (scores>100) using 69 genes (FC>1.5) by Enrichr[20]. Data depicts results from n = 3012 cells (2D RPE), n = 4380 cells (3D-oBRB RPE).

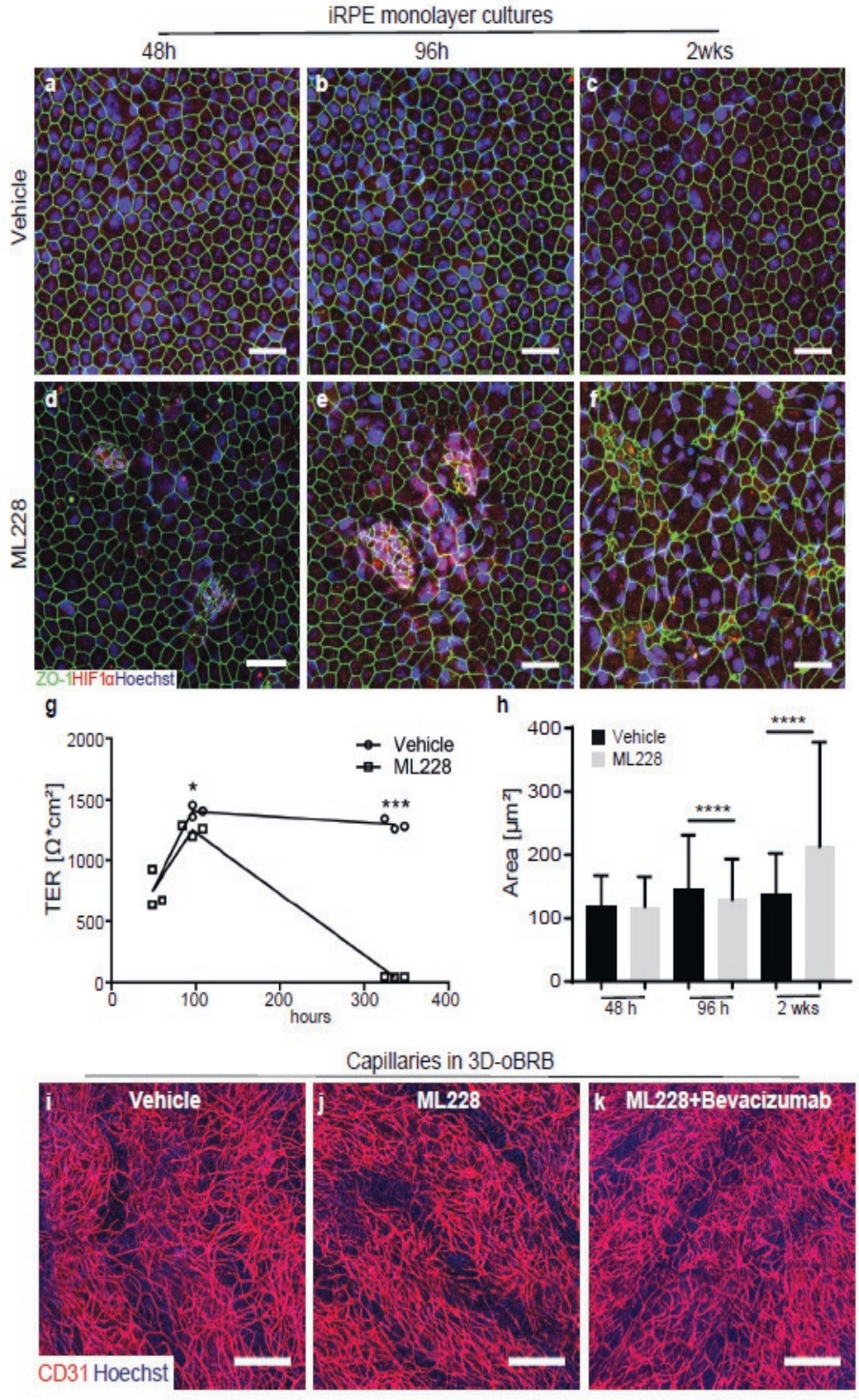
iRPE monolayer cultures
48h
96h
2wks
Vehicle
ML228
a
b
c
d
e
f
ZO-1HIF1αHoechst
g
TER [Ω*cm²]
2000
1500
1000
500
0
0
100
200
300
400
hours
Vehicle
ML228
*
***
h
Area [µm²]
400
300
200
100
0
Vehicle
ML228
****
****
48 h
96 h
2 wks
Capillaries in 3D-oBRB
i Vehicle
j ML228
k ML228+Bevacizumab
CD31 Hoechst

Supplementary Figure 12. ML228 and Bevacizumab treatment on 2D iRPE and 3D-oBRB. **A**-**F**: RPE monoculture at 48 hr (**A**,**D**), 96 hr (**B**,**E**), and 2weeks (**C**,**F**) from the beginning of ML228 (2 μM; 96hr) treatment, immunostained with HIF-1α (red), ZO-1 (green), and Hoeschst (blue). Vehicle treatment consisted of DMSO. Scale bars, 30 μm. (n = 3) **G**: TER measurement of 2D iRPE without or with ML228 treatment (n = 3). **H**: ZO-1 staining based morphometry analysis of individual cell area in vehicle and ML228 treated samples was performed, n = 7495. Error bars indicate standard deviation. **I**-**K**: images of deep choroidal regions of **I**, vehicle. **J**: ML228. **K**: ML228+bevacizumab treated 3D-oBRB, immunostained with CD31 (red) and Hoechst (blue) show no differences in deeper layers.
Scale bars, 350 μm. (n = 4)

List of authors with affiliations

In order of appearance in this thesis.

Céline Koster (CK)

*Department of Human Genetics Amsterdam, Section of Ophthalmogenetics, Amsterdam University Medical Centers (AUMC), University of Amsterdam (UvA), Location Meibergdreef, 1105 AZ Amsterdam, The Netherlands (NL)

Kimberley E. Wever (KW)

*Systematic Review Center for Laboratory Animal Experimentation (SYRCLE), Department for Health Evidence, Radboud Institute for Health Sciences, Radboud University Medical Center, 6525 GA Nijmegen, NL

Philip E. Wagstaff (PW)

*Department of Human Genetics Amsterdam, Section of Ophthalmogenetics, AUMC, UvA, Location Meibergdreef, 1105 AZ Amsterdam, NL

Koen T. van den Hurk (KH)

*Department of Human Genetics Amsterdam, Section of Ophthalmogenetics, AUMC, UvA, Location Meibergdreef, 1105 AZ Amsterdam, NL

Carlijn R. Hooijmans (CH)

*SYRCLE, Department for Health Evidence, Radboud Institute for Health Sciences, Radboud University Medical Center, 6525 GA Nijmegen, NL

*Department of Anesthesiology, Pain and Palliative Medicine, Radboud University Medical Center, 6525 GA Nijmegen, The Netherlands.

Arthur A. Bergen (AB)

*Department of Human Genetics Amsterdam, Section of Ophthalmogenetics, AUMC, UvA, Location Meibergdreef, 1105 AZ Amsterdam, NL

*Department of Ophthalmology, AUMC, UvA, Location Meibergdreef, 1105 AZ Amsterdam, NL

*Queen Emma Centre of Precision Medicine, AUMC, UvA, Location Meibergdreef, 1105 AZ, Amsterdam, NL

Colby F. Lewallen (CF)

*Georgia Institute of Technology, G.W. Woodruff School of Mechanical Engineering, Atlanta, GA 30313, United States of America (USA)

Mays Talib (MT)

*Department of Ophthalmology, Leiden University Medical Center, 2333 ZA Leiden, NL

Jacoline B. ten Brink (JB)
*Department of Human Genetics Amsterdam, Section of Ophthalmogenetics, AUMC, UvA, Location Meibergdreef, 1105 AZ Amsterdam, NL

Camiel J.F. Boon (CB)
*Department of Ophthalmology, AUMC, UvA, Location Meibergdreef, 1105 AZ Amsterdam, NL
*Department of Ophthalmology, Leiden University Medical Center, 2333 ZA Leiden, NL

Boris V. Stanzel (BS)
*Eye Clinic Sulzbach, Knappschaft Hospital Saar, 66280 Sulzbach/Saar, Germany
*Department of Ophthalmology, University of Bonn, 53113 Bonn, Germany

Kapil Bharti (KB)
*Ocular and Stem Cell Research Section, National Eye Institute (NEI), National Institutes of Health (NIH), Bethesda, MD 20892, USA
*NCATS, NIH, Bethesda, MD 20850, USA

Min Jae Song (MS)
*Ocular and Stem Cell Research Section, NEI, NIH, Bethesda, MD 20892, USA
*National Center for Advancing Translational Sciences (NCATS), NIH, Bethesda, MD 20850, USA

Russel Quinn (RQ)
*Ocular and Stem Cell Research Section, NEI, NIH, Bethesda, MD 20892, USA

Eric Nguyen (EN)
*Ocular and Stem Cell Research Section, NEI, NIH, Bethesda, MD 20892, USA

Christopher Hampton (CH)
*Ocular and Stem Cell Research Section, NEI, NIH, Bethesda, MD 20892, USA

Ruchi Sharma (RS)
*Ocular and Stem Cell Research Section, NEI, NIH, Bethesda, MD 20892, USA

Tea Soon Park (TP)
*Ocular and Stem Cell Research Section, NEI, NIH, Bethesda, MD 20892, USA

Ty Voss (TV)
*NCATS, NIH, Bethesda, MD 20850, USA

Carlos Tristan (CT)
*NCATS, NIH, Bethesda, MD 20850, USA

Claire Malley (CM)
*NCATS, NIH, Bethesda, MD 20850, USA

Anju Singh (AS)
*NCATS, NIH, Bethesda, MD 20850, USA
Roba Sejene (RS)
*Ocular and Stem Cell Research Section, NEI, NIH, Bethesda, MD 20892, USA

Devika Bose (DB)
*Ocular and Stem Cell Research Section, NEI, NIH, Bethesda, MD 20892, USA

Paige Derr (PD)
*NCATS, NIH, Bethesda, MD 20850, USA

Kristy Derr (KD)
*NCATS, NIH, Bethesda, MD 20850, USA

Sam Michael (SM)
*NCATS, NIH, Bethesda, MD 20850, USA

Francesca Barone (FB)
*Ocular and Stem Cell Research Section, NEI, NIH, Bethesda, MD 20892, USA

Arvydas Maminishkis (AM)
*Ocular and Stem Cell Research Section, NEI, NIH, Bethesda, MD 20892, USA

Ilyas Singec (IS)
*NCATS, NIH, Bethesda, MD 20850, USA

Marc Ferrer (MF)
*NCATS, NIH, Bethesda, MD 20850, USA

Author contributions

Chapter 1 ("General introduction") and **Chapter 6** ("General discussion, prospects and conclusions") of this thesis have been written by CK and extensively reviewed by AB and KB.

Chapter 2 ("A Systematic Review on Transplantation Studies of the Retinal Pigment Epithelium in Animal Models"): CK: study selection, data collection, analysis, interpretation of results, drafting of the manuscript; KW: study selection, data collection, search strategy, analysis, and review of the manuscript; PW and KH: study selection; CH: data collection, analysis and review of the manuscript; AB: critical review of the manuscript. All authors have read and agreed to the published version of the chapter.

Chapter 3 ("The Lrat$^{-/-}$ Rat: CRISPR/Cas9 Construction and Phenotyping of a New Animal Model for Retinitis Pigmentosa"): CK: conceptualization, formal analysis, investigation, original draft preparation, review and editing, project administration; KH: formal analysis, investigation, review and editing; CL: software, review and editing; MT and CB: patient data curation, review and editing; JB: investigation, review and editing; AB: conceptualization, investigation, supervision, funding acquisition, review and editing. All authors have read and agreed to the published version of the chapter.

Chapter 4 ("Sodium-iodate injection can replicate retinal degenerative disease stages in pigmented mice and rats: non-invasive follow-up using OCT and ERG"): CK: conceptualization, formal analysis, investigation, drafting of the manuscript, review and editing, project administration; KH: formal analysis, investigation, review and editing; JB: investigation, review and editing; CL: software, review and editing; BS: supervision, review and editing; KB: supervision, review and editing; AB: conceptualization, investigation, supervision, funding acquisition. All authors have read and agreed to the published version of the chapter.

Chapter 5 ("Bioprinted 3D Outer Retina Barrier Uncovers RPE-dependent Choroidal Phenotype in Advanced Macular Degeneration"): MS: conceptualization, formal analysis, investigation, drafting of the manuscript, review and editing, project administration; RQ: formal analysis, investigation, review and editing; EN, CH, RS, TP, CK, TV, CT, CM, AS, RD, DB, PD, KD, SM, FB, IS and MF: investigation, review and editing; AM: investigation, review and editing, supervision; KB: investigation, review and editing, supervision, funding acquisition. All authors have read and agreed to the published version of the chapter.

Graduate Schools:
AMC Graduate School for Medical Sciences
&
ONWAR Graduate School Neurosciences Amsterdam Rotterdam

Summary of PhD training, teaching and parameters of esteem

Céline Koster
March 2015 – September 2022
Promotor: Prof. dr. A.A.B. Bergen (AUMC, location AMC)
Co-promotor: Dr. K. Bharti (NEI-NIH)

1. PhD training

Course Name	**Year**	**Workload (hours / ECTs)**
General Courses		
Basic Laboratory Safety	2015	12 / 0.4
Practical Biostatistics	2015	40 / 1.4
Advanced qPCR	2015	20 / 0.7
Functional Imaging and Super Resolution	2015	50 / 1.8
Advanced Topics in Biostatistics	2016	60 / 2.2
Computing in R	2016	12 / 0.4
Basic Microsurgery Course (Groningen)	2016	25 / 0.9
Grant Writing Course (ONWAR)	2017	50 / 1.8
	Total (hours)	**269 / 9.6**

Specific Courses		
Functional Neuroanatomy	2015	40 / 1.4
In vivo Phenotyping of Mutant Rodents: Integrating Neural Activity, Neurochemistry, Heart Rate & Behavior	2015	50 / 1.8
BCRM: Current Issues in Clinical Neuroscience: The Neonatal Brain and Connectome	2017	42 / 1.5
Stem Cells and Organoids as Models for Tissue Differentiation and Eye Diseases	2017	5 / 0.2
	Total (hours)	**137 / 4.9**

Seminars, Workshops and Masterclasses	Year
Hands-on training Systematic Reviews of Animal Studies	2015
Master Class Kevin Eggan (VU/CNCR)	2015
Symposium Genome editing with CRISPR-Cas9 (AMC)	2016
Animal Welfare: Pain in Practice (IvD, VU)	2016
Westburg Takara: CRISPR/Cas9 (organization, AMC)	2016
Workshop and Masterclass Malcolm McLeod: Animal Experiments, better, faster and easier	2017
NEI Regenerative Medicine seminar series (online)	2020
Onderzoekssymposium Oogheelkunde Amsterdam UMC (oral presentation)	2020
Harry Blom Beraad: “Een verschil van dag en nacht”	2020
IXA valorisation seminar series (online)	2021
World CRISPR Day by Synthego (online)	2021
Harry Blom Beraad: “De invloed van het microbioom op dierproeven”	2021
Expert Class Governance Structure	2022
Whole Horse Dissection (Equine Studies)	2022

Presentations	Year
Wetenschapsdag Klinische Genetica AMC/VUmc (oral)	2016
Refereeravond Klinische Genetica AMC/VUmc (oral)	2016
ARVONED (oral)	2016
HydraXII, The European Summer School on Stem Cells & Regenerative Medicine (poster)	2016
ONWAR Annual Meeting (poster)	2016
ARVO (poster)	2017
Wetenschapsdag Klinische Genetica AMC/VUmc (poster)	2017
ARVO (poster)	2018
ONWAR Annual Meeting (oral)	2018
ARVO (oral)	2019
Boerhaave Symposium (oral)	2019
International DOG Symposium on AMD (poster)	2019
Wetenschapsdag Klinische Genetica AMC/VUmc (oral)	2019
Annual Amsterdam Neuroscience Meeting (poster)	2021

(Inter)national conferences	Year
Young Researcher Vision Camp 2015	2015
ONWAR Career Event	2015
ONWAR Annual Meeting	2015
Hydra XII, The European Summer School on Stem Cells & Regenerative Medicine	2016
Annual Amsterdam Neuroscience Meeting	2016
ONWAR Annual Meeting	2016
ARVONED	2016
ARVO 2017	2017

ARVO 2018	2018
BCF Career Event	2018
ARVO 2019	2019
International DOG Symposium on AMD	2019
BCF Career Event	2019
Annual Amsterdam Neuroscience meeting	2019
3D printing and additive manufacturing (online)	2020
DALAS biotechnische dagen	2021
Annual Amsterdam Neuroscience meeting	2021

2. Teaching

Supervising	**Year**
Internship Annemarijn Lukassen (HBO, final thesis).	2016
Internship Pesho Ismael (Literature thesis, Geneeskunde bachelor)	2017-2018
Internship Leon Begthel (HBO, final thesis, biotechnical)	2018-2019
Internship Koen van den Hurk (HBO, final thesis, biotechnical)	2019-2020
Internship Roos-Sanne Verkerk (HBO, final thesis, biotechnical)	2020-2021
Internship Thomas van der Horst (WO, final thesis, master: science, bussiness & innovation)	2022
Internship Eduard Siemerink (WO, final thesis, master: drug, discovery & safety, major: science in society)	2022

3. Parameters of Esteem

Grants	**Year**
ZonMW: Meer Kennis met Minder Dieren; Synthesis of Evidence	2017
ZonMW: translational travelgrant	2018
ZonMW: Meer Kennis met Minder Dieren; Synthesis of Evidence	2020

Awards and Prizes	**Year**
Best Poster Prize wetenschapsdag Klinische Genetica AMC/VUmc	2017
AMC Young Talent Fund	2017

4. Publications

Peer-reviewed	Year
Anna Bennis, Gerbren J. Jacobs, Lisa A.E. Catsburg, Jacoline B. ten Brink, ***Céline Koster***, Reinier O. Schlingemann, Jan C. van Meurs, Theo G.M.F. Gorgels, Perry D. Moerland, Vivi M. Heine and Arthur A. Bergen. 2017. "Stem Cell Derived Retinal Pigment Epithelium: The Role of Pigmentation as Maturation Marker and Gene Expression Profile Comparison with Human Endogenous Retinal Pigment Epithelium". *Stem Cell Reviews and Reports* 13, (5):659-669. https://doi.org/10.1007/s12015-017-9754-0	2017
Arthur A. Bergen, S. Arya, ***Céline Koster***, Matthew G. Pilgrim, Dagmara Wiatrek-Moumolidis, Peter J. van der Spek, Stefanie M. Hauck, Camiel J.F. Boon, Eszter Emri, Alan J. Stewart and Imre Lengyel. 2019. "On the origin of proteins in human drusen: The meet, greet and stick hypothesis". *Progress in Retinal Eye Research* 70: 55-84. https://doi.org/10.1016/j.preteyeres.2018.12.003	2019
Céline Koster, Kimberley E. Wever, Philip E. Wagstaff, Koen T. van den Hurk, Carlijn R. Hooijmans, and Arthur A. Bergen. 2020. "A Systematic Review on Transplantation Studies of the Retinal Pigment Epithelium in Animal Models". *International Journal of Molecular Sciences* 21, no. 8: 2719. https://doi.org/10.3390/ijms21082719	2020
Céline Koster, Koen T. van den Hurk, Colby F. Lewallen, Mays Talib, Jacoline B. ten Brink, Camiel J.F. Boon, and Arthur A. Bergen. 2021. "The Lrat$^{-/-}$ Rat: CRISPR/Cas9 Construction and Phenotyping of a New Animal Model for Retinitis Pigmentosa". *International Journal of Molecular Sciences* 22, no. 13: 7234. https://doi.org/10.3390/ijms22137234	2021
Céline Koster, Koen T. van den Hurk, Jacoline B. ten Brink, Colby F. Lewallen, Boris V. Stanzel, Kapil Bharti, and Arthur A. Bergen. 2022. "Sodium-Iodate Injection Can Replicate Retinal Degenerative Disease Stages in Pigmented Mice and Rats: Non-Invasive Follow-Up Using OCT and ERG". *International Journal of Molecular Sciences* 23, no. 6: 2918. https://doi.org/10.3390/ijms23062918	2022

Other	Year
Céline Koster, Ghazaleh Hajmousa, Anna Bennis, Reinier O. Schlingemann, Jan C. van Meurs, Frank D. Verbraak, Theo H. Smit, Jacoline B. ten Brink, Anneloor L.M.A. ten Asbroek, Vivi M. Heine and Arthur A. Bergen. 2017. "Towards an experimental stem cell-based therapy for Age-related Macular Degeneration". *Investigative Ophthalmology & Visual Science* 58, (8):1983.	2017
Céline Koster, Anneloor L.M.A. ten Asbroek, Jacoline B. ten Brink, Reinier O. Schlingemann, Jan C. van Meurs, Frank D. Verbraak, Theo H. Smit, Camiel J.F. Boon and Arthur A. Bergen. 2018. "Sodium iodate-induced retinal degeneration in small animal models for Age-related Macular degeneration". *Investigative Ophthalmology & Visual Science* 59, (9):6062.	2018
Céline Koster, Francesca Barone, Arvydas Maminishkis, Min Jae Song, Russell Quinn, Colby F, Lewallen, Jan C. van Meurs, Kapil Bharti and Arthur A. Bergen. 2019. "Transplantation of Bio-Printed Choroid-RPE Tissue into The Subretinal Space of Rats". *Investigative Ophthalmology & Visual Science* 60, (9):3275.	2019
Min Jae Song, Russell Quinn, Eric Nguyen, Christopher Hampton, Ruchi Sharma, Tea Soon Park, ***Céline Koster***, Ty Voss, Carlos Tristan, Claire Malley, Anju Singh, Roba Dejene, Devika Bose, Paige Derr, Kristy Derr, Sam Michael, Francesca Barone, Arvydas Maminishkis, Ilyas Singec, Marc Ferrer and Kapil Bharti. 2020. "Bioprinted 3D Outer Retina Barrier Uncovers RPE-dependent Choroidal Phenotype in Advanced Macular Degeneration". *In preprint*. https://doi.org/10.21203/rs.3.rs-135775/v1	2020

Funding

The printing and public distribution of this thesis has been made possible by the generous sponsorship of:

Mai Medizintechnik
Roland-Consult
MedicalWorkshop BV
Department of Human Genetics, Amsterdam UMC, location AMC

The work described in this thesis was funded by the following partners:

Stichting Uitzicht (UZ 2016-21) including:
Stichting Macula Degeneratie Nederland
Landelijke Stichting voor Blinden en Slechtzienden
Stichting Retina Fonds Nederland
Oogfonds
De Rotterdamse Stichting Blindenbelangen (#B20160043)
Stichting Blindenhulp
Stichting voor Ooglijders
Stichting Lijf en Leven (#42)
TKI-PPP Health Holland-Biogen Consortium (2020-1935)
ZonMw (114024111)
National Eye Institute (NEI) Intramural Funds (USA)
Department of Defense Grant (USA)

Dankwoord / Acknowledgments

Het is de hoogste tijd! Het boekje dat voor je ligt is het resultaat van een aantal jaren onderzoek. Lang niet alles wat ik heb gedaan staat in dit boekje, omdat ook lang niet alles is gelukt of nog niet is afgerond. Wat er wel in staat, daar ben ik ontzettend trots op! Het was een lange, soms frustrerende, uitdagende, maar ook voldoening gevende, interessante en leuke weg. Ik heb ontzettend veel geleerd en me op wetenschappelijk en persoonlijk vlak kunnen ontwikkelen.

Het is ontzettend moeilijk en bijna onmogelijk om mijn dankbaarheid in woorden te vangen. Er zijn teveel redenen om te bedanken en teveel mensen die ik zou willen bedanken. Ik ga een poging wagen. En bij deze ook iedereen, die ik hieronder niet persoonlijk noem, maar toch een bijdrage heeft geleverd aan mijn thesis, bedankt voor het advies, de gesprekken, de hulp op welke manier dan ook tijdens bijvoorbeeld conferenties of werkbezoeken. Elke input heb ik altijd enorm gewaardeerd.

Allereerst, en in het bijzonder, wil ik mijn promotor bedanken: Prof. dr. Arthur Bergen. Arthur, bedankt voor het creëren van een omgeving waar ik zelfstandig heb kunnen werken aan mijn projecten (natuurlijk met bepaalde sturing en instructies van jou). Dank je wel dat je altijd hebt geprobeerd om mijn focus te houden bij het afmaken van mijn promotietraject en mijn thesis en me niet liet afdwalen naar één van mijn “hobbyprojectjes” zoals jij die noemt. Bedankt dat ik tegelijkertijd ook de vrijheid heb gekregen die ik nodig had om sommige dingen op mijn manier aan te pakken.

Secondly, I would like to thank Dr. Kapil Bharti, my co-promotor. Kapil, I am so grateful that I was able to visit your lab in Bethesda a few times. I learned such a great deal from you and Arvydas. I developed skills that I will, for sure, use during the rest of my career. Arvydas, thank you for all your help, tips, trics, and, most importantly, your humor. I still have my red artificial intelligence machine that helps me answer all people’s questions. Colby, thank you for all your efforts in analyzing the ERG and behavioral data and your impressive and amazing skills in programming and machine-learning. I hope we can keep this collabolation going! Of course, my thanks also goes to all the Bharti/Maminishkis/Miller groupmembers at the NEI, who helped me make my time in Bethesda unforgettable. I hope we will meet again soon!

Graag zou ik ook bij deze de leden van mijn promotiecommissie willen bedanken. Prof. dr. Van Meurs, Prof. dr. Boon, Prof. dr. Mummery, Prof dr. Smit, Prof. dr. Verhaagen, Dr. Verbraak, Prof. dr. Tan en Prof. dr. Van Karnebeek, bedankt voor alle tijd die jullie hebben besteed aan het lezen en beoordelen van mijn thesis en dat jullie zitting hebben willen nemen in mijn promotiecommissie.

En dan: Jaco.. Wat moet ik zeggen. Ik denk dat je wel weet hoe belangrijk je bent geweest (en ook nog steeds bent) bij al mijn projecten. Je stond altijd klaar voor me, op meerdere vlakken, en dat doe je ook nog steeds. Je bent de eerste waar ik heen ren als er iets onduidelijk is of als ik iets zoek. Bedankt dat ik elke werkbespreking kan afsluiten met een lach omdat jij standaard “RTFM” en “Think Before You Start” roept. En dan hebben we ook nog de Nederlandse klassieker: “Eerst kijken, dan zeiken”. En je hebt eigenlijk ook altijd gelijk!

Anna, bedankt voor het “voor”onderzoek dat je hebt gedaan en al je harde werk. Ik heb veel gebruik gemaakt van alle kennis die jij tijdens je promotieproject hebt vergaard. Dr. Heine, Vivi, bedankt dat je me in het begin van mijn project hebt helpen opstarten en dat ik altijd bij je terug mocht komen voor vragen en input.

I would also like to thank all PhD-students and postdocs from the Bergen group at the AMC. Thank you, Phil, Reinier, Mark, Andrea and Isa for all fruitful discussions, anecdotes and stories. I hope that all your projects will be a success! My thanks also goes to all the former members of K2 including the ones from the Neurogenetics and the CFG. Thank you for all your input and learning curves.

Anneloor and Eszter, thank you for your help and critical input. Eszter, thank you for all the chats that we have, your companionship in the office, your little cheer-up-presents, and the endless bags of chocolate.

Nemanja, Sovann and Pete, thank you for helping me out in the beginning of my project and for setting up in the animal facilities.

Ook zou ik graag alle studenten bedanken die hun (afstudeer)stage tijdens mijn PhD-project hebben gedaan. Annemarijn, Pesho, Leon, Koen, Roos-Sanne, Thomas en Eduard jullie hebben bergen werk verzet en een grote bijdrage geleverd aan mijn projecten. Koen, bedankt voor al je werk dat je na je stage als biotechnisch analist doet en hebt gedaan. Ik vind het altijd gezellig om samen te werken! Roos, ontzettend leuk dat ook jij na je stage bij ons in de groep bent gebleven. Bedankt voor al je input en gezelligheid.

Lou, bedankt voor al je geduld als ik weer eens iets wilde bestellen bij een bedrijf dat niet in het systeem staat. Ook bedankt dat jij, als echte ICT-held, meerdere softwares weer werkend hebt gekregen op de AMC computers als de ICT-servicedesk er niet uit kwam. Patrick, bedankt voor al jouw praktische hulp in het lab en ook dat jij wel eens mijn kweken overnam als ik weer eens naar een congres ging!

Dan zou ik graag Dr. Van Schooneveld, Prof. dr. Boon en Dr. Talib willen bedanken. Mary, Camiel en Mays bedankt voor jullie waardevolle klinische input in mijn projecten!

Prof. dr. Van Meurs, en Drs. Van Overdam, Jan en Koen, bedankt dat ik altijd welkom ben in het Oogziekenhuis in Rotterdam om te leren van de indrukwekkende operaties die jullie uitvoeren. Ik hoop dat ik binnenkort weer een keer langs kan komen. Dr. Stanzel, Boris, thank you for having me in Bonn, showing me your lab, and sharing your knowledge.

Over de jaren heb ik veel samengewerkt met de dierverzorgers en het biotechnisch personeel van het UPC (in de VU) en het ARIA (in het AMC). Ik wil graag iedereen bedanken voor zijn/haar inzet voor mijn dieren en mijn experimenten. Natuurlijk zou ik ook graag alle leden van de IVD van beide locaties willen bedanken voor hun hulp en input.

En dan van collega's, collega-vrienden en mensen met wie ik samen heb gewerkt naar vrienden en familie.

Stephanie and Lisa, my paranimphs and two of my dearest friends. We met in the ONWAR program and in Vivi's lab, and we grew into three very good friends over the years. At work and in our private life, we walked almost the same path, and I am so glad and thankful that we were able to do this together. All three, we have very different personalities, but together it seems like we merge into one person. Even though we are distance-wise, not really close together, it feels like we are always close in my heart. Thank you for all your support and I hope that, despite the physical distance, we will stay in each other's lives.

Rachel, bedankt dat je zo goed voor Amke zorgt elke dag. Ook als ik even niet de mogelijkheid heb om meerdere keren in de week te komen. Ze heeft het onzettend goed bij jou en daar ben ik je heel erg dankbaar voor.

Mam, pap, bedankt dat jullie er altijd voor mij zijn en zijn geweest. Dat jullie me altijd hebben gesteund en me hebben geleerd dat ik mag zijn wie ik ben. Bedankt dat jullie altijd in me hebben geloofd en ervoor hebben gezorgd dat ik heb kunnen bereiken waar ik nu sta. Bedankt dat jullie nog altijd elke dag voor mij en mijn gezin klaar staan. Robbin, mijn broertje (alleen dan nog in leeftijd...), bedankt dat ook jij altijd voor me klaar staat. Ook al spreken we elkaar lang niet elke dag en zijn we uitgegroeid tot totaal twee verschillende personen, we kunnen elkaar altijd terugvinden. Angelique, samen met Robbin, vormen jullie een goed team. Jullie vullen elkaar ontzettend goed aan op een liefdevolle manier. Bedankt dat ook jij altijd voor me klaar staat en dat je ervoor hebt gezorgd dat dit boekje er zo ontzettend mooi uit is komen te zien! Alle credits hiervoor gaan zonder twijfel naar jou!

En dan als laatste, Arjan, mijn liefde. Ik ben ontzettend trots op wat we samen hebben bereikt en waar we in het leven staan. Ik had zonder jouw onvoorwaardelijke steun en (soms engelen-) geduld mijn PhD nooit op deze manier kunnen afronden. Het heeft wat voeten in de aarde gehad, maar het moment is nu eindelijk daar. Bedankt dat je me de ruimte hebt gegeven om hierop te kunnen focussen. Bedankt dat je er altijd voor me bent. Je bent een fantastische vader voor onze zoon. Ik houd van jou.

I'm more interested in the future than in the past, because the future is where I intend to live.

— Albert Einstein